CARBON ORE, RARE EARTH, AND CRITICAL MINERALS (CORE-CM) ASSESSMENT OF SAN JUAN AND RATON COAL BASINS: WHAT IS THE FUTURE POTENTIAL OF COAL IN THE SAN JUAN AND RATON BASINS, NEW MEXICO AND COLORADO

Edited by Virginia T. McLemore and Amy Trivitt

Virginia.McLemore@nmt.edu
Amy.Trivitt@nmt.edu

New Mexico Bureau of Geology and Mineral Resources
New Mexico Institute of Mining and Technology
Socorro, NM 87801

U.S. Department of Energy
Office of Fossil Energy and Carbon Management
Contract number DE-FE0032051
Project Performance Period: 10/01/2021 to 6/30/2025

New Mexico Bureau of Geology and Mineral Resources
Open-file Report OF-646
February 2, 2027

CONTRIBUTING AUTHORS

PRINCIPAL INVESTIGATORS

Virginia T. McLemore (Lead Research Scientist, Economic Geologist and Adjunct Professor)
Navid Mojtabai (Professor)

*student, **high school student

NEW MEXICO INSTITUTE OF MINING AND TECHNOLOGY (NMIMT)

New Mexico Bureau of Geology and Mineral Resources (NMBGMR)
Virginia T. McLemore
Amy Trivitt
Cynthia Connolly
Shari Kelley
Mark Leo-Russell
Bonnie Frey
Nels Iverson
Evan Owen (now with New Mexico Energy, Minerals, and Natural Resources)
Devlon Shaver (former student, Mineral Engineering Department)
Mark Mansell
Jacob Lewis

Mineral Engineering Department
Navid Mojtabai
William X. Chavez
*Megan Bodanie
*Valentina Robledo
*Richard Otoo
*Zohreh Kazemi Motlagh
*Lawrence Sarpong
*Sebastian Nipah
*Harriett Tetteh
*Abena Serwah

Earth and Environmental Science
Rachel Coyte
*Jacob Newcomer
*Sarah Moses
*Rebecca Boakye
*John Lempke
*J. Jones
R. Tsosie
*B. Detsoi

Petroluem Resource and Recovery Center (PRRC)
Sai Wang
Robert Bausch
James McLemore

MAGDALENA TEEN SCIENCE CAFÉ
Jim Sauer
**Shiloh Carter
**Nara Scott
**Gabe Carothers
**Karina Henderson
**Zeb Apachito
**Brittney King

SANDIA NATIONAL LABORATORIES (SNL)
Guangpring Xu
Jason Heath
Mark J Rigali

LOS ALAMOS NATIONAL LABORATORY (LANL)
Brent Goehring
Peter Watson
Isaac Mantelli

SONOASH
Claudio Arato
Brad MacKenzie

SAN JUAN COLLEGE (SJC)
Craig J. William

DEDICATION

Since the start of this project, two NMBGMR staff members passed away before their time, Mark Mansell (1962-2023, Bureau of Geology News) and Mark Leo-Russell (1959-2025, Bureau of Geology News). Both gentlemen were essential in aiding students working on this and other projects and made every effort to help them succeed. We would like to dedicate this report in their memory. Mark Mansell provided GIS, IT, and other technical support, and Mark Leo-Russell designed the database used in this and other critical minerals projects, as well as assisted in sample collection, photography, and IT support. Their expertise, humor, smiles, and willingness to assist everyone are missed and both have been difficult to replace. Rest in peace friends!

EXECUTIVE SUMMARY

This report summarizes results from the CORE-CM project in the San Juan and Raton basins of New Mexico and Colorado and ultimately begins to address what is the future of coal in the San Juan and Raton basins. The objective of this project was to determine the nonfuel carbon-based products (CBP), critical minerals, and rare earth elements (REE) potential in coal and related stratigraphic units in the San Juan and Raton basins and adjacent areas. This project delineated favorable geologic terrains and priority areas containing potential CBP, critical minerals, and REE deposits for the DOE mandate, which also is a priority of the NMBGMR and state of New Mexico. This project is important to the state because CBP, critical minerals, and REE resources must be identified before land use decisions are made by government officials. Future mining of CBP, critical minerals, and REE will directly benefit the economy of New Mexico. Furthermore, it is crucial to re-establish a domestic source of critical minerals and REE in the U.S. to help secure the nation's clean energy future, to reduce the vulnerability of the U.S. to material shortages related to national defense, and to maintain our global technical and economic competitiveness. In addition to these benefits, students at New Mexico Institute of Mining and Technology (NMT) and San Juan College were hired and trained to contribute to this project and for the future workforce.

New Mexico has a wealth of mineral resources with significant production and resources of oil, gas, copper, potash, molybdenum, uranium, geothermal, and coal. Oil and gas are the most important extractive industries in the state in terms of production and New Mexico ranked 2nd in oil production and 3rd in gas production in 2024. New Mexico ranked 14th in the U.S. in coal production in 2024. CBP include the nonfuel uses of coal, such as use in construction materials, aggregates (clinkers), resin, cement, soil additives (humate), asphalt additives, and products for the chemical industry. Synthesis of graphite and graphene is a potential nonfuel use of coal, both are critical minerals, and graphite was once mined in the Raton Basin. Humate is currently produced in the San Juan Basin and the industry could be expanded by the presence of abundant reserves. However, mineral production, including coal has decreased in recent years for many reasons.

The San Juan Basin, located in the southeast margin of the Colorado Plateau extends over northwestern New Mexico, northeastern Arizona, and southern Colorado. The Raton Basin is located in the northeastern portion of New Mexico and southeastern Colorado. Paved highways, gravel, and dirt roads access both two basins. The areas are mostly rural, and only a few ranches are within several miles of the coal fields. The climate is semiarid to arid. During the Late Cretaceous, the present San Juan and Raton basins were on the western edge of the Western Interior seaway, which extended from the Gulf of Mexico to the Arctic Ocean. Coal is found in Cretaceous sedimentary rocks in the San Juan and Raton basins. The stratigraphic units in the San Juan Basin dip inward from the bounding highlands toward the center of the basin, creating a trough-like feature. The Cretaceous sedimentary rocks in the San Juan Basin contain three major coal-bearing units: the Crevasse Canyon, Menefee, and Fruitland Formations. The Raton Basin is divided into coal camps.

A sampling plan, health and safety plan (HASP), standard operating procedures (SOPs) and sampling and laboratory methods were developed to obtain the project objectives. Samples were collected, prepared, and analyzed according to standard methods for each specific laboratory analysis. Samples are archived at the NMBGMR. Samples collected are complete, comparable, and representative of the defined population at the defined scale. A sufficient

number and quantities of samples were collected to obtain the project objectives. However, more samples will increase the confidence of the results and fill in data gaps.

Coal and humate samples in this study from the San Juan and Raton basins typically displayed relatively flat to slightly light REE enriched chondrite-normalized REE patterns. When normalized to NASC (North American Shale Composite), these coal and humate samples display flat REE patterns with no significant enrichment or depletion. The New Mexico coal and humate samples are relatively moderate to low in REE (<485 ppm TREE), Li (<94 ppm), V (<282 ppm), Co (<65 ppm), Ni (<77 ppm), Zr (<1336 ppm), Hf (<10 ppm), and other critical minerals compared to typical economic deposits. The coal and humate samples are similar in chemistry as the adjacent sedimentary rocks.

Another way to examine critical minerals and REE in coal deposits is to determine the amount of the element in coal ash instead of the whole-rock sample. Measuring REE and other critical minerals on the ash basis approximates the critical minerals content of the fly or bottom ash remaining after coal is burned at a power plant, where critical minerals could then be leached from the ash. Recovery of critical minerals from these materials during stabilization and closure could help offset closure costs and help with the demand for critical minerals. Concentrations of REE on ash basis are higher on average in lower (<10%) ash content samples. Coal ash samples in this study typically displayed relatively flat to slightly light REE enriched chondrite-normalized REE patterns, consistent with REE hosted by clay minerals, zircon, and monazite. When normalized to NASC (North American Shale Composite), these coal ash samples display flat REE patterns with no significant enrichment or depletion. Some of the highest total REE concentrations (ash basis) are found in coal ash from the closed La Plata mine in the Fruitland Formation (2,103 ppm), the closed Mentmore mine in the Gallup Sandstone (807 ppm), as well as the Crownpoint (1,684 ppm), Standing Rock (523 ppm), Barker Creek (528 ppm), Mt. Taylor (696 ppm), Star Lake (795 ppm), and Monero (1,026 ppm) coal fields in the San Juan Basin. The La Plata coal was used at the San Juan power plant (now closed). These concentrations are above the DOE recommended limit of 500 ppm TREE and could be economic in the future. Other concentrations of critical minerals are mostly below economic concentrations.

Many beach-placer sandstone deposits in the San Juan Basin contain high concentrations of Ti (29..4%), Zr (>1000 ppm), REE (>14,041 ppm TREE+Y), U (179 ppm), Th (>1000 ppm), Nb (1490 ppm), Fe (69.52%), Sc (92.7 ppm), Y (1795 ppm), and other elements; some of these concentrations are similar to economic cut-off grades. Estimated endowment of critical minerals in beach-placer sandstone deposits in the San Juan Basin amounts to >1.6 million metric tons of ore containing >150,000 metric tons TiO_2, >385,000 metric tons Cr, 830 metric tons Nb, >1.8 million metric tons V, >36,000 metric tons Zr and >10,000 metric tons total REE.

Sediment-hosted, stratabound copper deposits throughout the world are known to have locally elevated concentrations of various critical minerals and are the second most important source of copper production in the world after porphyry copper deposits. Selected samples were collected from sediment-hosted, stratabound copper deposits in the Nacimiento and Zuni Mountains to examine their critical minerals potential by determining their mineralogy and geochemistry. Some samples in the Nacimiento and Zuni Mountains have elevated heavy REE. Samples from the Coyote district are elevated in cobalt. Both Coyote and Zuni samples are elevated in heavy REE, vanadium, and uranium. The Eureka deposit has elevated barium. Bismuth is elevated in Zuni and Coyote samples.

The Grants uranium district has important uranium deposits that could be in production in the future. Some sandstone-hosted, limestone-hosted, and U-vein deposits are elevated in critical

minerals. Uranium, vanadium, and molybdenum were once produced from the deposits. An estimated 146 million short tons of ore containing >236 million lbs of uranium at grades ranging from 0.1-0.4 U_3O_8 are found in the sandstone-hosted deposits in the Grants uranium district. Future exploration should include evaluation of critical minerals in these deposits, especially for V, REE, Re from molybdenite, and Cs.

Mine wastes are high-volume heterogeneous material that remains from the extraction (mining) and processing (milling, refining) of a range of metalliferous and non-metalliferous mineral deposits. The types of mine wastes include waste rock or rock piles (mine dumps), tailings, overburden, low grade or subore stockpiles, slag, water, heap leach, coal ash, flue dust, and fly ash.

More than 133 million tons of coal ash are stored at the electric power generating plants in New Mexico. Millions of tons of coal waste rock (mine dumps) are found throughout New Mexico. Known critical minerals found in coal ash include REE, Sc, V, and others. Coal ash was sampled from some of the power plants. The overall REE content of these coal ashes is low; the highest values are below 300 ppm TREE. When compared to chemical analysis from other coal basins, San Juan Basin samples are similar. Known critical minerals found in coal ash include REE, Sc, V, and others.

Some of these mine wastes from older coal mine sites no longer in production contain elevated critical minerals, although below recommended exploration threshold values. Endowments for minerals such as Th, V, Y, and TREE are higher at the Thatcher and Law mines sites. The Thatcher waste rock contains approximately 0.5 ton of Th, 2.8 tonnes of V, 0.5 tonnes of Y, and 4.6 tonnes of TREE. The Law mine dump shows similarly elevated values, with about 0.1 tonnes of Th, 0.8 tonnes of V, 0.1 tonnes of Y, and 1.2 tonnes of TREE. In contrast, the Noci and Black Diamond mine dumps contain smaller endowments: Noci dump has roughly 0.02 tonnes of Th, 0.2 tonnes of V, 0.03 tonnes of Y, and 0.2 tonne of TREE, whereas Black Diamond dump has about 0.4 tonnes of Th, 1 tonnes of V, 0.2 tonnes of Y, and 1.4 tonnes of TREE. Although, some of the mine wastes show concentrations of some critical minerals above crustal abundance, the concentrations are below recommended exploration threshold concentrations and therefore, the concentrations and tonnages are probably too small to provide an economic resource.

The REE concentrations for water collected during this project are low for the one coal mine sampled. However, sampling of one coal mine is not representative. Throughout our work to measure REE in surface water, we have identified a significant gap of REE data for surface water. Continuing water quality surveys to close this gap are encouraged.

A long-range plan to compile information about critical minerals was developed for the USGS Earth MRI program and revised this year. This plan will guide future endeavors to examine critical minerals in New Mexico. See https://geoinfo.nmt.edu/staff/McLemore/projects/mining/REE/documents/NMBGMR_CM_Plan23v1_001.pdf.

Throughout the project some lessons were learned, and data gaps identified. A gap analyses is required for the entire project and will be performed in phase 2, if funded. Other coal fields in New Mexico should be examined, sampled and analyzed. There is no agreed upon method of geochemically analyzing coal and coal ash accurately. There is a lack of access to coal samples and ash at power plants. Additional samples are required to characterize many of the coal fields. Better resource estimation of critical minerals around areas such as coal mines requires more refined sampling spatially, which will help to better understand distribution of

critical minerals across the basin. Stratigraphic data from electric logs should be integrated with pXRF analyses and geologic models to improve the spatial distribution understanding of critical minerals. Cretaceous beach-placer sandstone deposits should be re-examined for their critical minerals potential.

Ultimately, the economic potential of critical minerals and REE in the San Juan and Raton basins and adjacent areas will most likely depend upon production of more than one commodity, maybe even from coal, humate, beach-placer, uranium, clinker and adjacent deposits.

TABLE OF CONTENTS

Contributing Authors 2
Dedication 3
Executive Summary 4
Table of Contents 8
Acknowledgements 14
1.0 Introduction 15
1.1 Critical Minerals and Rare Earth Elements (REE) (V.T. Mclemore) 16
1.2 Carbon Based Products (CBP) (V.T. Mclemore) 17
1.3 Project Objectives, Scope, and Justification (V.T. Mclemore) 20
1.4 Importance of Energy and Minerals in New Mexico (Task 4) (V.T. Mclemore) 21
1.5 The Coal Industry in New Mexico (Task 4) (V.T. Mclemore) 31
1.6 Other Industries in the San Juan and Raton Basins (V.T. Mclemore) 34
1.7 Summary of Findings 35
2.0 Physical and Geologic Setting (Task 2) (Mclemore, Badonie, and Robledo) 36
2.1 Vegetation and Terrain 36
2.2 Climate 36
2.3 Geologic Setting 37
2.4 Stratigraphy 37
2.5 Summary of Findings 41
3.0 Methods of Study 42
3.1 Databases and SOPs (V.T. Mclemore, A. Trivitt, and M. Leo-Russell) 42
3.2 Photography, Scanning, and Archiving of Samples (V.T. Mclemore, Z.K. Motlagh, R. Otoo, D. Shaver, H. Tetteh, A. Trivitt, and M. Leo-Russell) 42
3.3 Sampling of Solids (V.T. Mclemore and Z.K. Motlagh) 44
3.4 Logging of Drill Core (V.T. Mclemore, Z.K. Motlagh, A. Appah, A. Trivitt, and M. Bodanie) 49
3.5 Characterization 50
3.5.1 Petrography (Z.K. Motlagh, D. Shaver, and V.T. Mclemore) 50
3.5.2 Mineralogy Using Ultraviolet Lights (E.J. Owen) 50
3.5.3 Scintillation Counter/Gamma Ray Spectrometer (E.J. Owen) 51
3.5.4 Mineralogy By XRD (Z.K. Motlagh and R. Boakeye) 51
3.5.5 Chemical Analyses (V.T. Mclemore) 52
3.5.6 Electron Microprobe—New Mexico Bureau of Geology and Mineral Resources (N. Iverson) 52
3.5.7 Electron Microprobe—Sandia National Laboratory (G. Xu) 53

3.5.8 Paste pH (Z.K. Motlagh) 54
3.5.9 Specific Gravity (A. Serwah, Z.K. Motlagh, and V.T. Mclemore) 56
3.5.10 Sampling Procedures For Mining-Influenced Waters (B. Frey) 57
3.6 Quality Control (QA) and Quality Assurance (QC) (V.T. Mclemore) 60
3.7 Summary of Findings 62
4.0 Basinal Assessment REE and Critical Minerals in the San Juan and Raton Basins (Task 2) 63
4.1 Pre-Existing Data 63
4.1.1 Pre-Existing Chemical Analyses of Coal and Adjacent Strata (V.T. Mclemore) 63
4.1.2 Evaluation of Online Water Databases and Reports For Critical Element Potential (S. Kelley) 64
4.2 Minimum Concentrations of Critical Minerals For Exploration: How Good Is Good Enough? (R. Otoo and V.T. Mclemore) 65
4.3 Critical Minerals Potential of Coal Beds Based Using Whole-Rock Basis (V.T. Mclemore) 68
4.4 Characterization of Coal Maturity (G. Xu) 71
4.5 Critical Minerals Potential of Coal Beds On Ash Basis (V.T. Mclemore and E.J. Owen) 72
4.6 Critical Minerals Potential of Humates (V.T. Mclemore and J. Lempke) 77
4.7 Critical Minerals Potential of Beach-Placer Sandstones (V.T. Mclemore, G. Xu, A. Byrd, and E.J. Owen) 81
4.7.1 Introduction 81
4.7.2 Methods of Study 85
4.7.3 Evaluation of the Nure Data 86
4.7.4 Previous Investigations 86
4.7.5 Distribution in the San Juan Basin, New Mexico 88
4.7.6 Characterization 105
4.7.7 Geochemistry 108
4.7.8 Relationship To Coal Deposits 111
4.7.9 Potential Source Terrains 112
4.7.10 Origin of Beach-Placer Sandstone Deposits 112
4.7.11 Mineral-Resource Potential 113
4.7.12 Concluding Remarks 115
4.7.13 Future Work 115
4.8 Critical Minerals Potential of Clinkers (D. Shaver, G. Xu, and V.T. Mclemore) 115

4.8.1 Introduction 115
4.8.2 Mapping of Clinkers 119
4.8.3 Estimated Endowment 120
4.8.4 Critical Minerals in Clinkers 122
4.8.5 Petrography 124
4.9 Critical Minerals Potential of Clays (V.T. Mclemore and G. Xu) 126
4.10 Critical Minerals Potential of Black Shales (V.T. Mclemore and M. Rigali) 131
4.10.1 Introduction 131
4.10.2 Chemistry of Black Shales in the San Juan and Raton Basins 132
4.10.3 Future Studies 135
4.11 Critical Minerals Potential of Sandstone-Hosted Copper Deposits (V.T. Mclemore, E.J. Owen, and J. Newcomer) 135
4.11.1 Introduction 135
4.11.2 Mining History and Production 137
4.11.3 Description of Deposits 139
4.11.4 Critical Minerals 145
4.12 Sample Characterization, Nacimiento Mine (Task 5) (B. Goehring, P. Watson, I., and Mantelli) 145
4.12.1 Micro XRF (MXRF) and Element Co-Location 146
4.12.2 Summary 147
4.13 Critical Minerals Potential of Volcanic Ash Beds (D. Shaver and V.T. Mclemore) 148
4.14 Critical Minerals Potential of Uranium Deposits (V.T. Mclemore, R. Boakye, and Z.K. Motlagh) 153
4.14.1 Introduction 153
4.14.2 Description of Study Areas 157
4.14.3 Petrography and Mineralogy 162
4.14.4 Geochemical Analyses 163
4.14.5 Preliminary Conclusions 165
4.15 Critical Minerals Potential of the Cuba Manganese Deposits (V.T. Mclemore) 166
4.15.1 Introduction 166
4.15.2 Geologic Setting 168
4.15.3 Critical Minerals 168
4.15.4 Conclusions 172
4.16 Critical Minerals Potential of Perlite Deposits (E.J. Owen and V.T. Mclemore) 172

4.17 Evaluation of Drill Core in the San Juan and Raton Basins (M. Badonie, V. Robledo, and V.T. Mclemore) 176
4.17 Sources of REE and Critical Minerals in the San Juan and Raton Basins (V.T. Mclemore) 178
4.18 Basinal Assessment (Endowment of Critical Minerals) (V.T. Mclemore) 180
4.18.1 Assessment of Coal Field (V.T. Mclemore and Z.K. Motlagh) 180
4.18.2 Assessment of Beach Placer Deposits 181
4.19 Summary of Findings 182
5.0 Basinal Strategies For Reuse of Waste Streams (Task 3) 184
5.1 Types of Waste Streams (V.T. Mclemore) 184
5.2 Characterization of Waste Streams 185
5.2.1 Coal Ash (Power Plants) (D. Shaver and V.T. Mclemore) 185
5.2.2 Abandoned Mine Wastes (Z.K. Motlagh, R. Kelley, and V.T. Mclemore) ... 188
5.2.3 Mine-Influenced Waters From Lee Ranch Coal Mine (B. Frey) 201
5.2.4 Magdalena Leaching Tests (R. Coyte) 212
5.2.5 Acid Mine Drainage 219
5.3 Reuse Strategy 219
5.3.1 Reuse of Coal Waste Materials (G. Xu) 219
5.3.2 Sonash Reuse of Waste Materials (C. Arato) 219
5.4 Summary of Findings 219
6.0 Strategies For Infrastructure, Industries and Businesses (Task 4) (Mclemore and Arato) 221
7.0 Technology Assessment and Testing of New Techniques (Task 5) 222
7.1 Availability and Challenges of Infrastructure in the San Juan and Raton Basins (V.T. Mclemore) 222
7.2 Initial Technology Assessment (V.T. Mclemore) 222
7.3 Field Testing New Techniques and Technologies 224
7.3.1 Geochronology (N. Iverson and S. Moses) 224
7.3.2 Comparing Handheld X-Ray Fluoresce Instrument (pXRF) and Laboratory Analyses (Z.K. Motlagh) 226
7.3.3 Radiometric Surveys (E.J. Owen) 230
7.3.4 Correlation of Geophysical Logs, Laboratory, Chemical Analyses and pXRF (V.T. Mclemore and S. Fire) 230
7.3.5 Humates Used As A Filtration Medium For Uranium (B. Detsoi, B. Frey, V.T., Mclemore, J. Jones, and R. Tsosie) 234
7.3.6 Extraction of Alumina From Coal and Clays (J. Essary) 246
7.3.7 Machine Learning (Task 2) (B. Goehring, P. Watson, and I. Mantelli) 247

7.3.8 Technology Assessment of Extraction Techniques (Task 5) (B. Goehring, P. Watson, and I. Mantelli) 254
7.3.9 Snl Environmentally Benign Extraction (G. Xu) 259
7.4 Summary of Findings 260
8.0 Technology Innovation Center (Task 6) 261
9.0 Stakeholder Outreach, Education, and Work Force Development (Task 7) 262
9.1 Purpose (V.T. Mclemore) 262
9.2 Audience (V.T. Mclemore) 263
9.3 Workforce Development Plan (C. Connolly) 263
9.3.1 Foundation Supports 263
9.3.2 Background Research 263
9.3.3 Invest in the Workforce 263
9.3.4 Worker Training, Development, Retention, and Growth 264
9.3.5 Summary 264
9.4 What Has Been Accomplished (C. Connolly and V.T. Mclemore) 264
9.4.1 New Mexico State and Regional Education 264
9.4.2 Project Web Page 264
9.4.3 Historical Archives 265
9.4.4 Earth Matters 265
9.4.5 Rockin' Around New Mexico 265
9.4.6 Lite Geology 267
9.4.7 Post Cards From the Field 267
9.4.8 Lesson Plans 268
9.4.9 Displays and Exhibits in Local and Regional Museums, Earth Science Days and Other Events 268
9.4.10 Magdalena Science Café 268
9.4.11 Field Trips With Teachers 268
9.4.12 Field Trips With Community Groups 269
9.4.13 Field Trips With Cub Scouts 269
9.4.14 Earthscope Interns 269
9.4.15 Tribal Engagement 269
9.4.16 Technical Workshops 269
9.4.17 Public Field Trips 270
9.4.18 Other Publications 270
9.4.19 Participation in Geologic and Mining Engineering Conferences 270

9.4.20 Workforce Development 270
9.4.21 Mineral Kits For Teachers 270
9.4.22 Field Notes On the Geology of New Mexico 271
10.0 Lessons Learned, Challenges, Frustrations, and Data Gaps 272
11.0 Conclusions 273
12.0 References 274

Appendix 1. Acronyms, Conversions, and Glossary 289
Appendix 2. Project Publications, Theses, and Presentations 291
Appendix 3. Mining Districts in and Surrounding the San Juan and Raton Basins 294
Appendix 4. List of SOPsand Plans 295
Appendix 5. Description of Samples 296
Appendix 6. XRD Files 296
Appendix 7. Chemical Analyses (Solid) 296
Appendix 8. pXRF Data 296
Appendix 9. Geochemistry of Water Samples 296
Appendix 10. Particle Size Analyses 296
Appendix 11. Electron Microprobe and Analyses 296
Appendix 12. USGS Produced Water Data 296
Appendix 13. Geochronology 296
Appendix 14. Endowments of Critical Minerals in Coal Fields in the San Juan and Raton Basins 296
Appendix 15. SonoAsh Cementitious products memo 297
Appendix 16. Zero Waste Coal 297
Appendix 17. Batch capacity test and column tests 297

ACKNOWLEDGEMENTS

This report is part of on-going studies of mineral resources in New Mexico, supported by the New Mexico Bureau Of Geology and Mineral Resources (NMBGMR), J. Michael Timmons, director and state geologist. Current research is funded through a DOE, Carbon Ore, Rare Earth Elements, and Critical Minerals (CORE-CM) assessment of San Juan River-Raton coal basins, New Mexico (DE-FE0032051). Additional funding was by student grants from the New Mexico Geological Society, NMT Brightstar Scholarship, WAAIME (Women's Auxiliary to the American Institute of Mining Engineers), and Society of Mining, Metallurgy and Exploration, Inc. (SME). Compilation of data was partially funded by the U.S. Geological Survey (USGS) National Geological and Geophysical Data Preservation Program (NGGDPP) Grants No. G19AP00098, G20AP00105, G21AP10434, and G23AP00332. TEF (Technology Enhancement Fund) funding provided overhead funding for the project extension.

A team was formed to complete the tasks outlined in the contract and assistance by team members is greatly appreciated (listed in Contributing Authors). Thanks to the NMBGMR IT team, Jacob Lewis, Mark Leo-Russel, Jon Klaus, Phil Miller and Amy Dunn for keeping our computers and servers operating. Thanks to James McLemore (PRRC, NMIMT), Sha Lene Rodolph, Dan Koning (NMBGMR), Craig Williams (San Juan College), Shari Kelley (NMBGMR) and students of the NMBGMR Economic Geology group for assisting with sample collection and preparation. John Durica sampled waters from the Lee Ranch mine. Perlite samples from Socorro and Taos County were obtained from Dicalite Management Group, Socorro. Mark Leo-Russell assisted with database development. Mark Mansell provided technical support. Nels Iverson assisted with electron microprobe and geochronology data. William X. Chaves, Jr. assisted with petrographic analyses.

Earlier investigations on the Apache Mesa deposits were funded by a contract with the Jicarilla Apache Nation through the Division of Energy and Minerals Development, Assistant Secretary Indian Affairs (Grant A14AP00084). Thanks to the many landowners who allowed access to sampling for this project: NRA Whittington Center, Navajo Transitional Energy Co. (Kevin Talbott, Benson Chow), Stirling Spencer, Tyler Vandenburg (Meneffe Mining Corp.), Robert Newcomer, Ted Wilton, and Richard Carlton (Navajo Nation). Even though this DOE project was not directly funded by the USGS Earth MRI projects, many of the USGS sampling procedures and information on critical minerals was used in this report. **Any persons wishing to conduct geologic investigations on the Navajo Nation must first apply for and receive a permit from the Minerals Department, P.O. Box 1910, Window Rock, Arizona 6515 and telephone no. 928-871-6588.**

1.0 INTRODUCTION

The New Mexico Bureau of Geology and Mineral Resources (NMBGMR) and New Mexico Institute of Mining and Technology (NMIMT) led the San Juan and Raton basins Carbon Ore, Rare Earth, and Critical Minerals (CORE-CM) Initiative to explore the expansion and transformation of coal and coal-based resources within these basins to produce potential nonfuel carbon-based products (CBP), rare earth elements (REE), and other critical minerals. This project is one of 13 CORE-CM projects funded by the U.S. Department of Energy (DOE) to identify and quantify the distribution of critical minerals, including REE, in coal beds and related stratigraphic units in basins throughout the United States, including the San Juan and Raton basins (Fig. 1.1). This project is the first phase in a long-term program that will set the stage for future work by assessing resource, market, technology, and infrastructure knowledge; identifying knowledge gaps; developing a series of plans to be carried out in future work; and initiating stakeholder engagement.

FIGURE 1.1 CORE-CM projects in the United States (The Carbon Ore, Rare Earth, and Critical Minerals (CORE-CM) Initiative | netl.doe.gov). San Juan and Raton basins are area 4 in red.

The project's objectives were achieved through seven tasks. Task 1.0 included project management and planning activities that ensured all subsequent tasks were completed according to specified U.S. Department of Energy (DOE) timelines; methods are described in Chapter 3. In Task 2.0, a basinal resource assessment was performed coupling CBP, critical minerals and REE data with detailed geologic and stratigraphic data with machine learning approaches to identify potential critical minerals and REE resources within the San Juan and Raton basins and adjacent areas

(Chapters 2 and 4). Task 3.0 focused on the identification of potential waste streams that can be reused (Chapter 5). In Task 4.0, infrastructure, industries and businesses were identified that can support the development of these resources in the San Juan and Raton basins (Chapters 1 and 6)). Task 5.0 consists of a technology assessment, development, and field testing of new techniques and technologies to better characterize and assess critical minerals and REE potential (Chapter 7). Task 6.0 developed a plan to create a technology innovation center in the New Mexico to continue critical minerals and REE work into the future (Chapter 8). Task 7.0 included identifying stakeholders, planning outreach and education, and deploying outreach materials (Chapter 9). Acronyms, conversions, and glossary are in Appendix 1. A list of project publications, theses, and presentations generated through these activities is in Appendix 2. This introduction chapter provides the background for the report. Most of the data collected for the project are in attached appendices.

1.1 Critical Minerals and Rare Earth Elements (REE) (V.T. McLemore)

The growing market for alternative technologies like solar panels, wind turbines, batteries, magnets, electric cars, desalination plants, and carbon capture and storage require non-traditional elements for their manufacture. In December 2017, a presidential executive order (U.S. Presidential Executive Order (EO) No. 13817) was signed that required the Departments of Interior, Energy, and Defense to develop a list of critical minerals. In May 2018, the U.S. Department of the Interior (U.S. Geological Survey, USGS) published its first list of 35 critical minerals. That list was revised in 2022 and again in fall 2025. The critical minerals list now includes 60 minerals (Fig. 1.2). A *critical mineral* is a nonfuel mineral essential to the economic and national security of the U.S. that is from a supply chain that is vulnerable to disruption. Critical minerals are essential in the manufacture of products, the absence of which would have substantial consequences for the U.S. economy or national security. The term *mineral* used here is based upon the U.S. Mining Law of 1872, where minerals are defined as any mineral commodity of economic importance that could be removed from the ground, including aggregates, coal, oil, and gas (https://www.blm.gov/programs/energy-and-minerals/mining-and-minerals/about). As many as 75-100% of critical minerals are imported into the U.S. (Committee on Critical Mineral Impacts of the U.S. Economy, 2008; Subcommittee on Critical and Strategic Mineral Supply Chains Committee on Environment, Natural Resources, and Sustainability, 2018; U.S. Geological Survey, 2025) and many of these critical minerals are found in New Mexico (Fig. 1.2; McLemore and Gysi, 2023). Table 1.1 summarizes the critical minerals potential in New Mexico.

Rare earth elements (REE) include the 15 lanthanide elements (La, Ce, Pr, Nd, Pm, Sm, Eu, Gd, Tb, Dy, Ho, Er, Tm, Yb, Lu, atomic numbers 57-71), yttrium (Y, atomic number 39), and scandium (Sc, atomic number 21) (Fig. 1.1) and are commonly divided into two chemical groups, the light REE (La through Eu) and the heavy REE (Gd through Lu and Y). REE, zirconium (Zr), niobium (Nb), and beryllium (Be), are critical minerals that are essential in most of our electronic devices, such as cell phones, laptops, computer chips, hybrid/electric cars, etc. (Committee on Critical Mineral Impacts of the U.S. Economy, 2008; Long et al., 2010; McLemore, 2011, 2014). REE (Nd, Dy) are used in magnets and batteries, and cerium (Ce) is an important polishing agent. Other uses include wind turbines, solar panels, water purification, desalination, magnetic refrigeration, and phosphors for more efficient light bulbs. Most of the current world production of REE comes from China, but the U.S. has significant REE resources that have a potential for future development. Some of the REE and critical minerals resources are

found in New Mexico (McLemore and Lueth, 2017; McLemore and Austin, 2017; McLemore, 2018a, 2019), but they have not been important exploration targets in the past because demand has been met elsewhere. With the projected increase in demand for critical minerals, the New Mexico deposits, including coal, are being re-examined for the critical minerals potential, and several areas in the state are currently undergoing exploration.

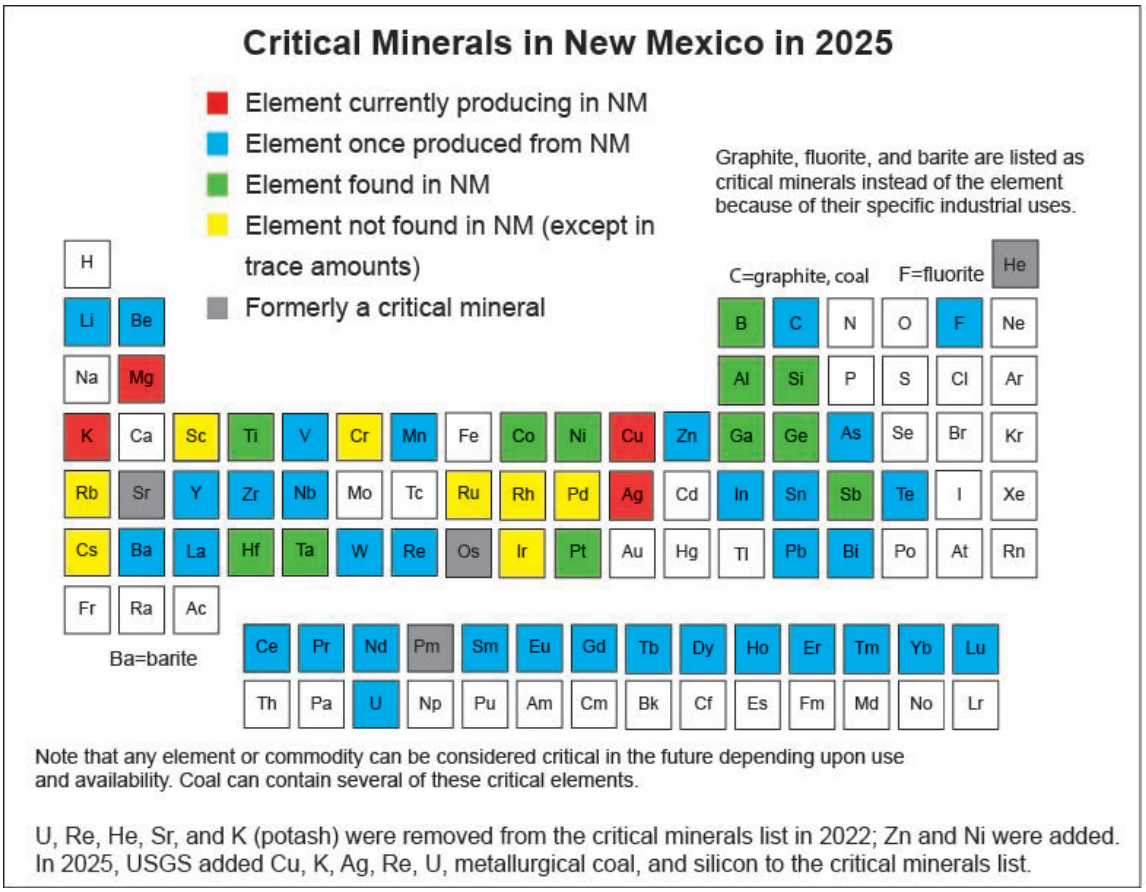

FIGURE 1.2 Critical minerals found in New Mexico (modified from McLemore and Gysi, 2023 using the final revised list of critical minerals released in fall 2025).

1.2 Carbon based products (CBP) (V.T. McLemore)

Carbon-based products (CBP) include the nonfuel uses of coal and associated rocks, such as use in construction materials, aggregates (including clinkers), cement, soil additives (including humate), asphalt additives, coal tar (resin), and products for the chemical industry. Coal also can be a potential source of graphite, a critical mineral that is a major component of batteries. Humate production is currently produced in the San Juan Basin and the industry is expected to grow as a result of the abundant reserves present (Fig. 1.3; Newcomer et al., 2021). Resin found in coal (Fig. 1.4) can be extracted and used in the manufacture of adhesives, waterproofing, and other uses. Coal also is a feedstock for the manufacture of chemicals, such as methanol, dimethyl, and others and coal is being investigated for carbon sequestration.

FIGURE 1.3 Menefee Mining Company humate mill (photograph by V.T. McLemore, 4/14/2023).

FIGURE 1.4 Amber resin in black coal, El Segundo mine (photograph by V.T. McLemore, 8/23/2022). Resin found in coal can be extracted and used in the manufacture of adhesives, waterproofing, and other uses.

TABLE 1.1 Critical minerals found or have potential in the San Juan and Raton basins and surrounding areas, New Mexico (modified from McLemore, 2019, 2020). Critical minerals in bold have been produced from the San Juan or Raton basins and surrounding areas (using the final revised list of critical minerals released in fall 2025).

Critical minerals	Is it found in New Mexico?	Is it found in the San Juan and Raton basins?	Was it produced from New Mexico?
Aluminum (bauxite, kaolinite) (Al)	?	?	Yes
Antimony (Sb)	Yes	No	Yes
Barium (barite) (Ba)	Yes	No	Yes
Beryllium (Be)	Yes	?	Yes
Bismuth (Bi)	Yes	No	Yes
Boron (B)	Yes	Yes	No
Cesium (Cs)	?	?	No
Chromium (Cr)	?	?	No
Cobalt (Co)	?	?	No
Copper (Cu)	yes	Yes	Yes
Fluorine (fluorite) (F)	Yes	Yes	Yes
Gallium (Ga)	Yes	?	No
Germanium (Ge)	?	?	No
Graphite (carbon)	Yes	Yes	Yes
Hafnium (Hf)	?	?	No
Indium (In)	Yes	?	No
Lead (Pb)	Yes	Yes	Yes
Lithium (Li)	Yes	?	Yes
Magnesium (Mg)	Yes	?	No
Manganese (Mn)	Yes	Yes	Yes
Nickel (Ni)	Yes	No	?
Niobium (Nb)	Yes	Yes	Yes
Platinum group elements (PGE: Pd, Pt, Os, Ir, Rh, Ru)	?	?	?
Potash (K)	Yes	No	Yes
Rare earth elements (REE), yttrium (Y)	Yes	Yes	Yes
Rhenium (Re)	Yes	No	?
Rubidium (Rb)	?	?	No
Scandium (Sc)	Yes	?	No
Silicon (Si)	No	No	No
Silver (Ag)	Yes	Yes	Yes
Tantalum (Ta)	?	No	No
Tellurium (Te)	Yes	No	Yes
Tin (Sn)	Yes	No	Yes
Titanium (Ti)	Yes	Yes	No
Tungsten (W)	Yes	No	Yes
Uranium (U)	Yes	Yes	Yes
Vanadium (V)	Yes	Yes	Yes
Yttrium (Y)	Yes	Yes	No
Zinc (Zn)	Yes	?	Yes
Zirconium (Zr)	Yes	Yes	Yes

1.3 Project objectives, scope, and justification (V.T. McLemore)

The San Juan and Raton basins are predominant Laramide structural basins in northern New Mexico and southern Colorado that host important energy resources and have produced significant amounts of coal, uranium, oil, and gas (Fig. 1.5). The purposes of this project are to:

- identify and quantify the distribution of critical minerals, including REE and CBP, in coal beds and related stratigraphic units in the San Juan and Raton basins (including coal, coal refuse, ash, coal seam, interstitial clays/shales, volcanic ash beds, acid mine drainage, associated sludge samples, mine dumps, process waters, etc.)
- identify and characterize possible sources of critical minerals and REE in the basins
- identify the coal mine wastes and nonfuel CBP that could contain critical minerals and REE
- characterize the critical minerals and REE in these materials
- determine the economic viability of extracting CBP, critical minerals and REE from these materials
- test and develop new technologies in identifying and quantifying critical minerals and REE in high-fidelity geologic models
- evaluate the basinal industry infrastructure and determine the economic viability of industrial upgrading.

To accomplish these objectives, a basinal resource assessment of the San Juan and Raton basins and adjacent areas is required. This assessment is needed to complete the DOE mandate to identify critical minerals potential in the U.S., including New Mexico, which could have economic benefits if the resources are mined. Favorable geologic terranes and priority areas containing critical minerals and REE are identified in this report.

Future mining of critical minerals and REE will directly benefit the economy of New Mexico. Mining companies working in these areas and the Navajo Nation are interested in understanding the potential for critical minerals on their properties. Residents of small communities in rural New Mexico are especially concerned about the mineral resources near their communities and this project will aid in their understanding of these resources. These data will increase our understanding of ore formation, mineral-resource potential, production, consumption, disposal, and how minerals and mineral extraction interact with the environment. State and Federal government decision makers, tribal governments, mining companies, and the public require this information for land use decisions, remediation prioritization, and to determine if some of these deposits can be mined now or in the future. Furthermore, it is crucial to re-establish a sustainable domestic source of critical minerals and REE in the U.S. to help secure the nation's clean energy future, reduce the vulnerability of the U.S to material shortages related to national defense, and to maintain our global technical and economic competitiveness. This project will train future geologists and engineers since undergraduate and graduate students will assist in data collection and analysis. The PI and other team members have a well-established history of mentoring students and contributing to diversity in the geoscience and mining engineering workforce (Student Theses (nmt.edu)).

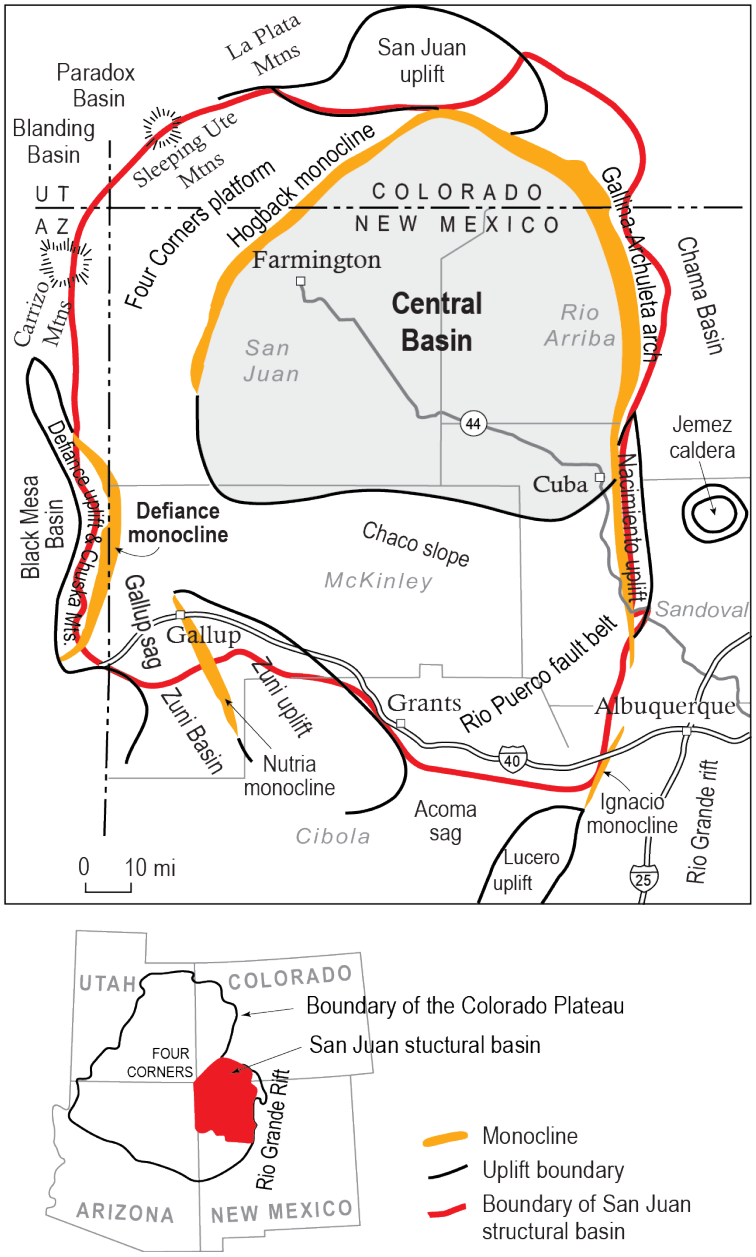

FIGURE 1.5 Structural features of the San Juan Basin and adjacent areas (from Hoffman, 2017).

1.4 Importance of energy and minerals in New Mexico (Task 4) (V.T. McLemore)

New Mexico's mineral wealth is among the richest endowments of any state in the U.S. Most of New Mexico's energy and mineral production comes from oil, gas, coal, copper, potash, industrial minerals, geothermal, and aggregates; past uranium production also was significant (Table 1.2, Fig. 1.6). Oil and gas are the most important extractive industries in New Mexico in terms of production and New Mexico ranked 2nd in oil production and 3rd in gas production in the U.S. during 2024 (https://www.eia.gov/state/print.php?sid=NM). In 2023, New Mexico's annual crude oil production reached just over 1.8 million barrels per day, ten times greater than it was in 2010. Electricity generated from wind farms is the largest electric energy source in New

Mexico (Fig. 1.6) and New Mexico ranks 7th in the U.S. in electricity generation from wind power in 2024 (https://nm-secm.org/new-mexico-electricity-generation/). Approximately 37% of New Mexico's total electricity net generation came from wind in 2024, and wind power was more than seven times greater than in 2014. Although uranium is no longer produced from New Mexico, New Mexico leads the U.S. in total uranium production from 1948 to 2002 and significant uranium resources remain (McLemore and Chenoweth, 2017) with several projects undergoing permitting (Tables 1.3, 1.4, Fig. 1.8). The first commercial geothermal electricity facility in New Mexico opened south of Lordsburg in 2013, with a capacity of 4-19 megawatts of electricity and New Mexico ranks 6th in geothermal resource potential (https://nm-secm-org/geothermal/). Hydrogen and biofuels also are being examined as potential energy sources. Critical minerals are essential in the energy transition from oil, gas and coal to non-CO_2 forms of electricity generation.

TABLE 1.2 Estimated total production of major commodities in New Mexico, in order of estimated cumulative value (data from USGS, 1902-1927; USBM, 1927-1990; Kelley, 1949; Northrop, 1996; Harrer, 1965; USGS, 1965; Howard, 1967; Harben et al., 2008; Energy Information Administration, 2023; Energy, Minerals and Natural Resources Department (EMNRD), 1986-2025; New Mexico Energy, Minerals and Natural Resources Department, 1986–2025). Figures are subject to change as more data are obtained (these are conservative estimates). *Oil and gas values are estimated from production data provided by EMNRD (2024). **Industrial minerals include the combined total of several industrial minerals (e.g., perlite, cement, decorative stone, pumice, zeolites, cement after 2013, etc.), but excluding potash and aggregates. *** Aggregates include only sand and gravel from 1951-1997, after 1997 aggregates include crushed stone and scoria. na—not available.

Commodity	Years of production	Estimated quantity of production	Estimated cumulative value ($)	Quantity of production in 2024*	Value in 2024 ($)*	Ranking in U.S. in 2024
Natural Gas	1921-2023	>162 trillion cubic ft	na	3.6 trillion cubic ft	na	3
Oil	1922-2023	>9.2 billion barrels	na	667 million barrels	na	2
Coal	1882-2024	>1.21 billion short tons	>$26.1 billion	7,203,935 short tons	$409,619,447	14
Copper	1804-2024	>12.7 million tons	>$28 billion	87,587 short tons	$738,547,109	3
Potash	1951-2024	125 million short tons	>$18 billion	440,717 short tons	$156,604,740	1
Uranium	1948-2002	>347 million pounds	>$4.7 billion	none	$0	
Industrial minerals**	1997-2024	61 million short tons	>$4.4 billion	1,946,741	$221,627,725	
Aggregates***	1951-2024	>790 short tons	>$3.8 billion	212,759,957	$222,676,359	
Cement	1959-2013		>$1 billion	Included in industrial minerals		
Molybdenum	1931-2013	>176 million pounds	>$852 million	2,384,509 pounds	$24,739,281	6
Gold	1848-2024	>3.4 million troy ounces	>$642 million	8,233 ounces	$19,657,902	9
Zinc	1903-1991	>1.51 million tons	>$337 million	none	$0	
Silver	1848-2024	>120 million troy ounces	not	156,119 ounces	$4,512,242	7

Commodity	Years of production	Estimated quantity of production	Estimated cumulative value ($)	Quantity of production in 2024*	Value in 2024 ($)*	Ranking in U.S. in 2024
Lead	1883-1992	>367,000 tons	>$56.7 million	none	$0	
Iron	1883-1962	8.2 million long tons	$17.3 million	512,323 short tons	$2,539,625	
Fluorspar	1909-1978	>721,000 tons	$12 million	none	$0	
Manganese	1883-1963	>1.9 million tons	$5 million	none	$0	
Barite	1918-1965	>37,500 tons	>$400,000	none	$0	
Tungsten	1940-1958	113.8 tons (>60% WO_3)	na	none	$0	
Niobium-tantalum	1953-1965	34,000 pounds of concentrates	na	none	$0	
TOTAL	2024	—	—	—	$1,773,145,524	24

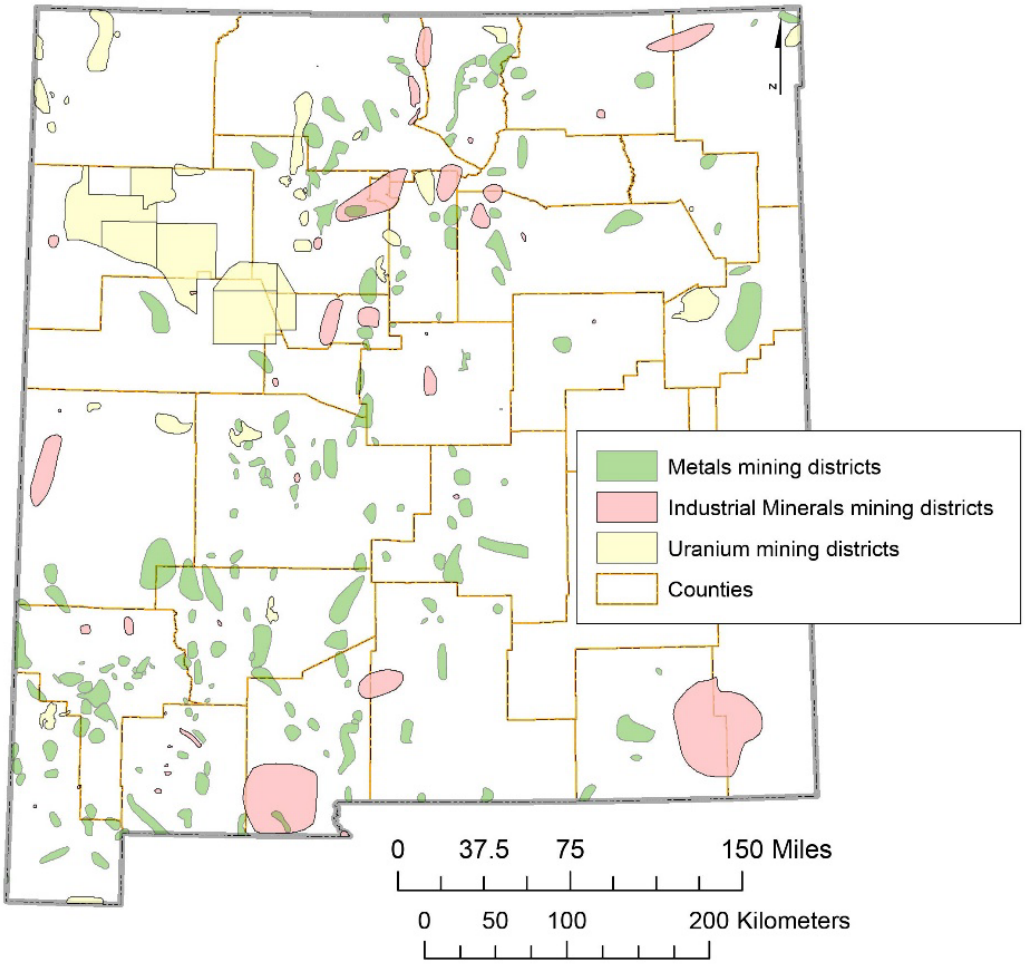

FIGURE 1.6 Mining districts in New Mexico (modified from McLemore 2017). Coal fields are shown in section 1.4.

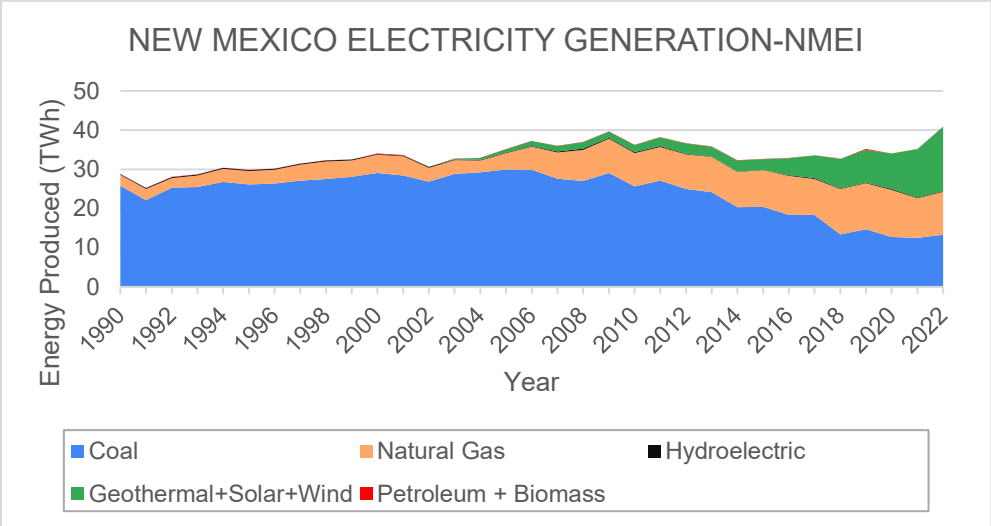

FIGURE 1.7 Electricity in New Mexico generated by source (data from https://nm-secm.org/new-mexico-electricity-generation/).

TABLE 1.3 Resource estimates of major uranium deposits in the Ambrosia Lake subdistrict. See McLemore et al. (2013) for references and other information. DD=decimal degrees.

NM Mines Database Id No	Deposit Name	Latitude (DD)	Longitude (DD)	Resource (short tons ore)	Grade (%U)	U lbs	Date of Estimate	Type of Estimate
NMMK0020	Borrego Pass	35.620119	107.94362	45,000,000	0.15		1983	historic
NMMK0035	Cliffside (Frosty Ox)	35.395569	107.74929	0	see NMMK0239		1985	historic
NMCI0251	East Area	35.279174	107.74755	388,434	0.25		2006	NI 43-101 measured and indicated
NMMK0712	East Roca Honda	35.373201	107.65319	2,750,000	0.175	9,625,000	1985	historic
NMCI0020	La Jara Mesa	35.280139	107.74489	1,555,899	0.23	7,257,817	2007	NI 43-101 measured and indicated
NMCI0027	Mt. Taylor	35.334977	107.63558	0	0.15-0.2	100,000,000	2012	historic
NMMK0142	Roca Honda	35.365717	107.6966	2,077,000	0.404	16,783,000	2012	NI 43-101 measured and indicated
NMMK0143	Roca Honda	35.363139	107.69961	3,900,000	0.19	14,700,000	2011	reported
NMMK0179	Section 13	35.348778	107.63547	710,000	0.17	2,400,000	2011	reported
NMMK0210	Section 24 (Treeline)	35.347278	107.74672	0	0.11	577,000		historic
NMMK0222	Section 26 (Elizabeth)	35.408972	107.76286	924,198	0.24	4,440,605		historic
NMMK0239	Section 31 (Frosty Ox)	35.398194	107.72336	303,695	0.165	1,002,160	1985	historic
NMMK0250	Section 35 (Elizabeth)	35.398861	107.75842	838,418	0.24	2,014,225	1985	historic
NMMK0340	West Largo	35.5257	107.92151	2,800,000	0.3	17,200,000	2011	reported
Total				61,247,644		175,999,807		

TABLE 1.4 Resource estimates of major uranium deposits in the Church Rock-Crownpoint subdistrict. See McLemore et al. (2013) for references and other information. DD=decimal degrees.

NM Mines Database Id No	Deposit Name	Latitude (DD)	Longitude (DD)	Resource (short tons ore)	Grade (%U)	U lbs	Date of Estimate	Type of Estimate
NMMK0025	Canyon	35.65699	108.20692	600,000	0.12	0	1983	historic
NMMK0034	Church Rock (Section 17)	35.62221	108.55273	8,443,000		0	2002	historic
NMMK0128	Church Rock ISL (Section 8)	35.63031	108.55064	3,060,000	0.11	6,500,000	2012	proven and probable reserves
NMMK0316	Church Rock-Section 4	35.6423	108.53346	2,564,000	0.11	5,502,000	1995	historic
NMMK0036	Crownpoint	35.68475	108.16042	9,477,000	0.102	19,205,000	2012	indicated
NMMK0040	Crownpoint ISL (Unit 1)	35.70668	108.22052	27,000,000		0	2002	historic
NMMK0346	Crownpoint-Section 24	35.68459	108.1677	4,800,000	0.16	15,300,000	2011	reported
NMMK0043	Dalton Pass	35.67849	108.26496	600,000	0.12	0	1983	historic
NMMK0044	Dalton Pass	35.6813	108.27829	200,000	0.1	0	1983	historic
NMMK0101	Mancos-Section 12	35.62645	108.58327	11,300,000	0.11	0		historic
NMMK0100	Mancos-Section 7	35.62894	108.58055	5,200,000	0.11	11,300,000	2011	reported
NMMK0111	Narrow Canyon	35.64484	108.29841	828,000	0.12	0	1983	historic
NMMK0117	NE Church Rock	35.65841	108.50853	2,250,000	0.15	0	1969	historic
NMMK0112	NE Church Rock 1	35.6665	108.50273	708,589	0.247	0	1983	historic
NMMK0114	NE Church Rock 2	35.67663	108.52621	2,850,000	0.19	0	1979	historic
NMMK0115	NE Church Rock 3	35.69756	108.54866	4,200,000	0.2	0	1983	historic
NMMK0126	Section 32-Dalton Pass	35.66422	108.23567	1,622,650	0.095	3,070,726	2009	NI 43-101 measured and indicated
Total				85,703,239		60,877,726		

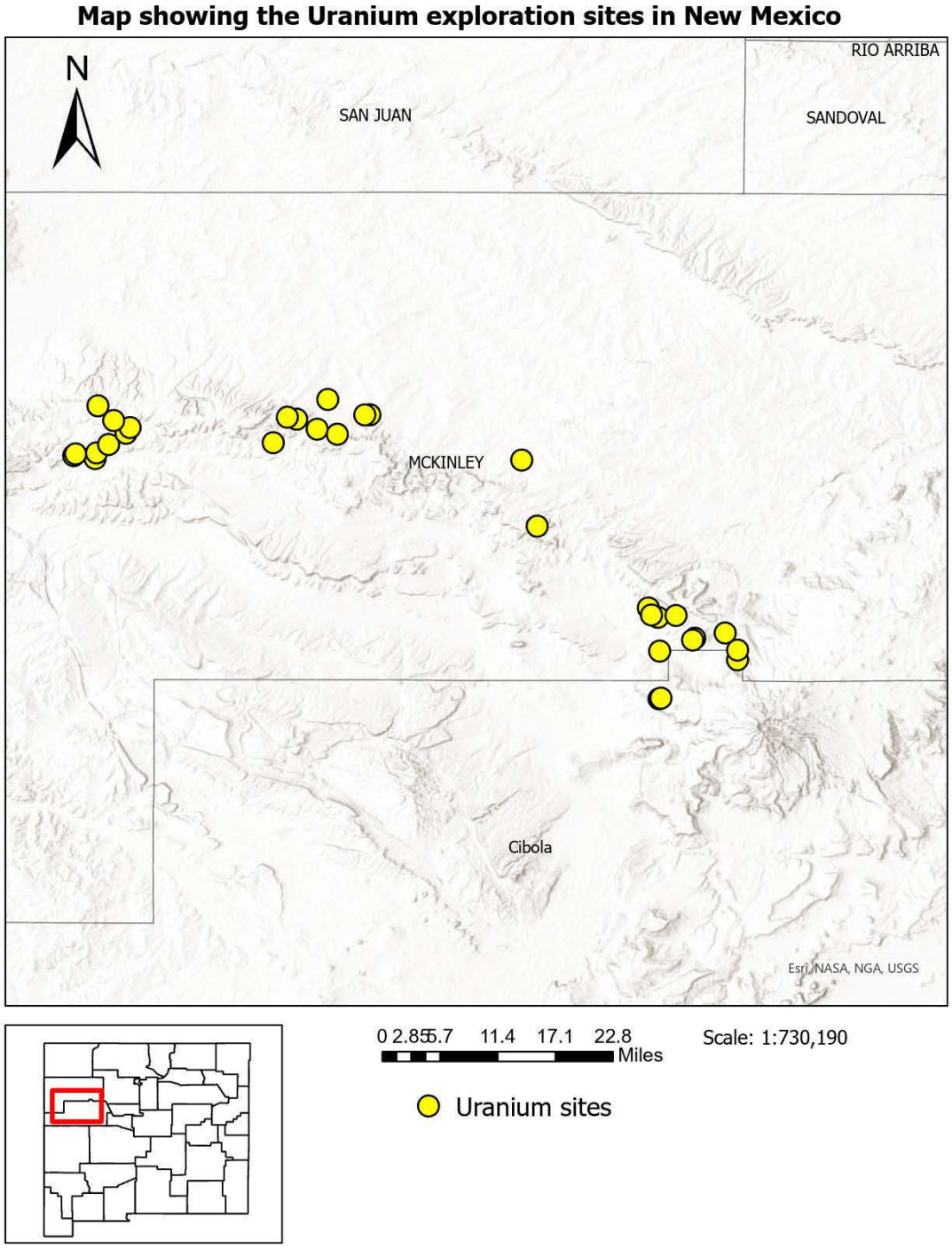

FIGURE 1.8 Major uranium exploration projects in the Grants uranium district, New Mexico.

New Mexico is home to 243 mining districts (Fig. 1.6; McLemore, 2017) and most of them contain critical minerals (Fig. 1.9). Active mines and exploration projects are shown in Figure. 1.10. An increase in exploration for critical minerals has occurred over the last five years (Fig. 1.11). In 2024, New Mexico ranked 14th in coal production in the U.S. and ranked 24th in the U.S. in nonfuel minerals production. Other commodities produced in the state include a

variety of industrial minerals, sulfuric acid, molybdenum, gold, uranium, and silver (U.S. Geological Survey, 2025). New Mexico ranks number one in potash and perlite production, and is one of the top six states in zeolite production. Furthermore, significant reserves of oil, gas, coal, uranium, copper, potash, molybdenum, other minerals and geothermal resources are identified in the state that could be produced in the future.

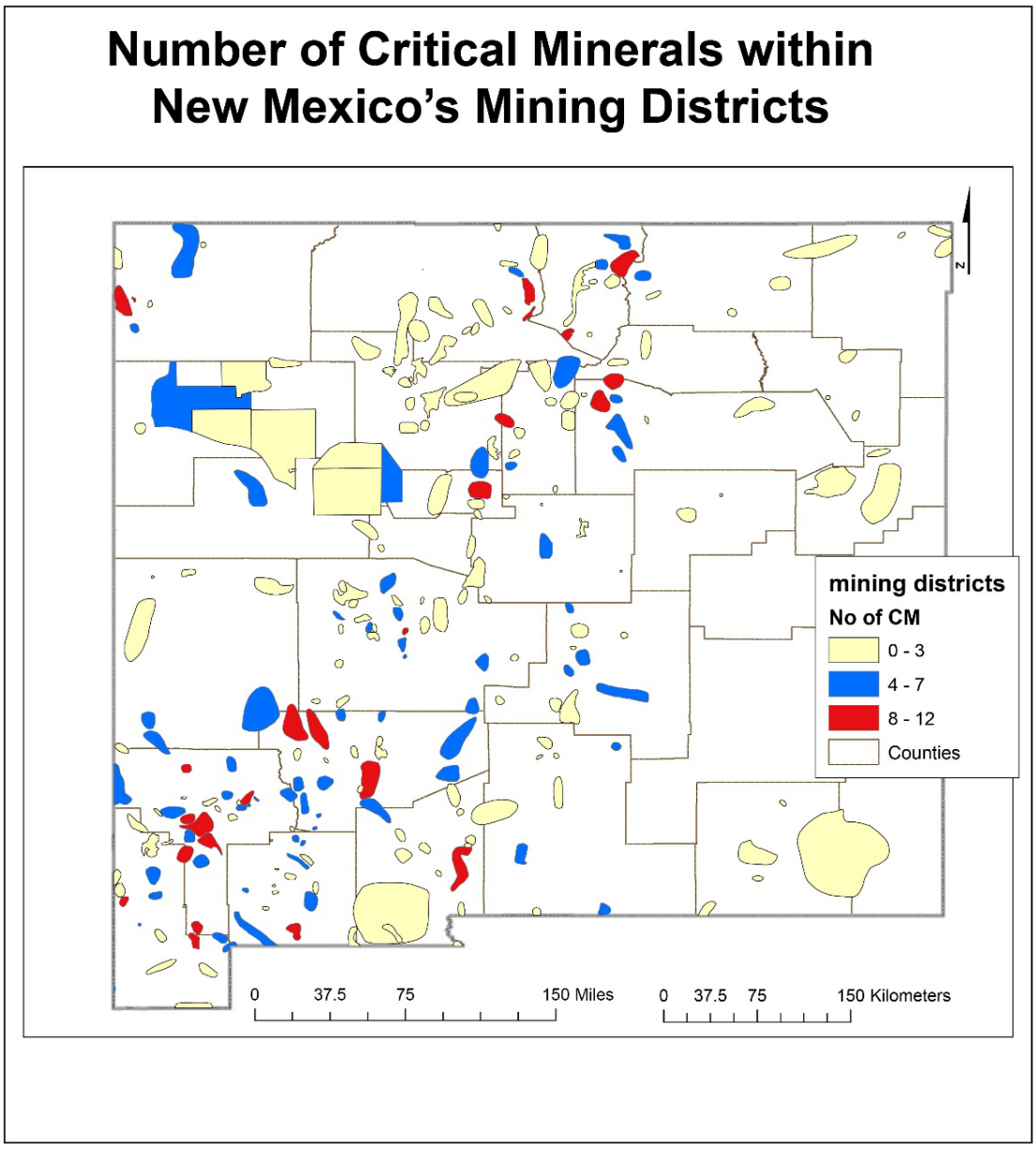

FIGURE 1.9 The number of critical minerals found in mining districts in New Mexico (modified from McLemore, 2017).

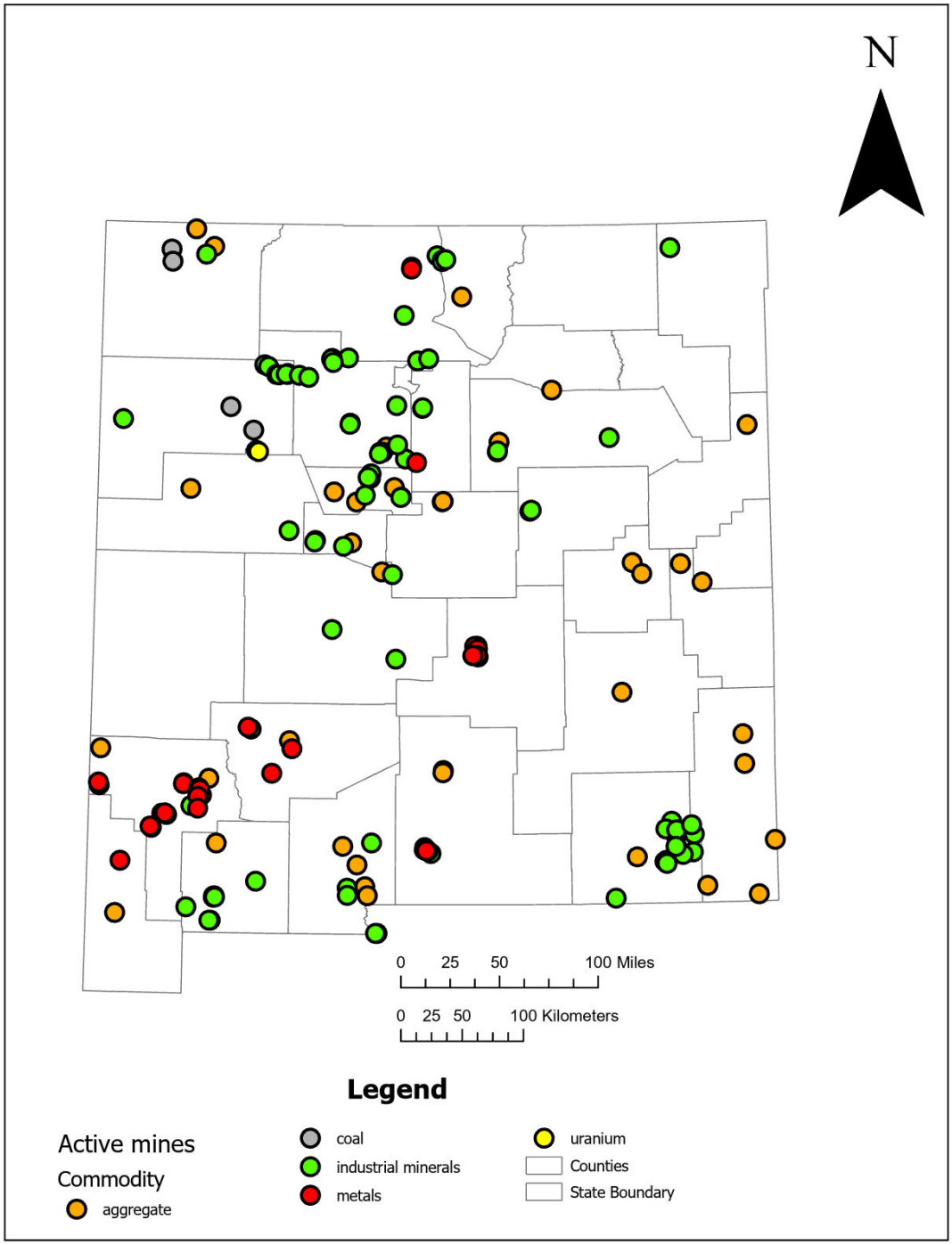

FIGURE 1.10 Active mines and exploration sites in New Mexico (not all aggregate mines are shown).

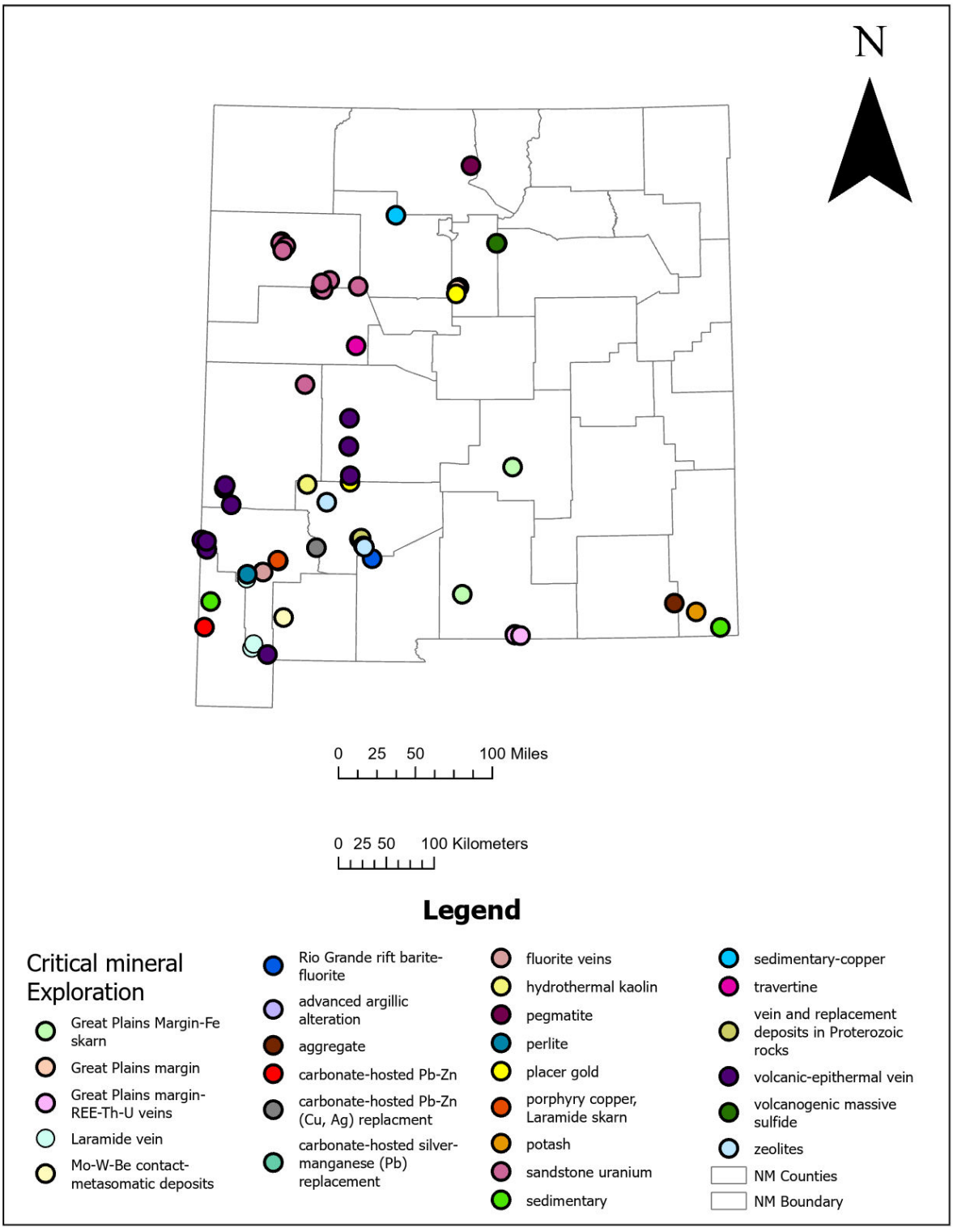

FIGURE 1.11 Critical minerals exploration projects in New Mexico (except for uranium, see Figure 1.9).

A healthy energy and mineral industry are vital to the economy of New Mexico and to maintenance of public education and services, but more important the extractive industries are necessary to maintain your way of life. Essentially, our present lifestyles are heavily dependent upon mining the various commodities that are used to manufacture everything we use. The minerals industries provide property and corporate income taxes, while their ~100,000 direct employees (including oil, gas, and mining) contributed millions of dollars of personal income taxes (EMNRD, 2025). The multiplier effect of dispersal of these wages through local economies increases their impact many fold.

The number of mines and value of produced minerals has continued to decline in recent years (Fig. 1.12). This decline is a result of numerous complex and interrelated factors; some of the more important factors include declining commodity prices, declining quality of ore (for example lower grades and more difficult ore to process), competition from throughout the world (i.e. a global market), and a shift in using alternative energy sources besides oil, gas and coal for generating electricity. Other factors have hampered new mines from opening in the state. These challenges include water rights issues, availability of water, public perceptions, and public opposition to petroleum drilling/production and mining, along with the complexity and length of time for the entire regulatory process to occur in the U.S. at local, state, and federal levels. All these factors add to the cost of mining, not only in New Mexico, but throughout the world.

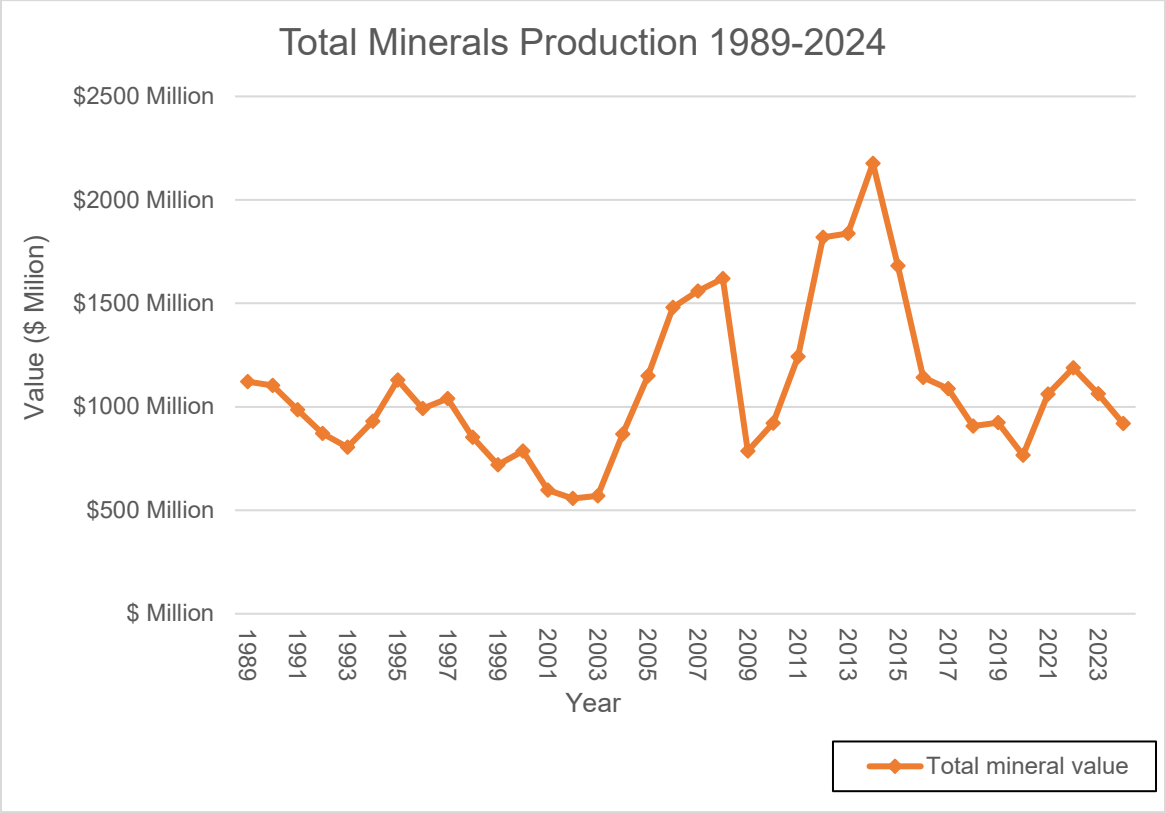

FIGURE 1.12 Production of minerals (total value excluding oil and gas production) from New Mexico (data from New Mexico Energy, Minerals and Natural Resources Department, 1989–2025).

1.5 The coal industry in New Mexico (Task 4) (V.T. McLemore)

Coal is a sedimentary rock that is composed of more than 50 wt% organic material and is formed by the compaction of decaying plant material deposited in ancient peat swamps or mires (Hoffman, 2017). Coal is readily combustible and is burned as a fuel in electrical power plants. Coal also is essential in the manufacture of steel, cement, carbon fibers and foams, medicines, tars, synthetic petroleum-based fuels, as well as home and commercial heating. Coal contains minerals that are noncombustible. These noncombustible minerals could contain REE and other critical minerals that could be recovered from coal mining or the coal ash remaining after the coal is burned. Some coal deposits worldwide are known to contain elevated concentrations of critical minerals, including REE (Dai and Finkelman, 2018; Finkelman et al., 2019; Scott and Kolker, 2019; Dai et al., 2021). In the future, the concentration of critical minerals, including REE, could be a factor in producing coal deposits. A basin-wide geochemical and mineralogical characterization study of New Mexico coals is needed to determine their potential as a resource for critical minerals.

Coal can be divided into different types based on carbon content. Anthracite contains approximately 86%-97% carbon content and generally has the highest heating value of the different subtypes. It is considered the highest rank of coal and can be described as hard, brittle, and black in color. It is used primarily for residential and commercial space heating (Speight, 2005). Bituminous coal contains approximately 45%-86% carbon content. It can be described as having a dark brown to black color. It also contains bands of coal that have bright or dull lusters. It is primarily used for fuel in steam-electric power generation, with substantial quantities also used for heat and power applications in manufacturing and to make coke (Speight, 2005). Subbituminous coal has a carbon content of 35%-45%. It has a large range of appearances from bright and black to a soft and crumbly dull brown color. Like bituminous coal, subbituminous coal is also used in steam-electric power generation. Lignite coal contains 25%-35% carbon content and has the lowest energy content. Lignite is considered the lowest coal rank and can be described as brown coal. It also is used in steam-electric power generation (Speight, 2005).

Coal was first mined in New Mexico by the Spanish in the 1600s to heat homes. Coal mining on a significant scale began in New Mexico in 1862, when U.S. Army troops from Fort Craig opened the Government mine in the Carthage coal field (Socorro County) to supply coal for smithing at Forts Seldon, Bayard, and Stanton and was later worked by Santa Fe Railroad in the 1870's for fuel and as coking coal used in manufacturing (Hoffman and Hereford, 2009). The Atchison, Topeka and Santa Fe Railway was responsible for most of the early development of many of the New Mexico coal fields to fuel its railroad operations. Coal mining continued to expand throughout New Mexico in the 1880s to supply the railroads, but production decreased during the Great Depression as coal demand fell while the oil and natural gas industries grew.

In the Crevasse Canyon Formation, coal had been previously mined in the Gallup, Crownpoint, Mount Taylor, Rio Puerco, and Zuni coal fields (Fig. 1.13, Table 1.5). The coal that comes from these coal fields is mostly subbituminous to bituminous. Gallup coal field has a long coal mining history dating from the early 1880s to approximately 1994. Gallup's coal is considered some of the best quality coals in the San Juan Basin (Hoffman, 2017). In the Menefee Formation, coal has been previously mined in the Hogback, Chaco Canyon, Chacra Mesa, La Ventana, San Mateo, Standing Rock, Monero, and Tierra Amarilla fields. Bituminous coal is predominant for most coal fields in the Menefee Formation but still some fields have subbituminous coals. The Fruitland Formation has had coal mined from all four of its coal fields:

Bisti, Fruitland, Navajo, and Star Lake. Two areas within the Bisti coal field have been withdrawn from mineral entry; both are wilderness areas managed by the U.S. Bureau of Land Management.

Surface mining of coal began in the San Juan Basin in 1881 with construction of the railroad. The Four Corners Generating Station near Farmington, northern San Juan Basin, was constructed in 1963 on Navajo Tribal Land and is still in production, using coal mined from the Navajo mine to generate electricity. It is scheduled to close in 2031. The San Juan Generating Station, also near Farmington, opened in 1973. At peak production, the San Juan Generating Station produced 1,848 megawatts of electricity to New Mexico, Arizona, California, and Utah (https://westmoreland.com/the-end-of-an-era-at-san-juan/). The San Juan Generating Station closed in 2022. The Escalante Generating Station was constructed in 1984 near Prewitt, New Mexico in the southern San Juan Basin and closed in 2020. Coal mined from the Lee Ranch and El Segundo mines supplied the Escalante Generating Station and supplies coal to generating stations in Arizona.

Humate is a high humic-acid-content material that is typically associated with weathered or oxidized coals and humic-rich mudstones and shales. Humates are weathered coal or highly organic mudstone that are found generally at the top of coal-bearing sequences (Newcomer et al., 2021). They can transition to coal at depth. Humates are locally called leonardite or weathered lignite; other terms are explained in Newcomer et al. (2021). Humate is brownish, a lighter color than black coal and contains more humic acid content than coal. Coal burns, whereas high quality humate dissolves in water, implying a high humic acid content. Humate is mined in the San Juan Basin from the Fruitland Formation (Newcomer et al., 2021).

In 2023, for the first time, natural gas surpassed the contribution of coal in New Mexico's total in-state electrical power generation (Table 1.2, Fig. 1.7). In 2024, New Mexico ranked 14th in coal production in the U.S., with a production of 7,987,232 short tons worth $226,590,974 (New Mexico Energy, Minerals and Natural Resource Department, 2025). This production came from the Navajo, El Segundo, and Lee Ranch mines in the San Juan Basin (Fig. 1.13). Total coal production from New Mexico is estimated as >1.21 billion short tons from 1882 to 2024 (Fig. 1.14; Tables 1.2, 1.5). New Mexico state revenues generated from coal production in 2024 amounted to $6,981,779, while federal revenues amounted to $1,222,326. Approximately 904 people were employed by the coal industry in 2024. However, coal production is decreasing because of mine closures due to closures of coal-fired electrical generating plants. Furthermore, the coal at some mines is deeper in the subsurface and more expensive to mine. New Mexico has approximately 28 million short tons of coal reserves at producing mines (https://www.eia.gov/state/print.php?sid=NM), accounting for 3% of the reserves in the U.S. Coal currently produced in New Mexico is used to generate electricity at power plants in New Mexico and Arizona.

Coal fields in the San Juan and Raton basins in New Mexico are summarized in Table 1.5 and shown in Figure 1.13. Not all coal fields were productive, never-the-less coal resources are estimated for most coal fields (Table 1.5). Several factors determine whether a coal deposit is economic today or in the future, which include: 1) geologic factors (quality, overburden thickness, coal thickness), 2) the technology available for extraction, 3) distance to a market, 4) available transportation network, 5) environmental issues, and 6) permitting. The closure of coal-fired power plants has resulted in decreased coal production, including the cancellation of planned mines. Throughout the history of coal mining in New Mexico, these factors have changed and continue to evolve. The availability of critical minerals and REE in coals and coal

ash could enhance the economic potential in the future. For example, Salt River Materials Group (SMRG) of Phoenix AZ has contracts for available fly ash in New Mexico and northeast Arizona for use as a component in their pozzolan products.

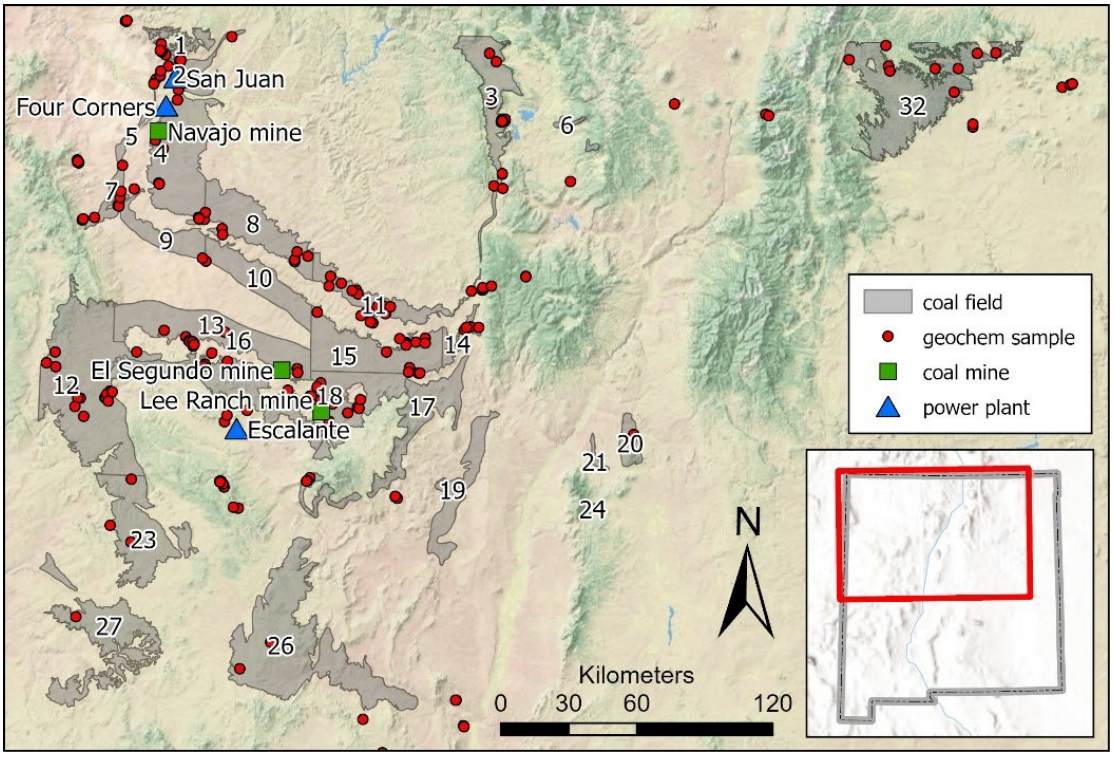

FIGURE 1.13 Location of coal fields in the San Juan and Raton basins, New Mexico (from Hoffman, 2017). Coal mines are surface operations except for the underground mine at the closed San Juan mine. Lee Ranch mine suspended operations in 2016 but reopened in 2024. Coal fields are listed in Table 1.5

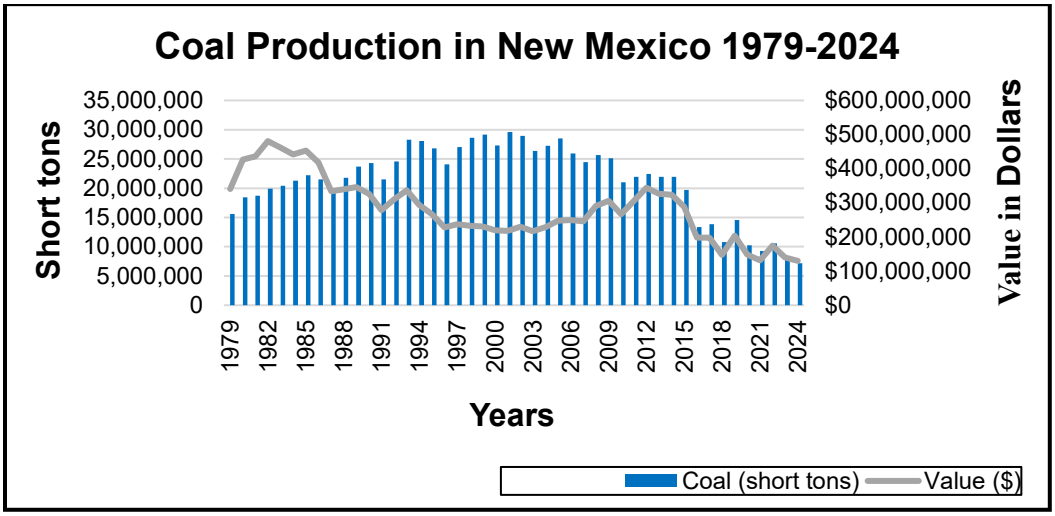

FIGURE 1.14 Coal production in New Mexico by year (data from USGS, 1902–1927; U.S. Bureau of Mines Mineral Yearbooks, 1927–1990; New Mexico Energy, Minerals and Natural Resources Department, 1986–2025; NMBGMR file data).

TABLE 1.5 Coal fields in the San Juan and Raton basins and adjacent areas studied in this project, delineated by Hoffman (1996, 2017). District Id numbers are from the New Mexico Mines Database (McLemore, 2010a, 2017). Red=no analyses at this time. Resource data from Hoffman (2017).

District Id	Coal field	Year of Discovery	Year of Initial Production	Year of Last Production	Estimated Cumulative Production	Formation	Demonstrated resources, million tons (Hoffman, 2017)
DIS257	Barker Creek	1882		1905		Menefee	183
DIS150	Bisti	1961	1980	1988	40,075,148	Fruitland	872
Arizona	Black Mesa						unknown
DIS208	Carthage	1856	1861	1963		Crevasse Canyon, Tres Hermanos	30
DIS181	Cerrillos	1835	1882	1962		Menefee	46.5
DIS259	Chaco Canyon	1905	1905		5,500,000	Menefee	46
DIS260	Chacra Mesa	1922		1945		Menefee	140
DIS118	Crownpoint	1905	1914	1951	20,758	Crevasse Canyon	663
na	Dakota	unknown			0	Dakota	unknown
DIS262	Datil	1913	1917	1940	66,980	Crevasse Canyon, Tres Hermanos	47
DIS155	Fruitland	1889	1889	2001	3,137,957,050	Fruitland	550
DIS119	Gallup	1881	1882	2001	121,522,629,885	Crevasse Canyon	610
DIS156	**Hogback**	1907	1907	1971	301,237	Menefee	66
DIS264	Jornada del Muerto	1910		1927		Crevasse Canyon	unknown
DIS174	La Ventana	1884	1904	1983		Menefee	263
DIS146	Monero	1882	1882	1970	5,277,552	Menefee	40
DIS016	Mount Taylor	1936	1952	1953	69,948	Crevasse Canyon	19
DIS157	Navajo	1933	1963	9999	4,714,689,147	Fruitland	1340
DIS258	**Newcomb**	1955				Menefee	126
DIS021	Raton	1820	1898	2002	954,470,032	Vermejo, Raton	unknown
DIS003	**Rio Puerco**	1901	1937	1944	139,555	Crevasse Canyon	25
DIS009	Salt Lake	1980	1987	1987	100,000	Moreno Hill	323
DIS121	San Mateo	1905	1983	2001	1,678,742,326	Menefee	385
DIS097	Sierra Blanca	1882	1899	1958	?	Crevasse Canyon	42
DIS261	Standing Rock	1934	1952	1958	?	Menefee	392
DIS158	Star Lake	1907			0	Fruitland	946
DIS263	**Tierra Amarilla**	1935	1955	1955	?	Menefee	4.5
DIS159	Toadlena	1950			0	Menefee	unknown
DIS124	Zuni	1908	1908	1926	16,010	Crevasse Canyon, Tres Hermanos	83
Total							7,242

1.6 Other industries in the San Juan and Raton basins (V.T. McLemore)

The primary industries in the San Juan Basin is production of oil and gas, and coal-bed methane is an important industry in the Raton Basin. Ranching, agriculture, and tourism also are important industries in both basins. Helium and geothermal resources have potential in both basins. Mining districts in or surrounding the San Juan and Raton basins are shown in Figure 1.6. Summary of the production and other information on the mining districts is in Appendix 3. Other industries support the minerals and agriculture industries are in both basins.

1.7 Summary of findings

- New Mexico has a wealth of mineral resources with significant production and resources of copper, potash, molybdenum, uranium, and coal.
- New Mexico ranked 14th in 2024 in the U.S. in coal production.
- Carbon-based products (CBP) include the nonfuel uses of coal, such as use in construction materials, aggregates (clinkers), resin, cement, soil additives (humate), asphalt additives, and products for the chemical industry. Synthesis of graphite and graphene is a potential nonfuel use of coal, both are critical minerals.
- Humate is currently produced in the San Juan Basin and the industry could be expanded by the presence of abundant reserves (Newcomer and Newcomer, 2021).
- Mineral production, including coal has decreased in recent years.

2.0 PHYSICAL AND GEOLOGIC SETTING (TASK 2) (V.T. MCLEMORE, M.N. BADONIE, AND V. ROBLEDO)

2.1 Vegetation and terrain

The San Juan Basin (Fig. 1.5), located in the southeast margin of the Colorado Plateau extends over northwestern New Mexico, northeastern Arizona, and southern Colorado. It also includes parts of the Jicarilla Apache, Ute Mountain, Southern Ute, Laguna Pueblo, Zuni Pueblo, and Navajo Indian Reservations. The Raton Basin is in the northeastern portion of New Mexico and southeastern Colorado. Paved highways, gravel, and dirt roads access both basins. The areas are mostly rural, with only a few ranches within several miles of the coal fields. Cell phone coverage is spotty or absent except on high peaks, ridges, and near communities. Some residents in the San Juan Basin do not have electricity or running water. The largest city in the Raton Basin is Raton while the San Juan Basin includes the cities of Grants, Gallup, Cuba, Farmington, and Bloomfield. The topography of both basins is flat to moderately rugged, with forested mesas. Adjacent mountains can be rough terrain with steep slopes. Vegetation ranges from piñon-juniper to scrub oak, and other bushes and grasses.

2.2 Climate

The climate of the San Juan and Raton basins is semiarid and high desert, with warm summers and cold winters (Table 2.1). Monsoon rains in the summer and snow in the winter provide the most precipitation. Meanwhile summer rains are occasionally intense and can cause mudslides and flash floods.

TABLE 2.1 Summary of climate data San Juan and Raton basins (from https://wrcc.dri.edu/summary/Climsmnm.html, accessed 5/31/2025).

	January	April	August	November	Annual
Cuba, NM					
Average high-temperature °F	41.9	62.4	83.2	53.0	63.8
Average low-temperature °F	10.0	26.2	48.8	17.7	28.5
Average precipitation in inches	0.84	0.74	2.32	0.73	13.15
Average snowfall in inches	8.0	1.1	0	2.4	28.6
Farmington, NM					
Average high-temperature °F	40.8	66.8	89.0	53.2	66.8
Average low-temperature °F	16.7	35.7	58.8	26.1	37.5
Average precipitation in inches	0.54	0.56	1.11	0.49	8.04
Average snowfall in inches	4.2	0.2	0	0.8	13.7
Grants, NM					
Average high-temperature °F	48.6	69.0	87.6	59.7	69.9
Average low-temperature °F	15.6	33.0	53.8	20.2	33.6
Average precipitation in inches	0.47	0.5	2.29	0.32	8.11
Average snowfall in inches	1.9	0	0	0.5	7.5
Raton, NM					
Average high-temperature °F	47.2	64.6	84.5	56.7	66.1
Average low-temperature °F	14.9	30.1	51.9	22.5	32.3
Average precipitation in inches	0.35	1.68	2.36	0.57	16.99
Average snowfall in inches	3.5	4.0	0	0	30.5

2.3 Geologic setting

During the Late Cretaceous, the present San Juan and Raton basins were on the western edge of the Western Interior seaway (Robinson-Roberts and Kirschbaum, 1995), which extended from the Gulf of Mexico to the Arctic Ocean. Complex fluvial systems transported sediments from volcanic and metamorphic sources in the Mogollon Highlands to the south and west into both basins. Cyclic transgressions and regressions of the marine seas resulted in a shift of the paleoshorelines. The shoreline of these interior seas was from the northwest to southeast portion of the state, which constantly migrated back and forth. During this period, there were three types of depositional environments, marine, coastal plain, and nonmarine deposits (Fig. 2.1). The San Juan Basin is an asymmetrical structural depression that is located on the southeast margin of the Colorado Plateau and is Upper Cretaceous to early Tertiary age. The basin covers more than 26,000 square miles of land and the center part of the basin is a circular, bowl-shaped depression (Brister et al., 2002).

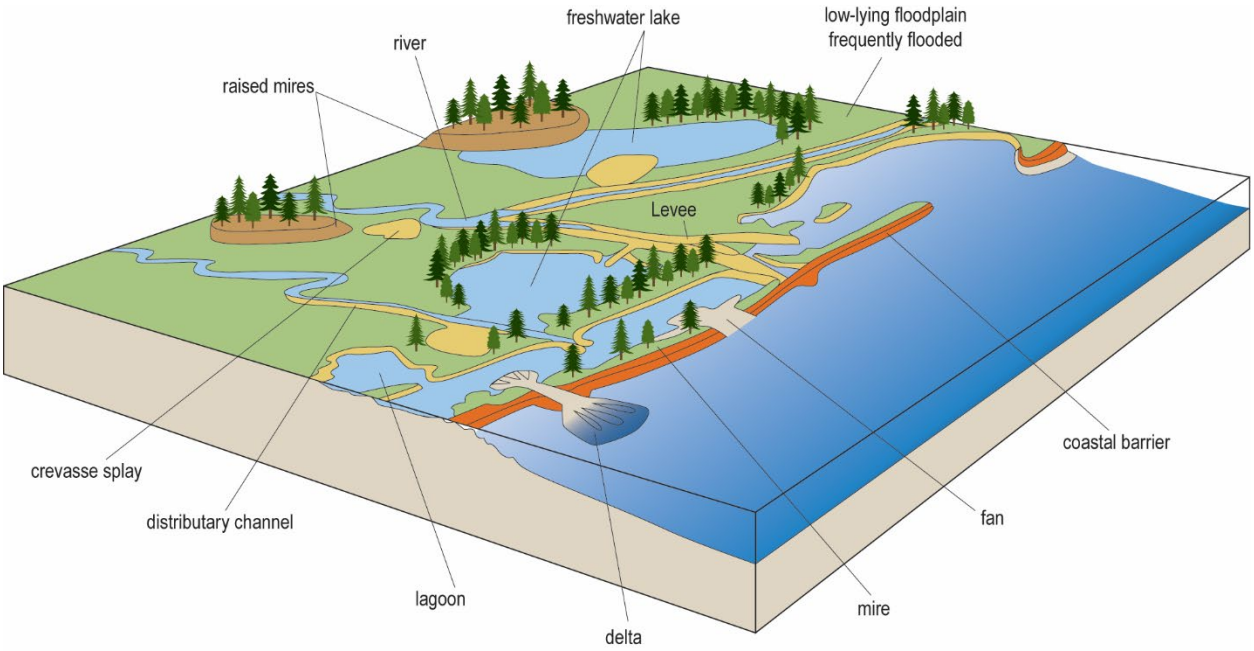

FIGURE 2.1 Depositional environments near coal swamps (Hoffman, 2017).

2.4 Stratigraphy

The stratigraphic units in the San Juan Basin dip inward from the bounding highlands toward the center of the basin, creating a trough-like feature (Fig. 2.2; Brister and Hoffman, 2002; Hoffman, 2017). The Cretaceous sedimentary rocks in the San Juan Basin contain three major coal-bearing units: the Crevasse Canyon, Menefee, and Fruitland Formations (Fig. 2.3). There are 26 defined coal fields in the San Juan Basin (Fig. 1.13; Tables 1.5, 2.2; Hoffman, 1996, 2017). The Raton Basin is divided into coal camps (Fig. 2.4).

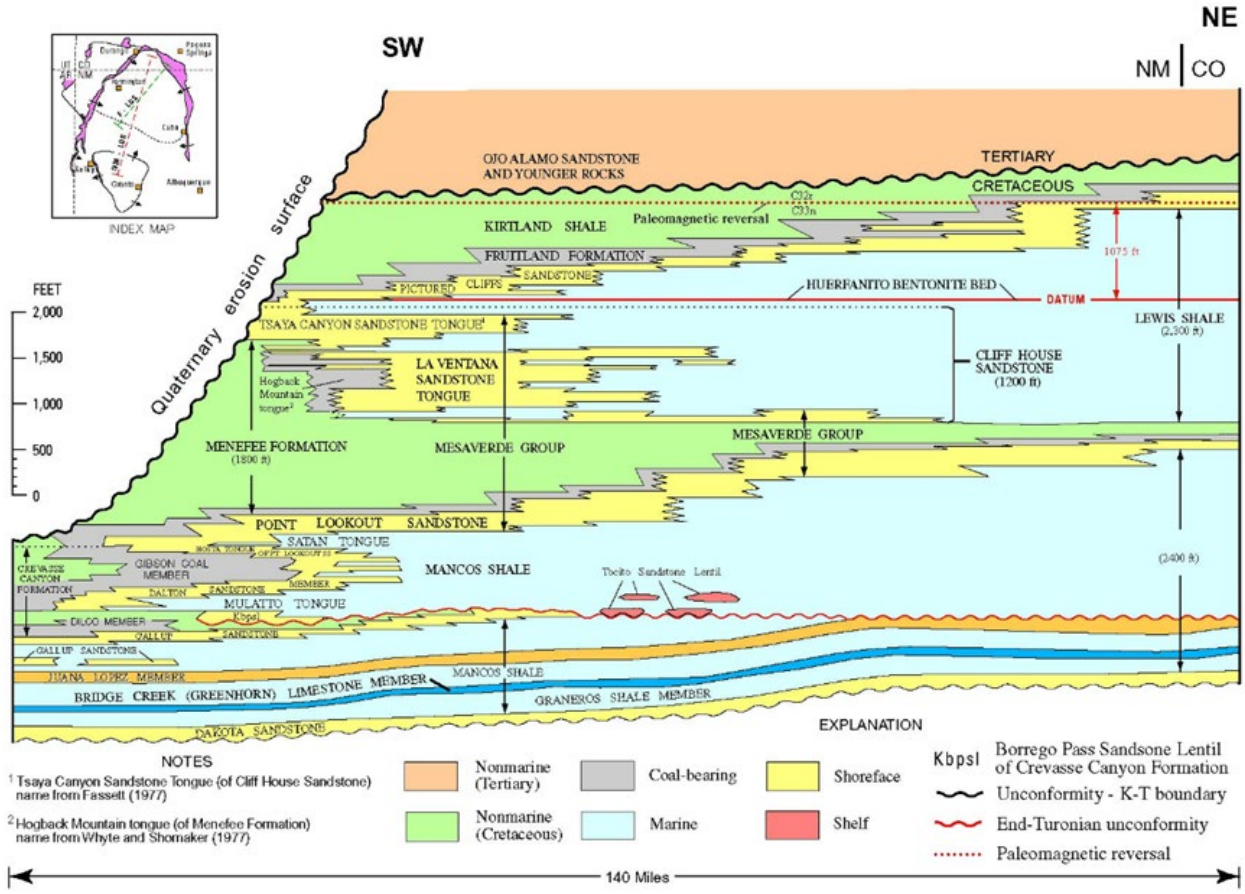

FIGURE 2.2 Stratigraphic section of the San Juan Basin (Hoffman, 2017).

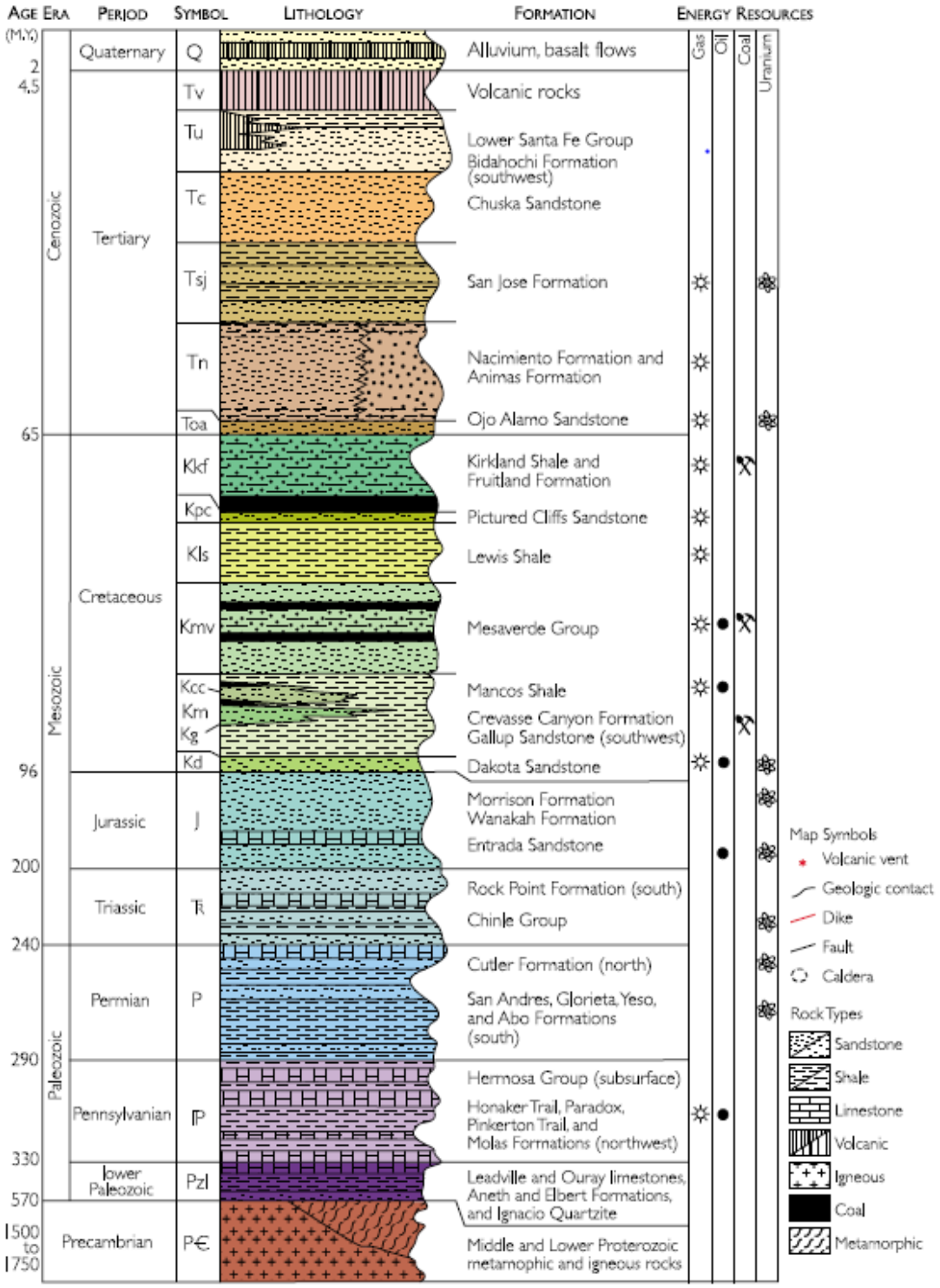

FIGURE 2.3 Stratigraphy of the San Juan Basin, New Mexico. Note the stratigraphic units that have gas, petroleum, coal, and uranium potential. Many of these same stratigraphic units have the potential for REE and other critical minerals (from Brister and Hoffman, 2002).

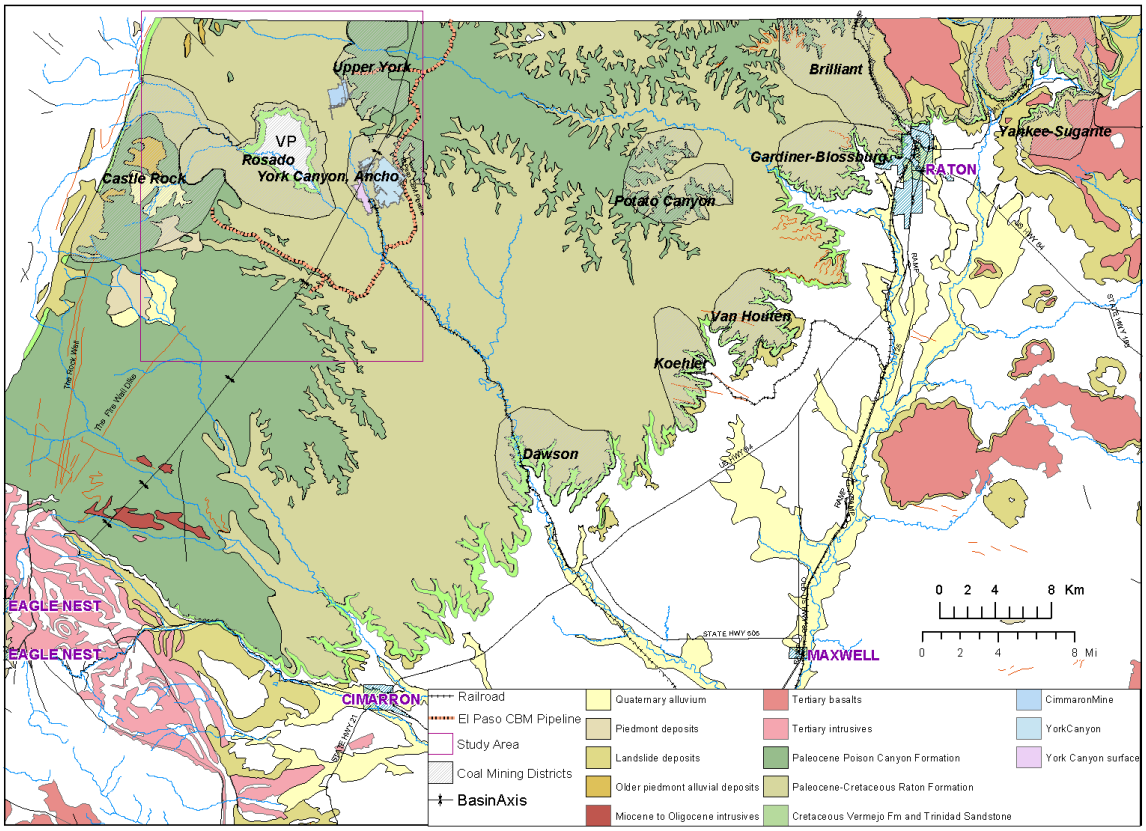

FIGURE 2.4 Geologic map of Raton Basin with coal camps (Hoffman, 2017).

TABLE 2.2 Coal fields in the San Juan Basin and outlier coal fields based on geologic formation. * indicates outlier fields. **Mount Taylor is the combination of East Mount Taylor and South Mount Taylor coal fields. The Dakota Formation also contains minor coal beds.

San Juan Basin coal-bearing formations		
Crevasse Canyon Formation coal fields	Menefee Formation coal fields	Fruitland Formation coal fields
Carthage*	Barker Creek	Bisti
Crownpoint	Chaco Canyon	Fruitland
Datil*	Chacra Mesa	Navajo
Gallup	Hogback	Star Lake
Jornada del Muerto*	La Ventana	
Mount Taylor**	Monero	
Rio Puerco	Newcomb	
Salt Lake*	San Mateo	
Zuni	Standing Rock	
	Tierra Amarilla	

2.5 Summary of findings

- The San Juan Basin, located in the southeast margin of the Colorado Plateau extends over northwestern New Mexico, northeastern Arizona, and southern Colorado. The Raton Basin is in the northeastern portion of New Mexico and southeastern Colorado.
- Paved highways, gravel, and dirt roads access both basins.
- The areas are rural, with only a few ranches within several miles of the coal fields.
- The climate is semiarid to arid.
- During the Late Cretaceous, the present San Juan and Raton basins were on the western edge of the Western Interior seaway, which extended from the Gulf of Mexico to the Arctic Ocean.
- Coal is found in Cretaceous sedimentary rocks in the San Juan and Raton basins.

3.0 METHODS OF STUDY

3.1 Databases and SOPs (V.T. McLemore, A. Trivitt, and M. Leo-Russell)

Databases were developed for this project. Initially, data were collected and stored in MS Access databases. Data collected were migrated to a MS SQL Server (SQLS) database, and the Access front-end forms were reworked to connect to the database server to increase reliability, efficiency, and security. Location, descriptions of samples, and other information from photographs taken in the field and thin sections are recorded in the SQL database. SOPs (Standard Operating Procedures) were developed for the project and provided in Appendix 4.

3.2 Photography, scanning, and archiving of samples (V.T. McLemore, Z.K. Motlagh, R. Otoo, D. Shaver, H. Tetteh, A. Trivitt, and M. Leo-Russell)

Photographs were taken of selected sample sites, test pits, trenches or long walls, drill cores, thin sections, and probe sections. Additional types of photographs were taken and stored with the database as appropriate. Digital cameras, phone cameras or film were used, with high resolution. Digital photographs and scans were taken at high resolution so that publication of the photograph will be possible. Photographs of all drillhole cores were obtained as a permanent record and for comparison with the descriptive log. Core photography was carried out before any core was removed for description and testing. Thin sections and probe sections were scanned and stored on the NMBGMR server. The following information was collected for photographs and scans:

- Sample number or some other identification in the field of view
- Ruler or some other object included in the photograph for scale
- GPS location.

Archiving of samples is necessary for future studies. Splits of samples were stored in plastic bags, labeled, and placed in well-labeled plastic buckets or wooden boxes. Shelves in the container were identified (Fig. 3.1, 3.2). A database was developed to inventory the samples and identify each sample by sample number, location in the storage facility, and other information (https://geoinfo.nmt.edu/staff/McLemore/documents/SampleStorageSpreadsheet%20V4%201-16-24.xlsx). Thin sections and probe sections were stored in the NMBMGR laboratories.

FIGURE 3.1 Storage facility with shelves of archived samples (photograph by D. Shaver).

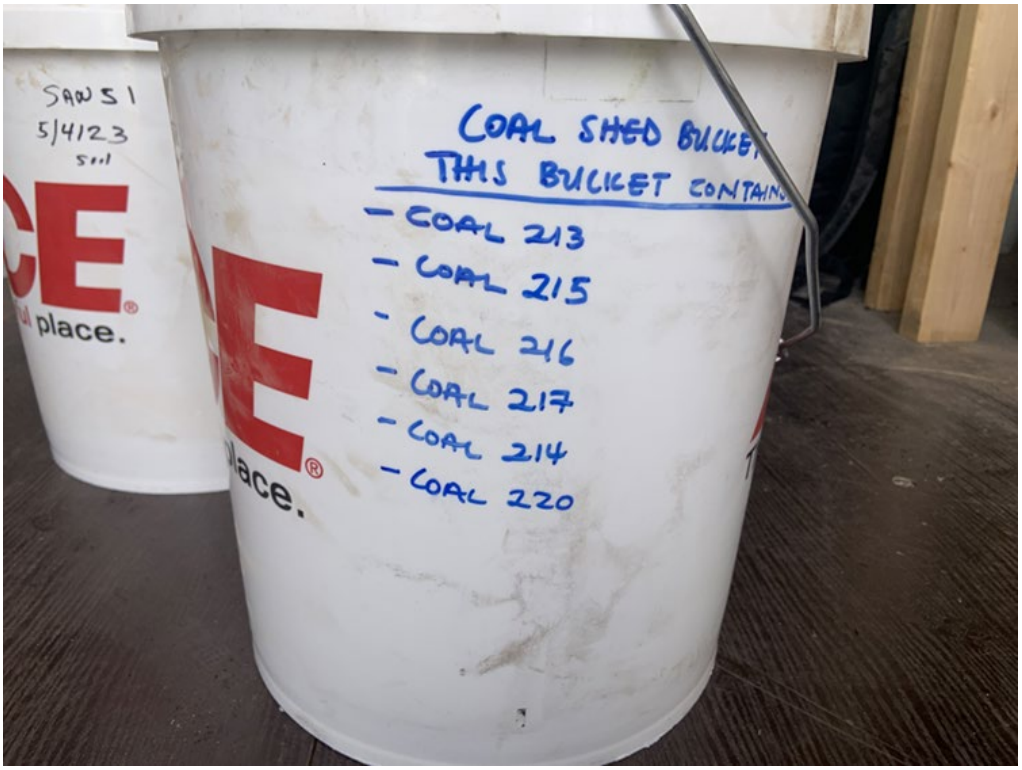

FIGURE 3.2 Each bucket was labeled with enclosed samples (photograph by D. Shaver).

3.3 Sampling of solids (V.T. McLemore and Z.K. Motlagh)

Before sampling, a site Health and Safety Plan (HASP) was written and reviewed by all field workers personnel (https://geoinfo.nmt.edu/geoscience/research/documents/145/HASP12.pdf). Sampling focused on outcrops, mine faces, stockpiles (Fig. 3.3), waste rock piles, stockpiles, and tailings; however, selected mineralized samples and slags were collected where present. Locally, steep slopes, ponding water, and other topographic challenges that present unsafe conditions arose, resulting in no sampling or revised sampling procedures to maintain safety standards. Summary of samples collected by coal field and types of samples are in Table 3.1. Descriptions, information on location, sources, types of samples, and other sampling information are in Appendices 5 and 6.

A sample is a representative portion, subset, or fraction of a body of material representing a defined population (Koch and Link, 1971; Wellmer, 1989; Davis, 1998; Neuendorf et al., 2005; Downing, 2008; McLemore et al., 2014; Smith et al., 2000; McLemore and Owen, 2024). A sample is a portion of the population studied and used to characterize the population. Collecting a representative sample of waste rock and other materials can be difficult because of the compositional, spatial, and size heterogeneity of the material.

Select samples include hand specimens of outcrops of mineralized rocks (including ore samples), grab samples of the mine wastes, and samples from individual cells from anywhere in a mine feature and are collected for specific purposes (such as to identify minerals or for geochemical analyses). The volume or number of samples collected is highly dependent on the type of laboratory test to be conducted and the availability of the sample. Weathering surfaces are removed from the rock samples. If the purpose of sampling is for geochemical analysis, the samples are broken into smaller chips. Select samples are collected directly from the outcrop, mine waste feature or the base of a slope to avoid sampling just float material. All samples are stored in well-labeled bags.

Mine waste features (defined as low-grade stockpiles (Fig. 3.3), mine waste rock piles, gob piles, tailings, slag, etc.) vary in size, shape, composition, the nature of the source material, waste management approaches, climate influence, and site accessibility. These variables affect safety and access considerations in sampling. The number of samples collected, the type of samples, sample locations, sample intervals, and other specific procedures depend on safety (Fig. 3.4, 3.5), the study's objectives, and equipment availability. These considerations dictated the systematic sampling procedures developed by the USGS (Smith and Huyck, 1999; Smith et al., 2000; USGS written communication, 2023; Acheampong-Mensah, 2024; McLemore and Owen, 2024).

A flow chart of the sampling and analytical methods used for solid samples is in Figure 3.6. Before going into the field and sampling, the features to be sampled were identified with satellite or other imagery, and the geology and topography of the sample site were examined. Site reconnaissance was utilized to determine the geography and topography of the sites more clearly. If a significant sample site or mine feature included topographical or other distinguishing features that suggested a change in composition or site management (e.g., benches, separate piles, tailings color, etc.), the feature was split into separate sample units. In some areas, a scintillation counter was used to identify more radioactive zones in the sample site as separate sample units. If the mine waste feature had discrete benches, each bench was considered an individual sampling unit.

FIGURE 3.3 Sampling a stockpile at El Segundo mine (photograph by V.T. McLemore, 7/20/22).

FIGURE 3.4 Sampling of high walls at El Segundo mine could not be performed safely (photograph by V.T. McLemore, 6/23/23).

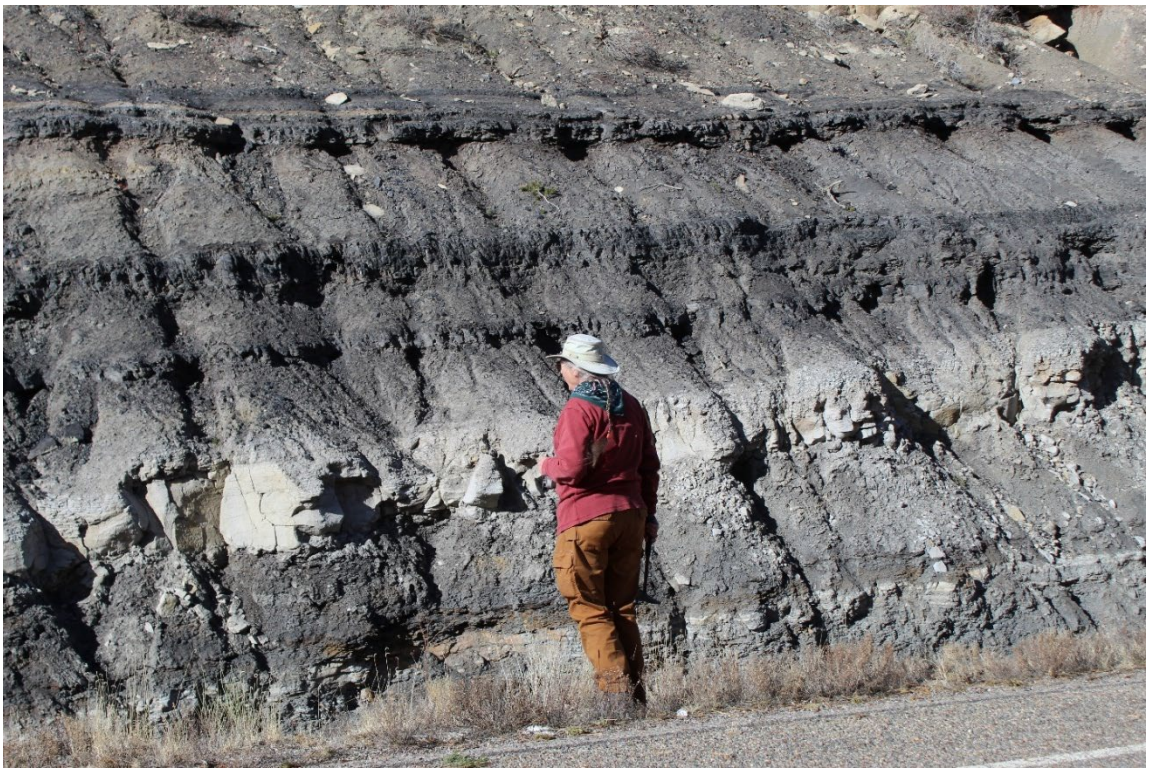

FIGURE 3.5 Road cuts offer excellent vertical sampling along many layers. Sampling at the top of the road cuts is not always possible because of safety (photograph by S.L. Rodolph, 1/13/2023).

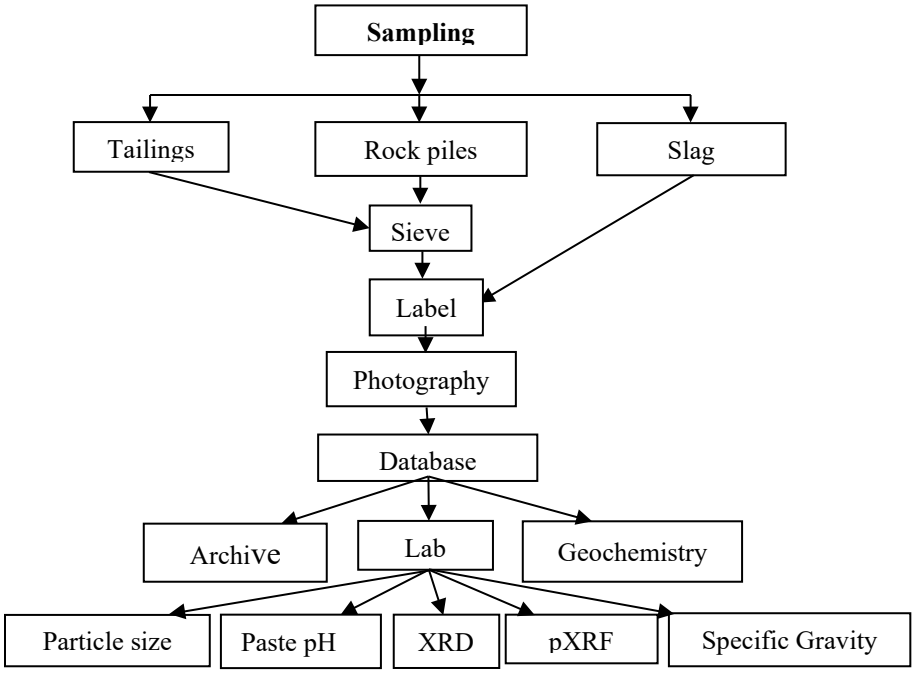

FIGURE 3.6 Flow chart for sampling and analytical analyses for solid samples.

TABLE 3.1 Summary of samples collected. Districts in red were not sampled.

District id	Coal field	Number of samples analyzed total	Number of coal (humate) analyzed	Number of samples from previous reports	Drill core available
DIS257	Barker Creek	9	8	0	no
DIS150	Bisti	65	18	3	yes
Arizona	Black Mesa	1	1	1	no
DIS208	Carthage	3	2	1	no
DIS181	Cerrillos	2	2	0	no
DIS259	Chaco Canyon	3	2	0	no
DIS260	Chacra Mesa	30	13	3	yes
DIS118	Crownpoint	12	8	0	no
na	Dakota	4	4	0	
DIS262	Datil	2	1	0	yes
DIS155	Fruitland	73	52	63	no
DIS119	Gallup	47	26	0	yes
DIS156	**Hogback**	0	0	0	no
DIS264	Jornada del Muerto	11	8	0	yes
DIS174	La Ventana	5	5	0	no
DIS146	Monero	25	18	6	yes
DIS016	Mount Taylor	8	6	0	no
DIS157	Navajo	32	17	2	yes
DIS258	**Newcomb**	3	0	0	no
DIS021	Raton	126	78	47	yes
DIS003	**Rio Puerco**	0	0		no
DIS009	Salt Lake	16	15	14	yes
DIS121	San Mateo	190	143	170	yes
DIS097	Sierra Blanca	8	3	0	no
DIS261	Standing Rock	8	4	0	yes
DIS158	Star Lake	45	28	0	yes
DIS263	**Tierra Amarilla**	0	0	0	no
DIS159	Toadlena	15	6	0	no
DIS124	Zuni	4	1	3	no
	Coal ash from power plants	7	5	2	
	Sedimentary copper	58	0	0	yes
	Uranium sandstone	22	0	23	yes
	Beach placer	131	0	89	yes
	Popotosa clay	20	0	20	yes
	Kline clay	6	0	6	
	Perlite	4	0	4	
	Manganese	4	0	4	
	Other samples	34	0	0	
	Total samples	1033	474	461	

When wet samples were collected, the samples were air dried at NMBGMR laboratories before sieving, and any particle agglomerates, which can form primarily upon drying a damp sample, were disaggregated before sieving. Chip samples (oversized material broken up to remove weathering surfaces) were collected from the material remaining after sieving (especially

for waste rock piles where a large percentage of the material is coarse) and placed into a separate bucket or bag and identified as a “coarse” (or oversized) sample. Finally, all the composite samples were thoroughly homogenized again and then transferred into appropriately labeled sample containers. Several buckets were used to homogenize the sample thoroughly. All holes were filled with the remaining material. This type of sampling poses no stability or erosion risks to the waste rock piles or tailings.

Select samples are rock samples collected for specific characterization purposes (mineral identification, chemical analyses, etc.). These samples are collected explicitly from hand specimens of mineralized rocks or ore samples, grab samples of the mine wastes, samples from individual cells of the waste feature, or samples from anywhere in the mine feature or outcrop. These samples were collected separately from the composite sample of mine features. The volume or number of samples collected is dependent on the type of laboratory parameter to be measured and the availability of the sample. Weathering surfaces were removed from rock samples and broken into smaller chips when sampled. Grab samples were collected directly from the outcrop, mine waste feature or along the slope.

Profile samples were generally collected along a vertical exposed section of a mine feature or road cut, if safe (Fig. 3.4). The soil profile was exposed by erosion, or a small pit was dug to reveal a profile. The pit's depth depended on the depth of the mine waste feature. A small trowel was used to gently clean the surface of the profile to prevent the edges from caving in. Lithological changes (i.e., color, thickness, depth texture, grain size, Munsell color, etc.) were identified and recorded in the field book. Samples were collected carefully by scraping directly into a well-labeled sample bag or decontaminated container (with the sampling depth labeled on the sample container) using a small trowel or scoop to avoid cross-contamination from different lithologies. In addition, samples were collected from the midpoint of the profile as much as possible to prevent mixing lithologies. A global positioning system (GPS) location or waypoint was assigned to the profile, and different sample IDs were assigned to each lithology or unit sampled in the profile.

Each container or sample bag was labeled with a permanent marker, at least twice on each container or sample bag. The sample label included a unique sampling identification number, collection date, and size fraction. Solid samples were stored at room temperature. Samples were then inventoried and submitted to the laboratories for analysis.

Gloves, dust masks, and reflective vests were used for sample collection. Before use, all equipment used for sampling (trowels, shovels, picks, buckets, sieves) were rinsed three times with deionized water and then air-dried. Disposable gloves were worn while sieving to prevent cross-contamination of the sample. After several sampling sessions, it was decided that several sieves needed to be available became sieves clogged with clay or dirt and to also allow for rapid subsample collecting while cleaned sieves were drying. Samplers used clean buckets for each sample rather than reusing buckets. All equipment (trowel, shovel, pick, buckets, sample bags, sieves) were rinsed with water and air dried to prevent cross-contamination of the sample. Sampling tools were constructed of materials suitable for environmental sampling (typically stainless steel, plastic, or aluminum) to avoid contamination.

Two splits of each sample were collected in the field: one split for chemical analyses submitted to a chemical laboratory and the second split archived at NMBGMR. The samples were transported from the field to NMBGMR, where each sample was prepared for laboratory analyses. Select samples were sent for preparation of polished thin sections. A summary of sample preparation for different laboratory analyses is in Table 3.2.

TABLE 3.2 Summary of sample preparation for laboratory analyses. XRF=X-ray fluorescence analyses. XRD=X-ray diffraction analysis. ICP=Induced-coupled plasma spectrometric analysis.

Laboratory analysis	Type of sample	Sample Preparation	Method of obtaining accuracy and precision
Petrographic analyses (Appendix 5)	Collected in the field, used split from chemistry sample	Uncrushed, typically smaller than gravel size material used, thin sections made of selected rock fragments	Not applicable
X-ray diffraction (XRD) analyses (Appendix 6)	Used select split from chemistry sample	Crushed	Compared to petrographic and electron microprobe analysis
Paste pH (Appendix 7)	Collected in the field, used split from chemistry sample	Uncrushed, typically smaller than gravel size material used	Use duplicates
Whole-rock chemical analysis (XRF, ICP, S/SO_4, other) (Appendix 7)	Collected in the field in separate bags, analysis performed on powdered samples	Crushed and pulverized	Use reference standards and duplicates
pXRF (Appendix 8)	Analyses on split from chemistry sample	Uncrushed, typically smaller than gravel size material used	Use reference standards and duplicates
Chemical analyses of water samples (Appendix 9)	Collected in the field in bottles	Refrigerated until analyzed	Use blanks, reference standards, and duplicates
Particle size analysis (Appendix 10)	Bulk samples collected in the field	Sample sieved for each size fraction weighed	Not applicable
Electron microprobe data (Appendix 11)	Collected in the field, used split from chemistry sample	Polished sections	See methods

3.4 Logging of drill core (V.T. McLemore, Z.K. Motlagh, A. Appah, A. Trivitt, and M. Bodanie)

NMBGMR retains drill core of coal deposits from 146 locations scattered throughout San Juan and Raton basins. Holes were selected based on coal field, completeness of the core, core description, and availability of geophysical logs. Drill core was photographed and logged describing the lithology, color, mineralogy, phenocryst size and shape, alteration, fracture intensity, and hardness. Grain size cards were used to determine phenocryst shape and rounding, and tables were used to determine alteration and fracture intensity. All core was photographed with hole, box, and depth information and then replaced in the original position. Samples were collected of the coal seams and layers above and below the coal seams. Drill core samples were split in half using a drill core splitter or saw. One half of the core was returned to the box to preserve the core. The other half was split into sufficient sizes for thin section preparation and chips for chemical analysis. Sampled intervals are indicated in the core box by a note denoting sampler, date, purpose, project, hole, box, and depth. Photographs of the core are found at https://photoarchive.nmt.edu/.

3.5 Characterization

3.5.1 Petrography (Z.K. Motlagh, D. Shaver, and V.T. McLemore)

Petrographic analyses were performed using standard petrographic techniques (hand lens, binocular microscope, polarizing microscope and reflective light microscope)**.** These analyses were supplemented by thin-section petrography, X-ray diffraction (XRD), pXRF, and whole-rock chemical analyses (Motlagh and McLemore, 2025). Hand sample descriptions, including mineralogy and texture of samples, sawed samples, and thin sections, were entered into the project database and briefly described in Appendix 5. Polished thin sections of selected samples of the host, altered, and mineralized rocks were made by commercial laboratories. Thin sections were scanned in plane and plane-polarized light, and selected photomicrographs were taken. The mineralogy of selected samples was determined by visual, petrographic, and X-ray diffraction (XRD) methods. Modal mineralogy was estimated using standard comparison abundance charts. Mineral concentrations and phase percentages, grain size, roundness, and sorting were estimated visually using standard charts (Appendix 5; Carpenter and Keane, 2016).

Bulk mineral identification can identify minerals in quantities greater than approximately 3%. Estimates of primary and secondary minerals were determined, cementation and alteration described, and mineralogy and lithology were described (Folk, 1974; Carpenter and Keane, 2016). Any special features were noted. Weathered waste rock piles and coal samples typically contain some amorphous material that XRD cannot identify (Smith et al., 2000). This material can be characterized by integrating XRD and geochemical data. Detailed petrography analysis using optical microscopy and SEM was performed on several representative samples at SNL. The reports are in Appendix 5.

3.5.2 Mineralogy using ultraviolet lights (E.J. Owen)

Long (365 nm) and short (254 nm) wavelength ultraviolet light sources can aid in mineral identification. Some minerals fluoresce distinct colors under either or both of these wavelengths, though most fluorescent minerals favor 254 nm wavelength. Minerals fluoresce due to fluorescent activators and co-activators, elements that substitute within their crystal structure, a notable example being Mn^{2+} in many minerals. Orange fluorescing calcite is attributed due to this activator, Mn^{2+} substituting for Ca^{2+}, in the structure. A few minerals are intrinsically fluorescent due to their crystal structure, for example, scheelite ($CaWO_4$). Fluorescent minerals can be indicators of the presence of critical minerals, directly or indirectly. Zircon ($ZrSiO_4$), a source of Zr and Hf, commonly fluoresces yellow-orange under 254 and 365 nm wavelengths and can be present in large amounts in heavy-mineral sandstones. Many secondary U minerals fluoresce bright green under 254 and 365 nm wavelengths and could be an indicator of critical minerals such as V in some sedimentary-hosted deposits. Resinite, or coal resin, is a naturally occurring resin found in some coals that could be economically extracted from some coal deposits. This low-density substance is generally translucent yellow to orange and is generally brightly fluorescent green, though it can also fluoresce yellow, orange, or red-brown (Tabet et al., 1995).

3.5.3 Scintillation counter/gamma ray spectrometer (E.J. Owen)

Scintillation counters are instruments for measuring gamma radiation and are more sensitive than Geiger counters. A dense crystal (generally NaI(Tl), sodium iodide doped with thallium) produces a very small emission of photons when bombarded with a gamma ray. A photomultiplier tube amplifies this signal, which can then be paired with a rate counter to output rate in counts per second (cps), generally. The more sophisticated gamma ray spectrometer is at its core a scintillation counter, but an onboard spectrometer determines the energy of incoming gamma rays because the photon emissions from the scintillation crystal are proportional to the incoming gamma rays. The energy of gamma rays is characteristic of the radionuclides that produce them, and thus these instruments can infer the decay series present in the sample being measured. In geological applications, K, U, and Th are the main naturally occurring elements with radioactive isotopes that can be measured with a gamma ray spectrometer. For CORE-CM studies, the presence of U and Th are significant as other critical minerals can associate with these elements, either in the same minerals that contain U and Th, or in other minerals that occur with the radioactive minerals. For example, zircon ($ZrSiO_4$) and monazite ($[Ce,La]PO_4$) can both accommodate U and Th in their crystal structures, causing them to be radioactive. Zircon can also substitute REE and Hf in its crystal structure, making it a source for other critical minerals besides Zr; monazite is a primary REE mineral. Both minerals can be found in high concentrations in heavy-mineral sandstones, which can be found in the vicinity of some coal seams. Scintillation counters and gamma ray spectrometers also can aid in geologic mapping. Each lithologic unit in an area will have a particular background radioactivity associated with it. For example, quartz-rich or carbonate sedimentary rocks generally have very low background radioactivity. The background radioactivity of shales can be significantly higher due to K found in clay minerals, as well as U found in some black shales. Igneous rocks can vary widely with respect to background radioactivity, but alkaline rocks are generally more radioactive due to significant concentrations of K. Using a scintillation counter in the field can help identify contacts between rocks of differing background radioactivity, ash beds, and faults (some of which can be slightly enriched in U). These instruments are also very useful in mapping the extent of heavy mineral sandstones. Techniques can also be quickly developed and employed to estimate the content of combined U and Th, Zr, and Ti in hand samples from a particular deposit, provided some geochemical data for these elements from the deposit exist or can be collected (Owen and McLemore, 2024).

3.5.4 Mineralogy by XRD (Z.K. Motlagh and R. Boakeye)

Mineralogy of selected samples was determined using X-ray Diffraction (XRD). Either whole rock or specific mineral separations were powdered to perform XRD analysis using the PANanalytical X'Pert Pro Diffractometer at the NMBGMR XRD laboratory. Analyses were conducted using 45 kV X-ray beam tension and 40 mA X-ray beam current. A diffractogram is produced (Fig. 3.7). X'Pert HighScore Plus software was used to interpret the XRD data by comparing measured X-ray peak intensities and matching the patterns to a Powder Diffraction File database that correspond to specific mineral structures. XRD data are presented in Appendix 6.

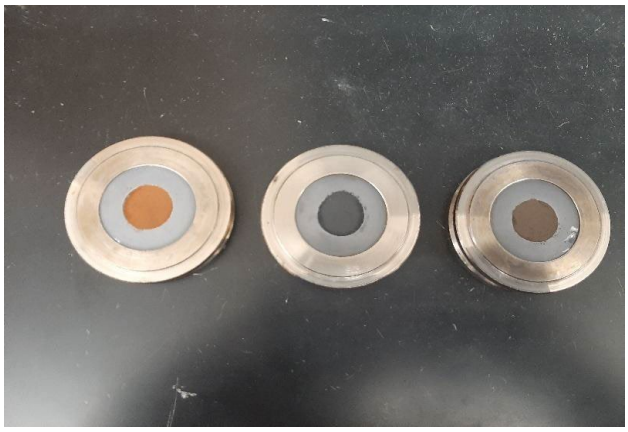

FIGURE 3.7 Sample holder containing prepared samples

3.5.5 Chemical analyses (V.T. McLemore)

Geochemical data are a critical part of evaluating critical minerals resources. Sample preparation and geochemical analyses of solid samples collected for this study were performed by commercial laboratories. Analytical methods are described in the spreadsheet with the geochemical analyses (Appendix 7). Duplicate samples and reference standards were analyzed (Appendix 7); the uncertainty of most analyses is generally <5%.

Chemical plots were created using ioGAS-64 (ioGAS™ - REFLEX (reflexnow.com). REE plots are typically normalized to a standard, such as chondrite or North American Shale Composite (NASC) in order to remove the systematic zig-zag patterns due to the Oddo-Harkins effect, which is hard to interpret. Normalization produces a smoother curve that is easier to interpret. Box and whisker plots are similar to histograms and provides visual representations of data distribution, illustrating the minimum and maximum ranges as whiskers along with the median value and quartile ranges as boxes of a given dataset. Other plots and descriptive statistics can be created using ioGAS-64 and are used in this report. Correlation diagrams plot one element verses another element. In some cases, the elements do show a correlation, in other cases, the elements show no correlation between them. Downhole vertical plots show the distribution of elements vertically down a drill hole, with 0 ft representing the surface and the depths indicated.

3.5.6 Electron microprobe—New Mexico Bureau of Geology and Mineral Resources (N. Iverson)

Samples with high measured total REE and Zr concentrations were analyzed for the major and minor element compositions of feldspars, zirconosilicates and REE-bearing phases. All preparation work was completed at the NMBGMR electron microprobe lab. Rock samples were cut to billet size, set in plastic ring molds, backfilled with Spurr 4-part epoxy, and cured at 80ºC for four hours. Some of the samples dated using the $^{40}Ar/^{39}Ar$ dating method needed further characterization and a subset of the picked grains were analyzed on the electron microprobe. These samples were mounted in leucite 4-hole mounts, backfilled with Spurr 4-part epoxy and cured. Cured samples were then polished using diamond polishing wheels (168 µm, 63 µm and 30 µm) and finished with diamond polishing powder slurry on Buehler polishing cloth (15 µm, 6 µm) down to 1 µm and coated with approximately 20 nm of carbon.

Prepared samples were analyzed using the Cameca SX-100 electron microprobe with four wavelength dispersive spectrometers (WDS) located at the NMBGMR. Backscattered electron (BSE) images were used to observe textures, identify bright phases with high mean atomic number, and assess REE phase abundance. WDS qualitative element scans and WDS X-ray maps were used to identify the mineral phases. Major, minor, and trace element concentrations were collected on specific mineral phases using a 20 nA beam current and an accelerating voltage of 15 kV. Amphiboles and oxides were analyzed with a 1μm beam diameter, 10 μm for monazite, bastnäsite and feldspars, and 20 μm for clinker matrix. The microprobe was calibrated using kaersutite and Kakanui hornblende, orthoclase, ilmenite, VG568 rhyolite, siderite, apatite and albite standards. Calibration minerals, counting times, and spectrometer crystals can be found in the footnote of Appendix 11.

3.5.7 Electron microprobe—Sandia National Laboratory (G. Xu)

Micro-sampling via Dremel

To preserve sample heterogeneity, localized sampling is needed. A Dremel tool was used to drill powders from the selected features using diamond drill bit. The resulting powder is collected and used for further analysis by microwave digestion, XRD analyses and leaching experiments. Therefore, the data might differ from the bulk analyses.

Microwave multi-acid digestion

A microwave multi-acid digestion process (REFs) was utilized resulting in total to near-total digestion of the powdered starting materials. Microwave system, MiniWave, is utilized to dissolve the samples quickly. About 100 mg of the individual powdered samples were loaded into Teflon tubes and then filled with a mixture of concentrated acids: 6 mL concentrated HNO_3 + 2 mL concentrated HCl + 3 mL concentrated HF. Teflon tubes were then sealed using a cap and plunger. The rack with 6 tubes was then loaded into the microwave digester (MiniWave) and locked into place. The digestion temperature was ramped up to 190°C and then held at that temperature for 15 minutes before allowing the samples to cool down to ambient temperature. The process is often repeated 2-3 times to make sure the sample is nearly or completely digested. The final solution was then transferred to Teflon beakers and dried overnight at 85°C. Subsequently, 20 mL 2% HNO_3 was added to each dried solid residue (cake) and sonicated for 10 minutes. After determining the cake was in solution by visual inspection. Once it is in solution is then ready to be diluted for ICP-MS analysis. The measured concentrations of the individual critical elements by ICP-MS enable the determination of their concentration in the sample of interest. A significant majority of the material will be dissolved so the method is resulting in near total sample digestion.

Assessing Critical Element Recovery Using Citric Acid Leaching

To evaluate the recoverability of individual critical elements, various concentrations of citric acid solution were used to extract these elements from powdered samples using a process developed by Sandia National Laboratories. Citric acid with or and without $MgSO_4$ additions were added into 30 mL deionized water before mixing with 0.5 g of sample powder. The resulting solution/solid mixture was placed in an oven at 70°C for one week. The mixture was stirred daily. After one week, the leachate solution was sampled and diluted with 2% HNO_3 for ICP-MS analysis. Percent recovery for individual critical elements are reported in Appendix 5.

Vibration spectroscopy (Raman and Infrared spectroscopy)

Raman and infrared spectra were obtained for several coal or coal-rich samples to understand the maturity. The micro-Raman analysis was performed on XploRA+ whereas the attenuated total reflectance (ATR) was obtained using IS50 infrared spectrometer.

Scanning electron microbe

Polished thin sections were produced by commercial laboratories and subsequently were examined on an Oxford Instrument TSCAN SEM equipped with Energy Dispersive X-ray Spectrometry (EDX). by Oxford Instrument. The detailed analyses for samples Coal2, Coal 9, Pop1 and Far2 are provided attached in Appendix 5.

X-Ray CT

Samples (Coal2, Coal 9, Pop1 and Far2) were analyzed by Zeiss Xradia 520 Versa with pixel resolution of 77.8 micron per pixel with low resolution and 14.9 micron per pixel with high resolution. The CT analysis results are presented in Appendix 5.

3.5.8 Paste pH (Z.K. Motlagh)

Upon exposure to air, water, and bacteria commonly occurring sulfide minerals (predominantly pyrite (FeS_2)) can oxidize and break down to form acid drainage. The acid drainage enables various metals within the minerals to dissolve into the ground and surface water. A sample is typically considered “acid generating” if the resulting pH is less than 4 (Borden, 2001). To determine the pH of the pore water produced by the dissolution of secondary mineral phases on the surfaces of oxidized rock particles, paste tests on mine waste samples are used to evaluate the geochemical behavior of mine waste materials subject to weathering under field conditions (Fig. 3.8).

FIGURE 3.8 Paste pH test setup for analyzing coal samples.

The following materials are required for conducting paste pH tests.

- A pH meter with a combination pH electrode (Fig. 3.9)
- pH 4 and pH 7 calibration standards
- Stirring rod
- 50 mL glass beaker
- Distilled or deionized water
- Sieve (No. 10)
- Scale
- Graduated cylinder
- Laboratory measurements (solids) forms

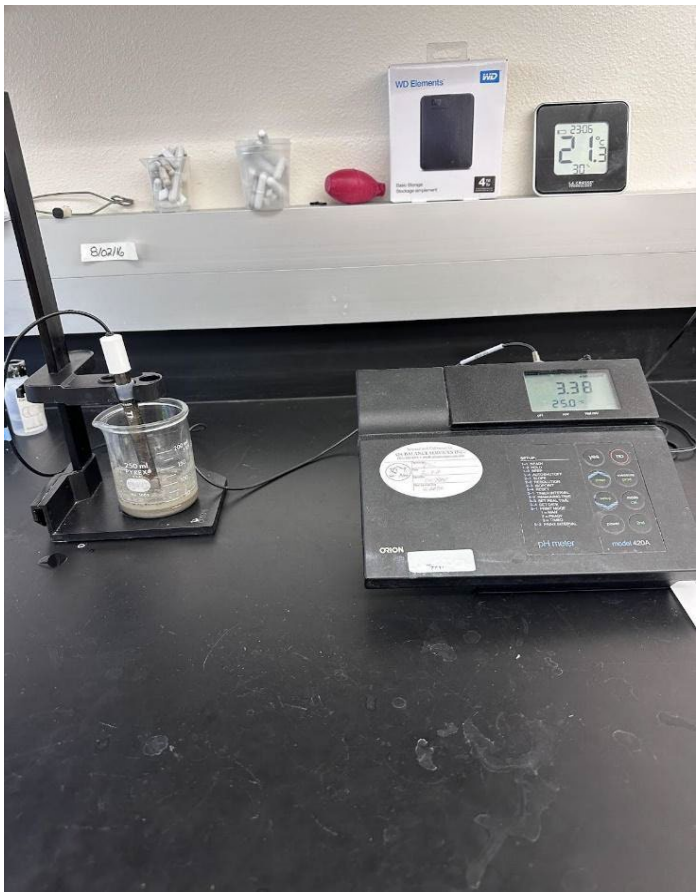

FIGURE 3.9 The pH meter with a combination pH electrode is measuring the pH of a coal paste sample.

First, the pH meter is calibrated using standard solutions. Approximately 25 grams of fine sample particles (less than 1 mm) were placed in a clean beaker and combined with 25 mL of deionized water. The mixture was stirred and left to stand for 10 minutes. A fizz test was performed to find out how much hydrochloric acid (HCl) needs to be added to a 2 g sample in order to digest carbonate (and other neutralizing minerals). The pH meter probe was inserted, and measurements were recorded. Probes and containers were rinsed with deionized water between tests. Probes were rechecked every 20 tests to ensure accuracy.

3.5.9 Specific gravity (A. Serwah, Z.K. Motlagh, and V.T. McLemore)

Specific gravity was measured and used with mine waste volume estimates to estimate the tonnage of the mine waste together with the mine waste characterization. The specific gravity was performed using the ASTM D854-02 method or the Standard Test Methods for Specific Gravity of Soil Solids by Water Pycnometer. A total of 13 samples were measured. The samples were air-dried. The specific gravity of the samples was calculated through the equation:

$$Gs= \frac{A}{B-C}, \text{ where}$$

A: Dry Weight

B: Wet weight

C: Submerged weight.

3.5.10 Sampling procedures for mining-influenced waters (B. Frey)

Water bodies at mine sites offer an opportunity to evaluate and determine if mineral extraction of REE and other critical minerals from mine-influenced waters can be feasible or even economical. Meanwhile, the technology to extract REE continues to develop (e.g., Hermassi et al., 2022), making mine-influenced waters a potentially viable source for REE production.

The NMBGMR Economic Geology Program includes water resources in its investigations, such as in this project. Six water samples were taken from two mining districts, Hillsboro and Steeple Rock, with a team of at least one staff member and two to three students who followed USGS sampling protocols (SOP 101). Of the two water samples taken at Hillsboro, one was from the pit lake at the Copper Flat mine, and one from ponding seep water collected from a nearby small cliff face. Four water samples were taken in the Steeple Rock district: water from an adit at the Center mine, water from two different adits at the Carlisle mine, and surface runoff water from a stock tank above Carlisle mine. For water samples, additional information must include:

- Checklist of samples collected for water samples
- Field parameters (pH, T, SC, ORP, DO) and associated calibration, check standard information
- Filtration system used
- Flow measurement technique and source of data.

Methods for water sample collection and preservation are derived from the USGS National Field Manual for the Collection of Water-Quality Data (NFM; Wilde, 2011; full report at https://www.usgs.gov/mission-areas/water-resources/science/national-field-manual-collection-water-quality-data-nfm). See specifically chapters A1, A2, A3, A4, A5, and A6 in the USGS manual for details of the collection processes used by NMBGMR. Depending on the type of site sampled (for example, pit lake, adit drainage), additional equipment may be needed to collect the water sample (for example: boat, sampling pole, etc.). Generally, water will be extracted via a peristaltic pump, into a filtration unit, or directly into a bottle, although alternate methods, such as syringe filtration, are acceptable. Field parameters (pH, temperature, specific conductance, dissolved oxygen, oxidation-reduction potential) should be measured when water samples are collected.

Five splits were taken for each water sample for five different analyses (Table 3.3). All splits were collected in 125 mL plastic bottles, most splits were filtered, several splits received nitric acid for preservation, and all splits were kept on ice after sampling. Depending on analytical requirements, water was collected via a peristaltic pump into a filtration unit or directly into a bottle; syringe filtering was done on samples that caused clogging in the peristaltic pump filter. Field parameters (pH, temperature, specific conductance, dissolved oxygen, oxidation-reduction potential) were measured on pre-calibrated instruments when water samples were collected. Depending on the type of site sampled (for example, pit lake, adit drainage), additional equipment may need to be used to collect the water sample (e.g., sampling pole, acid-washed containers, etc.).

TABLE 3.3 Overview of types of bottles, preparation, and preservation for water samples. Filtration pore size is 0.45 mm.

Analysis	Bottle *	Filtration	Preservation
Metals and cations, raw (RA)	125 mL plastic bottle	None	1% v/v nitric acid
Metals and cations, filtered (FA)	125 mL plastic bottle	Filter (0.45 μm)	1% v/v nitric acid
Precious metals	125 mL plastic bottle	Filter (0.45 μm)	1% v/v nitric acid
Anions	125 mL plastic bottle	Filter (0.45 μm)	Chill at 4 °C
Alkalinity/acidity	125 mL plastic bottle	Filter (0.45 μm)	Chill at 4 °C

*Certified contaminant-free HDPE sample bottles were purchased; thus, no pre-cleaning was needed on sample bottles.

Personal protective equipment (PPE)

Clean, nitrile (or similar) gloves were worn when handling equipment that comes in contact with water samples and during field parameter collection. Safety glasses were worn on site**.** If samples were collected in underground workings, hard hats, glasses, and other appropriate PPE were used.

Bottle sets

Each sample collected was distributed into a set of five 125-mL HDPE bottles as detailed in Table 3.3 and analyzed for: 1) alkalinity, 2) anions, 3) trace filtered acidified (FA), 4) trace unfiltered acidified (RA), and 5) precious metals. One exception was the stock pond above Carlisle mine, which was so high in suspended solids that only half a bottle for FA trace metals could be filtered (with about 20 filters by syringe filtering), and only full bottles for alkalinity and RA trace metals were collected.

Pre-cleaned bottles were purchased from the supply company, so the project team performed no precleaning. Before sample bottles were filled, they were rinsed with the sample three times. The “raw” metals and cations bottle was not filtered before preservation acid was added; analysis of this split was intended to capture total suspended solids. The “filtered” metals and cations bottle was filtered before preservation acid was added, analysis of this split targeted total dissolved solids. Bottles were rinsed three times with sample water before collecting the sample and were filled to the top as much as possible, leaving minimal headspace in the bottle.

Bottles were labeled in the laboratory or field before field sampling, and waterproof labels with some information (filtration, acidification, etc.) were preprinted on the labels. Each bottle was uniquely labeled with the site name, collection date and time, and the analysis and associated preservation. Abbreviations for special handling were included; for example, unfiltered metals/cations were labeled with the suffix “-RA” for “raw (unfiltered), acidified.” Filtered metals/cations were labeled with the “-FA” suffix for “filtered, acidified.” Filtered anions were labeled with the suffix “-FU” for “filtered, unacidified.” Filtered alkalinity splits were labeled with the suffix “-FALK” for “filtered alkalinity.”

Pumps and tubing

An Alexis peristaltic pump from Proactive Environmental Products was used for this project. The pump tubing was acid-washed and rinsed with deionized water before every trip. Several sections (varying from 3 to 26 feet, the maximum suction lift length) were taken on every sampling trip so a clean section could prevent carryover between sites. Although every site

had its dedicated tubing, enough DI water was taken along in the field so that tubing could be rinsed between sample sites if more clean sections were needed than were provided. Before taking a water sample, one liter of sample water was pumped through the tubing without collecting to rinse the tubing clear between samples.

Filters—Reusable polypropylene filter holders with 0.45 mm filters were used, except where high solids water required syringe filtering. The filtration type was noted in the field sheet.

Preservation—After sampling, all sample bottles were closed tightly to prevent leakage and stored in plastic bags to prevent melted ice or dirt from contaminating the samples. Samples were placed in a cooler with ice in the field and during shipping. If shipping could not be done immediately after fieldwork, the samples were placed in a lab refrigerator until shipment. Sample splits that needed acidification upon collection were acidified to 1% nitric acid in the field (see Table 4) with concentrated, ultra-high-purity nitric acid (HNO_3). The amount of acid needed was calculated as 1 mL added to each 125 mL bottle filled to the shoulder. The acid was applied using a pipette, clean pipette tips, a PTFE bottle for acid, or a PTFE dropper bottle calibrated in the laboratory for how many drops approximately equals mL of acid. The closed bottle was shaken after the acid was added to the bottle.

Water sampling QA/QC

Duplicates and blanks—Deionized water (DI water) was brought into the field to collect at least one field blank for each day of a sampling event. The entire sample collection protocol was followed with DI water, including rinses and filling a complete set of sample bottles. A duplicate sample was collected at least once per day per sampling trip or once per every 20 samples if more than 20 samples were collected in a single sampling event, following the same sampling protocol as a routine sample. These QC splits were transported, stored, and shipped to the Denver laboratory along with the other samples and analyzed as samples.

Field parameters

Specific conductance, pH, temperature, and oxidation-reduction potential (ORP) were measured in the field with a YSI ProPlus multimeter. Dissolved oxygen was measured with a ProSolo meter. Meters were calibrated the night before the fieldwork or in the field before measurements are taken. The calibration was rechecked on-site before the water source was measured.

Field parameters were measured in situ (electrodes placed directly into the water source), using care not to collect the water samples simultaneously to prevent contamination by disturbing the surrounding sediment.

- Meters were calibrated using the following solutions:
- pH was calibrated using buffers of 4.01, 7.00 and 10.01
- Specific conductance – 1413 µS/cm standard
- ORP – 445.4 mV standard
- Optical dissolved oxygen (ProSolo meter) was calibrated in water-saturated air per the manufacturer's instructions.

The samples were then transported from the field to NMBGMR and inventoried before being shipped for laboratory analyses. Laboratory methods are detailed on the USGS National Water Quality Laboratory website: https://www.usgs.gov/labs/national-water-quality-laboratory.

3.6 Quality control (QA) and quality assurance (QC) (V.T. McLemore)

The samples and field data (including field observations and measurements) are the basic component of the data collection and interpretation, which ultimately leads to the project conclusions. Therefore, it is important to understand the spatial and geological context and to describe the types of samples collected, sample preparation, and sample analyses. The purpose of this section is to describe the QA/QC procedures to support the accuracy and precision for the geochemical (Appendices 7, 9, 10) and mineralogical analyses obtained by NMBGMR. The data were obtained from the various laboratories and at least 10% of the data were validated or checked by an additional staff member to assure the data were entered into the database properly. If during validation, data were found to be entered incorrectly, the error was immediately corrected. This section only describes the sample collection and preparation of samples collected during the project. The QA/QC procedures for the electron microprobe laboratory at NMIMT are explained at http://geoinfo.nmt.edu/labs/microprobe/home.html (accessed 6/16/2025).

The determination of total error of a measurement depends upon several parameters, including the sample error and analytical error (Rollinson, 1993; Schreuder et al., 2004). The sample error is the error that results from studying the collected sample instead of the entire population and depends upon completeness, comparability, and representativeness, as defined below:

• *Completeness*—the comparison between the amount of valid, or usable, data originally planned to collect, versus how much was collected.

• *Comparability*—the extent to which data can be compared between sample locations or periods of time within a project, or between projects.

• *Representativeness*—the extent to which samples depict the true condition or population being evaluated

Sample error is the error caused by observing a single sample instead of the whole population and typically is dependent upon the sample-to-sample variation that is controlled by collecting a sample of suitable size relative to the heterogeneity of the sampled material, as well as a sufficient number of samples to characterize the population (Wellmer, 1989).

All analytical measurements are incorrect at some level and are measured against an agreed upon standard of analysis. It is just a question of how large the errors are compared to an agreed upon standard of accuracy, but if those errors are acceptable. These are typically defined in the original sampling plan. Analytical error is the error that results from laboratory analysis, is typically reported by the laboratory, and is defined by precision and accuracy.

Precision is the degree of agreement among repeated measurements of the same characteristic and is monitored by multiple analyses of many sample duplicates and internal standards. It can be determined by calculating the standard deviation, or relative percent difference, among samples taken from the same place at the same time (i.e. duplicates and triplicates, Fig. 3.10). *Accuracy* measures how close the results are to a true or accepted value and can be determined by analyzing certified reference standards as unknown samples and comparing with known certified values (Fig. 3.10).

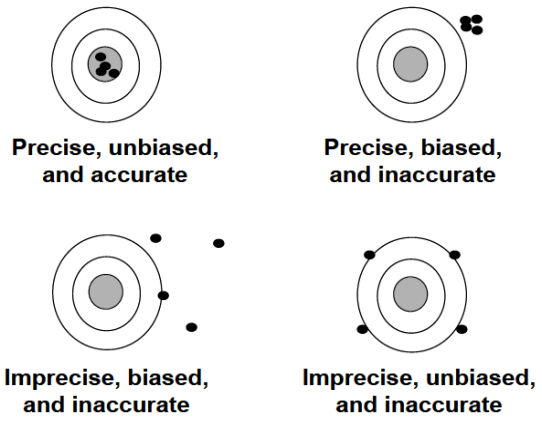

FIGURE 3.10 Diagram illustrating the difference between precision, bias, and accuracy.

Two types of standards, certified standards and internal, were used. Laboratories used certified standards, which are commercial standards with certified values as determined by round robin analyses at numerous certified laboratories. The certified standards are expensive, so internal standards also were submitted with each batch. The internal standards are samples collected and analyzed by different methods and over several years' time. Numerous duplicates and triplicates were submitted blind to the laboratory and analyzed with each sample batch to compare and assess analytical precision, accuracy, and representativeness. Detection limits can vary between laboratories and even samples. Uncertainty of analyses is generally <5% of duplicate samples and standards that were analyzed.

The sum of major oxides should total between 98 and 101% (Appendix 7), however, many samples have lower or higher totals. Extreme totals are found mostly in mineralized samples, especially samples with high F, Ba, Pb, or Cu. The precision of analyses is acceptable (within 10%) for samples where multiple analyses of the same sample were obtained (Table 3.3). For every 10 samples submitted, a duplicate sample was analyzed; these analyses compared within 10% (see Appendix 7 for additional data).

There are numerous reasons why duplicate samples and standards do not always reproduce precisely. Some samples, such as rhyolite and basalt, grind into a powder more easily than other samples, such as stream-sediment samples and nepheline syenites. Fusion techniques required for XRF analyses vary from lab to lab and can differ between different personnel that could result in variations between sample pairs. Analytical error is higher for analyses with concentrations close to the detection limit. In addition, dump samples and alluvium are very heterogeneous and difficult to completely homogenize. Most variations between duplicate samples are probably a result of sample inhomogeneities and analytical errors related to low concentrations of trace elements.

Accuracy of the data is how close the measured value is to the true or accepted value. Analyzing certified standards as unknown samples and comparing these values with certified values can monitor accuracy. Each laboratory is responsible for the accuracy of the data they produce, and the laboratory's QA/QC protocols are available upon request from the project manager. In general, analyses obtained from the laboratories agree with certified values of certified standards and precision is excellent between multiple analyses (see documentation in Appendix 7).

Differences between certified standards and duplicate pairs do exist. Generally, no corrective procedures could be applied to solid samples. Variation in preparation of the glass disk used in the XRF analysis is a major cause of these differences (Johnson et al., 1999). Nugget effects can account for variations in copper (Cu), iron (Fe), lead (Pb), sulfur (S), zinc (Zn), and zirconium (Zr), observed in some pairs of samples. An example of the nugget effect is where a small grain of native gold or other mineral occurs in one split and not the other split and thus produces a higher concentration. Another variation between certified values and the results provided by the laboratories is a result of different analytical techniques. ICP requires acid digestion and analysis of a liquid-based solution. In some cases, not all of the solid will be completely digested and can result in a lower value than that obtained by certified values generated using XRF, ICP or instrumental neutron activation analysis (INAA).

Samples were collected, prepared, and analyzed according to standard methods for each specific laboratory analysis. Samples are archived at the NMBGMR. Samples collected are complete, comparable, and representative of the defined population at the defined scale. Precision and accuracy are measured differently for each field and laboratory analysis (parameter). Effective sampling and analysis help plan the field program and the control of accuracy and precision. This provides a large, high-quality set of observations and measurements that are adequate to support the interpretations and conclusions of this report. Field and laboratory audits by the PI were performed to ensure that procedures were followed.

3.7 Summary of findings

- A sampling plan, HASP, SOPs and sampling and laboratory methods were developed to obtain the project objectives.
- Samples were collected, prepared, and analyzed according to standard methods for each specific laboratory analysis.
- Samples are archived at the NMBGMR. Samples collected are complete, comparable, and representative of the defined population at the defined scale.
- A sufficient number and amounts of samples were collected to obtain the project objectives. However, more samples will increase the confidence of the results.

4.0 BASINAL ASSESSMENT REE AND CRITICAL MINERALS IN THE SAN JUAN AND RATON BASINS (TASK 2)

This section includes results of the basinal assessment. Initial assessments of potential CORE-CM resources were determined for existing data in the literature for coal and adjacent strata and waters in the San Juan and Raton basins and adjacent areas. Samples were collected and analyzed, and assessments were determined for 12 types of deposits (Fig. 4.1): 1) coal beds (whole rock), 2) coal beds (ash basis), 3) humates, 4) beach placer sandstones, 5) clinkers, 6) clays, 7) black shales, 8) sandstone-hosted copper deposits, 9) volcanic ash, 10) uranium deposits, 11) manganese deposits, and 12) perlite deposits. See methods section (chapter 3) for descritpion of methods and section 3.55 includes a description of the chemical plots.

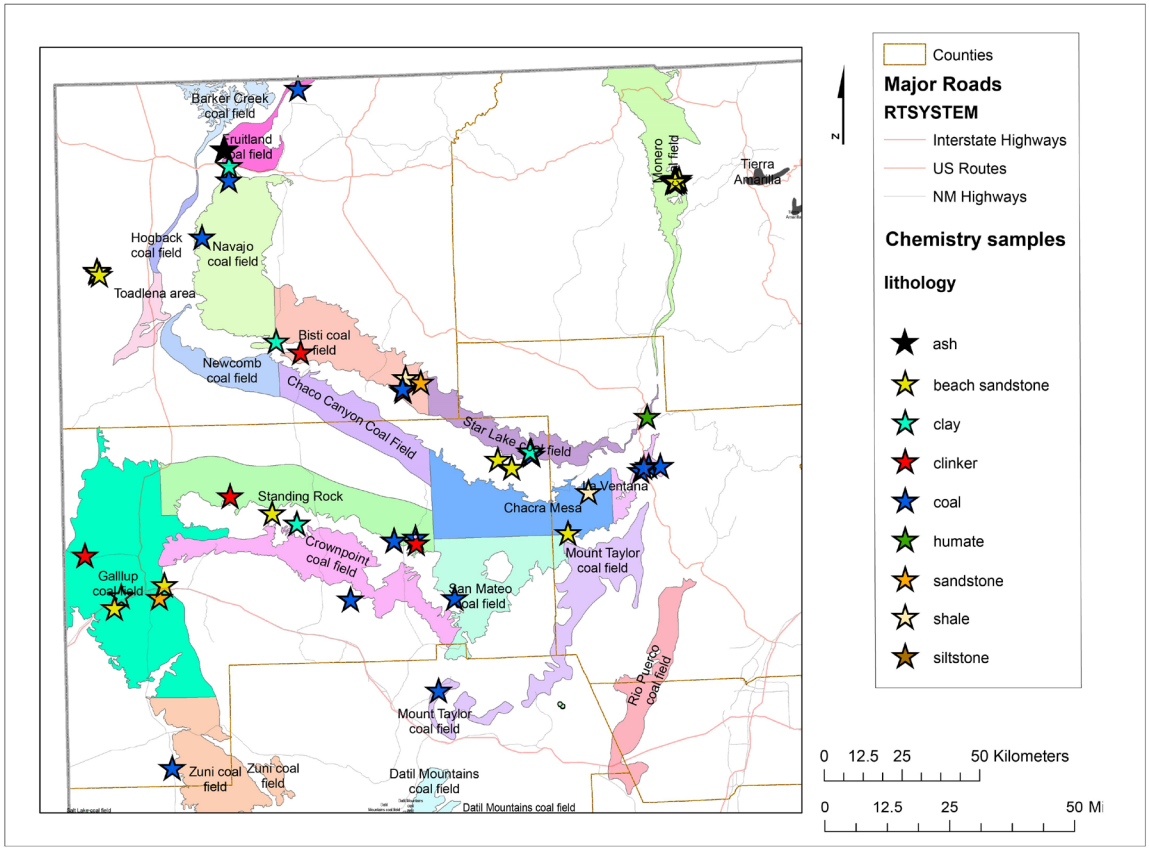

FIGURE 4.1 Location of samples analyzed for chemistry (Appendix 7) in the San Juan Basin.

4.1 Pre-existing data

4.1.1 Pre-existing chemical analyses of coal and adjacent strata (V.T. McLemore)

As part of the USGS national coal resource assessment program, chemical data were obtained from the USGS (including the USGS Coal Quality Database) and other sources for the Colorado Plateau, which includes Colorado, Utah, New Mexico, and Arizona. Details of sample collection and analyses are in Affolter (2009). There are more than 40 coal fields in the Colorado Plateau, but the USGS reported chemical data for only 19 coal fields that were considered high

priority. Additional geochemical data were compiled from other references, including Affolter et al. (2011), Araya (1993), Baker, (1989), Kendrick (1985), and Taggart et al. (2016). The focus of these studies was to analyze the geochemistry of major and trace elements of coals found throughout New Mexico. The pre-existing geochemistry data have been included in the chemistry data (Appendix 7). Legacy data has been compiled and used as a baseline for comparison and guidance. Since much of the earlier published data is inconsistent and of variable quality; only a subset of data are included (Appendix 7).

The coals in the San Juan and Raton basin exhibit light-REE chondrite normalized REE patterns, similar to many coal deposits world-wide. The coal samples show good correlation between TREE and Si and several critical elements. A strong correlation may suggest the elements are within similar mineral phases that contain TREE and critical minerals. These correlations appear to be typical of similar correlations of TREE and other elements in sedimentary rocks, especially beach placer sandstone deposits. Chemical analyses of coal deposits from the literature (including the USGS coal quality database) are not always accurate and must be used with caution. However, chemical analyses from the prior literature do provide guides for interpretations and areas to prioritize for resampling.

4.1.2 Evaluation of online water databases and reports for critical element potential (S. Kelley)

The most recent version of the produced water database was downloaded from the USGS website on January 5, 2022 (Appendix 12). Data from Black Mesa, the Las Vegas/Bravo Dome area and the Raton and San Juan basins were extracted from the larger database. The evaluation was further refined to focus on data from the San Juan and Raton basins. Most of the data from the Raton Basin are from Colorado. Trace element data were available for the following elements: B, Ba, Br, Cr, F, Li, Mn, Ni, and Zn. The data are summarized in Table 4.1. Data from wells in Arizona, Utah, and Colorado that penetrate the Mississippian, Pennsylvanian, and Permian sections indicate elevated Li concentrations in dolomite and limestone units (22.81 to 55.92 ppm).

TABLE 4.1 Ranges of trace element concentrations (ppm) from the USGS produced waters database.

Coal Basin	Formation	B	Ba	Br	Cr	Li	Mn	Ni	Zn
San Juan	Dakota	3.02	0.04-15.18						0.02-0.35
	Fruitland	0.05-2.1	0.17-58.13	0.22-56.0	0.1-1.0				
	Gallup Sandstone	3.05	0.14-0.63						
	Mesaverde		0.05-8.07						
	Mesa Verde-Dakota		0.25-15.56						
	Pictured Cliffs Ss	2.02	0.9-86.3						
	Point Lookout Ss	2							
	Devonian McCracken					13.26	83.15		
Raton	Raton coal	0.05-0.39	0.14-2.47	0.1-0.26	0.1-1.25	0.01-0.34	0.01-0.16	0.01-2.61	
	Raton-Vermejo	0.05-4.7	0.09-27.4	0.04-41.08	0.01-3.71	0.02-0.99	0.05-1.61	0.01-0.11	0.01-0.39
	Vermejo Coal	0.05-4.0	0.16-3.57	0.09-69.6	0.01-1.2	0.01-1.0	0.01-1.5	0.01-0.02	0.01-3.9

Snyder et al. (2003) examined water chemistry in the Fruitland Formation near the Colorado-New Mexico state line. Unfortunately, that data set only contains isotopic data and does not have trace-element chemistry. Langman et al. (2012) sampled two seeps in the San Mateo region on the northwest side of Mt. Taylor that have elevated B and Li concentrations. The San Mateo seep is warm (~25°C). Samples collected in Aug. 2009 had Li concentrations of 17 and 66 ppm and samples collected in May 2010 have Li concentrations of 78 and 51 ppm. Langman et al. (2012; table 6 therein) determined that the Menefee Formation has higher concentrations of B, FE, Li, Mn, V, and Zn groundwater compared to groundwater in other rock units in the area.

The New Mexico Energy, Minerals, and Natural Resources Department (EMNRD) has a data set of water samples collected at coal mines collected on a regular basis starting in the 1979 through 2015. The samples were collected from wells, springs, and ponds on the mine property. The coal mines with water that has elevated concentrations of critical elements are presented in Table 4.2. Additional data is available on the EMNRD website for 2016–2022 for the San Juan coal mine, but critical elements concentrations are low.

TABLE 4.2 Coal mines with elevated concentrations of critical elements (ppb) in water collected by EMNRD.

Mine name	Al	As	Ba	Be	Co	Cr	F	Mn	Ni	V	Zn
Ancho	83.92					104-150.7					
Carbon No.2	87						2280	210			
El Segundo											2.6-14.3
Fence Lake		12		22				1542			
Gateway	36.4-82.2										
La Plata	120-1843										
Lee Ranch	29-703	5.79			0.45-0.96				23	0.7-1.7	
Mckinley								65.4-490			
San Juan			21.6-1501					154			
York Canyon						117-146	80-212				

4.2 Minimum concentrations of critical minerals for exploration: How good is good enough? (R. Otoo and V.T. McLemore)

This section proposes a practical way to decide whether early exploration results for critical minerals are “good enough” to justify advancing an exploration project. Critical minerals are produced from primary ore deposits as well as secondary sources (e.g. cobalt from battery recycling, platinum group metals from catalytic converters). They also can be extracted as byproducts or recovered from unconventional sources, such as coal and coal combustion products (e.g., fly ash). However, as critical minerals continue to face increasing global demand, mineral exploration for new deposits becomes an important tool in ensuring long-term supply security. To determine whether the concentration of critical minerals in a deposit can justify spending further resources on an exploration target, it is necessary to evaluate and understand established cut-off grades of actively operating mines and exploration sites. These cut-off grades provide a benchmark for assessing whether exploration targets contain sufficiently high concentrations for economic consideration.

In exploration, the preliminary cut-off grade acts as an early filter to guide resource allocation toward promising targets. Cut-off grade is dynamic and shaped by multiple factors including, logistical, geological, economic, and technological. Larger deposits depend upon high

grades and tonnages and include lower cut-off grades because economies of scale. Whereas smaller deposits typically require higher grades to remain viable. Mining and processing methods also play a significant role. For instance, brine evaporation in lithium extraction generally allows for lower cut-off thresholds compared to more expensive hard-rock mining techniques with higher cutoff grades. Additionally, the recovery of valuable byproducts or coproducts such as niobium or uranium can offset production costs and effectively lower the required cut-off grade of the primary mineral.

This study reviewed active mines and exploration sites across different deposit types to establish concentration thresholds for exploration targets (Otoo et al., 2025). Exploration thresholds are set at approximately 70% of the lowest cut-off grade used in comparable active mining or exploration operations. For example, Greenbushes mine in Australia, which is one of the largest and highest-grade pegmatite lithium deposits, reports cutoff grades between 0.5 and 0.7% Li_2O (SEC, 2023). Similar projects with cut-off grades around 0.4% Li_2O could still be considered attractive for further exploration, depending on deposit size, mining and processing methods, and other economic factors. This approach helps align exploration with realistic economic standards and reduces the risk of pursuing sub-economic deposits.

Another example, the Mountain Pass carbonatite deposit in California uses a cut-off grade of approximately 2% total rare earth oxide (TREO) for its mining operations. However, the lower-bound industry cut-off grade for rare earths is around 0.8% TREO. Therefore, setting an exploration threshold at 70% of this lower-bound cut-off of an active mine can be considered justifiable for comparable deposit types. However, the DOE established a concentration of 500 ppm TREE that can serve as a realistic exploration target for coal-hosted REE deposits, given their distinct geological setting and extraction considerations (U.S. Department of Energy, 2022).

Incorporating established cut-off grades as benchmarks for mineral exploration strategies can enhance the effectiveness of target prioritization and increase the chances of successful mines. This approach can be achieved by categorizing deposits of active mines and exploration sites into low, medium and high targets based on their cut-off grades, which provide a structured framework for exploration. By regularly updating benchmarking data to reflect evolving market conditions, operational costs, and technological advancements, exploration values can be set at 70% of the lowest cut-off grade of operating mines to ensure that potential deposits compare with operational thresholds.

Tonnages and cut-off grades of economic deposits vary with the commodity and type of deposits (Fig. 4.2; Table 4.3). For example, what is economic for REE in carbonatites (10-15% TREE) differs from potentially economic values in coal deposits (500 ppm TREE). It also is important to compare chemical compositions to crustal abundance and cut-off grades (Otoo et al., 2025a, b).

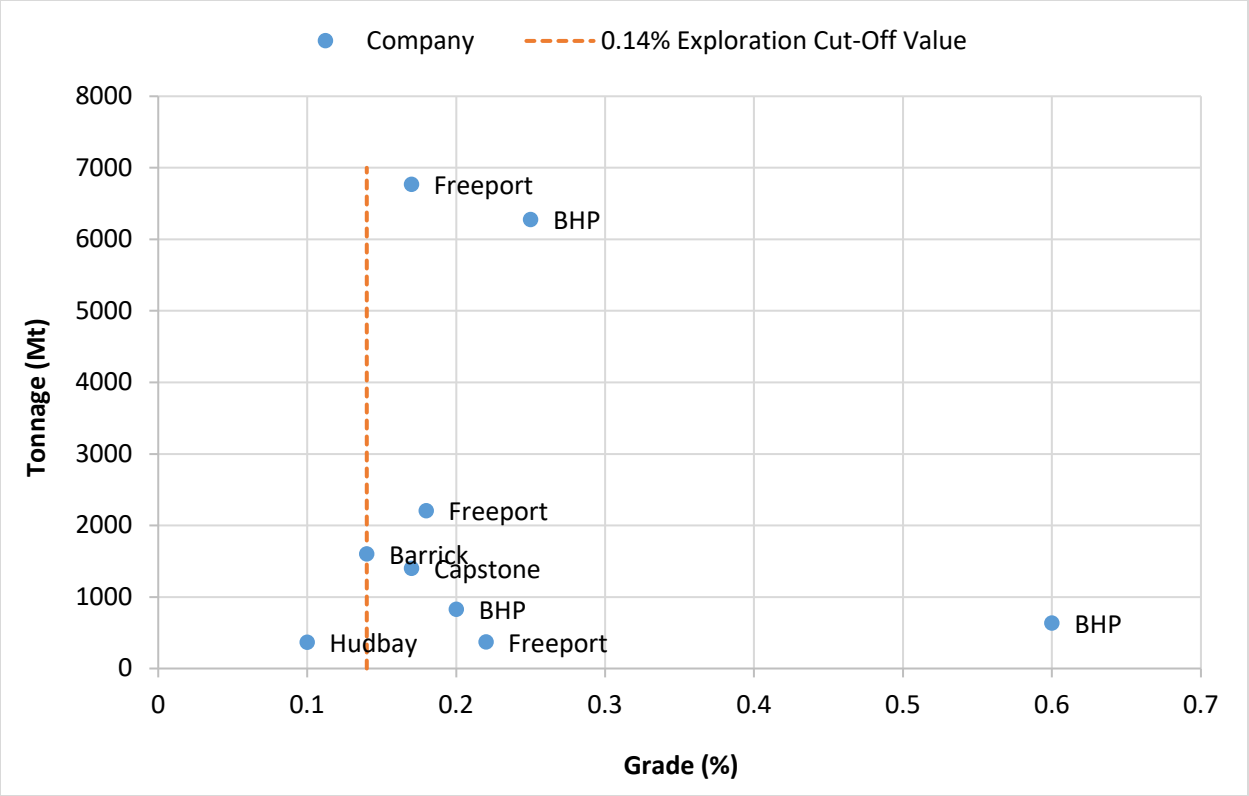

FIGURE 4.2 Comparison of copper grades and tonnages across selected companies.

TABLE 4.3 Concentration of trace elements (ppm, except where noted) within the upper continental crust (Rudnick and Gao, 2003; Hu and Gao, 2008) and recommended exploration values. *DOE recommended value. ** recommended by Dai and Finkelman (2018). ppm—parts per million. ppb—parts per billion.

Element (ppm, unless noted)	Shaw et al. (1967, 1976)	Gao et al. (1998)	Taylor and McLennan (1985, 1995)	Wedepohl (1995)	Rudnick and Gao (2003)	Hu and Gao (2008)	Recommended crustal abundance values (ppm)	Cut-off grades for various economic Deposits (ppm or stated)	Recommended exploration value (ppm)
Li	22	20	20		21	41	41	320 (brine), 4000 (pegmatite)	224 (brine), 2800 (pegmatite)
Co	12	17	17		17.3	15	15	0.14%	980
Ni	19	38	44		47	34	34	0.6%	0.42%
Cu	14	32	25		28	27	27	0.2%	0.14%
Zn	52	70	71		67	75	75	2.2%	1.5%
As		4.4	1.5	2	4.8	5.7	5.7		100
Cd	0.075	0.079	0.098	0.102	0.09	0.06	0.06		100
Se		0.15	0.05	0.083	0.09		0.09		100
Y	21	17.4	22		21		21	300**	210
Ag (ppb)		55	50	55	53		0.0053		0.1
Ga	14	18	17		17.5	18.6	18.6		100
Ge		1.34	1.6	1.4	1.4	1.3	1.3		100
Ce	65.6	66.4	64		63		63		500
Sc								100*	70
TREE								2.4%	500*

Element (ppm, unless noted)	Shaw et al. (1967, 1976)	Gao et al. (1998)	Taylor and McLennan (1985, 1995)	Wedepohl (1995)	Rudnick and Gao (2003)	Hu and Gao (2008)	Recommended crustal abundance values (ppm)	Cut-off grades for various economic Deposits (ppm or stated)	Recommended exploration value (ppm)
Hg	0.096	0.0123		0.056	0.05		0.05		100
Ti	0.524	1.55	0.75	0.75	0.9	0.55	0.55		0.1%
Be	1.3	1.95	3	3.1	2.1	1.9	1.9	300	210
Zr	237	188	190		193		193	2000**	1400
Nb	26	12	12		12	11.6	11.6	300**	210
Sb		0.3	0.2	0.31	0.4	0.075	0.075	1000	700
Ta	5.7	0.74	1	1.5	0.9	0.92	0.92		100
W		0.91	2	1.4	1.9	1.4	1.4	1500	1050
Pb	17	18	17	17	17		17	1.5%	1.05%
Th	10.3	8.95	10.7		10.5		10.5		1000
V	53	98	107	53	97	106	106	3000	2100
U	2.45	1.55	2.8		2.7	2.6	2.6	1300	910

4.3 Critical minerals potential of coal beds based using whole-rock basis (V.T. McLemore)

Samples were collected from coal fields in the San Juan and Raton basins and adjacent areas (Table 3.1, Fig. 4.1; McLemore and Owen, 2025). Chemical analyses and descriptive statistics are in Appendix 7. Coal and humate samples in this study typically displayed relatively flat to slightly light REE enriched chondrite-normalized REE patterns (Fig. 4.3; whole-rock basis). When normalized to NASC (North American Shale Composite; Gromet et al., 1984), the coal and humate samples display flat REE patterns with no significant enrichment or depletion (Fig. 4.4). Box and whisker plots (Figs. 4.5, 4.6, 4.7) show the concentrations of REE, scandium, and lithium, respectively. See section 3.5.5 on descriptions of chemical plots used in this report. The coal and humate samples contain less than 500 ppm total REE. Scandium concentrations average 4 ppm with one sample containing as much as 76 ppm. Concentrations of lithium average 17 ppm, though one sample contains as much as 94 ppm (Appendix 7). The New Mexico coal and humate samples are relatively moderate to low in REE (<485 ppm TREE), Li (<94 ppm), V (<282 ppm), Co (<65 ppm), Ni (<77 ppm), Zr (<1336 ppm), Hf (<10 ppm), and other critical minerals compared to cut-off grades of economic deposits (Table 4.3). The coal and humate samples are similar in chemistry as the adjacent sedimentary rocks.

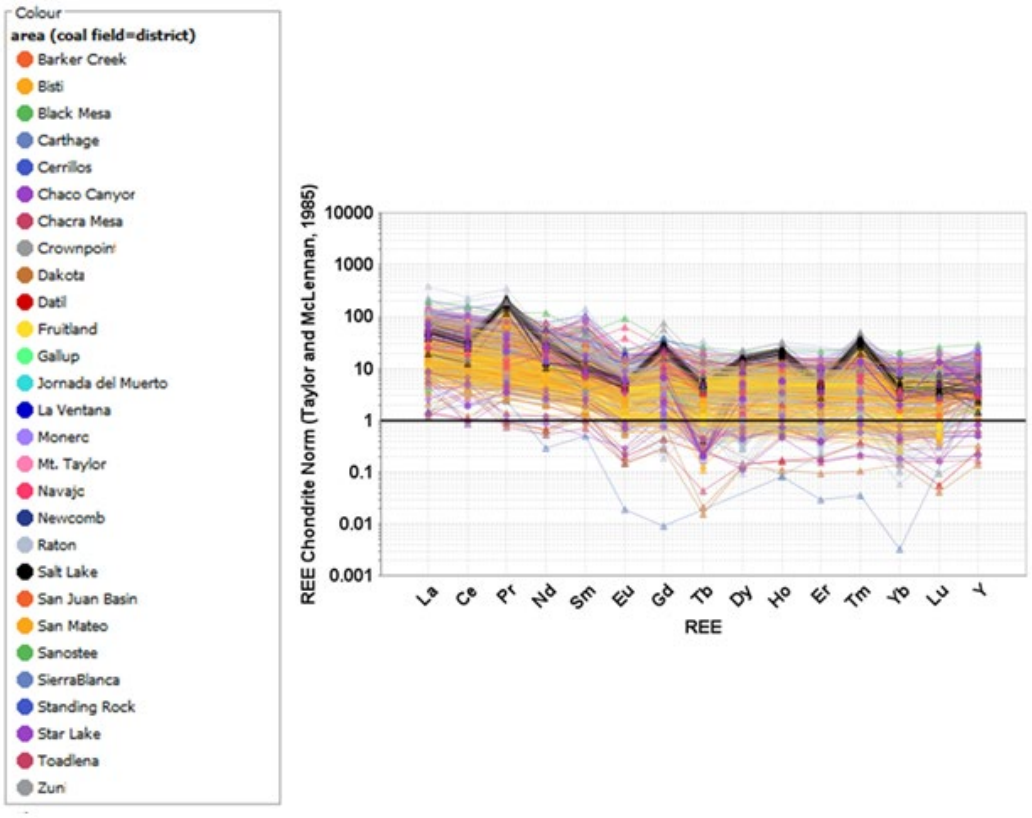

FIGURE 4.3 Chondrite-normalized REE plot for coal and humate in the San Juan and Raton basins by coal field. Chemical analyses are in Appendix 7. Chondrite values from Taylor and McLennan (1985).

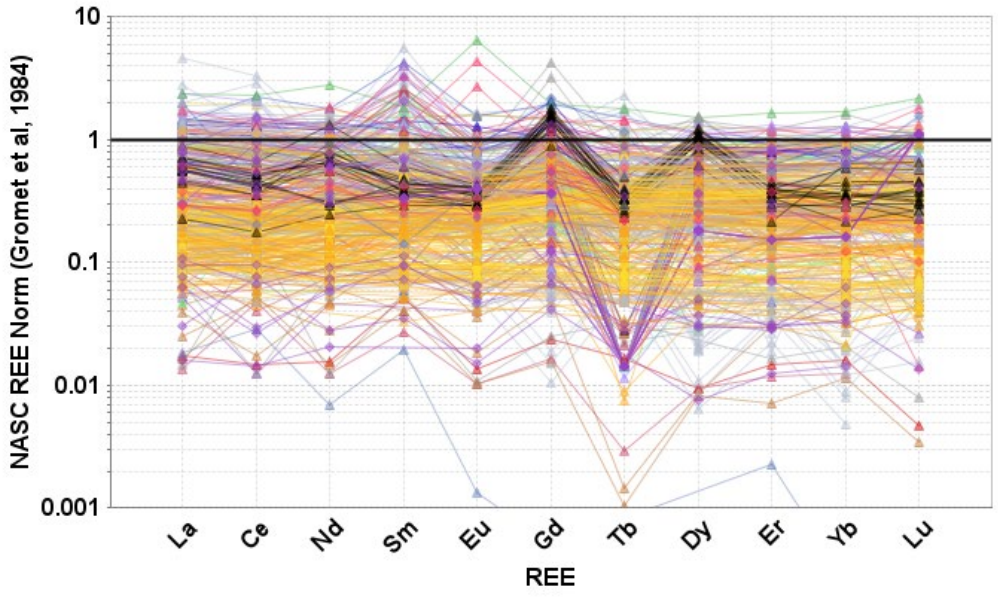

FIGURE 4.4 NASC-normalized REE plot for coal and humate in the San Juan and Raton basins by coal field. Chemical analyses are in Appendix 7. Legend is in Figure 4.3. NASC=North American Shale Composite (values from Gromet et al., 1984).

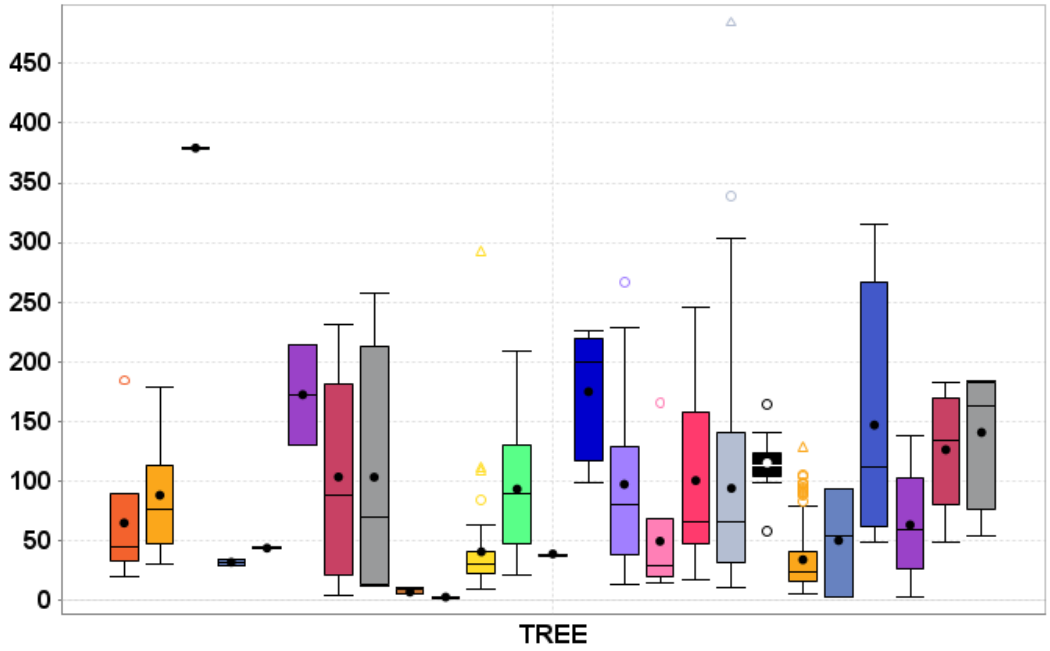

FIGURE 4.5 Total REE box and whisper plot of coal and humate samples from the San Juan and Raton basins. Chemical analyses are in Appendix 7. Legend is in Figure 4.3. The TREE is below the recommended value for exploration of 500 ppm REE (Table 4.3).

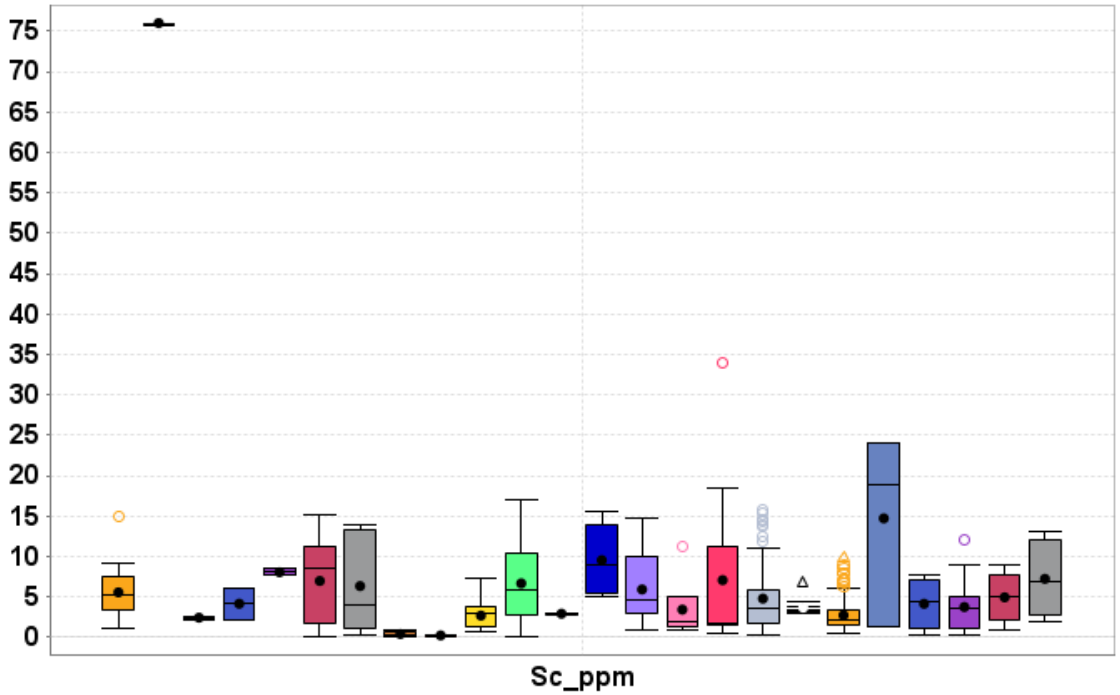

FIGURE 4.6 Sc box and whisper plot of coal and humate samples from the San Juan and Raton basins. Chemical analyses are in Appendix 7. Legend is in Figure 4.3. Only one sample is above the recommended value for exploration for Sc of 70 ppm (Table 4.3).

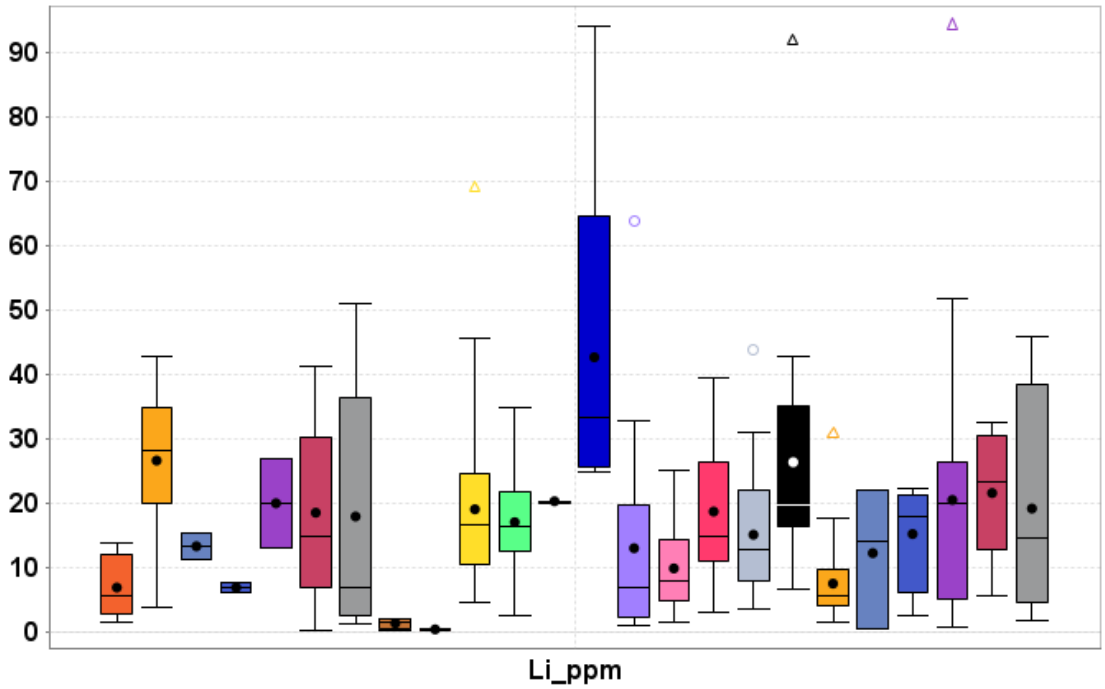

FIGURE 4.7 Li box and whisper plot of coal and humate samples from the San Juan and Raton basins. Chemical analyses are in Appendix 7. Legend is in Figure 4.3. The samples are below the recommended value for exploration for Li of 2800 ppm (Table 4.3).

4.4 Characterization of coal maturity (G. Xu)

Vibration spectroscopy can reveal the maturity grade of coal (e.g., Quirico et al., 2005; Craddock and Sauerer, 2022; Craddock et al., 2015). ATR spectra and Raman spectra have been obtained on six coal samples and one humate from Lee Ranch mine (Figs. 4.8, 4.9). As coals mature, aromatic C-H and C=O peaks increase whereas aliphatic C-H peaks decrease. Similarly in Raman spectra, the larger separation between G (graphite) and D bands indicate higher maturity. Both ATR and Raman spectra suggest high maturity of these coal samples.

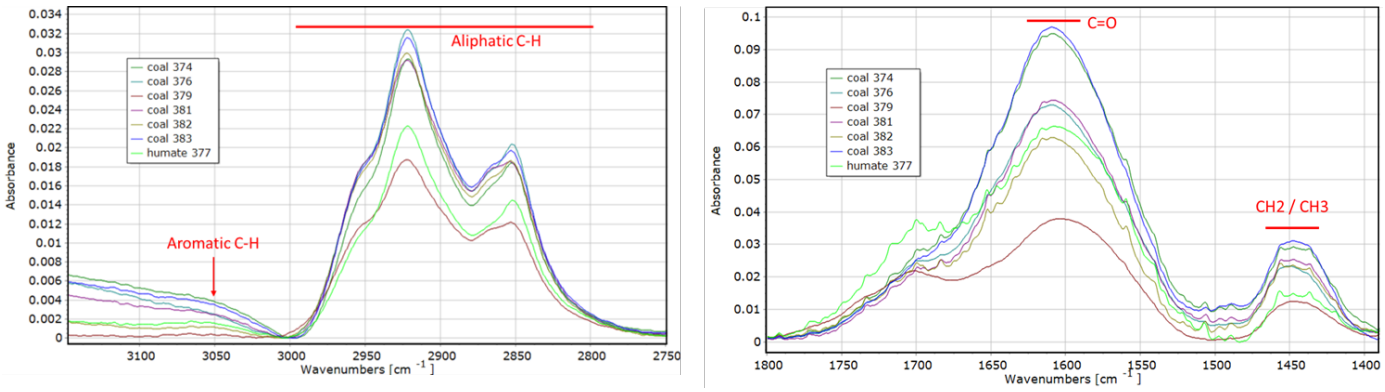

FIGURE 4.8 ATR spectra showing aliphatic (left) and aromatic carbon (right).

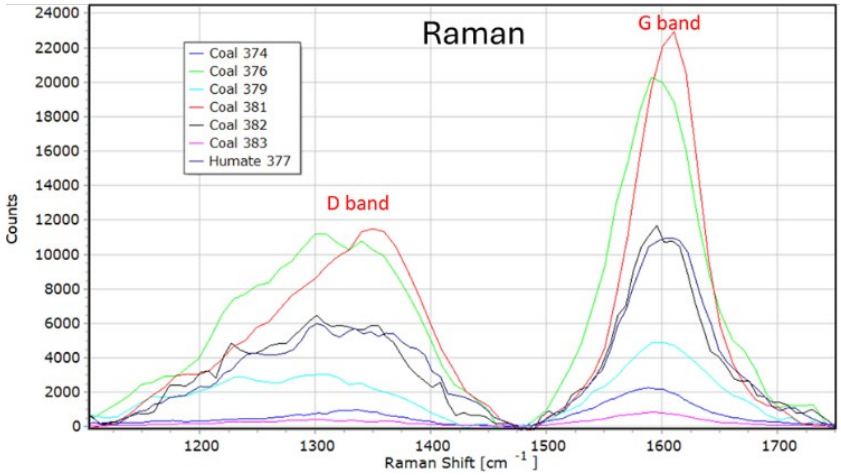

FIGURE 4.9 Raman spectra showing the D and G bands.

4.5 Critical minerals potential of coal beds on ash basis (V.T. McLemore and E.J. Owen)

Another way to examine critical minerals and REE in coal deposits is to determine the amount of the element in coal ash instead of the whole-rock sample (McLemore and Owen, 2025). Measuring REE and other critical minerals on the ash basis approximates the critical mineral content of the fly or bottom ash remaining after coal is burned at a power plant, where critical minerals could then be leached from the ash (Geboy et al., 2013; Scott and Kolker, 2019; Dodbida and Fujita, 2023). Furthermore, coal ash wastes stored in ponds and landfills at current and former coal-burning power plants in New Mexico represent an environmental liability. Recovery of critical minerals from these materials during stabilization and closure could help offset closure costs and help with the demand for critical minerals.

Figure 4.10 shows the locations of coal samples (McLemore and Owen, 2025) and Figure 4.11 shows a typical coal seam. Chemical analyses and descriptive statistics are in Appendix 7. Concentrations of REE on ash basis are higher on average in lower (<10%) ash content samples (Fig. 4.12). Coal ash samples in this study typically displayed relatively flat to slightly light REE enriched chondrite-normalized REE patterns (Fig. 4.13), consistent with REE hosted by clay minerals, zircon, and monazite. When normalized to NASC (North American Shale Composite; Haskin and Haskin, 1966), these coal ash samples display flat REE patterns with no significant enrichment or depletion (Fig. 4.14). Box and whisker plots (Figs. 4.15, 4.17, 4.18) show the concentrations of REE, scandium, and lithium, respectively. On an ash basis, these coal samples generally contain less than 500 ppm total REE, though some samples contain as much as 2,103 ppm. Scandium concentrations are generally less than 30 ppm, with some samples reaching as high as ~80 ppm. Concentrations of lithium average around 20 ppm, though several samples contain as much as ~90 ppm (Appendix 7).

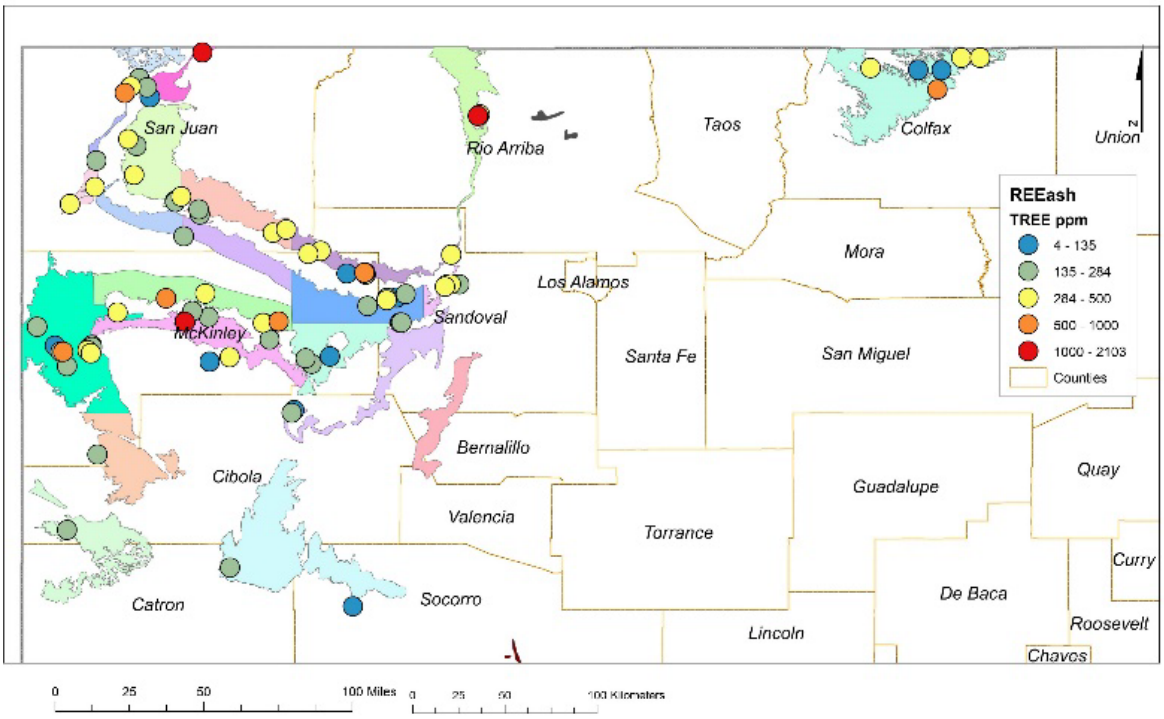

FIGURE 4.10 REE in coal ash in the San Juan and Raton basins (McLemore and Owen, 2025). See Table 1.5 for names of coal fields.

FIGURE 4.11 Coal bed at Van Hootten coal camp, Whittington Center, Raton Basin (sample COAL27a, photograph by V.T. McLemore). This sample contained 982 ppm total REE in the ash (Appendix 7).

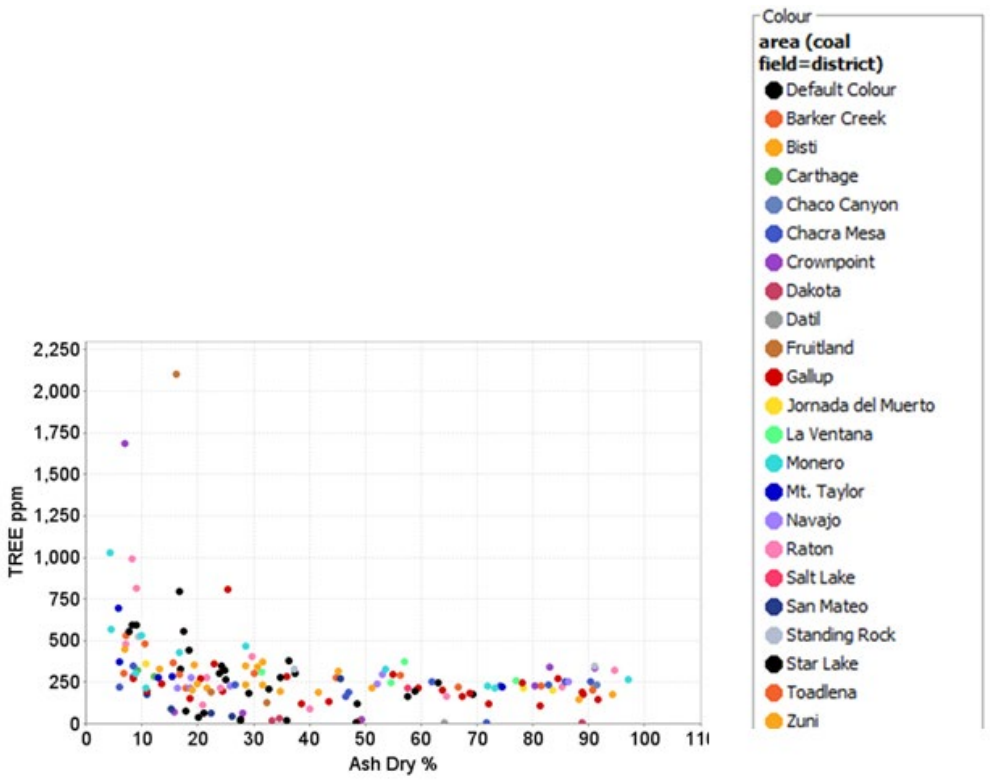

FIGURE 4.12 Total REE vs. ash content of coal samples from the San Juan and Raton Basins (McLemore and Owen, 2025). Note higher TREE are found in samples with lower ash contents.

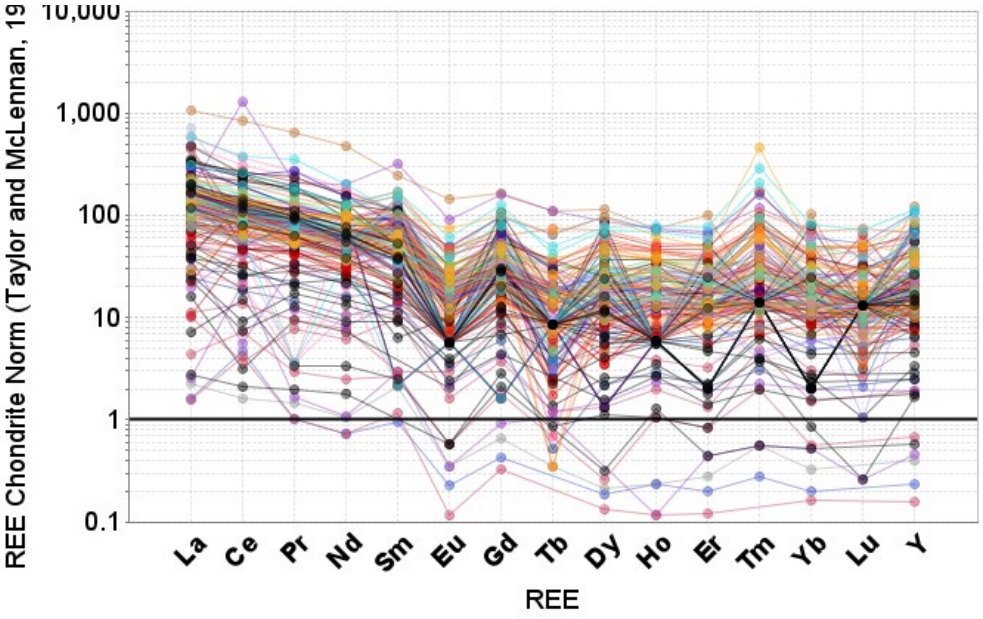

FIGURE 4.13 Chondrite-normalized REE diagram of New Mexico coals (McLemore and Owen, 2025). Legend of colors in Figure 4.12. Chondrite values from Taylor and McLennan (1985).

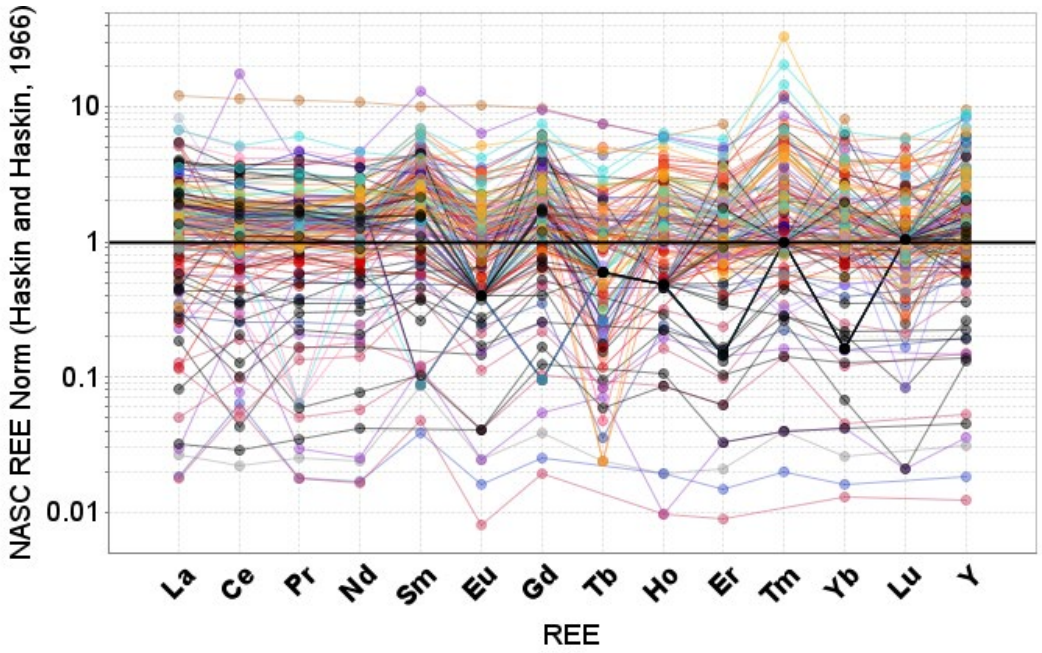

FIGURE 4.14 Plot of New Mexico coal samples normalized to North American Shale Composite (NASC) (concentrations from Haskin and Haskin, 1966). Legend of colors in Figure 4.12.

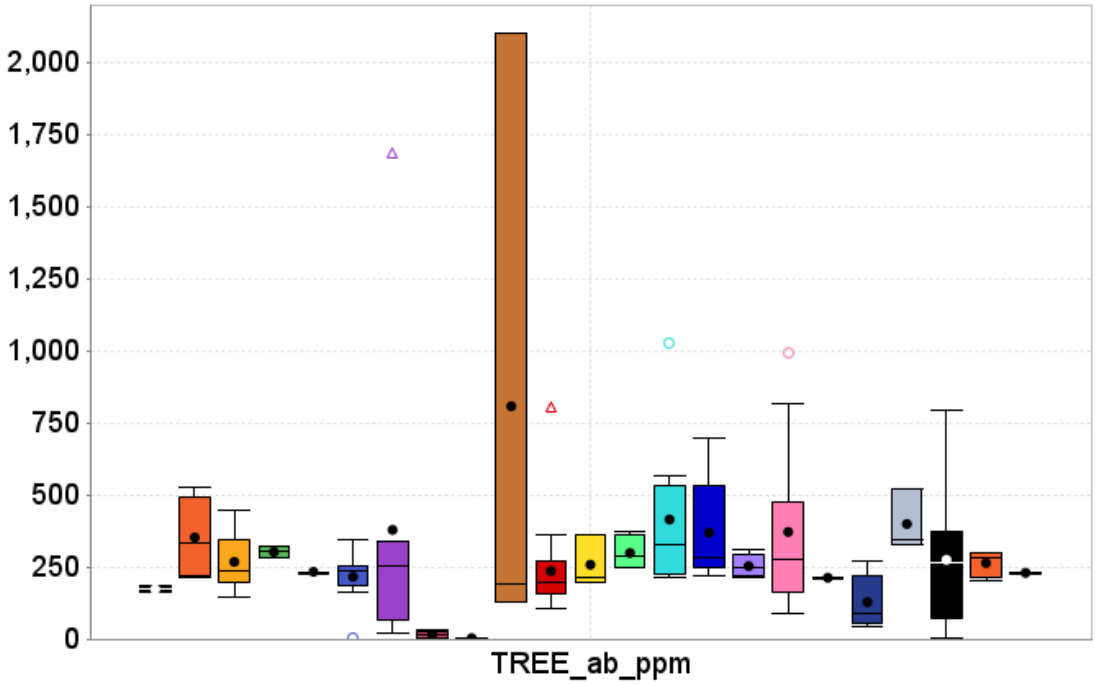

FIGURE 4.15 Box and whisker plot of TREE (ash-basis, in ppm) by coal field (McLemore and Owen, 2025). Legend of colors in Figure 4.12.

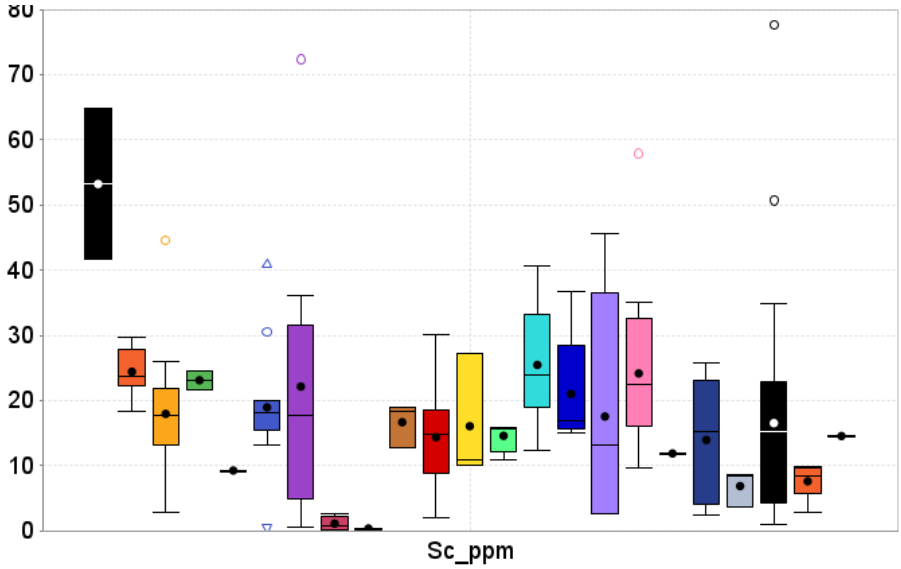

FIGURE 4.16 Box and whisker plot of Sc (in ppm) by coal field (McLemore and Owen, 2025). Legend of colors in Figure 4.12. The black field is Star Lake. There appears to be an inverse correlation between Sc abundance and TREO. Only a few samples exceed the recommended value for exploration for Sc of 70 ppm (Table 4.3).

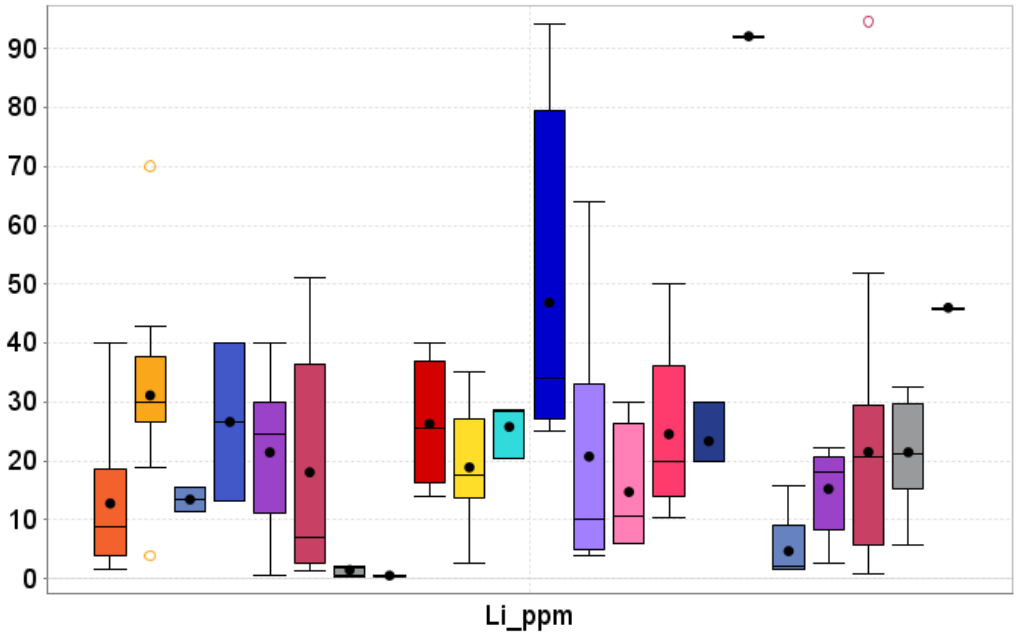

FIGURE 4.17 Box and whisker plot of Li (in ppm) by coal field (McLemore and Owen, 2025). Legend of colors in Figure 4.12. The blue field is La Ventana. The samples are below the recommended value for exploration for Li of 980 ppm (Table 4.3).

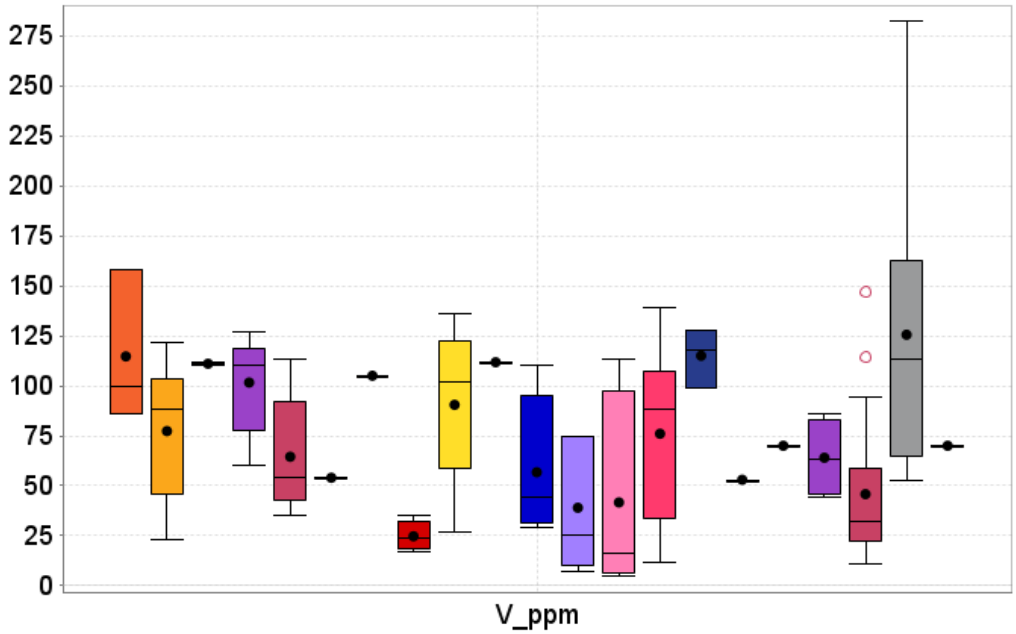

FIGURE 4.18 Box and whisker plot of V (in ppm) by coal field (McLemore and Owen, 2025). Legend of colors in Figure 4.12. The gray field are samples from Toadlena. The samples are below the recommended value for exploration for V of 2100 ppm (Table 4.3).

The DOE considers samples containing >500 ppm REE potentially economic in the future (U.S. Department of Energy, 2022). Some of the highest total REE concentrations (ash basis) are found in coal ash from the closed La Plata mine in the Fruitland Formation (2,103 ppm), the closed Mentmore mine in the Gallup Sandstone (807 ppm), as well as the Crownpoint (1,684 ppm), Standing Rock (523 ppm), Barker Creek (528 ppm), Mt. Taylor (696 ppm), Star Lake (795 ppm), and Monero (1,026 ppm) coal fields in the San Juan Basin (McLemore and Owen, 2025). The La Plata coal was used at the San Juan power plant (now closed). Other concentrations of critical minerals are mostly below economic concentrations (Table 4.3).

4.6 Critical minerals potential of humates (V.T. McLemore and J. Lempke)

New Mexico has significant deposits of humates, predominantly in the Fruitland and Menefee formations in the eastern San Juan Basin (Fig. 4.19). Humate, when used as a lithologic term, includes oxidized coals and lignites, organic-rich mudstones and clays, and the concentrations of humic substances locally found in sandstones. Humate is commonly associated with both weathered coal and lignite, particularly in southwestern U.S. (McLemore and Austin, 2017; Newcomer et al., 2021). The humic-acid content of lignite decreases rapidly as coal rank increases and oxidation decreases. Organic-rich mudstones primarily within the coal-bearing sequences generally have a lower humic acid content than either the oxidized lignites or coals. Humates can transition to coal at depth (Fig. 4.20). They also are termed leonardite or weathered lignite; other terms are explained in Newcomer et al. (2021). Humate can be distinguished from coal by its brownish color, higher humic (and fulvic) acid content and its higher solubility in water (high-quality humate dissolves in water).

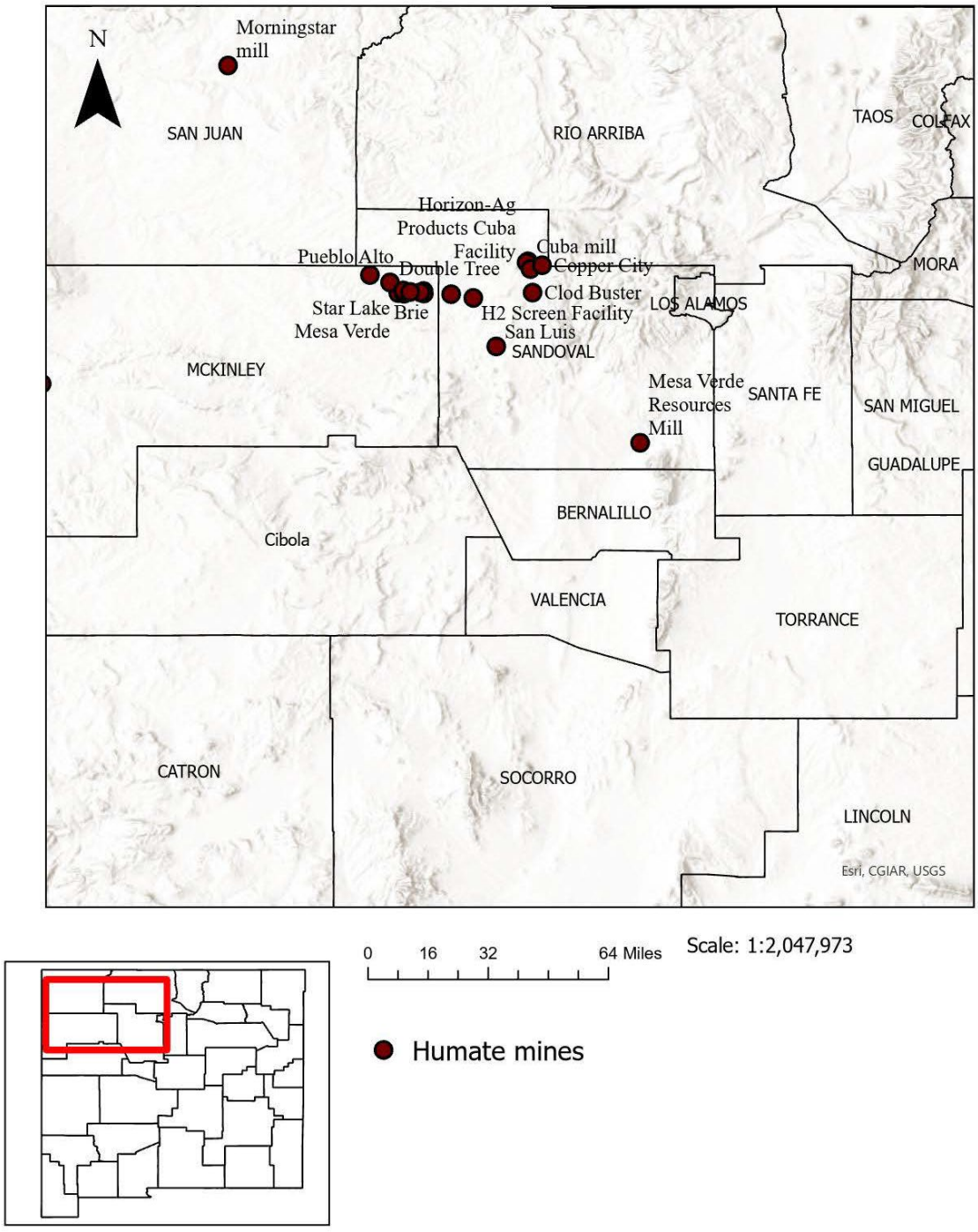

FIGURE 4.19 Location of humate mines in the San Juan Basin, New Mexico.

FIGURE 4.20 Humate mine in the San Juan Basin. Note the brownish color. Sample Coal143 (photograph by V.T. McLemore).

Humate is used as a soil conditioner, in medicinal products, a dispersant and viscosity control in oil-well drilling muds, a stabilizer for ion-exchange resins in water treatment, and a source of water-soluble brown stain for wood finishing. The primary use of humates is as a soil amendment, but humates are not beneficial for every type of soil, particularly soils already rich in clay. The humic and fulvic acids in humates are organic colloids, which are similar in their sorption behavior to clay minerals. They increase water retention and the cation exchange capacity of the soil. Humate also lowers the pH of alkaline soil, thus increasing plant nutrient availability and stimulating growth of microorganisms (Hoffman et al., 1995). Humates are used in drilling mud for increased circulation. Humates are most beneficial on sandy soils lacking in clay material. More importantly, humates can readily chemically complex and transport REE, U, and other metals in soil, surface water, humates and coals (Sonke, 2006).

Mining of humate in New Mexico began in 1970 and total production amounts to more than 900,000 metric tons of humate. Humate is produced from ~10 mines and mills in New Mexico. The Horizon Ag Products mine and mill are south of Cuba. Menefee Mining operates one pit and a mill near Cuba. The mining operations, processing site, and transportation facility of U-Mate International, Inc. are in the Gallup area. The Eagle Mesa mine is near Cuba and the Morningstar mine is in San Juan County. The Jaramillo humate mine in McKinley County is under development by Anasazi Stone LLC. Both El Segundo and Navajo mines also produce some humate. Approximately 12.1 billion short tons of humate resources are present within the San Juan Basin (Newcomer et al., 2021).

Humate sample Coal159 was used to assess the digestion of humate. About 0.5 gram of coal Coal159 was placed into 12 g DI H_2O, but it was found that very little material was dissolved and REE were not detected in the leachate by ICP-MS analysis. On the other hand, when 0.5 gram of Coal159 was placed into 6 mL of 0.1M NaOH, most of the material was

dissolved. However, when the solution was titrated to pH neutral for ICP-MS analysis the solution became reddish and opaque and thus ICP-MS could not be analyzed.

Critical minerals in humate are generally low and similar to critical minerals concentrations in coal samples. The REE also are low (Fig. 4.21).

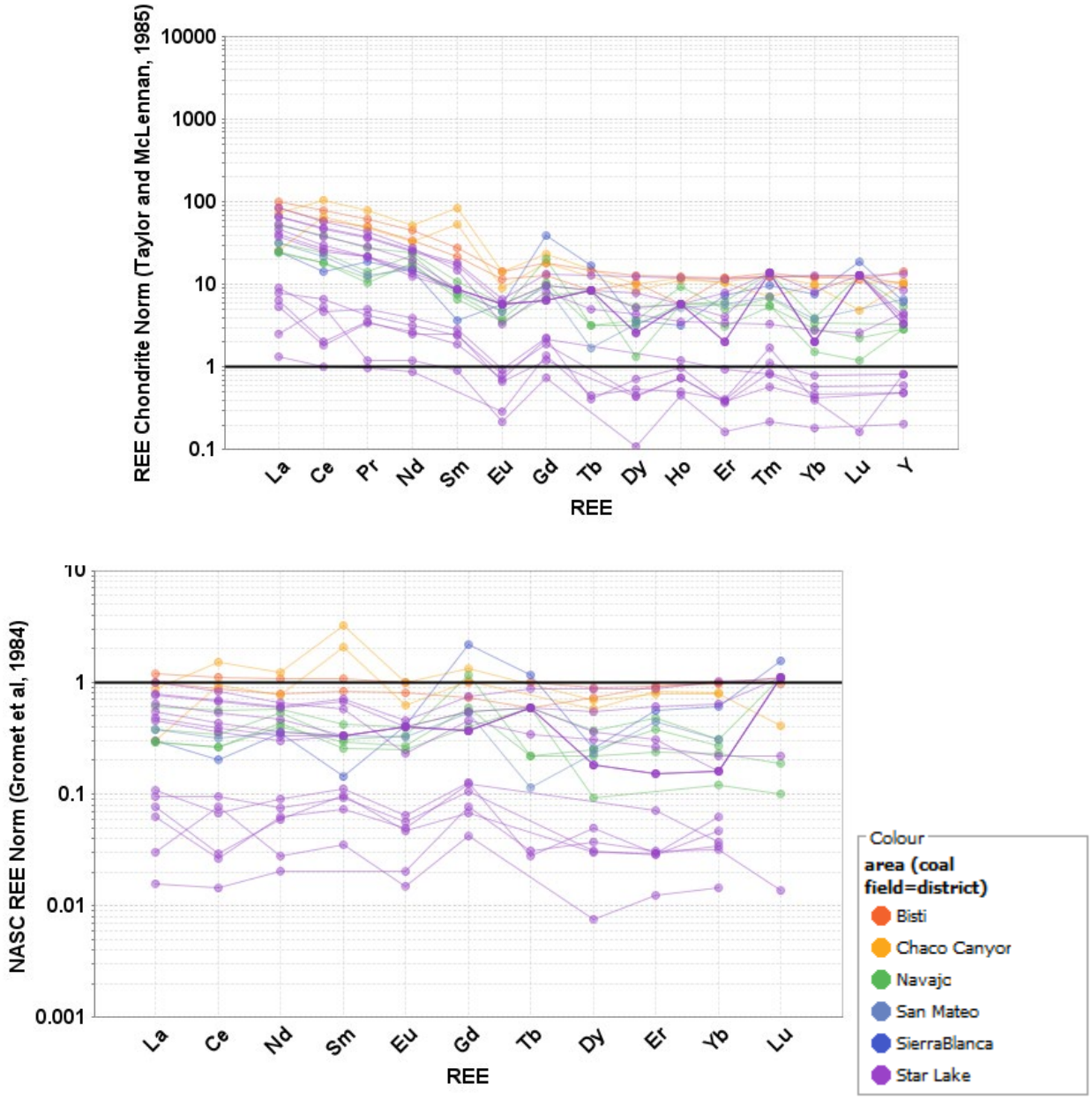

FIGURE 4.21. Chondrite-normalized REE plot and NASC-normalized REE plot of humate samples. Chondrite values from Taylor and McLennan (1985). NASC values from Gromet et al., 1984).

4.7 Critical minerals potential of beach-placer sandstones (V.T. McLemore, G. Xu, A. Byrd, and E.J. Owen)

4.7.1 Introduction

Beach-placer sandstone deposits are accumulations of heavy, resistant minerals (i.e. high specific gravity) that form on upper regions of beaches or in long-shore bars in a marginal-marine environment (Fig. 4.22). They form by mechanical concentration (i.e. settling) of heavy minerals by the action of waves, currents, and winds (Bryan et al., 2007). Specifically, beach-placer sandstones form in the upper part of the high-tide swash (wave) zone, in the foreshore zone, and in the sand dunes where they are remobilized by winds and waves, especially after storm surges (van Gosen et al., 2014, 2016).

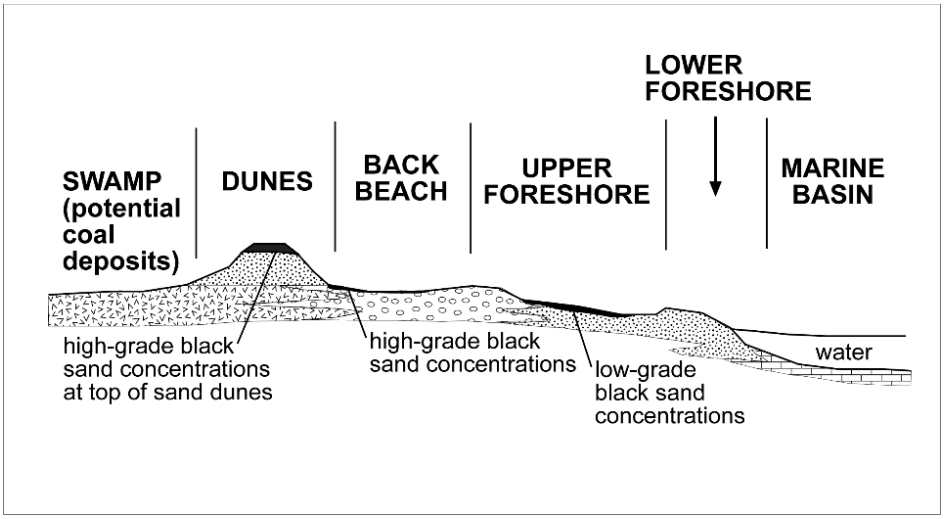

FIGURE 4.22 Idealized cross-section of formation of beach-placer sandstone deposits (modified from Houston and Murphy, 1970, 1977).

Detrital heavy minerals comprise approximately 50-60% of the sandstones and typically consist of titanite, zircon, magnetite, ilmenite, monazite, apatite, rutile, xenotime, garnet, and allanite, among other minerals. Most of these minerals have a high specific gravity exceeding 4. Although beach-placer sandstone deposits are found in strata of all ages; the deposits in the San Juan Basin in New Mexico are restricted to Late Cretaceous rocks belonging to the Gallup, Dalton, Point Lookout, and Pictured Cliffs Sandstones (Table 4.4; Chenoweth, 1957; Houston and Murphy, 1970, 1977; Brookins, 1977; McLemore, 2010; McLemore and Robinson, 2016; McLemore et al., 2016; Owen and McLemore, 2024). These formations are characterized by nearshore facies deposited during transgressions and regressions of the Western Interior Seaway. The beach-placer sandstones in New Mexico are black, dark gray, to olive-brown, resistant to erosion, and radioactive due to radioactive zircon, monazite, apatite, and thorium minerals. Anomalously high concentrations of Ti, Fe, Nb, Th, U, Zr, Sc, Y, and REE are characteristic of these deposits. Dow and Batty (1961) reported the known deposits in the San Juan Basin (Fig. 4.23, Table 4.4) contain an estimated resource of 4.3 million metric tonnes of ore containing 12.8% TiO_2, 2.1% Zr, 15.5% Fe and less than 0.10% ThO_2 ().

Modern examples are found along the Atlantic Coast, USA (Koch, 1986; Carpenter and Carpenter, 1991; Pirkel et al., 2009), southeastern Australia (Roy, 1999; Reid et al., 2013), west

coast of South Africa (Philander and Rozendall, 2015), Tartous in Syria (Kattaa, 2002), and Andhra Pradesh, India (Rao et al., 2008). In these localities, beach placers are mined for titanium-bearing minerals, zircon, and locally, monazite (a Ce-bearing REE mineral). India is currently mining monazite from modern beach-placer sandstones for REE (Kramer-Miller, 2015). Some reported reserves of economic deposits are listed in Table 4.5. Other potential commodities include niobium, chromium, thorium, and REE. Similar Upper Cretaceous heavy mineral, beach-placer sandstone deposits are found throughout Montana, Wyoming, Utah, Arizona, and Colorado (Table 4.5; Dow and Batty, 1961; Houston and Murphy, 1970, 1977; Zech et al., 1994).

Many of these elements are critical minerals, are increasingly becoming more important in our technological society, and are used in many of our electronic devices, such as cell phones, computer monitors, televisions, wind turbines, etc. (Table 4.6; Morteani, 1991; Long et al., 2010; McLemore, 2011, 2015). The white color and high refractive index of titanium make it an important ingredient in pigment in paint, plastics, and paper (Force, 1991, 2000; Jones, 2009). Zircon is important in the refractory industry (Jones, 2009). REE are used as catalysts in the chemical industry, and in glass, re-chargeable batteries, magnets, lasers, TV color phosphors, solar panels, and wind turbines. As the demand for some of these elements increases because of increased demand and short supplies, the dollar value per ton of ore rises, enhancing deposit economics. Detailed mapping and exploration drilling of some of these deposits are essential to fully evaluate the economic potential (Bingler, 1968; Segerstrom and Henkes, 1977).

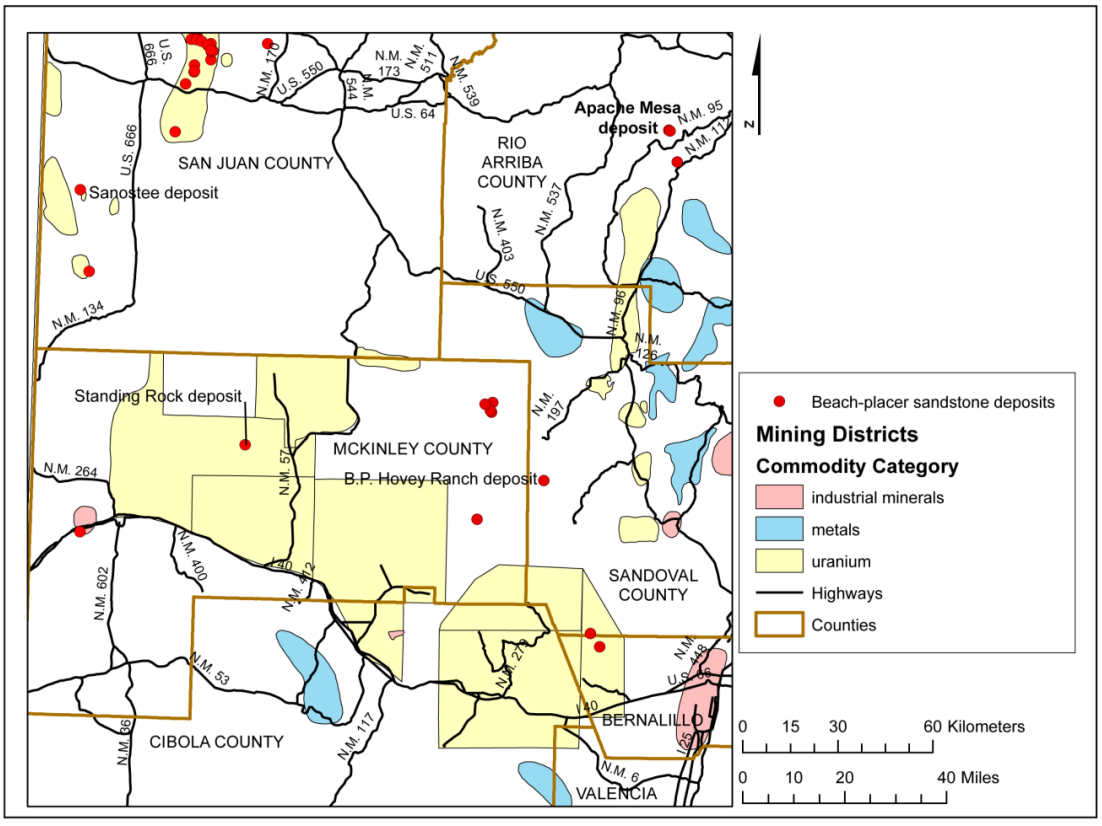

FIGURE 4.23 Location of Late Cretaceous heavy mineral, beach-placer sandstone deposits in the San Juan Basin, New Mexico.

TABLE 4.4 Heavy mineral, beach-placer sandstone deposits in the San Juan Basin, New Mexico (U.S. Bureau of Mines and U.S. Atomic Energy files; Chenoweth, 1957; Dow and Batty, 1961; Houston and Murphy, 1970, 1977; Brookins, 1977; McLemore, 1983, 2016). New geologic mapping has occurred since the deposits were first described and, therefore, the host sandstone could be different than first described. The mine identification number (Mine id) is from the New Mexico Mines Database (McLemore et al., 2005a, b).

Mine id	County	Name (aliases)	Latitude	Longitude	Host formation
NMBE0005	Bernalillo	Herrera Ranch	35.187111	107.050083	Point Lookout Sandstone (?)
NMSA0049	Sandoval	Herrera Ranch	35.224111	107.082667	Gallup Sandstone
NMSA0028	Sandoval	B.P. Hovey Ranch (Torreon Wash)	35.659444	107.252639	Point Lookout Sandstone
NMMK0060	McKinley	Farr Ranch (Star Lake)	35.880167	107.434778	Pictured Cliffs Sandstone
NMMK0061	McKinley	Farr Ranch (Star Lake)	35.875139	107.461444	Pictured Cliffs Sandstone
NMMK0062	McKinley	Farr Ranch (Star Lake)	35.857444	107.443472	Pictured Cliffs Sandstone
NMMK0063	McKinley	Farr Ranch (Star Lake)	35.852611	107.438889	Pictured Cliffs Sandstone
NMMK0072	McKinley	Gallup (Defiance, Torrivio Anticline)	35.481639	108.870778	Gallup Sandstone
NMMK0108	McKinley	Miguel Creek Dome	35.546028	107.482889	Crevasse Canyon Formation-Dalton Sandstone Member
NMMK0261	McKinley	Standing Rock (Flat Top Hill)	35.745389	108.301667	Point Lookout Sandstone
NMRA0001	Rio Arriba	Apache Mesa (Airborne Anomaly 1, Stinking Lake)	36.665	106.825417	Point Lookout Sandstone
NMRA0002	Rio Arriba	Apache Mesa (Airborne Anomaly 3, Stinking Lake)	36.574028	106.793944	Point Lookout Sandstone
NMRA0003	Rio Arriba	Apache Mesa (Airborne Anomaly 2, Stinking Lake)	36.662528	106.821278	Point Lookout Sandstone
NMSJ0002	San Juan	Airborne Anomaly 4 (Barker Dome)	36.892313	108.25757	Pictured Cliffs Sandstone
NMSJ0003	San Juan	Airborne Anomaly 5	36.772	108.545667	Point Lookout Sandstone
NMSJ0004	San Juan	Airborne Anomaly 6	36.826306	108.515417	Point Lookout Sandstone
NMSJ0005	San Juan	Airborne Anomaly 7	36.883444	108.470806	Point Lookout Sandstone
NMSJ0006	San Juan	Airborne Anomalies 8, 9	36.874116	108.460203	Point Lookout Sandstone
NMSJ0007	San Juan	Airborne Anomalies 10, 11	36.869486	108.453519	Point Lookout Sandstone
NMSJ0008	San Juan	Airborne Anomaly 12	36.86586	108.457431	Point Lookout Sandstone
NMSJ0009	San Juan	Airborne Anomaly 13, 14, 15	36.881206	108.450158	Point Lookout Sandstone
NMSJ0010	San Juan	Airborne Anomaly 16, 17, 18	36.891513	108.49564	Point Lookout Sandstone
NMSJ0011	San Juan	Airborne Anomaly 19, 20, FA1	36.904199	108.512519	Point Lookout Sandstone
NMSJ0012	San Juan	Airborne Anomaly 21	36.932931	108.513809	Point Lookout Sandstone
NMSJ0013	San Juan	unknown	36.92975	108.506778	Point Lookout Sandstone
NMSJ0014	San Juan	Airborne Anomaly 22, 23 (Salt Creek Wash)	36.953889	108.530278	Point Lookout Sandstone
NMSJ0015	San Juan	unknown	36.951222	108.526472	Point Lookout Sandstone
NMSJ0016	San Juan	Airborne Anomaly 24	36.953639	108.551722	Point Lookout Sandstone
NMSJ0017	San Juan	Airborne Anomaly 32	36.955474	108.614891	Point Lookout Sandstone

Mine id	County	Name (aliases)	Latitude	Longitude	Host formation
NMSJ0018	San Juan	Airborne Anomaly 33	36.973486	108.614159	Point Lookout Sandstone
NMSJ0019	San Juan	Airborne Anomaly 34	36.957985	108.615112	Point Lookout Sandstone
NMSJ0020	San Juan	Airborne Anomaly 35	36.964092	108.614879	Point Lookout Sandstone
NMSJ0021	San Juan	Airborne Anomaly 36	36.894443	108.521101	Point Lookout Sandstone
NMSJ0022	San Juan	Airborne Anomaly 37	36.921983	108.511314	Point Lookout Sandstone
NMSJ0023	San Juan	Airborne Anomaly 46	36.634045	108.577897	Point Lookout Sandstone
NMSJ0037	San Juan	Deposit 2	36.971746	108.559063	Point Lookout Sandstone
NMSJ0038	San Juan	Deposit X-Y	36.84282	108.456884	Point Lookout Sandstone
NMSJ0054	San Juan	Hogback (Elmer Davidson, Willie Davidson)	36.809722	108.516667	Point Lookout Sandstone
NMSJ0088	San Juan	Sanostee	36.44894	108.898049	Gallup Sandstone
NMSJ0095	San Juan	Toadlena	36.227892	108.867162	Gallup Sandstone

TABLE 4.5 Ore reserves for other heavy mineral beach-placer sandstone deposits in the world. Iluka ore reserves are from (Iluka, 2014).

Area	Total deposit (metric tonnes)	Year	Ilmenite % ($FeTiO_3$)	Rutile % (TiO_2)	Leucoxene % ($(Fe,Mg,Mn,Ti)O_3$)	Zircon % ($ZrSiO_4$)
Apache Mesa, NM	120,564	2016	<3	-	-	<1
Atlantic Seaboard (Iluka)	19,700,000	2014	60	-	-	18
Eucla Basin, Australia (Iluka)	114,600,000	2014	27	4	-	51
Perth Basin, Australia (Iluka)	313,300,000	2014	59	5	-	10
Murray Basin, Australia (Iluka)	12,000,000	2014	47	19	-	13
Grande Côte, Senegal, West Africa	1,915,000	2015	-	2.5	3.2	10.7

TABLE 4.6 Some uses of selected commodities found in Cretaceous heavy mineral, beach-placer sandstone deposits in New Mexico. Price is from U.S. Geological Survey (2016) for 2015. Na=not available

Commodity	Primary Mineral	Specific Gravity	Price ($/metric ton)	Selected Uses
Titanium	Rutile (TiO_2), leucoxene (TiO_2), ilmenite ($FeTiO_3$)	4.2–5.0	110 (ilmenite)-840 (rutile)	white pigment found in toothpaste, paint, paper, glazes, and some plastics, heat exchangers in desalination plants, alloys in aircraft, welding rods
Zirconium	Zircon ($ZrSiO_4$)	4.7	1050 (zircon)	ceramic tiles, bricks used to line steel making furnaces, mold and chill sands, alloying agent in steel, laboratory crucibles
Iron	Magnetite (Fe_3O_4)	5.2	na	additive in cement, iron ore, steel
REE	Monazite ($(Ce,La,Y,Th)PO_4$	4.9–5.3	na	catalyst, glass, polishing, re-chargeable batteries, magnets, lasers, glass, TV color phosphors, solar panels, wind turbines
Niobium	Trace element in other minerals	na	na	used in alloys including stainless steel, superconducting

Commodity	Primary Mineral	Specific Gravity	Price ($/metric ton)	Selected Uses
				magnets for particle accelerators, MRI scanners
Chromium	Chromite ($FeCr_2O_4$)	4.5–4.8	na	Stainless steel
Uranium	Monazite $(Ce,La,Y,Th)PO_4$	4.9–5.3	na	fuel for nuclear reactors to generate electricity, projectiles, shielding of radioactive materials
Thorium	Monazite $(Ce,La,Y,Th)PO_4$	4.9–5.3	na	fuel for thorium-reactors
Yttrium	Monazite $(Ce,La,Y,Th)PO_4$, xenotime YPO_4	4.9–5.3, 4.4–5.1	na	additive in alloys to increase strength, microwave filters, lasers, catalyst
Staurolite	Staurolite (Fe, Mg, $Zn)_2Al_6O_6(SiO_4)_4(O,OH)_2$	3.6–3.8	na	abrasive
Kyanite	Kyanite (Al_2SiO_5)	3.6–3.7	290	refractory products (bricks, mortars, kilns, molds), brake shoes, clutch facings, porcelain
Garnet	Garnet $(Fe,Mn,Ca)_3 \cdot Al_2(SiO_4)_3$	3.4–4.2	na	abrasive

This section summarizes previous investigations of the geology and economic viability of Cretaceous beach-placer sandstones in the San Juan Basin, New Mexico (McLemore, 1983; 2010; Zech et al., 1994; McLemore and Robinson, 2016; McLemore et al., 2017; Owen and McLemore, 2024), as well as presenting new analyses, mapping and identifying additional investigation needed to assess their economic potential. The purposes of this chapter are to: 1) describe the heavy mineral, beach-placer sandstone deposits in the San Juan Basin in New Mexico, 2) summarize the formation, tectonic setting, stratigraphy, and possible sources of these deposits, 3) summarize their association and relationship to coal deposits, 4) summarize their economic potential (especially critical minerals), and 4) identify areas that require additional investigation in order to assess their economic potential. This report presents unpublished geochemical analyses of selected deposits (Appendix 7) and builds upon previous reports that have been written describing these deposits and their formation. Published geochemical analyses are by Green et al. (1980) and Zech et al. (1994). Detailed mapping of selected deposits by the authors, Dow and Batty (1961), Bingler (1963, 1968), Zech et al. (1994), and others as cited.

4.7.2 Methods of study

Data used in this report are compiled from a literature review, field investigations, and includes results previously unpublished. Some of the deposits were mapped and samples were collected. The Apache Mesa area was mapped according to standard geologic mapping techniques (Lahee, 1961; Carpenter and Keane, 2016) at 1:6,000 scale in 2015 (McLemore et al., 2016**)**. Drilling at Apache Mesa began on August 18, 2015 and was completed on August 25, 2015; drill logs are in McLemore et al. (2016). Mineralized samples were collected at the surface and from drill core. Chemical analyses are in Appendix 7. Polished thin sections of selected samples from beach-placer deposits throughout the San Juan Basin were examined using standard petrographic techniques that included examination of the texture and mineralogy. Any resource or reserve data presented here are historical data and are provided for information purposes only and do not conform to Canadian National Instrument NI 43-101 requirements.

The handheld scintillation counter was used in combination with a handheld GPS to create ground radiometric surveys over selected areas. Survey grids were not planned before

field work, but rather surveyed “on the fly”, with the edges of the survey extent generally defined by a return to background radiation values. The scintillation counter was held at waist height and was allowed to equilibrate at each station. The reading at each station (in counts per second, cps) was recorded on a handheld GPS. Station spacing varied between site, but generally was ~15 m over mineralized zones up to 50 m over unmineralized areas. Radiometric maps were created using Esri ArcGIS Pro.

Unlike most types of deposits, mineral sands are generally reported in terms of percentage of minerals, specifically percent ilmenite, rutile, zircon, and so forth (Table 4.7) (Kattaa, 2002; Jones and O’Brien, 2014). However, there was not enough funding, equipment, or time to determine quantitative mineral composition, so the chemical analyses were used to calculate ore reserves for this report. TiO_2 was used as a proxy for the amount of ilmenite, rutile, and leucoxene. Zr was used as a proxy for the amount of zircon. Total REE (TREE) was used as a proxy for the amount of monazite.

4.7.3 Evaluation of the NURE data

A regional geochemical database of stream sediments exists for the state of New Mexico that was generated from reconnaissance surveys as part of the U.S. Department of Energy’s National Uranium Resource Evaluation (NURE) program during 1974-1984 (McLemore and Chamberlin, 1986). The NURE data are typically arranged by 1x2-degree quadrangles, although the Grants uranium district was sampled and evaluated in greater detail. Parts of four 1x2-degree quadrangles cover the San Juan Basin: Shiprock, Gallup, Albuquerque, and Aztec. The main purposes of the NURE program were to provide an assessment of the nation's uranium resources and to identify areas favorable for uranium mineralization. The NURE data were not designed to reveal uranium or other mineral deposits, but if the NURE data are used with caution, the data can be used to identify areas of potential geochemical interest for further study. Ultimately, field examination of these identified areas must be conducted. Zumlot (2006) and Zumlot et al. (2009) presented an evaluation of the NURE data for the entire state.

NURE geochemical data aided in the exploration of modern beach-placer deposits in Georgia, North Carolina, and Virginia (Koch, 1986; Carpenter and Carpenter, 1991). However, preliminary examination of the NURE stream-sediment geochemical data in the San Juan Basin in areas of known heavy mineral, beach-placer sandstone deposits indicated no significant geochemical anomalies. That is probably explained by: 1) the Cretaceous deposits in New Mexico are much smaller than the large modern deposits along the Atlantic coast, 2) the sampling density in the San Juan Basin was not detailed enough to locate such small deposits, and 3) streams draining from the deposits in the San Juan Basin were not sampled for the NURE program. There are numerous single-element geochemical anomalies of Zr, Ti, REE, and Th scattered throughout the San Juan Basin that could be indicative of undiscovered heavy mineral, beach-placer sandstone deposits, but significant detailed field examination is required to verify those anomalies, which will be examined in future studies.

4.7.4 Previous investigations

Most of the Cretaceous heavy mineral, beach-placer sandstone deposits in New Mexico were discovered during airborne gamma-ray radiometric surveys in the 1950s by the U.S. Atomic Energy Commission (Murphy, 1956; Chenoweth, 1957) and originally were simply

identified as airborne anomaly number 1, 2, and so forth. The airborne anomalies were subsequently verified by field examinations that are documented by a series of Preliminary Reconnaissance Reports (PRR; see McLemore, 1983). Nearshore facies in Late Cretaceous transgressive-regressive sequences throughout the Rocky Mountain region locally host similar beach-placer sandstone deposits. Murphy (1956) described some of the deposits in adjacent states and recommended additional investigation. Chenoweth (1957), Dow and Batty (1961), Overstreet (1967), and Brookins (1977) summarized the stratigraphy and physical and chemical attributes of the deposits in the San Juan Basin. Bingler (1963, 1968) described the Sanostee and the deposits at Apache Mesa (formerly Stinking Lake). Houston and Murphy (1970, 1977) described the depositional environment of the deposits. Zech et al. (1994) described the deposits on the Ute Indian Reservation and included detailed chemistry of most of the deposits (Appendix 7, McLemore, 2010). McLemore et al. (1988a, b) discussed the REE potential of beach-placer sandstone deposits. McLemore et al. (2016) and McLemore and Robisson (2016) examined the Apache Mesa deposits, including new drilling. The deposits at Apache Mesa were originally named the Stinking Lake deposits after a nearby lake by William Chenoweth (Chenoweth, 1957). The name of the deposits was changed from Stinking Lake to Apache Mesa at the request of Tribal members (McLemore et al., 2016). Owen and McLemore (2024) described recent radiometric surveys of some of the deposits. New geologic mapping for this project has occurred since the deposits were first described and, therefore, the host sandstone could be different than first described, primarily because of the intertonguing nature of the transgressive-regressive sandstone units (Fig. 4.24).

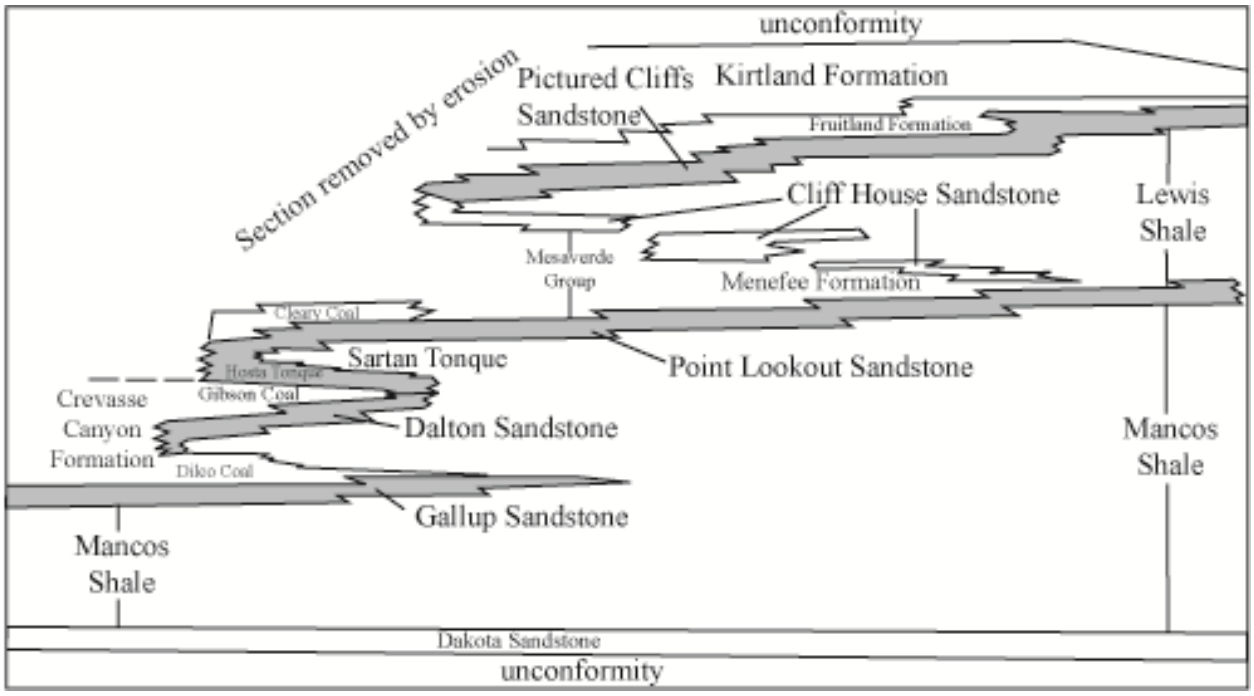

FIGURE 4.24 Stratigraphic framework and nomenclature of the Late Cretaceous sedimentary rocks in the San Juan Basin (simplified from Molenaar, 1989; Craigg et al., 1990; Fassett, 1977, 2000). Gray-shaded sandstone units are hosts of known beach-placer sandstone deposits in the San Juan Basin.

4.7.5 Distribution in the San Juan Basin, New Mexico

Most of the heavy mineral, beach-placer deposits define local depositional trends of the beaches at the time of deposition. The shoreface sandstone deposits in the San Juan Basin were formed both during transgression and regression of the western edge of the Western Interior Seaway (Robinson-Roberts and Kirschbaum, 1995; Fassett, 2000) and are similar to deposits in Australia (Roy, 1999). Beach-placer deposits have not been recognized in Late Cretaceous sand dunes in the San Juan Basin. The majority of the beach-placer sandstone deposits in New Mexico are discontinuous, lenticular- or crescent-shaped, radioactive, well-cemented, medium-grained to very fine-grained, well sorted, and without crossbedding. They are found in dark-colored sandstones, including olive-gray, rust-brown, brownish-black to maroon, and occasionally are called black-sandstone deposits. Host formations include the Gallup Sandstone, Dalton Sandstone Member of the Crevasse Canyon Formation, Point Lookout Sandstone, and Pictured Cliffs Sandstone (Fig. 4.24). Many of the Cretaceous shoreface sandstone beds containing beach-placer deposits either form the resistant caps of mesas or are overlain by black shale and coal or Quaternary sedimentary deposits.

Gallup Sandstone

The Gallup Sandstone is the oldest of the sandstone units hosting beach-placer sandstone deposits in the San Juan Basin (Fig. 4.24) and forms regressive beach deposits overlain by transgressive offshore-bar deposits (Campbell, 1971, 1979). Locally, the Gallup Sandstone is mapped as the Torrivio Member and an unnamed lower member (Millgate, 1991).

Gallup deposit, McKinley County (NMMK0072, Mine Id number from the New Mexico Mines Database)

The Gallup (also known as Defiance or Torrivio Anticline) deposit, in section 32, T15N, R19W, west of Gallup and south of Interstate 40 (Fig. 4.23, 4.25, Table 4.5), is in an olive-green to dark-brown to gray, medium- to fine-grained, well to moderately sorted, heavy-mineral sandstone bed with rounded to subrounded grains and no cross bedding and lies on top of a white to buff, cross bedded, medium-grained sandstone bed in the Gallup Sandstone. The deposit trends N25°W intermittently for 457 m (Fig. 4.25), is less than 30 m wide, up to 1.2 m thick, and is overlain by black to gray shale and thin coal beds. The deposit contains monazite, ilmentite, rutile, brookite, anatase, leucoxene, magnetite, and zircon (Allen, 1956; Sun and Allen, 1957; Chenoweth, 1957; this report). A sample from the deposit (#2391) contained the highest REE concentrations of beach-placer sandstone samples analyzed, containing 4250 ppm La and 8375 ppm Ce (Appendix 7). Resources are estimated as 5400 metric tonnes containing 0.6% TiO_2 and 6.5% Fe (USBM files).

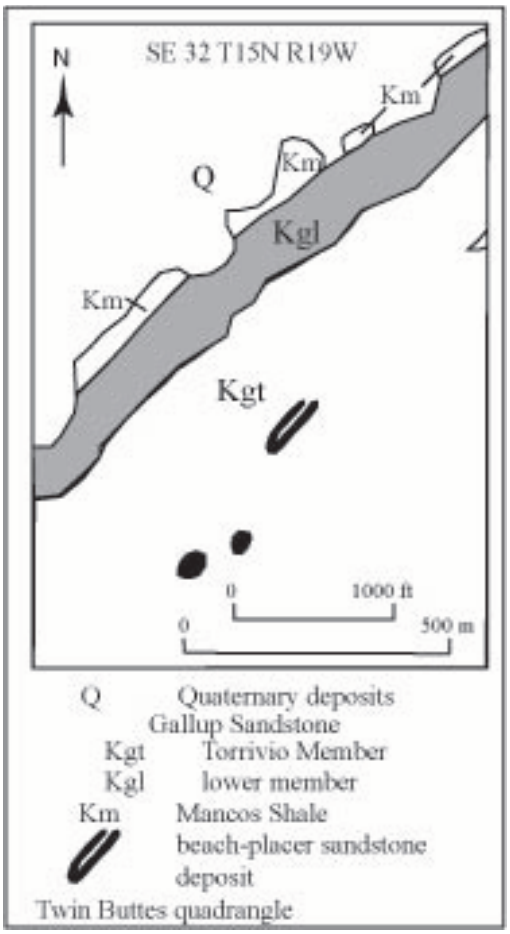

FIGURE 4.25 Geologic map of the Gallup beach-placer sandstone deposits. Mapping of the deposit was by V.T. McLemore in 2009. Sedimentary geology simplified from Millgate (1991).

Sanostee deposit, San Juan County (NMSJ0088)

The largest exposed beach-placer sandstone deposit in New Mexico is the Sanostee deposit, which lies along the top of a mesa northwest of Sanostee, New Mexico on the Navajo Indian Reservation (Fig. 4.23, 4.26, Table 4.4; Bingler, 1963; Force, 2000). The Sanostee deposit is in an olive-green-gray to dark brown to black, medium- to fine-grained, well to moderately sorted, heavy-mineral sandstone bed with rounded to subrounded grains and no cross bedding that overlies a white to buff, cross bedded, medium-grained sandstone, with local rust staining within the Gallup Sandstone. This deposit formed in a regressive shoreface environment. The deposit trends N30°W, dips 5-10°W, is approximately 2400 m long (Fig. 4.26), 152-183 m wide, 1-4 m thick, and is overlain by black to gray shale. The deposit occurs in two separate zones forming a resistant, cliff-forming ledge along the mesa (Fig. 4.26, 4.27; Force, 2000; V.T. McLemore, field mapping, 2010). Bingler (1963) described six discrete zones based upon exposure and stratigraphy. The deposit contains ilmentite, magnetite, hematite-ilmenite, zircon, tourmaline, garnet, hematite, staurolite, apatite, barite, sphene, and rutile (Fig. 4.28; Bingler, 1963; Force, 2000; Force et al., 2001; this report).

A radiometric survey of the Sanostee deposit (Fig. 4.27) consisted of 234 stations focused around the ledges of the mesa where the most mineralized sandstones were exposed. The survey

shows a 1200-meter-long, northwest trending zone of mineralization that is likely shallowly buried under the thicker portion of the mesa and eroded away entirely between the central and northwestern portion of the deposit. The survey also shows a nearly 200-meter-long, narrow mineralized zone southwest of the main zone of mineralization, also trending northwest. The most radioactive stations were above 2000 cps, with the highest value of 4500 cps located on the ledge at the very northwest extent of the survey. It is possible that these mineralized zones extend along strike to the northwest and may be buried deeper. Extension to the southeast is also possible, but the mesa cliffs out around 600 meters from the southern end of the surveyed area.

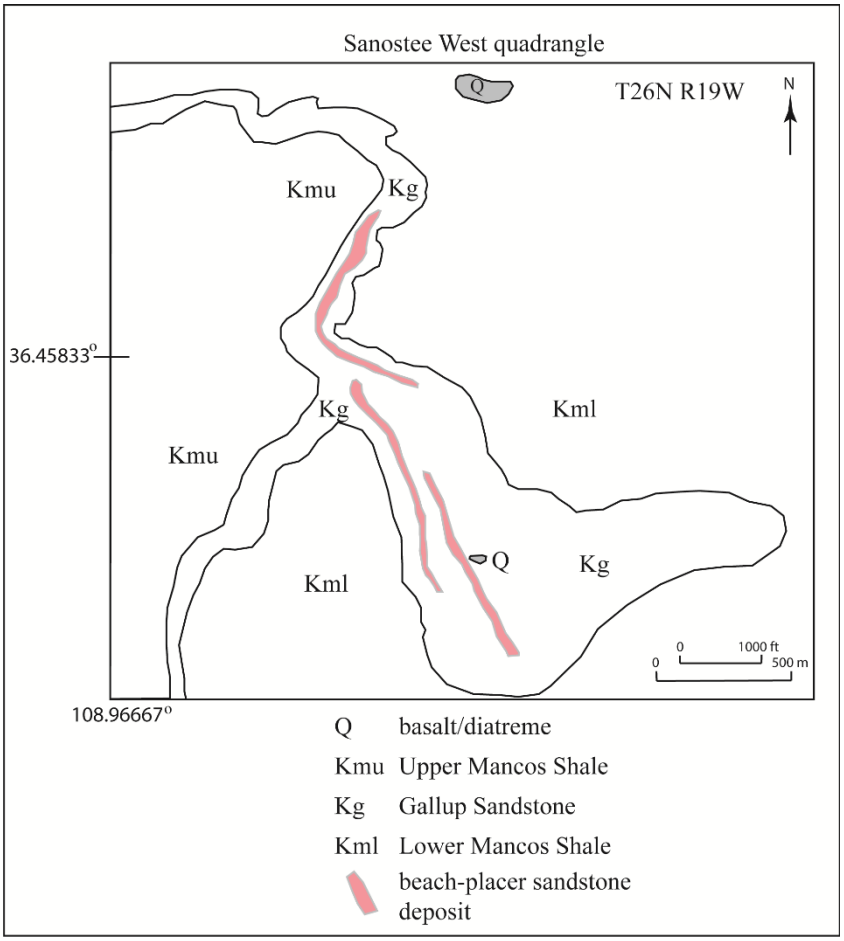

FIGURE 4.26 Geologic map of the Sanostee beach-placer sandstone deposits, in section 31, T26N, R19W, McKinley County, New Mexico. Mapping of the deposit was by V.T. McLemore in 2009, modified from Beaumont (1954), Dow and Batty (1961), Bingler (1963), and Force (2000).

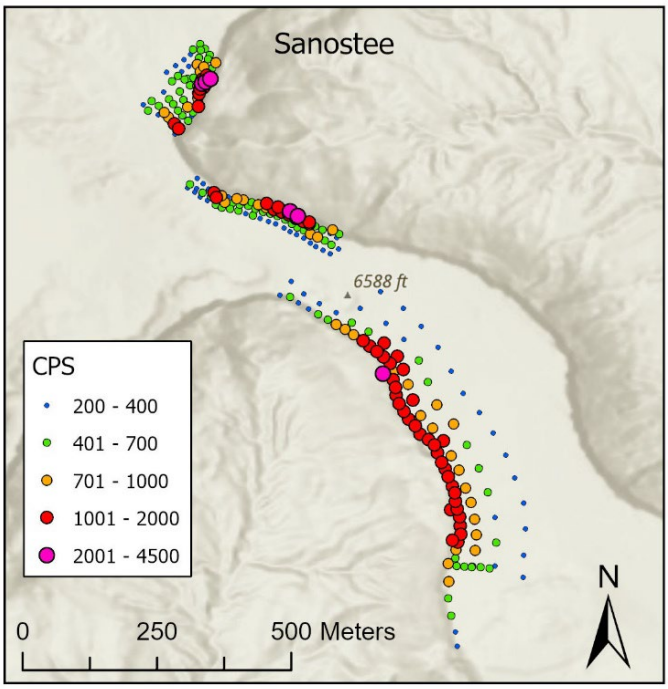

FIGURE 4.27. Beach-placer sandstone at Sanostee, McKinley County, New Mexico (photograph by V.T. McLemore).

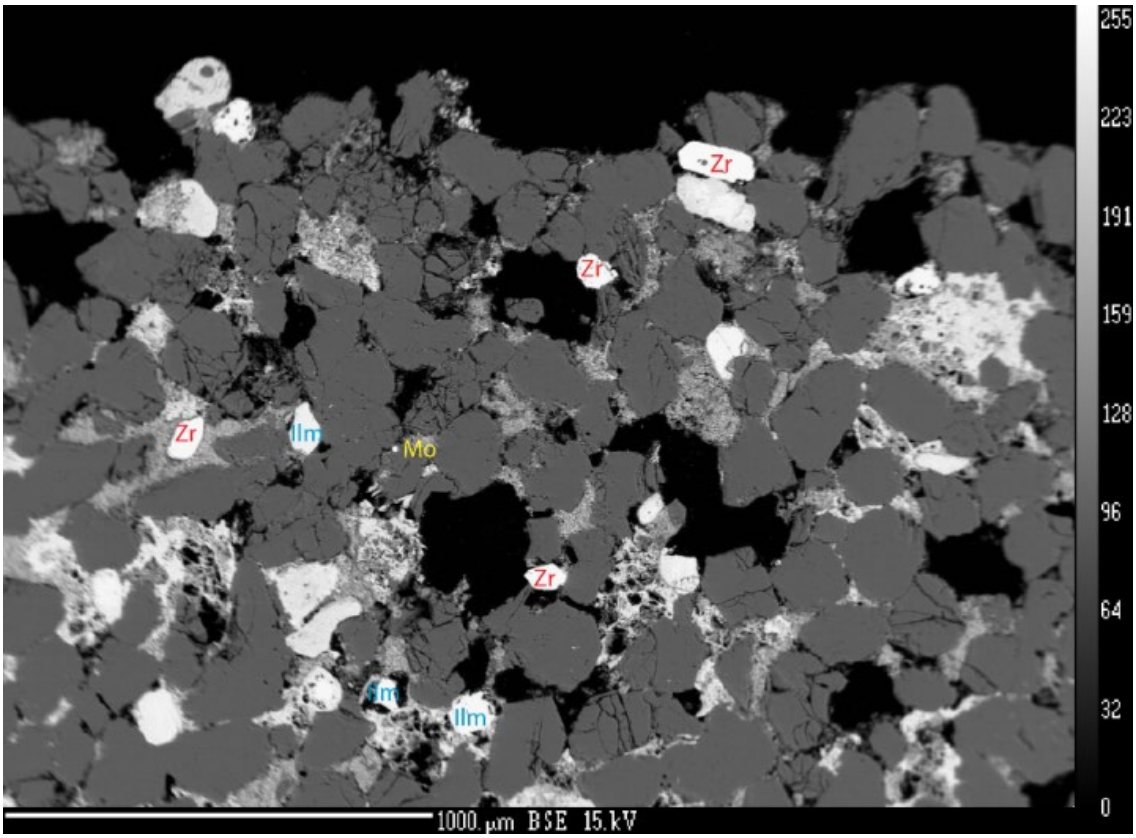

FIGURE 4.28 Electron microprobe photograph showing distribution of zircon, ilmenite and monazite grains in sample SAN6 (Sanostee). Zircon grains are labeled in red, ilmenite in blue, and monazite in yellow. Mottled, lighter colored cement is iron oxide (hematite). Dark gray grains are mainly quartz. Black areas are pore spaces (photograph by A. Robisson).

Toadlena, San Juan County (NMSJ0095)

The Toadlena deposit, near Toadlena, New Mexico is located on the Navajo Indian Reservation (Fig. 4.23, Table 4.4), consists of olive-green to gray sandstone that is approximately 457 m long and 0.6-2.4 m thick, trends N20°E, and consists of ilmenite, magnetite, and monazite (Chenoweth, 1957; Archer, 1957). The host is the Gallup Sandstone exposed along the steeply dipping hogback. Dow and Batty (1961) reported a sample containing 0.4% TiO_2, 11% Fe, and 530 ppm Th. Resources are estimated as 2300 metric tonnes of 0.11% Fe, 0.4% TiO_2, and 0.06% ThO_2 (USBM files). This deposit could not be found in 2023.

Herrera Ranch, Sandoval County (NMSA0049)

One of the Herrera Ranch deposits (also known as the Anaconda deposit) is within a bluff to gray sandstone bed belonging to the Gallup Sandstone and is found in section 31, T12N, R12W in the southeastern San Juan Basin (Fig. 4.23, Table 4.4; Chenoweth, 1957). It is approximately 0.3 m thick, 15 m wide, and 61 m long and trends N20°E. No chemical analyses are available for this deposit. The other Herrera Ranch deposit is in Point Lookout Sandstone.

Dalton Sandstone

Miguel Creek Dome, McKinley County (NMMK0108)

The Miguel Creek Dome deposits in section 8, T15N, R6W (Fig. 4.23, Table 4.4) are the only known deposits within the Dalton Sandstone member of the Crevasse Canyon Formation. The deposits consist of two small lenses within green-gray to olive-gray sandstone (Chenoweth, 1957). The largest deposit is 67 m long, 37 m wide, 0.5 m thick, trends N40°E, and consists of ilmenite, magnetite, quartz, zircon, and monazite. Only limited chemical analyses are available for this deposit (Appendix 7, McLemore, 2010), and additional sampling is required to fully characterize this deposit. Resources are estimated as approximately 610 metric tonnes of 0.4% ZrO_2, 4% TiO_2, 17.2% Fe and 0.03% ThO_2 (USBM files).

Point Lookout Sandstone

The Point Lookout Sandstone crops out around the margins of the San Juan Basin, forms cliffs or caps mesas or resistant dip slopes and hogbacks, is of variable thickness (12-127 m), and is a regressive sandstone (Hollenshead and Pritchard, 1961; Talbot and Frost, 1979; Craigg et al., 1990; Devine, 1991; Zech et al., 1994). It conformably overlies the Mancos Shale and is overlain by the Menefee Formation (Fig. 4.24). The Point Lookout Sandstone was deposited in upper shoreface, foreshore, washover, and eolian environments (Zech, 1982; Zech et al., 1994). In the northern part of the San Juan Basin, the heavy mineral, beach-placer sandstone deposits are at the top of the Point Lookout Sandstone and trend N55-60°W (Figs. 4.23, 4.29).

Herrera Ranch, Bernalillo County (NMBE0005)

The second deposit on the Herrera Ranch is in section 16, T11N, R2W (Fig. 4.23, Table 4.4) and is in brown-gray sandstone belonging to the Point Lookout Sandstone. The deposit is small, less than 1 m thick and only a few tens of meters long. No chemical analyses are available for this deposit.

B.P. Hovey Ranch, Sandoval County (NMSA0028)

The P.B. Hovey Ranch deposit (also known as the Torreon Wash deposit) is in section 34, T17W, R4W (Fig. 4.23, 4.29, Table 4.4). The deposit is in brown- to olive-gray, medium grained, well to moderately sorted sandstone (Fig. 4.30) and is approximately 100 m long and 0.6-1.5 m thick (Fig. 4.29). There are two zones of beach-placer deposits at the B. P. Hovey Ranch locality (McLemore, 1983, fig. 26). Drilling suggests that this deposit continues to the northwest (Chenoweth, 1957). Only limited chemical analyses are available for this deposit (Appendix 7, McLemore, 2010), and additional sampling is required to fully characterize this deposit.

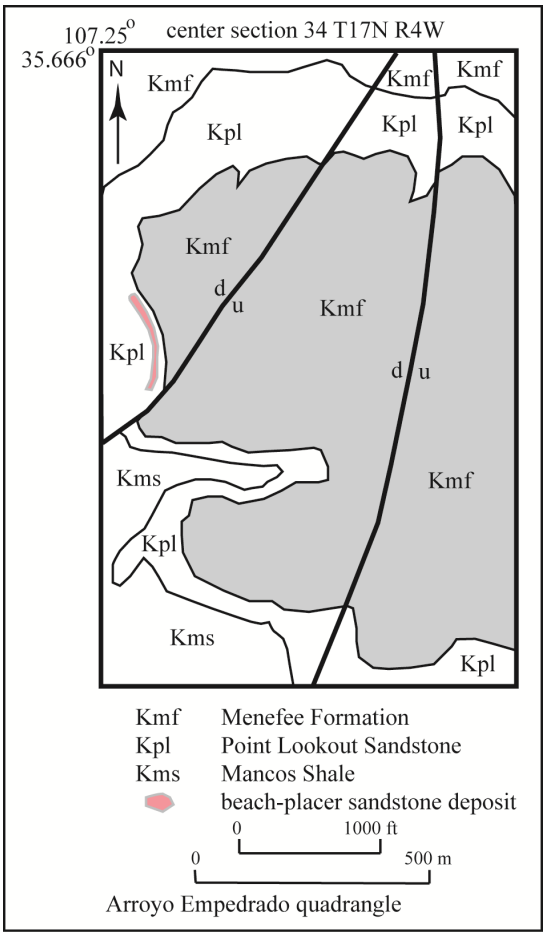

FIGURE 4.29 Geologic map of the B.P. Hovey beach-placer sandstone deposit, Sandoval County, New Mexico. Mapping of the deposit was by V.T. McLemore in 1981 and 2015. Sedimentary geology is modified from Tabet and Frost (1979).

FIGURE 4.30 Beach-placer sandstone at B.P. Hovey, Sandoval County, New Mexico (photograph by V.T. McLemore).

Standing Rock (Flat Top Hill) deposit, McKinley County (NMMK0261)

The Standing Rock (also known as Flat Top Hill) deposit, in section 35, T18N, R14W, also on the Navajo Indian Reservation (Fig. 4.23, 4.31, Table 4.4), is in a dark orange-brown to yellow to black, medium- to fine-grained, well to moderately sorted, heavy-mineral sandstone lens with no cross bedding resting on top of a lower sandstone bed in the Point Lookout Sandstone. It caps the mesa top of Flat Top Hill (Fig. 4.31; Chenoweth, 1957; Kirk and Sullivan, 1987) and overlies a white to buff, cross bedded, medium-grained sandstone bed (Fig. 4.32). It is as much as 1.5 m thick, 30 m wide, and consists of at least two lenses striking N50°W for approximately 1500 m. Calcite veining cuts the sandstone deposit locally. The deposit contains monazite, ilmenite, anatase, leucoxene, rutile, zircon, and magnetite.

The survey of the Flat Top Hill deposit (Fig. 4.33) consists of two separate mineralized zones that lie on strike with each other. Flat Top Hill, host to what is referred to here as Flat Top Hill East deposit, is an 800-meter-long, northwest oriented mesa with distinct incisions on its northeast face. The extension of this deposit, referred to as Flat Top Hill West, lies roughly 1.6 kilometers to the northwest on a less prominent, narrow ridge roughly 1.3 kilometers long. The radiometric survey of Flat Top Hill East consisted of 273 stations and shows that the most radioactive zones lie on the “fingers” that extend to the northeast. The highest values reach 760 cps. Elevated values are also found on the wider, southeastern portion of the mesa. As radioactivity decreased in lower elevation portions of the mesa, it is likely that the mineralized horizon has been locally eroded. The survey of Flat Top Hill West was comprised of 75 stations. The most radioactive zones are generally confined to the southwestern edge of the ridge, with the highest value reaching 420 cps. This deposit appears to be less mineralized or more eroded (or both) than Flat Top Hill East. No other apparent northwest trending mesas or ridges appear in the vicinity of Flat Top Hill, so it is unlikely that these deposits continue elsewhere.

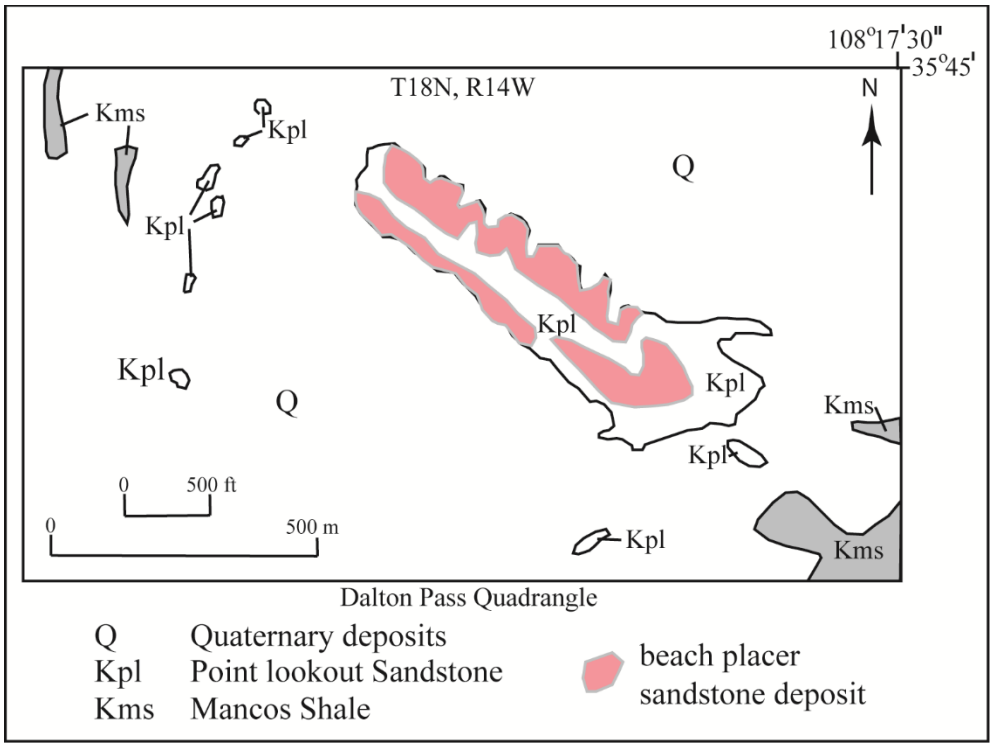

FIGURE 4.31 Geologic map of the Standing Rock beach-placer sandstone deposit in section 35, T18N, R14W, McKinley County, New Mexico. Mapping of the deposit was by V.T. McLemore in 2009, sedimentary geology modified from Kirk and Sullivan (1987).

FIGURE 4.32 Beach-placer sandstone at Standing Rock, McKinley County, New Mexico (photograph by V.T. McLemore).

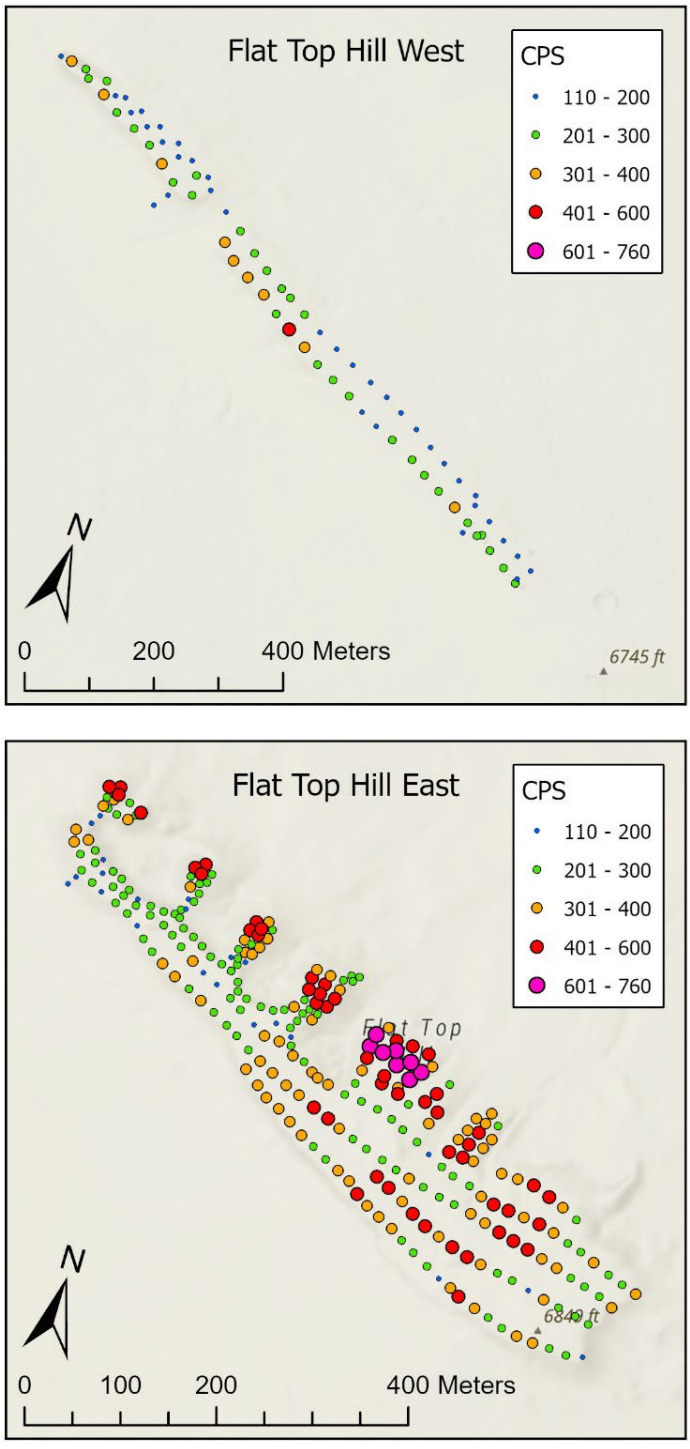

FIGURE 4.33 Ground radiometric survey of the Flat Top Hill East and West Deposits (Owen and McLemore, 2024). Flat Top Hill East shows the most mineralized zones along the "fingers" extending towards the northeast. Flat Top Hill West is less mineralized, with its most elevated values lying on the southeast edge of the ridge.

Hogback, San Juan County (NMSJ0054)

The Hogback deposit in section 15, T30N, R16W (Fig. 4.23, 4.34, Table 4.4), is the only deposit to have yielded production. In 1954, a test shipment of 8 short tons of ore was shipped to an AEC ore-buying station by Willie Davidson (McLemore, 1983). This shipment yielded 3 lbs of 0.02% U_3O_8 and 23 lbs of V_2O_5 The deposit is in an olive-green-gray to dark brown to black, medium- to fine-grained, well to moderately sorted, heavy-mineral sandstone lens with no cross bedding within the Point Lookout Sandstone. The deposit dips 10°E, is overlain by black to gray shale and coal, and overlies a white to buff, cross- bedded, medium-grained sandstone bed (Fig. 4.34). The deposit is approximately 0.3-0.6 m thick, 91 m long, and contains ilmentite, magnetite, and zircon. At least four additional similar deposits are found in the Point Lookout Sandstone along the Hogback area west of Farmington (Chenoweth, 1957; Strobell et al., 1980).

The Hogback deposit is so named because it lies along the Hogback near Shiprock. The radiometric survey over the deposit (Fig. 4.35) consists of 82 stations on a southeast sloping hill on the west side of Coal Mine Creek. Unlike the other surveyed deposits, the Hogback deposit appears to exhibit less topographic control than the deposits found on relatively prominent mesas or ridges. The radiometric anomaly forms a north to northwest feature roughly 200 meters long. The most radioactive zone within the anomaly reaches 1500 cps. An even more radioactive zone was located 120 meters northeast of the main surveyed area and reached 4000 cps. This zone appeared to be a stockpile of mineralized sandstone from historic prospecting efforts.

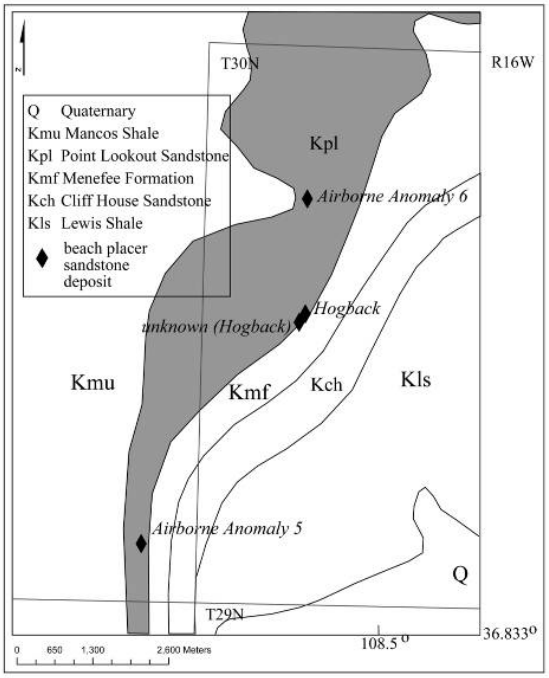

FIGURE 4.34 Geologic map of the Hogback beach-placer sandstone deposit. Mapping of the deposit was by V.T. McLemore in 2009, sedimentary geology modified from Strobell et al. (1980) and New Mexico Bureau of Geology and Mineral Resources (2003).

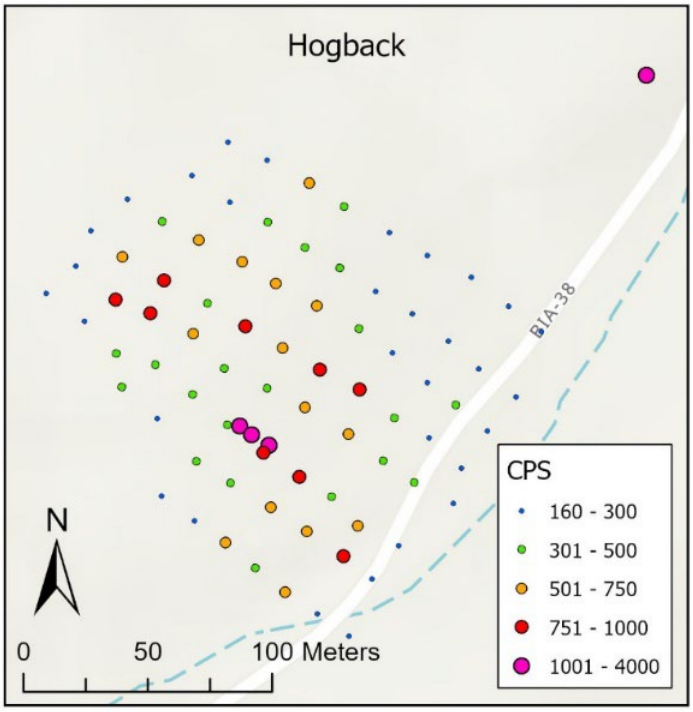

FIGURE 4.35 Ground radiometric survey of the Hogback deposit showing a north to northwest trending radiometric anomaly. A possible stockpile of mineralized sandstone lies to the northeast of the main survey area.

Ute Indian Reservation (Mesa Verde)

Beach-placer sandstone deposits are found in 29 separate localities in the upper Point Lookout Sandstone in and adjacent to the Ute Indian Reservation in southern Colorado and northern New Mexico (Fig. 4.23, 4.36, Table 4.4; Chenoweth, 1957; Dow and Batty, 1961; Zech et al., 1994). This is the largest cluster of closely spaced deposits in the San Juan Basin, although most are small tonnage and grade or are covered by recent dune sands or talus. The deposits are purplish-gray and typically trend N55-60ºW, are up to 2.3 m thick, and are a few tens of meters to more than a kilometer long (Zech et al., 1994). REE are elevated above crustal abundance, but below recommended threshold values (Fig. 37). Detailed chemical analyses (Appendix 7) are from Zech et al. (1994).

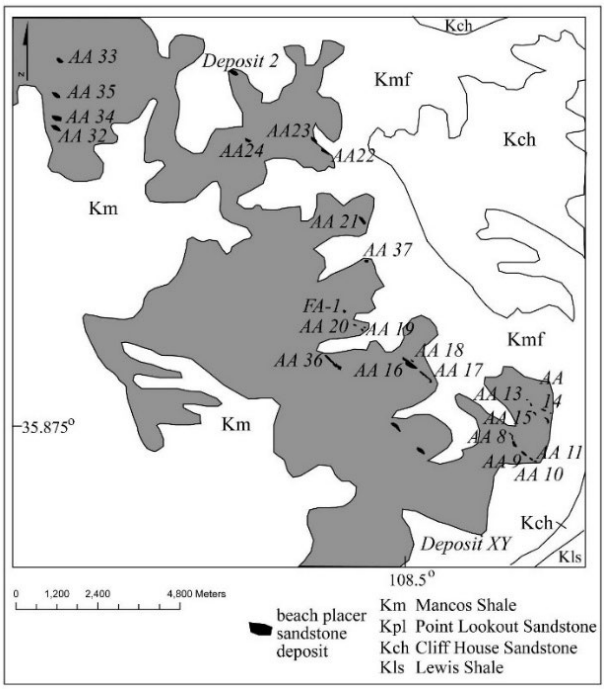

FIGURE 4.36 Geologic map of the beach-placer sandstone deposits on the Ute Indian Reservation and adjacent area (modified from AEC records; Strobell et al., 1980; Zech et al., 1994; New Mexico Bureau of Geology and Mineral Resources, 2003).

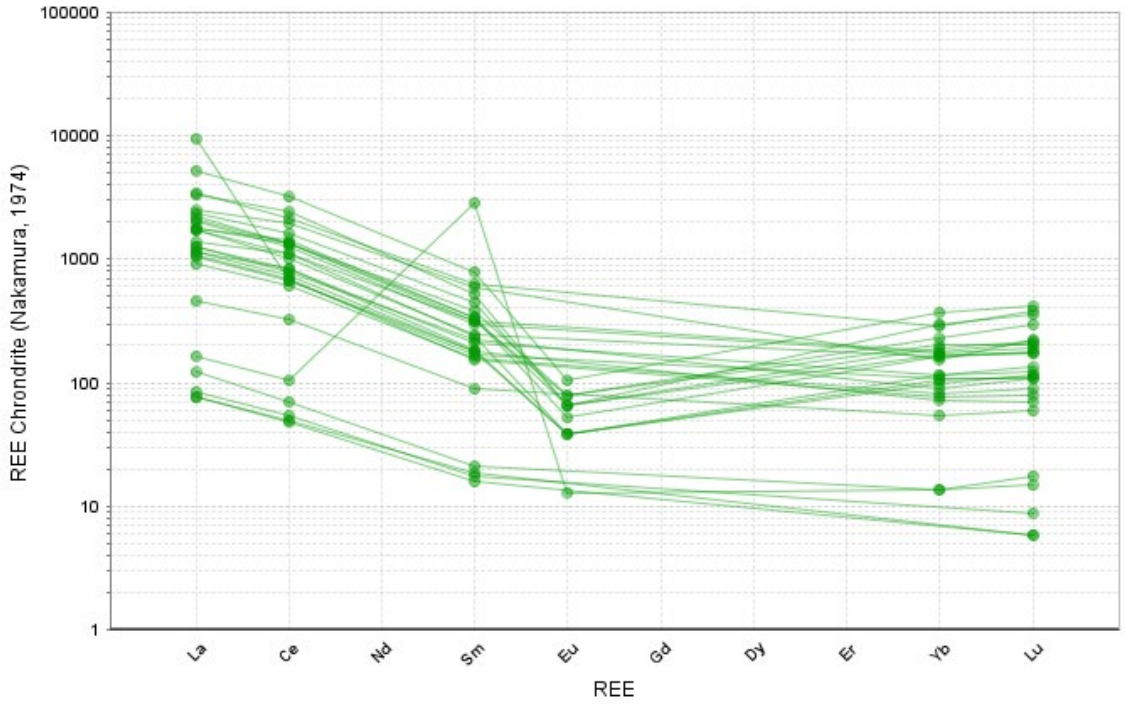

FIGURE 4.37 Chondrite-normalized REE plot of samples from the Ute Reservation. Chondrite values from Taylor and McLennan (1985).

Apache Mesa (Airborne Anomalies 1-3, Stinking Lake), Rio Arriba County (NMRA0001, 3)

The Apache Mesa (Airborne Anomalies 1-3 deposits) are in section 3, T28N, R1E and section 2, T27N, R1E, on the Jicarilla Apache Reservation in the eastern San Juan Basin (Fig. 4.23, 4.38, Table 4.4) and are in the Point Lookout Sandstone (Bingler, 1968; McLemore and Robisson, 2016; McLemore et al., 2016). The original naming of these deposits as airborne anomalies followed by a number is as designated by the airborne survey and the field reconnaissance reports. The deposits are lenses, approximately 213-914 m long and 0-2.4 m thick, and are found at the top of a 3.7-m thick, gray to yellow-white to reddish-brown, fine- to medium-grained, cross-bedded quartz sandstone (Figs. 4.38, 4.39, 4.40, 4.41). The heavy mineral sandstone is reddish-purple to olive-brown, well cemented, and contains iron oxide minerals, leucoxene, zircon, tourmaline, rutile, magnetite, and ilmenite.

The majority of the black-sandstone samples are detrital and composed mostly of quartz, some lithic fragments, feldspar, and heavy minerals. Alteration and weathering of grains is apparent in these samples, although the intensity varies. Cementation is composed mostly of iron oxide and some silica. Petrographic, chemistry, and electron microprobe results confirm the presence of iron oxides, ilmenite, rutile, zircon, monazite, xenotime, garnet, and illite in these beach-placer sandstone deposits (Figs. 4.40, 4.41; McLemore et al., 2016). The heavy mineral grains are oblong, rounded, and somewhat altered. The albite grains are blockier and less altered than the more rounded quartz. The zircon grains are very fractured and blocky. Some of the ilmenite grains are zoned and much of the ilmenite is either altered partially to hematite or is in solid solution series with hematite. A few grains of chromite, and one grain of gold with a silver-rich rim, also are found in the Apache Mesa deposits. Although, some individual analyses of samples from Apache Mesa contain high concentrations of TiO_2 (15%), Cr (590 ppm), Nb (260 ppm), Zr (>10,000 ppm), Th (258 ppm), and total REE (2,692 ppm; Fig. 4.42); the Apache Mesa beach-placer sandstone deposit is overall much smaller, thinner and lower in trace element constituents

The Apache Mesa beach-placer sandstone deposit contains 132,900 short tons (120,564 metric tons) of ore with grades of 3% TiO_2, 108 ppm Cr, 46 ppm Nb, 2,187 ppm Zr, 40 ppm Th, and 522 ppm total REE. Modern, economic beach-placer sandstone deposits are typically greater than 10 million short tons of greater than 2% heavy minerals and are mined by open-pit methods. Geologic mapping and drilling indicate that the Apache Mesa beach-placer sandstone deposits are too small and low grade to be economic in today's market. No further investigation is recommended at this time.

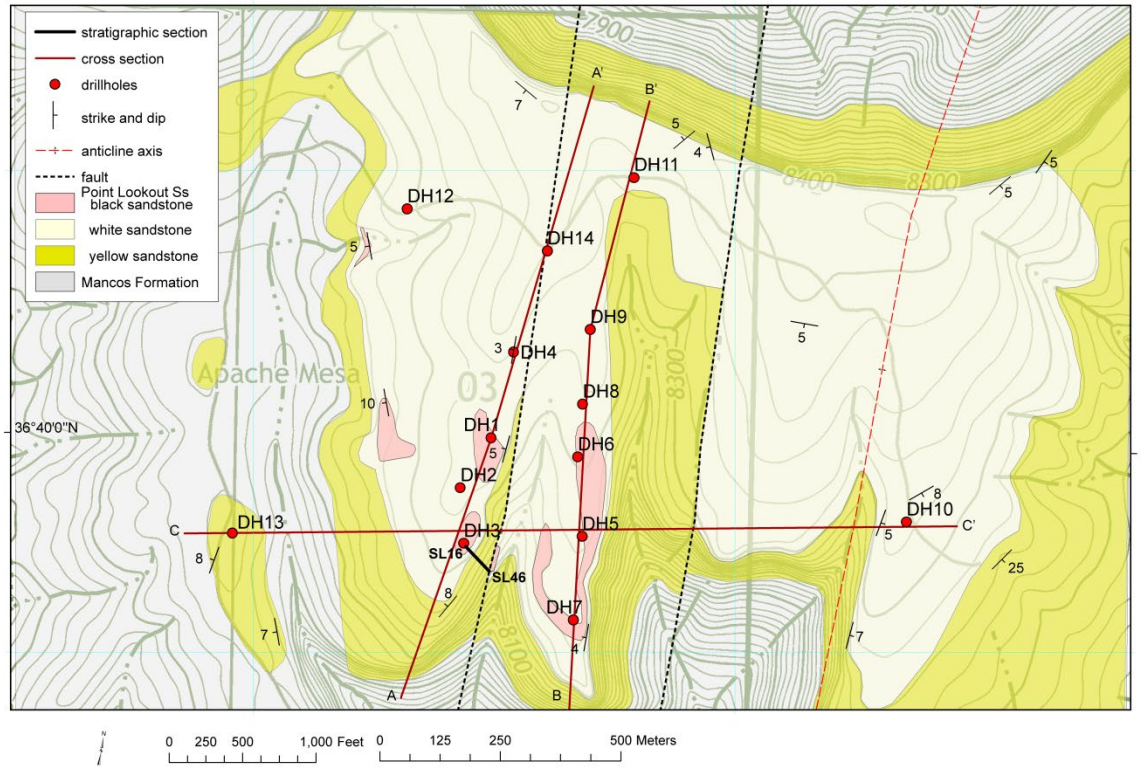

FIGURE 4.38 Geologic map and location of drill holes for chemical analyses. Details and cross sections are in McLemore et al. (2016).

FIGURE 4.39 Beach-placer sandstone deposit overlying the white sandstone in the Point Lookout Sandstone at Apache Mesa (photograph by V.T. McLemore).

FIGURE 4.40 Close-up of beach-placer sandstone at Apache Mesa (photograph by V.T. McLemore).

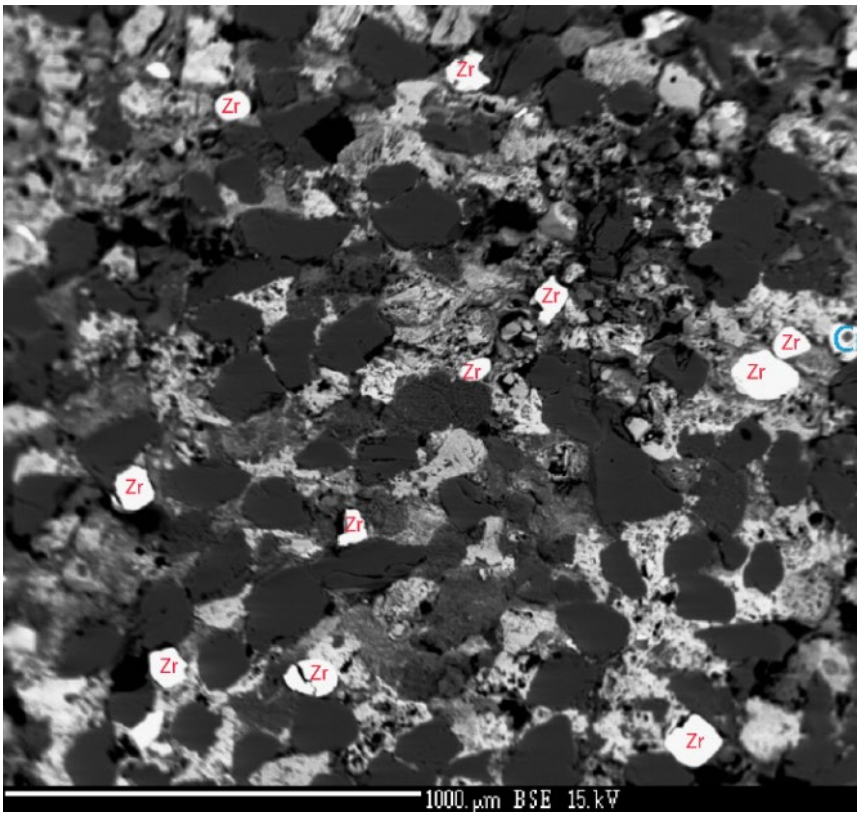

FIGURE 4.41 Electron microprobe picture of sample SL 16 (Apache Mesa). Zircon grains are labeled in red. Chromite is labeled in blue. Mottled, lighter colored cement is iron oxide (hematite). Dark grains are mainly quartz (photograph by A. Robisson).

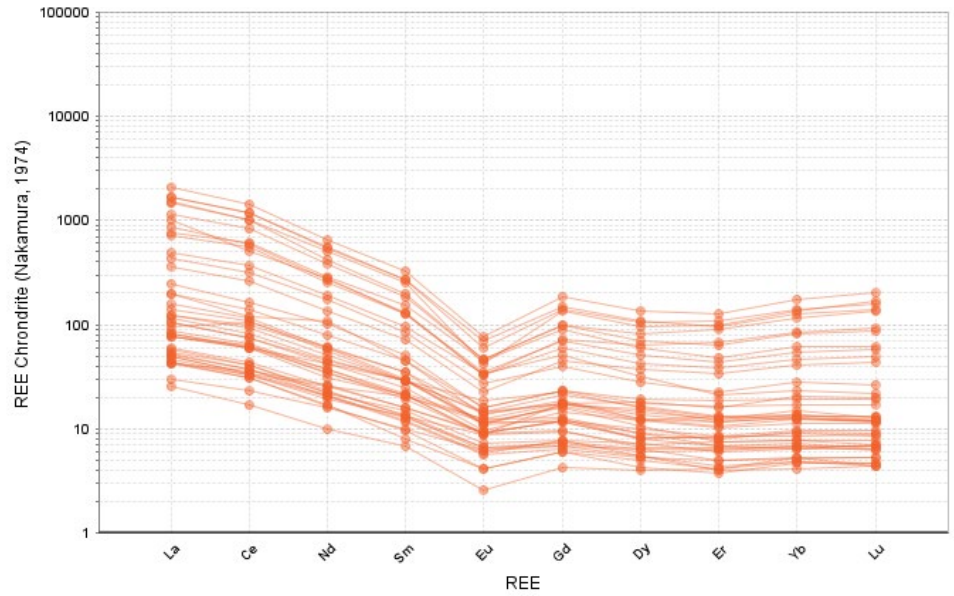

FIGURE 4.42 Chondrite-normalized REE plot of samples from the Apache Mesa. Chondrite values from Nakamura, 1974).

Pictured Cliffs Sandstone

The Pictured Cliffs Sandstone is a regressive shoreface sandstone that is up to 30 m thick and outcrops nearly around the entire periphery of the San Juan Basin (Fassett, 2000). The Pictured Cliffs conformably overlies the marine Lewis Shale and is overlain by the coal-bearing Fruitland Formation.

Farr Ranch (Star Lake), McKinley County (NMMK0060, 61, 62, 63)

The Farr Ranch deposits, in sections 13, 14, 15, 23, 25, and 26, T19N, R6W (Fig. 4.23, Table 4.23), are in the Pictured Cliffs Sandstone, which consists of an upper zone of thick beds of yellow-gray to gray-orange, cross-bedded, fine- to medium-grained, well sorted friable sandstone beds overlying a lower zone of alternating thin beds of yellow-brown to brown, fine-grained, sandstone to siltstone and gray to dark-gray shale (Scott et al., 1980). The heavy mineral, beach-placer sandstones are found in several beds forming low bluffs, up to 18 m thick, trending N60°W, and contain U, Th, REE, Ti, Fe, and Zn. One sample contained 10.23% TiO_2 and 12.98% Fe_2O_3 (Appendix 7). The largest deposit is approximately 1066 m long and 46 m wide (Murphy, 1956).

The Farr Ranch deposit (Fig. 4.43) lies on a 1.2-kilometer-long, northwest trending, southwest sloping mesa with a steep northeast face. 71 stations were surveyed over this deposit. The zones of highest radioactivity were located on the northwest-central portion of the mesa and reached 1200 cps. Similar to Flat Top Hill, lower elevations on the mesa corresponded with lower radioactivity, suggesting erosion of the mineralized sandstone.

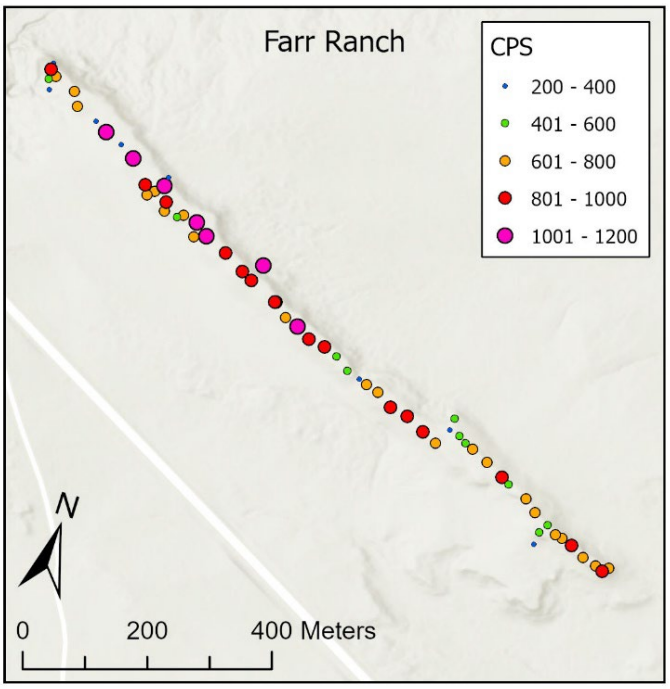

FIGURE 4.43 Geologic map of the Farr Ranch beach-placer sandstone deposits.

Barker Dome, San Juan Basin (NMSJ0002)

The Barker Dome deposits (also known as Airborne Anomaly 4), section 13, T31N, R14W (Fig. 4.23, Table 4.4) are in brown-gray Pictured Cliffs Sandstone. These deposits are less than 1 m thick and a few tens of meters long (Chenoweth, 1957). No chemical analyses are available for this deposit.

4.7.6 Characterization

Detailed characterization work focused on the Cretaceous beach-placer sandstone from Farr Ranch (Star Lake) in San Juan Basin, New Mexico. The sandstone placer deposit, Far2, is layered in mineral compositions alternating from dominantly quartz and feldspar with almost no zircon to ilmenite- and anatase-rich layer with abundant zircon (Fig. 4.44). The main heavy minerals present are zircon, ilmenite, hematite and anatase (Figs 4.45, 4.46). These mineralogical variations are accompanied by different concentrations of critical minerals. For example, the ilmenite- and anatase-rich layer have total REE ~2.85% whereas the quartz and feldspar layer has less than 0.2% (Fig. 4.47). Due to their similarly high densities, zircon, ilmenite, anatase and hematite are concentrated, leading to high concentration of critical minerals other than REEs, such as 1.2% Ni and 0.7% Zr.

The critical minerals distributions in sandstone were mapped using laser ablation-inductively coupled plasma-mass spectrometry (LA-ICP-MS) with a NWR193 laser unit connected to a Thermo Scientific TQ ICP-MS, and raw count rates were converted to concentration information using measurements of USGS standard samples (Fig. 4.48). The chemical compositions of minerals were further determined using LA-ICP-MS under spot mode (Fig. 4.49). As expected, there are large element variations on the ablated sample surface because

different minerals are rich in different sets of CMs. This information will guide the leaching and recovery strategy. As shown in Figure 4.49 iron oxides have the highest REE whereas ilmenite has high Nb, V, Mn, Zn contents.

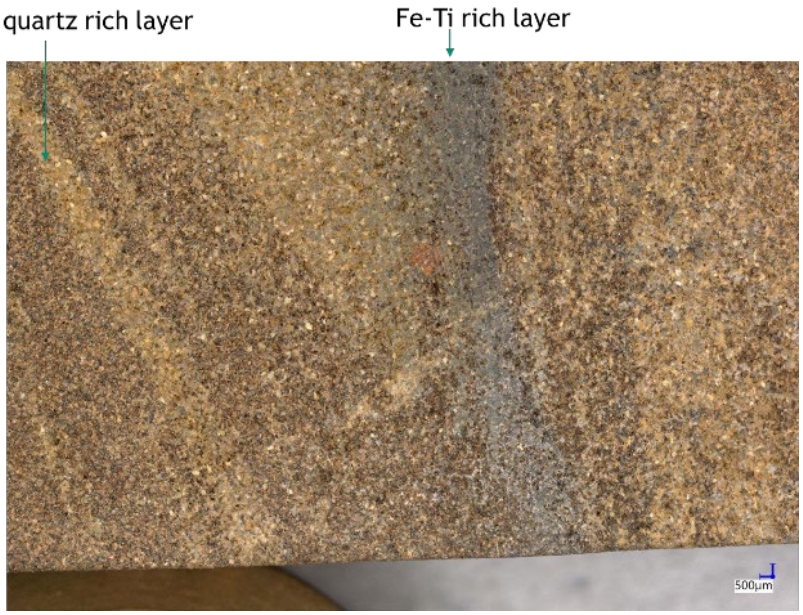

FIGURE 4.44 Layered mineralogy between quartz-rich layer (light color) and ilmenite + anatase rich layer (dark/grey color) for beach placer sample Far2.

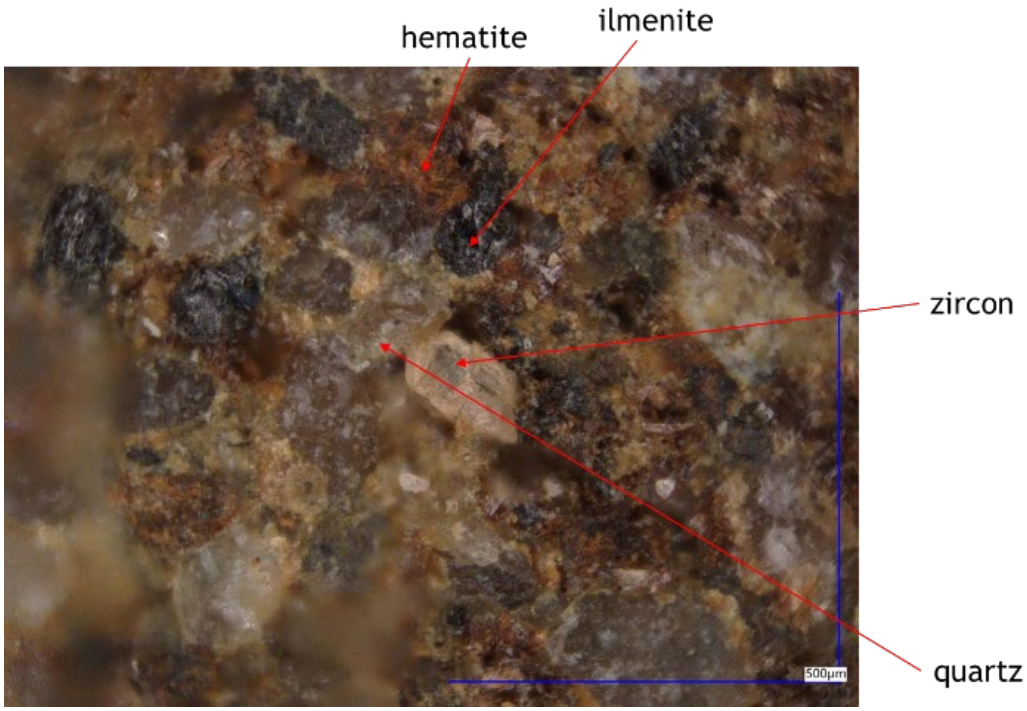

FIGURE 4.45 Major mineralogy components, quartz, ilmenite, hematite, zircon were identified using laser induced breakdown spectroscopy for beach placer deposit sample Far2.

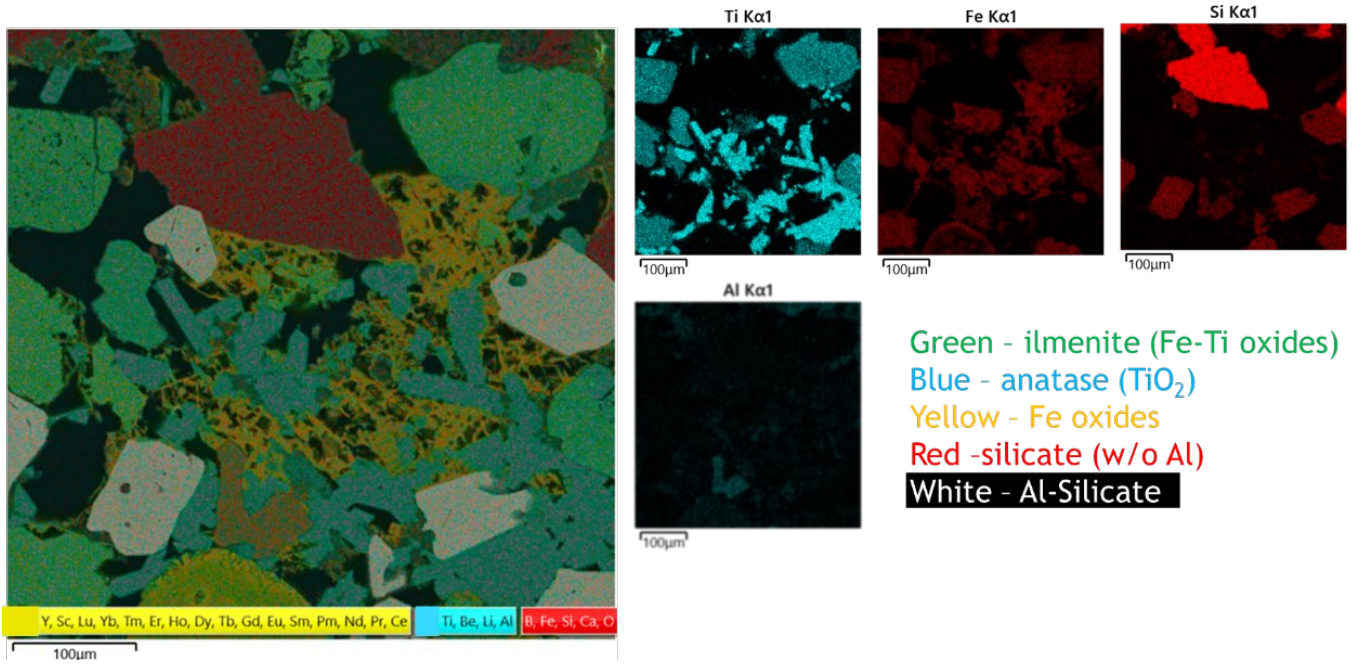

FIGURE 4.46 SEM EDX analysis for beach placer deposit sample Far2. Besides zircon, five endmember minerals were identified: qu3artz (in red color), ilmenite (in blue color), anatase (in blue color), iron oxides (in yellow color) and Al-bearing silicate, likely plagioclase and/or feldspar, in white-reddish color.

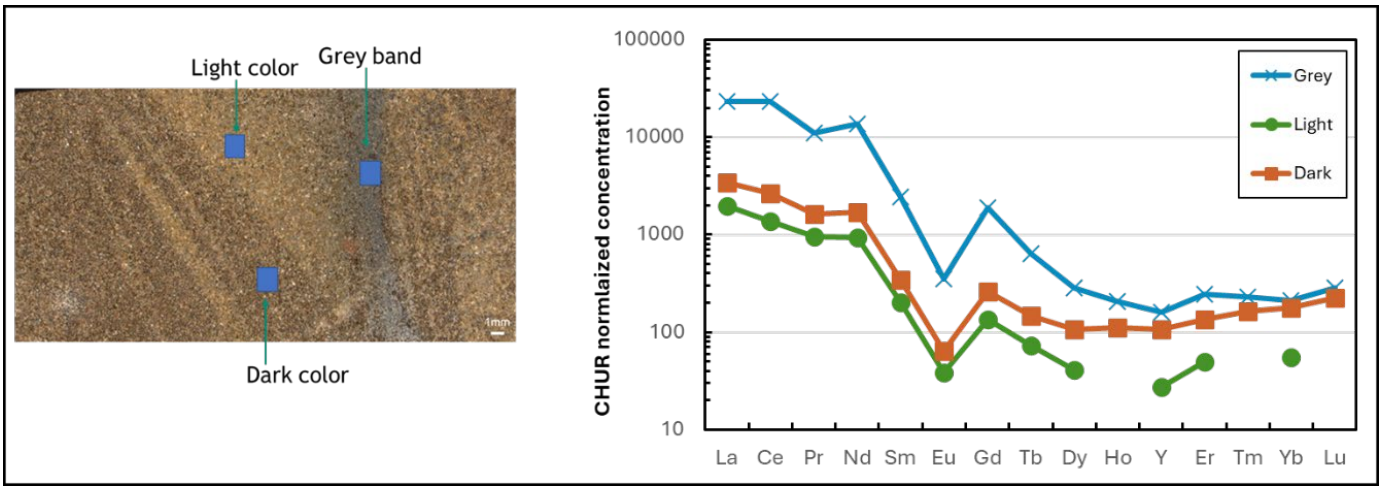

FIGURE 4.47 REE distribution patterns for ilmenite/anatase rich grey band, light color layer, and dark colored. Through localized sampling, the total REEs for these three locations are analyzed. The light color layer has total REEs 1984 ppm, dark color has 3820 ppm and grey band has 28,507 ppm.

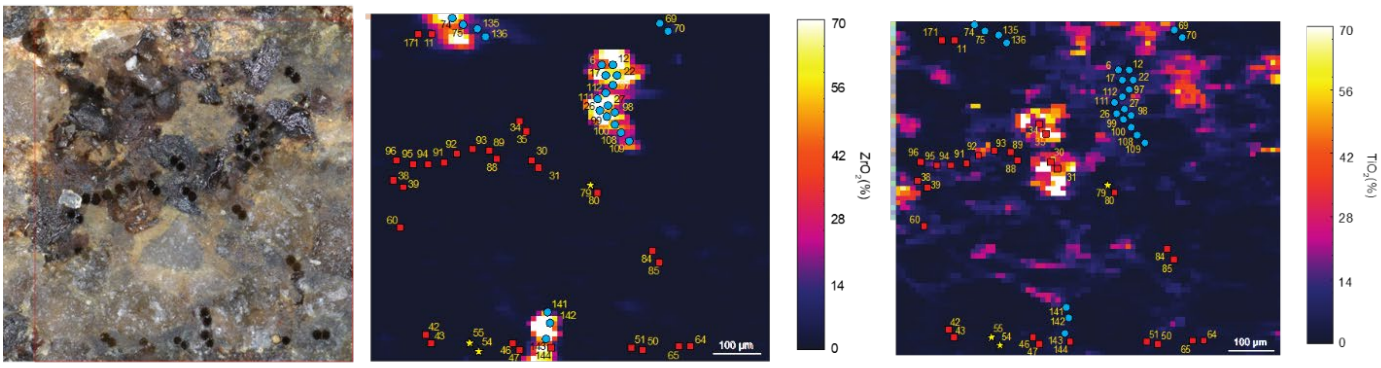

FIGURE 4.48 (left) optical image showing the laser holes after the LA-ICP-MS analyses for sample unpolished sample Far2. The middle and right panels are Zr and Ti distribution mapping. The blue/red/yellow labels are classified based on principal component analysis. The blue endmember is zircon.

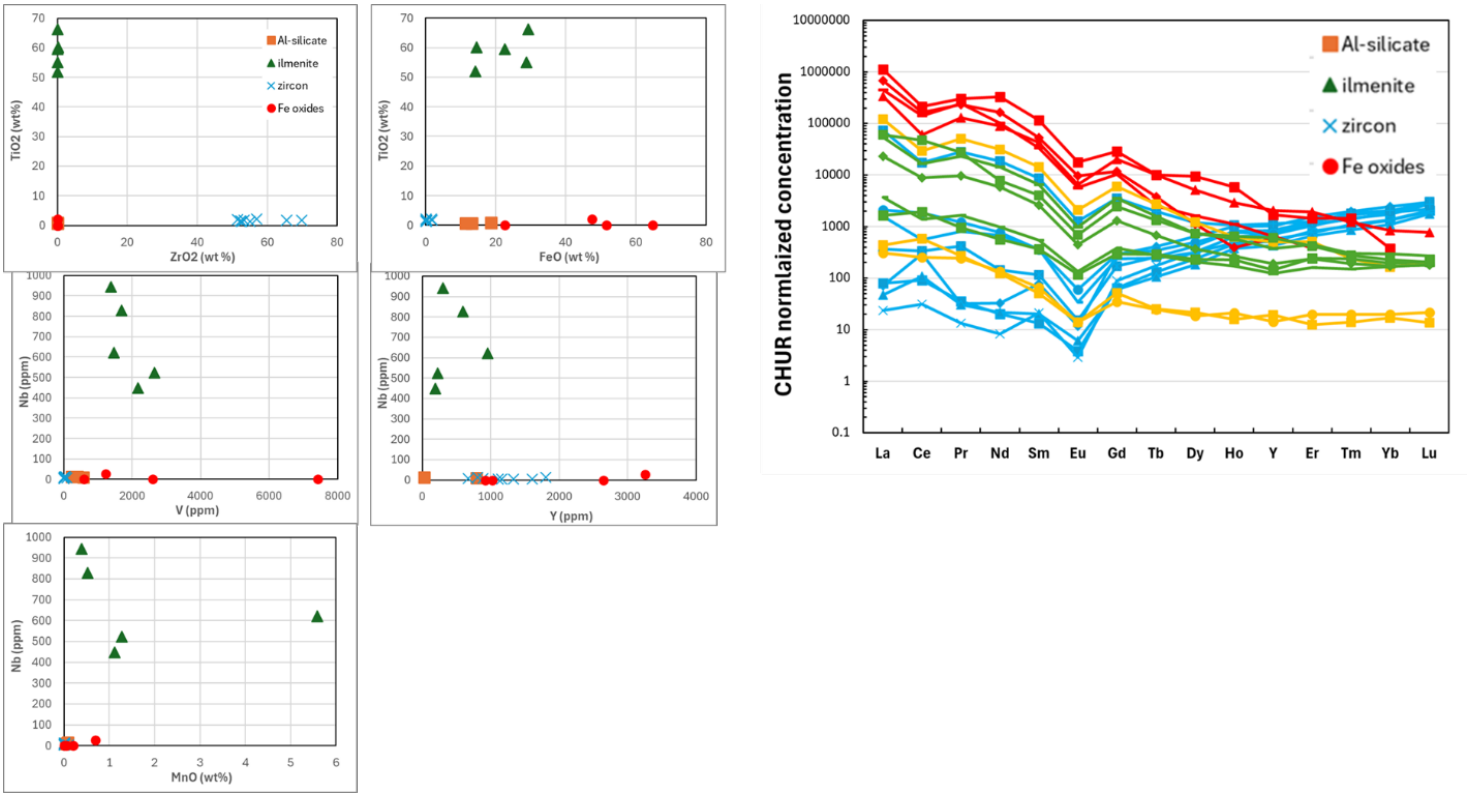

FIGURE 4.49 Critical mineral contents in four endmember minerals: zircon, ilmenite, Fe oxides and Al-bearing silicate for sample Far2.

4.7.7 Geochemistry

Chemical analyses of selected beach-placer deposits are in Appendix 7 and include new analyses as well as analyses reported in the literature. Descriptive statistics are in Table 4.7, including ranges in selected elements. Ti, Fe, Cr, Nb, Th, U, Zr, Sc, and REE (Fig. 4.50) are found in high concentrations in these deposits. Pierson correlation coefficients indicate strong

correlations (Table 4.7) between TiO_2, Cr, Nb, Th, Y, Zr, and REE (Fig. 4.51), which is consistent with the known mineralogy of the deposits, predominantly reflecting ilmenite, monazite, zircon, and other heavy minerals. Many of the beach-placer deposits likely contain monazite, since they are all radioactive and monazite is the primary radioactive mineral. The REE plots exhibit light-REE chondrite-normalized enriched patterns, typically with negative Eu anomalies (Fig. 4.50).

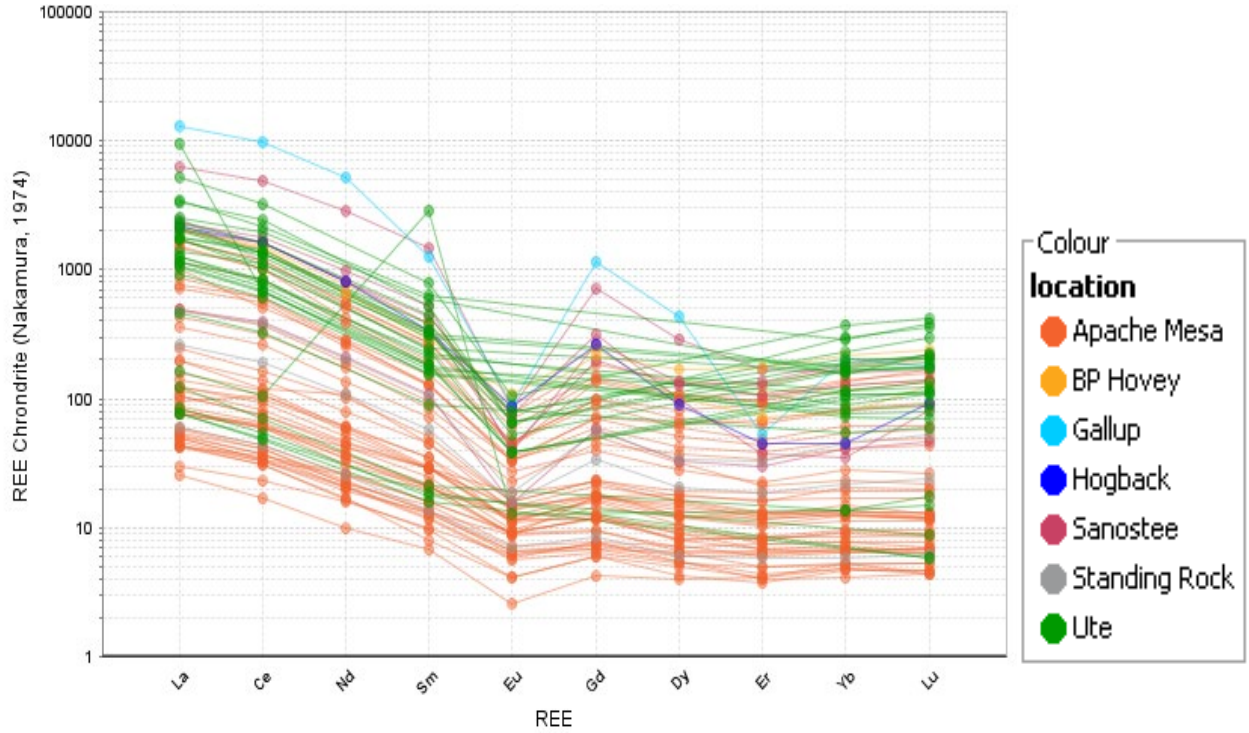

FIGURE 4.50 Chondrite-normalized REE plots of selected beach placer sandstone deposits. Chondrite values from Nakamura, 1974).

TABLE 4.7 Summary statistics of selected elements in beach-placer sandstones.

N=93	SiO_2%	Fe_2O_3T%	TiO_2%	Hf (ppm)	Th (ppm)	U (ppm)	Zr (ppm)	TREE+Y (ppm)
Minimum	4.67	0.30	0.08	1.4	2.44	0.9	43	47
Maximum	96.13	69.52	29.4	1630	>1000	179	>1000	14,041
Mean	58.99	19.47	5.42	176	129	20.9	3913	1473
Median	63.38	12.77	2.39	38.9	31.6	7.8	1730	502

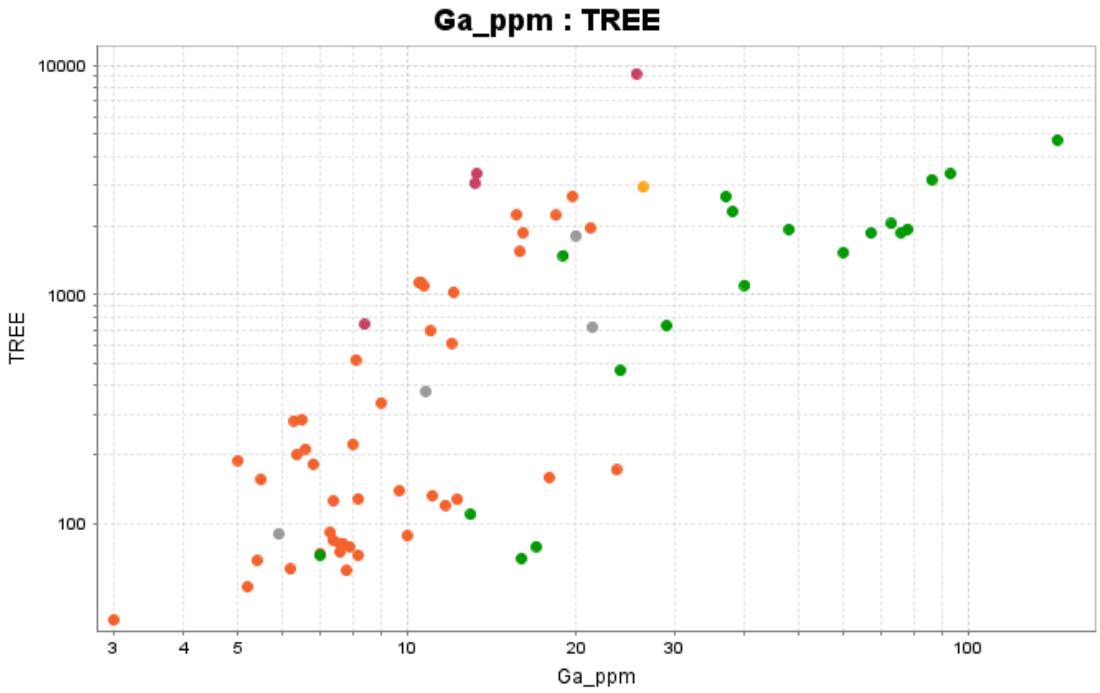
Ga_ppm : TREE
10000
1000
100
TREE
3
4
5
10
20
30
100
Ga_ppm

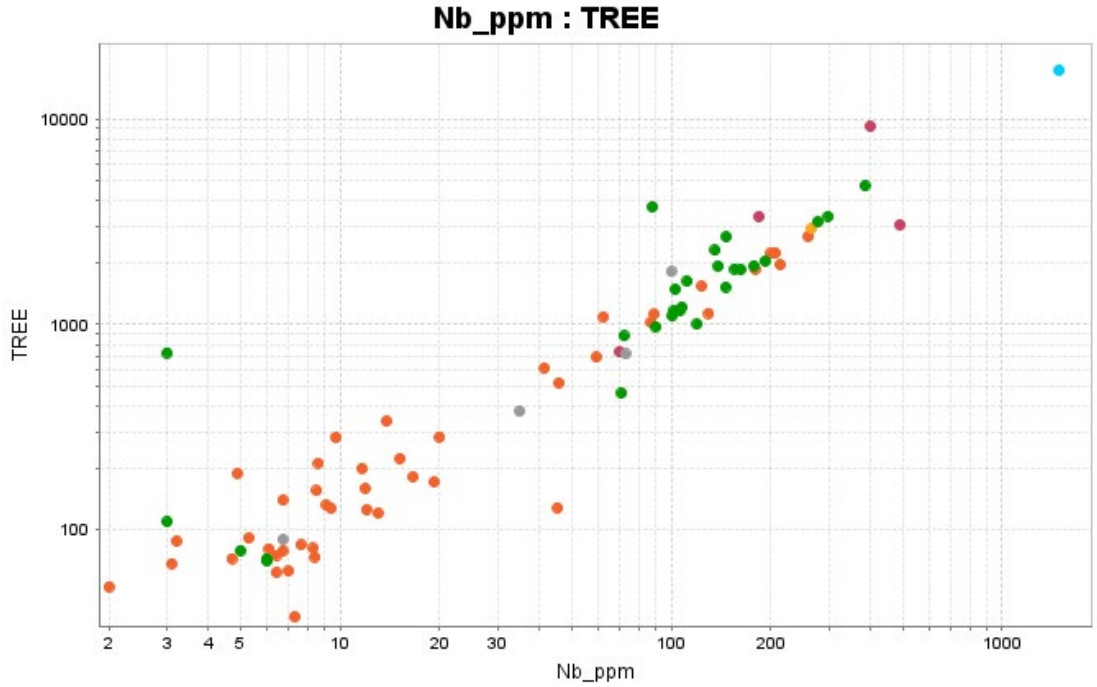
Nb_ppm : TREE
10000
1000
100
TREE
2
3
4
5
10
20
30
100
200
1000
Nb_ppm

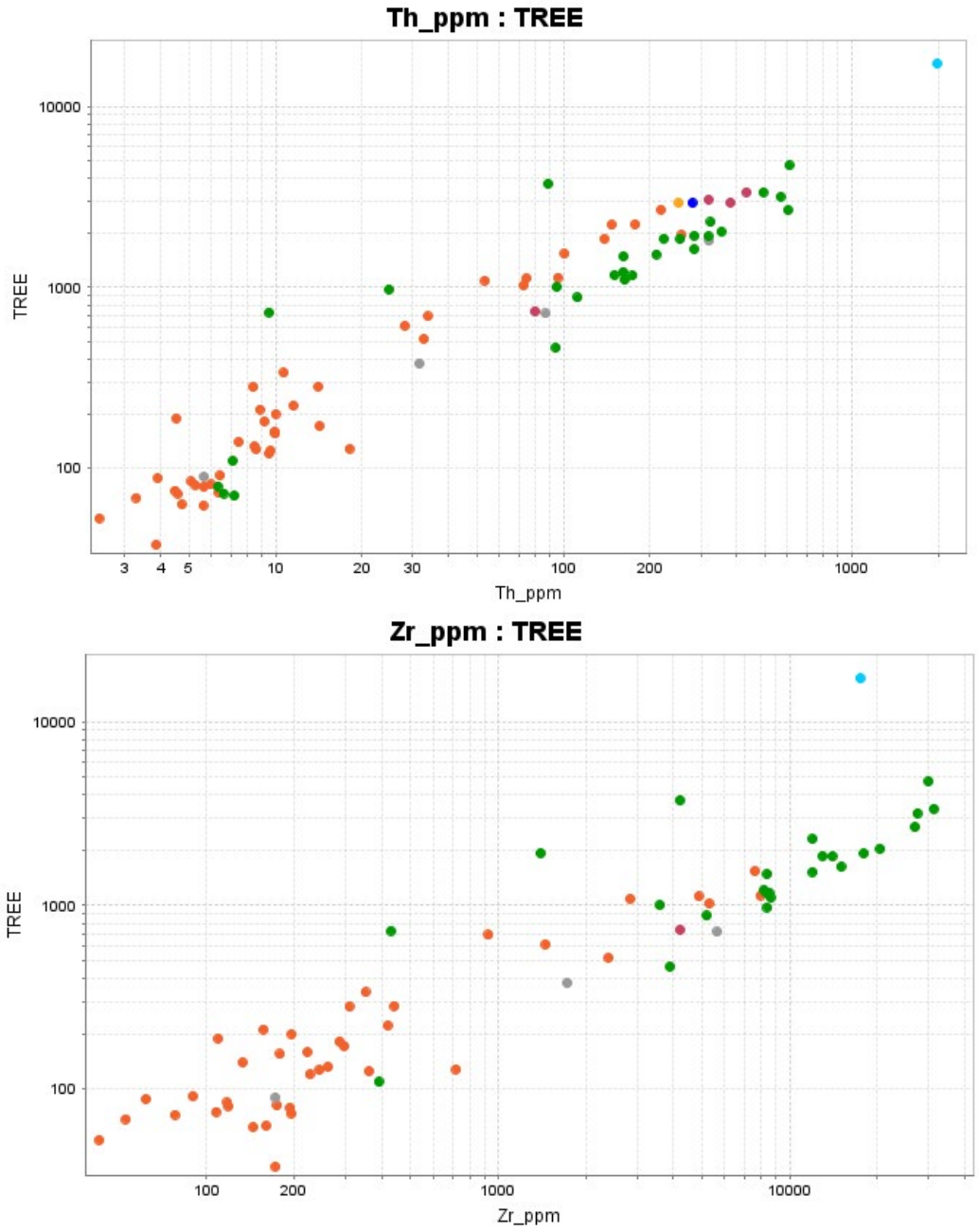

FIGURE 4.51 Scatter plots of various elements vs. total REE (TREE), showing the varability between deposits.

4.7.8 Relationship to coal deposits

The Cretaceous beach-placer sandstones in the western U.S. are typically underlain by nearshore marine sandstone and overlain by nonmarine fine-grained sandstone, carbonaceous shale, and coal (Houston and Murphy, 1977). Coal deposits overlie beach-placer sandstone deposits at Apache Mesa, New Mexico (McLemore et al., 2016) and in the Fox Hills Sandstone in Colorado (O'Keeffe et al., 2020).

4.7.9 Potential source terrains

The whole-rock geochemical compositions of the beach-placer deposits are consistent with a granitic and/or metamorphic source terrain. Proterozoic granitic rocks, including syenites are exposed in the Zuni Mountains on the southern edge of the San Juan Basin (Goddard, 1966; McLemore and McKee, 1989; Strickland et al., 2003) and could be a source if exposed during the Cretaceous. Dickinson and Gehrels (2009) determined the ages of detrital zircons found in Jurassic sedimentary rocks in the San Juan Basin and found that most of the detrital zircons were from basement rocks older than 285 Ma. Some researchers have suggested that Jurassic arc volcanism formed the Mogollon Highlands, south and west of the San Juan Basin, and this highland was the source of the Grants uranium in the Jurassic Morrison Formation (Fig. 4.52). This volcanic highland persisted into the Cretaceous and very well could have been a source of the heavy minerals in the beach-placer deposits in the San Juan Basin. Recycling of older sediments is likely. Detailed chemical analyses of the heavy minerals, such as ilmenite and zircon, within the beach-placer sandstone deposits are one method of determining the source of those minerals (Darby, 1984; Lloyd et al., 2005; McLimans et al., 2005). U-Pb dates of detrital zircons also aid in defining the source (Dickinson and Gehrels, 2009).

4.7.10 Origin of beach-placer sandstone deposits

The Cretaceous heavy mineral, beach-placer sandstone deposits discussed herein have many physical and chemical characteristics that are similar to modern beach-placers, including host rock, mineralogy, chemistry, and depositional environment (Houston and Murphy, 1970, 1977; Zech et al., 1994; Roy, 1999). These deposits formed by gravitational settling of the heavy minerals during wave action and currents that form beaches and offshore sand bars (Fig. 4.22; Houston and Murphy, 1970, 1977; Zech et al., 1994; Roy, 1999). The deposits in eastern Australia were formed during low rates of clastic supply and long periods of weathering and abrasion of beach deposits (Roy, 1999). Transgressive and regressive shoreline movements, such as occurred in Late Cretaceous time in the San Juan Basin area, result in the formation of extensive shoreface-sandstone deposits covering thousands of square kilometers. Once the shoreface sandstone deposits are deposited, they are covered by continental deposits, which preserves them unless later erosion exposes them. In examination of titanomagnetite placer deposits along the coast of New Zealand, sorting by size rather than weight appeared to be more important in concentrating the heavy minerals (Bryan et al., 2007). The heavy minerals tend to concentrate in the upper 30 m of the beach, decreasing in concentration seaward. In the seaward region, the undertow removed the finer and lighter minerals, whereas in the landward region, wind transported the finer or lighter minerals away. Riptides and undertow currents erode beach deposits and subsequently remove the lighter minerals, leaving the heavier minerals behind. The Srikurmam ilmenite placer deposit in Andhra Pradesh area in India is confined between two major rivers (Rao et al., 2008) and local drainages could have controlled the formation of beach-placer deposits in New Mexico. Destruction and reworking of older beach-placer deposits can occur only until they are covered by continental deposits.

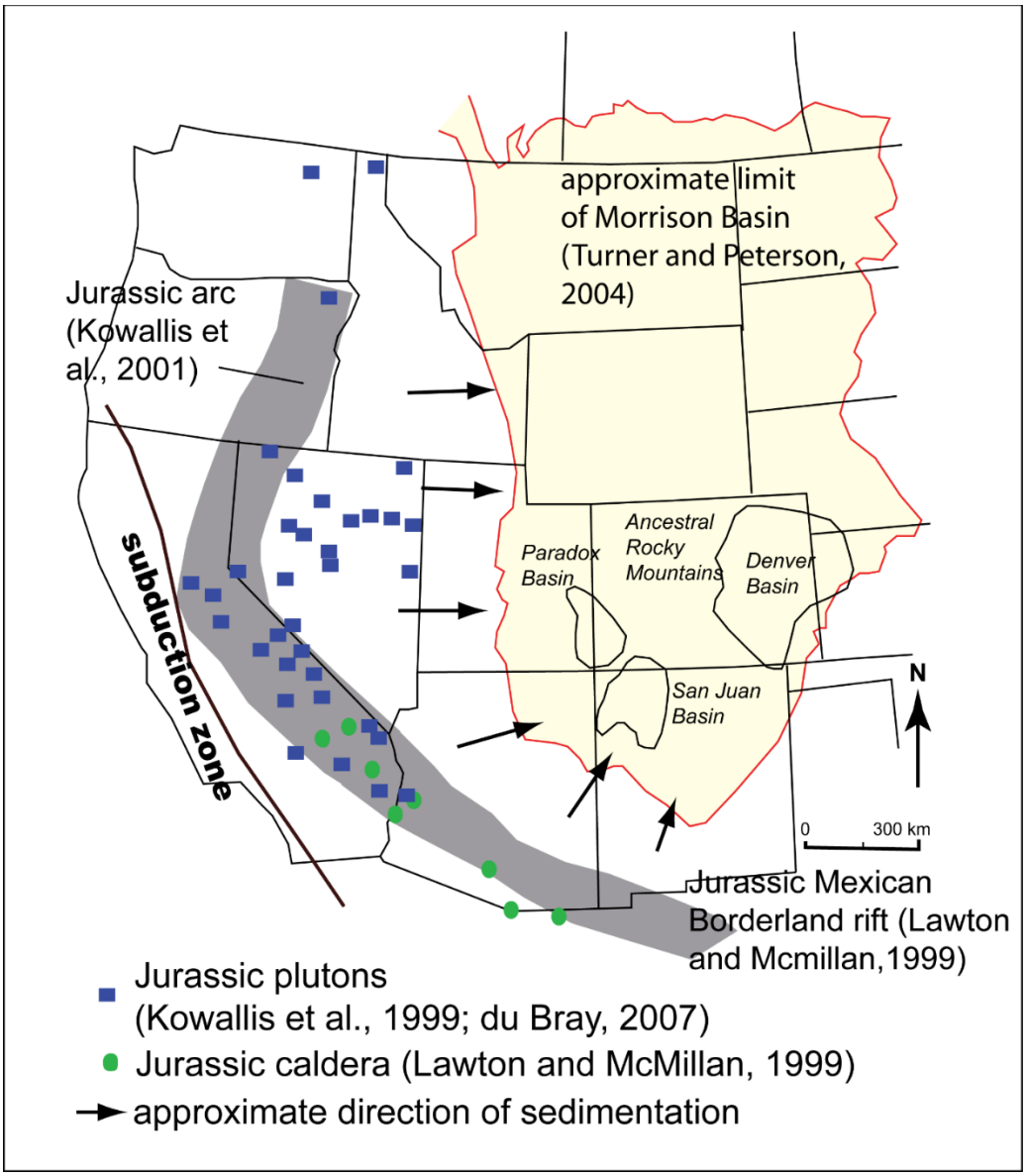

FIGURE 4.52 Approximate location of the Jurassic arc in relation to the Morrison Basin. This arc provided a highland consisting of granitic rocks that could have been a source for the Cretaceous beach-placer sandstone deposits in the San Juan Basin. Modified from Lawton and McMillan (1999), Kowallis et al. (1999, 2001), Turner and Peterson (2004) and du Bray (2007).

4.7.11 Mineral-resource potential

Many beach-placer sandstone deposits in the San Juan Basin contain high concentrations of Ti, Zr, REE, U, Th, Nb, Ta, Fe, Sc, Y, and other elements (Table 4.7, Appendix 7). Selected geochemical analyses are in Appendix 7 and McLemore (2010); maximum values for selected elements are in Table 4.7. Many of the deposits are on Indian reservation land. Additional deposits probably remain undiscovered in the San Juan Basin; at least three drill holes are suspected of having similar deposits (Chenoweth, 1957).

Titanium-bearing minerals (ilmenite, rutile, leucoxene) are the more important economic minerals in these heavy mineral, beach-placer sandstone deposits and TiO_2 is used in pigments (i.e. coatings and paints, plastics, cosmetics, textiles, glazes, etc.), metal alloys, and other applications. A titanium resource typically contains 1% or more ilmenite or rutile at recoverable grain size, typically in unconsolidated deposits (Force, 2000). Zirconium, REE, and Fe could be by-product minerals. Titanium is found in the San Juan Basin deposits in ilmenite, titanomagnetite, titanohematite, rutile, anatase, and brookite. Much of the ilmenite is either altered partially to hematite or is in solid solution series with hematite, which complicates processing (Force et al., 2001). Titanium varies in concentration from 16% to 32% in the San Juan Basin deposits (Appendix 7; Chenoweth, 1957; Zech et al., 1994). Force (2000) estimated the contained titanium resource of the Sanostee deposit as 700,000 metric tonnes of Ti ore and does not consider any other deposit in New Mexico to have any resource potential because of small size and low grade. These deposits need further drilling to fully evaluate their potential, considering today's economic market.

Zirconium is another potentially important economic element and is mostly found in zircon and, locally ilmenite. It is used in abrasives, ceramics, refractories, foundry applications, welding rod coatings, nuclear fuel industry applications, and other applications. Most of the deposits in the San Juan Basin contain zircon, which could be recovered for some applications only as a by-product. Impurities in zircon that could be recovered include Th, U, REE, and Hf.

Modern beach-placer sand deposits in Australia, India, South Africa, and the U.S. contain 0.1-2% monazite and are mined for REE (Morteani, 1991). In the San Juan Basin deposits, the REE are mostly found in monazite, although apatite, zircon, sphene, xenotime, allanite, and epidote also contain minor amounts of REE. However, the grades and tonnages of the San Juan Basin deposits are currently too low compared to commercial deposits (Table 4.5, 4.7), but the REE could be recovered as by-products, especially if the deposits contain higher concentrations of a specific high-value REE (McLemore, 2010).

Uranium and Th are typically found in anomalously high concentrations in heavy mineral, beach-placer sandstone deposits (Table 4.7), but the concentrations are not of economic values today. Most of the U and Th in the San Juan Basin deposits are in zircon and monazite, although U and Th also are found in apatite and iron oxide minerals (Zech et al., 1994). Uranium is used mostly as fuel for nuclear power plants and, if the technology is developed, Th also could be become commercially viable as a fuel for nuclear power plants.

Niobium and Ta also are found in some of these deposits and could be recovered as a by-product. Gold was found in small amounts in the samples collected in this study, by McLemore et al. (2016), and reported by Zech et al. (1994) and could be economic as a by-product. Although Zn is found in high concentrations in the samples reported by Zech et al. (1994), probably in magnetite and other iron-oxide minerals, the values are not of economic importance. Chromium is found in high concentrations, probably in ilmenite and magnetite, however the high Cr concentrations can adversely affect the milling process (Zech et al., 1994). Scandium is found in elevated concentrations, which could be recovered only as a by-product of other production. Garnet is found in many of the deposits, but the garnet is generally too small in grain size and in low concentrations to be considered economic.

4.7.12 Concluding remarks

It is unlikely that any of the heavy mineral, beach-placer sandstone deposits in the San Juan Basin will be mined in the near future because of small tonnage, low grades, high degree of cementation through lithification, high iron content, and distance to processing plants and markets. The Energy Fuels uranium mill in Blading, Utah is recovering REE from modern beach placer sandstone deposits. However, as the demand for some of these elements increases because of increased demand and short supplies, the dollar value per ton of ore may rise, enhancing deposit economics. Mapping and exploration drilling of some of these deposits, especially the Sanostee deposit and the deposits on the Ute Mountain Ute Indian Reservation in the northern San Juan Basin could be warranted to fully evaluate the economic potential. Ultimately, economic potential will most likely depend upon production of more than one commodity. Not only do these deposits represent potential future economic resources, they also help define local depositional trends of the Cretaceous beaches. Potential sources of these deposits include Proterozoic granitic and metamorphic rocks, such as those found in the Zuni Mountains, the Jurassic arc volcanism and magmatism forming the Mogollon Highlands to the south and west, and recycling of older sediments.

4.7.13 Future work

Beach-placer sandstone deposits are generally overlain by nonmarine fine-grained sandstone, carbonaceous shale, and coal deposits. These placer deposits could provide REE and other critical minerals resources in addition to the REE and critical minerals in nearby coal deposits. Furthermore, the placer deposits could provide supporting evidence for identifying source areas for both the placer and coal deposits. Age determinations of heavy minerals within the deposits, such as zircon and monazite, also will aid in defining their source area.

Preliminary examination of the NURE stream-sediment data revealed numerous single-element geochemical anomalies of Zr, Ti, REE, Sc, and Th scattered throughout the San Juan Basin; these areas need to be examined and sampled. Chenoweth (1957) identified three wells drilled for oil or gas with gamma anomalies in the Cretaceous sandstones, suggesting that these could be buried heavy mineral, beach-placer sandstone deposits. Further detailed examination of other geophysical logs of wells is needed to locate potential deposits.

4.8 Critical minerals potential of clinkers (D. Shaver, G. Xu, and V.T. McLemore)

4.8.1 Introduction

Clinkers in the San Juan Basin are formerly sedimentary rocks that have undergone alteration after deposition (Shaver, 2025). They surround coal seams and have undergone pyro-metamorphization after exposure to extreme temperatures due to natural burning of coal. Coal seams would catch fire at exposed surfaces through various means, such as spontaneous combustion, the result of the oxidation of pyrite, natural wildfires or lightning strikes igniting the exposed coal. The fires spread extensively underground, burning up to temperatures of 1000°C (Cosca et al., 1989) and drawing oxygen through fractures in the rock. The intense heat from the fires burn organic material from the surrounding sedimentary units, as well as melting silicates and clay minerals to form glasses. Iron minerals in the sedimentary rocks oxidizes, giving the

rocks a reddish orange to yellowish appearance, dependent on which iron mineral is present (Fig. 4.53, 4.54, 4.55, 4.56). The chemical makeup of these rocks has never been extensively studied until now since they are being examined as a potential resource for REE and critical minerals due to their proximity to large coal deposits.

FIGURE 4.21 Clinker sample from El Segundo mine (photograph by D. Shaver). Note the red coloration indicating the presence of iron oxides.

FIGURE 4.54 Sampling a clinker deposit at El Sequndo mine (photograph by V.T. McLemore).

FIGURE 4.55 Clinker deposit in the San Juan Basin, mine for road aggregate (photograph by S.L. Rodolph, 1/13/2023).

FIGURE 4.56 Clinker deposit in the San Juan Basin, mine for road aggregate (Photograph by S.L. Rodolph, 1/13/2023).

Clinker deposits in the San Juan Basin are Late Cretaceous in age and are associated with the Menefee and Crevasse Canyon formations of the Mesa Verde Group, and the Fruitland Formation (Speer and others, 1977), where the most abundant coal formations in the San Juan basin are found. The most common rocks found in these formations are medium- to fine-grained sandstones and very fine-grained mudstones and shales. The lithologies present with the coal seams vary depending on what geological depositional processes were going on in that area. The most common rocks are sandstones to shales. The clinkers themselves are sedimentary rocks near coal seams that caught fire and burned underground, causing pyro-metamorphization that had varied effects depending on the rocks and temperatures they were exposed to. Some clinkers only underwent low temperature exposure, estimated to be 400-500°C and resulting in the removal of organic material and oxidation of iron oxide minerals (Fig. 4.57). Other samples were heavily affected, undergoing temperatures of 1000°C and partially melting, resulting in high glass contents and glassy minerals like cristobalite forming, taking on a bubbly slag like texture, on the verge of becoming paralava rocks (Fig. 4.57) (Hoffman,1996). However, the exact conditions that cause the formation of clinker are currently not fully understood, as the time frame of how long these rocks were exposed to high temperatures is not known.

FIGURE 4.57 Sample COAL274, showing partially melted high temperature clinker, transitioning from clinker to paralava (photograph by D. Shaver).

Industrially, San Juan Basin clinkers have been used as aggregates for road and drainage usage due to their availability and ease of use in the San Juan Basin. Clinkers are used as cement additives and aggregates for roads in areas where other aggregates are less common and clinker is more readily available (Hoffman 1996, Permutrade, 2023), for use in construction, and some specific clinkers are refined down to powders as additives for glass and metal working processes (Wilson et al., 2018).

4.8.2 Mapping of clinkers

Clinker deposits in the San Juan Basin were mapped through ArcGIS mapping software by digitizing coal resource maps, and total reserves were estimated by calculating estimated volume and using measured specific gravity (Fig. 4.58). A list of all digitized maps is available (Table 4.8) and all were sources from the USGS Warehouse database. Data on some areas of the San Juan Basin coal fields was not available so clinker resources in these areas were not able to be mapped and estimated.

TABLE 4.8 ArcGIS georectified quadrangle maps of coal resources.

Quadrangle	Year	Open File report
Cuba	1985	79-623
San Pablo	1985	79-634
La Ventana	1985	79-1038
Headcut Reservoir	1985	79-1043
San Luis	1985	79-1044
Arroyo Empedrado	1985	79-1045
Wolf Stand	1985	79-1045
Tinian	1985	79-625
Canada Calladita	1985	79-626
Cerro Parido	1985	79-627
El Dado	1985	79-634
Mesa Cortada	1985	79-629
Mesita del Gavilan	1985	79-630
Rincon Marquez	1985	79-631
Whitehorse Rincon	1985	79-632
Mesita Americana	1985	79-633
Cerro Alesna	1985	79-635
San Luca Dam	1985	79-636
Piedra de la Aguila	1985	79-1039
Hospah	1985	79-637
Whitehorse	1985	79-1040
Seven Lakes NE	1985	79-638
Kin Nahzin Ruins	1985	79-639
Orphan Annie Rock	1985	79-1041
Mesa De Los Toros	1985	79-1122
Laguna Castillo	1985	79-640
Seven Lakes	1985	79-1042
Seven Lakes NW	1985	79-1123
Kin Klizhin Ruins	1985	79-1047
Nose Rock	1985	79-641
Heart Rock	1985	79-642
Crownpoint	1985	79-1125
Milk Lake	1985	79-1377
La Vida Mission	1985	79-1378
The Pillar 3	1985	79-1379
Red Lake Well	1985	79-1380
Standing rock	1985	79-1381
Oak Spring	1985	80-27
Hard Ground Flats	1985	80-28
Big Rock Hill	1985	80-29
Twin Lakes	1985	80-30
Tse Bonita School	1985	80-31
Samson Lake	1985	80-32
Gallup West	1985	80-33
Gallup East	1985	80-34
Bread Springs	1985	80-35
Manuelito	1985	80-36
Borrego Pass	1985	80-37
Casamero Lake	1985	80-38
Twin Buttes	1985	80-39
Pinehaven	1985	80-40
Upper Nutria	1985	80-41

Clinker outcrops follow closely established coal seams and can be used as an exploration tool to locate coal seams. If a clinker formation is found, coal was at one point present at that location before burning. Due to how small clinker outcrops typically are, with the largest measured clinker outcrop only reaching several hundred meters in size, it can be assumed that more coal resources nearby.

4.8.3 Estimated endowment

Clinkers are relatively small with the largest outcrops only a few hundred meters in length at most (Fig. 4.59). Samples were measured for specific gravity (Table 4.9).

SG=(Mass sample/volume sample)/(mass water/volume water)

With an average calculated specific gravity of 1.922 g/cm^3, the values of estimated endowment can be calculated by multiplying the gravity against the measured area of clinker that was mapped and the estimated thickness of the clinker deposits.

ore volume (V) = area x avg thickness
ore tonnage (kg)= V x Density factor/specific gravity)

An endowment of 12,524,000 tonnes of clinker was estimated for 1-meter-thick beds, a value that can double and triple depending on thickness of clinker layers present.

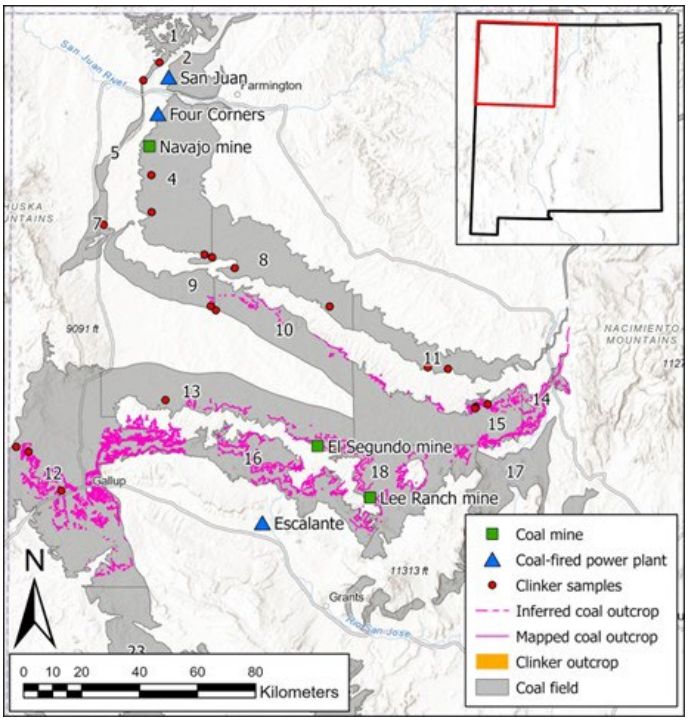

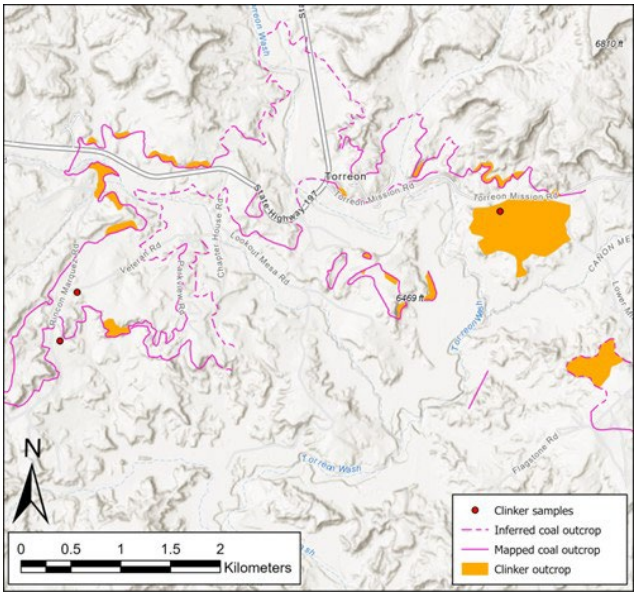

FIGURE 4.58 Top figure showing outcrops of digitized coal deposit quadrangle maps of the San Juan coal fields using Arc GIS (top 1=Barker Creek, 2=Fruitland, 3=Monero, 4=Navajo, 5=Hogback, 6=Tierra Amarilla, 7=Toadlena Area, 8=Bisti, 9=Newcomb, 10=Chaco Canyon, 11=Star Lake, 12=Gallup, 13=Standing Rock, 14=La Ventana, 15=Chacra Mesa, 16=Crownpoint, 17=Mt. Taylor, 18=San Mateo, 19=Rio Puerco, 20=Cerillos, 21=Hagan, 22=Zuni, 23=Salt Lake, 24=Datil). Bottom figure showing clinker samples and outcrops.

FIGURE 4.59 View of black coal transitioning to red clinker (sample COAL9c, photograph by V.T. McLemore).

TABLE 4.9 Specific gravity results of clinker samples.

Sample Name	A: Dry Weight (g)	B: Wet Weight (g)	C: Submerged Weight (g)	Gs: Specific Gravity
COAL 138	1991.5	2159.0	1143.7	1.96
COAL28	1985.5	2166.5	1183.5	2.02
COAL36	1999.5	2082.0	1129.4	2.10
COAL 140	1828.5	1904.5	859.4	1.75
COAL 102	1969.0	2157.0	1050.1	1.78

4.8.4 Critical minerals in clinkers

Clinkers and associated sedimentary rocks from the San Juan Basin exhibit minor REE enrichment with slight preferences for LREE relative to HREE values (Fig. 4.60). The composition of clinkers overlaps that of adjacent sedimentary rock types, especially clay, shale, and sandstone, indicating little to no difference between the clinkers and the unaltered rocks.

Comparing chemistry of clinkers to Average Upper Crust for Sedimentary Rock concentrations, some of the critical minerals and REE concentrations are enriched or depleted (Fig. 4.61). Clinkers and San Juan sedimentary rocks are moderately enriched in REE in comparison to established average upper crustal concentrations. Similar comparisons for REE can be made between the clinker and adjacent strata using the Average European Shale values

(Fig. 4.62); most samples of both clinkers and San Juan sedimentary strata are depleted in comparison to established European Shale values.

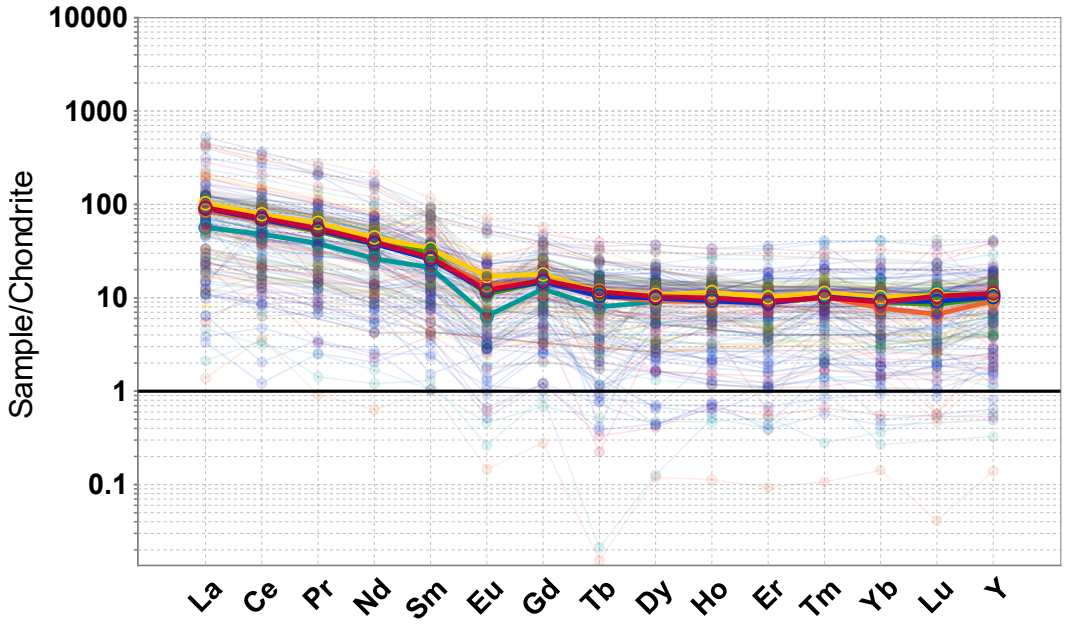

FIGURE 4.60 Chondrite-normalized patterns of clinkers and adjacent sedimentary rock samples. REE of clinker samples overlap the sedimentary rocks from the same region. Blue = Coal. Red = Clinker, Orange = Clay, Green = Humate, Yellow = Sandstone, Teal = Shale. Chondrite values from Taylor and McLennan (1985).

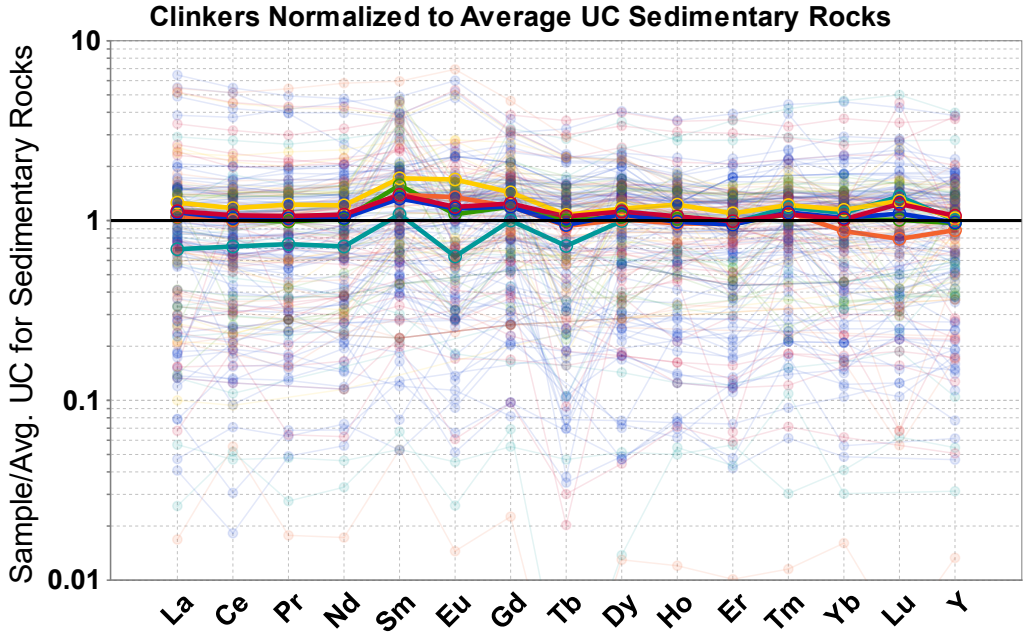

FIGURE 4.22 REE plot of clinker samples normalized to Average Upper Crust for Sedimentary Rocks.

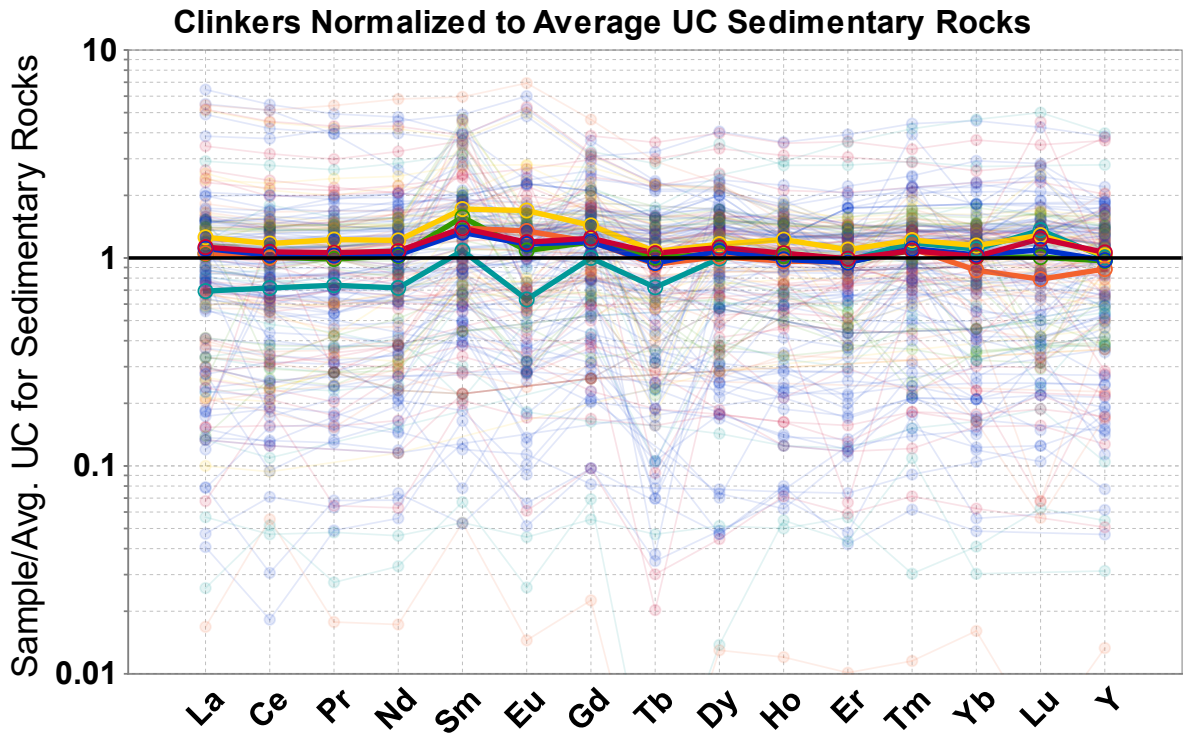

FIGURE 4.62 REE in clinker samples normalized to Average European Shale.

The highest measured REE concentration in clinker rocks is relatively low with only 639 ppm TREE, however a positive correlation occurs between Al_2O_3 and TREE, which suggests that REE may be found in or absorbed onto clay minerals. However, due to the low concentrations detected and relative lack of other minerals seen in clinkers, these rocks are probably not a source of critical minerals and would not be economic to exploit. Chemical analysis shows that clinkers do not contain economic values of REE or critical minerals, and the REE values that are present are mostly dependent on the original rock type of the clinker before it underwent pyro-metamorphosis. The concentrations of most clinkers are below cut-off grades and recommended exploration thresholds (Table 4.3). They are likely to remain an inexpensive aggregate resource in areas where they are present and as an industrial additive in some cases.

4.8.5 Petrography

Sample Coal9 is a clinker that has been subjected to detailed petrography, XRD and SEM study (Appendix 11). The primary minerals identified by XRD are quartz (64.4%), feldspar (plagioclase, 18.5%), hematite (8.4%,) Fe-Ti oxides and TiO_2 (8.7%) (Figs. 4.62, 4.63, 4.64). Coal 9 has total REE of 343 ppm, presumably contained in hematite and/or Fe-Ti oxides including TiO_2. The leaching test in section 5 shows that majority of REEs cannot be recovered with citric acid.

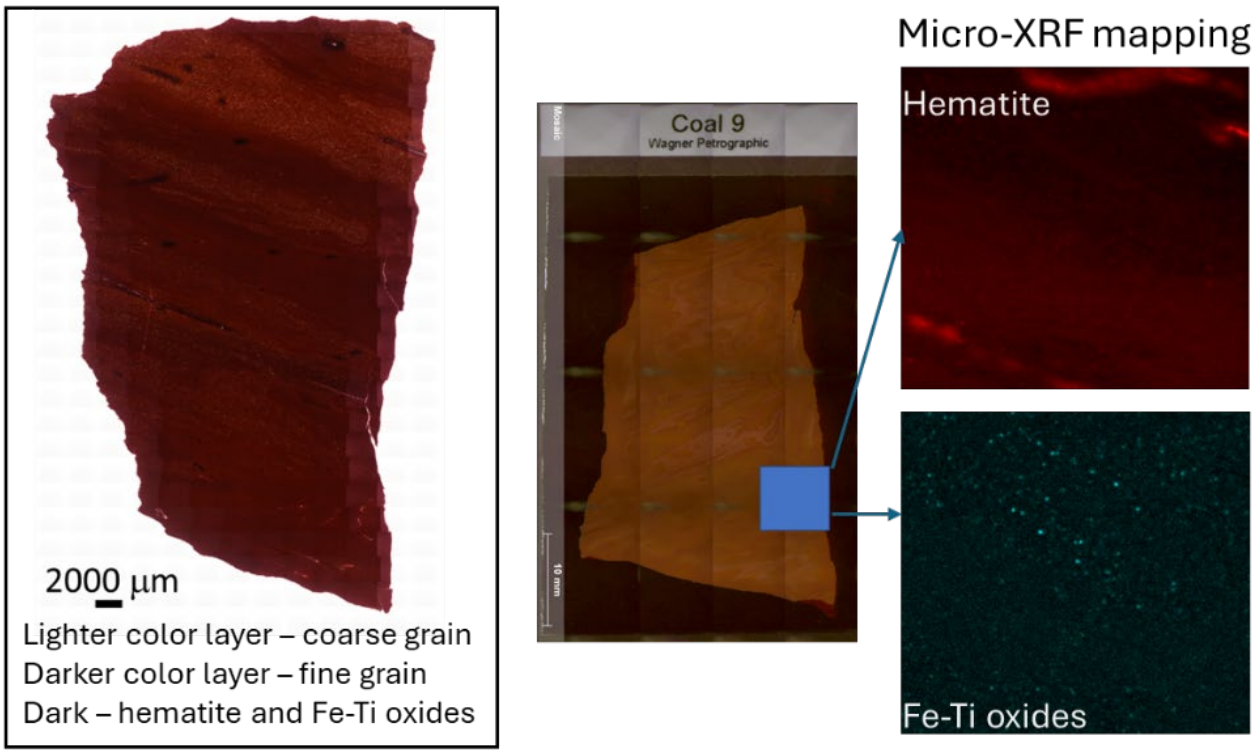

FIGURE 4.63 Coal 9 petrography images and micro-XRF mapping the distribution of hematite and Fe-Ti oxides.

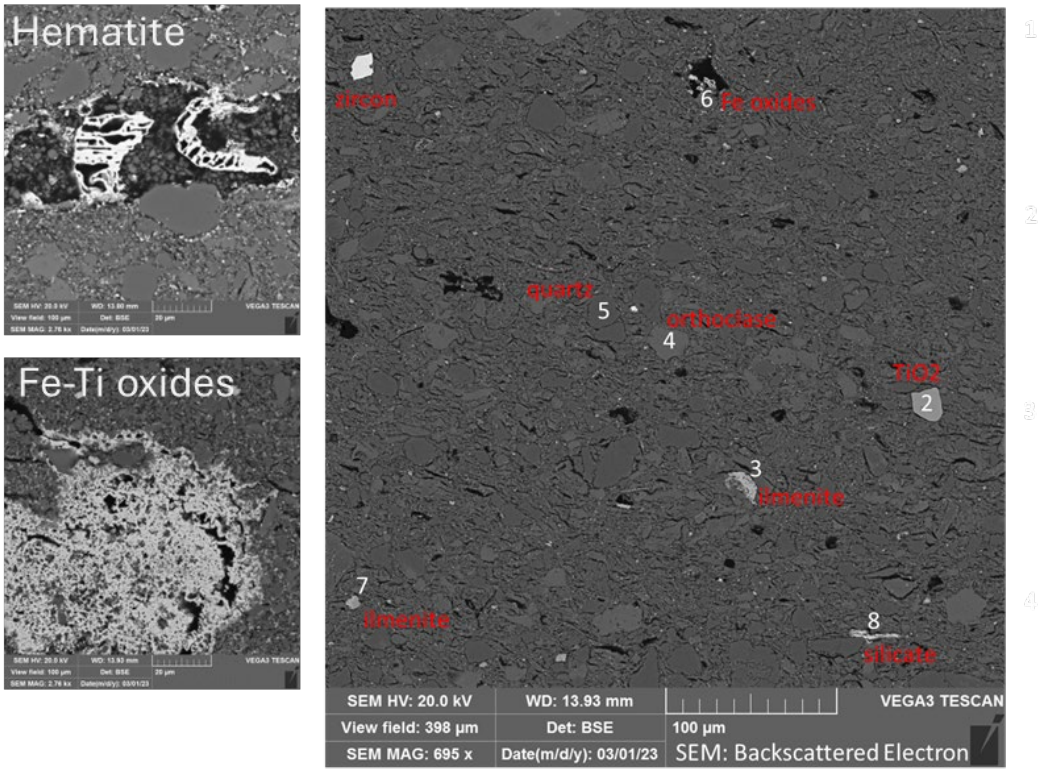

FIGURE 4.64 Coal 9 SEM images showing hematite, Fe-Ti oxides and anatase.

4.9 Critical minerals potential of clays (V.T. McLemore and G. Xu)

Clays were collected throughout the San Juan and Raton basins (Appendix 7), especially if found beneath coal seams (Fig. 4.65). Clay samples also were collected from the Popotosa Formation near Socorro (Fig. 4.66), where Li concentrations were reported and from the Kline Mountain kaolinite deposit in the Black Range, Sierra County (Appendix 7). The concentrations of most critical minerals in clay samples are below the below cut-off grades and recommended exploration thresholds (Figs. 4.67, 4.68, 4.69, Appendix 7, Table 4.3). Additional clay samples will be collected in phase 2, if funded.

Detailed petrography, CT and SEM analyses were performed for sample Pop1, which has > 563 ppm total REEs and more than 10,000 ppm Sr. The detailed reports are in Appendix 11. CT images show the linear feature of the high-density mineral, which is identified as a mixture sulfate and phosphate (Figs. 4.70, 4.71) that are hosting Sr.

FIGURE 4.65 Underlay beneath clinker in San Juan Basin (sample Coal10b, photograph by V.T. McLemore).

FIGURE 4.66 Clay from Popotosa Formation, Sevellita Wildlife Refuge (sample Pop1, photograph by V.T. McLemore).

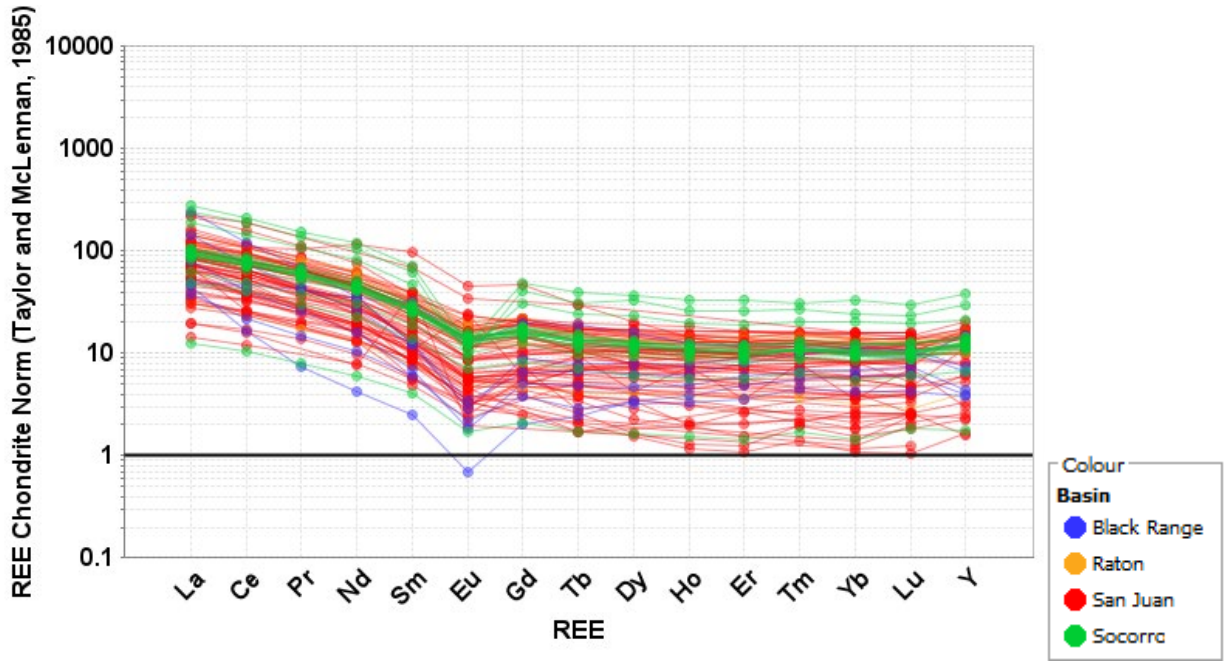

FIGURE 4.67 Chondrite-normalized patterns of clay samples. Chondrite values from Taylor and McLennan (1985).

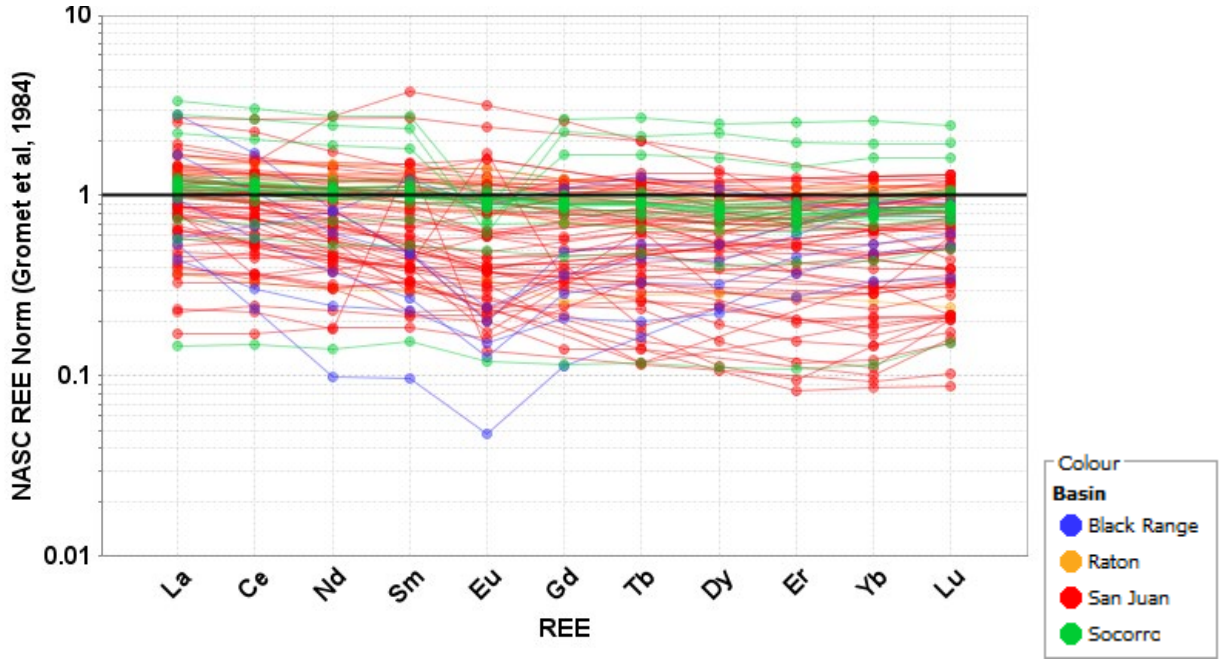

FIGURE 4.68 NASC-normalized patterns of clay samples. NASC (North American Shale Composite, values from Gromet et al., 1984).

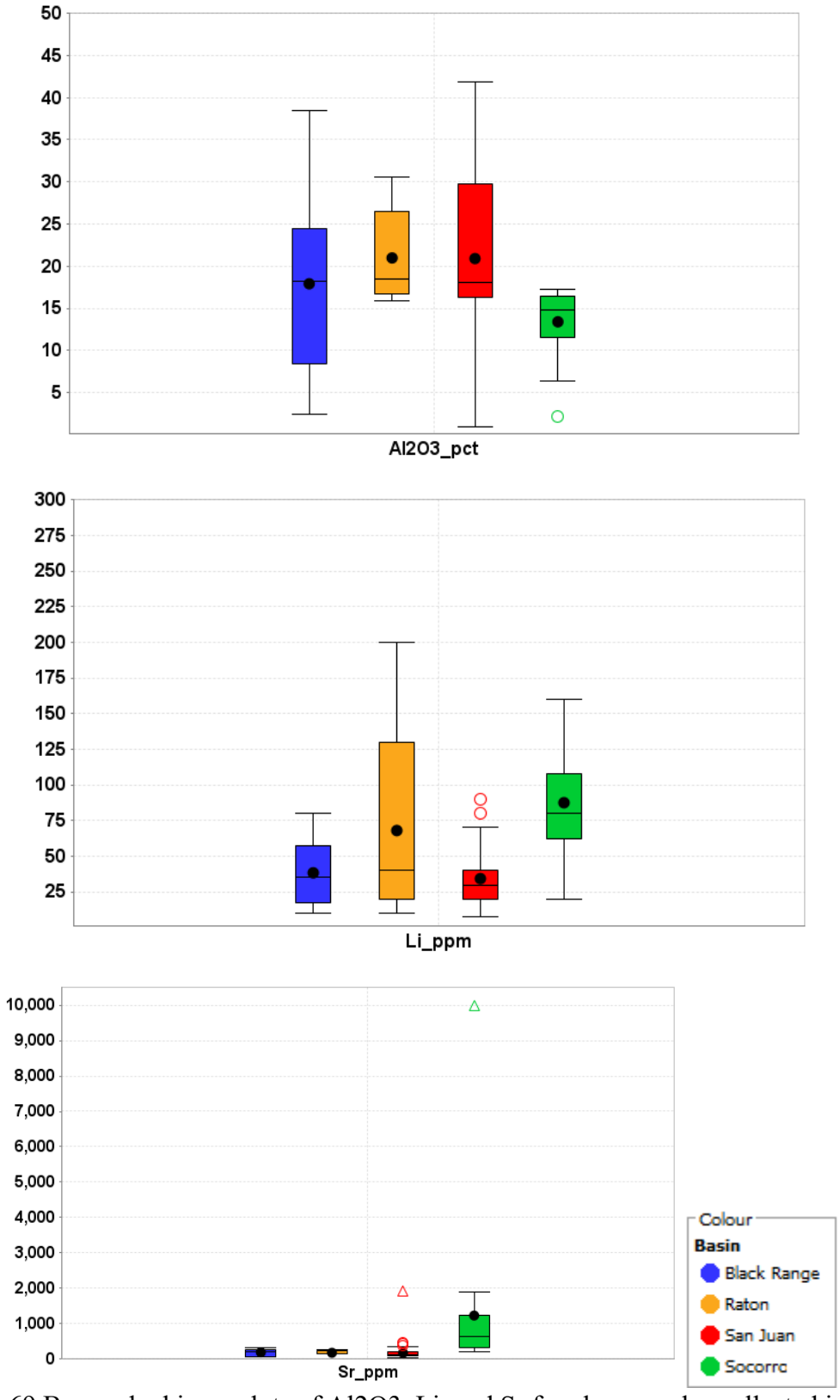

FIGURE 4.69 Box and whisper plots of Al2O3, Li, and Sr for clay samples collected in northern New Mexico.

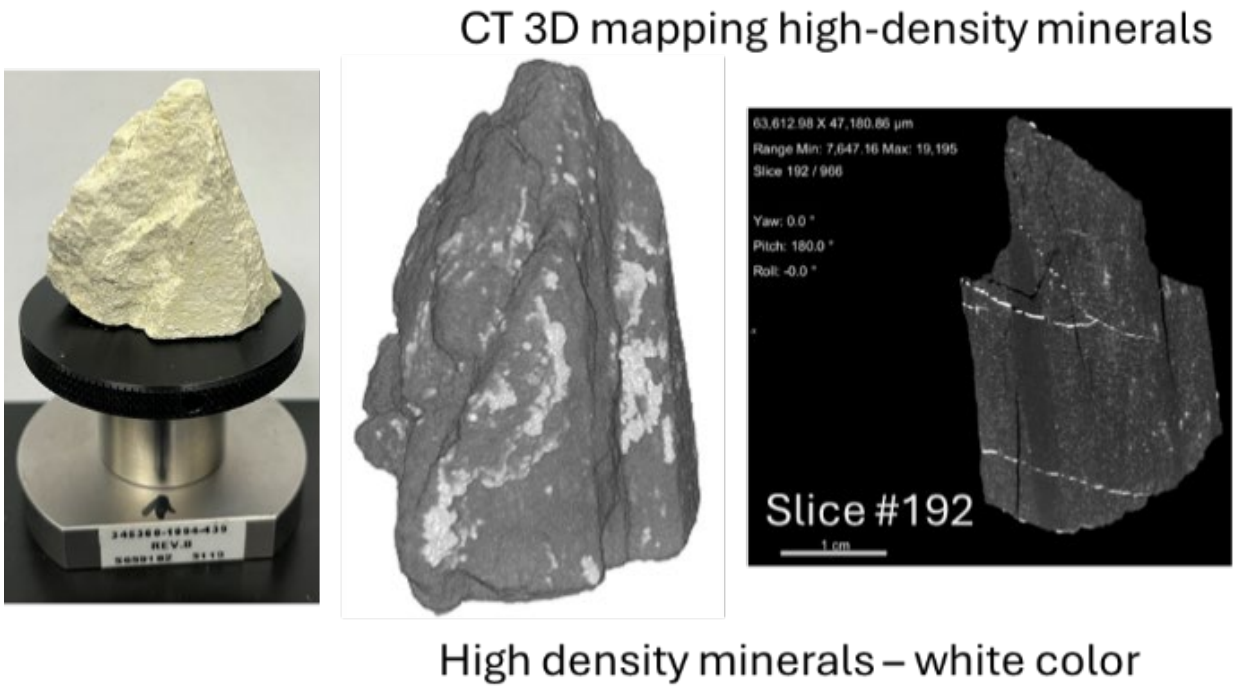

FIGURE 4.70 3D CT images showing the distribution of high-density minerals for sample Pop1.

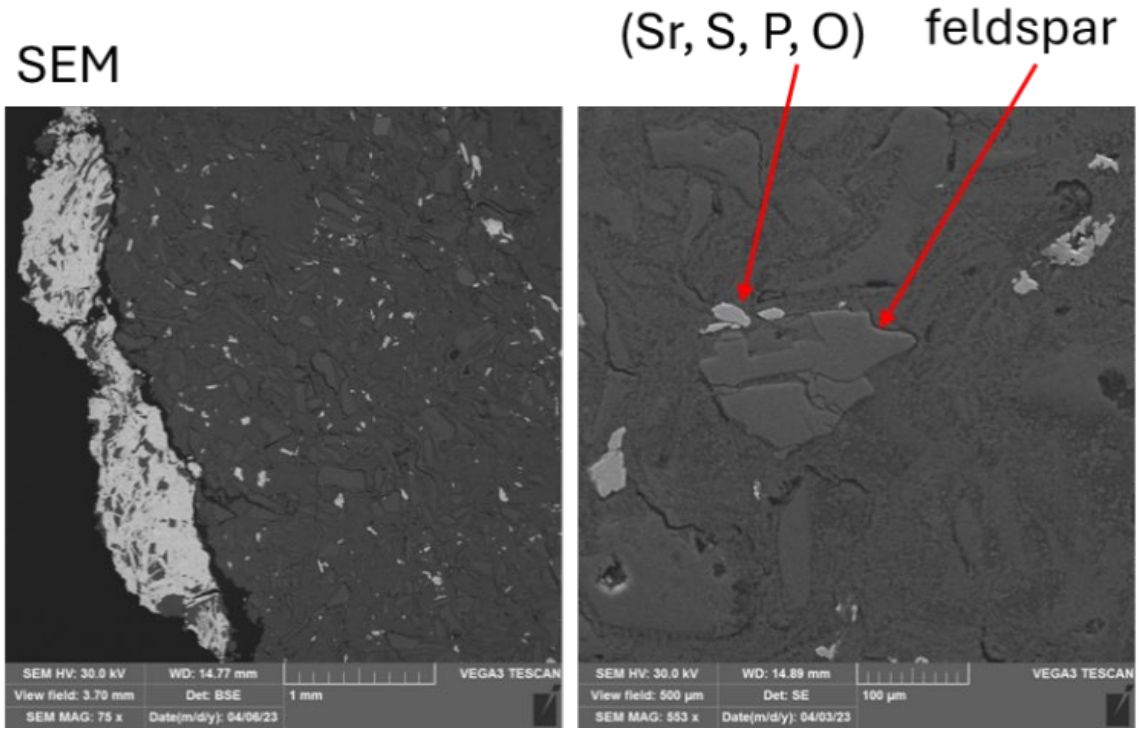

FIGURE 4.71 Y-3. SEM analysis identified major strontium hosted minerals: sulfate and phosphate.

4.10 Critical minerals potential of black shales (V.T. McLemore and M. Rigali)

4.10.1 Introduction

Black shales, particularly those that qualify as organic matter rich, have long been recognized as source rocks for the generation of oil and gas deposits globally. More recently with the advent of horizontal drilling and fracking technologies, they are being recognized as reservoir rocks and resulting in a substantial resurgence of oil and gas production in the U.S. particularly in the Permian and Delaware basins of southwest New Mexico and Texas.

In addition to their primary roles in hydrocarbon generation and as hydrocarbon reservoir rocks, they have long been studied for their unusual accumulations of metals such as uranium, vanadium, molybdenum, zinc and many others. These shales dubbed metalliferous black shales (MBS) were a focus of intense study by the USGS and university collaborators in the 1980's and 1990's not only to understand the origins of their unusual metal concentrations but also to assess their potential as ore deposits (Holland, 1979; Leventhal and Hosterman, 1982; Desborough et al., 1984; Coveney and Glascock 1989; Quinby-Hunt et al., 1989: Huyck, 1990; Leventhal, 1993; Large, 2012).

There are examples of mining MBS for base metals and uranium. The Alum Shale in Sweden that has been mined for small amounts of vanadium during World War II and more recently for uranium in the 1950s to 1980s (Dyni, 2006). The Talvivaara polymetallic black shale has been mined since 2008 (Loukola-Ruskeeniemi et al., 2013). This relatively low-grade ore deposit (averaging 2200 ppm Ni, 1300 ppm Cu, 200 ppm Co, and 5000 ppm Zn) is economically produced using large-scale open pit mining in combination with bioleaching technology resulting in relatively low production costs. In Nevada, the Gibellini Facies of the Woodruff Formation is a metalliferous black shale that contains significant quantities of vanadium (~3000 ppm average grade) along with significant quantities of zinc and nickel (Desborough et al., 1984). It is under development and if successful it has the potential to become the only primary vanadium mine in the U.S. (Gibellini Vanadium Project, 2019).

With the resurgence of oil and gas production in the U.S., Rigali and Krumhansl (2019) analyzed data on the metal contents of oil and gas producing shales across the U.S. and determined that the vast majority of these shale deposits contained metal-bearing intervals that make them by definition metalliferous black shales (Huyak, 1990). However, few of these shales contained enough metals to make them viable as mining prospects based on their assessment of conventional mining cut-off grades. It is important to note that Rigali and Krumhansl's (2019) assessment did not consider the possibility of solution mining with or without the use of directional drilling and fracking technologies now commonplace in the oil and gas industry.

In 2022 a SNL-NETL DOE funded project led by Xu and Rigali (contributors on this report) was initiated to assess the feasibility of solution mining MBS intervals in the Marcellus and Bakkan Shales. The final report (in preparation) suggests that solution mining of MBS may be feasible but more research including pilot-scale field studies and detailed technoeconomic analyses are required to establish the viability of this approach for the economic mining of base and critical metals.

Rare earth element concentrations of black shales have become a subject of considerable interest as a result of recent studies. Work by Bamburak et al. (2013) revealed that a sample from the Gammon Ferruginous Member of the Upper Cretaceous Pierre Shale in southwestern Manitoba contains 0.225% light REE and 0.124% heavy REE. The latter constitute 35.5% of the

total REE. Further, it was shown that the sample has 3178 ppm TREE or 3844 ppm total rare earth oxides (TREO); and the heavy REE content is >1000 ppm, which accounts for >30% of TREE. Further, the recent discovery of the Minamitorishima deposits near Japan (Takaya et al., 2018) reveals elevated concentrations of critical elements (including Ni, Co and REE with significant enrichments in heavy REE) hosted in modern fine-grained pelagic sediments off the coast of Minamitorishima Island. This has encouraged an effort to identify ancient analogs for these deposits in the geologic record. Pelagic sediments are frequently the precursors of fine-grained sedimentary rocks including shales. A recent paper by Thompson (2024) of ancient pelagic sediments of the Western Interior Cretaceous Basin of North America from Nebraska, Wyoming, the Dakotas and into Canada (southern Manitoba) reports significant REE concentrations with TREO amounts >2000 ppm. Such REE deposits have not been reported to date in New Mexico, but shales and pelagic sedimentary rocks represent both a research opportunity and potential exploration target for the state.

4.10.2 Chemistry of black shales in the San Juan and Raton basins

As a first step in exploring the resource potential of black shale deposits, 76 samples were collected for this project to examine the critical minerals content (Appendix 7) of black shale samples at several locations within the Raton (Fig. 4.72) and San Juan basins. Statistics are summarized in Table 4.10 and summarized in Figures 4.73 and 4.74. Although, some concentrations are above crustal abundance, none are above exploration or cut-off grades (Table 4.3) and are not considered metal bearing shales.

TABLE 4.10 Descriptive statistics of selected critical minerals in shale samples collected from the San Juan and Raton basins (data in Appendix 7). Average crustal abundance from Rudnick and Gao (2014).

Statistic	C%	Ba	Co	Cr	Cs	Cu	Ga	Li	Mo	Ni	Pb	Th	U	V	Zn	TREE
Count	36	71	72	69	60	48	48	49	38	49	48	71	67	47	71	75
Count Null	39	4	3	6	15	27	27	26	37	26	27	4	8	28	4	0
Minimum	0.04	37.9	0.5	2.5	0.08	3	0.6	0.24	0.5	0.5	1	0.25	0.18	5	1.6	5.64
Maximum	50.1	8066	105	105	19.1	126	38.7	90	33	52	58	43.2	13	371	250	343.2
Mean	4.38	680	10	43	8	29	20	30	3.39	16.6	23	12.69	5	123	74	136
Median	1.245	358	8.115	42.53	9.59	26.75	20.05	30	2	12	23	12.81	4.47	108	62	137.47
Avg crustal abundance		624	17	92	4.9	28	17.5	21	1.1	47	17	10.5	2.7	97	67	147

FIGURE 4.72 Black shale deposits along I-25 near Raton (Sample Coal15a, photograph by V.T. McLemore).

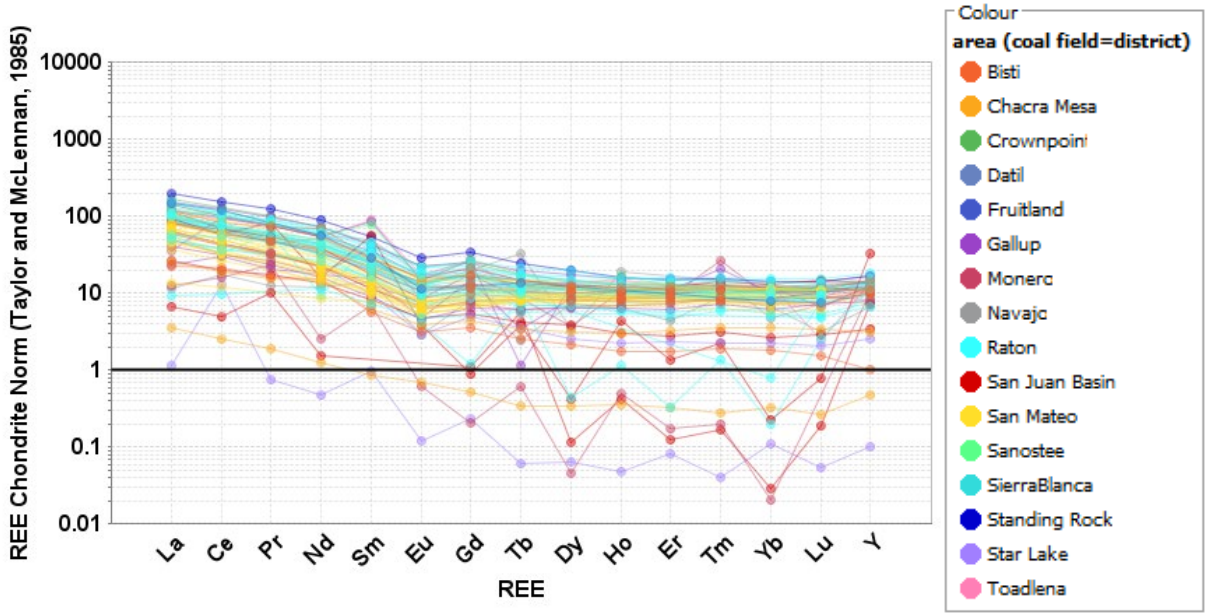

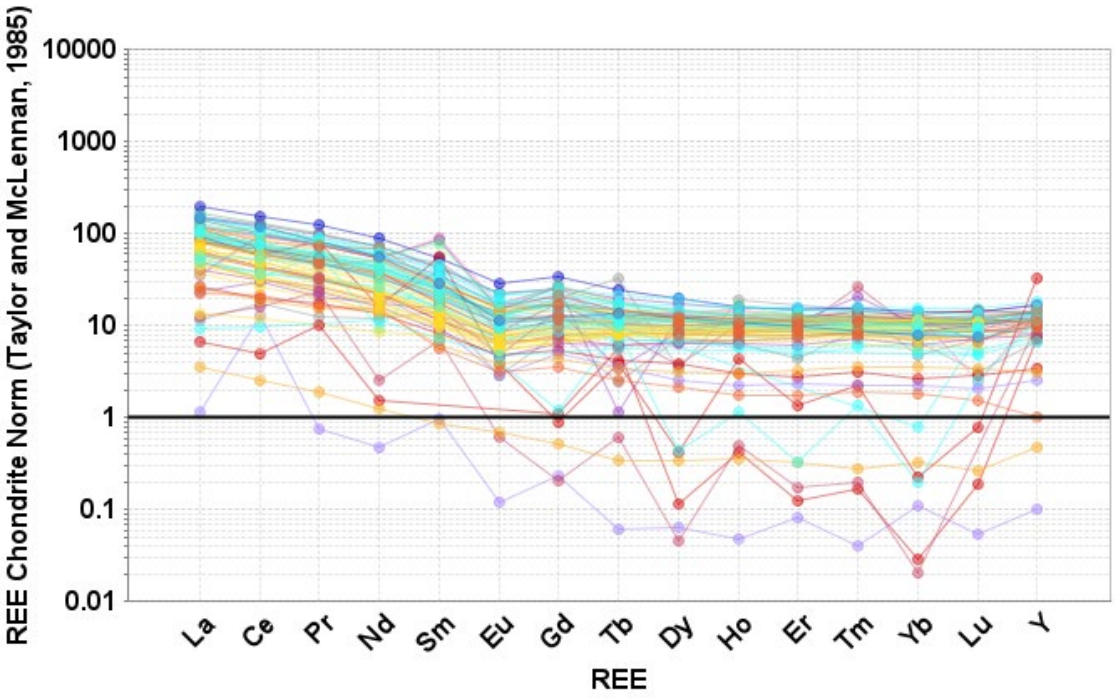

FIGURE 4.73 Chondrite-normalized REE plot of shales collected from San Juan and Raton basins (chondrite values from Taylor and McLennan, 1986).

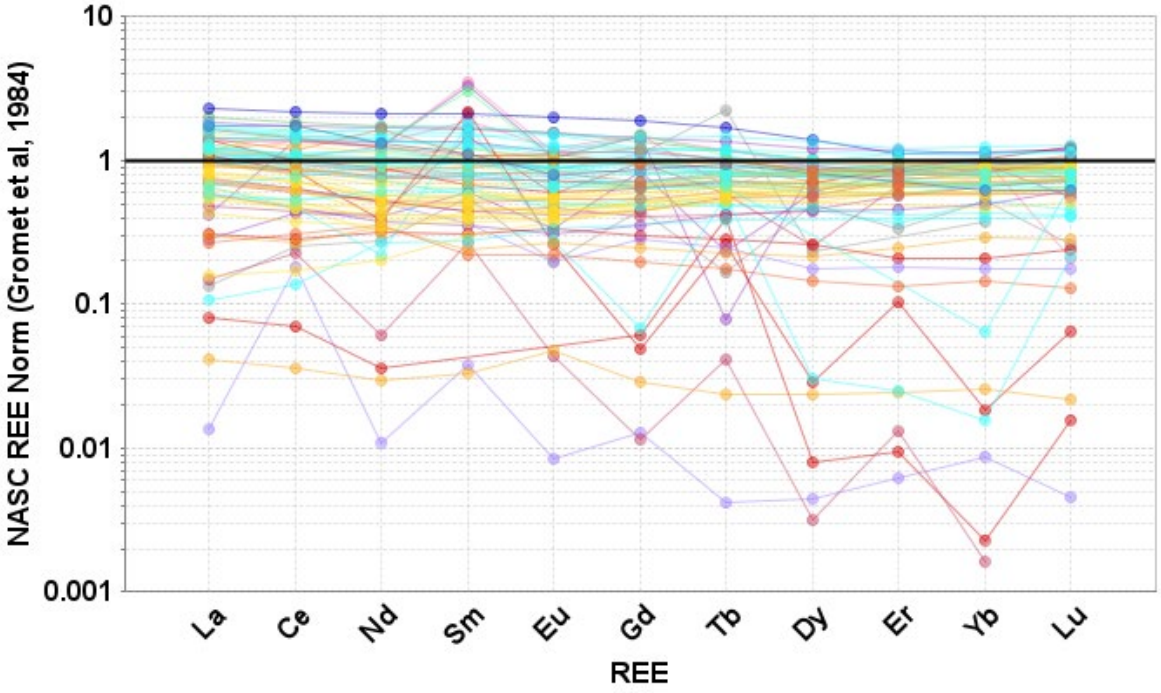

FIGURE 4.74 NASC-normalized REE plot of shales collected from San Juan and Raton basins (NASC values from Gromet et al., 1984). Legend in Figure 4.72.

4.10.3 Future studies

It is recommended to sample additional shales in the basins, especially the Delaware Basin. Future research includes examine pelagic equivalents in New Mexico in the northern Cretaceous Interior Seaway. Could the REE-enriched pelagic sediments be the deep-water sediment equivalent of the placer beach sands (Santosee etc.)?

4.11 Critical minerals potential of sandstone-hosted copper deposits (V.T. McLemore, E.J. Owen, and J. Newcomer)

4.11.1 Introduction

Sediment-hosted, stratabound copper deposits are bodies of copper minerals found as disseminations, cement, and veinlets in bleached sandstones, siltstones, shales, and limestones within or marginal to thick clastic red-bed sequences (Hayes et al., 2015; McLemore and Lueth, 2017) and are the second most important source of copper production in the world after porphyry copper deposits (Hayes et al., 2015). Three subtypes of sediment-hosted, stratabound copper deposits in the world are recognized by host lithologies and corresponding reductants:

- reduced-facies type (black to gray to green shale, siltstone, mudstone, or carbonaceous siltstone containing solid amorphous organic matter and pyrite)
- sandstone-type (gray, well-sorted, fine- to coarse-grained sandstone containing petroleum, probably sour gas in most cases)
- red-bed type (Hayes et al., 2015).

The term *sediment-hosted, stratabound copper deposits* is used here as suggested by the USGS (Hayes et al., 2015; Marsh et al., 2016). These deposits also have been called stratabound sedimentary-copper deposits (McLemore and Lueth, 2017), sediment-hosted Cu-Ag-Co, shale-hosted copper, red bed copper (Soulé, 1956), or sandstone copper deposits (Soulé, 1956; Phillips, 1960; Cox and Singer, 1986).

Numerous mining districts are found throughout New Mexico (Fig. 4.75; Table 4.11) that contain sediment-hosted, stratabound copper and silver, and locally lead, zinc, uranium, vanadium, cobalt, and molybdenum in Pennsylvanian, Permian, or Triassic poorly to moderately sorted fluvial sandstones, conglomerates, and shales containing carbonized plant debris, including fossil logs (McLemore, 2017; McLemore and Lueth, 2017). Most deposits in New Mexico are of the red-bed type (Hayes et al., 2015; McLemore and Lueth, 2017). The majority of sediment-hosted, stratabound copper deposits in New Mexico occur at or near the base of individual sedimentary layers within these sediments. Some deposits are in sedimentary rocks that unconformably overlie mineralized Proterozoic granitic rocks (McLemore, 1983, 2013; McLemore and Lueth, 2017).

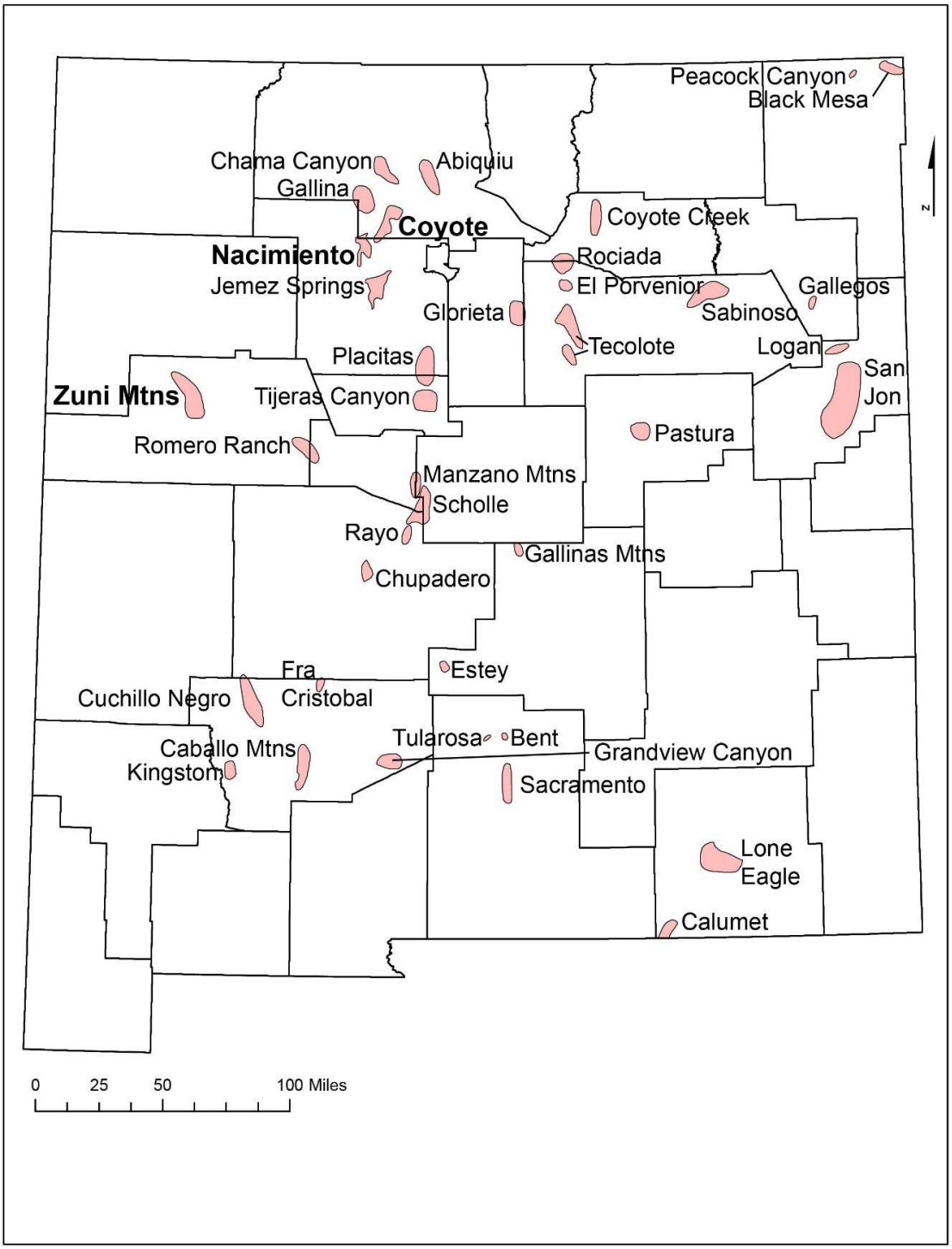

FIGURE 4.75 Sediment-hosted, stratabound copper deposits formed during Paleozoic to Mesozoic time in New Mexico (from McLemore and Lueth, 2017). Names in bold text are discussed in this report.

TABLE 4.11 Sediment-hosted, stratabound copper deposits in New Mexico, ranked by estimated copper production (McLemore, 2017). Bold type = discussed in this report. * = production includes that from other types of deposits. [1]TRs-Santa Rosa Formation, TRc-Chinle Formation, Pa-Abo Formation, Pb-Bursum Formation, PPs-Sangre de Cristo Formation, Py-Yeso Formation.

District	County	Estimated Copper Production (lbs)*	Estimated Silver Production (Oz)	Host Rock[1]
Pastura	Guadalupe	13,578,214	42,500	TRs
Nacimiento	Sandoval	7,561,567	>75,000	TRc, Pa
Scholle	Socorro, Valencia	1,122,468	8,200	Pa, Pb
Coyote	Sandoval	462,000	841	Pc
Estey	Lincoln	444,000	124	Pa
Sacramento	Otero	260,570	891	Pa
Glorieta	Santa Fe	50,000	—	PPs
Lone Eagle	Eddy	35,236	21	Py
*Zuni Mountains	Cibola	30,484	260	Pa
Jemez Springs	Sandoval	19,200	159	Pa
Tecolote	San Miguel	19,112	128	PPs
Coyote Creek	Mora	10,100	48	PPs
Romero Ranch	Valencia	9,300	24	Pa
*Placitas	Sandoval	2,441	48	Pa
Black Mesa	Union	800	10	TRs

Other deposits: Tijeras Canyon (Bernalillo), Gallegos (Harding), Gallinas (Lincoln), Tularosa (Otero), Logan (Quay), Red Peak (Quay), Abiquiu (Rio Arriba), Chama Canyon (Rio Arriba), Gallinas (Sandoval, Rio Arriba), El Porvenir (San Miguel), Rociada (San Miguel), Caballo Mountains (Sierra), Cuchillo (Sierra), Chupadera (Socorro), Rayo (Socorro), Peacock Canyon (Union), Sabinoso (San Miguel)

Critical minerals found in sediment-hosted, stratabound copper deposits include copper, zinc, vanadium, cobalt, gallium, uranium, and other minor commodities (Hayes et al., 2015; Marsh et al., 2016). Globally, sediment-hosted, stratabound copper deposits are the most important sources of cobalt (Hayes et al., 2015).

The copper deposits of the Nacimiento Mountains were mined by Native Americans and Spanish settlers perhaps as early as the 1500s. Larger-scale mining in the Nacimiento district did not occur until the 1880s. Two mining districts are associated with the copper deposits in the Nacimiento Mountains: Nacimiento and Coyote mining districts (Fig. 4.75). The Nacimiento mine is known for mineral collecting of copper minerals replacing fossil logs and wood and azurite spheres (Ottea and Uhl, 2020).

4.11.2 Mining history and production

The Nacimiento Mining Co. was formed about 1868 to examine deposits in the Nacimiento Mountains. Later, the Juratrias Mining Co. and Senorito Mining Co. explored and mined parts of the Nacimiento deposit by both surface and underground mining techniques in the early 1900s; at least two small smelters were constructed in the area to process the ores. Interest in the district faded after 1917 (Ottea and Uhl, 2020), only to increase again in the late 1960s. In 1971, Earth Resources Company constructed a mill and concentrator and began an open pit mine excavation and production at the Nacimiento mine (formerly the Copper Glance-Cuprite patented claims) after an extensive exploration program. A 2722 metric ton/day mill was built to handle the estimated reserves of 807 million metric tons of 0.71% Cu (Talbott, 1974; Woodward

et al., 1974). There was also a flotation circuit to concentrate the copper sulfides during Earth Resources Company operations. The deposit was mined by open-pit methods.

In 1973, there was release from the tailings dam into Señorito Creek, followed by issues with high-wall instability in the open pit and falling copper prices; in 1975, the company ceased production. The property was operated by various companies through the 1970s. In the early 1980s, Leaching Technology Inc. attempted to mine the deposit by in situ recovery methods using sulfuric acid, but poor results, low recovery from wells, and environmental concerns have hampered the project. Contaminated groundwater in the open pit area was pumped and effectively treated onsite by the U.S. Forest Service beginning in about 2007, and the treated water was discharged to Señorito Creek. A plume of sulfuric acid remains in the subsurface.

Production from the district is shown in Table 4.12. Historic reserves are reported for the Nacimiento mine and amount to 5.4 million metric tons of ore at a grade of 0.56% Cu and an additional 11.8 million metric tons of ore at a grade of 0.48% Cu as of May 2, 1980 (NMBMGR file data).

Little is known about the mining history of the Coyote district. The known deposits are small. Some production was recorded in 1956–1957, included in Table 4.12.

Base and precious metals were found in the Zuni Mountains circa 1900, and at least two metals mills and one leaching operation were built in the district. Total reported metals production from the district amounts to more than 30,000 pounds Cu, 260 oz Ag, and 2 oz Au from 1923 to 1965 (Table 4.13); additional copper, gold, and silver production probably occurred during the late 1800s from sediment-hosted deposits and veins in Precambrian rocks (McLemore, 1989, 2013).

TABLE 4.12 Reported metals production from the Nacimiento and Coyote mining districts, Nacimiento Mountains, Sandoval and Rio Arriba Counties (from USGS, 1902–1927; U.S. Bureau of Mines Mineral Yearbooks, 1927–1990; McLemore, 1989, 2017; NMBGMR file data). Production data can change as better data are obtained. Blank = no reported production. W = withheld or not available.

Year	Ore (short tons)	Copper (lbs)	Gold (oz)	Silver (oz)	Lead (lbs)	Zinc (lbs)	Total value ($)	Comments
Nacimiento mining district								
1880-1900		6,300,000		63,000			$700,000	
1904	467	846		52			$190	
1911	10	5,731		46			$741	
1916	130	26,276		274			$6,684	
1917	20	12,901		153			$3,648	Nacimiento mine
1918	6	10,935		118			$2,819	
1919	166	100,000		1,317			$20,075	
1920	89	53,821		700			$10,666	
1929								withheld
1943		4,000		45			$552	
1945		2,000		28			$290	
1950		6,000		10			$1,257	
1951		4,000		11			$978	
1955		600,00		410			$22,751	

Year	Ore (short tons)	Copper (lbs)	Gold (oz)	Silver (oz)	Lead (lbs)	Zinc (lbs)	Total value ($)	Comments
1956		548,200		7,564			$239,831	Eureka mine
1957		421,700		1,392			$128,912	
1959	75	6,000		55			$1,658	
1960	277	12,000		99			$3,505	
1961	99	2,000		23			$1,362	
1964	1,010	6,000					$1,923	Nacimiento mine
1967, 1971–1975								withheld, Nacimiento mine
TOTAL REPORTED 1880–1964	27,704	7,582,410		75,297			$1,147,842	Nacimiento mining district
ESTIMATED TOTAL 1880–1975		7,700,000	1	76,000	1,783	463	$1,500,000	Nacimiento mining district
Coyote mining district								
1956–1957		462,000		841	W		$4,000	Coyote mining district

TABLE 4.13 Reported metals production from the Zuni Mountains mining district, Cibola County (from USGS, 1902–1927; U.S. Bureau of Mines Mineral Yearbooks, 1927–1990; McLemore, 1989, 2017; NMBGMR file data). Production data can change as better data are obtained. . — = no reported production. W = withheld or not available.

Year	Ore mined (short tons)	Gold (oz)	Silver (oz)	Copper (lbs)	Total value ($)
1905	W	—	—	W	W
1923	16	—	36	4,884	748
1925	30	—	27	3,300	487
1930	57	—	57	6,600	880
1937	59	—	88	11,000	1,399
1940	12	—	28	2,700	325
1959	—	2	12	W	81
1963	W	—	W	W	W
1965	15	—	12	2,000	901
Total (excluding withheld values)	189	2	260	30,484	4,821

4.11.3 Description of deposits

Various types of deposits are found in the Nacimiento and Coyote mining districts in the Nacimiento Mountains. The largest deposits are sediment-hosted, stratabound copper deposits that occur in the Agua Zarca Sandstone Member of the Chinle Formation (Triassic); smaller deposits occur in the Madera (Pennsylvanian), Abo, and Cutler Formations (Permian) in the Coyote district. The copper deposits in the Triassic sandstones in the Nacimiento district are found in large, braided stream complexes in the Agua Zarca Sandstone Member of the Chinle Formation (LaPoint, 1979, 1983) and are less arkosic than Pennsylvanian-Permian deposits in the Coyote district.

The largest copper deposit in the Nacimiento district is at the Nacimiento mine, where the host rock is white, poorly cemented arkosic conglomeratic sandstone, 23 to 30 m thick. Kaolinization is present. The sandstones consist primarily of quartz, feldspar with local chert, magnetite, muscovite, zircon, chlorite, and biotite. Copper minerals are associated with carbonaceous material. Much of the deposit occurs at the surface; the deepest mineralized zones are at least 274 m and deeper. The deposit is bounded by the El Cajete fault to the north and the Bluebird fault to the south (Woodward et al., 1974). Both disseminated deposits and high-grade, mineralized fossil logs are present. In the disseminated deposits, the sulfide to oxide ratio is 1:3 above the water table and 10:1 below the water table, where most of the copper is as chalcocite (NMBGMR file data). Chalcocite occurs as discrete anhedral grains and replacement of the organic material (Talbott, 1974). Pyrite and native silver are present locally throughout the deposit and the oxidized portion contains malachite, chrysocolla, azurite, cuprite, antlerite, spangolite, native silver, silver sulfides, and native copper (Table 4.14; Talbott, 1974; Woodward et al., 1974; LaPoint, 1979). Uranium and barite are present locally but only in trace amounts (Appendix 7; McLemore, 1983; McLemore et al., 2024). Large, mineralized fossil logs up to several meters long have been replaced by chalcocite, locally preserving the woody cell structure (Fig. 4.76). In some places, the logs were replaced by pyrite followed by bornite and chalcocite, then finally replaced by covellite (Woodward et al., 1974). The adjacent carbonaceous shales typically are not mineralized. Copper content varies, with some deposits containing as much as 40–50% Cu. Gold is rare (typically less than 1 ppb). Similar but smaller sedimentary-copper deposits are found in the Agua Zarca Member at the San Miguel and Eureka mines (Fig. 4.77, 4.78), where sphalerite is found in addition to the copper minerals. Note that zinc is a critical mineral.

TABLE 4.14 Mineralogy of the sediment-hosted, stratabound copper deposits in the Zuni and Nacimiento Mountains. X = XRD (this study), E = EMPA (this study), O = optical petrography (this study), M = Mindat.org. Elements in red are critical minerals.

Mineral Name	Mineral Formula	Nacimiento Mountains	Zuni Mountains
Azurite	$Cu_3(CO_3)_2(OH)_2$	O, M	E, M
Barite	$BaSO_4$	E	E, M
Bornite	Cu_5FeS_4	O, M	
Chalcocite	Cu_2S	X, E, O, M	M
Chalcopyrite	$CuFeS_2$		M
Chrysocolla	$Cu_{2-x}Al_x(H_{2-x}Si_2O_5)(OH)_4 \cdot nH_2O$, $x < 1$	E, M	E, M
Copper, native	Cu		M
Covellite	$Cu^{+}{}_4Cu^{2+}{}_2(S_2)_2S_2$	X	M
Djurleite	$Cu_{31}S_{16}$	M	
Hematite	Fe_2O_3		M
Malachite	$Cu_2(CO_3)(OH)_2$	X, E, M	M
Pyrite	FeS_2	X, E, M	X, E, M
Silver, native	Ag	M	M

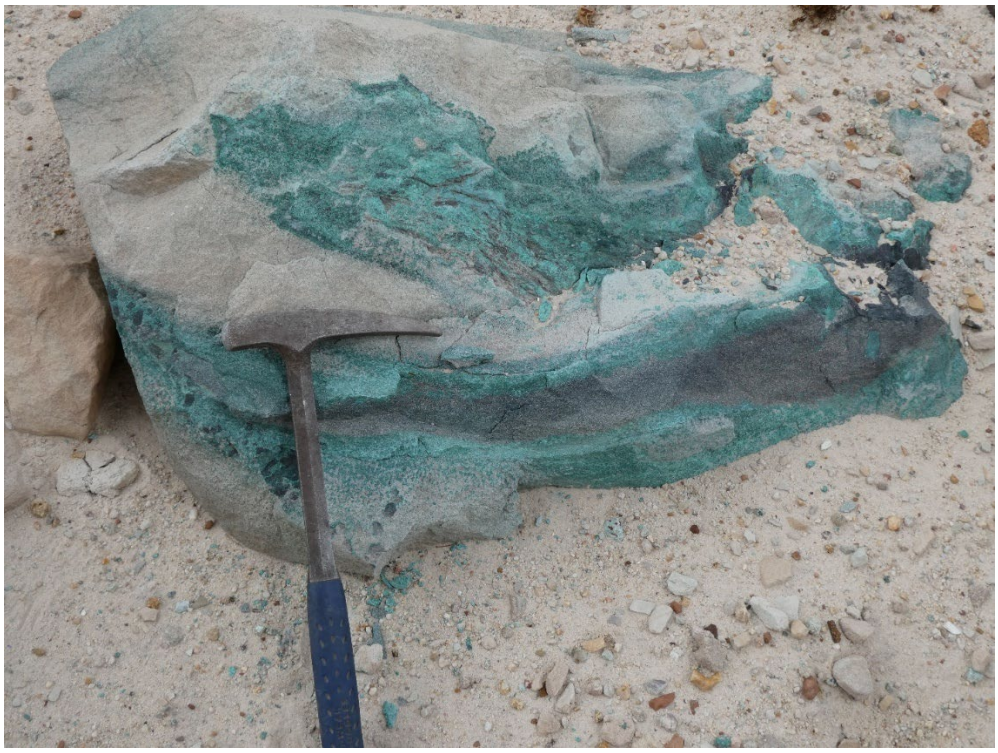

FIGURE 4.76 Green malachite and chrysocolla and black tenorite associated with black organic material in sandstone at the Nacimiento mine (photograph by V.T. McLemore).

FIGURE 4.77 Green malachite and chrysocolla in sandstone at the Eureka mine (mine id number NMRA0092a, photograph by V.T. McLemore, https://photoarchive.nmt.edu/?r=11881&k=f9123002a8).

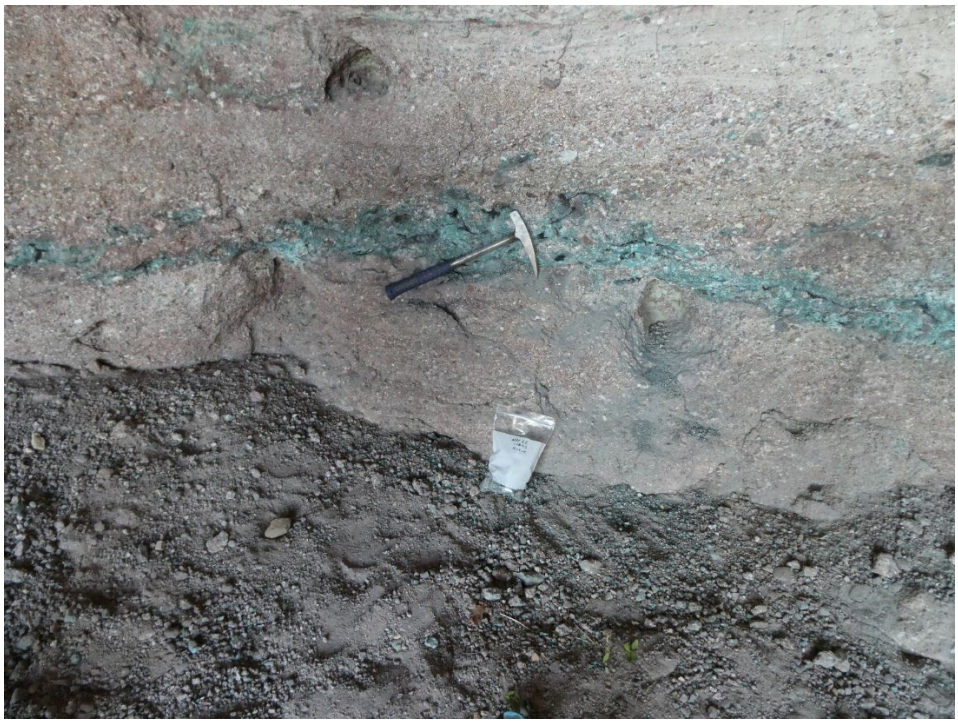

FIGURE 4.78 Green malachite and chrysocolla and black tenorite associated with black organic material in sandstone at the Eureka mine (sample NAC22, photograph by VT. McLemore, https://photoarchive.nmt.edu/?r=11882&k=550e610ace).

Additional sediment-hosted, stratabound copper deposits containing uranium and vanadium are found in the Pennsylvanian and Permian Madera, Abo, and Cutler Formations throughout the Nacimiento Mountains (Soulé, 1956; McLemore, 1983; Woodward, 1987), but they are small and uneconomic. The copper deposits in the Pennsylvanian-Permian beds are typically more arkosic than Triassic deposits and are found in small, meandering stream channels. Silver is rarely as abundant in Permian deposits as in Triassic deposits (Appendix 7). Uranium concentrations are higher in Permian deposits than Triassic deposits (Chenoweth, 1974).

Types of deposits in the Zuni Mountains include 1) veins and replacements in Proterozoic rocks, 2) sediment-hosted, stratabound copper deposits, 3) fluorite veins, 4) REE-Th-U metasomatic bodies (episyenites), 5) high-calcium limestone, 6) volcanic cinders (scoria), and 7) iron deposits (McLemore, 2013, 2017). In the Zuni Mountains, copper deposits are found in both Proterozoic granite and gneiss and Permian Abo Formation sandstones and shale (Schrader, 1906; Lindgren et al., 1910; McLemore et al., 1986). The copper deposits typically are found in bleached pink or light-gray sandstones, siltstones, and conglomerates of the Pennsylvanian (?)-Permian units deposited unconformably on the Proterozoic rocks in the Copper Hill area. At one locality, the Proterozoic granite beneath the mineralized conglomerate consists of thin veinlets and disseminations of malachite and chalcocite. Fluorite-barite veins locally cut the copper deposits (Fig. 4.79). The deposits are predominantly in the Abo Formation (Permian), but some replacements of the Pennsylvanian rocks also are found. The mineralized bodies typically occur as lenses or blankets of disseminated and/or fracture coatings of copper minerals, predominantly chalcocite, malachite, and azurite with local uranium minerals, galena, sphalerite, chalcopyrite,

and barite. Ore minerals in these sediment-hosted, stratabound copper deposits are typically associated with organic debris and other carbonaceous material. Locally, sedimentary features such as bedding, crossbedding, paleochannels, and intraformational slumping also appear to control mineralization. The copper deposits are found in small, meandering stream channels and tend to be discontinuous, small, and low grade. The average thickness of mineralized zones is less than 2 m, but as many as four horizons or zones are found. Malachite, azurite, and chalcocite with local pyrite, quartz, and galena are disseminated within shear zones within the granite and gneiss. Malachite, azurite, chalcocite, and local chalcopyrite are disseminated or along thin seams within pore spaces in and cementing conglomerate, sandstone, and shale of the Abo Formation directly overlying the Proterozoic rocks. Copper minerals also replace fossil wood, carbon layers, and thin shales locally with carbonates.

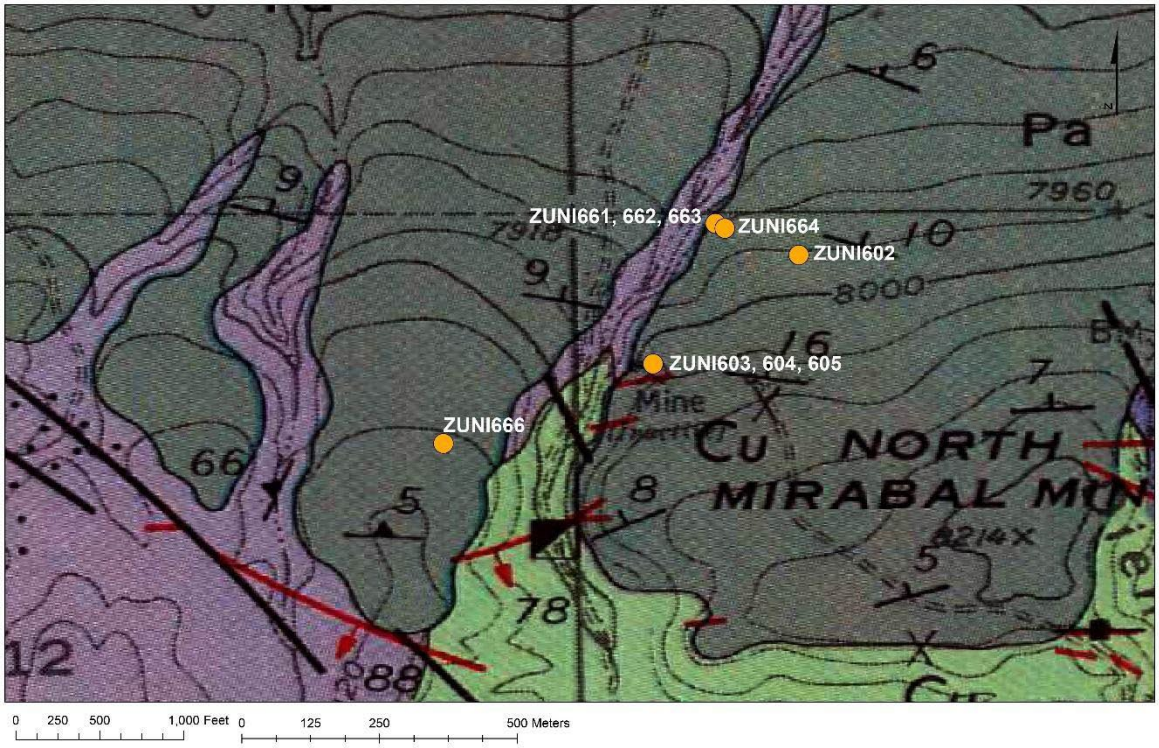

FIGURE 4.79 Location of samples collected from the Copper Mountain area, Zuni Mountains. Geologic map from Goddard (1966). Lithologic units (oldest to youngest): gg (green) = gneissic granite, ap (purple) = porphyritic aplite, Pa (dark gray) = Permian Abo Formation, red lines = fluorite veins. Yellow circles are sample locations. Coordinates and chemical analyses for each sample are in Appendix 7.

The mineralogy of mineral deposits found in the Nacimiento and Zuni Mountains is presented in Table 4.15, and chemical analyses are in McLemore et al. (2024) and Appendix 7. Electron microprobe analyses of chalcocite in replaced wood from the Nacimiento mine show an average of ~400 ppm Ag (up to ~600 ppm Ag) substituting within the mineral (Table 4.15). While native silver has been reported from the Nacimiento mine, none was observed in the studied samples. EMPA analyses of pyrite from the Nacimiento mine show an average of 1900 ppm Pb (Table 4.15). Chalcocite and pyrite are the dominant sulfide minerals present in replaced wood from the Nacimiento mine (Fig. 4.80). Minor amounts of secondary iron-copper and

copper minerals fill late fractures (Fig. 4.80). More analytical work, including XRD will be needed to confidently identify these phases.

TABLE 4.15 Summary of electron microprobe analyses data.

Chemistry of chalcocite from the Nacimiento Mine (n = 12)				
Cu	Fe	Ag	S	Total
75.36±1.2	0.38±0.35	0.04±0.02	22.75±3.06	98.53±2.52
Chemistry of pyrite from the Nacimiento mine (n = 4)				
Fe	Pb	S	Total	
46.46±0.14	0.19±0.05	53.63±0.23	100.27±0.4	

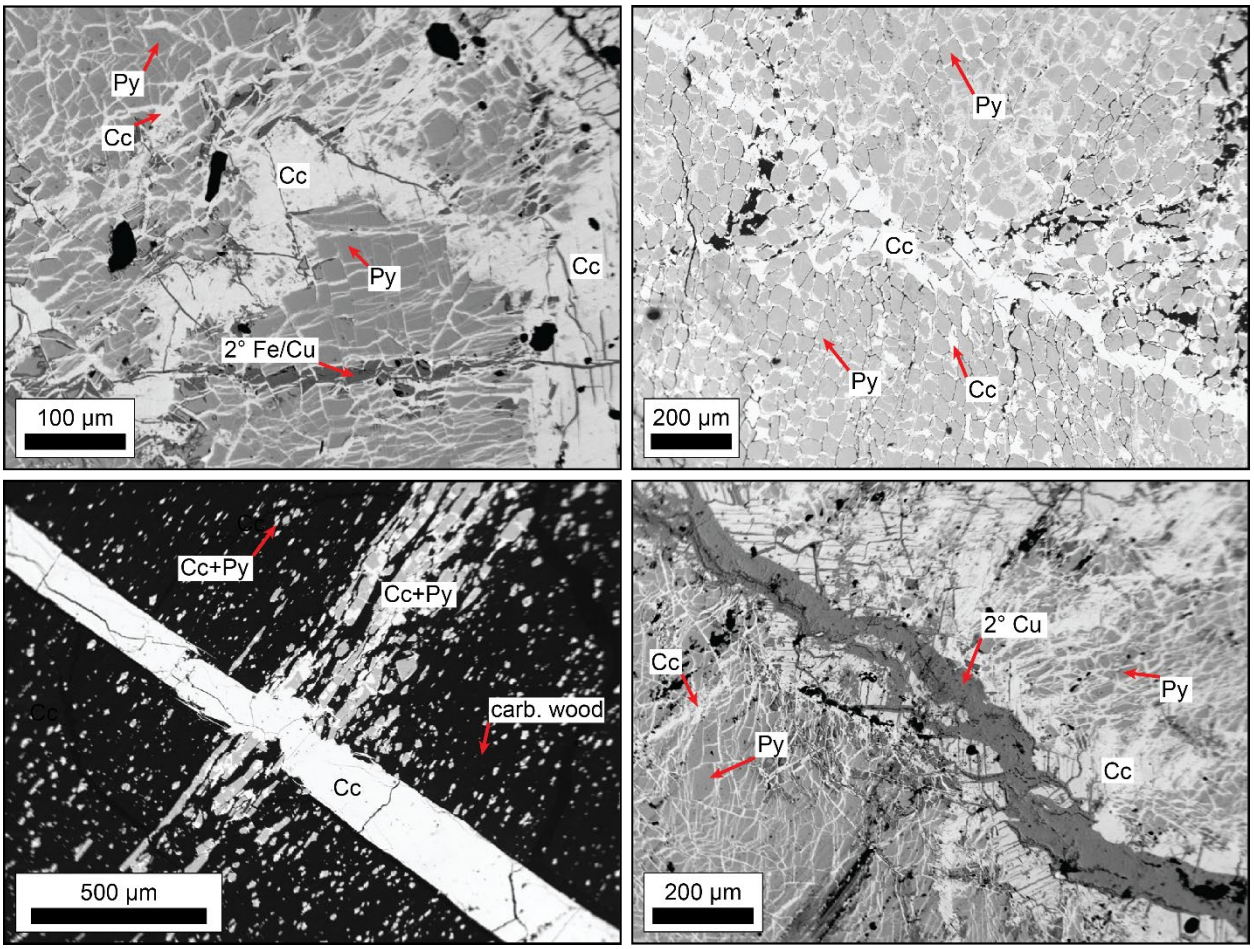

FIGURE 4.23 Backscattered electron images (BSE) of chalcocite and pyrite replaced wood from the Nacimiento mine. (a) Chalcocite veinlets cutting and replacing pyrite that has replaced wood. Late secondary iron-copper veinlets are also observed (NAC4). (b) Chalcocite veinlets cut and replace pyrite which shows preserved plant cellular structure (NAC A). (c) Chalcocite and pyrite locally replace carbonized wood and are cut by a sharp chalcocite vein (NAC B). (d) A late, secondary copper vein (possibly spertiniite, though additional analyses are needed to confirm) cuts chalcocite, replacing pyrite along fractures (NAC4). Cc = chalcocite, Py = pyrite, 2° = secondary (iron-copper or copper minerals).

4.11.4 Critical minerals

Sediment-hosted, stratabound copper deposits throughout the world are known to have locally elevated concentrations of various critical minerals including cobalt, zinc, vanadium, uranium, gallium, germanium, indium, platinum group metals, rhenium, and possibly REE. Geochemical and mineralogical studies are required to properly evaluate whether a deposit has elevated critical minerals.

Selected samples were collected from sediment-hosted, stratabound copper deposits in the Nacimiento and Zuni Mountains to examine their critical minerals potential by determining their mineralogy and geochemistry (Table 4.15; Appendix 7). Some samples in the Nacimiento and Zuni Mountains have elevated heavy REE. Samples from the Coyote district are elevated in cobalt; preliminary electron microprobe data suggest trace amounts of cobalt within chalcocite. Both Coyote and Zuni samples are elevated in heavy REE (Fig. 4.81), vanadium, and uranium. Arsenic is found in many of the samples (McLemore et al., 2024). The Eureka deposit has elevated barium. Bismuth is elevated in Zuni and Coyote samples.

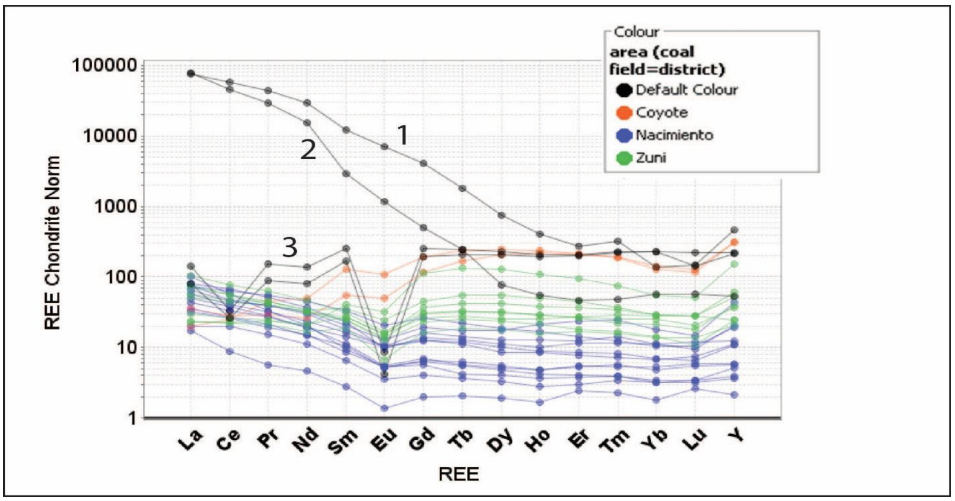

FIGURE 4.24 Chrondite-normalized REE plot. Chondrite values from Taylor and McLennan (1985). Black lines are representative REE analyses of major deposits in production, for comparison. 1 = Mt. Weld laterite deposit (https://lynasrareearths.com/wp-content/uploads/2019/05/Increase_in_Mt_Weld_Resource_Estimate_1068363.pdf), 2 = Mountain Pass, Ca carbonatite deposit (Verplanck et al., 2014), 3 = Zudong, China, ion-adsorption clay deposit (Li et al., 2019).

4.12 Sample Characterization, Nacimiento mine (Task 5) (B. Goehring, P. Watson, I., and Mantelli)

As part of the basin specific technology development, the concentration and distribution of REE and other critical minerals within a sample of the copper sandstones from the Nacimiento mine were characterized. This work is motivated by the fact that the hosting characteristics will ultimately inform the potential extraction technologies applicable to materials from the San Juan Basin. Here we applied micro XRF to generate elemental maps and stoichiometric ratios of elements.

4.12.1 Micro XRF (mXRF) and element co-location

Micro x-ray fluorescence (mXRF) is an emerging technique to simply and rapidly perform relatively high resolution (20 micron) elemental mapping of samples without the complications often associated with similar techniques such as EDS SEM techniques. Therefore, it can provide rapid analysis of materials on typically shorter time frames than EDS SEM and/or on samples that otherwise are not conducive to such techniques. Here, the potential is examined for mXRF to provide such analyses of GGRB and similar materials and further inform what elements are present, where they are hosted, and potentially the hosting composition (Fig. 4.82). Note that because of the complexity of mXRF and more generally XRF spectral interpretations, some of the observed Ce may be artificial occurrences and could be Ti. However, the Ce is associated with other elements commonly associated with REE and therefore the occurrence and observation likely is real. All discussions and images below are strictly qualitative owing to the lack of a suitable matrix matched standard. Quantitative results will require further development and testing.

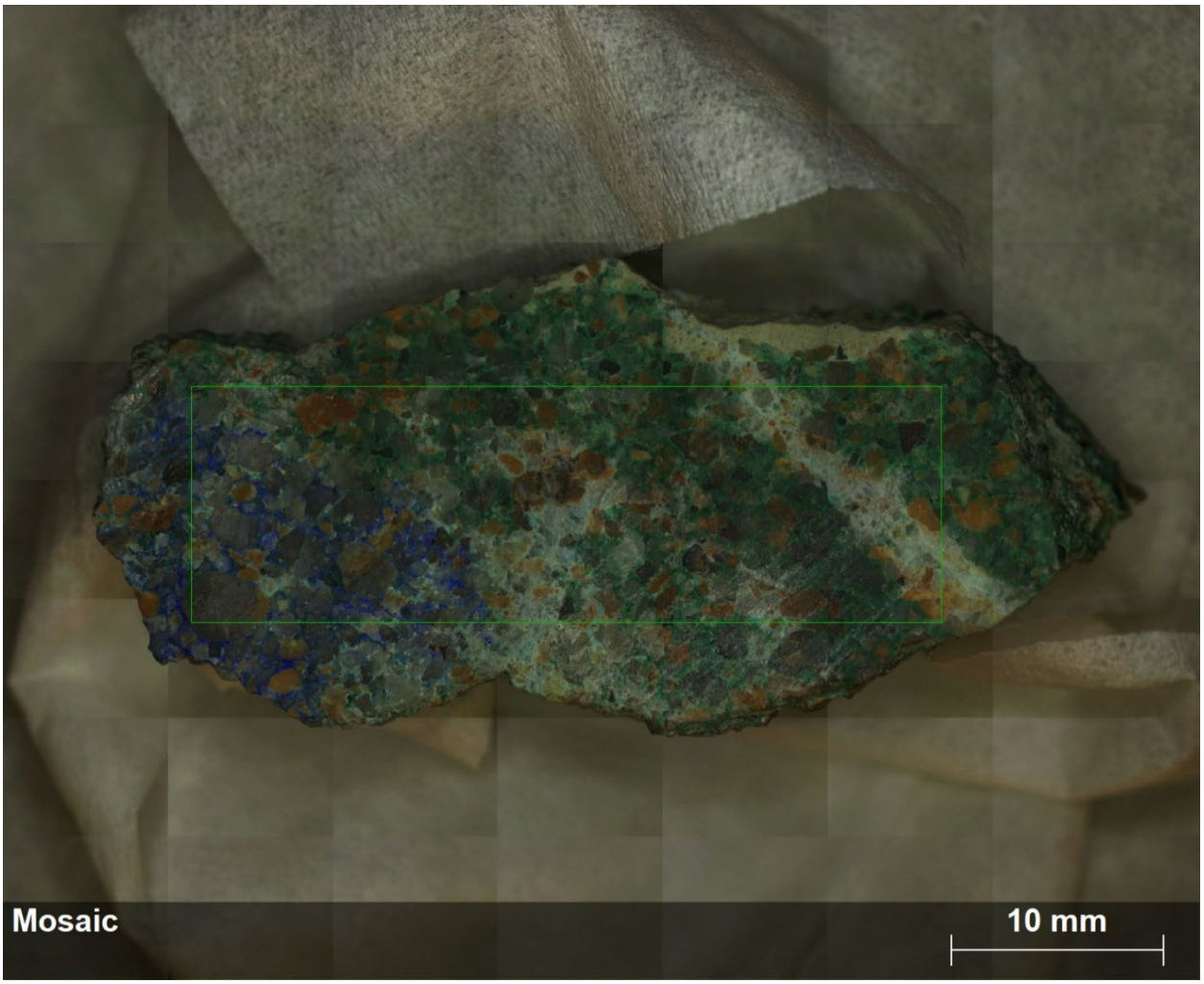

FIGURE 4.82 Stitched mosaic image of the rock and scan area (green rectangle). The target surface of the Cu-bearing sandstone was cut and lightly polished prior to analysis.

4.12.2 Summary

A hand sample (Fig. 4.83, Table 4.16) was analyzed via the Bruker M4 Tornado µXRF instrument with a Rh X-ray tube. Detecting REE using energy dispersive XRF (EDXRF) can present some challenges due to many interfering K lines in the 4–8 keV range and high background signal. This data represents only a qualitative analysis of absence/presence. Figure 4.83 shows a graphical representation of the distribution of select elements. The color bar is scaled 0-100 and is relative to the range of intensities observed for that element. Therefore, it should be interpreted simply as presence or absence more or less of a given element.

While the above obviously limits quantitative assessment, it does provide important information on the physical location of economical minerals/elements and more specificity regarding the important elemental co-associations. The former is important for assessing how an element of interest might best be liberated and the latter providing important insight into potential future characterization of an economic resource.

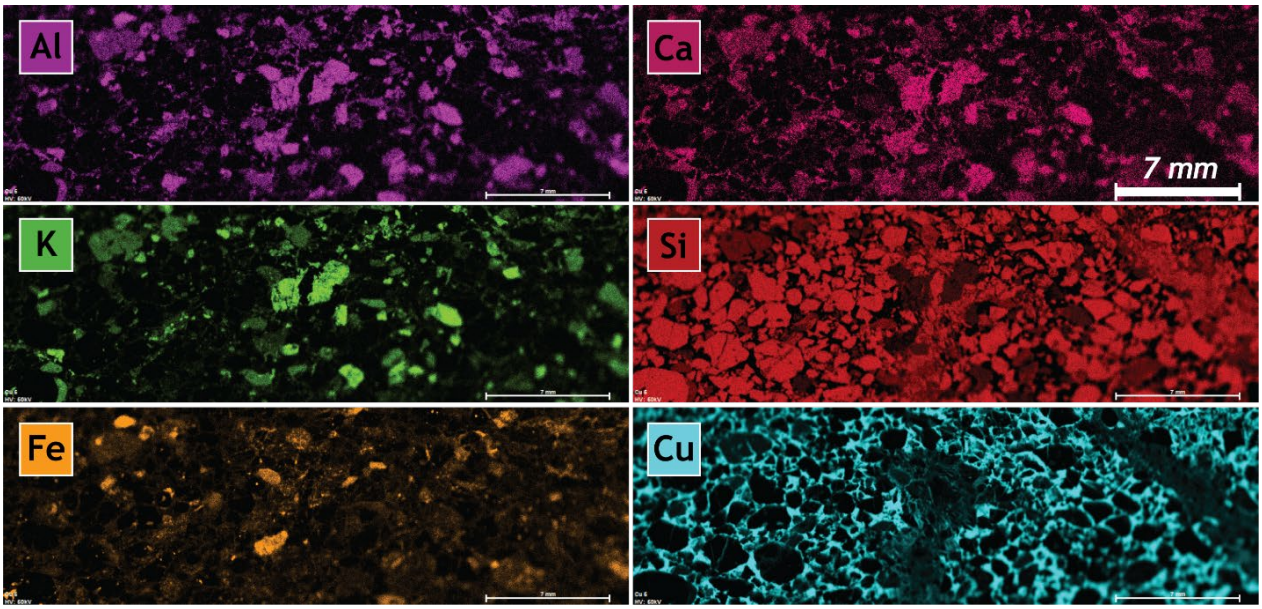

FIGURE 4.83 Color intensity maps of major and minor elements from the Cu-bearing sandstone.

TABLE 4.46 Quantitative results of major, minor, and trace elements averaged from 5x5 blocks of points. No detectable REE+Y was observed at the detection limits of the instrument.

Element	Net	wt.%	norm. wt.%	norm. at.%	Error in wt.% (1σ)
Silicon	39326607	45.52365	73.42335	82.10115	0.00726
Sulfur	60572	0.04141	0.06679	0.06541	0.00017
Aluminum	1672658	3.11364	5.02186	5.84515	0.00241
Potassium	3400022	2.54700	4.10795	3.29963	0.00138
Iron	2541698	0.20416	0.32928	0.18517	0.00013
Copper	141381549	10.31735	16.64046	8.22383	0.00087
Rubidium	243208	0.02709	0.04370	0.01606	0.00005
Titanium	406577	0.08483	0.13683	0.08974	0.00013
Manganese	184312	0.01812	0.02923	0.01671	0.00004
Calcium	303954	0.12434	0.20055	0.15715	0.00023
	Sum:	62.0016	100	100	

4.13 Critical minerals potential of volcanic ash beds (D. Shaver and V.T. McLemore)

Volcanic ash beds are the result of volcanic eruptions across multiple periods of time, and they can vary in thickness, texture, and grain sizes in the geologic layers they are found. Volcanic ash samples were collected in the San Juan Basin to determine their critical minerals and REE potential and as a possible source for critical minerals in coal and adjacent strata.

Ten samples of volcanic ash from four coal fields in the San Juan Basin were collected and analyzed (Fig. 4.84). Six samples were collected from the surface and four samples from drill core. Most volcanic ash samples are thin, white beds of fine-grained volcanic ash (Fig. 4.85). The overall REE content of these ashes is low; a sample from Mt. Taylor has the highest concentrations of REE. Uranium concentrations are low, less than 100 ppm (Fig. 4.86). Vanadium concentrations are below crustal abundance values (150 ppm) (Fig. 4.87). Lithium concentrations are high in comparison to crustal abundance (Fig. 4.88, 4.89). The low concentrations of critical minerals indicates that most volcanic ashes do not have any economic potential and are not a potential source of critical minerals in adjacent strata. However, the Star Lake sample is elevated in Li (250 ppm).

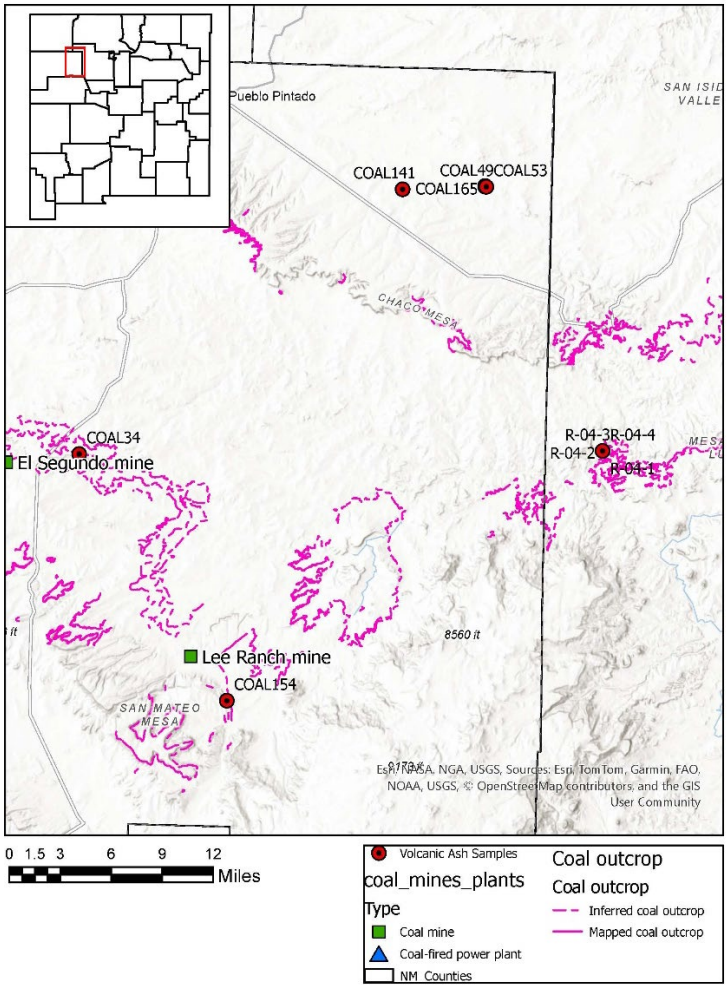

FIGURE 4.25 Locations of volcanic ash samples collected in the San Juan Basin.

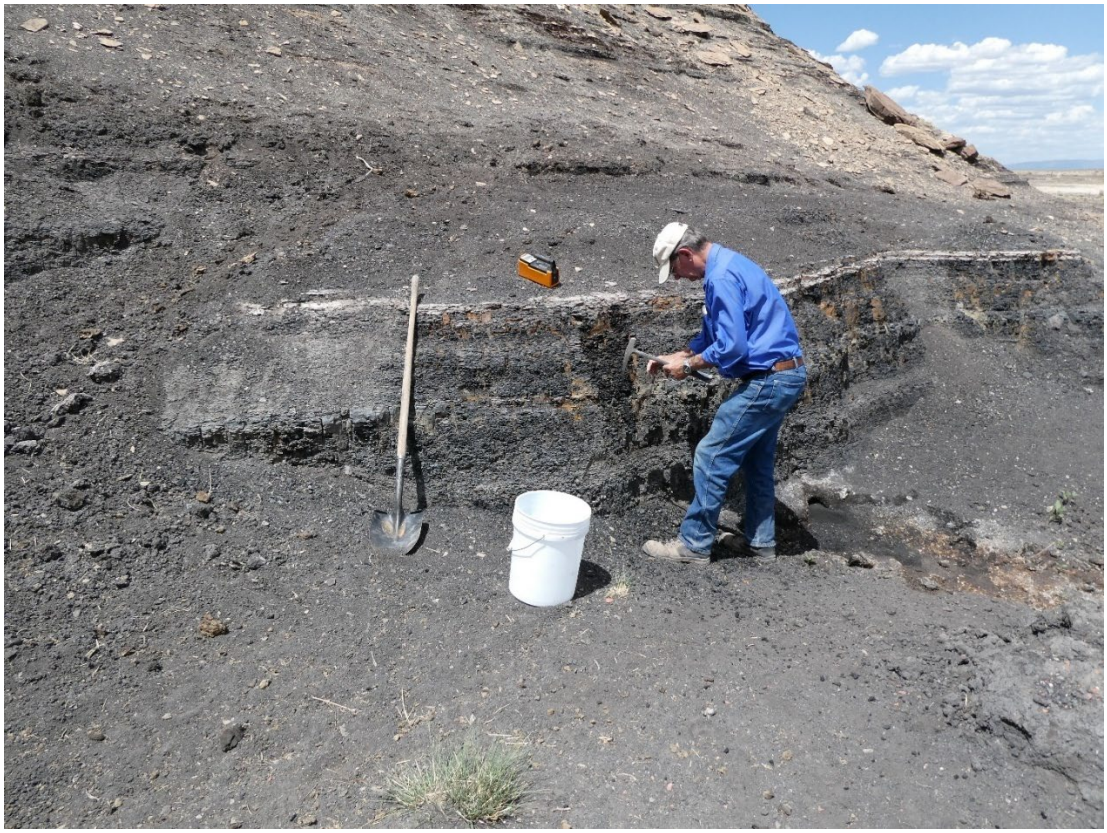

FIGURE 4.85 Coal with white volcanic ash bed, San Juan Basin (photograph by V.T. McLemore).

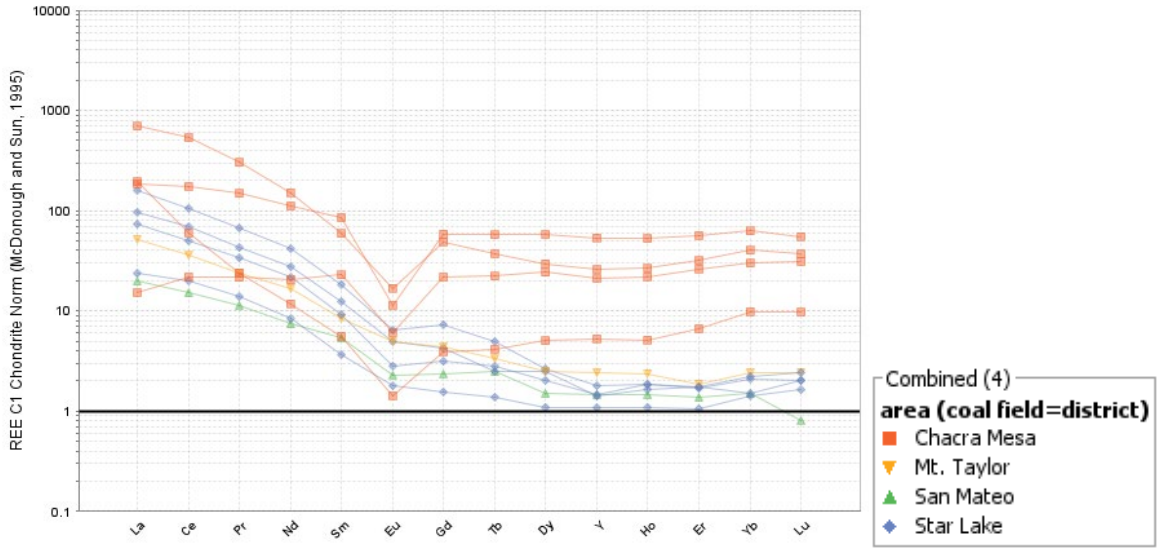

FIGURE 4.86 Chondrite normalized REE plot of volcanic ashes (chondrite values from McDonough and Sun, 1995).

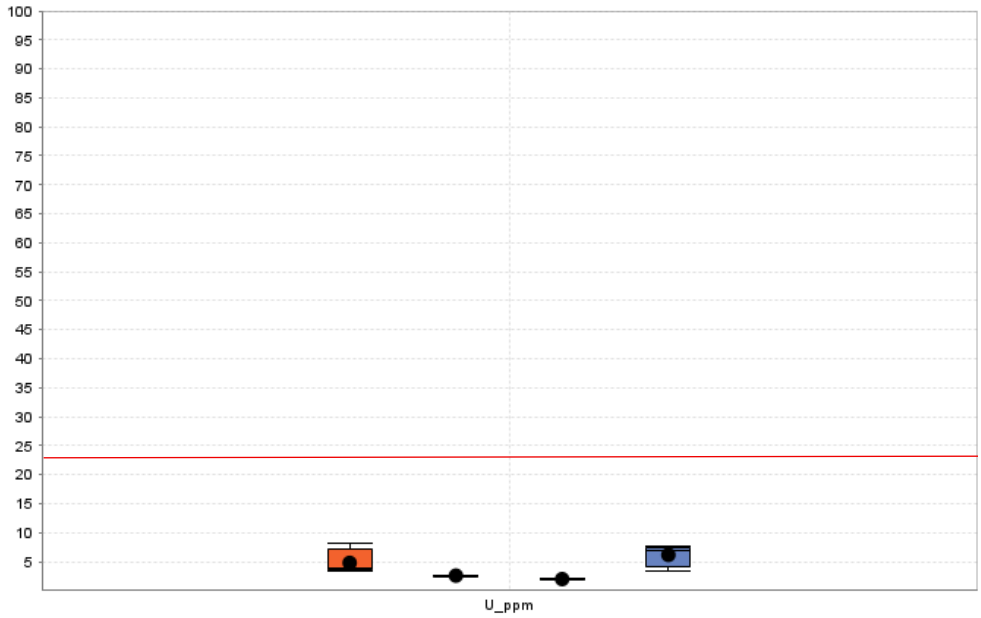

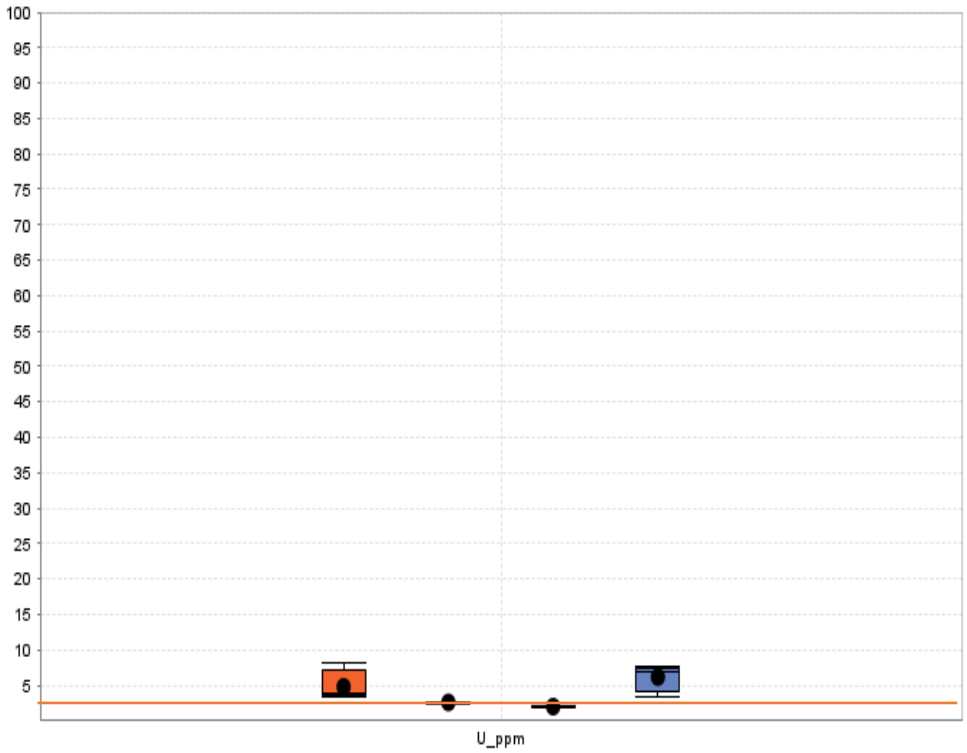

FIGURE 4.87 Uranium box plot of volcanic ashes. Red line is average crustal abundance. Legend in Figure 4.86. These concentrations are below exploration threshold values (Table 4.3).

FIGURE 4.88 Vanadium box plot of volcanic ashes. Red line is average crustal abundance. Legend in Figure 4.86. These concentrations are below exploration threshold values (Table 4.3).

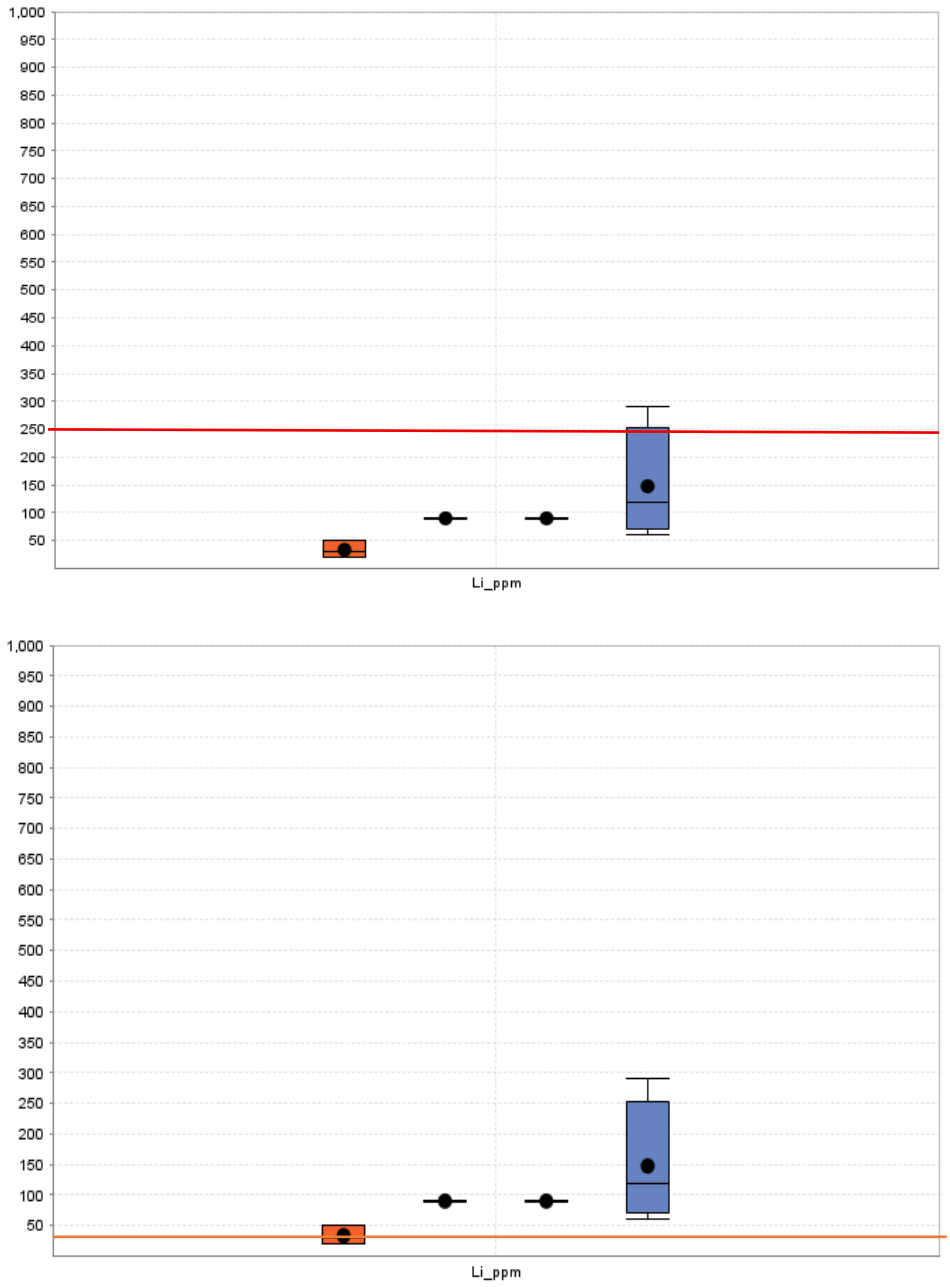

FIGURE 4.89 Lithium box plot of volcanic ashes. Red line is average crustal abundance. Legend in Figure 4.86. These concentrations are below exploration threshold values (Table 4.3).

4.14 Critical minerals potential of uranium deposits (V.T. McLemore, R. Boakye, and Z.K. Motlagh)

4.14.1 Introduction

Sandstone-hosted uranium deposits primarily constitute historical uranium production within the Grants uranium district of the San Juan Basin in northwestern New Mexico (Fig. 4.90, 4.91; McLemore, 2007; McLemore et al., 2013; McLemore et al., 2016). These deposits are formed when uranium, dissolved in groundwater precipitates in the void spaces of sandstone matrix under reducing conditions (McLemore and Chenoweth, 2017). These deposits are primarily epigenetic, stratabound concentrations of uranium in fluvial, lacustrine, and deltaic sandstones and are part of the Morrison Formation, specifically the Westwater Canyon Member (McLemore, 2007). Three types of sandstone-hosted uranium deposits are recognized in the Westwater Canyon Member of the Morrison Formation:

- Primary sandstone-hosted uranium deposits (prefault, trend, blanket and black-band ores), form blanket-like, parallel ore bodies along trends. These deposits are typically less than 2.4 m thick, and averages more than 0.20% U_3O_8 and have sharp-to-ore boundaries.
- Redistributed (post-fault/stack/roll-front/secondary) deposits. These deposits are younger, discordant, asymmetrical and irregularly shaped bodies, typically thicker than 2.4 m with diffuse contacts, and often vertically stacked along faults.
- Remnant-primary sandstone uranium deposits were preserved within less permeable sandstones after the oxidizing waters that formed redistributed uranium deposits had passed. These are similar to primary deposits but difficult to locate due to sporadic occurrence within oxidized sandstone. (McLemore, 2007; McLemore et al., 2013; McLemore et al., 2016).

Other sandstone uranium deposits include the tabular sandstone uranium-vanadium deposits in the Salt Wash and Recapture Members of the Morrison Formation, redistributed uranium deposits in the Cretaceous Dakota Sandstone, roll-front sandstone uranium deposits and sedimentary sandstone uranium deposits (McLemore, 2007). Historically, sandstone uranium deposits were mined in the Ambrosia Lake subdistrict by conventional underground and open pit mining methods. Critical minerals in these sandstone-hosted uranium deposits include uranium, vanadium and copper (McLemore et al., 2013; 2026).

Production from uranium deposits is shown in Table 4.17 and 4.18. Table 4.19 show types of uranium deposits in New Mexico. In addition, 9,076,207 lbs of V_2O_5 at grades of 0.03-1.8 V_2O_5 were recovered from sandstone and limestone uranium deposits in the Ambrosia Lake subdistrict (Atomic Energy file data, V.T. McLemore). The total estimated uranium resources in New Mexico are recorded as 409,122,587 pounds of U_3O_8 (lbs U_3O_8) with additional undetermined resources remaining. The Department of Energy (DOE) in 2008, classified uranium reserves into forward-cost categories of $50 and $100 per pound. At a forward-cost of $50 per pound, New Mexico has 64 million short tons of ore at a grade of 0.14% U_3O_8 totaling 174 million pounds of U_3O_8. At a forward-cost of $100 per pound, New Mexico has 186 million short tons of ore at a grade of 0.105% U_3O_8 totaling 390 million pounds of U_3O_8 (McLemore and Chenoweth, 2017). Uranium districts are shown in Figure 4.90 and the Grants uranium district in Figure 4.91.

TABLE 4.57 Uranium production from 1947–2002 by type of deposit from New Mexico and total U.S. production (McLemore and Chenoweth, 1989, 2003. From McLemore and Chenoweth, 2017). [1]Production rounded to the nearest 1,000 pounds.

Type of deposit	Production (lbs U3O8)	Period of production (Years)	Production total in NM (%)
Primary, redistributed, remnant sandstone uranium deposits (Morrison Formation, Grants district)	330,453,000[1]	1951–1988	95.4
Mine water recovery (Morrison Formation, Grants district)	9,635,869	1963–2002	2.4
Tabular sandstone uranium deposits (Morrison Formation, Shiprock district)	493,510	1948–1982	0.1
Other Morrison Formation sandstone uranium deposits (San Juan Basin)	991	1955–1959	—
Other sandstone uranium deposits (San Juan Basin)	503,279	1952–1970	0.1
Limestone uranium deposits (Todilto Formation2, predominantly Grants district)	6,671,798	1950–1985	1.9
Other sedimentary rocks with uranium deposits (total NM)	34,889	1952–1970	—
Vein-type uranium deposits (total NM)	226,162	1953–1966	—
Igneous and metamorphic rocks with uranium deposits (total NM)	69	1954–1956	—
Total in New Mexico	927,917,000[1]	1947–2002	100
Total in United States	927,917,000[1]	1947–2002	NM is 37.5 of total U.S.

TABLE 4.68 Uranium production and types of deposits by district or subdistrict in the San Juan Basin, New Mexico (McLemore and Chenoweth, 1989, and updated production from 1988–2002 as estimated by the authors. From McLemore and Chenoweth, 2017).

District (District ID)	Production (lbs U_3O_8)	Grade (U_3O_8%)	Period of production (years)	Types of deposits
Grants district				
Laguna (DIS014)	>100,600,000	0.1–1.3	1951–1983	A, C, E
Marquez (DIS015)	28,000	0.1–0.2	1979–1980	A
Bernabe Montaño (DIS012)	None			A
Ambrosia Lake (DIS115)	>211,200,000	0.1–0.5	1950–2002	A, B, C, E
Smith Lake (DIS122)	>13,000,000	0.2	1951–1985	A, C
Church Rock-Crownpoint (DIS117)	>16,400,000	0.1–0.2	1952–1986	A, B
Nose Rock (DIS120)	None			A
Chaco Canyon (DIS116)	None			A

TABLE 4.19 Classification of uranium deposits in New Mexico (modified from McLemore and Chenoweth, 1989; McLemore, 2001, 2009). Deposit types in bold are found in the Grants uranium district. Deposit types in red are discussed in this report.

I. Peneconcordant U deposits in sedimentary host rocks

A. Morrison Formation (Jurassic) sandstone U deposits

- **Primary, tabular sandstone U-humate deposits in the Morrison Formation**
- **Redistributed sandstone U deposits in the Morrison Formation**
- **Remnant sandstone U deposits in the Morrison Formation**
- Tabular sandstone U-vanadium deposits in the Salt Wash and Recapture Members of the Morrison Formation

B. Other sandstone U deposits

- **Redistributed U deposits in the Dakota Sandstone (Cretaceous)**
- **Roll-front sandstone U deposits in Cretaceous and Tertiary sandstones**
- Sedimentary U deposits
- Sedimentary-copper deposits
- **Beach placer, thorium-rich sandstone U deposits**

C. Limestone U deposits

- **Limestone U deposits in the Todilto Formation (Jurassic)**
- Other limestone deposits

D. Other sedimentary rocks with U deposits

- **Carbonaceous shale and lignite U deposits**
- Surficial U deposits
- Fracture-controlled U deposits

E. Vein-type U deposits

- Copper-silver (U) veins (formerly Jeter-type, low-temperature vein-type U deposits and La Bajada, low-temperature U-base metal vein-type U deposits)
- **Collapse-breccia pipes (including clastic plugs)**
- Volcanic epithermal veins
- Laramide veins
- Arsenide 5-element veins

II. Disseminated U deposits in igneous and metamorphic rocks

F. Igneous and metamorphic rocks with disseminated U deposits

- Pegmatites
- Alkaline rocks
- Granitic rocks
- Carbonatites
- Miscellaneous
- Carbonatites
- Miscellaneous

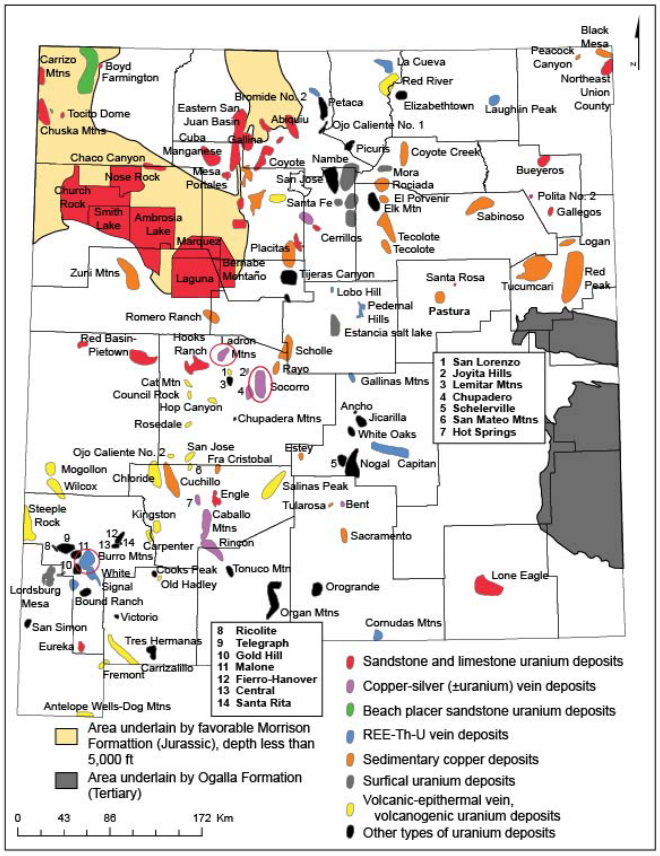

FIGURE 4.90 Uranium deposits in New Mexico (McLemore and Chenoweth, 1989, 2017). Red circle identifies location of Socorro, Ladron Mountains and Black Hawk districts. Samples were also collected from the Grants district shown in red polygons in northwestern New Mexico.

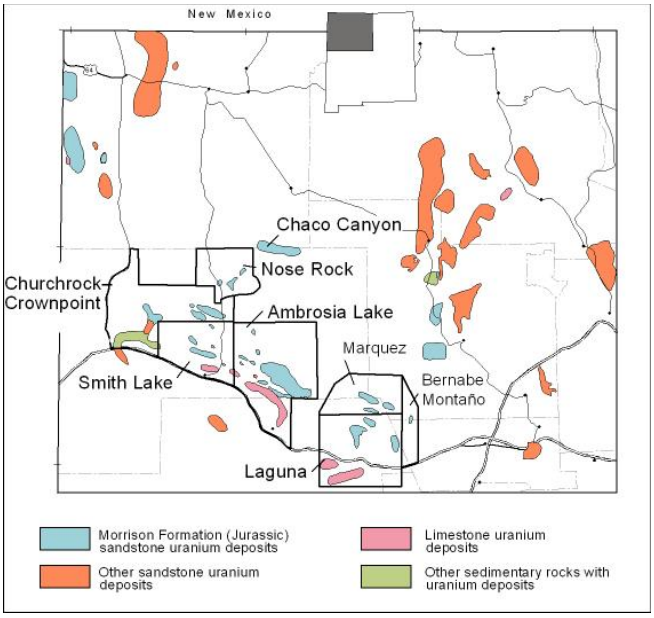

FIGURE 4.91 Grants U district (McLemore and Chenoweth, 1989).

New Mexico produced over 347 million pounds of uranium and more than 9 million pounds of vanadium between 1948–2002. Early uranium and vanadium minerals discovery were in the Carrizo Mountains, San Juan County in 1918 and was driven by the radium market for medicinal purposes. These discoveries were in a sandstone unit and was later named the Salt Wash Member of the Morrison Formation. Mining permits were restricted on the Navajo Reservation but became available by the Congressional Act of June 30, 1919. Vanadium Corporation of America (VCA) acquired leases in the Carrizo Mountains and started producing vanadium ore from 1942–1947. Uranium was secretly recovered from these ores by the Manhattan Engineer District (MED) from 1943–1945 (McLemore and Chenoweth, 2017).

Samples were collected from uranium deposits in Grants and Ladron Mountains districts and Saint Anthony mine (NMCI0047) to determine their critical minerals potential by examining their mineralogy and chemistry. Some samples in the Grants districts show elevated levels of U, V and Mo compared to the average crustal abundance.

4.14.2 Description of study areas

Grants uranium district, McKinley, Cibola, and Sandoval Counties

Sandstone uranium deposits account for most of the uranium production from the Grants district and the most significant deposits are those in the Morrison Formation, specifically the Westwater Canyon Member, where more than 169,500 short tons of U_3O_8 were produced from 1950 to 2002 (McLemore and Chenoweth, 1989, 2017). In contrast, production from other sandstone uranium deposits in New Mexico amounts to 234 short tons U_3O_8 (1948-1970, McLemore and Chenoweth, 1989, 2017).

Primary sandstone-hosted uranium deposits, also known as prefault, trend, blanket, and black-band ores, are found as blanket-like, roughly parallel ore bodies along trends, mostly in sandstones of the Westwater Canyon Member (Fig. 4.92, 4.93). These deposits are characteristically less than 2.4 m thick, average more than 0.20% U_3O_8, and have sharp ore-to-waste boundaries. The largest deposits in the Grants uranium district contain more than 30 million lbs of U_3O_8.

Redistributed sandstone-hosted U deposits, also known as post-fault, stack, secondary, and roll-type ores, are younger than the primary sandstone-hosted U deposits. They are discordant, asymmetrical, irregularly shaped, characteristically more than 2.4 m thick, have diffuse ore-to-waste contacts, and cut across sedimentary structures. The average deposit contains approximately 18.8 million lbs U_3O_8 with an average grade of 0.16% U_3O_8. Some redistributed U deposits are vertically stacked along faults.

Limestone uranium deposits are found in the Todilto limestone. Uranium is found only in a few limestones in the world, but the deposits in the Jurassic Todilto Formation are some of the largest and most productive. Uranium minerals were found in the Todilto Formation in the early 1920s, although it was Paddy Martinez's discovery in 1950 that resulted in development of the Grants district. From 1950 to 1981, mines in the Grants district yielded 6,671,798 lbs of U_3O_8 from the Todilto Formation, amounting to approximately 2% of the total uranium produced from the Grants district (McLemore and Chenoweth, 1989, 2017).

Limestone is typically an unfavorable host rock for uranium because of low permeability, porosity, and lack of precipitation agents, such as organic material. However, a set of unusual geological circumstances allowed the formation of uranium deposits in the Todilto Formation

(McLemore and Chenoweth, 2017). The organic-rich limestones were deposited in a sabkha environment (a coastal mudflat or sandflat environment in a semiarid to arid climate) on top of the permeable Entrada Sandstone. The overlying sand dunes of the Summerville or Wanakah Formation locally deformed the Todilto muds, producing the intraformational folds in the limestone. Uraniferous waters derived from a highland to the southwest migrated through the Entrada Sandstone. Groundwater migrated into the Todilto Formation by evapotranspiration or evaporative pumping. Uranium precipitated in the presence of organic material within the intraformational folds and associated fractures in the limestone.

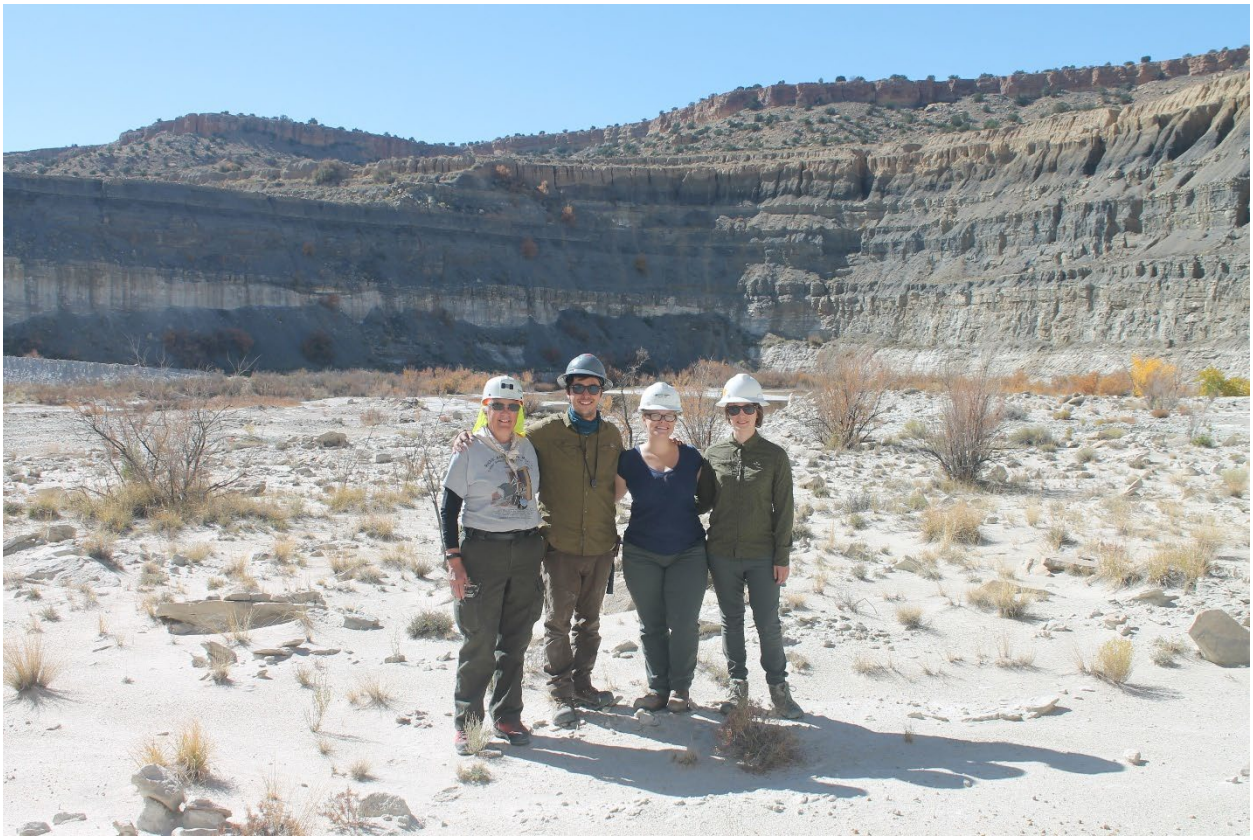

FIGURE 4.92 Sandstone beds with uranium minerals at the St. Anthony mine (photograph by V.T. McLemore, 10/27/2017).

FIGURE 4.93 Black uranium ore at the St. Anthony mine (photograph by V.T. McLemore, 10/27/2017).

Jeter mine, Ladron Mountains, Socorro County

North and McLemore (1986) originally classified two deposits in New Mexico as supergene-copper- uranium (silver) deposits: La Bajada (NMSF0024) and Jeter (NMSO0023, Ladron Mountains). McLemore (1983) and McLemore and Chenoweth (1989) described them as Jeter-type low-temperature, vein-type U deposits and La Bajada-type low-temperature, U-base metal, vein-type U deposits. Similar copper-silver vein deposits have been identified in other areas in New Mexico and the deposit type has been renamed Rio Grande Rift (RGR) copper-silver (±U) vein deposits (McLemore and Lueth, 2017; McLemore and Chenoweth, 2017). These vein deposits were formed at low temperatures, near-surface, and along Tertiary-age faults in Rio Grande Rift basins.

Veins at the Jeter mine are along faults and appear to be controlled by the distribution of carbonaceous mudstone (Fig. 4.94) Collins and Nye, 1957). Uranium is found along the Jeter fault, which is a gently-dipping, normal fault that places upper Santa Fe Group fanglomerates against Proterozoic Capirote granite. Only uranium and vanadium were produced from the Jeter mine (McLemore, 1983).

FIGURE 4.26 Caved Jeter mine adit (photograph by V.T. McLemore, 8/19/2016).

Socorro district, Socorro County

The Socorro mining district (McLemore and Chenoweth, 1989; McLemore, 2017), was first prospected during the late 1950s and has been known by several names, including Encarnacion, Agua Torres, Carthage, Little Davie, Lucky Don, and Marie districts. It is estimated that approximately $70,000 worth of uranium and vanadium were produced from Rio Grande Rift Cu-Ag (U) vein deposits (McLemore, 2017; McLemore and Chenoweth, 2017).

The Lucky Don and Little Davie mines were discovered in the early 1950's by E.R. Caprio. The Little Davie mine was operated by Holly U Corporation in 1955. Also known as the Bonanza mine, the Lucky Don mine was active during 1955-1956 and again during 1960-1963.

Uranium in the Little Davie and Lucky Don mines are hosted by limestones of the San Andres Formation. An adit was originally driven into the San Andres Formation for about 30 to 40 ft at Lucky Don, and it was later blasted after the ore run out. Today the mine consists of a cut face approximately 170 ft long, 4 short adits cut in the quarry face, a wooden loading bin and three waste rock piles with a volume of approximately 32,000 ft^3. Ore was blasted, hand sorted and trammed to a 15 to 20 short ton ore chute on the side of the hill. Total production from the Lucky Don mine amounted to 965 short tons of ore, yielding 4,168 lbs of U_3O_8 and 3,309 lbs of V_2O_5.

The Little Davie mine includes a 6 ft deep pit, a face cut and a waste rock pile (Fig. 4.95, 4.96). Ore from Little Davie was loaded into a pickup and hauled to the ore chute at Lucky Don. Equipment used in mining included a 125 cubic ft per minute compressor, a jackhammer, wheelbarrows, and picks and shovels. Total production from the Little Davie mine amounted to 17 short tons yielding 60 lbs of U_3O_8 and 71 lbs of V_2O_5.

FIGURE 4.95 Little Davie mine (photograph by V.T. McLemore, 8/9/2016).

FIGURE 4.96 Yellow uranium minerals in silicified breccia at the Little Davie mine (photograph by V.T. McLemore, 8/9/2016).

4.14.3 Petrography and mineralogy

Uranium ores in New Mexico, especially the Grants sandstone deposits, have been difficult to characterize mineralogically because of the association with organic material and much of the uranium is amorphous or too fine-grained to identify (McLemore and Chenoweth, 2017; Li, 2018; Caldwell, 2018; Pearce, 2020). Carnotite and tyuyamunite have been well known from throughout New Mexico deposits (McLemore and Chenoweth, 2017). The Todilto uranium deposits are known for spectacular specimens of uranophane and santafeite (McLemore and Chenoweth, 2107). A partial list of minerals from the Grants district are in Table 2 and minerals from the Black Hawk district are listed in Table 4.20.

TABLE 4.20 Minerals identified by McLemore and Chenoweth (2017), Caldwell (2018), Pearce (2020) and others with their respective chemical formulas. Elements in red are critical minerals (Fig. 1.2).

Group	Mineral Name	Formula
Silicate	Coffinite	$U(SiO_4)_{1-x}(OH)_{4x}$
Oxide	Uraninite (pitchblende)	UO_2
Hydroxy-Oxide	Schoepite	$(UO_2)_8O_2(OH)_{12}•12H_2O$
	Meta-Schoepite	$UO_3•1\text{-}2H_2O$
	Studtite	$[(UO_2)O_2(H_2O)_2](H_2O)_2$
Uranyl-Sulfate	Zippeite	$K_4(UO_2)_6(SO_4)_3(OH)_{10}•4H_2O$
	Natrozippeite	$Na_4(UO_2)_6(SO_4)_3(OH)_{10}•4H_2O$
	Jachymovite	$(UO_2)_8SO_4(OH)_{14}•13H_2O$
Uranyl-Phosphate	Autunite	$Ca(UO_2)_2(PO_4)_2•10H_2O$
	Meta-Autunite	$Ca(UO_2)_2(PO_4)_2•2\text{-}6H_2O$
	Meta-Ankoleite	$K_2(UO_2)_2(PO_4)_2•6(H_2O)$
	Chernikovite	$(H_3O)_2(UO_2)_2(PO_4)2•6(H_2O)$
	Phurcalite	$Ca_2(UO_2)_3O_2(PO_4)_2•7(H_2O)$
	Sabugalite	$HAl(UO_2)_6(PO_4)_4•16H_2O$
Uranyl-Carbonate	Andersonite	$Na_2Ca(UO_2)(CO_3)_3•6\ H_2O$
	Cejkaite	$Na_4(UO_2)(CO_3)_3$
	Oswaldpeetersite	$(UO_2)_2CO_3(OH)_2•4(H_2O)$
Uranyl-Vanadate	Carnotite	$K_2(UO_2)_2(VO_4)_2•3H_2O$
	Meta-Tyuyamunite	$Ca(UO_2)_2\ (VO_4)_2•(3\text{-}5)H_2O$
	Tyuyamunite	$Ca(UO_2)_2V_2O_8·(5–8)H_2O$
Sulfate	Gypsum	$CaSO_4•2H2O$
	Hexahydrite	$MgSO_4$
	Hydronium-Jarosite	$(H_3O)Fe_3(SO_4)_2(OH)_6$
	Natrojarosite	$NaFe_3(SO_4)_2(OH)_6$
	Minasragrite	$(VO)SO_4•5H_2O$
Vanadate	Magnesiopascoite	$Ca_2MgV_{10}O_{28}•16H_2O$
Carbontate	Calcite	$CaCO_3$
Sulfide	Pyrite	FeS_2
Molybdate	Ilsemannite	$Mo_3O_8•n(H_2O)$
Native Metal	Selenium	Se
	Uranophane	$(Ca(UO_2)_2(SiO_3OH)_2·5H_2O)$
	Santafeite	$(Ca,Sr,Na)_3\ (Mn^{2+}, Fe^{3+})\ 2Mn^{4+}\ 2(V^{5+}O_4)\ 4(OH,O)\ 5·2H_2O$

4.14.4 Geochemical analyses

Chemical analyses of selected critical minerals and uranium concentrations in the samples are in Appendix 7 and Figures 4.97, 4.98, 499, and 4.100. Elevated uranium and vanadium are present in all samples (Fig. 4.98, 4.99, 4.100). Elevated Cu and Cs are found in the Jeter samples. Although the total REE in all samples are below economic grades, some samples from Black Hawk district and sandstone-hosted uranium deposits (St. Anthony mine) are elevated heavy REE (Fig. 4.97). Elevated Cs is found in samples from the Jeter mine.

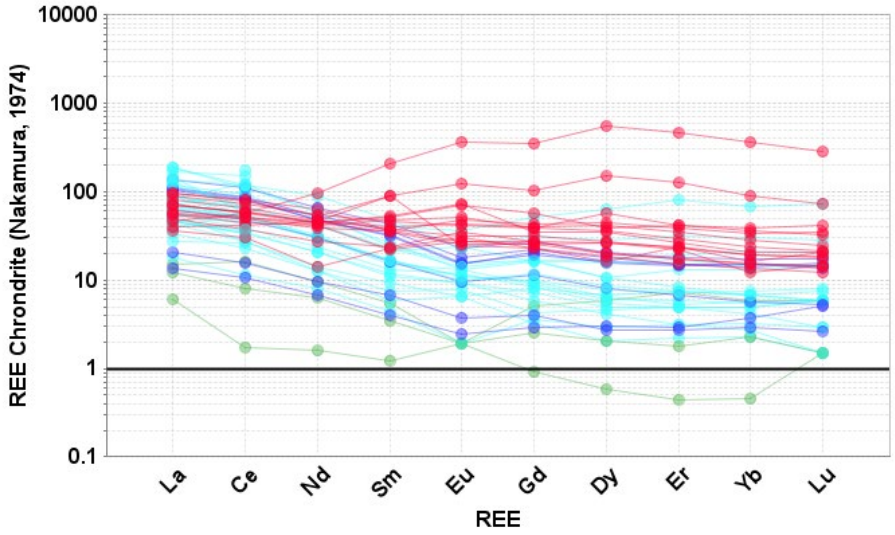

FIGURE 4.97 Chondrite-normalized REE plot of selected uranium samples (chondrite values from Nakamura, 1974). Note the enriched heavy REE for some of the 5-element veins and sandstone-hosted U samples.

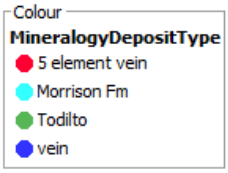

FIGURE 4.98 Co-Ni plot of selected uranium samples. Note the strong correlation and elevated values for the 5-element veins.

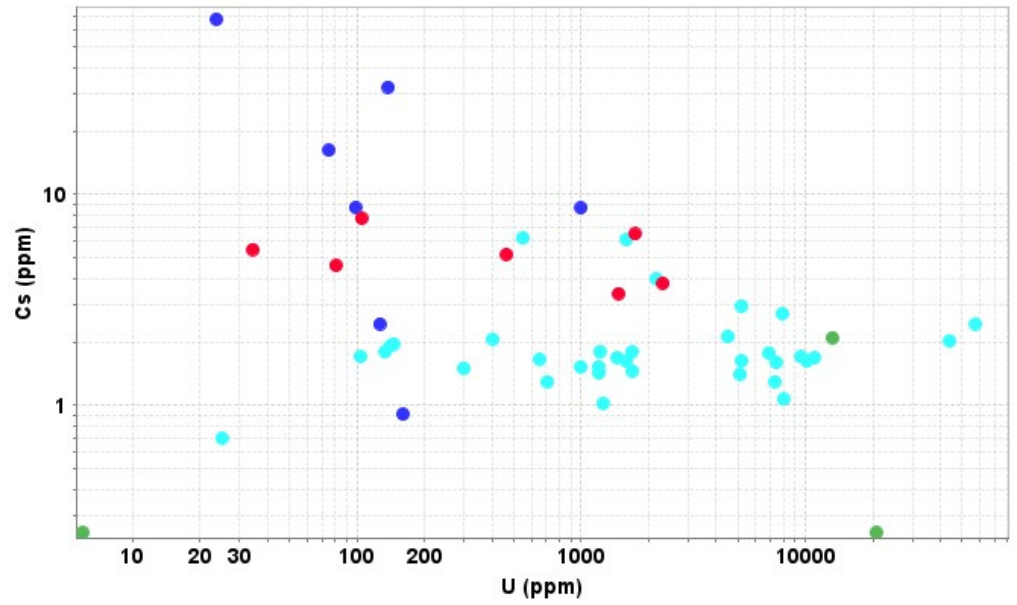

FIGURE 4.27 Cs-U plot of selected uranium samples. Note the elevated Cs for the U-veins from samples from the Jeter mine.

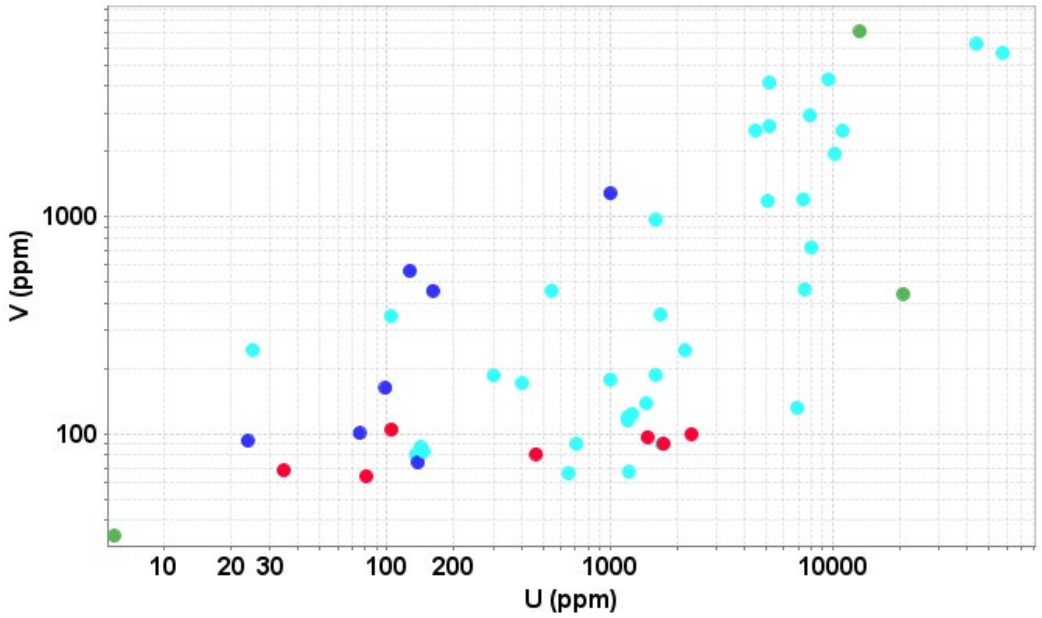

FIGURE 4.28 U-V plot of selected uranium samples. Note the elevated U and V in many samples.

4.14.5 Preliminary conclusions

Some sandstone-hosted, limestone-hosted, and U-vein deposits are elevated in critical minerals. One sandstone-hosted sample contained 0.3 ppm Re (critical mineral), 659 ppm Se and 408 ppm Mo. Some samples are elevated in heavy REE. Elevated Cu and Cs are found in the

Jeter samples. An estimated 146 million short tons of ore containing >236 million lbs of uranium at grades ranging from 0.1-0.4 U_3O_8 are found in the Grants uranium district (Tables 1.3, 1.4). Future exploration should include evaluation of critical minerals in these deposits, especially for V, REE, Re from molybdenite, and Cs.

4.15 Critical minerals potential of the Cuba Manganese deposits (V.T. McLemore)

4.15.1 Introduction

The Cuba Manganese mining district is north of Cuba in Sandoval County, New Mexico (Fig. 4.101; McLemore et al., 1984; McLemore, 2017, 2025). Four small sedimentary manganese deposits have been found and yielded production (Table 4.21). Economically, manganese is essential to the chemical and manufacturing industries because of important chemical and metallurgical properties, such as desulfurizing, deoxidizing, and alloying. Manganese is classified as a critical mineral by the U.S. government, because there is no current manganese production in the U.S. and supply chain disruptions are likely (Cannon et al., 2017). Reexamination of the mineral resources in the sedimentary manganese deposits in the Cuba Manganese district is warranted considering today's economic importance of critical minerals, which are essential in most of our electronic devices.

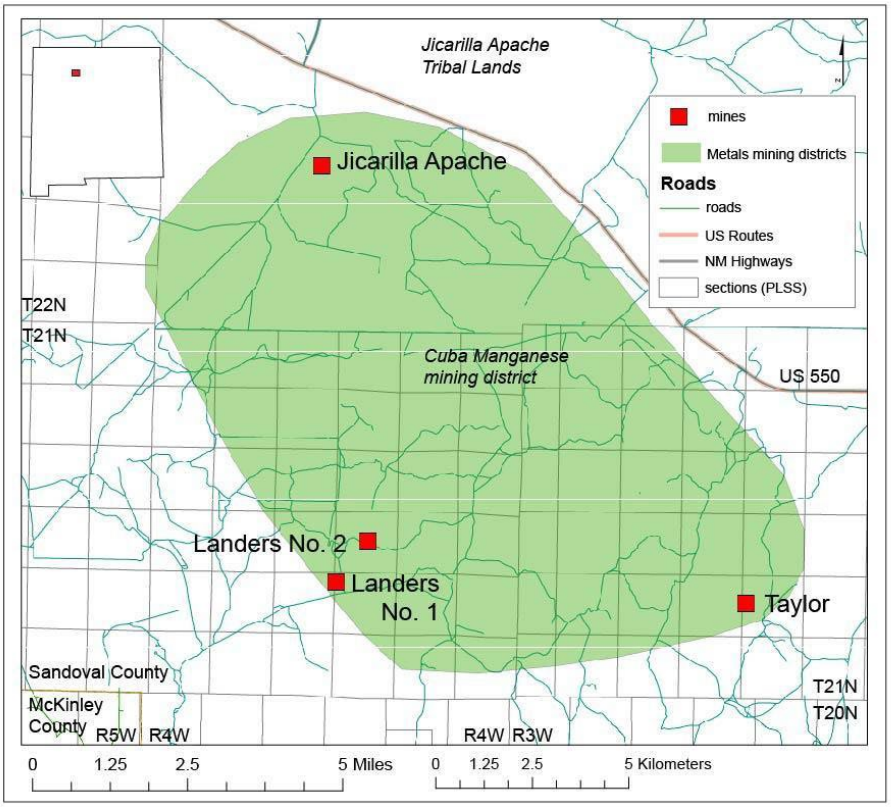

FIGURE 4.101 Location of manganese mines (i.e., deposits) in the Cuba Manganese mining district, Sandoval County, New Mexico. District boundaries modified from McLemore (2017).

TABLE 4.21 Production from mines in the Cuba Manganese mining district (U.S. Bureau of Mines, 1942–1959; Farnham, 1961; Dorr, 1965). W = withheld production. Mine ID is from the New Mexico Mines database.

Year	Mine ID	Mine	Latitude, longitude	Production (long tons)	Grade Mn%
1942	NMSA0302, NMSA0303	Landers No. 1 and 2	36.025199, −107.25302; 36.0348139, −107.2439777	2242	41
1944–1945	NMSA0366	Taylor	36.021371, −107.134455	896	38
1952–1955	NMSA0302, NMSA0303	Landers No. 1 and 2	36.025199, −107.25302; 36.0348139, −107.2439777	68	38
1957–1958	NMSA0302, NMSA0303	Landers No. 1 and 2	36.025199, −107.25302; 36.0348139, −107.2439777	271	41
1957–1958	NMSA0056	Jicarilla Apache	36.1229321, −107.2588777	309	36
1958–1959	NMSA0302, NMSA0303	Landers No. 1 and 2	36.025199, −107.25302; 36.0348139, −107.2439777	w	w
Total				3786	

Four mine sites (i.e., deposits) are found in the Cuba Manganese district (Fig. 4.101): Landers No. 1, Landers No. 2, Taylor, and Jicarilla Apache (locations are in Table 4.21). In 1926, W. Crook staked the first claims, but production did not occur until 1942 (Farnham, 1961). Only the Landers No. 1 and Taylor deposits were examined and sampled in 2024; the roads were washed out leading to Landers No. 2 and the Jicarilla Apache deposit is in the Jicarilla Apache Nation. Sample information is in Table 4.22 and Appendix 7.

TABLE 4.22 Location and brief description of samples collected from the Cuba Manganese district, Sandoval County, New Mexico. Latitude and longitude are in WGS83.

Sample Id	Date collected	Date analyzed	Chem Lab File No.	Latitude	Longitude	Method collected	Sample source	Sample description
Coal370	10/9/2024	11/14/2024	RE24294640	36.021371	−107.134455	composite	outcrop	Mn from dump, Taylor
Coal371	10/9/2024	11/14/2024	RE24294640	36.025199	−107.25302	select	outcrop	Mn nodules, Landers No. 1
Coal372	10/9/2024	11/14/2024	RE24294640	36.025199	−107.25302	composite	outcrop	Mn sandstone bed, Landers No. 1
Coal373	10/9/2024	11/14/2024	RE24294640	36.025199	−107.25302	select	outcrop	fossil log, Landers No. 1

The Landers No. 1 and No. 2 mines (also known as Crook No. 1 and Crook No. 2) were first mined in 1942 by R.E. Anderson of the Good Luck Mining Co. Ore was shipped to the Deming manganese stockpile. Between 1952 and1955, Sterling C. Landers operated the mines until the Deming manganese stockpile closed in 1955. J.F. McRee then operated the mines. The mines consisted of open pits and trenches.

The Taylor mine (also known as Miller) was located in 1941 by Joel Taylor and leased to T.B. Everhart and D.B. Miller in 1943 (Fig. 4.102). Everhart and Miller mined the deposit in 1944 and 1945 by surface pits and trenches and shipped the ore to a mill near the paved highway. J.F. McRee then operated the mine again in 1957.

The Jicarilla Apache mine was operated by J.F. McRee in 1957 under a lease from the tribe. The ore was shipped to Socorro (Farnham, 1961).

FIGURE 4.102 Reddish-brown manganese at the Taylor mine (photograph by V.T. McLemore, 10/9/2024).

4.15.2 Geologic setting

The four manganese deposits are hosted in the Paleogene San Jose Formation, which is predominantly sandstone with interbedded shales deposited by mostly streams and floodplains (Smith and Lucas, 1991). Manganese ore is generally found in 1–2 m-thick stratiform or blankets of rounded to subrounded manganese nodules in shale or fine-grained sandstone, generally in pods less than 100 m long, few meters wide, and only thousands of metric tons in size. Farnham (1961) reported the manganese mineralization as psilomelane (a general term for a group of hard black manganese oxide minerals). XRD analyses indicated the primary manganese mineral is pyrolusite (McLemore, 2025). Other major minerals in the deposits include quartz, hematite/goethite, a spinel group mineral, clay, and albite.

The Cuba Manganese deposits formed in reducing conditions where anoxic waters mixed with shallow oxygen-rich waters, creating reducing conditions which allowed the manganese to precipitate (Force and Cannon, 1988; Cannon et al., 2017). Stratigraphic studies by Smith and Lucas (1991) indicated that similar anoxic conditions were found in local stratified, lacustrine-deltaic environments in the San Jose Formation. These environments are rare in the San Jose Formation and not expected to contain large resources of manganese.

4.15.3 Critical minerals

Manganese concentrations of samples collected from two of the deposits range from 5 to >39% MnO; whereas arsenic ranges from 3.5 to 206 ppm (Tables 4.23 and 4.24; Appendix 7). Barium (6,190 to >10,000 ppm) and cobalt (32 to 354 ppm) are elevated in these deposits (Fig. 4.103; Table 4.24), but these concentrations are too low to be economic. Rare earth elements and

other critical minerals are at normal concentrations for sedimentary deposits and are not economic (Fig. 4.104; Table 4.24). The Cuba Manganese deposits are small in tonnage and currently have no economic potential. There are no additional critical minerals known in the Cuba Manganese mining district as indicated by the chemical analyses (Tables 4.23 and 4.24). There is potential for finding additional subsurface sedimentary manganese deposits in the area, but they are likely to be small in tonnage and uneconomic because the local stratified, lacustrine-deltaic environments in the San Jose Formation hosting the manganese deposits are too small (Smith and Lucas, 1991) for the millions of tons of manganese ore needed to form an economic manganese deposit.

TABLE 4.23 Chemical analyses of major elements (in wt %) of samples collected from the Cuba Manganese district. Locations and brief descriptions of samples are in Table 1. Fe_2O_3T = total iron reported as Fe_2O_3. Major oxides were determined by XRF (X-ray fluorescence), S and C by combustion analysis by induction furnace, and LOI (loss on ignition) by furnace at 500ºC after sample was pre-dried at 105ºC.

Sample ID/element	Coal370	Coal371	Coal372	Coal373
SiO_2	16.57	10.78	75.31	94.85
TiO_2	0.15	0.17	0.36	0.01
Al_2O_3	4.53	2.91	7.89	0.23
Fe_2O_3T	26.85	13.40	1.82	3.05
MnO	33.80	>39	5.29	0.12
MgO	0.16	0.13	0.36	0.03
CaO	1.22	1.00	0.59	0.06
Na_2O	0.09	0.08	1.43	0.09
K_2O	0.46	0.41	2.61	0.07
P_2O_5	0.72	0.66	0.06	0.03
LOI	10.65	10.69	2.46	0.77
S	0.40	0.50	0.04	0.22
C	0.10	0.05	0.04	0.14
Total oxides	95.7	79.78	98.26	99.67

TABLE 4.24 Chemical analyses of trace elements (in ppm) of samples collected from the Cuba Manganese district. Locations and brief descriptions of samples are in Table 1. ME-MS81 = lithium borate fusion prior to acid dissolution followed by ICP-MS analysis. ME-MS42 = aqua regia digestion followed by ICP-MS analysis. F-ELE81a = KOH fusion and ion selective electrode. Au-ICP21 = aqua regia digestion followed by ICP-MS analysis. ME-4ACD81 = four acid digestion followed by ICP-MS analysis. TREE=total (sum) of REE.

Sample ID/element	Coal370	Coal371	Coal372	Coal373	Method of analysis
F	780	700	180	30	F-ELE81a
Au	<0.001	<0.001	0.003	0.001	Au-ICP21
Ag	<0.5	<0.5	<0.5	<0.5	ME-4ACD81
As	206	150.5	3.5	71.1	ME-MS42
Ba	>10,000	>10,000	6190	491	ME-MS81
Bi	0.18	0.2	0.08	0.01	ME-MS42
Cd	1.1	1.5	1.9	<0.5	ME-4ACD81
Co	323	354	32	3	ME-4ACD81
Cr	16	12	20	25	ME-MS81
Cs	1.18	1.18	2.11	0.07	ME-MS81
Cu	49	70	6	3	ME-4ACD81
Ga	22.6	34.6	12.5	1.8	ME-MS81
Ge	4.8	2.9	1.1	2.7	ME-MS81
Hf	2.49	1.62	11.3	0.2	ME-MS81
Hg	0.041	0.049	0.02	0.014	ME-MS42
In	0.024	0.021	0.011	<0.005	ME-MS42
Li	10	20	20	10	ME-4ACD81
Mo	3	1	<1	3	ME-4ACD81
Nb	3.55	3.74	9.41	0.35	ME-MS81
Ni	51	72	8	2	ME-4ACD81
Pb	89	69	16	65	ME-4ACD81
Rb	21.5	16.7	81.8	2.3	ME-MS81
Sb	2.13	1.87	0.07	1.42	ME-MS42
Sc	5.9	4.7	2	0.3	ME-MS42
Se	1.1	0.4	0.2	0.3	ME-MS42
Sn	0.5	0.7	0.8	<0.5	ME-MS81
Sr	567	1080	304	69.6	ME-MS81
Ta	0.2	0.2	0.7	<0.1	ME-MS81
Te	0.16	0.2	0.01	0.01	ME-MS42
Th	8.5	4	8.7	0.58	ME-MS81
Tl	1.37	2.2	0.24	1.36	ME-MS42
U	10.2	8.73	2.39	0.26	ME-MS81
V	74	122	30	9	ME-MS81
W	1.5	2.2	1.1	<0.5	ME-MS81
Y	25.2	40.4	21.6	2.5	ME-MS81
Zn	150	135	58	4	ME-MS81

Sample ID/element	Coal370	Coal371	Coal372	Coal373	Method of analysis
Zr	110	71	485	10	ME-MS81
La	45.90	39.50	32.70	2.80	ME-MS81
Ce	180.50	140.00	72.00	5.40	ME-MS81
Pr	8.91	12.25	8.49	0.75	ME-MS81
Nd	33.40	51.40	34.40	2.70	ME-MS81
Sm	7.13	10.50	6.16	0.77	ME-MS81
Eu	1.54	2.09	1.22	0.14	ME-MS81
Gd	6.38	9.98	4.96	0.72	ME-MS81
Tb	1.01	1.50	0.69	0.09	ME-MS81
Dy	5.19	8.13	3.86	0.54	ME-MS81
Ho	1.06	1.56	0.76	0.11	ME-MS81
Er	3.08	4.46	2.41	0.30	ME-MS81
Tm	0.39	0.62	0.33	0.05	ME-MS81
Yb	2.62	3.40	2.31	0.19	ME-MS81
Lu	0.35	0.46	0.35	0.04	ME-MS81
TREE	297.46	285.85	170.64	14.60	Sum of REE

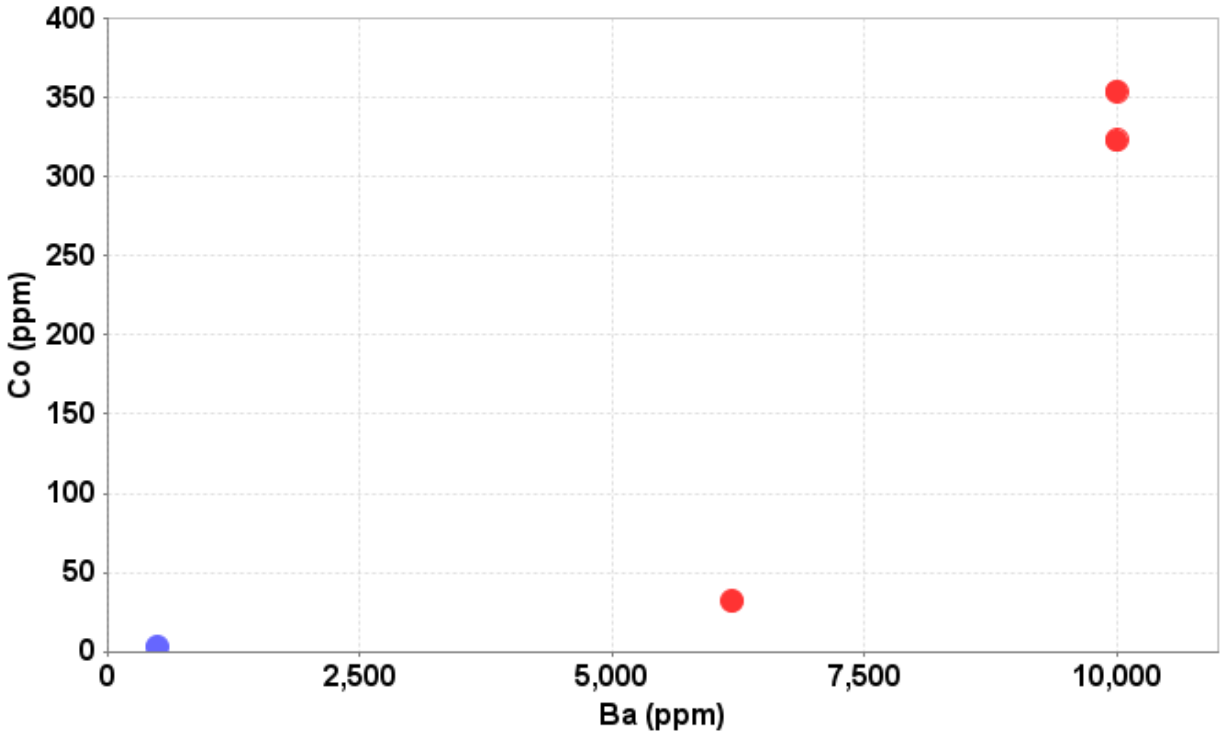

FIGURE 4.103 Co versus Ba plot of samples from the Cuba Manganese district. Co and Ba are in ppm. Chemical analyses are in Appendix 7.

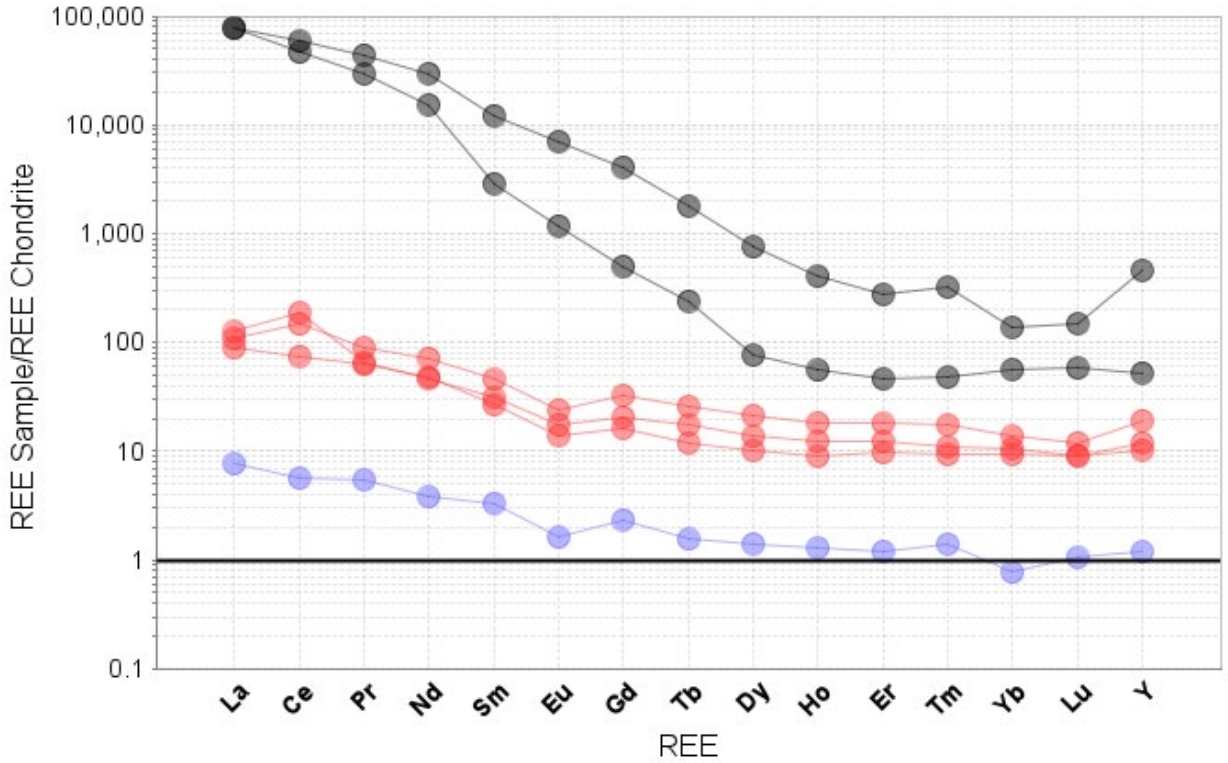

FIGURE 4.104 Chondrite-normalized REE plot for samples from the Cuba Manganese district showing the relatively low concentrations of REE compared to REE deposits currently in production. Chemical analyses are in Table 4. Blue = manganese deposits. Red = petrified wood. Chondrite values from Taylor and McLennan (1985). Black lines are representative REE analyses of major deposits in production, for comparison. 1 = Mt. Weld laterite deposit, 2 = Mountain Pass, Ca carbonatite deposit (Verplanck et al., 2014).

4.15.4 Conclusions

The Cuba Manganese deposits form in small, local lacustrine-deltaic environments where anoxic waters mixed with shallow oxygen-rich waters, creating reducing conditions that allowed the manganese to precipitate. Although, the Cuba Manganese district has manganese concentrations similar to economic deposits (>39% MnO), the deposits are small in tonnage and have no economic potential at this time. Barium and cobalt are elevated in these deposits, but the concentrations are too low to be economic. There are no additional critical minerals known in the Cuba Manganese mining district.

4.16 Critical minerals potential of perlite deposits (E.J. Owen and V.T. McLemore)

New Mexico is a significant producer of perlite (McLemore and Austin, 2017). Some of these deposits are found in and near the San Juan Basin (Fig. 4.105) and could have potential for critical minerals or could be a potential source of critical minerals in the coal and adjacent strata.

The industrial term perlite refers to any volcanic glass that expands appreciably by vesiculation under an appropriate heat-treating method and includes some obsidians, pitchstones, vitrophyres, as well as the expanded product. Perlite is associated with young (Paleogene or younger) felsic volcanic rocks, as the glassy phases are relatively unstable and devitrify via

crystallization with age. Perlite, as the expanded product, has a diverse range of applications, including lightweight plasters and mortars, insulation, ceiling tiles, filtration, and as a soil amendment. Perlite deposits of developed or potential commercial value are found in the western half of New Mexico related to rhyolitic volcanic fields at or near eruptive centers. New Mexico leads the nation in perlite production (McLemore and Austin, 2016). A list of New Mexico perlite deposits with descriptions can be found in McLemore and Austin (2016).

Four samples of raw perlite were collected from three perlite deposits in New Mexico to assess the critical minerals potential of the material in the state (Fig. 4.106). These deposits include the Dicalite mine in Socorro (https://www.dicalite.com/about/), the Grants perlite mine near Grants, and the El Grande perlite mine in Taos County. Chemically, the perlite contains predominantly SiO_2 (68-74 wt. %), with lesser Al_2O_3 (11-13 wt. %), H_2O (3-10 wt. %), K_2O (~4 wt. %), and Na_2O (up to ~4 wt. %). The Socorro perlite is classified as dacite based on the TAS classification diagram (Fig. 4.107; Le Maitre, 1989), while the Grants and El Grande samples are classified as rhyolites.

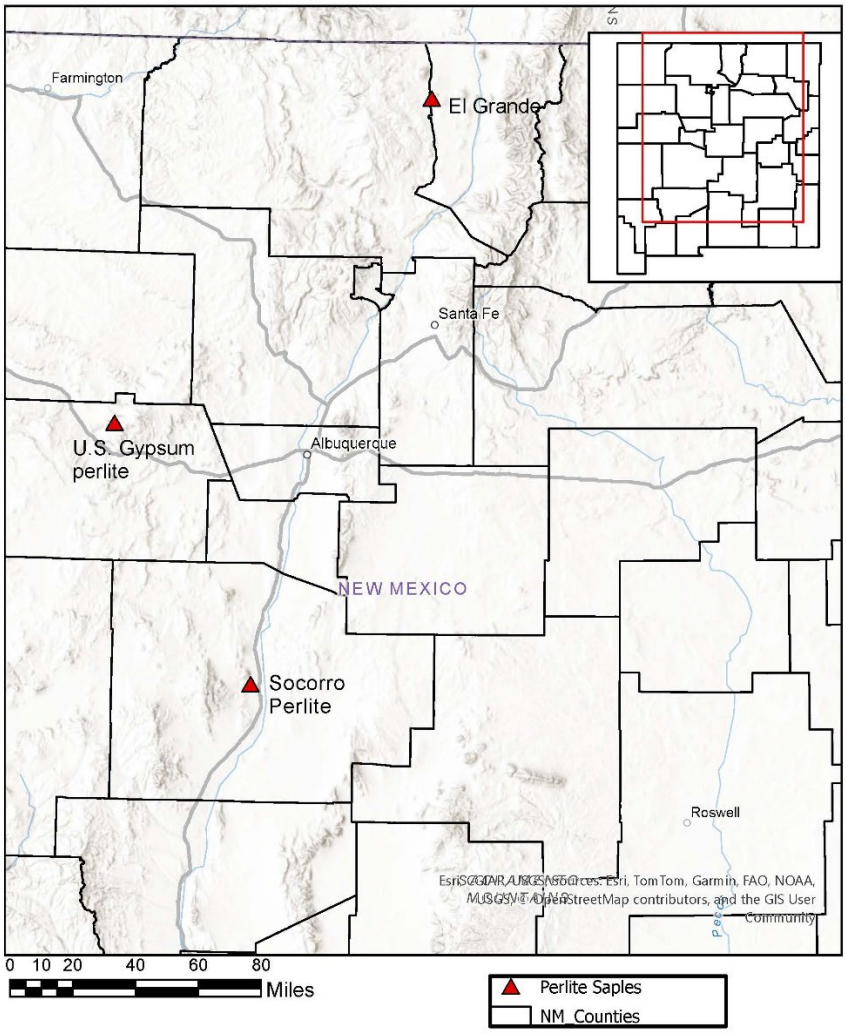

FIGURE 4.105 Location of perlite in New Mexico.

FIGURE 4.106 Socorro perlite (white) mine (photograph by V.T. McLemore, 6/26/20).

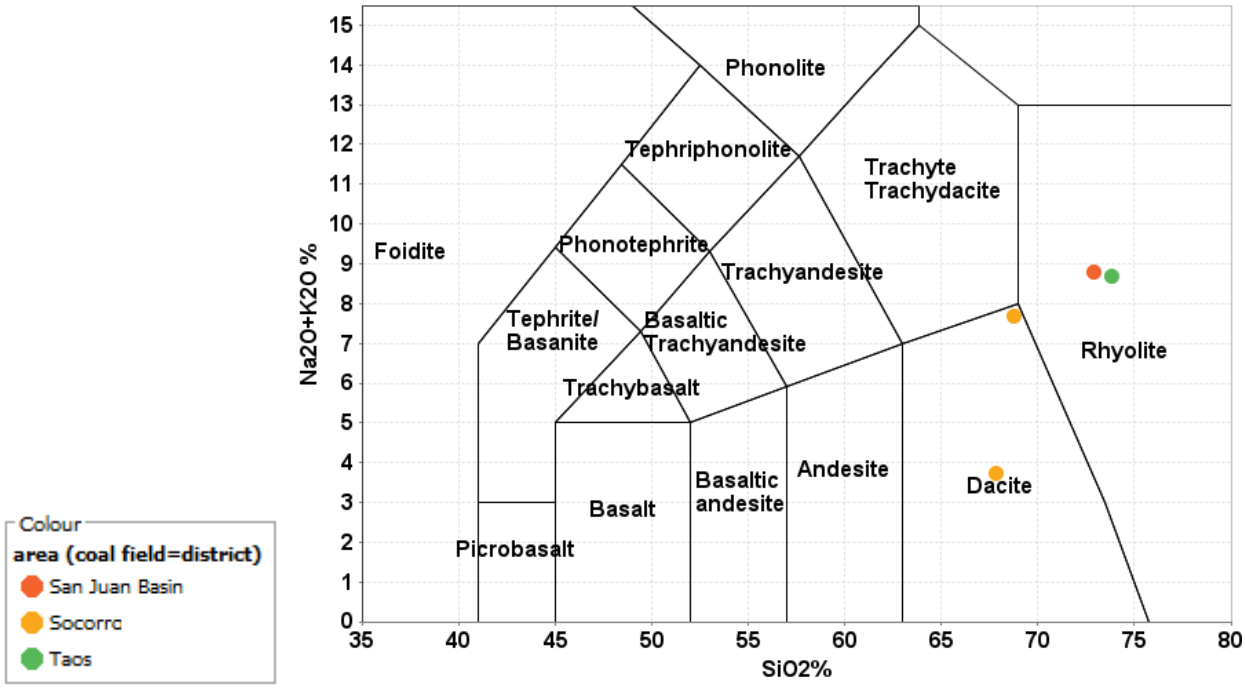

FIGURE 4.29 Total alkali-silica (TAS) classification diagram from Le Maitre (1989) showing Socorro perlite classified as dacite, while Grants and El Grande perlite are classified as rhyolite.

The critical minerals potential of perlite based on these samples is quite low, with most critical minerals at or below average crustal abundance values (Table 4.25; Rudnick and Gao, 2003; Hu and Gao, 2008). Normalizing the perlite samples to C1 chondrite (Fig. 4.108; McDonough and Sun, 1995) show two distinct patterns of minor REE enrichment: LREE enrichment (up to around 100 times chondritic values) relative to HREE (Socorro samples) and uniform REE enrichment up to around 40 times chondritic values (Grants and El Grande samples). Both patterns show distinct negative Eu anomalies. Nonetheless, these values are too low to be of economic significance for critical minerals. At this time, no further investigation into the critical mineral potential of perlite in New Mexico is recommended.

TABLE 4.25 Comparison of critical mineral concentrations in average perlite and average upper continental crust (UCC). Units in parts per million (ppm) except where noted.

Perlite n=4	Avg. perlite	Avg. UCC abundance		Avg. perlite	Avg. UCC abundance		Avg. perlite	Avg. UCC abundance
TiO_2 (%)	0.10	0.64	Nb	73.2	11.6	La	22.4	31
Al_2O_3 (%)	12.38	15.40	Ni	4	34	Ce	46.2	63
MgO (%)	0.40	2.48	Rb	266	94	Pr	5.2	7.1
K_2O (%)	4.03	2.80	Re (ppb)	<1	0.02	Nd	19	27
As	3.2	5.7	Sb	0.093	0.075	Sm	4.5	4.7
Ba	297	624	Sc	1	14	Eu	0.3	1
Bi	0.65	0.23	Sn	7.7	2.2	Gd	4	4
Co	2	15	Sr	152	320	Tb	0.8	0.7
Cr	7	73	Ta	9.5	0.9	Dy	5.1	3.9
Cs	6.8	4.9	Te	<0.01	0.027	Ho	1.08	0.83
Cu	52	27	U	7.2	2.6	Er	3.5	2.3
Ga	22.9	18.6	V	13	106	Tm	0.59	0.37
Ge	2.1	1.3	W	2.3	1.4	Yb	4.34	2.34
Hf	5.8	5.3	Y	40	21	Lu	0.71	0.36
In	0.021	0.066	Zn	85	75			
Li	60	41	Zr	131	193			

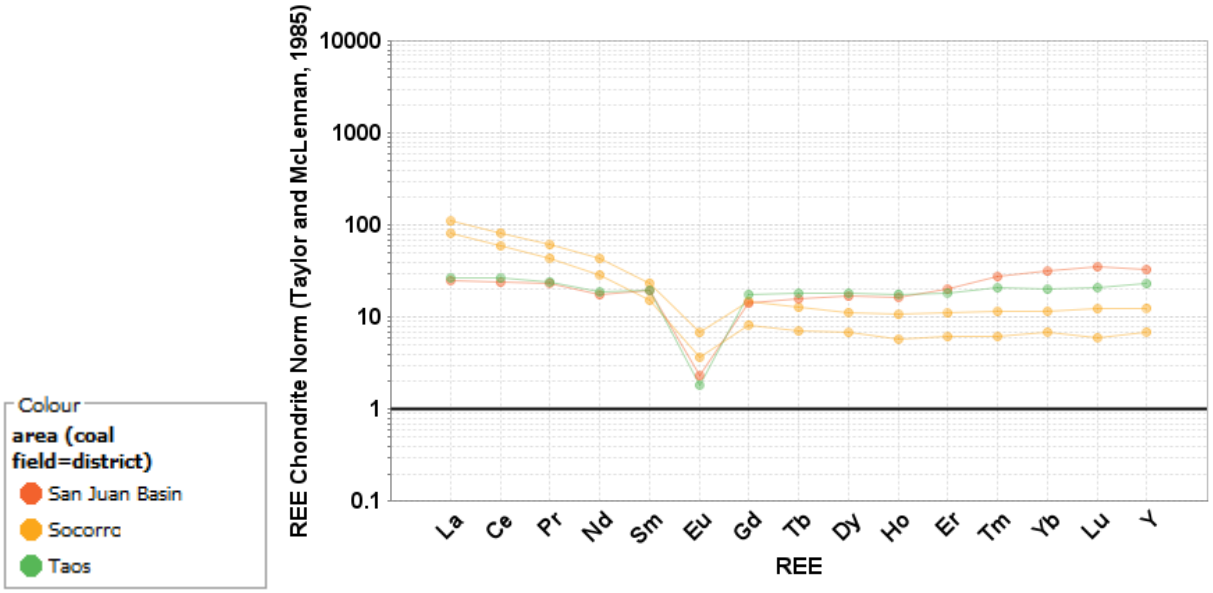

FIGURE 4.108 Chondrite normalized REE diagram (Taylor and McLennan, 1985) showing two distinct patterns for perlite. Socorro perlite is relatively LREE enriched, while Grants and El Grande perlites are uniformly enriched. All samples show a distinct negative Eu anomaly.

4.17 Evaluation of drill core in the San Juan and Raton basins (M. Badonie, V. Robledo, and V.T. McLemore)

More than 3000 ft of drill core stored at the NMBGMR core facility has been logged, photograph, and sampled as part of this project (Fig. 4.109, 4.110). Sample descriptions and chemical analyses are in Appendix 7. In addition, several theses in past years have sampled and described drill core; those data are in Appendix 7. Photographs of the core are found at https://photoarchive.nmt.edu/.

The drill core indicates an immature depositional environment with a macerals-rich matrix, angular quartz, twinned feldspar, kaolinite, muscovite, plant fragments, and oxidation evidence with mixed detrital sources including zircon, rutile, and framboidal pyrite. Examination of drill core has shown no apparent trend of elements downhole with changes in lithology. The element concentrations of coal and sedimentary rocks above and below the coal seams are similar in composition (Fig. 110, Appendix 7). However, it does appear that thinner coal seams (less than 6 inches) had higher TREE+Y totals compared to thicker coal seams.

Additional study of drill core is recommended, especially as drilling programs occur at the active coal mines.

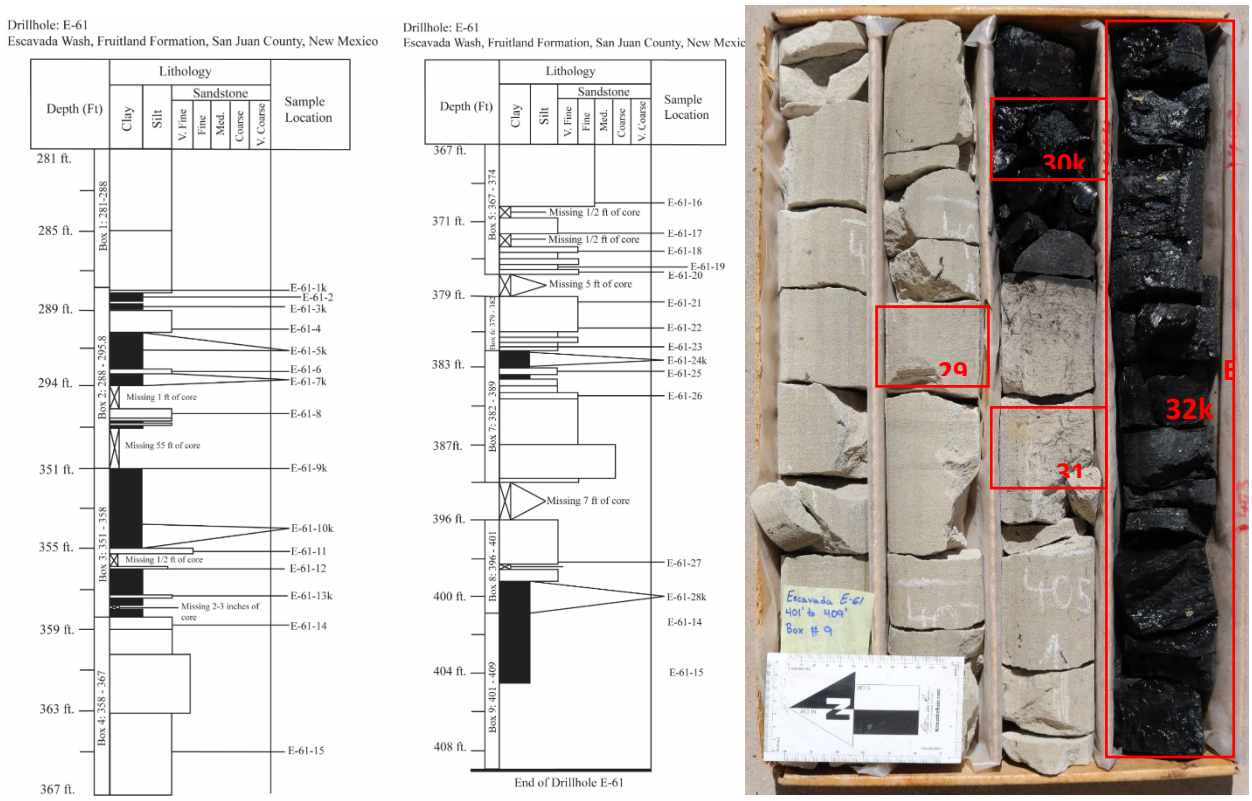

FIGURE 4.109 Stratigraphic column of drill hole E-61 for depth 281-367 ft (left) and 367-408 ft and photograph of core from 401-409 ft (right). Missing core indicated by X. (by M. Badonie).

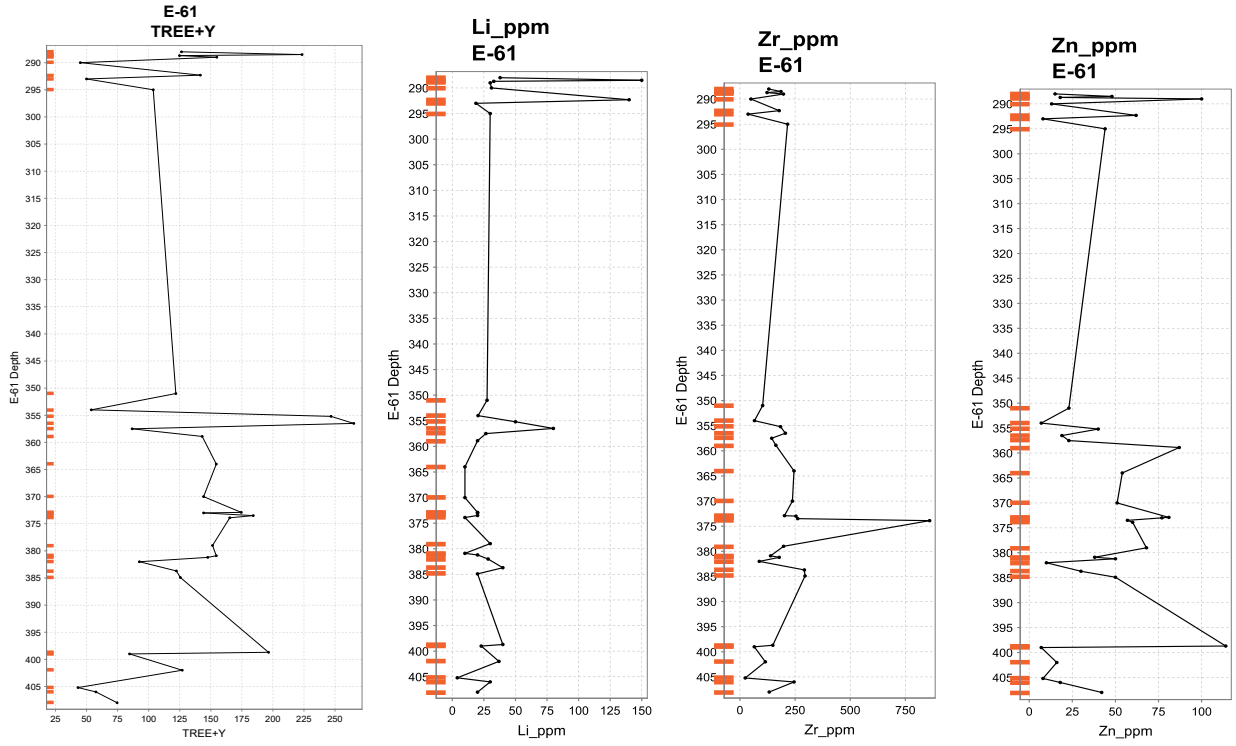

FIGURE 4.110 Chemical plots showing concentrations vertically downhole, for drill hole E-61.

4.17 Sources of REE and critical minerals in the San Juan and Raton basins (V.T. McLemore)

Understanding the source of REE and critical minerals in the San Juan and Raton basins is important in evaluating the resource potential of REE and critical minerals. However, the source of the REE and critical minerals in the San Juan and Raton basins is not well constrained. Uranium is found in Jurassic rocks in the San Juan Basin and could provide insights into the source of REE and critical minerals, since they locally are found together (McLemore and Chenoweth, 2017). Vanadium, a critical mineral, is found with most of the uranium deposits in the San Juan Basin (McLemore and Chenoweth, 2017).

Three possible theories of sources of REE, uranium, and critical minerals in New Mexico have been identified:

- Adjacent highlands consist of Proterozoic granitic rocks enriched in REE, uranium, and critical minerals. Both basins also have a relatively high heat flow, which provides elevated temperatures that enhance mobilization of REE, uranium, and critical minerals. The Zuni and Nacimiento Mountains lie south and east of the San Juan Basin and the Sangre de Cristo Mountains lies west of the Raton Basin. Erosion of the Proterozoic rocks could contribute detrital REE, uranium, and critical minerals to the San Juan and Raton basins. Sediment-hosted, stratabound copper deposits are found overlying all three highlands (see section 3.3.1 above) and could provide detrital material during Late Cretaceous times.
- Volcanic and igneous rocks in the San Juan and Raton basins, although younger than the Late Cretaceous coal and adjacent strata, could result in contributing REE and critical minerals into the groundwater, which then migrates into the coal and adjacent strata after deposition. A similar weathering process is proposed by Murphy et al. (2023) in the Williston Basin, North Dakota, where rocks above the REE-enriched lignites were leached by weakly acidic meteoric waters, which transported REE and other elements into organic complexes in the underlying lignites.
- Volcanic rocks erupted from a Jurassic-Late Cretaceous arc volcanism (Fig. 4.111), which formed southwest of the San Juan Basin, and deposited ash over much of the region during the formation of the coal deposits. REE, uranium, and critical minerals could be leached from the Jurassic volcanic rocks, Jurassic ash, and the Precambrian granites; these waters then migrated into the San Juan and Raton basins. Waters then mixed with pore water containing REE, uranium, and critical minerals that was leached from the detrital volcanic ash in the host sediments. The mineralized groundwater migrated into the coal and sandstones and precipitated.

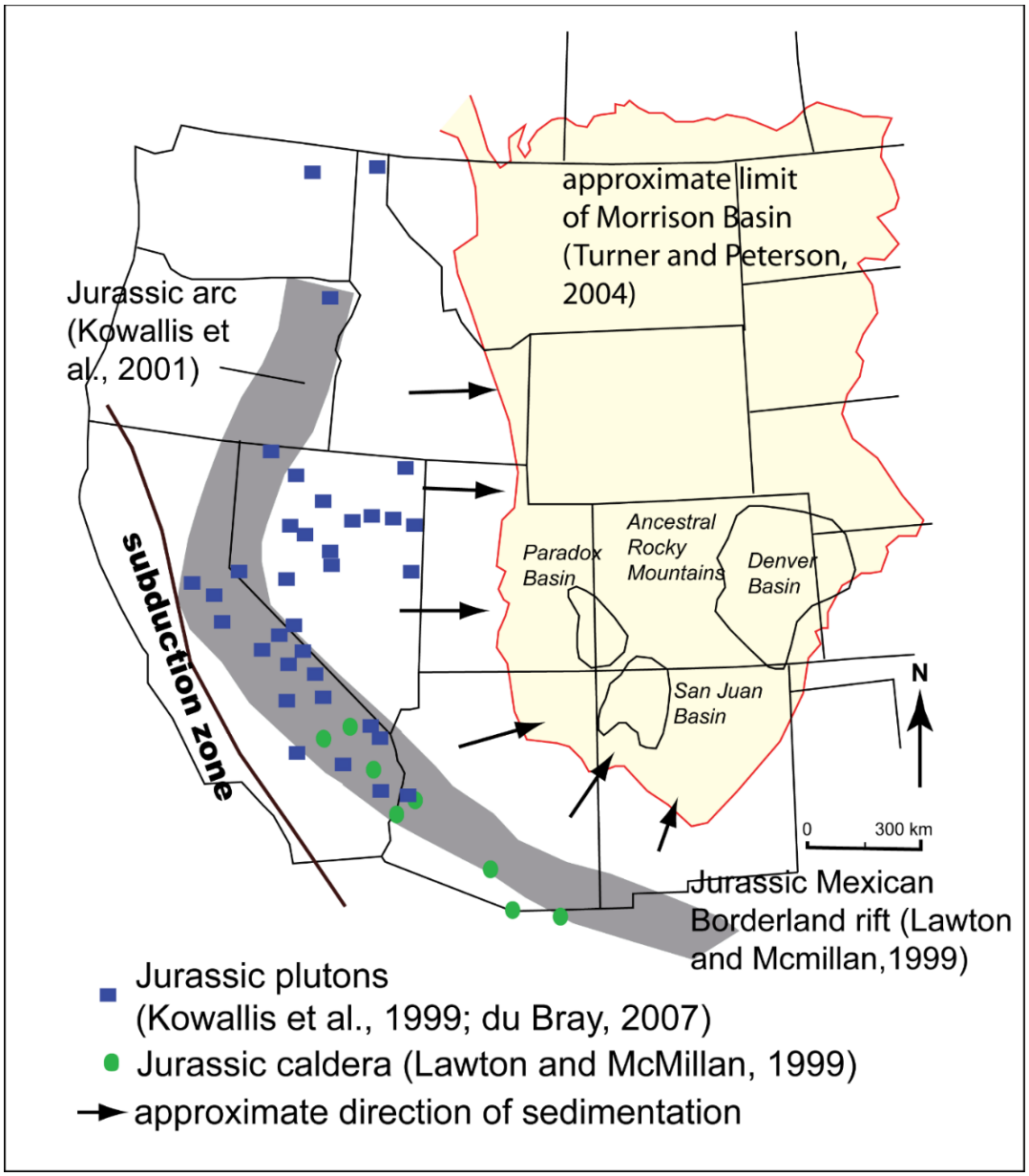

FIGURE 4.111 Approximate location of the Jurassic arc in relation to the San Juan Basin. The gray polygon represents the chain of volcanoes formed during the Jurassic Period, with the Morrison Basin in beige. Three subbasins also are delineated, including the Grants uranium district in the southern San Juan Basin. Modified from Kowallis et al. (1999), du Bray 2007), Lawton and McMillan (1999). The Jurassic Mexican borderland rift is from Lawton and McMillan (1999). Modified from McLemore and Chenoweth (2017).

The recognition that there are potential different sources of REE, uranium, and critical minerals and different mechanisms of mineral deposition (i.e. geologic processes), complicates understanding the complexity and local variations within the basins. These hypotheses will be tested in the future, if funded for phase 2.

4.18 Basinal Assessment (Endowment of critical minerals) (V.T. McLemore)

4.18.1 Assessment of coal field (V.T. McLemore and Z.K. Motlagh)

Method of calculation of endowment critical minerals in coal fields

Data required for calculating reserves and resources are summarized in Table 4.26. The endowment is an estimate of various critical minerals and REE in each coal field in the San Juan and Raton basins. Since rigorous statistical resource and reserve calculations are not possible because sufficient data are not available, endowment is the term used in this report. Hoffman (2017) estimated the coal resources for each coal field. The concentration (i.e. grade) of the critical minerals and REE of interest was determined by the average of the concentration of samples collected within a particular coal field.

TABLE 4.26 Required data for calculating the endowment of a potential mineral deposit.

Required data	Description	Source
Grade	The concentration of the mineral or commodity in the ore deposit	Average of samples collected from the coal field (Appendix 7)
Amount of coal	Tons of coal for each coal field	Determined by Hoffman (2107)

These are simple calculations that do not account for metallurgical considerations or particle size distributions (Jones and O'Brien, 2014). Tonnage estimates are dry tonnage without any account of moisture. No cut-off grade was used. No metallurgical or marketing factors were accounted for. Open pit or shallow underground mining was assumed. These grade and tonnage calculations do not conform to Canadian 43–101 criteria (http://web.cim.org/standards/documents/Block484_Doc111.pdf, accessed 6/1/16) and are only preliminary estimates.

Assessment and ranking of coal fields

Endowments for each coal field are in Appendix 12 and summarized in Table 4.27 for selected coal fields and critical minerals.

TABLE 4.27 Endowments for coal fields in San Juan and Raton basins, New Mexico (Appendix 12).

District Id	Coal field	Demonstrated resources, million tons (Hoffman, 2017)	avg. Cu (ppm)	metric tons of Cu	avg. Li (ppm)	metric tons of Li	avg. U (ppm)	metric tons of U	avg. V (ppm)	metric tons of V	avg. TREE (ppm)	metric tons of TREE
DIS150	Bisti	872	18	16,078	27	23,312	6	5,450	61	52,998	88	76,885
DIS259	Chaco Canyon	46	18	805	20	925	8	368	105	4,807	172	7,931
DIS260	Chacra Mesa	140	19	2,632	19	2,609	7	980	102	14,220	103	14,484
DIS118	Crownpoint	663	14	9,471	18	11,962	7	4,420	65	42,764	103	68,488
DIS262	Datil	47	21	987	1	24	11	517	105	4,935	3	130

District Id	Coal field	Demonstrated resources, million tons (Hoffman, 2017)	avg. Cu (ppm)	metric tons of Cu	avg. Li (ppm)	metric tons of Li	avg. U (ppm)	metric tons of U	avg. V (ppm)	metric tons of V	avg. TREE (ppm)	metric tons of TREE
DIS155	Fruitland	550	16	9,067	19	10,540	2	1,318	21	11,733	41	22,427
DIS119	Gallup	610	24	14,335	17	10,467	5	2,762	87	53,261	93	56,927
DIS174	La Ventana	263	27	6,996	43	11,251	46	12,001	57	14,925	175	46,007
DIS146	Monero	40	13	508	13	525	4	146	42	1,672	97	3,893
DIS016	Mount Taylor	19	11	211	10	190	3	57	27	521	50	942
DIS157	Navajo	1340	16	20,979	19	25,201	4	5,829	72	96,097	100	134,626
DIS021	Raton		24		15		3		74		94	
DIS009	Salt Lake	323	18	5,879	26	8,552	4	1,234	27	8,691	115	37,215
DIS121	San Mateo	385	10	3,803	8	2,933	2	885	20	7,562	34	13,145
DIS261	Standing Rock	392	18	6,991	15	6,007	5	1,848	81	31,556	147	57,624
DIS158	Star Lake	946	19	18,104	21	19,496	5	4,381	39	36,819	63	59,891
DIS124	Zuni	83	19	1,575	19	1,600	5	387	45	3,774	141	11,685

4.18.2 Assessment of beach placer deposits

Estimated endowment of critical minerals in beach placer sandstone deposits in the San Juan Basin amounts to >1.6 million metric tons of ore containing >150,000 metric tons TiO2, >385,000 metric tons Cr, 830 metric tons Nb, >1.8 million metric tons V, >36,000 metric tons Zr and >10,000 metric tons total REE (Table 4.28). These grade and tonnage calculations do not conform to Canadian 43–101 criteria (http://web.cim.org/standards/documents/Block484_Doc111.pdf) and are only preliminary estimates.

TABLE 4.28 Endowment of critical minerals and REE for selected beach placer deposits in the San Juan Basin, New Mexico.

Area	Metric Tons of Ore	Metric Tons TiO_2	Metric Tons Cr	Metric Tons Nb	Metric Tons V	Metric Tons Zr	Metric Tons REE
Star Lake	179,860	21,979	143	30.9	69.9	1253	603
Standing Rock	438,330	17,446	148	18.2	302	1224	174
Hogback	61,030	4,949	25.7	8.43	29.5	397	153
Sanostee	865,740	102,936	67.6	215	186	7079	3333
Apache Mesa	109,405	3,282	1.299	558		26,365	6,296
Total	1,654,365	150,592	385.599	830.53	1,806,173	36,318	10,559

4.19 Summary of findings

- The pre-existing geochemistry data have been included in the chemistry data (Appendix 7) and legacy data was compiled and used as a baseline for comparison and guidance. However, much of the previously published data is inconsistent and of variable quality and only a small subset of data are included in this project (Appendix 7).
- Tonnages and cutoff grades of economic deposits vary with the commodity and type of deposits. For example, what is economic for REE in carbonatites (10-15% TREE) differs from potentially economic in coal deposits (500-1000 ppm TREE). It is important to compare chemical compositions to crustal abundance or cut-off grades to determine what is good enough for exploration.
- Samples were collected from 25 coal fields in the San Juan and Raton basins. Coal and humate samples in this study typically displayed relatively flat to slightly light REE enriched chondrite-normalized REE patterns. When normalized to NASC (North American Shale Composite), these coal and humate samples display flat REE patterns with no significant enrichment or depletion. The New Mexico coal and humate samples are relatively moderate to low in REE (<485 ppm TREE), Li (<94 ppm), V (<282 ppm), Co (<65 ppm), Ni (<77 ppm), Zr (<1336 ppm), Hf (<10 ppm), and other critical minerals compared to normal economic deposits (Table 4.3). The coal and humate samples are similar in chemistry as the adjacent sedimentary rocks.
- Another way to examine critical minerals and REE in coal deposits is to determine the amount of the element in coal ash instead of the whole-rock sample. Measuring REE and other critical minerals on the ash basis approximates the critical mineral content of the fly or bottom ash remaining after coal is burned at a power plant, where critical minerals could then be leached from the ash. Recovery of critical minerals from these materials during stabilization and closure could help offset closure costs and help with the demand for critical minerals. Concentrations of REE on ash basis are higher on average in lower (<10%) ash content samples. Coal ash samples in this study typically displayed relatively flat to slightly light REE enriched chondrite-normalized REE patterns, consistent with REE hosted by clay minerals, zircon, and monazite. When normalized to NASC (North American Shale Composite), these coal ash samples display flat REE patterns with no significant enrichment or depletion. Some of the highest total REE concentrations (ash basis) are found in coal ash from the closed La Plata mine in the Fruitland Formation (2,103 ppm), the closed Mentmore mine in the Gallup Sandstone (807 ppm), as well as the Crownpoint (1,684 ppm), Standing Rock (523 ppm), Barker Creek (528 ppm), Mt. Taylor (696 ppm), Star Lake (795 ppm), and Monero (1,026 ppm) coal fields in the San Juan Basin. The La Plata coal was used at the San Juan power plant (now closed). Other concentrations of critical minerals are mostly below economic concentrations.
- Many beach-placer sandstone deposits in the San Juan Basin contain high concentrations of Ti, Zr, REE, U, Th, Nb, Ta, Fe, Sc, Y, and other elements. Estimated endowment of critical minerals in beach placer sandstone deposits in the San Juan Basin amounts to >1.6 million metric tons of ore containing >150,000 metric tons TiO_2, >385,000 metric tons Cr, 830 metric tons Nb, >1.8 million metric tons V, >36,000 metric tons Zr and >10,000 metric tons total REE.
- Selected samples were collected for this project to examine the critical minerals content of black shale samples at several locations within the Raton and San Juan basins. Although,

some concentrations are above crustal abundance, none are above exploration or economic grades and are not considered metal-bearing shales.

- Selected samples were collected from sediment-hosted, stratabound copper deposits in the Nacimiento and Zuni Mountains to examine their critical minerals potential by determining their mineralogy and geochemistry. Some samples in the Nacimiento and Zuni Mountains have elevated heavy REE. Samples from the Coyote district are elevated in cobalt; preliminary electron microprobe data suggest trace amounts of cobalt within chalcocite. Both Coyote and Zuni samples are elevated in heavy REE, vanadium, and uranium. Arsenic is found in many of the samples. The Eureka deposit has elevated barium. Bismuth is elevated in Zuni and Coyote samples.
- The low concentrations of critical minerals indicates that most volcanic ashes do not have any economic potential and are not a potential source of critical minerals in adjacent strata. However, the Star Lake sample is elevated in Li (250 ppm).
- The Grants uranium district has important uranium deposits that could be in production in the future. Some sandstone-hosted, limestone-hosted, and U-vein deposits are elevated in critical minerals. One sandstone-hosted sample contained 0.3 ppm Re (critical mineral), 659 ppm Se and 408 ppm Mo. Some samples are elevated in heavy REE. Elevated Cu and Cs are found in the Jeter samples. An estimated 146 million short tons of ore containing >236 million lbs of uranium at grades ranging from 0.1-0.4 U_3O_8 are found in the Grants uranium district (Tables 1.3, 1.4). Future exploration should include evaluation of critical minerals in these deposits, especially for V, REE, Re from molybdenite, and Cs.
- The Cuba manganese deposits form in small, local lacustrine-deltaic environments where anoxic waters mixed with shallow oxygen-rich waters, creating reducing conditions that allowed the manganese to precipitate. Although, the Cuba manganese district has manganese concentrations similar to economic deposits (>39% MnO), the deposits are small in tonnage and have no economic potential at this time. Barium and cobalt are elevated in these deposits, but the concentrations are too low to be economic. There are no additional critical minerals known in the Cuba manganese mining district.
- New Mexico is a significant producer of perlite and some of these deposits are found in and near the San Juan Basin and were sampled to determine if there was any potential for critical minerals or could be a potential source of critical minerals in the coal and adjacent strata. The industrial term perlite refers to any volcanic glass that expands appreciably by vesiculation under an appropriate heat-treating method and includes some obsidians, pitchstones, vitrophyres, as well as the expanded product. However, the critical minerals potential of perlite based on the collected samples is quite low, with most critical minerals at or below average crustal abundance values.
- Basinal assessment is in Appendix 12 and Table 4.27.

5.0 BASINAL STRATEGIES FOR REUSE OF WASTE STREAMS (TASK 3)

This section includes descriptions, characterization, and potential reuses of waste streams (fly ash, bottom ash, CO_2 from coal-fired plants, acid mine drainage (AMD), tailings, mine waste, etc.) associated with coal and other mining. Samples were collected and analyzed, and assessments were determined for coal ash, abandoned mine wastes, and mine waters. Potential reuse strategies are discussed. Many of these legacy mines have existing mine wastes generated during mineral production, which could have potential for critical minerals, especially since the actual mineral production was generally for precious and base metals and not critical minerals. Therefore, any critical minerals that are found in a mineral deposit could be also found in the mine wastes.

5.1 Types of waste streams (V.T. McLemore)

Mine wastes are high-volume heterogeneous material that remains from the extraction (mining) and processing (milling, refining) of a range of metalliferous and non-metalliferous mineral deposits (Fig. 5.1). Generally, mine wastes are noneconomic and considered a hazard. Mined material is defined as ore (material above cutoff grade), cut-off grade is the concentration of the commodity above which it is economic (Table 4.3). The types of mine wastes include:

- Waste rock or rock piles (bedrock that has been mined or removed to access the ore)
- Tailings (fine-grained material remaining after processing/removing the ore)
- Overburden (material generally covering the mineral deposit)
- Low grade or subore stockpiles (below but near cut-off grade)
- Slag (smelter waste, mostly metallic deposits)
- Water (all stages of mining, including acid mine drainage)
- Heap leach (ore pile that is leached for commodities)
- Coal ash, flue dust, and fly ash (ash remaining after coal is burned).

The San Juan Basin hosts abundant coal resources (Hoffman and Jones, 1998; Hoffman, 2017) and coal mining has been continuously developed over a century (Chapter 1). The coal ash remaining after burning at the generating stations was either stored in ash ponds at the generating stations or returned to the mine to backfill the open pits. Approximately 59 million tons of coal ash are stored at the San Juan Generating Station (DOE) and an unknown amount of coal ash are stored at other generating stations (Navajo and Escalante Generating Stations). Millions of tons of coal waste rock are found throughout New Mexico. Known critical minerals found in coal ash include REE, Sc, V, and others. Recently active coal mines are under reclamation and these mine wastes are not available for remining. The AMLB, tribes, and BLM have reclaimed some of these legacy mine features, but many that operated before the 1970s remain unreclaimed. Mine waters and acid drainage are potential waste streams, but New Mexico has an arid climate and not much water or acid mine drainage is available.

Sample preparation and laboratory methods are described in Chapter 5.

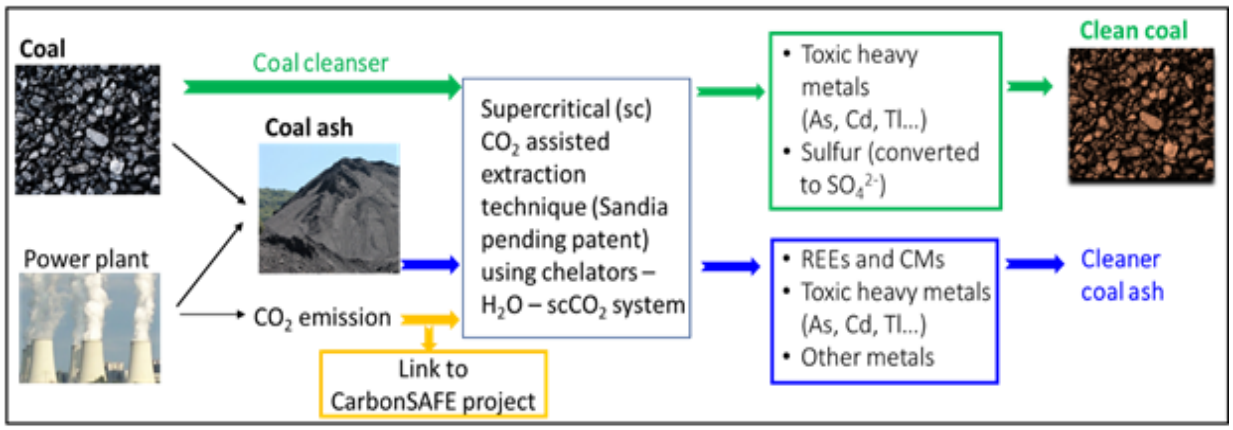

FIGURE 5.1 Illustration of pathway for reuse of waste streams related to coal-burning power plants.

5.2 Characterization of waste streams

5.2.1 Coal ash (power plants) (D. Shaver and V.T. McLemore)

Coal ashes are the product remaining after coal has burned, either naturally through fires in coal bearing regions, or by burning coal to produce steam in power plants. Coal ash can be used industrially to produce aggregates for use in construction, road work and gypsum production (Reedy and other, 2023). Coal ashes in New Mexico are found in the San Juan Basin, either as native ashes from coal fires or as Coal Combustion Products (CCP) and these ashes are being analyzed for their potential to contain critical minerals and REE.

Three coal power plants have operated in New Mexico, primarily receiving coal directly from the San Juan Basin (Fig. 5.2). These plants are Escalante, Four Corners, and San Juan. Currently the Four Corners is the only powerplant still in operation under Navajo Tribal ownership. These powerplants operated from the 1980's to the early 2020's when the demand for renewable energy began to increase (Table 5.1). During the operations period, these powerplants received and produced millions of tons of coal. More than 133 million tons of coal ash are stored at the plants (Table 5.1)

TABLE 5.1 Summary of coal generating stations in New Mexico

Coal Basin	Year operation started	Operation ended	Coal delivered (short tons)	Ash Produced (short tons)
Escalante	1984	2020	30,848,070	5,313,139
Four Corners	1972	2021	333,574,453	73,551,888
San Juan	1973	active	241,201,560	54,395092
Total			605,624,083	133,260,119

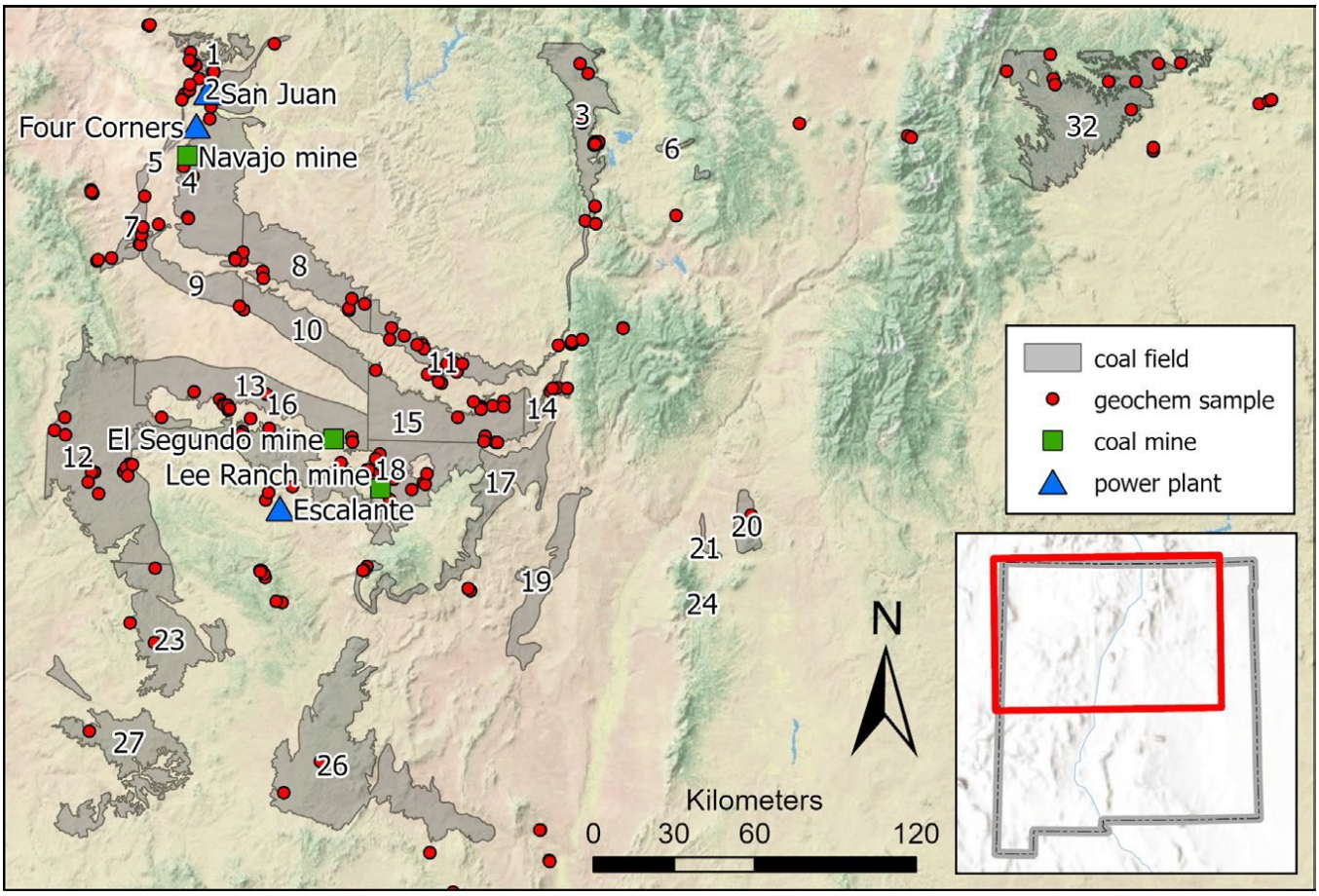

FIGURE 5.2 Location of coal mines, coal generating stations, and geochemistry samples in New Mexico.

Eight samples of coal ashes from the San Juan Basin have been examined. Six of these samples were collected from the power plants, whereas two samples are older samples from a previous study (Taggart et al., 2016). Geochemical plots of the ashes are shown in Figures 5.3, 5.4, and 5.5. The overall REE content of these ashes is low; the highest values are below 300 ppm TREE. When compared to chemical analysis from other coal basins (Fig. 5.6; Taggart et al., 2016), San Juan Basin samples are similar, with the exception of the App samples, which are higher in REE content.

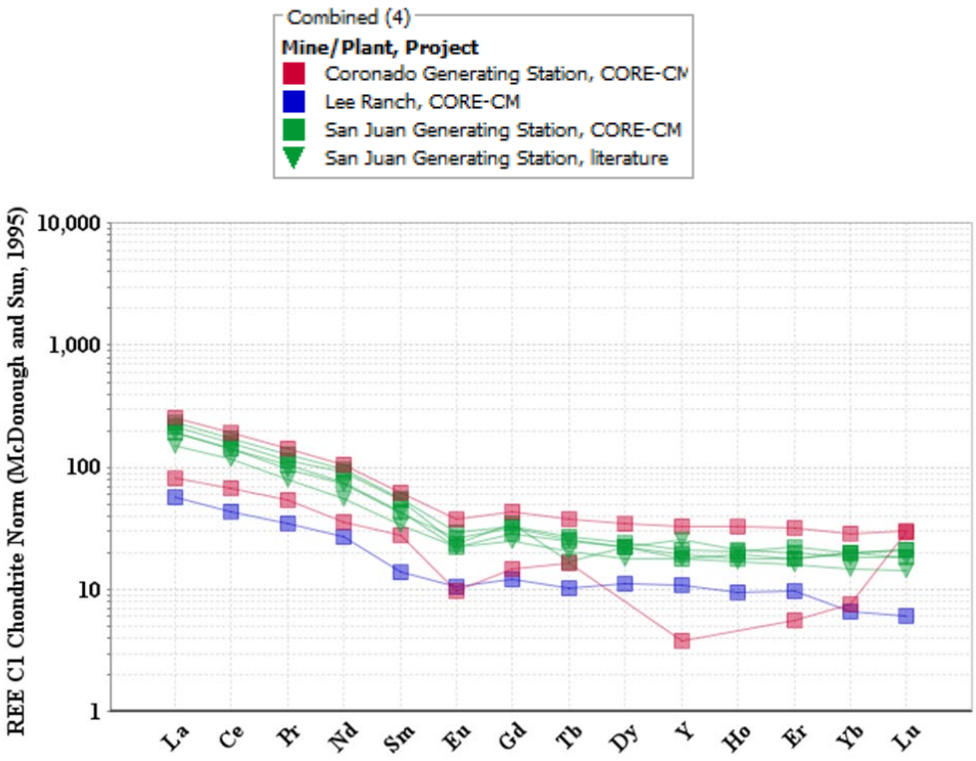

FIGURE 5.3 Chondrite-normalized REE diagram of coal ash samples collected for this report and coal ash samples from Taggart (2016) (chondrite values from McDonough and Sun, 1995).

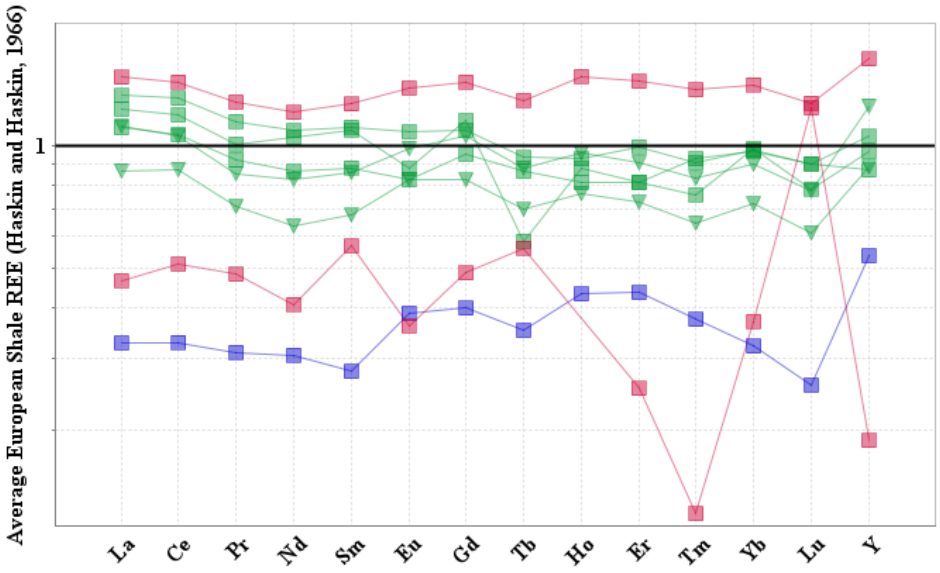

FIGURE 5.4 REE normalized to Average European Shale plots of coal ash samples (values from Haskin and Haskin, 1966). Legend in Figure 5.3.

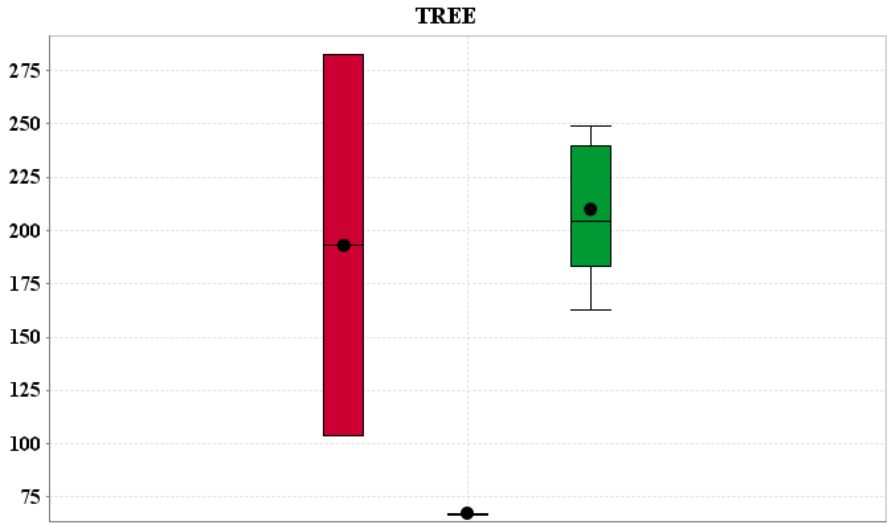

FIGURE 5.5 Box and whisper plot of total REE of coal ash samples. Legend in Figure 5.3.

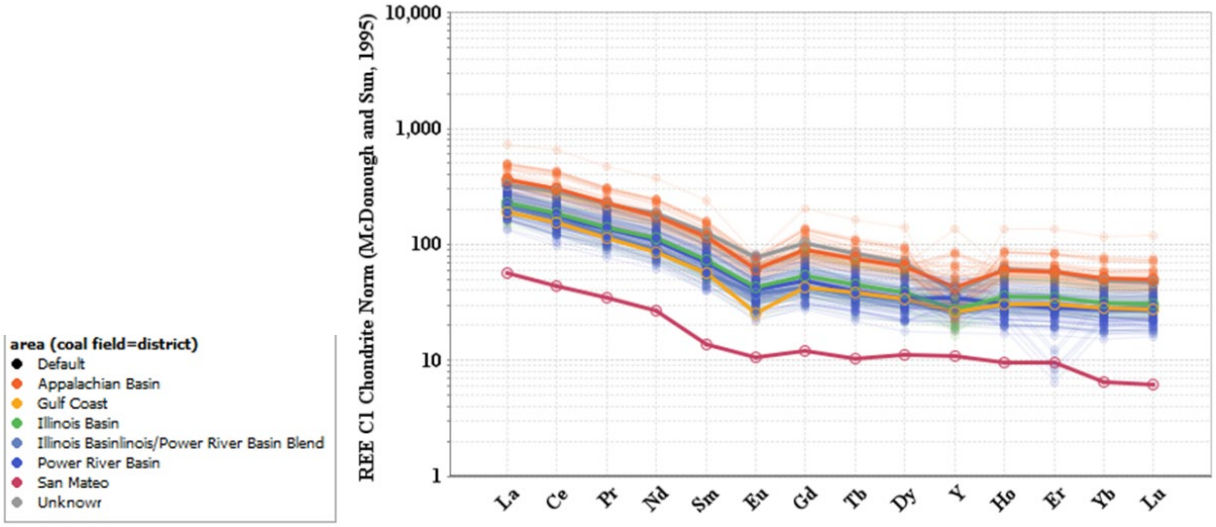

FIGURE 5.6 Chondrite-normalized REE diagram of coal ash samples collected for this report and coal ash samples from Taggart (2016) from other coal basins (McDonough and Sun, 1995).

5.2.2 Abandoned mine wastes (Z.K. Motlagh, R. Kelley, and V.T. McLemore)

There are hundreds of inactive coal mines throughout New Mexico that were never reclaimed after production because the mines were not required to be reclaimed until the 1990s. The AMLB is currently reclaiming many of these inactive coal mines. Many of these mines have existing mine wastes generated during mineral production. These wastes could have potential for critical minerals, especially since the actual mineral production was generally for precious and base metals, not critical minerals. Several coal mine waste piles were sampled for this project to evaluate the critical minerals potential using USGS protocols (McLemore et al., 2025; Campbell et al., 2025).

Geology

Areas were selected were based upon type of deposit, accessibility, production history, and presence of mine waste materials (Fig. 5.7). Descriptions of each area are below.

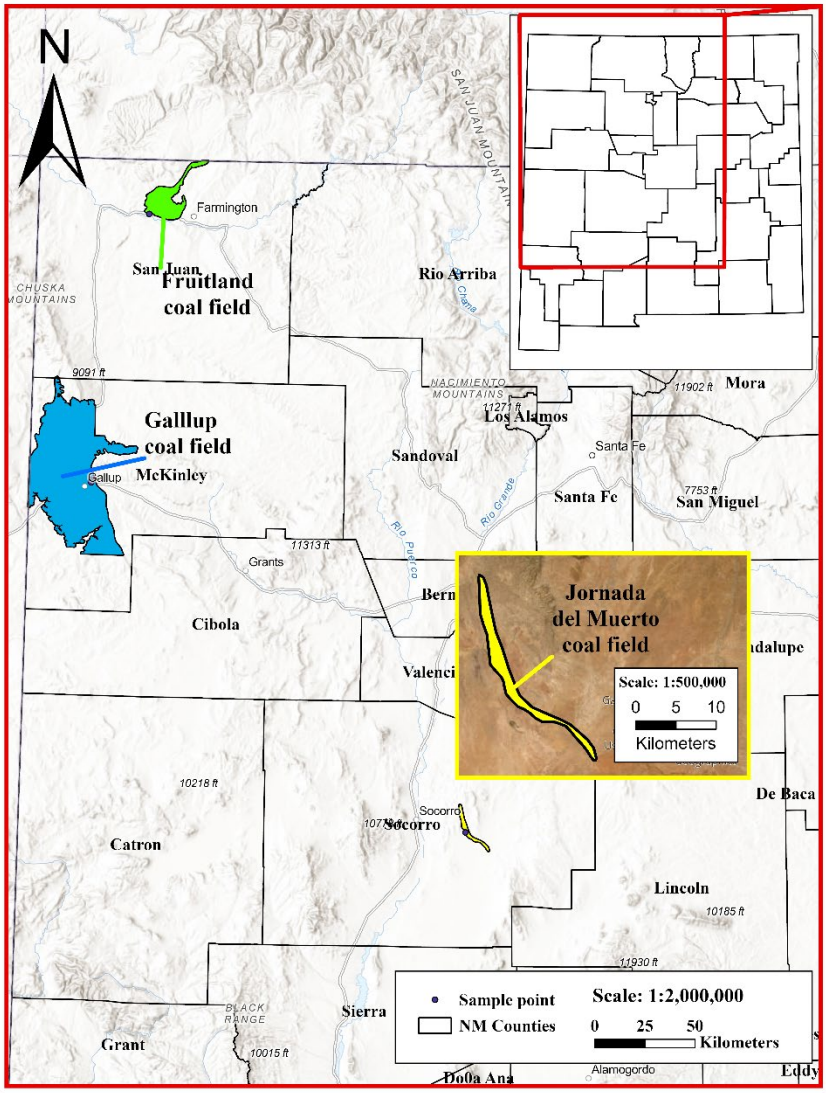

FIGURE 5.7 Location of mine waste samples from Jornada del Muerto (Socorro County), Fruitland (San Juan County), and Gallup (McKinley County) coal fields.

Black Diamond mine, Fruitland coal field, San Juan County

The Black Diamond mine was a major surface operation in Fruitland coal field of the San Juan Basin, San Juan County. Coal mining in the area began in the late 1800s and expanded during the 1900s with the development of regional rail and power infrastructure. Production in the Fruitland coal field was historically modest compared to major basin operations such as the Navajo or Lee Ranch mines but contributed to local energy supply (Hoffman et al., 1993; Hoffman and Jones, 1998).

The Fruitland sequence within Fruitland field is characterized by shale with minor sandstone in the southernmost drill sites. In addition, there are minor carbonaceous shales in the sequence. Four coal zones identified in the Fruitland field, each separated by layers of shale, siltstone, and sandstone, but only three of these zones contained coal beds thicker than 2.5 ft (Hoffman, et al., 1993). The simple structural geology of the basin and the sheer volume of coal, with original resources in the billions of tons, made this a premier coal province (Averitt, 1973). It exemplifies the large-scale industrial mining that dominated the region, primarily supplying fuel for power generation. The mine targeted the thick, laterally continuous seams of the Upper Cretaceous Fruitland formation, a world-class coal unit deposited in a widespread upper delta plain setting (McLemore, 1993; Fassett and Hinds, 1971). As a representative of this giant deposit, waste rock from the Black Diamond mine is important for assessing the critical minerals endowment of a high-volume, stable depositional system and serves as a key endmember in a comparative study of New Mexico's coal-bearing strata.

The Fruitland coals yield 8,500 to 10,500 Btu per pound, in general, and contain up to 35 percent ash as received. Sulfur content is generally less than 0.7 percent (Shomaker et al., 1971). Coal waste rocks were sampled from Fruitland coal field for this project (Fig. 5.8).

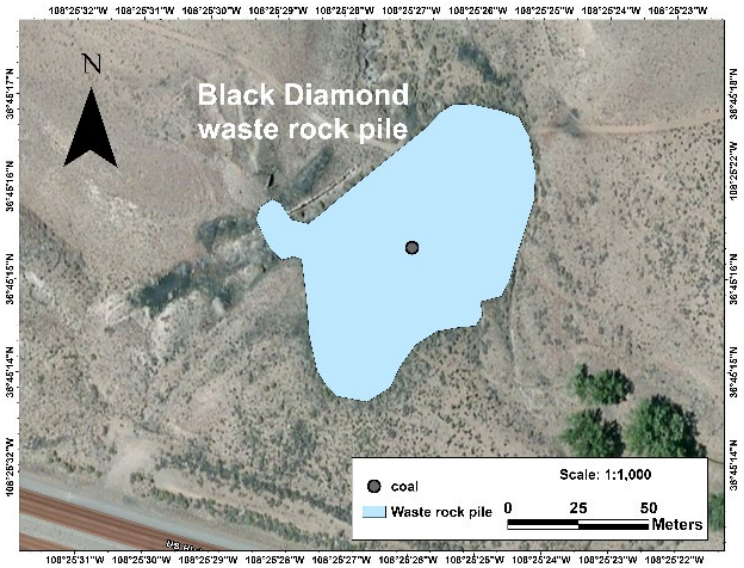

FIGURE 5.8 Waste rock pile sample location from Black Diamond mine in Fruitland coal field.

Law mine, Jornada del Muerto coal field, Socorro County

The Law mine, located in Jornada del Muerto coal field of Socorro County, is an example of a small, fault-bound coal field (Fig. 5.9). The mine includes a 1,080-ft-long slope, with the lower half affected by sagging and collapsing timbers. According to USGS records, the mine workings consisted of a main slope driven toward the southwest and a parallel back slope that branched off about 225 ft from the portal (Tabet, 1979). The area is within the Rio Grande Rift, where strong faulting and steeply tilted rock layers make exploration and mining challenging. In the past, only two small mines operated in the Jornada del Muerto coal field. Operations at Law mine stopped in 1927 after faulting displaced the coal seam at the back of the mine, making further extraction impossible (Hoffman, 2017).

The mine accessed thin, lenticular coal seams within the Upper Cretaceous Crevasse Canyon Formation (Fig. 5.9), which were deposited in a fluvially-influenced coastal setting (Osburn, 1983; Tabet, 1979). These strata are exposed on the steeply dipping limb of the Prairie Springs anticline, where extensive faulting led to the mine's abandonment in the late 1920s after the target seam was lost (Tabet, 1979).

There are no official records showing how much coal was ever produced from the Jornada del Muerto coal field, but evidence suggests that at least two small mines or exploration sites once operated there (Tabet, 1979). Law mine extracted coal from a seam about 4 ft thick (Tabet, 1979). Coal waste rocks were sampled from Jornada del Muerto coal field for this project (Fig. 5.10).

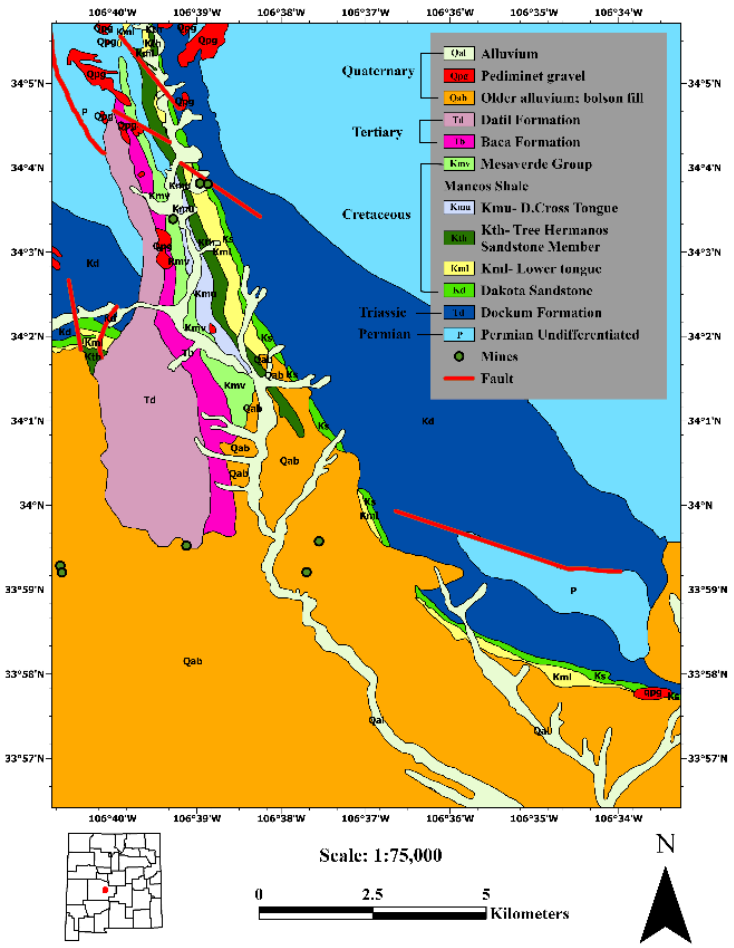

FIGURE 5.9 Geology of Jornada del Muerto coal field, Socorro County, New Mexico, digitized and modified from (Tabet, 1979).

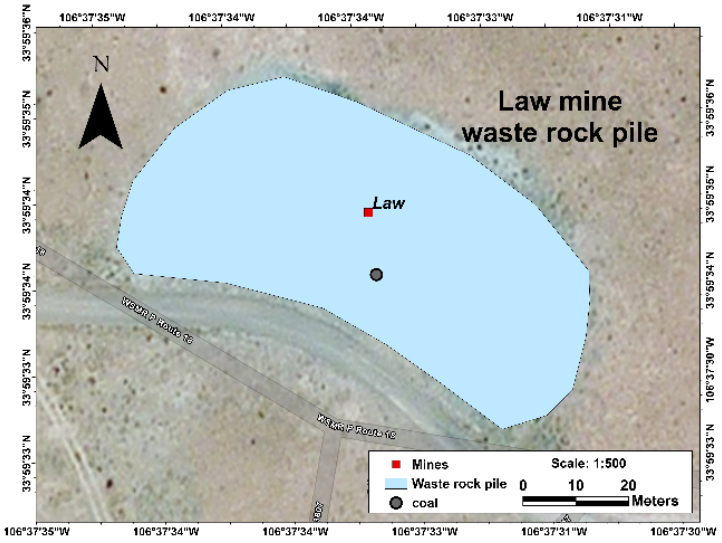

FIGURE 5.10 Waste rock pile sample location from Law mine in Jornada del Muerto coal field.

Thatcher and Noci mines, Gallup coal field, McKinley County

The historic Thatcher and Noci mines are located within the Gallup coal field on southern of the San Juan Basin in McKinley County (Hoffman, 2017). The coal has been mined underground in the Gallup coal field. Mining was active from the 1880s through the approximately 1994. Coal from Gallup coal filed is considered some of the best quality coal in San Juan Basin ((New Mexico Territorial and State Mine Inspector, 1882–1962; Hoffman, 2017)

In the Gallup coal field, coal occurs within several rock units of the Mesaverde Group. These include the Gallup Sandstone, the Dilco Coal Member of the Crevasse Canyon Formation, and the combined Cleary and Gibson coal members of the Menefee and Crevasse Canyon Formations (Fig. 5.11; Shomaker et al., 1971)

Between 1882 and 1961, a total of about 33.3 million short tons of coal was produced from the Gallup coal field (New Mexico Territorial and State Mine Inspector, 1882–1962). Coal waste rocks were sampled from Gallup coal field for this project.

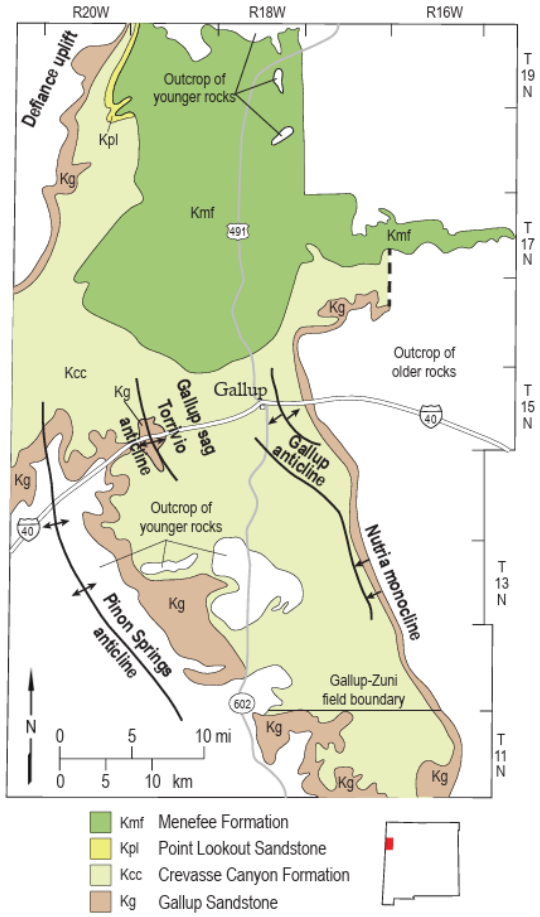

FIGURE 5.11 Geology map of Gallup coal field from (Shomaker et al. 1971).

Mineralogy of waste materials

Mineralogy of six coal mine waste samples was determined by examining under a microscope and using powdered X-ray diffraction (XRD) analysis. XRD results are represented in a stacked bar chart (Fig. 5.12). Quartz (SiO_2), kaolinite ($Al_2Si_2O_5(OH)_4$) and gypsum ($CaSO_4 \cdot 2H_2O$) are the predominant minerals. Mica ($KAl_2(AlSi_3O_{10})(OH)_2$) and jarosite ($KFe_3(SO_4)_2(OH)_6$) are identified in the Law mine samples. Montmorillonite ($((Na,Ca)_{0.33}(Al,Mg)_2(Si_4O_{10})(OH)_2 \cdot nH_2O)$) is found in the samples from Noci mine. Nontronite ($Na_{0.3}Fe^{3+}_2(Si,Al)_4O_{10}(OH)_2 \cdot nH_2O$) and mica ($KAl_2(AlSi_3O_{10})(OH)_2$) are detected in the Law mine samples.

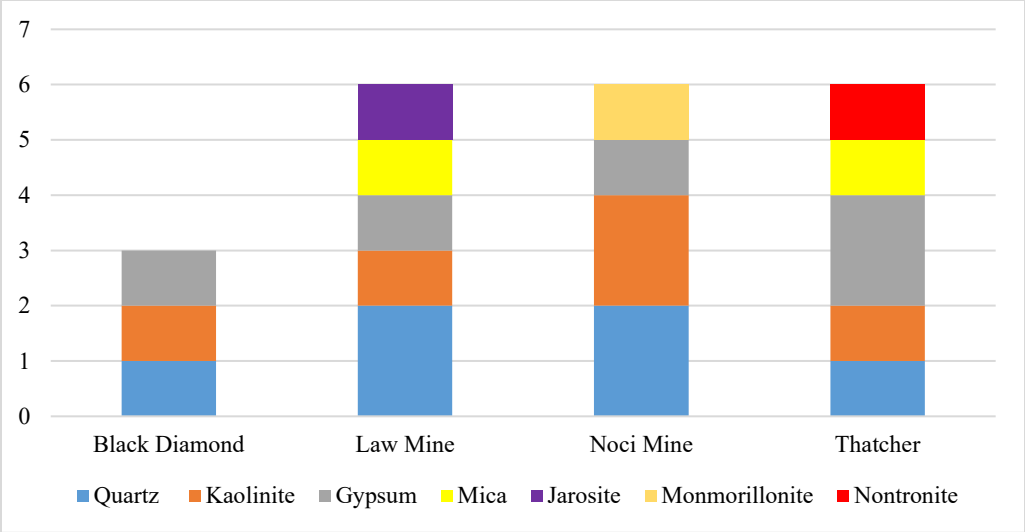

FIGURE 5.12 Histogram of XRD results of coal mine waste.

Geochemical analyses of waste materials

Seven coal mine dump samples were submitted for whole-rock geochemical analyses (Appendix 7). Table 5.2 shows statistical summary of these mine waste samples. Figure 5.13 shows a spider plot of chondrite normalized REE plot. The results show samples are slightly enriched in light REE, up to 200 times chondritic values, but below recommended exploration threshold values (Table 4.3).

TABLE 5.2 Statistical summary for Black Diamond, Law, Noci, and Thatcher mines waste dump samples.

Coal Mine		Ba (ppm)	Cu (ppm)	Th (ppm)	V (ppm)	Y (ppm)	Zn (ppm)	TREE
Black Diamond	Min	450	15	10	25	5	20	-
	Max	450	15	10	25	5	20	-
	Mean	450	15	10	25	5	20	-
	Median	450	15	10	25	5	20	-
Law Mine	Min	10	20	15	122	20	80	-
	Max	14	25	20	122	22	80	-
	Mean	12	20	18	122	22	80	-
	Median	12	20	18	122	22	80	-
Thatcher	Min	155	10	10	88	20	60	150
	Max	395	15	18	128	20	73	250
	Mean	275	10	15	108	20	67	200
	Median	275	10	15	108	20	67	200
Noci Mine	Min	80	15	10	104	18	35	120
	Max	330	20	15	104	18	70	210
	Mean	205	20	14	104	18	53	165
	Median	205	20	14	105	18	53	165

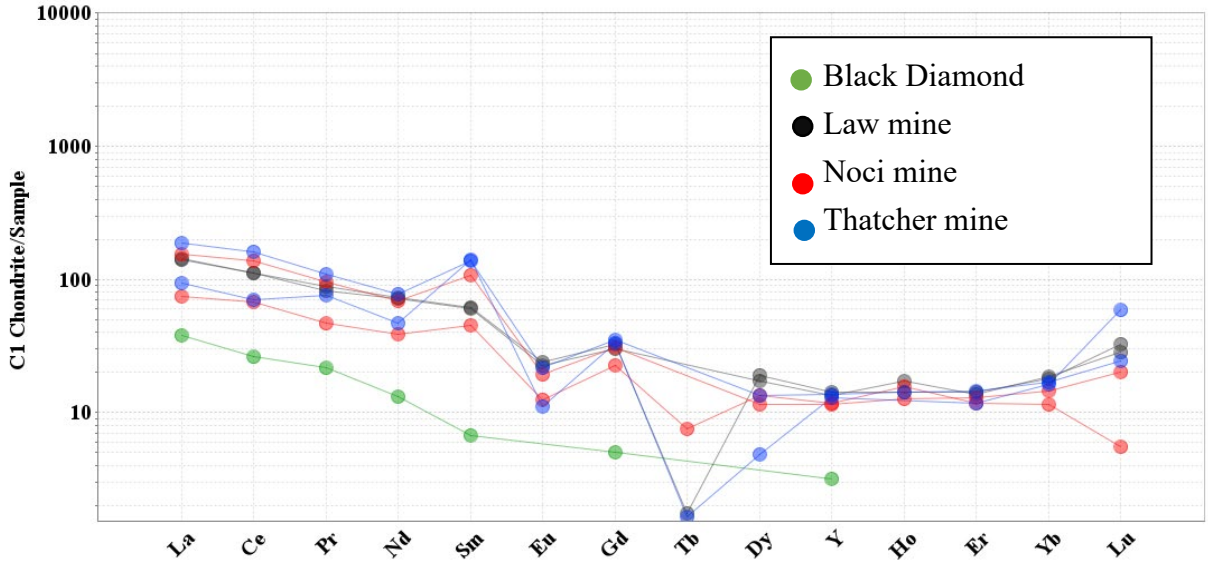

FIGURE 5.13 Chondrite-normalized REE plot of Black Diamond, Law, Noci, and Thatcher mines waste rock samples (McDonough and Sun, 1995).

The box plots in Figure 5.14 show Th concentrations for coal samples from Black Diamond, Law, Noci, and Thatcher mines samples. The red horizontal line at 10.5 ppm represents the average crustal abundance of Th (Rudnick and Gao, 2003. In this figure, the Noci (red), Law (black), and Thatcher (blue) samples show elevated value of Th compared to average crustal abundance. The Black Diamond sample (green) plots below the detection threshold.

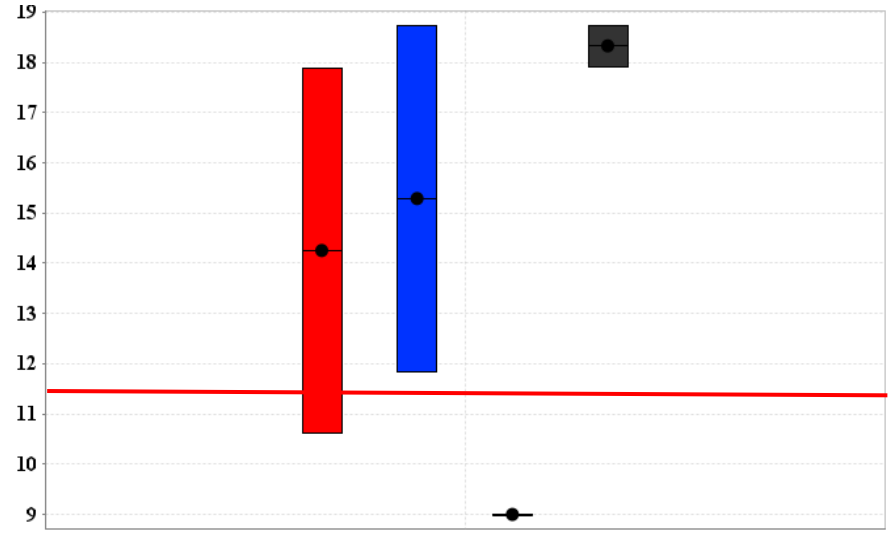

FIGURE 5.14 Box plots compare the thorium (Th) concentrations of Black Diamond, Law, Noci, and Thatcher mines waste rock samples compared to average crustal abundance. Legend in Figure 5.13.

The box plots in Figure 5.15 show V concentrations for coal samples from Black Diamond, Law, Noci, and Thatcher mine samples. The red horizontal line at 106 ppm represents the average crustal abundance of V, as reported by Rudnick and Gao (2003). In this figure, both the Thatcher (blue), and Law (black), samples show elevated value of V compared to average crustal abundance. The Black Diamond and Noci Mine samples plot below the detection threshold.

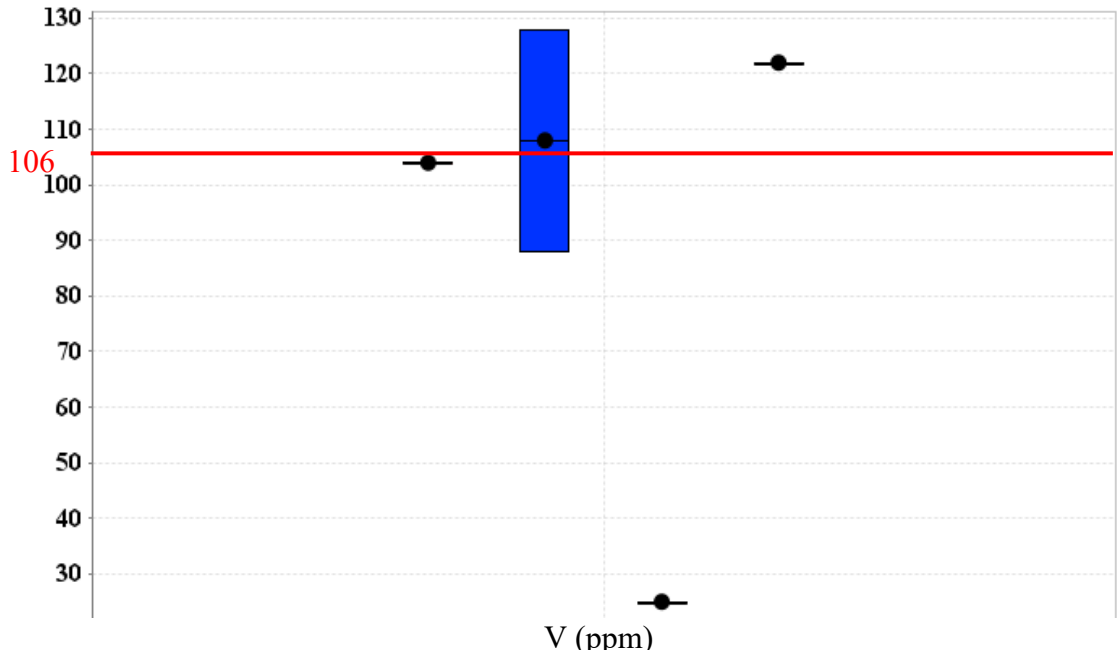

FIGURE 5.15 Box plots compare the vanadium (V) concentrations of Black Diamond, Law, Noci, and Thatcher mines waste rock samples compared to average crustal abundance. Legend in Figure 5.13.

Particle size fraction of waste materials

Two samples, Coal115 and Coal126 were selected for paricle size fraction analyze to compare concentrations of critical minerals in different size fractions. The procedure was performed according to ASTM D422-63 standard test methods for particle size analyses of soils using stainless-steel sieves, specifically No. 4 (4.75 mm), No. 14 (1.40 mm), No. 40 (0.417 mm), No. 60 (0.246 mm), No. 80 (0.177 mm), and No 200 (0.074 mm). The particle size distributions and data are in Appendix 10.

The geochemical analysis of the particle size fractions (Fig. 5.16) shows variations in distribution of critical minerals with respect to particle size. In Coal115, the concentrations of Cu, Th, Y, and Zn show an increasing trend from the finer to the coarser fractions. Coal126 shows the same pattern for some minerals like Th and Y, enrichment in the finer fractions, whereas Cu and Zn concentrations decrease as the sieve opening size increases.

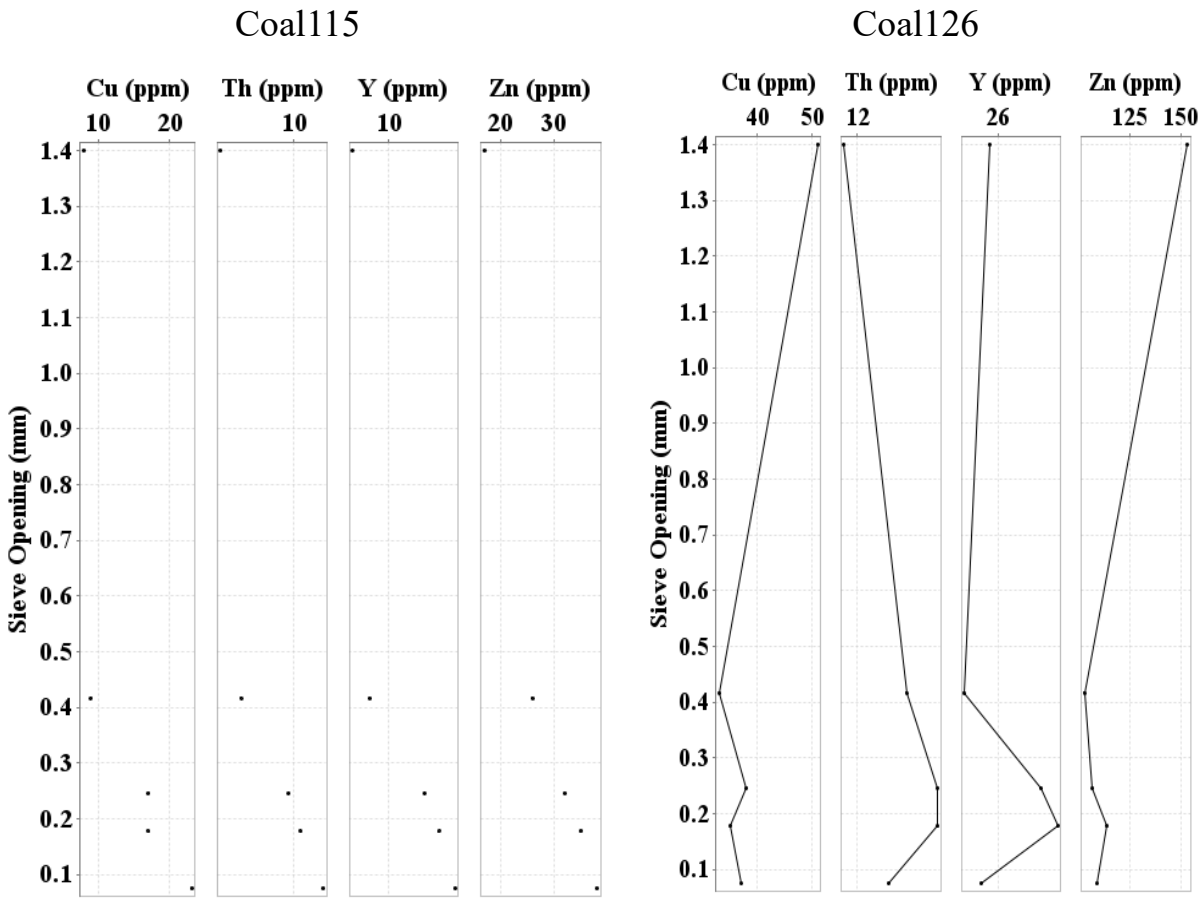

FIGURE 5.16 Variation in minerals concentrations (Cu, Th, Y, and Zn) with particle size for Coal115 and Coal126.

Critical Minerals Endowment of waste materials

Each mine feature was mapped using a combination of field survey (using handheld GPS, measuring tape, and/or Brunton compass), topography, LiDAR, and GIS tools. The survey points were entered in ArcPro. Dimensions used to calculate area of waste material are estimated based on field measurements approximations and GPS data. For the waste piles estimated with GPS data, a handheld GPS unit was used to take GPS waypoints of the waste pile footprints. Using the GPS data, a geographic information system (GIS) program, ArcGIS Pro, and LiDAR data were used to extrapolate the surface area of the waste pile footprints. Estimated depth of materials and volume of mine waste features were made through visual observation, topography, and LiDAR data. Figures 5.17 and 5.18 show locations of subsamples, area and volume of mine waste features at Jornada del Muerto, and Gallup coal fields. Details are in Tables 5.3 and 5.4.

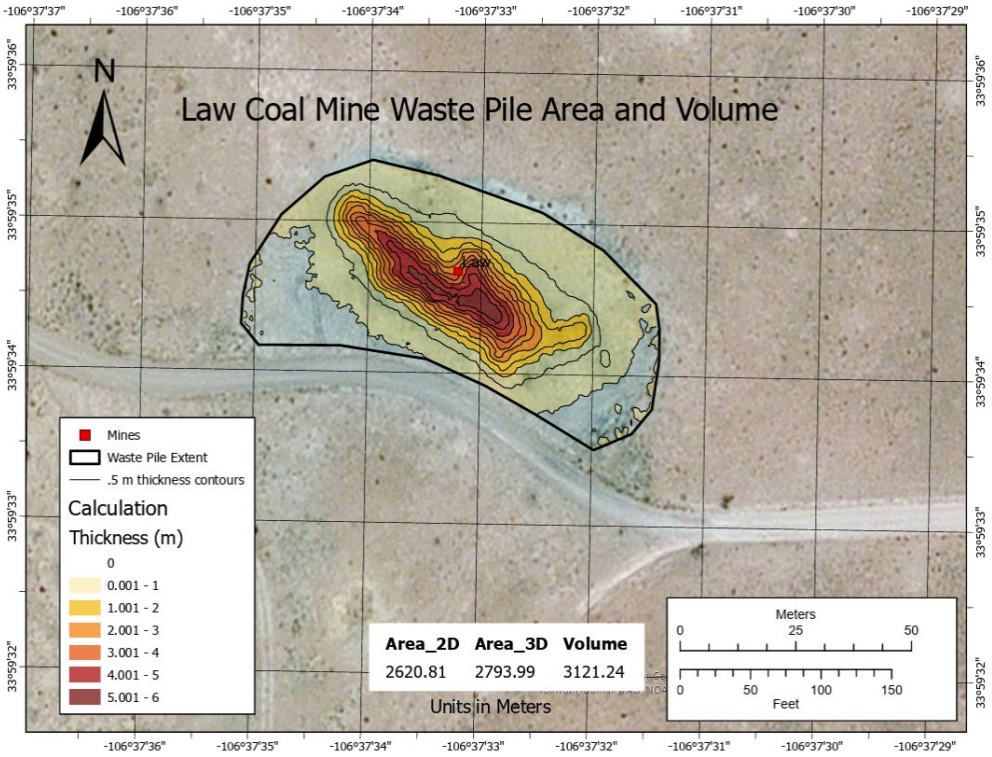

FIGURE 5.17 Location of area and volume of mine wastes at Jornada del Muerto coal field, Law mine (map by R. Kelley).

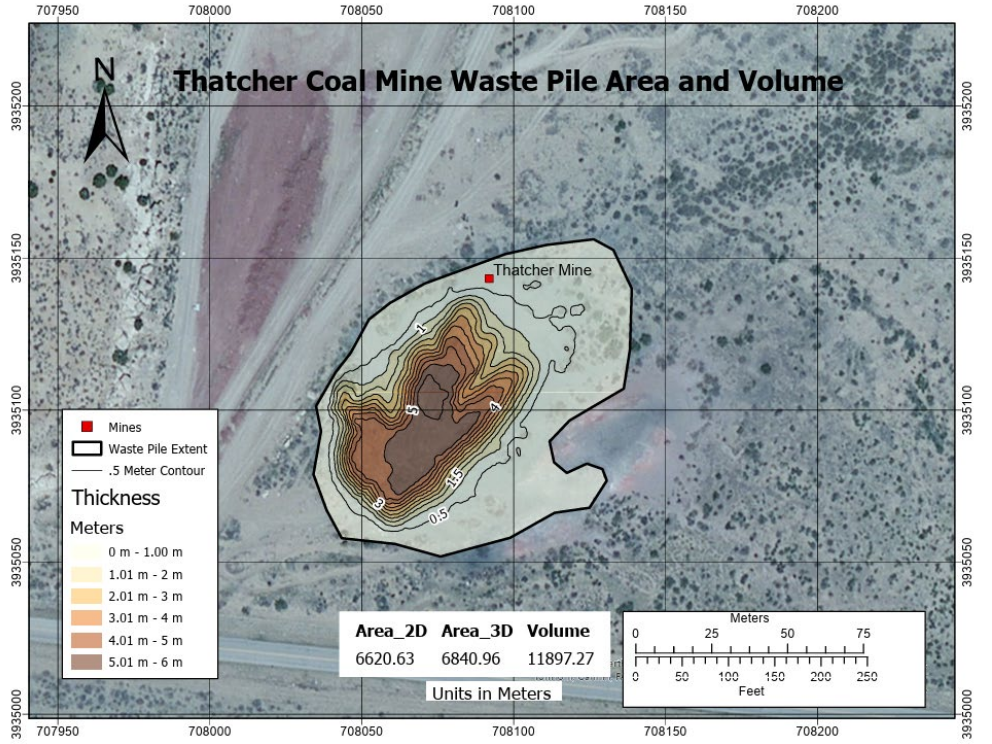

FIGURE 5.18 Location of area and volume of mine wastes at Gallup coal field waste rock piles at Thatcher mine (map by R. Kelley).

To assess the approximate amount of critical minerals potential in the mine wastes of Black Diamond, Law, Noci, and Thatcher mines waste dumps, it is essential to estimate the mineral endowment of the area. Mineral endowment is determined by multiplying the mass of the material (tonnage) by its mineral concentration (grade).

The thickness of mine waste areas is approximated based on field observation. The tonnage is then obtained by applying a specific gravity value, which is derived from laboratory measurements. Parameters are presented in Table 5.3.

TABLE 5.3 Parameters used to calculate for endowments

Parameters	Black Diamond	Law	Noci	Thatcher
Area (m^2)	5,855	2,620	797	6,620
Thickness (m)	3.05	6	0.91	6
Specific gravity	2.18	2.18	2.18	2.18
Volume (m^3)	17,847	3,120	730	11,900
Mass (tonnes)	38,906	6,800	1,590	25,940

By applying geochemical data endowments of metal content are estimated. These estimations are presented in Table 5.4.

TABLE 5.4 Black Diamond, Law, Noci, and Thatcher mine waste dump endowments

Endowment (tonnes)	Ba	Cu	Th	V	Y	Zn	TREE
Black Diamond	17.5	0.6	0.4	1	0.2	0.8	1.4
Law	0.01	0.6	0.1	0.8	0.1	0.5	1.2
Noci	0.3	0.03	0.02	0.2	0.03	0.1	0.2
Thatcher	7.1	0.3	0.4	2.8	0.5	1.7	4.6

Paste pH tests and Net Acid Generation of waste materials

Static tests are geochemical analyses to predict the potential of a waste sample to produce acid. The generation of acid in sulfidic wastes can be determined by Net Acid Generation (NAG) tests. To enable waste sorting, the NAGpH value is typically plotted against the Neutralization Potential Ratio (NPR) value (Fig. 5.19).

The Acid Potential (AP) is measured by analyzing the sample for its sulfur content. The Neutralization Potential (NP) is determined by analyzing the acidity consumption of a sample in acid (HCl or H_2SO_4). Net Neutralization Potential (NNP) gives the waste's capacity to neutralize any acid generated and is the difference between the Acid Potential and the Neutralization Potential. The ratio NP/AP, known as the Neutralization Potential Ratio (NPR) (Lottermoser, 2010).

$$\text{AP (kg } CaCO_3\text{/tonnes)} = \text{wt.\% S} \times 31.25$$
$$\text{NP (total C)} = \text{wt.\% C} \times 83.3$$
$$\text{NNP} = \text{NP} - \text{AP},$$
$$\text{NPR} = \text{NP/AP}$$

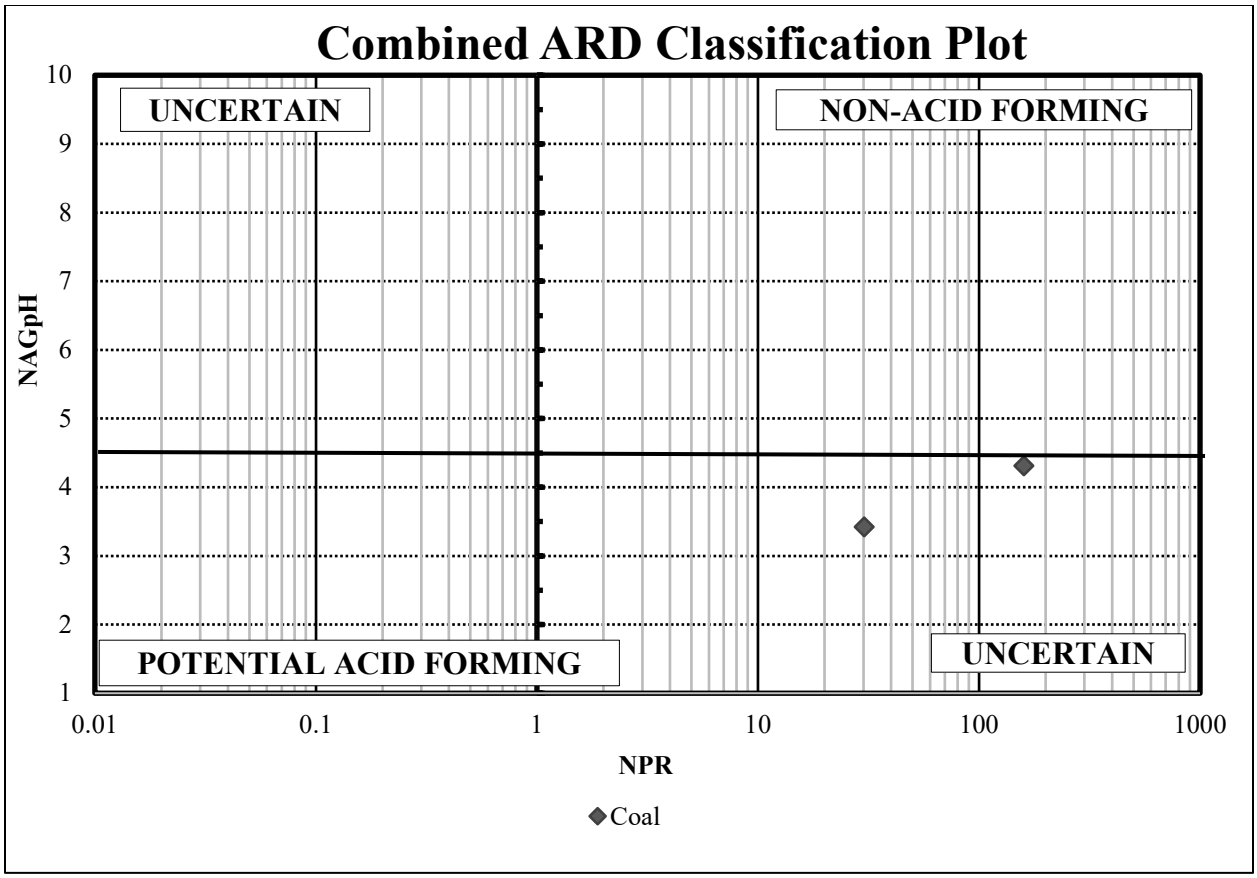

FIGURE 5.19 Combined ARD classification of Black Hawk district mine waste rock samples, Hillsboro district tailing samples, and Steeple Rock district mine waste rock samples and coal mine waste samples from Fruitland, Jornada del Muerto, and Gallup coal fields.

Significant findings

The mineralogical and geochemical characteristics of the coal mine waste samples from Black Diamond, Law, Noci, and Thatcher mines provide information on distribution and values of critical minerals in coal mine wastes in New Mexico. The XRD results show that quartz, kaolinite, and gypsum are the dominant mineral phases across all sites, suggesting that the mine wastes are primarily composed of detrital silicate and secondary sulfate minerals. In the Law mine samples, the presence of mica and jarosite show local oxidation under acidic conditions. Whole-rock geochemical analyses demonstrate that these mine wastes are slightly elevated in in several critical elements, notably Th, V and TREE. The chondrite-normalized REE plot show slightly elevated in light REE, with concentrations reaching up to 200 times chondritic values. Box plots of Th and V concentrations show variability among the mine sites. Thorium concentrations in the Noci, Law, and Thatcher mines dump samples exceed the average crustal abundance of 10.5 ppm, whereas the Black Diamond sample is below detection. Similarly, V concentrations are above the crustal average (106 ppm) in the Thatcher and Law mines samples, while Noci and Black Diamond mines samples show lower values.

The estimated critical mineral endowments, based on measured concentrations, specific gravity, and field observations, show metal content potential among the sites. Endowments for minerals such as Th, V, Y, and TREE are higher at the Thatcher and Law mines sites. The

Thatcher waste rock contains approximately 0.5 ton of Th, 2.8 tonnes of V, 0.5 tonnes of Y, and 4.6 tonnes of TREE. The Law mine dump shows similarly elevated values, with about 0.1 tonnes of Th, 0.8 tonnes of V, 0.1 tonnes of Y, and 1.2 tonnes of TREE. In contrast, the Noci and Black Diamond mine dumps contain smaller endowments: Noci dump has roughly 0.02 tonnes of Th, 0.2 tonnes of V, 0.03 tonnes of Y, and 0.2 tonne of TREE, whereas Black Diamond dump has about 0.4 tonnes of Th, 1 tonnes of V, 0.2 tonnes of Y, and 1.4 tonnes of TREE.

The different particle size fraction analyses imply different mineral associations and geochemical behaviors. Coal115 shows enrichment of Cu, Th, Y and Z in finer fractions, while Coal126 shows higher concentrations of Cu and Zn in coarser particles. The acid generation characteristics show uncertainty about acid producing potential among the samples. Although, some of the mine wastes show concentrations of some critical minerals above crustal abundance, the concentrations are below recommended economic concentrations (Table 4.3) and therefore, the concentrations and tonnages are probably too small to provide an economic resource.

5.2.3 Mine-influenced waters from Lee ranch coal mine (B. Frey)

Introduction

Water bodies offer an opportunity to further evaluate rare earth elements (REE) and other critical minerals (CM) at mine sites. They can indicate possible CM reserves at a given mine site, and they can help determine if CM extraction from mine waters can be economic. Previous investigations in metal mines found REE present in concentrations as much as 1000 times higher than natural water sources; some water concentrations may be economical for REE extraction (e.g., Hermassi et al., 2022). Similar studies at coal mines have potential to indicate the presence of REE in coal.

For this reason, the NMBGMR Economic Geology Program includes water resources in its investigations, including for this coal project. Grab samples were collected in 1-L Nalgene bottles at one coal mine and during an outreach event at a metal mine; these samples were submitted for analysis by the NMBGMR Analytical Laboratory. They included five pit-lake water samples from the Lee Ranch coal mine (Fig. 5.20) and four samples from the Nacimiento copper mine (Fig. 5.21).

The Lee Ranch coal mine is a closed coal mine northwest of San Mateo, New Mexico, on the west side of Mt. Taylor. The mine extracted coal from the Menefee Formation (Hoffman and Jones, 2011). Water samples were collected in 2023 and 2024 by mine staff, and in addition to sampling at four pit lakes, a fifth reclaimed pit was sampled.

The Nacimiento samples were collected in the Nacimiento coal mine in 2024 by NMBGMR staff during a K-12 teacher tour, a CORE project outreach event (https://geoinfo.nmt.edu/news/home.cfml?id=718). Three of the samples were collected from pit lakes, and the fourth was collected from a flume of treated water being released to Senorito Creek. Photos of the sampling locations (marked in Fig. 5.22) are shown in Figures 5.23, 5.24, 5.25, and 5.26.

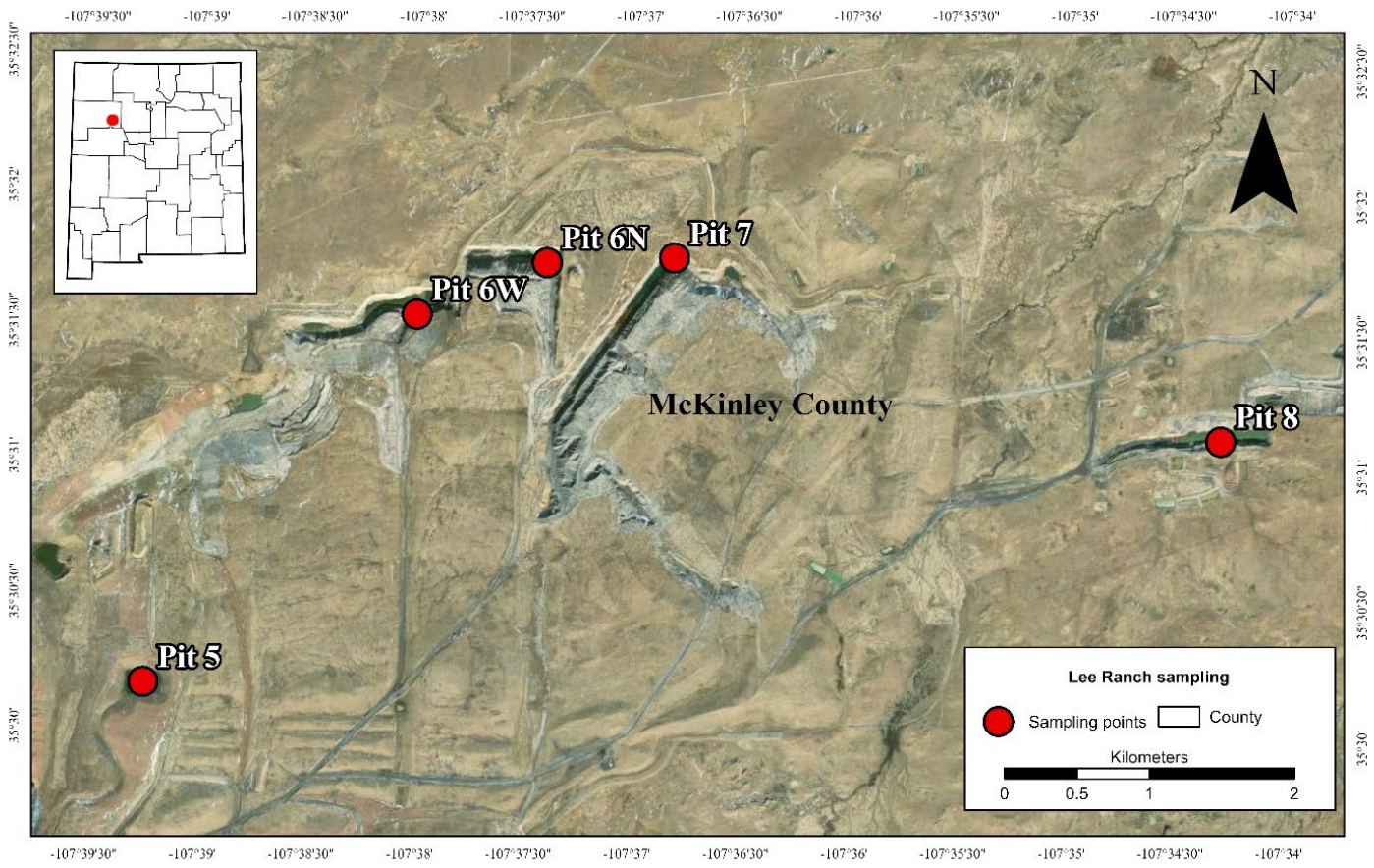

FIGURE 5.20 Six water samples were taken from several pit lakes at the Lee Ranch coal mine for inorganic analysis.

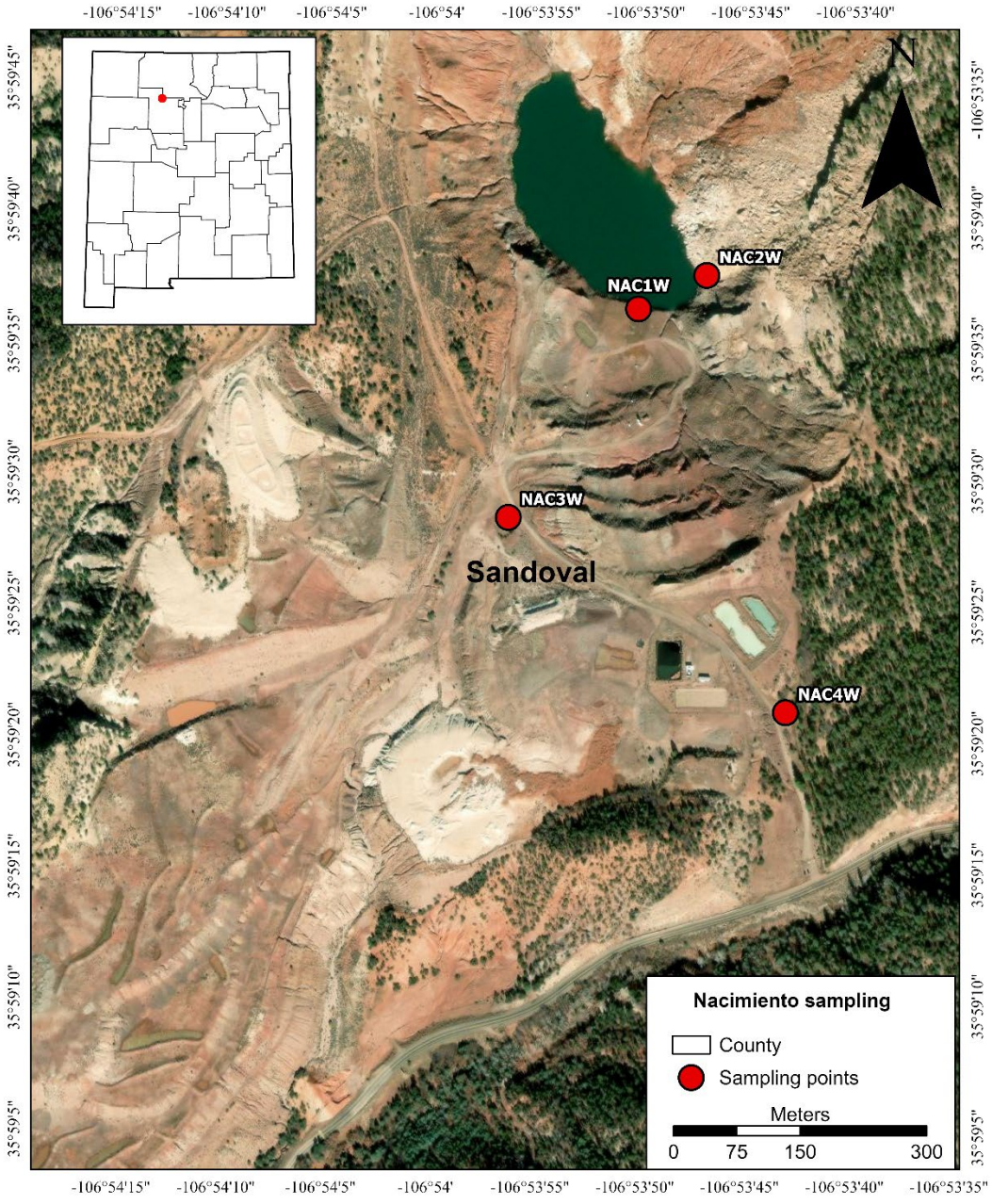

FIGURE 5.21 Four water samples were collected at the Nacimiento mine in Sandoval County for inorganic analysis.

FIGURE 5.22 Water sample site at the Nacimiento pit lake (NAC1W).

FIGURE 5.23 Water sample site on the Nacimiento pit lake (NAC2W).

FIGURE 5.24 Sampling location of NAC3W water sample, taken at a pit lake near the Nacimiento mine.

FIGURE 5.25 Sampling location of the NAC4W water sample, taken at the flume where water drained into the creek from the water treatment plant.

Methods

No field measurements, filtration or preservation were made at the sites, and specifications for sampling, other than filling a bottle, are unknown. The following splits were made in the laboratory:

- a 250 mL split that was stored in a refrigerator for measurements of anions, pH, specific conductance and alkalinity

- a 125-mL split that was acidified to pH 1 with ultra-high-purity nitric acid in preparation for metals analysis. Acidification was done at least 18 hours in advance of analysis.

All splits were made into precleaned HDPE bottles and labeled with the lab's tracking number. Sample log in, data entry, and report production were made through the laboratory's LIMS system (SampleMaster / confience). Analyses were completed on unfiltered samples and included alkalinity, anions, major cations, trace metals and REE. Table 5.4 lists the analyses made for this project, along with instrumentation and methods. Personal protective gear (gloves, eye protection and lab coats) were worn when handling samples and reagents that have pH below 4.3.

TABLE 5.5 Analytical methods of water samples collected at Lee Ranch Coal Mine and Nacimiento Mine. IC = Ion Chromatography; ICP-OES = Inductively Coupled Plasma Optical Emission Spectroscopy; ICP-MS = Inductively Coupled Plasma Mass Spectroscopy. Analyses on ICP

Analysis	Constituents	Instrument	EPA Methods
Specific conductance	Specific conductance	YSI 3200 Conductivity Instrument	EPA Method 120.1
pH	pH	Metrohm 904 Titrando Autotitrator	EPA Method 150.1
Alkalinity	HCO3, CO3	Metrohm 904 Titrando Autotitrator	EPA Method 310.1
Anions	Cl, SO4, NO3, NO2, Br, PO4, F	Dionex ICS-500 IC	EPA Method 300.0
Major and minor cations	Na, K, Ca, K, Mn, Fe, Sr, Si, Ba	Agilent 5900 ICP-OES	EPA Method 200.7
Trace metals	Ag, Al, As, Be, B, Cd, Cr, Co, Cu, Fe, Li, Pb, Mo, Ni, Se, Sb, Sn, Th, Ti, U, V, Zn	Agilent 7900 ICP-MS	EPA Method 200.8
Rare earth elements	Ce, Dy, Er, Eu, Gd, Ho, La, Lu, Nd, Pm, Pr, Sm, Tb, Tm, Y, Yb	Agilent 7900 ICP-MS	EPA Method 200.8
Hardness		By calculation	Standard Methods
Total dissolved solids		By calculation	Standard Methods

QC samples

Analyses on IC, ICP-OES and ICP-MS include quality assurance samples such as blanks, standards and duplicates, analyzed at a rate of 5%, which are used by laboratory personnel to determine if an instrument problem or matrix effect is causing a problem with analysis. If analyses are outside required parameters, the problem are resolved before continuing with analyses. To aid in interpreting the water data taken for this project, results were compared to data collected in other projects in New Mexico:

Pit, seep and adit samples from the Steeple Rock and Hillsboro mining districts in southern New Mexico by the NMBGMR Economic Geology team

A Rio Grande sample taken from near Fort Craig, Socorro County, New Mexico (Newton, 2004)

A Rio Grande water sample taken at Valle de Oro, Albuquerque, as part of a USGS project (Beisner et al., 2024)

San Juan River samples taken during a USGS project (WQP, 2021).

Results

The chemical constituents of water samples collected in this project are in the tables in Appendix 9. A piper diagram (Fig. 5.27) and an REE spider diagram (Fig. 5.28) are used to interpret the analytical data of the samples.

Major Constituents

Water samples from the Lee Ranch coal mine (red icons on Fig. 5.27) plot as "older" water, which have had a longer interaction with gypsum, have had a longer period for cation-exchange activity, and contain notable amounts of dissolved Na^{+} and SO_4^{2-}. This is compared to the "younger" waters (black icons for rivers, streams and springs on Fig. 5.27) that have more recent input from precipitation and have mainly interacted with $CaCO_3$ (calcite), a common soluble mineral. Cow Creek is likely the youngest water of the group, sourced in the Pecos Mountains near North San Ysidro. Waters from the Lee Ranch coal mine, which sourced coal from the Cretaceous Menefee Formation, plot similarly to well water sourced in the Menefee Formation in the San Juan Basin (Fig. 5.28; Kelley et al., 2014), which also show a trend of low Ca, high sodium and potassium, and high sulfate, low carbonate and bicarbonate.

The water from Lee Ranch Pit 5 (red circle, Fig. 5.27), a reclaimed area, is the exception, plotting as a calcium sulfate water. This is similar to metal mine waters (olive and blue) collected by the NMBGMR Economic Geology team, which plot at the top of the diamond plot. These are mine-related surface water and adit samples taken at the Steeple Rock and Hillsboro mining districts and which exhibit chemistry that is typical for mine waters.

The Nacimiento water samples (neon green icons, Fig. 5.27) track similarly to the river and spring samples (black icons on Fig. 5.27) on the Piper diagram, with the exception of higher sulfate values that one would predict sourced from copper sulfides. Nacimiento NAC4W, a treated lower-TDS water being released to the Senorita Creek, diverges from the other Nacimiento samples and plots closer to the river and spring waters on the plot.

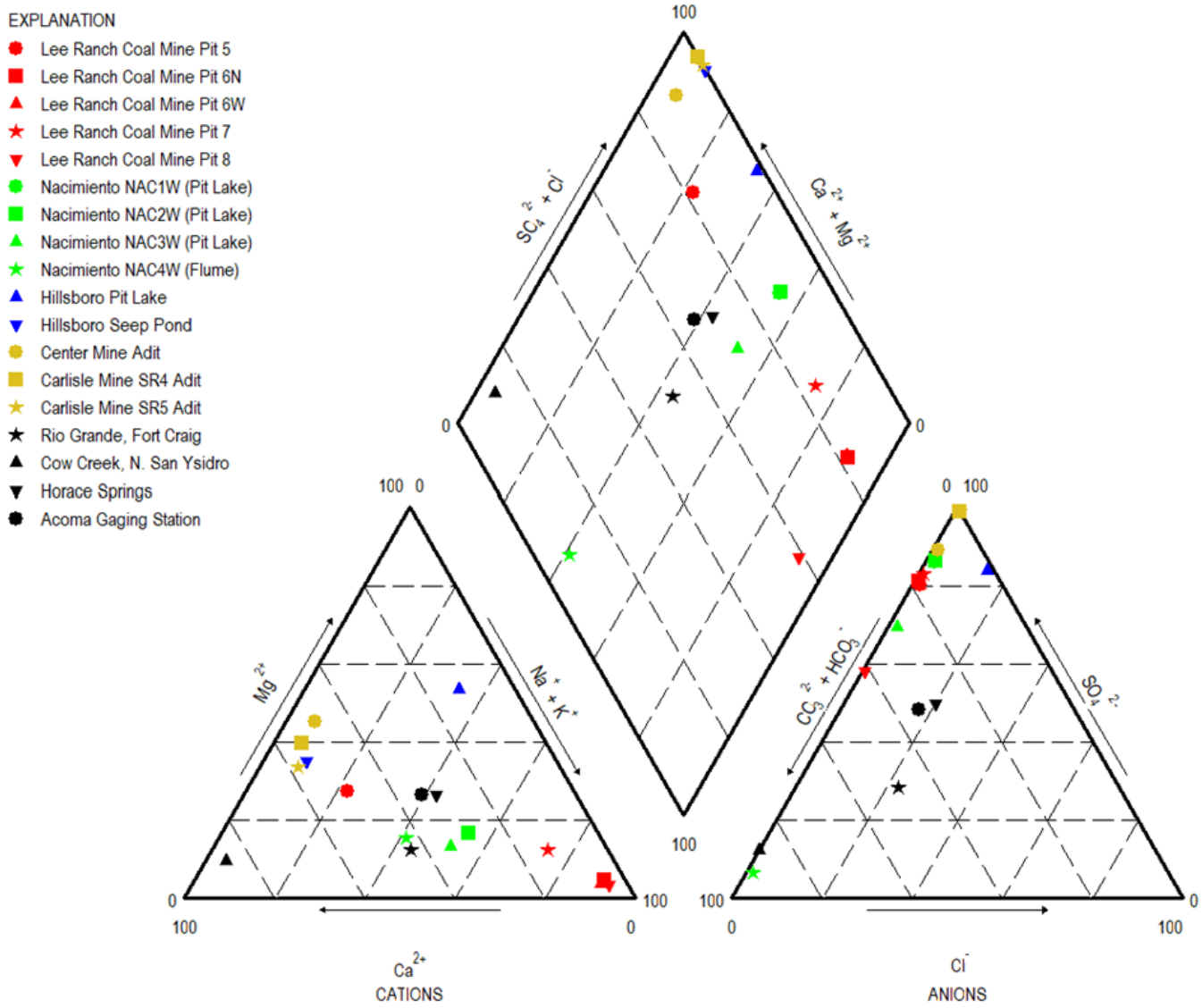

FIGURE 5.26 Data from Lee Ranch Coal Mine and Nacimiento copper mine plotted on a Piper diagram using GW_Chart (Winston, 2000). Also plotted are data from Hillsboro, Center, and Carlisle mines, and water data from the Rio Grande, Cow Creek, Horace Springs and the Acoma Gaging Station in Canada del Ojo, east of Albuquerque. Arrows along each axis indicate an increasing percentage of the given constituent(s).

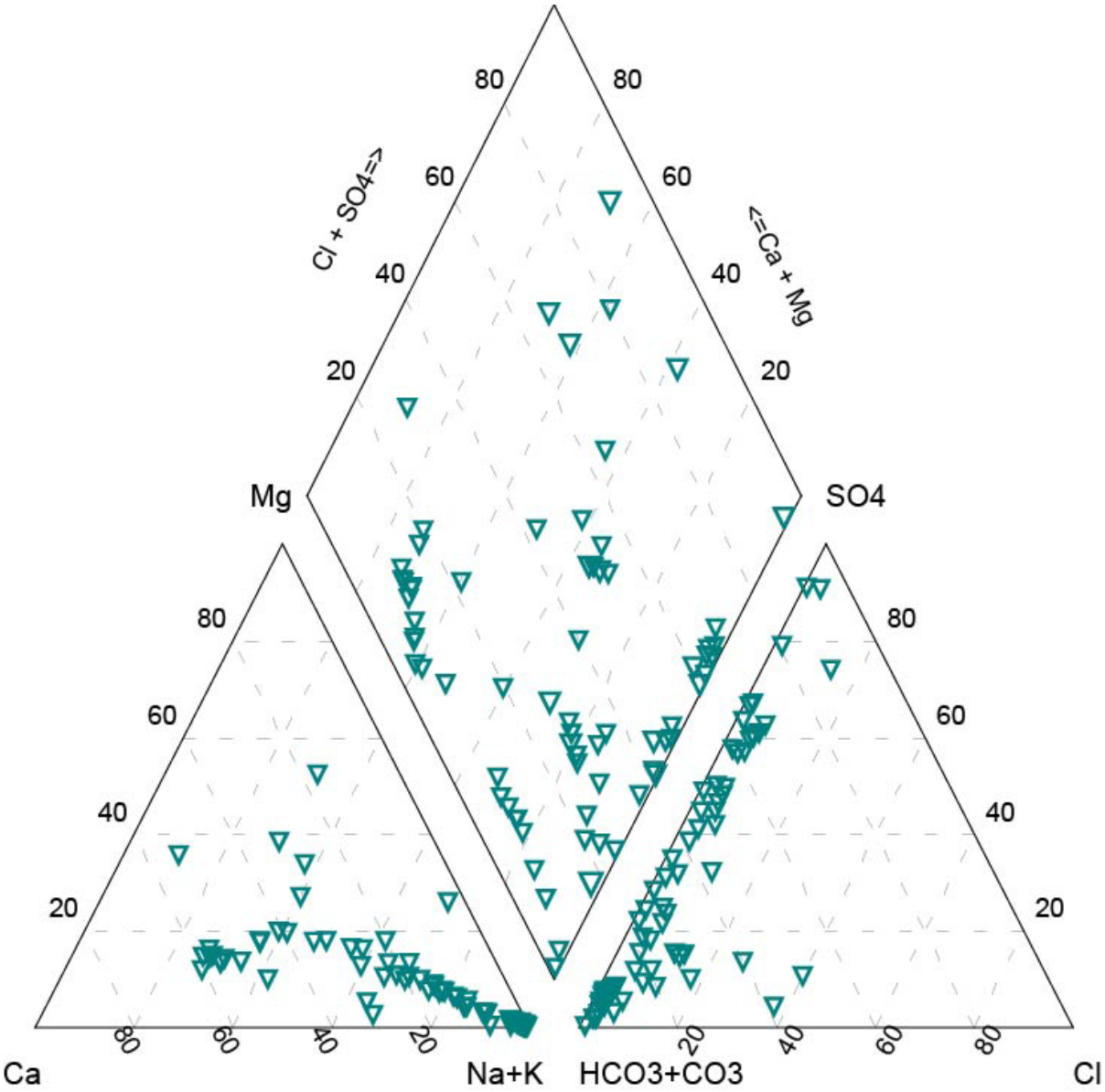

FIGURE 5.27 Piper Diagram for well water samples sourced in the Menefee Formation in the San Juan Basin (Modified from Kelley et al., 2014). Surface water samples from the Lee Ranch Coal Mine pits show low Ca, high sodium and potassium, and high sulfate, low carbonate and bicarbonate, similar to these water samples.

Rare Earth Elements

Rare earth element concentrations in the Lee Ranch coal mine samples were low (Fig. 5.29) and comparable to naturally occurring surface water bodies (grey icons, Fig. 5.30). Like other data gathered around New Mexico, the light REE (lanthanum through samarium) have elevated values relative to the heavy REE (europium through lutetium). Water from metal mine sites have been shown to have elevated REE, relative to the Lee Ranch coal mine samples, as shown in Fig. 5.30. Also included in Figure 10 are data from several river sites unaffected by mining activity to contrast with water from mine sites. The Lee Ranch coal mine samples fall

into the same range as these river data (Figs. 5.29 and 5.30). The data would greatly benefit from water samples from other coal mines; however, one of the limitations of this project was the aridity of New Mexico; although staff visited several other coal mines, no other standing water could be sampled.

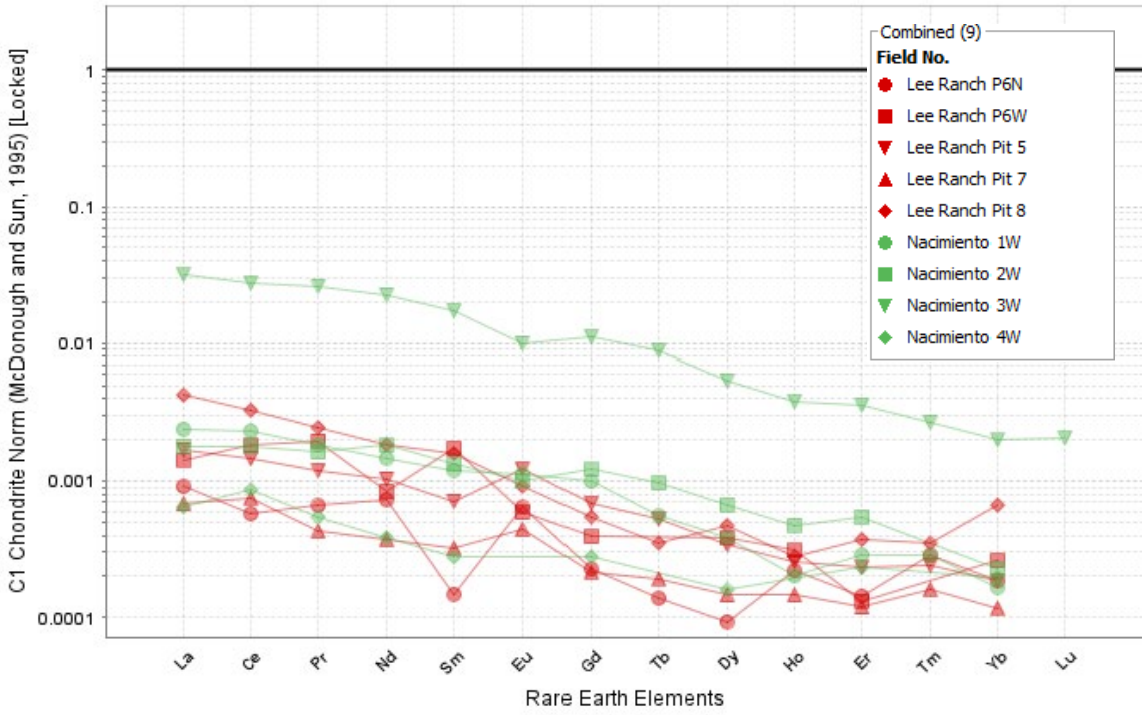

FIGURE 5.28 Chondrite normalized REE graph of water data from Lee Ranch coal mine and Nacimiento copper mine. REE data from the coal mine are notably low Relative to Nacimiento sample 4W and data from mine sites in Figure. 5.29

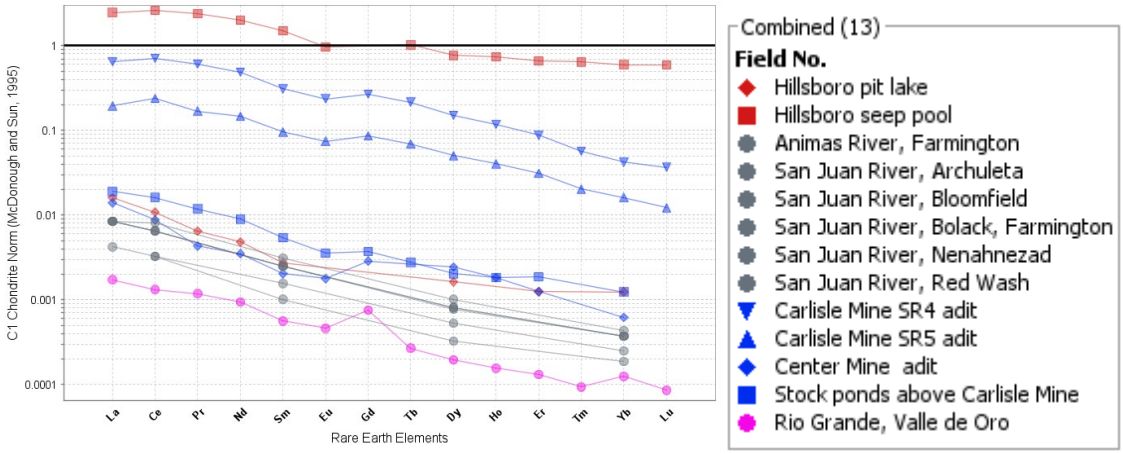

FIGURE 5.29 Chondrite normalized REE graph of water data from three mines in southwestern New Mexico (Hillsboro, Carlisle and Center) and several river sites along the San Juan River and the Rio Grande. The y-axis is scaled to match Figure 5.28 for ease of comparison

Water quality

This project also presented an opportunity to evaluate the quality of water at coal mine sites, specifically looking at total dissolved solids (TDS, Table 5.3) and metals (Table 5.4).

TDS is an important indicator of water quality. Within this project, TDS tended to be well above naturally occurring surface waters and US EPA Secondary Drinking Water Standards (those related to aesthetic considerations such as taste, color and odor). TDS in the pit waters of the Lee Ranch coal mine were between 1000 and 4000 ppm TDS, comparable to mine adit and seep waters (Hillsboro, Center and Carlisle). The water from Lee Ranch pit 5, which has been reclaimed, is an exception and is comparable to the spring water.

TABLE 5.6 Total dissolved solids (TDS) levels of pit water of the Lee Ranch coal mine (red text), river sources from around New Mexico (green text), and metal mine sources.

Project location	Sample ID	TDS (ppm)
Lee Ranch coal mine	Pit 5	733
Lee Ranch coal mine	Pit 6N	3560
Lee Ranch coal mine	Pit 6W	2620
Lee Ranch coal mine	Pit 7	2400
Lee Ranch coal mine	Pit 8	1570
Nacimiento mine	NAC1W	1710
Nacimiento mine	NAC2W	1720
Nacimiento mine	NAC3W	643
Nacimiento mine	NAC4W	987

Mine and River Samples	TDS (ppm)
Hillsboro mine pit lake	12068
Hillsboro mine seep pond	4175
Center mine adit	3222
Carlisle mine SR4 adit	1814
Carlisle mine SR5 adit	1451
Rio Grande, Fort Craig	400
Cow Creek, North San Ysidro	116
Horace Springs	766
Acoma Gaging Station	630

Several inorganic elements and compounds are regulated in drinking water by the U.S. EPA. We list these regulated constituents in Table 5.7, along with their maximum allowable contaminant level, and the measured concentrations in waters from the Lee Ranch coal mine and the Nacimiento copper mine. Only a couple of exceedances were identified, and only in the Nacimiento copper mine samples (orange cells in Table 5.7); 0.031 mg/L uranium in NAC2W and 25.9 mg/L fluoride in NAC4W. The high level of fluoride in NAC4W is concerning because of its release as treated water to the Senorito Creek.

TABLE 5.7 Exceedances of US EPA Maximum Contaminant Levels for Drinking Water. Orange shading = greater than EPA maximum contaminant limit for drinking water. ND = Not detectible above the lab's reporting limit. * = Not detectible above the lab's detection limit (=RL*10)

Parameter	EPA MCLs (mg/L)	LR Pit 5	LR Pit 6 N	LR Pit 6 W	LR Pit 7	LR Pit 8	NAC1W	NAC2W	NAC3W	NAC4W	Reporting limit (mg/L)
Nitrate (as NO3)	44	ND	ND	5.56	ND	ND	ND	ND	ND	ND	0.5
Nitrite (as NO2)	3	ND	ND	ND	ND	ND	ND	ND	ND	ND	0.5
Fluoride	4.0	0.48	1.4	1.3	0.73	1.35	1.75	1.89	0.41	***25.9***	0.5
Antimony	0.006	ND	ND	ND	ND	ND	ND	ND	ND	ND	0.005
Arsenic	0.010	ND	ND	ND	ND	ND	ND	ND	0.0028	ND	0.005
Barium	2	0.101	0.081	0.036	ND	0.054	0.076	0.076	0.123	0.029	0.05
Beryllium	0.004	ND	ND	ND	ND	ND	ND	ND	ND	ND	*0.001
Cadmium	0.005	ND	ND	ND	ND	ND	ND	0.0012	0.0031	ND	*0.0004
Chromium	0.1	ND	ND	ND	ND	ND	ND	ND	ND	ND	0.005
Selenium	0.05	ND	ND	0.01	ND	ND	0.016	0.017	ND	ND	0.01
Thallium	0.002	ND	ND	ND	ND	ND	ND	ND	ND	ND	*0.001
Uranium	0.03	ND	0.0064	0.0076	ND	ND	0.0295	***0.031***	0.0174	ND	0.005

Concluding thoughts

The REE concentrations for water collected during this project are low for the one coal mine sampled. However, sampling of one coal mine is not representative. Throughout our work to measure REE in surface water, we have identified a significant gap of REE data for surface water. Continuing water quality surveys to close this gap are encouraged for several reasons:

We have learned from the legacy of uranium mining in New Mexico that background data is critical to understanding the impact of mining and in facilitating legacy cleanup

Surveying for REE and other critical minerals may lead to the identification of other critical minerals resources

REE can be used as tracers in hydrologic systems, and with water resources in New Mexico becoming more and more impacted by drought and increasing temperatures, such tools for understanding our hydrologic systems is becoming more and more necessary for providing the water needed by our communities and our industries

Combining critical minerals analysis with general water chemistry and other chemical constituents can help guide extractive technologies.

5.2.4 Magdalena leaching tests (R. Coyte)

Experimental Design

Students at the Science Café in Magdalena constructed columns for leaching experiments on samples from four waste piles from the Kelly mine in Magdalena, New Mexico (Figs. 5.30, 5.31, 5.32, 5.33, 5.34). In the lab, the students placed the <2 mm material in columns (Fig. 5.35) and ran deionized water through the columns to learn what metals were environmental available in the piles during precipitation events. Each column consisted of a clear high-density

polyethylene (HDPE) tube fitted with a polyvinyl chloride (PVC) cap secured with silicone at one end. A brass hose fitting, threaded on one side, was installed into the PVC cap, and a clear hose with a hose clamp was attached to the brass fitting to collect and retain fluid in a reservoir (Fig. 5.35).

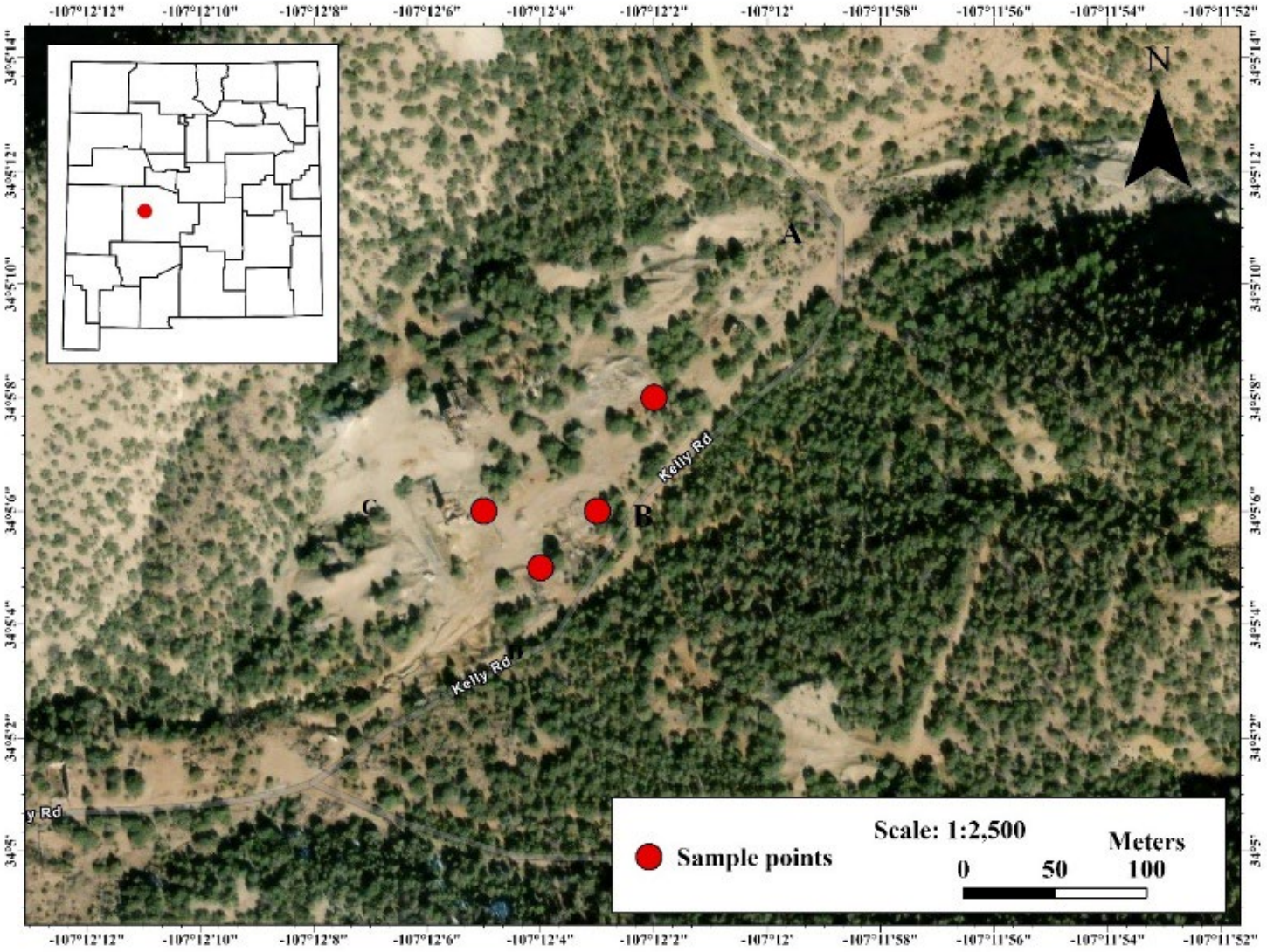

FIGURE 5.30 Location of sample sites in the Magdalena district.

FIGURE 5.31 Training Magdalena Teen Science Café students to sample piles at Kelly mine near Magdalena, New Mexico, March 2024 (photograph by B. Frey).

FIGURE 5.32 Magdalena Teen Science Café students sieving material from mine waste piles at Kelly mine near Magdalena, New Mexico, March 2024 (photograph by B. Frey).

FIGURE 5.33 Magdalena Teen Science Café (MTSC) students participate in mine waste sampling at Kelly mine near Magdalena, New Mexico (photograph by B. Frey).

FIGURE 5.34 Experimental leaching column setup constructed by students at the Science Café in Magdalena. Each column consists of a clear HDPE tube with a PVC cap sealed with silicone at the base. A brass hose fitting, threaded into the PVC cap, connects to a clear hose secured with a hose clamp, allowing fluid collection in a reservoir.

Inside the HDPE tube, a small plastic cup with four drilled holes in its base was affixed using silicone adhesive. This configuration created a separation between the soil and the fluid reservoir at the base of the tube. Four identical apparatuses were constructed for the experiment.

Students standardized the soil column height in each tube to 17 inches, and ran a precipitation simulation protocol, administering 0.25 inches of distilled water daily to each tube. This simulated rainfall continued until sufficient water was collected in the reservoirs to facilitate subsequent analyses, 250 mL in total. The collected water samples were delivered to NMT for chemical analysis.

Results

The total dissolved solids (TDS) in water from all column experiments were high (exceeding 2000 mg/L), and the pH was consistently low (below 6). Column A had the highest TDS by far, measuring 42,700 mg/L. Due to its high TDS, significant dilution was required for analytical chemistry, leading to some analytes falling below detection limits.

Because no reference column with unimpacted sediment was prepared, groundwater collected by the USGS from a nearby location in Socorro was used as a reference to illustrate water chemistry trends (Fig. 5.36). This reference groundwater represents a typical Na-Cl groundwater. In contrast, the leachate from the column experiments resembled mine drainage, characterized by high sulfate concentrations and elevated levels of various metals compared to most natural waters.

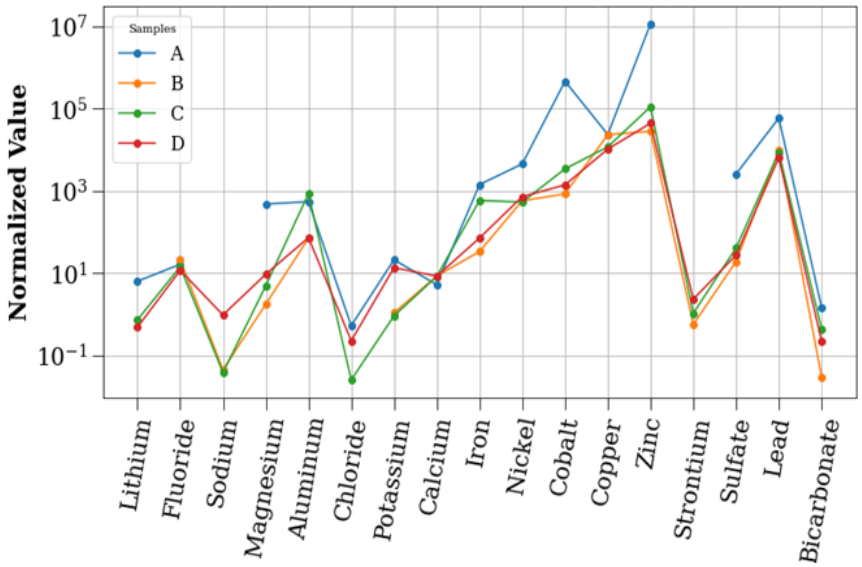

FIGURE 5.35 Comparison of water chemistry between the leachate from column experiments and reference groundwater collected by the USGS from a nearby location in Socorro, New Mexico. The reference groundwater, representative of typical Na-Cl water, contrasts with the mine drainage-like leachate from the columns, which exhibited high sulfate concentrations and elevated metal levels. Elemental patterns were broadly consistent across experiments, with Columns B and C displaying similar chemistries dominated by sulfate, zinc, and calcium. Column D had the lowest TDS but elevated nitrate, while Column A had the highest TDS, with sulfate, zinc, magnesium, and manganese as dominant analytes. All leachates were enriched in heavier row 4 transition metals (Mn, Fe, Ni, Co, Cu, Zn) and post-transition metals (Pb, Al), with no detectable Cr or V.

Elemental patterns were broadly consistent across the four experiments (Fig. 5.35). Columns B and C exhibited the most similar water chemistries, with sulfate, zinc, and calcium as the dominant analytes, and comparable TDS levels. Column D had the lowest TDS among the experiments. In addition to high sulfate, calcium, and zinc, it also contained elevated nitrate concentrations. Column A, with the highest TDS, was dominated by sulfate, zinc, magnesium, and manganese. All samples were highly enriched in the heavier row four transition metals (Mn, Fe, Ni, Co, Cu, Zn), though with no detectable Cr or V, as well as the post-transition metals Pb and Al.

Rare earth elements (REE) were analyzed after normalizing to chondrite values (Fig. 5.37). Column A contained the highest REE concentrations of the four experiments and displayed a slight enrichment in heavy REEs (HREE) relative to light REE (LREE). The other three experiments shared similar REE patterns, with a steadily decreasing trend and enrichment in LREE over HREE. A slight europium (Eu) depletion was observed in Columns A, B, and C, but this pattern was not present in Column D.

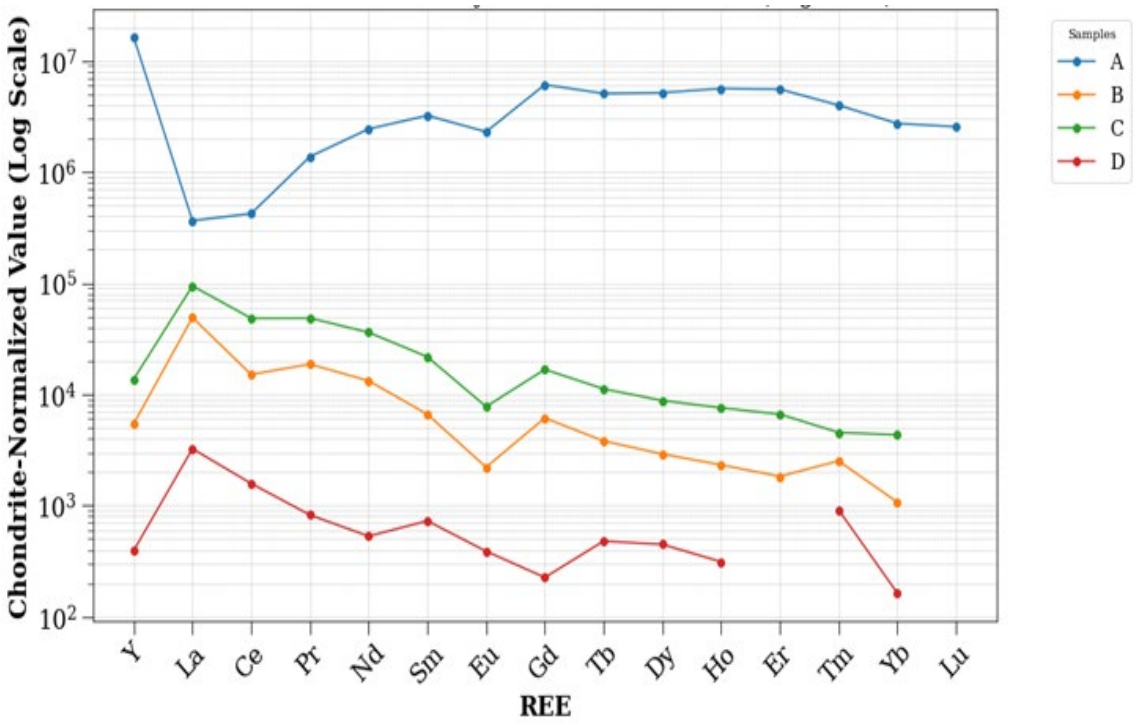

FIGURE 5.36 Chondrite-normalized rare earth element (REE) patterns for leachate from the column experiments. Column A exhibited the highest overall REE concentrations and a slight enrichment in heavy REEs (HREE) relative to light REEs (LREE). In contrast, Columns B, C, and D displayed similar REE trends, with steadily decreasing concentrations and enrichment in LREE over HREE. A slight europium (Eu) depletion was observed in Columns A, B, and C, while Column D did not exhibit this pattern.

Discussion

The Kelly mine, a former lode Zn-Pb-Cu-Ag-Au mine, is a known source of enriched metal and sulfate-bearing minerals. XRD data confirmed the presence of zinc sulfate minerals in high concentrations (Appendix 6), aligning with the leachate chemistry, which was highly enriched in zinc and sulfate, as well as in lead and copper. The acidic pH of the water from these tailings further promotes the mobilization of these elements, creating favorable conditions for their dissolution and transport.

Several elements in the leachates are particularly noteworthy due to their dual significance; they are designated as critical minerals by the USGS, including nickel, cobalt, zinc, and copper, and they pose environmental risks due to their high solubility in water. This solubility enhances the potential for these elements to be mobilized and transported into surrounding ecosystems, posing a risk to environmental and human health.

Adding to this concern are the exceptionally high concentrations of toxic elements such as cadmium and lead in the leachates—several orders of magnitude above drinking water standards. While the leachates themselves are not a direct drinking water source or representative of one, their potential to seep into groundwater or surface water represents a serious risk to local water supplies, including those serving the nearby town of Magdalena. However, the arid climate of the region slows the rate of mobilization by water, offering some mitigation. Yet, it is important to recognize that this does not eliminate the risk entirely. Over time, even in dry

conditions, these elements can migrate into the environment. This underscores the need for a more comprehensive study to model the likely rate and extent of element migration from the tailings. Such a study should account for local hydrology and provide a detailed understanding of the distribution and volume of tailings in the area. These insights would be invaluable for predicting long-term impacts and informing effective management strategies to safeguard regional water resources.

5.2.5 Acid mine drainage

Acid mine drainage does not occur in appreciable amounts in the San Juan and Raton basins.

5.3 Reuse strategy

5.3.1 Reuse of coal waste materials (G. Xu)

Recovery of critical minerals from coal ash and reuse of the residual coal ash in the cement industry presents a promising opportunity to enhance critical minerals sustainability while addressing waste management challenges. By employing environmentally benign leaching processes to extract REE, it can simultaneously reduce the concentration of toxic metals such as arsenic, lead, and mercury, resulting in cleaner residual coal ash. New Mexico coal ash, i.e., from power generating stations in the Four Corner area, do not have high REE but they do contain other critical minerals with economic potential, such as, gallium (up to 40 ppm).

5.3.2 Sonash reuse of waste materials (C. Arato)

SonoAsh is actively engaged with private New Mexico companies to build additive partnerships for Phase 2 of the CORE-CM program, if funded. SonoAsh continues to develop a separate ion exchange membrane program in collaboration with the University of Maryland. Additional reuse strategies developed by SonoAsh is summarized on their web site (Coal Ash Processing Solutions | SonoAsh). SonoAsh has direct experience around taking the waste streams (i.e. ash, coal and fly) for regional product development. While the sources of potential sources appear to be available in New Mexico, SonoAsh and the project team were unable to source material from sources and near Farmington or elsewhere in New Mexico.

5.4 Summary of findings

- Mine wastes are high-volume heterogeneous material that remains from the extraction (mining) and processing (milling, refining) of a range of metalliferous and non-metalliferous mineral deposits. The types of mine wastes include waste rock or rock piles, tailings, overburden, low grade or subore stockpiles, slag, water, heap leach, coal ash, flue dust, and fly ash.
- Coal ash was sampled from some of the power plants. The overall REE content of these ashes is low; the highest values are below 300 ppm TREE. When compared to chemical analysis from other coal basins, San Juan Basin samples are similar.

- More than 133 million tons of coal ash are stored at the electric power generating plants in New Mexico. Millions of tons of coal waste rock are found throughout New Mexico. Known critical minerals found in coal ash include REE, Sc, V, and others.
- Endowments for minerals such as Th, V, Y, and TREE are higher at the Thatcher and Law mines sites. The Thatcher waste rock contains approximately 0.5 ton of Th, 2.8 tonnes of V, 0.5 tonnes of Y, and 4.6 tonnes of TREE. The Law mine dump shows similarly elevated values, with about 0.1 tonnes of Th, 0.8 tonnes of V, 0.1 tonnes of Y, and 1.2 tonnes of TREE. In contrast, the Noci and Black Diamond mine dumps contain smaller endowments: Noci dump has roughly 0.02 tonnes of Th, 0.2 tonnes of V, 0.03 tonnes of Y, and 0.2 tonne of TREE, whereas Black Diamond dump has about 0.4 tonnes of Th, 1 tonnes of V, 0.2 tonnes of Y, and 1.4 tonnes of TREE.
- Although, some of the mine wastes show concentrations of some critical minerals above crustal abundance, the concentrations are below recommended economic concentrations and therefore, the concentrations and tonnages are probably too small to provide an economic resource.
- The REE concentrations for water collected during this project are low for the one coal mine sampled. However, sampling of one coal mine is not representative. Throughout our work to measure REE in surface water, we have identified a significant gap of REE data for surface water. Continuing water geochemistry surveys to close this gap are encouraged.
- While the sources of potential sources appear to be available in New Mexico, SonoAsh and the project team were unable to source material from sources and near Farmington or elsewhere in New Mexico.

6.0 STRATEGIES FOR INFRASTRUCTURE, INDUSTRIES AND BUSINESSES (TASK 4) (V.T. MCLEMORE AND C. ARATO)

SonaAsh, one of the CORE-CM partners, is a processing engineering company utilizing coal ash processing technologies to transform environmental liabilities into valuable assets (https://sonoash.com). SonoAsh specializes in technologies that transforms coal combustion residuals into valuable resources for the construction industry, such as using coal ash in cement manufacture (Appendix 15, 16). SonoAsh has worked on relationships, such as with John Elling's Santa Fe analytical lab, and related projects, as well as with partnerships with a large ($100 m/y) Farmington-area industrial company. SonoAsh has worked to create a network of technical, production and infrastructure partners throughout the USA for its planned network of fly ash beneficiation efforts to create state-of-the-art, high margin secondary cementitious materials (SCMs) as well as a proprietary carbon concentrate of selected critical and REE metals for susbsequent IP to be developed for extraction and recovery in a national network of facilities, with significant engagement from New Mexico in plants planned for Maryland, West Virginia, North Carolina, Colorado, among others. Sonoash also was accepted into the initial DOE/MESC cohort of 14 U.S. companies, receiving $2 million in technical assistance through DOE, working with independent engineering firms to work initial cost estimates (Class IV) for San Juan County. Additional strategies will be explored in phase 2, if funded.

7.0 TECHNOLOGY ASSESSMENT AND TESTING OF NEW TECHNIQUES (TASK 5)

This section describes availability and challenges of infrastructure in the San Juan and Raton basins and the state of the industry. It also includes laboratory and computer modeling of new techniques in evaluating coal resources and future potential and applications.

7.1 Availability and challenges of infrastructure in the San Juan and Raton basins (V.T. McLemore)

The mining industry in New Mexico, including the San Juan and Raton basins was discussed in Chapter 1 of this report. Information on mining districts in and surrounding the San Juan and Raton basins is in Appendix 3. Much of the required infrastructure (highways, railroads, power transmission lines, etc.) needed for economic development is available in the region, mostly near Farmington, Gallup, Grants, Raton, and other populated areas. However, infrastructure in less-populated, rural New Mexico, especially the tribal lands, is not as well developed. Many areas in rural New Mexico do not have paved roads, available running potable water, internet, cell phone, etc. Many federal, state, and tribal agencies are addressing these deficiencies.

7.2 Initial technology assessment (V.T. McLemore)

Coal production has decreased in New Mexico (Fig. 1.11) with the closure of major power plants (Escalante and San Juan generating plants). Only the Four Corners power plant remains in operation, which is located on Navajo Tribal Lands and operated by Navajo Transitional Energy Co. (NTEC; https://navenergy.com/four-corners-power-plant/). The closure of the coal mines and power plants has resulted in decreased employment and revenues for the area. Although the oil and gas industries have employed many of the former coal workers, additional industries are needed to continue economic stability in the area. The Four Corners Economic Development Center has developed plans and strategies to continue stability of economic development in the area (https://www.4conernsed.com). The mining districts in and surrounding the San Juan and Raton basins are idle, but some of them have critical minerals potential (Appendix 7).

Other initiatives are needed as well. Much of the infrastructure once used to transmit energy from the conventional power plants could be used to transmit energy from wind and solar installations. Several entities and projects elsewhere in the U.S. exist that show examples of what can be developed in the San Juan and Raton basins include:

Energy Fuels, Inc. has a mill in Blanding, Utah that recovers uranium, vanadium and REE and plans to recover titanium and zirconium for beach-placer sandstone deposits (https://investors.energyfuels.com/2022-04-13-Energy-Fuels-Hits-Critical-Mineral-Trifecta-in-Rare-Earths,-Uranium-Vanadium-Now-Performing-Commercial-Scale-Partial-Rare-Earth-Separation). Energy Fuels, Inc. has properties in the Grants uranium district, New Mexico (https://energyfuels.com/roca-honda-project/).

Lynas Corporation is building a new rare earths processing facility in Seadrift, Texas, to develop a domestic supply of rare earths for U.S. commercial and defense manufacturers (https://lynasrareearths.com/wp-content/uploads/2023/11/Lynas-USA-May-2025.pdf).

MP Materials is the owner of California's Mountain Pass Mine, the only operating REE mine in the United States. MP Materials plans to process REEs at a facility in California and produce rare-earth magnets at a factory in Texas (https://mpmaterials.com/facilities/).

Rare Element Resources, Ltd., has been developing the Bear Lodge REE mine in Wyoming and has been working on a REE demonstration facility in Wyoming (https://www.rareelementresources.com/bear-lodge-project/).

UCore Rare Metals, Inc. (https://ucore.com/), is developing the Bokan Mine in Alaska and is also working on a demonstration plant in Ontario.

Another future economic opportunity in the San Juan and Raton basins is centered around carbon capture and storage. NETC is developing carbon capture technology at their Four Corners power plant (Figs. 7.1, 7.2). Other potential businesses that could employ carbon capture technologies are summarized by a New Mexico legislature handout (ALFC 072121 Item 11 Brief_Carbon Sequestration at NM Power Plants.pdf). Maintaining economic security in these areas require all these initiatives and more.

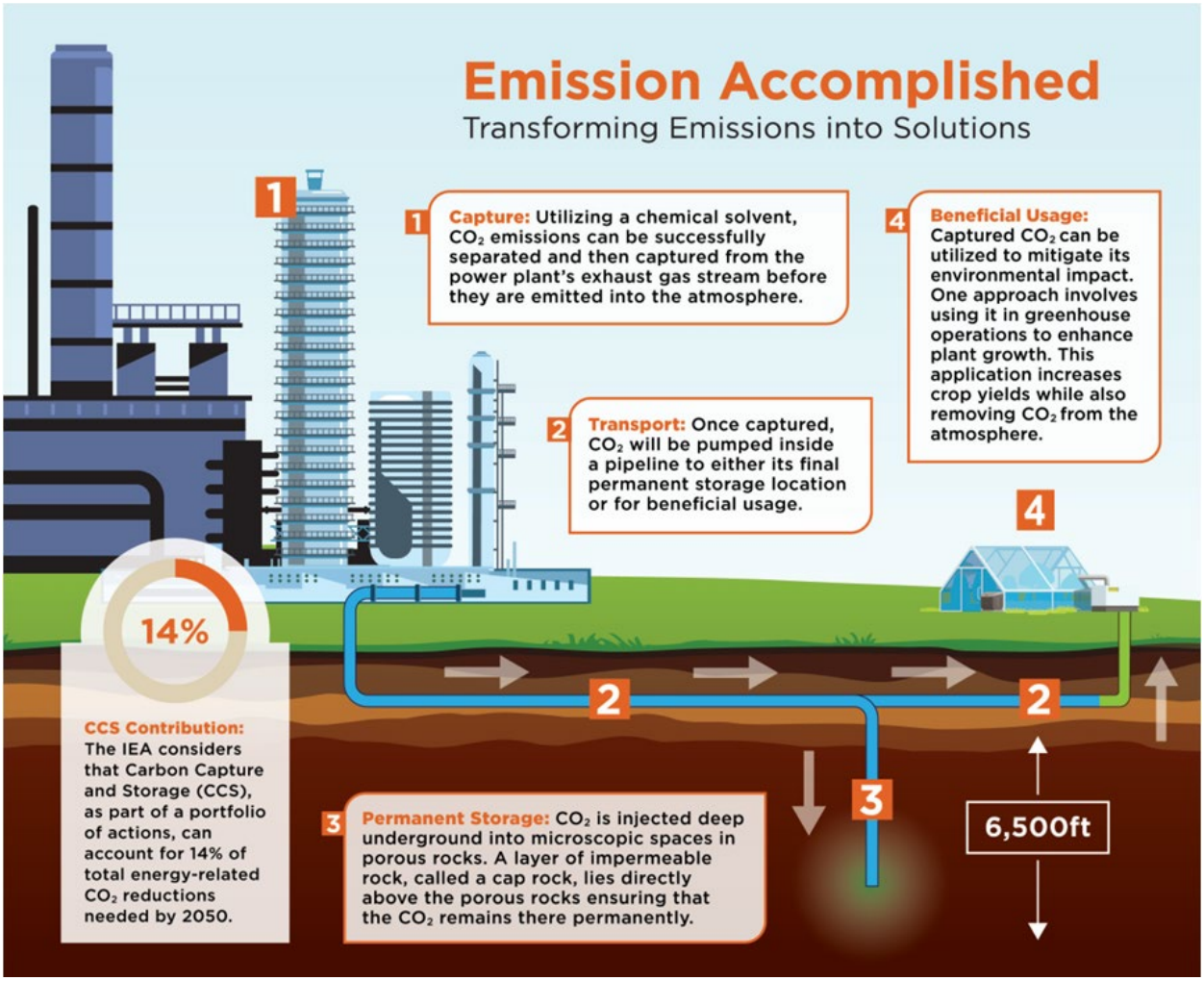

FIGURE 7.1 Graphic showing NTEC plans to incorporate carbon capture and storage at their Four Corners power plant (from https://navenergy.com/wp-content/uploads/2024/10/211654_CARBON.pdf).

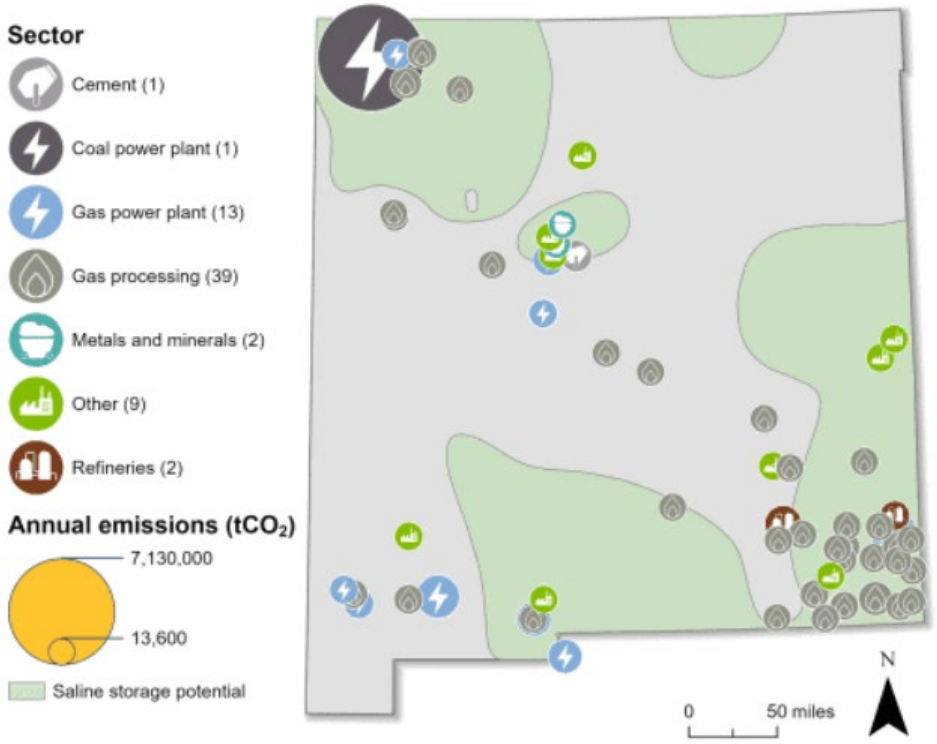

Sources: EPA GHGRP, 2024. Bauer et al., NATCARB, 2018.

FIGURE 7.2 Industries in New Mexico that could utilize carbon capture technologies (from New Mexico - Carbon Capture Ready).

7.3 Field testing new techniques and technologies

During this project several opportunities arose to explore and test new techniques and technologies in exploration, characterization and recovery of critical minerals. These projects are summarized below.

7.3.1 Geochronology (N. Iverson and S. Moses)

The $^{40}Ar/^{39}Ar$ geochronology method was performed on three clinker samples at the New Mexico Geochronology Research Laboratory (NMGRL). Coal samples were crushed in the jaw crusher and then a disk mill. The crushed material was sieved using 20, 40 and 60 mesh sieves, with the finest material being archived. Samples were rinsed in deionized water and in ultrasonic bath to remove all adhering particulates. Samples were then decanted, rinsed and placed in an oven to dry. This process enables the removal of contamination of fine particulate matter that clings to the intermediate grains of the clinker sample.

The dry samples were sent through the Frantz magnetic separator, whereafter they then underwent another ultrasonic bath but this time in hydrochloric acid to be then rinsed, decanted and dried. Dry samples were picked using a binocular microscope (approximately 50 mg of groundmass or glassy grains) and loaded into trays for irradiation, specifically into 8-hole aluminum disks with interspersed flux monitors of FC-2 (28.201 Ma, Kuiper et al., 2008).

Samples were then sent to the Oregon State University reactor in Corvallis, Oregon (NM-345) for a 30-hour irradiation. Samples were analyzed at NMGRL after irradiation and loaded into a 37-hole stainless steel laser tray and step-heated using a Photon Machine 810 nm diode laser. The extracted gas was cleaned using a cold trap at -198°C and a D50 getter, before being analyzed with a Thermo-Fisher Helix Multi-Collector ("Felix") mass spectrometer. All FC-2 standards underwent single-crystal laser fusion using a Photon Machine CO_2 laser and Ar isotopes were collected on a Thermo-Fisher Argus VI multi-collector mass spectrometer. Both instruments analyze the same internal gas standards: atmospheric air samples with a $^{40}Ar/^{39}Ar$ ratio of 295.5 (Nier, 1950), and an NMGRL gas "cocktail" with a $^{40}Ar^*/^{39}Ar$ ratio of 6.600975 to monitor detector drift and collector intercalibration. Procedural blanks were run for air, cocktail, and unknowns, which involves running the procedure without firing the laser or letting any sample gas into the extraction line.

Results

Three samples of clinker were dated to establish the age of pyrometamorphism (Table 7.1). All sample data was reduced using PyChron Software package PyCrunch 20.1.1 (Ross, 2014). Two subsamples from Coal140, a glassy black phase and brick colored groundmass phase. Only a brick-colored groundmass phase was dated for Coal102. Between 9.80 to 10.66 mg of each sample was loaded into a 37-hole stainless steel laser tray and step heated. Between 14 and 21 incremental heated-steps were used to maximize spectral resolution and maintain enough extracted gas for a precise measurement. All samples had complicated spectra with negative and positive portions of the spectra. Multiple aliquots were tried to improve resolution and precision. Coal140-A produced an age of 0.03±0.11 Ma. Both aliquots of Coal140-A produced plateau ages, however one was positive and one was negative (Coal-140A-02 was -0.82±0.41 Ma). Inverse-isochron analysis shows that the sample is atmospheric (does not contain extraneous argon) and also produced essentially a zero-age (Coal-140A-01 was 0.001±0.1 Ma and Coal-140A-02 was 0.4±0.2). Therefore, the glassy sample is considered to be zero age. Coal140-B (groundmass) did produce an imprecise inverse-isochron age (3.0±0.5 Ma). The groundmass is still atmospheric in composition and several steps were removed (A-J) because they contained no gas. This does overlap with the integrated spectrum age of 2.4+0.6 Ma. The inverse-isochron age is the preferred age due to the very complicated spectrum. This age is very imprecise and contained very low radiogenic yield (<3% *40Ar). The age of 3.0±0.5 Ma is potentially highly inaccurate and is considered a maximum age. Coal102 has a climbing spectrum, low heat steps are negative age (upwards of -11 Ma) and has a climbing spectrum to over 10 Ma. One aliquot produced an isochron age of 1.6±0.7 Ma with a very high MSWD (~155). The other aliquot could not generate an inverse-isochron age because the regression line would not intersect the x-axis. Because of these problems 1.6 Ma is the preferred age. All of these ages should be considered highly inaccurate maximum ages.

TABLE 7.1 Summary of $^{40}Ar/^{39}Ar$ geochronology of selective clinker samples from the San Juan Basin. See Appendix 11 for plots and tables.

Sample ID	Material Analyzed	Apparent Age (Ma) (Error 2σ)	MSWD	$^{40}Ar/^{36}Ar$ Intercept	Method
Coal140-A	Glass	0.03 ± 0.11	0.53	295.7±0.4	Plateau
Coal140-B	Groundmass	3.0 ± 0.5	21.78	295.2±0.4	Inverse Isochron
Coal102	Groundmass	1.6 ± 0.7	155.73	296.3±0.6	Inverse Isochron

Discussion

Dating two different phases from the same sample can provide insight into the measurements and allow closure temperature to be observed. For Coal140, dating both the glassy phase and the groundmass allowed us to see if the sample type affected the dating. In this case, the glass provided a plateau age at 0 Ma. Essentially, saying that pyrometamorphism of these samples happened so recently that there is no measurable amount of radiogenic argon in the sample. Which is corroborated by the -1% to <2% radiogenic ^{40}Ar measured in the sample. In contrast, the groundmass sample provided an age upwards of 3.0±0.5 Ma. Meaning the pyrometamorphism has more likely happened anytime in the last ~3Ma. However, there is not enough precision on the measurement or high enough radiogenic yield (<3% $*^{40}Ar$) to give a robust answer. All samples contained sufficient K content to produce a viable age (0.5 to 0.7 wt. % and 2 to 2.5 wt. % K_2O for Coal 140 and Coal 102, respectively). The age of the coal deposits are Late Cretaceous in age (see section 4.9 for details) and while dating these samples no steps within the argon spectrum were anywhere near the age of the deposit. Meaning that the age of the deposit was completely reset during pyrometamorphism and there is no evidence of inherited grains or Ar gas in the sample like other studies dating pyrometamorphism with the K-Ar system (Peretyazhko et al., 2018). Therefore, it is reasonable to assume that the pyrometamorphism was sufficiently hot enough and long enough to allow all of the previous radiogenic ^{40}Ar to be diffused/lost from the host rock. All of the ages should be considered a maximum age. Meaning that the pyrometamorphism of this coal seam happened in the recent past and not several to 10's of million years ago. To better understand the age of pyrometamorphism of these younger samples with low K_2O content, it may be advantageous to use zircon (U-Th)/He ages, as long as the samples are completely reset (Reiners et al., 2011).

7.3.2 Comparing handheld X-ray fluoresce instrument (pXRF) and laboratory analyses (Z.K. Motlagh)

Introduction

When determining the concentration of major and trace elements in samples, accurate and reliable results are essential. Hand-held or portable X-ray fluorescence (pXRF) instruments have been used in geochemical, mining, industrial, environmental, and archaeological applications to collect compositional data in the field since 1985 (Bosco, 2013; Young et al., 2016). X-ray fluorescence (XRF) analysis is a non-destructive method used to measure the chemical composition of materials by directing X-rays of a specific energy at a sample. This interaction causes the atoms in the material to emit fluorescent X-rays at energies characteristic of the elements present. Portable or handheld X-ray fluorescence (pXRF) instruments can save time and provide in situ chemical analyses to select the most appropriate samples for a broader study. While laboratory geochemical analyses will remain the standard for high-quality geochemical analyses, pXRF instruments help obtain rapid, in situ compositional data of field samples for preliminary evaluation of the sites.

The pXRF instrument has limitations and must be used with caution. The limit of detection is 5-100 ppm for elements with atomic number 19 (K) to 68 (Pb) and is not suitable for very low concentrations of elements lighter than 19 (K) (Barago et al., 2022). Newer instruments can be calibrated to obtain elemental analyses for elements greater than atomic number 68, but

ultimately, the results should be compared to high-quality geochemical laboratory analyses. Variations in the sample matrix (e.g., silicate, sulfide, or organic-rich), soil moisture, particle size, density, sample preparation (powdered versus hand sample), and other sample heterogeneities can affect the accuracy of the pXRF instrument (Barago et al., 2022). Interferences between elements (overlap of characteristic X-ray emission lines) can also affect the accuracy. The manufacturer calibrated the instrument used in this study to analyze silicate-based samples. Certified reference materials were used during this study for pXRF analytical validation and quality control.

In this project, selected samples obtained from the field were analyzed using the pXRF instrument, and a split was submitted to the ALS for high-quality geochemical laboratory analyses. This comparative data set (Appendix 8) can be used to evaluate the level of agreement between elemental concentrations in samples analyzed by PXRF in comparison with results obtained from laboratory whole-rock geochemistry analysis.

Methods

A statistical approach used to evaluate correlation and systematic differences between laboratory and pXRF results. Concentration data for each element were first log10-transformed to reduce the influence of skewness and heteroscedasticity that are typical of geochemical datasets spanning wide concentration ranges. This transformation helps stabilize variance and improves the validity of parametric statistical tests.

For each element, linear regression analysis was performed between the log-transformed laboratory concentrations and the corresponding pXRF concentrations in io-GAS64. The coefficient of determination (r^2) was used to assess the strength of the linear relationship. Higher r^2 values reflect stronger proportional agreement between the two methods, while low values indicate poor predictive capability of pXRF relative to laboratory analysis.

In addition to regression, a two-sample t-test was applied to the log-transformed datasets to determine whether the mean concentrations measured by pXRF differed significantly from those obtained by laboratory methods in Stata17 software. The p-values were used to evaluate statistical equivalence: values below 0.05 indicate a significant difference between methods (systematic bias), whereas values above 0.05 suggest no statistically detectable difference in central tendency.

$$H_0: \mu\_lab = \mu\_pXRF$$
$$H_1: \mu\_lab \neq \mu\_pXRF$$

where μ_lab and μ_pXRF represent the mean log10-transformed concentrations of laboratory analysis and pXRF, respectively.

Under these hypotheses, any difference between methods is attributed to random variation. Rejection of H_0 ($p < 0.05$) shows that $\mu\_lab \neq \mu\_pXRF$, which means there is a statistically significant difference between the two analytical methods. Failure to reject H_0 ($p \geq 0.05$) suggests that the mean concentrations from the two methods are not significantly different at the chosen confidence level.

The number of paired observations (n) was reported for each element to indicate dataset size, and pXRF limits of detection (LOD) were included to provide context for measurement sensitivity, particularly for low-concentration elements where analytical uncertainty is higher.

Results

The comparison shows that pXRF results have generally poor agreement with laboratory measurements, with only limited evidence of meaningful correlation for a few elements like S and As (Fig. 7.3). Most r^2 values are very low (≤0.50), indicating that pXRF concentrations do not reliably track laboratory concentrations across the sample range. Elements such as As, Cu, Mo, Nb, Ni, and Y exhibit essentially no linear relationship (r^2 near zero), meaning pXRF results for these elements in coal behave almost independently of lab values. Cr displays the highest correlation ($r^2 = 0.81$), and S and V show moderate correlations (≈0.6), but the t-test results indicate statistically significant differences between pXRF and lab means for nearly all elements ($p < 0.05$) (Table 7.2). V is the only element where the t-test does not show a significant difference.

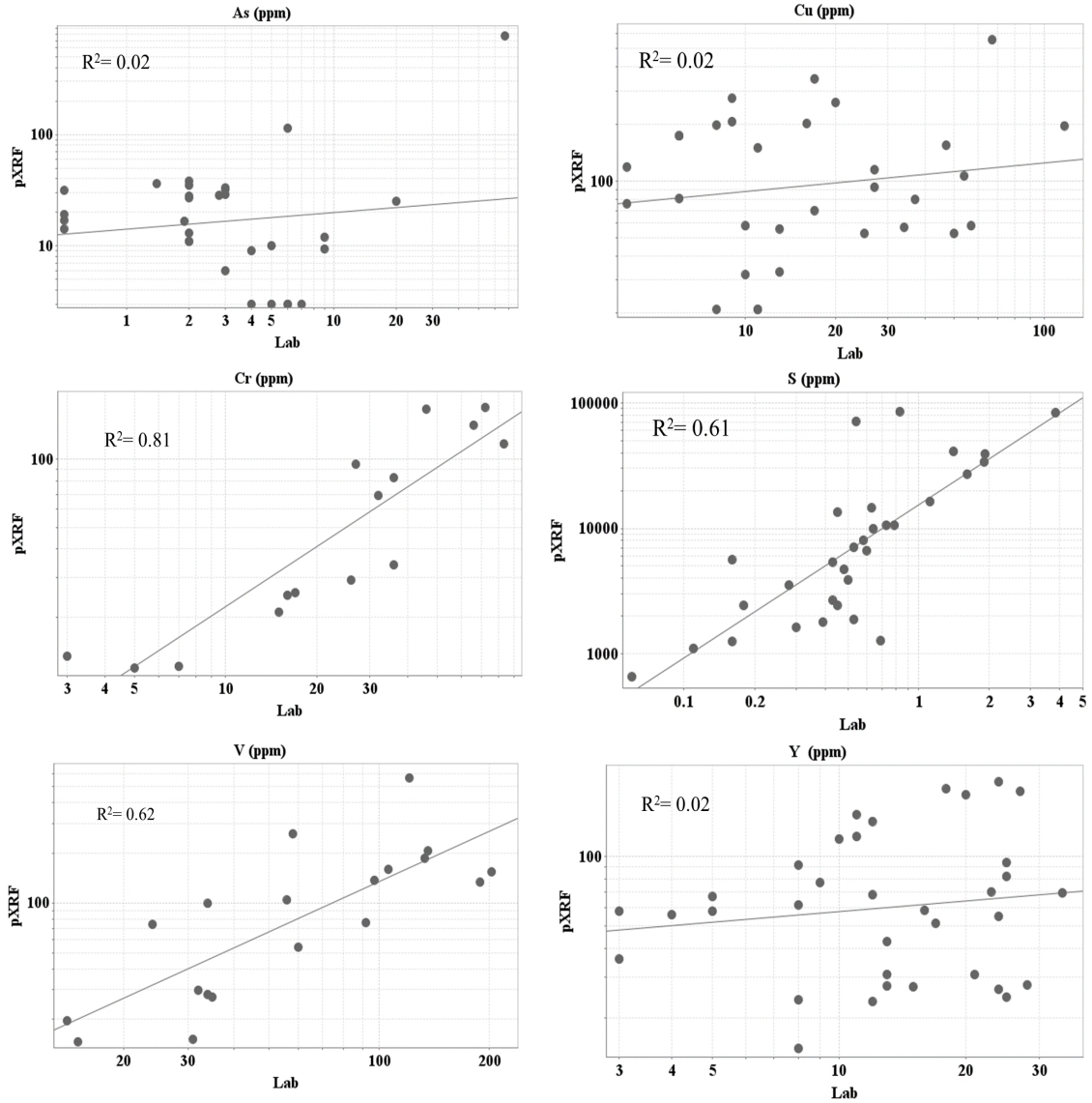

FIGURE 7.3 Scatterplots comparing log-transformed PXRF and laboratory concentrations for As, Cu, Cr, S, V, and Y in coal samples.

In Table 7.2, most of the elements have p-values as 0.000, which shows that coal samples pXRF and lab measurements do not have the same mean concentrations. This confirms that, even if some elements show moderate or strong correlations in regression (like Cr), the pXRF results are consistently offset relative to lab values and cannot be considered directly interchangeable for coal samples.

V is the only element with a p-value above 0.05 (p = 0.065). For V, the null hypothesis cannot be rejected, meaning there is no statistically detectable difference between the pXRF and laboratory mean concentrations at the chosen significance level. However, this does not prove the methods are identical; it only indicates that any difference is not large enough to be distinguished from random variability given the dataset size.

TABLE 7.2 Statistical summary of comparability on lab-pXRF for coal samples. Linear regression and t-test performed on log 10-transformed data. n, amount of data.

Element	n	Lab concentration range (ppm)		PXRF concentration range (ppm)		r^2 lab-PXRF	*t*-Test	PXRF LOD (ppm)
		Min	Max	Min	Max		*p*-Value	
As	26	1	67	3	771	0.06	0.000	2.05
Cr	15	3	83	12	170	0.81	0.000	4
Cu	31	4	117	21	556	0.02	0.000	3.5
Mo	15	1	7	7	63	0.00	0.000	1.5
Nb	24	2	22	11	83	0.03	0.000	1.2
Ni	36	2	17	9.5	238	0.05	0.000	6.5
Pb	20	4	29	8	877	0.30	0.000	4.8
Rb	28	2	148	14	185	0.61	0.000	1.05
Sr	36	16	494	35	7088	0.34	0.000	1.2
V	19	14	203	15	567	0.62	0.065	1.7
Y	35	3	34	15	210	0.02	0.000	0.8
Zn	36	2	109	4	238	0.28	0.000	5.5

The Certified Reference Materials (CRMs) shows that PXRF performance under controlled conditions is generally strong with most elements. Ag, As, Cu, Ni, Y, Zn, and U all show high coefficients of determination ($r^2 \approx 0.85–0.999$) (Table 7.3). This shows that the instrument can produce results that increase and decrease in line with the true concentrations when matrix interference is low.

TABLE 7.3 Statistical summary of comparability on lab-PXRF for CRM samples. Linear regression and t-test performed on log 10-transformed data. n, amount of data.

Element	n	Lab concentration range (ppm)		PXRF concentration range (ppm)		r^2 lab-pXRF1	*t*-Test	pXRF LOD (ppm)
		Min	Max	Min	Max		*p*-Value	
Ag	5	0.3	209	16	193	0.855	0.332	6.5
As	5	5.2	722	11	499	0.915	0.424	2.05
Cu	16	9.2	1,348	10	2,628	0.971	0.136	3.5
Ni	8	8.2	252	17	376	0.957	0.166	6.5
Pb	5	17.5	25.2	11.7	44	0.007	0.799	4.8
U	7	39.6	1,779	47	2,198	0.999	0.000	2.5
Y	13	0.7	133	1.5	163	0.923	0.043	0.8
Zn	10	6.7	108	11.9	103	0.995	0.009	5.5
Zr	8	7	143	17.5	418	0.648	0.001	2.5

Conclusions

The comparison between laboratory and pXRF results demonstrates for coal and CRM samples show that pXRF performance is controlled by sample matrix. In certified reference materials, most elements show strong linear relationships with certified concentrations that show pXRF measurements are reliable with true values under controlled and homogeneous conditions.

In contrast, the coal sample shows poor comparability between pXRF and laboratory results. Most elements exhibit weak or negligible correlations, showing that pXRF does not consistently track laboratory concentration trends in this matrix. Additionally, t-test results show significant differences between methods for nearly all elements. Only a few elements (Cr, s, and V) show moderate relationships, and even those vary too much to be considered reliably measurable by pXRF.

There are some factors that affect pXRF performance like matrix composition, grain size, moisture content, sample homogeneity, surface condition, etc. In coal samples, high carbon content absorbs incident and fluorescent X-rays (Vladimir et al., 2024), reducing signal intensity, especially for light and trace elements. Other factors like differences in particle size, poor sample homogeneity, and surface roughness can influence how deeply X-rays penetrate and means the small pXRF analysis spot may not represent the bulk composition. Future efforts using a different instrument are planned, if phase 2 is funded.

7.3.3 Radiometric surveys (E.J. Owen)

A handheld scintillation counter was also used in combination with a handheld GPS to create ground radiometric surveys over selected study areas. Survey grids were not planned ahead of time, but rather surveyed “on the fly”, with the edges of the survey extent generally defined by a return to background radiation values. This allowed the anomalies to more or less define themselves as they were surveyed. The scintillation counter was held at waist height and was allowed to equilibrate at each station. The reading at each station (in counts per second, cps) was recorded on a handheld GPS. Station spacing varied between sites, but generally was ~15m over mineralized zones and up to 50 m over unmineralized areas. Radiometric maps were created using Esri ArcGIS Pro.

7.3.4 Correlation of geophysical logs, laboratory, chemical analyses and pXRF (V.T. McLemore and S. Fire)

A preliminary correlation of descriptive drill logs, geophysical logs (Fig. 7.4), laboratory chemical analyses (Fig. 7.5), and pXRF chemical analyses was examined as part of this project (Fire et al., 2024). In theory some elements such as U, Th, and K should correlate with gamma logs because concentrations of these elements produce the variability in the gamma logs. If other elements correlate well with U, Th, or K, then those elements should also correlate with the gamma logs. However, preliminary results indicated downhole plots of the handheld pXRF geochemistry cannot be directly correlated with the geophysical survey for hole H-16 (Figs. 7.6; Fire et al., 2024). Additional study using a more precise pXRF and additional drill holes is planned for phase 2. If the correlation between certain elements and the gamma logs is correct, then this correlation is important in developing machine learning techniques to map and predict

the presence of certain elements, particularly critical minerals, in the subsurface across the basins.

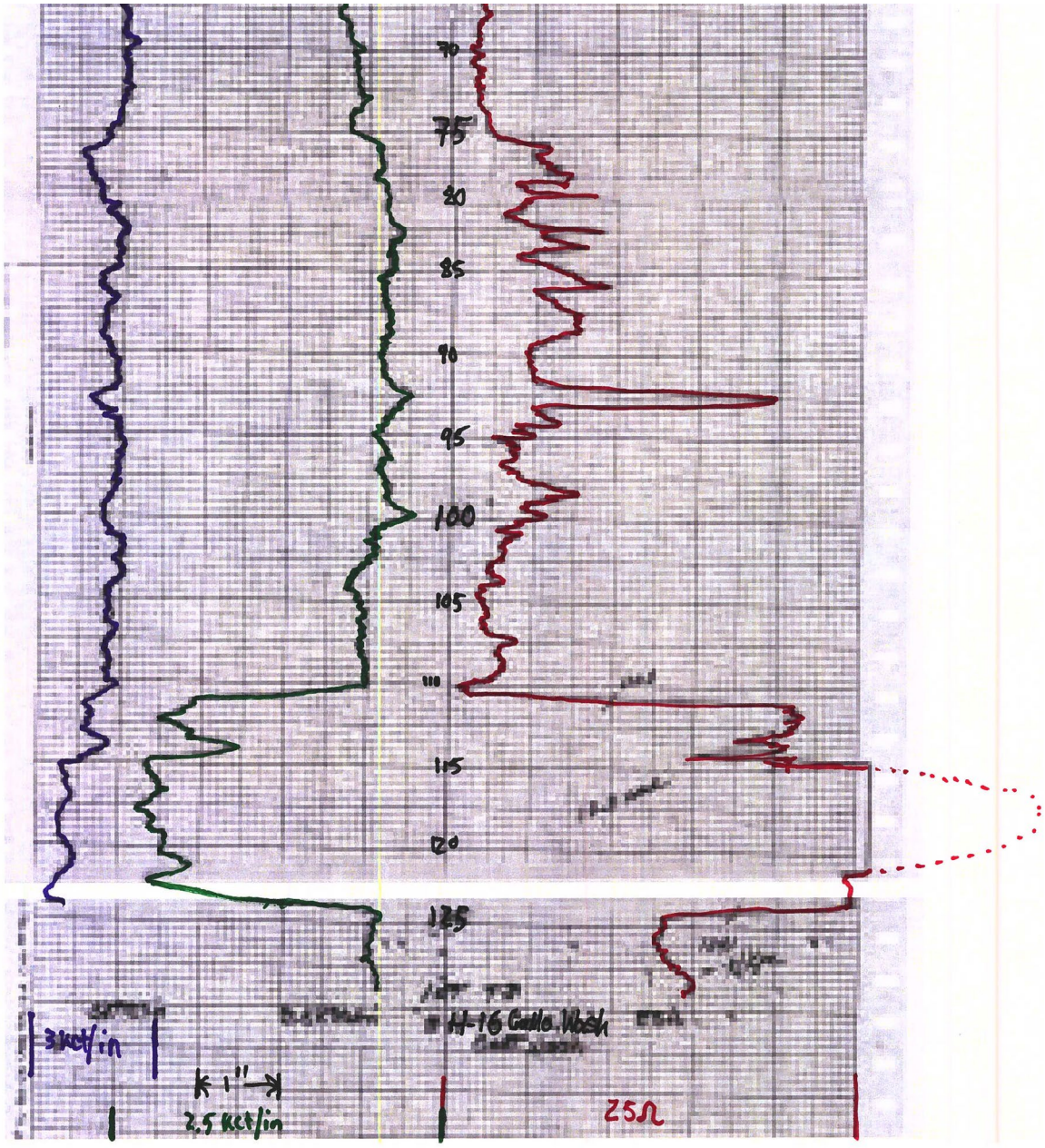

FIGURE 7.4 A geophysical log showing, from left to right, natural gamma, density, and resistivity for drill hole H-16X.

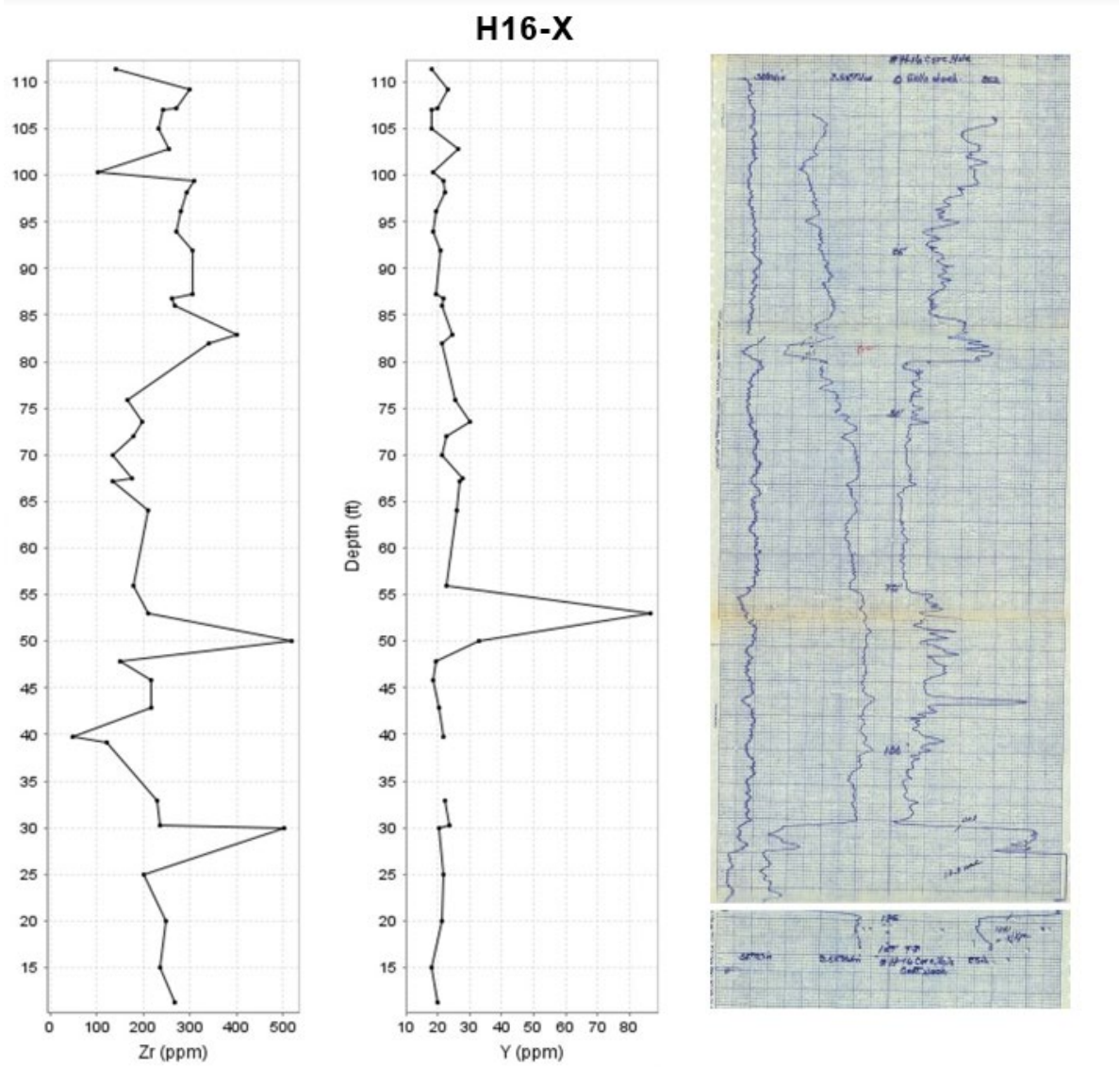

FIGURE 7.5 Zr (ppm), Y (ppm) and geophysical logs with depth for drill hole H-16X. Zr and Y were analyzed using the pXRF (see chapter 4 for details on methods). Note the lack of correlation between the chemistry and geophysical logs.

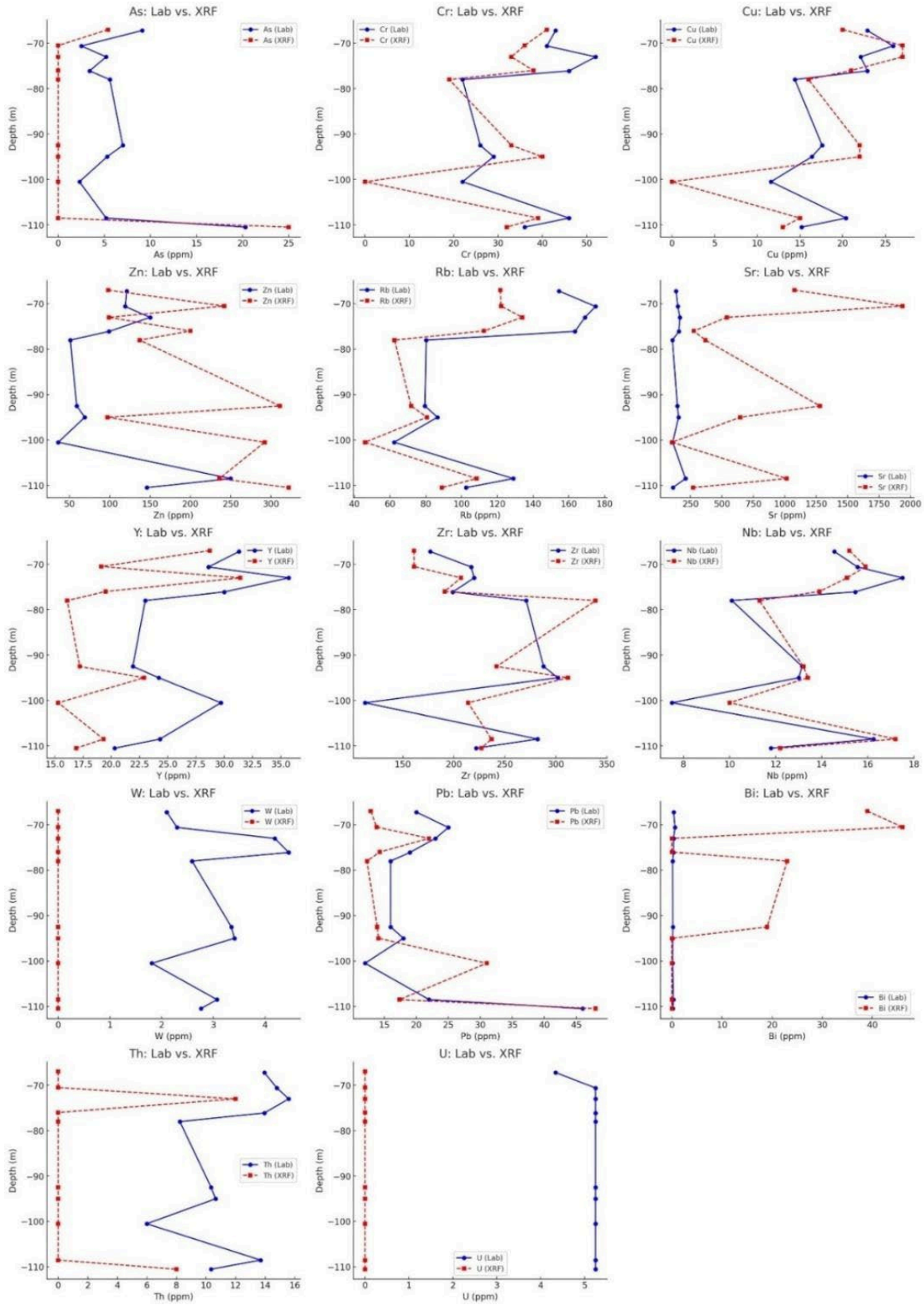

FIGURE 7.6 Comparison of pXRF-obtained (red) and lab-determined (blue) elemental concentrations vs. depth for hole H-16.

7.3.5 Humates used as a filtration medium for uranium (B. Detsoi, B. Frey, V.T., McLemore, J. Jones, and R. Tsosie)

Introduction

Uranium is element 92 on the periodic table and a member of the F-elements as an actinide. Uranium, initially called "Uranus," was named after the planet Uranus. Uranus was named after the Greek god in charge of the heavens and the sky (Carnevale, 2023). Discovered by German chemist M.H. Klaproth, the discovery of uranium was an accident while analyzing pitchblende samples from the Joachimsthal silver mine (Office of Nuclear Energy, 2023). Uranium was a vital element in the nuclear era, with its use in the atomic bomb and other nuclear devices developed around that time. Much like the mortals in Greek mythology, we were gifted an item of raw power and blissfully unaware of its power and destruction. Through the use of nuclear weapons, nuclear energy, and other household items, the demand for uranium was high. At this time of high demand, mining for this resource damaged the land surrounding the mines.

Uranium contamination surrounding mining sites is common for the sites hosting these mines. The ecological damages include contamination of the soil surrounding the mine, contamination of groundwater, and acid mine drainage (Committee on Uranium Mining of Virginia, 2023). Remediation attempts to tackle the problem. The available commercial filtration systems are reverse osmosis and ultrafiltration systems. Filtration systems for a household are available; smaller reverse osmosis systems can be installed that range from $150-$300 if installed personally, or professionally installed prices range from $2,000 to $5,000 (Brower, 2021). These point-of-use systems can only filter out 7-14 gallons per day of clean water for the household (Brower, 2021). With this project, I will explore using humates as a medium for household filtration.

Humates are weathered coal and primarily composed of nutrient-rich plant material. Its primary use is in agriculture and farming since it is rich in nutrients and amino acids and can retain water in the soil (Kim and Kim, 2014). Humic acid can be extracted from humate samples when fractionalized properly (Kim and Kim, 2014), an area of interest in uranium remediation. Tests where humic acid is used as a coating on colloidal silica have shown promise in effectively removing uranium from groundwater sources (Delarosa et al., 2019). Another study using iron coated with humic acid placed into a water filtration column showed that these humic acids could pull out heavy metals such as lead and copper from a water solution (Lai and Chen, 2001), and this media is being studied for other uses. Savannah River Site has been looking into using humates to filter their acid drainage by a pump-and-treat technique that allows them to use humates to filter out heavy metals in their acid drainage (Gudavalli et al., 2020). Since this is a relatively new approach, information on the process is limited. The research goal discussed in this paper is the application that humates can have in the filtration and remediation of uranium-contaminated water sources.

Methods

All solutions produced in this project were analyzed on an Agilent 7900 ICP-MS using the no-gas mode. Inductively coupled plasma mass spectroscopy (ICP-MS) serves to analyze aqueous samples with an argon plasma used to atomize and ionize them before separating the

ions by their mass-to-charge ratio in the quadrupole analyzer and detecting them with an electron multiplier detector. The approach to this project has three parts: processing coal samples, batch capacity, and column tests. Each step is essential to the next. To ensure the project's success, each phase was done in triplicate to provide the best results. Below are the details behind each process. The data are in Appendix 17.

Part One: Processing of coal samples

Researchers from the NMBGMR collected coal samples from several coal mines. These samples were cataloged and kept in storage until needed. Each sample in our storage has had full metal trace and analysis done on them at external labs; all of this data is kept in a joint spreadsheet we can access. This information was used to find a humate sample low in uranium and thus would not contribute significantly to uranium waste accumulation during this project. Once the sample was retrieved from storage, the humate chunks were processed manually by mortar and pestle (Fig. 7.6), and the sample was sieved through a No. 10 (2mm) sieve (Fig. 7.7) and then split and homogenized through the cut and quarter process. Once this is done, the sample is placed in a clean bag and set on the bench with the bag open for 24 hrs to ensure the sample is dry. The sample bags were then re-sealed and ready for experimental use.

FIGURE 7.7 Processing of Coal 289 via mortar and pestle (left) and the sieving process (right).

The humate samples were chosen based on uranium concentration within the sample, looking for a low concentration so that the sample selected could absorb the most amount of uranium from the solution. The initial humate sample chosen for this project was given the unique identifier “Coal 42,” per the CORE-CM coal project SOPs. Coal 42 was obtained from the Star mines outside Cuba, New Mexico. The uranium concentration of Coal 42, measured at the University of Kentucky laboratories, was 2.13 ppm. Partway through this project, we had to choose a new humate sample because there was not enough Coal 42 to use in both the batch capacity test and the construction of a column. Coal 289, a sample from Navajo Mines outside of Hogback, New Mexico, was chosen for the remainder of the study. The uranium concentration was below the detection limit (0.14 ppb; University of Kentucky laboratory).

We also prepared the uranium solutions in 1% nitric acid for the initial testing. We diluted the stock solution to 500 ppb uranium in nitric acid and then diluted it down to the 15 ppb, 30 ppb, and 50 ppb solutions. Once the error of making the stock solutions in nitric acid was recognized, we made the solutions again following the same process but in RO water instead. All solutions used in this experiment were stored at room temperature.

Part Two: Batch Capacity

Water spiked with uranium was introduced to a small amount of humate sample in a batch capacity test, which is designed to see how well and how much the humate material can absorb the uranium present in the solution. This allows us to gauge how much the humate samples may be able to absorb in the experiment. We chose a starting solution of 15 ppb, 30 ppb, and 50 ppb because we wanted to mimic a water sample with uranium concentrations near the EPA limit of 30 ppb while also going above (50 ppb) and below that limit (15 ppb). Solutions were made from a 1000 ug/mL stock solution (PlasmaCal Uranium 1000 µg/mL in 4% HNO_3) diluted with 18 MOhm reverse-osmosis water (RO water). After the stock solutions were ready, we measured 10 g of humate sample into a 40 mL vial and then added 30 g of spiked solution by mass. The samples were then placed in a shaker for 24 hours at 150 rpm at room temperature (Fig. 7.8).

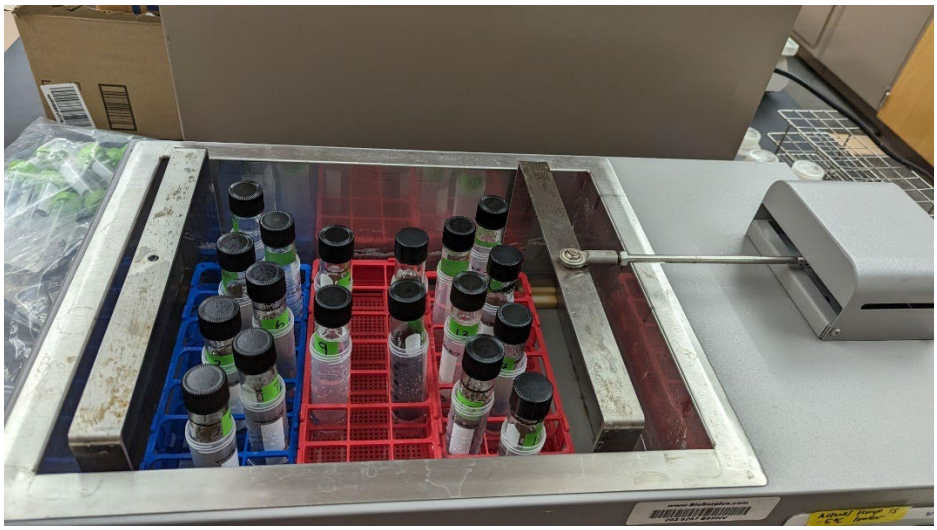

FIGURE 7.8 Batch Capacity testing using a shaker

The fine particles of the humate samples became suspended in water during shaking, so the samples were centrifuged at 500 rpm for 20 minutes to get the humate to settle out of solution, thus allowing the solution to be decanted with minimal suspended solids. After the solutions were decanted, they were filtered using a Pall 0.45 µm Nylon syringe filter and acidified to a pH of 1 before analysing on the ICP-MS. Filtering ensured the debris would not clog the instrument nebulizer, and the acidification ensured the metals were dissolved in the solution. Data collected on the ICP-MS was reviewed to determine the uranium concentration in the spiked solution.

One problem we faced was an issue with the filters we were using. Our spiked RO samples showed surprisingly low recovery of uranium. We realized the filtered samples did not match the concentration of the non-filtered solution. This showed us an issue with our nylon filters pulling out the uranium solution. Upon switching to the acetate filters, we found that the concentrations were still low and that the filter was pulling most of the uranium from the solution. This prompted us to examine the amount of uranium absorption of the nylon and

acetate filters. Our solution was to decant the liquid from the vials of the batch capacity test and then acidify the solution before filtering it. This resolved our issue with the concentration levels.

Part Three: Column Tests

The columns used in this experiment were designed to maximize the porosity and surface area of the humates, to best allow the leaching of uranium. A 1:1 ratio of sand (Fisher Ottawa Sand Standard, 20-30 Mesh) and humates by mass. This ratio was chosen based on a previous test to maximize the most contact with the humates while optimizing the flow rate. This also ensured that the flow rate through the column could be continuous and not cause a pressure build-up in the columns. Humates naturally retain water because of the humic acid and the fine particulates of the material, an important characteristic for agricultural use. In this instance, sand was chosen to aid in the flow rate of the solution through the columns by providing additional porosity to the substrate. Using a spare test tube, the humates and sand were measured into it and kept as close to one another in mass. Once the masses were equal, the test tube was capped and shaken by hand to mix the two substrates for about a minute. This ensured that the samples were homogenized. After that, they were placed into the columns, and this step was repeated until the columns were full.

The column design (Figs. 7.8 and 7.9) was modified from Lara et al. (2018). Using this setup, four solutions were fed through the column and collected after passing through the column to measure the amount of uranium absorbed by the column over time and how much is being released back into the solution. The solutions being fed into the column were RO water spiked with uranium, with concentrations of 15 ppb, 30 ppb, and 50 ppb, followed by the 500 ppb stock solution at the end. After each solution and before the next solution was added, the columns were flushed with RO water for 12 hours and then left in a static soak for the next 24 hours before being used again with the next solution. Each sample collected was acidified with 5% nitric acid and left overnight at room temperature on the bench. Each sample was centrifuged at 500 rpm for 20 minutes, decanted and analyzed on ICP-MS. The data is analyzed, and adjustments are made to make the columns more efficient.

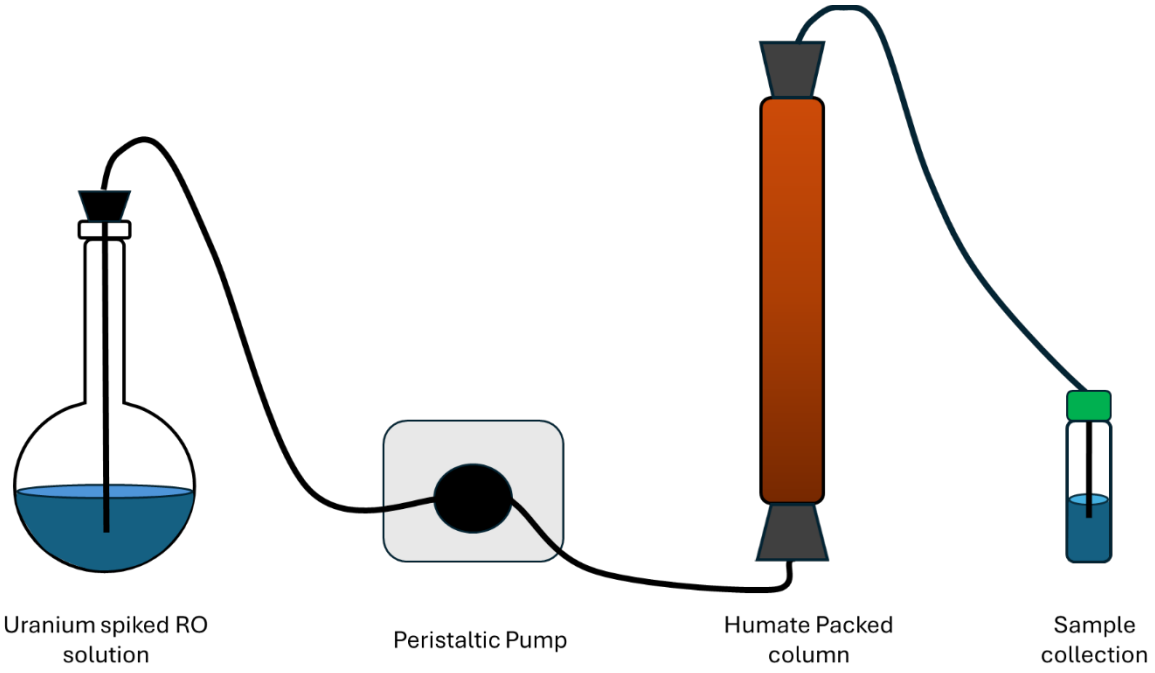

FIGURE 7.9 The diagram for the column setup.

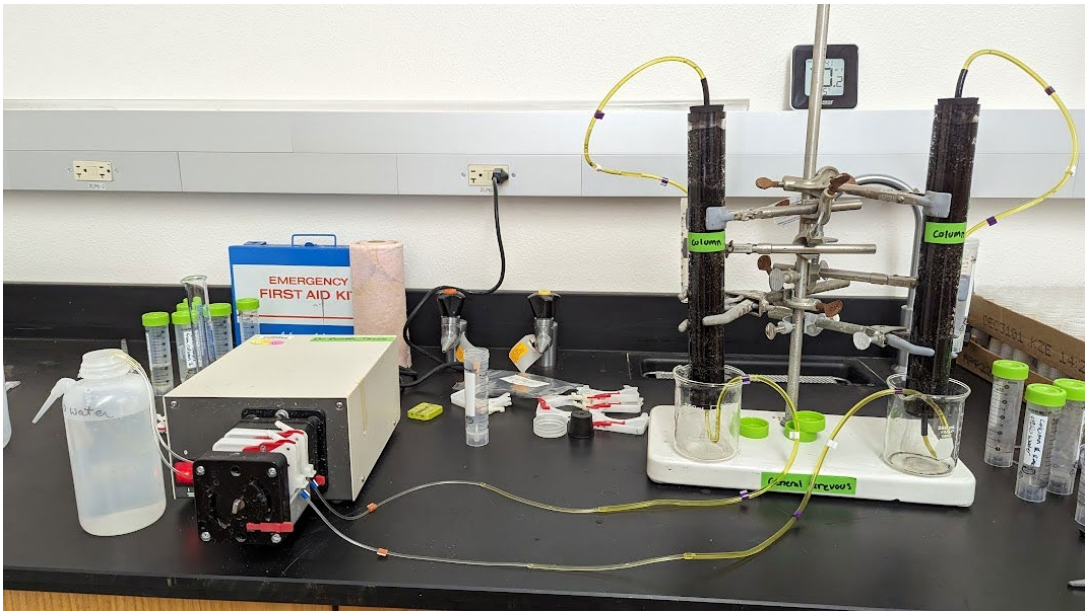

FIGURE 7.10 Column filter set up with peristaltic pump.

We used an acrylic column with an inner diameter of 1.25", an outer diameter of 1.50 inch, and 12 inch in length for the main body (Fig. 7.10). Size 6.5 rubber stoppers with a single hole in the stopper were used to seal the column once packed. All the stoppers and tubes were washed thoroughly, placed in an acid bath for 26 hours, rinsed with DI water, and allowed to dry. The fluid flowing up and through the top of the column ensured that the solutions would have the best amount of contact with the humates in the column before being pushed through the top and into the collection tubes. This process ensures that the humates in the column properly absorb the

solution as it passes through the columns. The decision to pass solutions from the bottom up also allowed us to keep the humates from flowing out of the system as it pushed through. The set up is shown in Figure 7.11.

FIGURE 7.11 Columns in the initial priming stage, with acrylic columns and filter set up with an initial water addition from the top. The humate fill for this sample was one part Coal 289 from Navajo Mine in Fruitland, New Mexico, and one part Ottawa sand.

Once the columns were constructed, they were charged with RO water using a 100 mL syringe in preparation for the experiment. Since this was the first time doing this, the columns were charged manually using a syringe to push RO water through the lines and the column. Two funnels were placed on top of the columns to ensure that water was making its way through the entire column and allowed air bubbles to rise without allowing any air pockets to form in the columns. The columns were left in a static soak for 24 hours before being placed on a peristaltic pump, allowing the columns to absorb the water and work out any air bubbles stuck inside the columns. This initial flush also allowed us to measure how much fluid would come out of the column per hour and to select collection containers according to the volume. The pump we used had two settings of high flow (155 rpm) and low flow (7 rpm) rates, respectively. Once this was done, the columns were ready to use.

A sample was collected from the columns every hour (give or take 30 minutes) for 12 hours. Once the samples were collected, they were labeled with the times they were collected and numbered in sequence. After collecting all samples, they were acidified with 5% nitric acid and left to sit on the bench for 24 hours. The samples were centrifuged for 20 minutes and decanted into smaller collection vials. From there, the samples were diluted by 1:20 to be run on the ICP-MS for analysis.

Results

With the size of this project, we had to split up data collection throughout the three parts. Each step aids in the success of the next, so analysis was conducted at each step. As structured above, the following results are presented in three parts.

Part 1: Sample Processing

As mentioned before, we had an issue selecting the filters we would be using on this project. This issue was recognized once we ran the samples through the ICP-MS and realized that the concentration of the original stock solutions was lower than the filtered stock solution. As mentioned above, there is a stock solution blank that is run alongside the humate samples, which goes through the same process as the humate sample and is used as a standard for testing. However, after finding that more uranium was extracted by the acetate filters, we switched back to the nylon filters. See Table 7.4 for data showing the differences between the two filter materials.

TABLE 7.4 The uranium concentrations of the solution from a non-filtered solution are compared to that of the solution that passed through an acetate filter and a nylon filter.

Desired Concentration	Unfiltered Solution	Acetate Filter	Nylon Filter
15	12.980	0.319	6.109
30	28.905	1.815	13.665
50	45.498	3.590	24.964
500	496.407	499.349	565.000

Since this experiment is based on solutions in parts per billion, having a good filter was vital. For the best result, we decided to centrifuge, decant, acidify, and then filter the solution with nylon filters.

Part 2: Batch Capacity Test

The batch capacity tests were conducted both with the Coal42 sample and the Coal289 sample. The first batch capacity test was conducted using Coal42, and due to a slight miscommunication on how to carry out the test, it was initially performed using nitric acid instead of RO water. The data from the first batch capacity test in nitric acid is displayed in Table 7.5.

TABLE 7.5 Data from the batch capacity test of Coal42 using 1% HNO_3.

Sample Name	Uranium Content (ppb)	Vanadium Content (ppb)
Humate Blank	0.001	0.174
50 ppb Uranium	0.001	0.157
30 ppb Uranium	0.003	0.301
15 ppb Uranium	0.002	0.312

The initial data demonstrated that the uranium content was dropping, which is what we wanted to see. Since uranium and vanadium have similar electron behavior, we checked to see if the vanadium content remained consistent. What we found was that the uranium concentrations and vanadium concentrations were reacting inversely to one another through the reaction.

The batch capacity test was rerun with spiked RO water samples at the predetermined concentrations of 50 ppb, 30 ppb, and 15 ppb. The initial data is displayed in Table 7.6.

TABLE 7.6 Data from the batch capacity test using an RO water solution on Coal42.

Sample Name	Uranium (ppb)	Vanadium (ppb)
Humate Blank	0.053	2.510
15 ppb Uranium	0.160	2.410
30 ppb Uranium	0.287	2.293
50 ppb Uranium	0.530	2.160

We ran low on Coal42 after these initial tests, so we switched to a different humate sample, Coal289. The resulting data showed the same trends as the Coal 42 sample (Table 7.7).

TABLE 7.7 Data from the batch capacity test of Coal289

Sample Name	Uranium (ppb)	Vanadium (ppb)
Humate	0.037	3.623
15 ppb Uranium	0.823	3.330
30 ppb Uranium	1.910	3.390
50 ppb Uranium	2.630	3.220

The vanadium and uranium content of the resulting Coal289 solutions fluctuated much more than the Coal42 sample. The initial concentration of V in the sample is also below the detection limit (0.12 ppb) of the humate sample.

Part 3: Column Tests

During the column tests, we ran the solutions through the columns in a 12-hour process in three experiments, each with a different concentration of uranium solution, starting with the lowest concentration of the spiked solution (15 ppb) to the highest concentration of our spiked solution (50 ppb).

One of the first things we measured was the uranium concentration of the columns themselves, by running an RO water rinse through the column. Since this humate sample had very low levels, we expected to see that. The rinse cycle for the columns was about six hours per collection.

As seen in Figure 7.12, the uranium concentrations in each column are at or below 0.250 ppb of uranium. The initial flush of the columns was done only using RO water, so the uranium from the columns is the naturally occurring uranium in the humates. After the initial

measurements of the columns were made, the columns were then connected to the 15 ppb spiked uranium solution, and the first 12-hour sample collection was underway. The data from this collection cycle is in Figure 7.13.

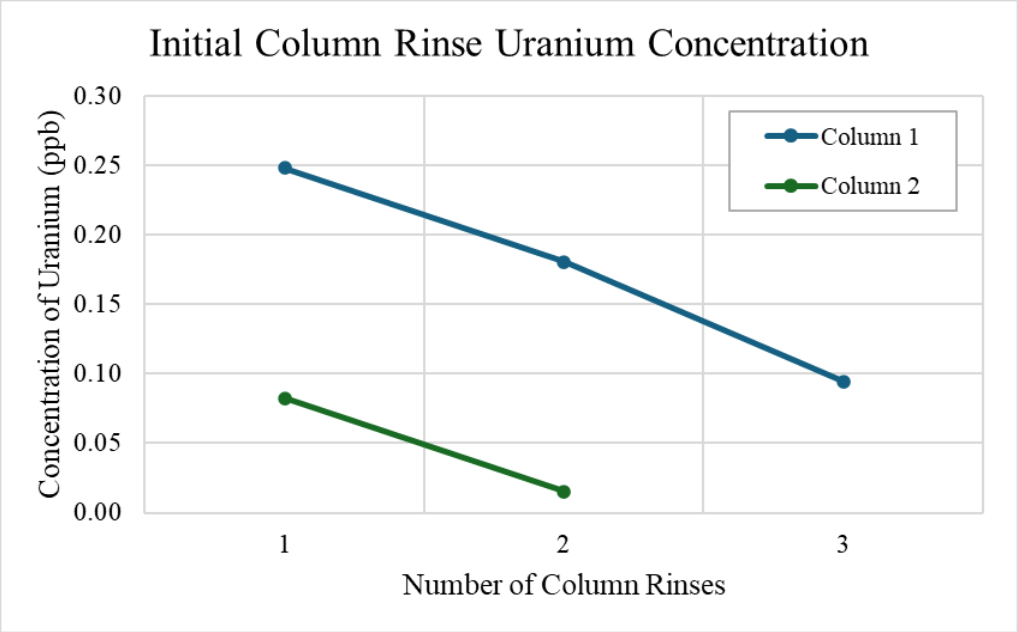

FIGURE 7.12 Uranium concentrations of Column 1 and Column 2 during their initial RO rinses. The concentration of the third rinse of Column 2 was below detection limit.

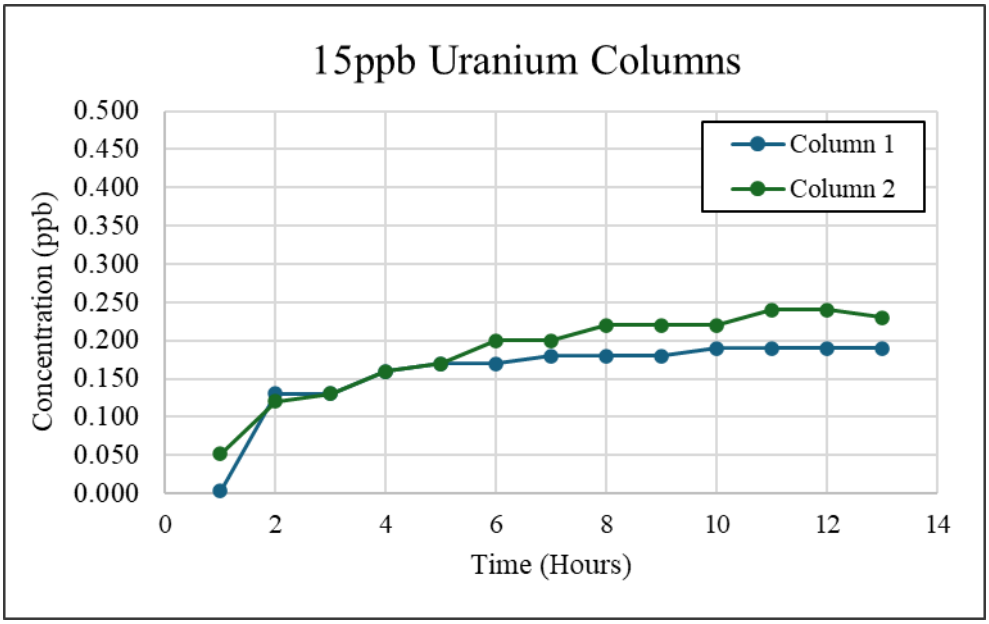

FIGURE 7.13 Data of the uranium concentrations of solution released from each column over the 12-hour test, 15 ppb solution.

The initial run of the 15 ppb solution through columns 1 and 2 was a success. The concentrations of the uranium in Column 1 spiked at the second-hour mark to 0.130 ppb of uranium and then came down. After the fourth hour, the concentration began to even out at nearly 0.200 ppb and remained below that level until the completion of the test. In Column 2, the spike at the second-hour mark went up to 0.120 ppb and then kept climbing up to 0.250 ppb of uranium. Unlike the first column, Column 2 kept climbing in terms of allowing uranium to pass through. We initially thought the uranium levels would be lower but not as low as a quarter of a part per billion in the solution.

Since the 15 ppb data was promising, we collected the 30 ppb Uranium solution using the same process. The data from that experiment is displayed in Figure 7.14. For the experiment with the 30 ppb solution, the concentrations of uranium fluctuated quite drastically within Column 2. In the first hour, uranium concentration spiked to 0.379 ppb; at the six-hour mark, the concentration spiked to 0.442 ppb, and once again, at the 11th-hour mark, it spiked to 0.423 ppb. The constant fluctuation of uranium concentration levels in that column did call for concern. However, the fluctuations were below 0.500 ppb and trended downwards after the spikes. Column 1 only had one spike to 0.136 ppb of uranium.

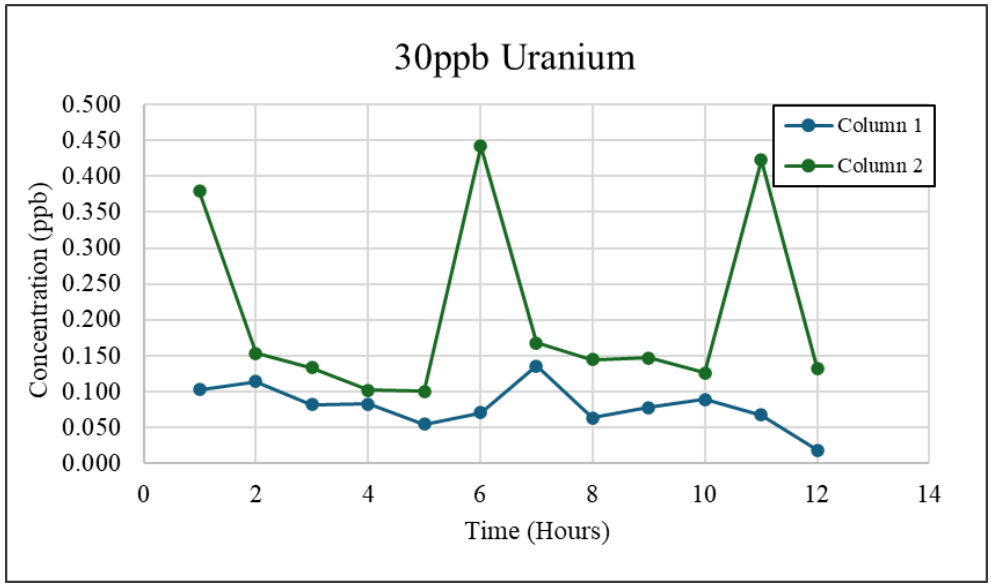

FIGURE 7.14 Data of the uranium concentrations of solution released from each column over the 12-hour test, 30 ppb solution.

We proceeded with the test with the 50 ppb uranium solution. The data from the 50 ppb uranium solution is displayed in Figure 7.15. The uranium concentration from the columns in this run was still about half of a part per billion. This time, fluctuation in the concentrations was more prominent in Column 1, reaching a level of 0.448 ppb. Column 2 also had a spike that reached a level of 0.407 ppb but could stabilize and remain more consistent throughout the testing. As seen in the data above, the uranium concentrations managed to spike at the fifth hour and then proceeded to trend downwards to above 0.250 ppb in the solution.

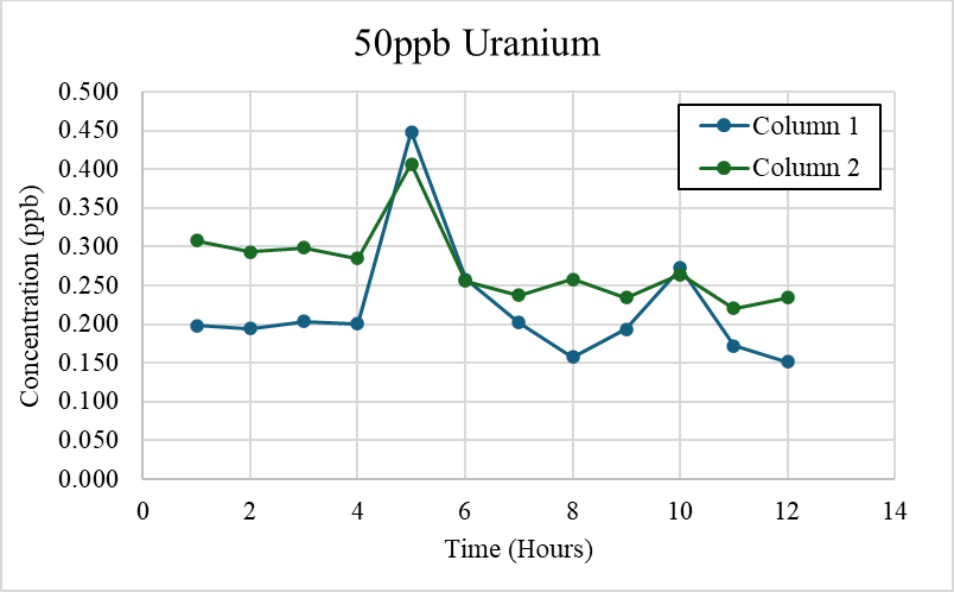

FIGURE 7.15 Data of the uranium concentrations of solution released from each column during the 12-hour test, 50 ppb solution.

Since the concentration of uranium from the columns remained below 1 ppb and reflected similar patterns, the decision to see how well the columns would handle the 500 ppb stock solution was made to see if that would make the uranium concentrations spike higher than 1 ppb. The results from this test were taken in a shorter period due to time constraints. The results are in Fig. 7.16.

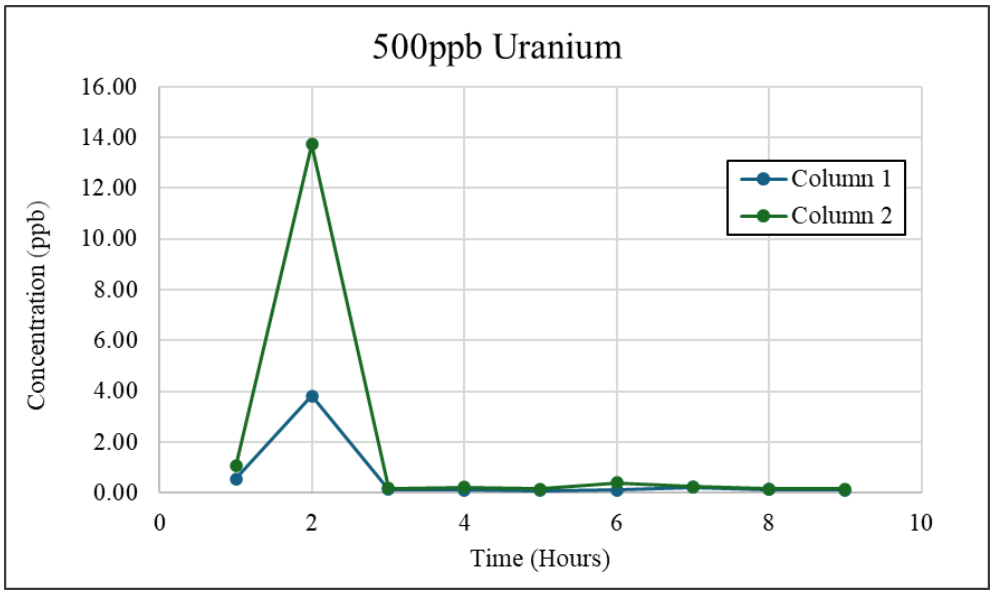

FIGURE 7.16 Data of the uranium concentrations of solution released from each column over the 12-hour test, 500 ppb solution.

Discussion

The processing phase of this project was by far the most tedious part; however, when it was done properly, the rest of the experiment ran smoothly. The main focus was on choosing a sample based on the availability of the humate and on the uranium concentration within the humate. Every experiment must start with the proper tools and items to ensure a successful experiment.

The results of the batch-capacity tests indicate poorer uranium adsorption by humates than the results of the column tests. During the batch capacity test, the water did not flow through the humates, but rather was mixed with the humates in a shaker bath. The solution may not have come in as much contact with the humates in the batch capacity test as it did in the column test, thus, having an overall different result than the column test. However, the uranium absorption during the batch-capacity tests wasn't that far off from the concentration of the sample collected from the column tests.

The data from the column test indicates that the uranium is not only being taken out of the solution but being done in a way that is so effective that the concentration remains below one ppb, which far exceeds the result we had in mind. Even moving up in the concentration of the solution to 500 ppb has shown that the humic materials retain the uranium reasonably well and can bring it down into a range that is still acceptable in terms of the EPA regulations for drinking water (30 ppb).

One cause for concern was the rapid fluctuations of the column concentrations in the subsequent tests of the 30 ppb and 50 ppb solutions. Based on what was observed in the graphs, if we had changed out the columns to fresh columns for each experiment, the experiment may have yielded different results. Due to time constraints though, using a freshly packed column was not an option for us, so we used the same columns repeatedly for each run, flushing them for 24 hours after each run. The heterogeneity of the substrates used could explain why Columns 1 and 2 had different results. As mentioned, the columns were a 1:1 ratio by weight humate and sand, measured into a vial, and shaken to mix before being placed into the columns. This process was done as precisely as possible; however, combining two substrates of different textures and densities makes it hard to gauge how well they mix, especially after being placed into the columns.

Conclusions

The rising cost to obtain clean water in various homes and communities was the driving force behind this research. Because I am from an area where our drinking-water sources are dwindling, my goal was to see if humates can be used as a feasible option for water filtration sometime in the future. Humates are commonly used to nurture crops and promote crop growth and are used in several farms in the area. When not used in agricultural applications, humates tend to be discarded. Now that we have seen the results, we can look into using humates as a filtration option for future work.

Our initial theory was that the humates may be able to remove some uranium from the water. At best, our hopes were to see that the filters were removing some of the uranium from the water; they exceeded our expectations. Seeing that the solution concentration can reach upwards of 500 ppb and still produce concentrations below the EPA drinking water limit of 30 ppb, when

it does exceed the detection limit, suggests we can push the concentration of the starting solution even higher.

Aside from the time constraints we were under, using the same column over and over was a great test run to test how many times these columns could be used before becoming ineffective, thus showing the sustainability of the method. We did not reach that limit; further tests are needed to test the limit of the media.

Future Work

What is the future use of humates in filters? Where is it going? How is it doing this? We can continue to answer these questions with further research. The difference in behavior between uranium and vanadium in the solution is another thing that should be tested, particularly as it relates to redox conditions. Is uranium being oxidized or reduced? These are all great questions to remember as this research moves forward.

When pulling apart my columns, I broke down the components into 1-inch sections to see where the uranium was collecting the most in the system. One thing that I hope for further investigation is seeing the chemical aspect of the reaction taking place in the columns, finding out what in the column is binding the uranium to the humates, and even solving the question of whether the reaction taking place is a redox reaction through further tests and analysis.

Another thing to test is the maximum concentration of uranium that the columns can handle by increasing the concentration of uranium spiked solution, to see the limits of concentration that the humates can handle; for example, can we increase the concentration to parts per million. Using actual contaminated water from communities near mine sites would be another solution to test in the humate filters. Further tests could also help us better understand the fluctuations (concentration spikes) that occurred during the 12-hour column tests.

I would also like to run multi-day experiments with multiple collections, which allows us to see how much uranium is flushing out of the columns. Along with this, testing is done to see what flow rate from the peristaltic pump would be ideal for prolonged usage. Seeing how these columns handle for longer durations will allow us to see what limits these columns can handle.

One last thing that I think would be great to explore is how temperature affects the results of the filtration effectiveness. Living in the desert, we have high temperatures some days and low temperatures at night, so seeing how this affects the columns' effectiveness would be interesting, especially when it comes to using them in further tests.

Humates have been limited to agricultural use for years. With this project, we have seen that humates have numerous, effective possibilities for water filtration. Hopefully, in the future, we can see how we can use these columns in the practical aspects, such as in using them to filter out uranium from contaminated water in communities all around contaminated uranium mine sites.

7.3.6 Extraction of alumina from coal and clays (J. Essary)

Extracting aluminum (Al_2O_3) from ore is no easy task. Aluminum bonds so well with other elements that two different processes are needed. The Bayer Process converts ore to Al_2O_3 and the Hall-Heroult Process converts Al_2O_3 to aluminum (Flint et al., 1946).

The Bayer process converts the aluminum ore, known as bauxite, into Al_2O_3 and a byproduct known as red mud. It has a relatively low energy cost compared to other processes

that can be used, which is why it is still used today. It does, however, have two drawbacks: the red mud is a caustic waste product and the process only works on bauxites that have a low amount of silicon dioxide in them (known as low-silica bauxites).

The Hall-Heroult process is the method that is used to remove oxygen. This process requires a tub, graphite electrodes, heat, electricity and very corrosive fluoride containing salts. The aluminum metal is pulled down toward the graphite cathode that lines the bottom of the tube, while the oxygen is pulled up toward the anode where it reacts with the graphite electrodes creating CO_2 which can then be released into the environment or gathered and used for other things.

Unfortunately, despite how much aluminum there is in the earth's crust it is becoming a rare commodity. This is because the world is running low on low-silica bauxites. The USGS lists aluminum as a critical mineral. There are other processes that can be used for the extraction of Al_2O_3 instead of the Bayer process, and what is even better: these processes don't require bauxite to work.

The most promising of these processes is the Lime-Sinter-Leach process, which can extract Al_2O_3 from any of the other ores available such as clay and feldspar. It works by combining lime (the same material that is found in seashells and limestone) with any finely ground aluminum-containing rock or clay then heating the mixture upwards of 1300°C. The lime and heat break down the bonds in the ore leaving behind insoluble calcium containing compounds. Afterward, the mixture is mixed with washing soda and water. This causes the Al_2O_3 in the sample to dissolve into the washing soda solution. It is then separated from the non-alumina material. The Al_2O_3 is then removed from the washing soda solution by reacting it with CO_2 and then processing it further to purify it. Afterward, it can be run through the Hall-Heroult process to convert it to aluminum metal.

Al_2O_3 was extracted from kaolinite for various localities, coal clinkers from the San Juan Basin and nepheline syenite from the Cornudas Mountains using the lime-sinter process (Essary, 2025). This process combines each sample with lime by mixing them and pressing them into pellets, then heating them at $1360^{O}C$, which under the right conditions, results in a fine powder that can then be leached with Na_2CO_3. The resulting calcium-silicate slurry is filtered out leaving behind a solution of sodium aluminate ($NaAlO_2$) that when mixed with CO_2 gas reduces to a precipitate of gibbsite ($Al(OH)_3$), while simultaneously lowering the pH. Filtering and washing the precipitate in acetic acid ensures that the precipitate is purified, which can then be analyzed using XRD to verify identification of the substance. From this research (Essary, 2025), it was discovered that self-pulverization of the pellets requires the formation and conversion of meyenite into its several polymorphs and that the sample also requires heating to the melting point of its highest melting phase in order to achieve complete disintegration, though further research still needs to be done.

7.3.7 Machine Learning (Task 2) (B. Goehring, P. Watson, and I. Mantelli)

Introduction

The report below summarizes initial efforts made by Los Alamos National Laboratory to develop state of the art machine learning aided approaches for resource characterization for the San Juan and Raton Basins with regards to critical mineral and rare earth element resources in coal and coal associated deposits. The techniques discussed below were developed with heavy

reliance on existing data sets (e.g., USGS CoalQual) owing to much of the new resource characterization measurements not being available until late in the project lifecycle. Regardless, the progress made serves to establish methods and have identified critical strengths and weaknesses to be applied in future work.

Below we present interim estimates of Rare Earth Elements and Yttrium (REEY) concentrations throughout the Powder River Basin (PRB) in San Juan and Raton Basins of Wyoming, which were produced by an application of machine learning and other data science techniques using currently available geochemical data. The data was gathered from United States Geological Survey (USGS) sources: more specifically CoalQual [https://ncrdspublic.er.usgs.gov/coalqual/] and the Core Research Center (CRC) [https://www.usgs.gov/core-research-center]. Additionally, as data became available, we incorporated proprietary data from mining partners and geochemical analyses lead by NMT.

As a significant fraction of the data was presented on a whole-coal basis, and did not include information about ash percentages, we performed and present our results as whole coal concentrations, contrary to the commonly reported ash basis. This allowed us to maximize the amount of data used in the analysis. All samples originally in ash-basis were converted to whole coal concentrations before their inclusion in the analysis. Performing this analysis using a whole-coal basis had additional benefits. Further, as we have worked with the ML methods used here, we find that working in a whole coal basis provides further predictive power when paired with traditional coal analyses. A preliminary analysis in ash-basis produced results that were spatially inconsistent, long tailed, and strongly influenced by coal grade. A whole-coal analysis produces results that are more spatially consistent and can be more directly used for resource characterization. Further, we argue that the whole-coal based analysis will yield further insight with respect to geologic interpretations based on traditional coal interpretive techniques, as well as empower future data fusion techniques (discussed below).

The methodology for REEY estimation consisted of four major steps:

1. Preprocessing of the Data: The data were cleaned and made consistent for analysis purposes. Also, Centered Log Ratio (CLR) transformations were applied to the major/minor elements and the trace elements separately to control for the compositional nature of the data, as well as the differences in magnitude of concentration between these groups of elements.
2. ML Assisted Matrix Factorization: The input data included 45 different element concentrations. Given the legacy nature of the data used, many entries were blank due to limitations in the original geochemical analysis. A Nonnegative Matrix Factorization + k-means (NMFk) algorithm was applied to reduce the number of variables, find geochemical patterns related to REEY, and fill-in the missing values (Fig. 7.17). This algorithm discovers an optimal factorization of the original data and breaks it down into a collection of patterns common in the data. Future work may need to use other standarization alogorithms since NMFk is very linear.
3. Geospatial Interpolation: Once the geochemical signals were determined, we estimated their distribution by applying an anisotropic gaussian process (GP) model. Mathematically this approach is very similar to well-accepted kriging methods but uses an optimization algorithm to fit the spatial predictions to the existing data, instead of relying on a fit manually determined by an analyst using semi-variograms.

4. Refactorization: This step produced the final results by refactoring and un-transforming the interpolation results to reconstitute the original input variables, including the constituents of REEY.

Results

1. Finding Geological Signal with ML Assisted Matrix Factorization (NMFk)

Applying the NMFk algorithm to the cleaned and transformed geochemical data identified a set of four reasonable geological signals (see Fig. 7.17). Of note are the grouping of REE+Y in signal 3 along with Al and Si. This latter observation suggests that Si+Al+Y may serve as useful pathfinder elements for future field-based determinations using tools such as pXRF. For areas with sparse data refinement will need to be made to incorporate sparsity constraints by possibly using mineralogical associations to group elements. These constraints can either be expert informed or can be determined using techniques such as x-ray diffraction, but further analysis and modeling is needed.

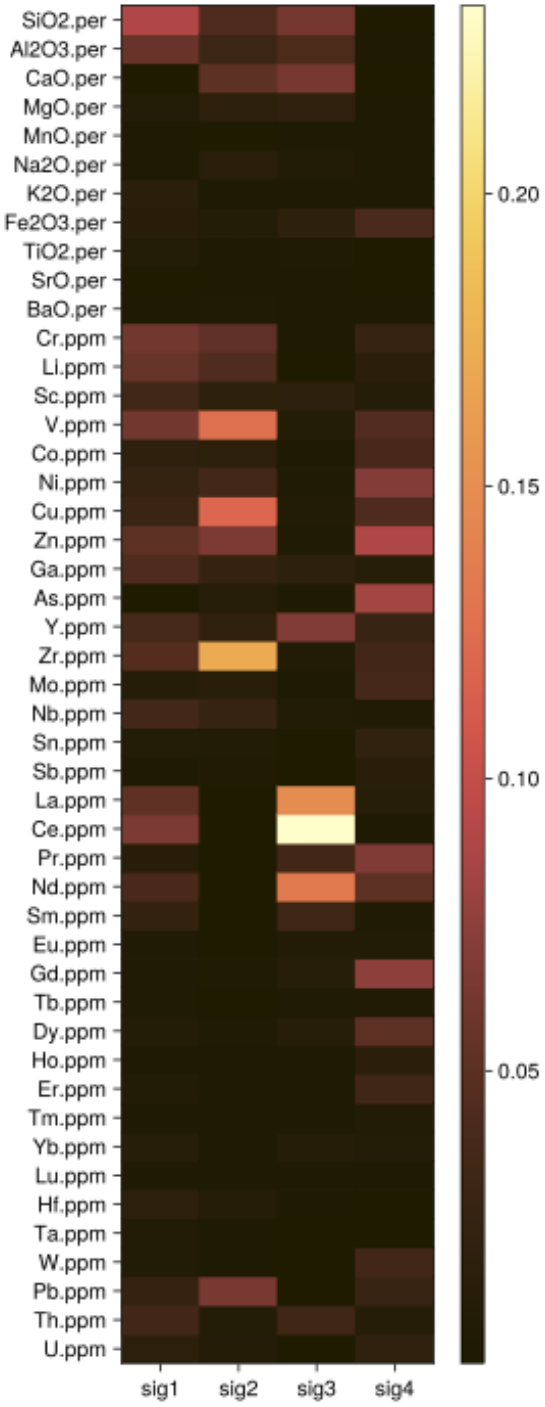

FIGURE 7.17 Geological signals discovered by NMFk. Important to note is that all REE+Y are co-associated. The current figure is not for the San Juan data modeled here, but rather for a Powder River Basin coal mine. The color bar represents the importance of a given element within of the identified k-means cluster or signatures. Recombination of the signatures provides the predictive power as new data is developed.

There are also interesting correlations between the different geological signals (see Fig. 7.18), mostly expressed as anti-correlations between related minerals. For example, Signal 1 tends to occur with Signals 2, and Signal 4 (REE+Y signal) tends to also occur with Signal 2 which suggests that REEY tends to be associated with Zircons and other transition metals many of which are CMM by the DOE and USGS definition.

Further, Figure 7.18 shows that the incorporation of additional signals does not significantly improve the RMSE and thus we settled on four NMFk signals as a balance.

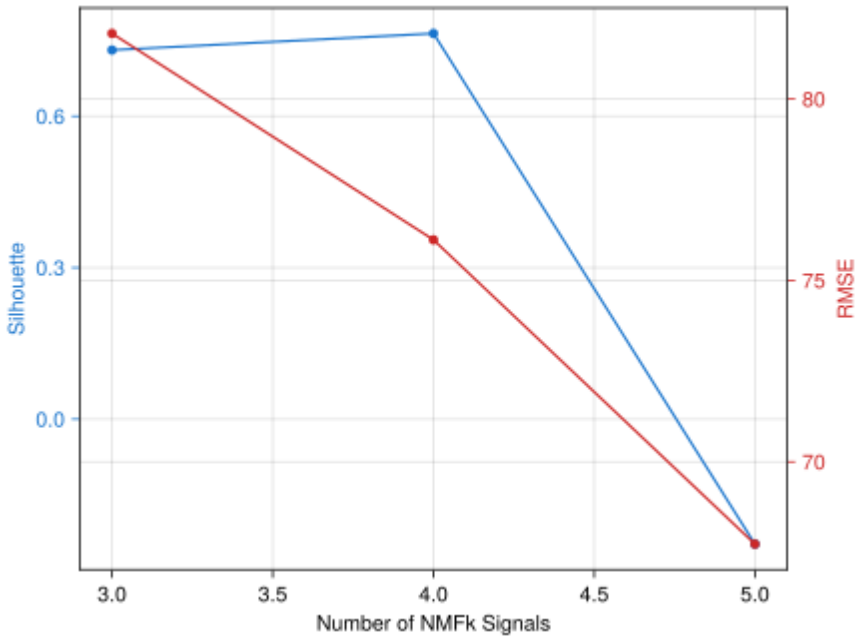

FIGURE 7.18 Histogram of Predicted REEY values in the PRB.

REEY Predictions

The kriging process used to determine the spatial distribution of the five geochemical signatures was applied to an area within the available data to prevent extrapolation. The spatial interpolation was applied to a 1000 m x 1000 m x 20m grid across this domain ignoring locations above the surface

A map of the summarized REEY predictions is shown in Figure 7.19. For each point in the map, the maximum REEY prediction in depth is plotted. There is an interesting SE-NW striking trend of elevated REEY concentrations within the San Juan Basin. Local highs are also observed within the Raton basin. It is important to interpret the 2D results with caution given the data limited nature of the dataset so anywhere there is data there will naturally be elevated concentrations.

Discussion

Overall, these preliminary results show that the chosen methodology has promise. The identified geological signals produced by NMFk are conducive to expert analysis and are consistent with known geochemical patterns. This is particularly impressive when considering

that the NMFk process is an unsupervised machine learning algorithm, which simply finds patterns in the data and is not guided or constrained by the user. Further work may implement such guidance given the data limited nature. Also, the statistical distribution of the REEY estimates is reasonable, and produces a range of realistic predicted values.

However, there remain steps that can be taken to make these results more compelling. First, more data should be incorporated into this analysis. As more geochemical data becomes available from CORE-CM, we should be able to improve the accuracy and spatial consistency of these results. Additional types of data should also be investigated to improve the applicability of this methodology. High quality geochemical analyses are expensive and time consuming to develop and thus will remain uncommon. If geophysical information from core logs, or geochemical estimates from XRF could be incorporated into this analysis, the findings may be more easily applied in new areas. However, as new data sources are added, new methods of data fusion and processing may need to be explored. The NMFk algorithm currently used for dimension reduction and the imputation of missing values is linear by definition and will not be able to capture any non-linear relationships expected between geochemical concentrations and geophysical logs, for example. Alternative, non-linear methods, perhaps based on neural-network based autoencoders, should be developed and evaluated as an alternative to NMFk.

Also, it should be noted that the REEY estimates presented here are not currently validated. Accuracy of these estimates should be determined because of the sparsity of the data available. Traditional validation methods may be to restrictive with small datasets. Additionally, a better understanding of the uncertainties associated with the REEY estimates should be developed. Error is introduced by both the NMFk process and the signal interpolation. To better understand knowing where additional data is needed and how these models can be used for mineral exploration the error propagation needs to be quantified.

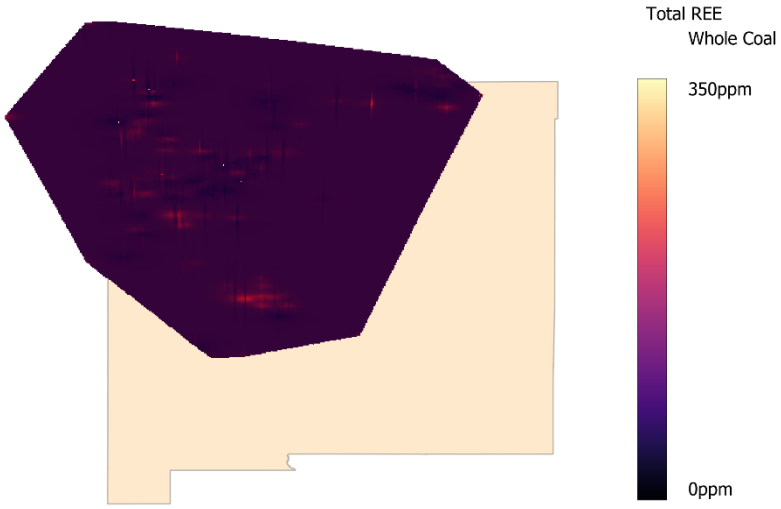

FIGURE 7.19 Spatial distribution of REEY concentrations on a whole-coal basis. Rendered in 2D by taking maximum concentration in depth at each point.

Conclusions and key takeaways

We have made good initial progress on machine learning based modeling of REE/CM distribution in the New Mexico CORE-CM domain. We tested model development using the SmartTensors machine learning package. Anisotropy is the norm within the data and highlights the need for additional data much as possible; however, we can also explore potential solutions in data presentation. Figure 7.20 highlights the challenge of not only x-y anisotropy but also the limited data in the depth dimension, which further enhances the x-y anisotropy. Finally, additional work is needed in handling textual geo data, for example lithologic descriptions, formation names, etc.

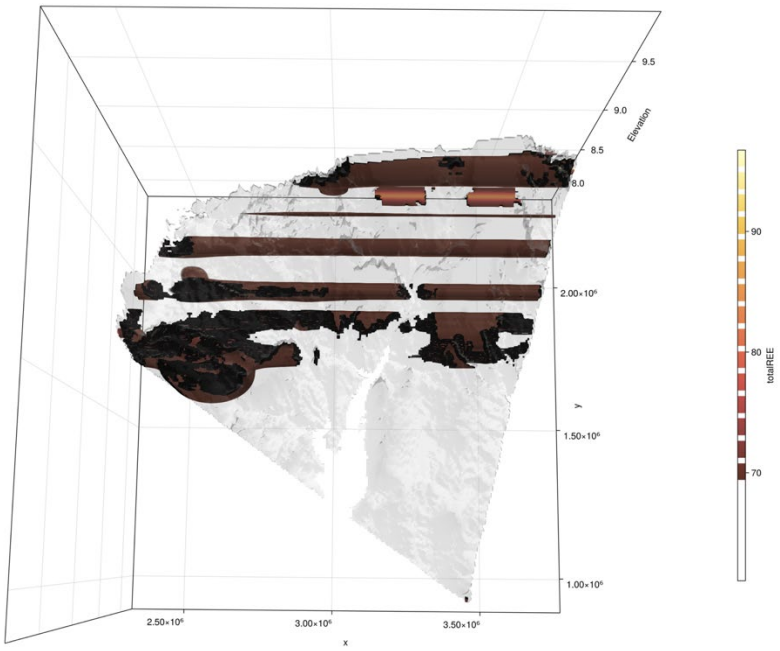

FIGURE 7.20 3D representation of RREY predictions. Notice how elongated the predictions are along the x axis and how our predictions max out at 100ppm. This isn't surprising given the statistical distribution of the limited training data used, and potentially how untrustworthy the depth values are.

Successes

- Built a proof-of-concept model that can predict concentrations of REE/critical minerals across the region
- Combined unsupervised ML techniques with geostatistics to learn signatures of REE/ critical minerals and map them spatially
- The current set of data provide useful information for horizontal variation in REE concentration.

Key Challenges

- Data limitation is the principal challenge especially in the vertical direction causing strong anisotropy in resulting data models.
- Overall lack of samples to generate tall skinny matrices, which are preferred in ML models. Currently have too many variables for the number of samples, resulting in model runs not always replicating adequately.
- Incorporation of geologic textual information needs advancement (e.g., natural language models).
- Legacy ash percentages are only reported about quarter of the time, making analysis on a whole coal basis limited and overall limits the data set size.
- This combination of factors means that while we're starting with ~1000 samples, only 140 have ash percentages and reported depths, which come from ~32 different locations.

Future work

- Incorporating detailed stratigraphic information and improving the way we represent geologic information in the model.
- How much data is too much? In this case it is not too many samples but rather too many variables as possible signals.
- Connecting the existing model with a GIS framework. We have some initial, promising progress on the GIS front, but there's a lot more to do.
- Improving the way we deal with anisotropy in the vertical direction.

7.3.8 Technology Assessment of extraction techniques (Task 5) (B. Goehring, P. Watson, and I. Mantelli)

Los Alamos National Laboratory (LANL) investigated methods for REE separation from coal, coal waste streams, and other potential REE sources. We have focused on three main areas. These can be broken down into the complicated issues of extraction of bulk REE vs separation of the REE themselves, further development of LANL developed hydrothermal extraction technology, and brief list of other technologies being pursued for REE extraction and or separation. Additionally, as part of the LANL hydrothermal approach, we have documented current uses of REE-fluorides as potential direct to market uses of REE separates.

For all REE extraction and separation approaches detailed below, a key observation is that beneficiation, removing waste to increase concentration of minerals, especially of raw ore is crucial to lower overall costs associated with REE isolation. In general, the solubility (or lack thereof) means that REE and many critical minerals require acidic solutions to liberate elements from host mineral phase. Such approaches have obvious disadvantages in terms of financial and environmental costs.

There is active research in a variety of approaches centering around bioleaching, acidic leaching/digestion, and alkali treatment. Important to these new approaches is that they benefit subsequent additional extraction steps or REE separation steps, as the base starting point for most are acidic or basic solutions. LANL methodology needs an acidic starting solution, even if

dilute. The hydrothermal system approach, however, has relative insensitivity to the primary ligand, but is best characterized using HCl and H_2SO_4. A more complete understanding of REE mineral thermodynamics at low and mid temperatures and pressures is needed (e.g., Migdisov et al., 2009; Migdisov et al., 2014; Migdisov et al., 2019). We will elaborate in more detail on tests run to date, but we could see for example a potential flowsheet being bioleaching of pyrite in coal material to generate sulfuric acid, this sulfuric acid then is collected from a heap leach (or possibly in situ leach) and subsequently serve as the sulfate-based feedstock for LANL hydrothermal extraction.

LANL Hydrothermal Extraction

As summarized in Strzelecki et al. (2022), LANL began to take a nature-based approach to potential REE separations (Fig. 7.21). This was motivated by the observation that in REE hosting mineral deposits, there are known elevated P and T conditions and that these lead to the precipitation of almost fluorite minerals and furthermore there is elemental fractionation along the aqueous flow path. The resulting experiments led to a patented process for the efficient sequestration of REE from an acidic aqueous solution via exchange with fluorite and precipitation of REE enriched fluorocerite.

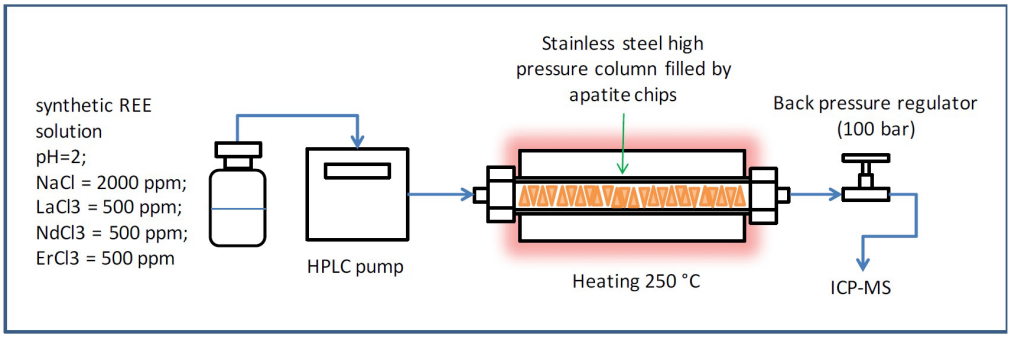

FIGURE 7.21 Schematic diagram of test-bench scale hydrothermal extraction system developed at LANL. Key next steps are scaling to industrial scale.

The current setup is at the test-bench scale and relies on high pressure pumping of a REE pregnant solution (chloride or sulfate based) through a Teflon lined steel tube at 200-250ºC (Fig. 7.22, 7.23). The acidic solution reacts with the fluoride and subsequently exchanges cationic species, forming fluorocerite and liberating Ca as the primary ion in the solution exciting the column. Early experiments showed that there is nearly complete extraction of the REE. Further, subsequent examination of the fluorite/fluorocerite mixture in the column showed that there was fractionation of the REE along the length of the column, where the light REE (La) was predominantly in the first third of the column, the middle REE (Nd) in middle third, and heavy REE (Er) in the final third of the column.

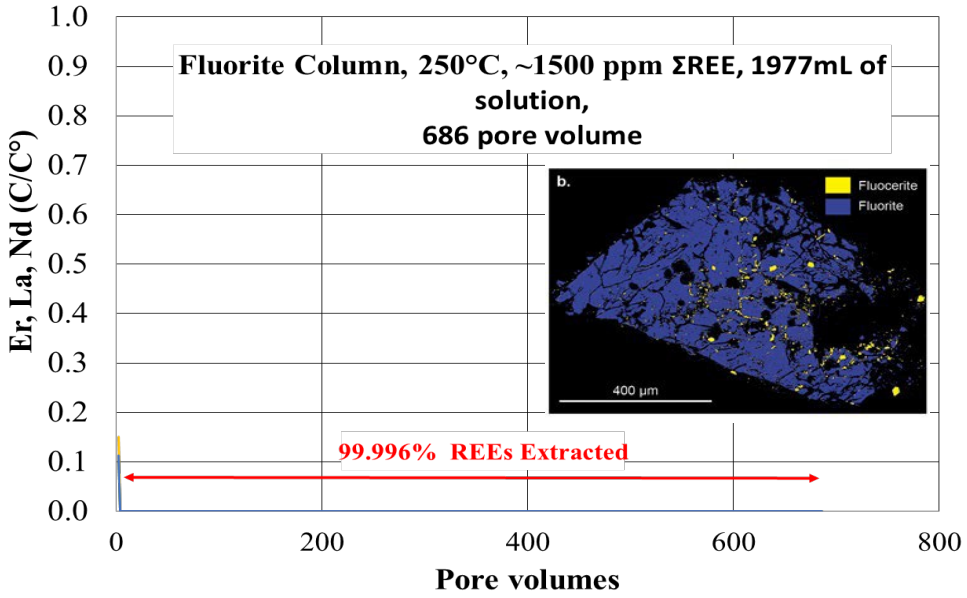

FIGURE 7.22 Demonstration of near complete extraction of REE from solution into fluorocerite. Main mechanism hypothesized is that of fracturing and replacement along all new fractured surfaces, resulting in a volumetric effect.

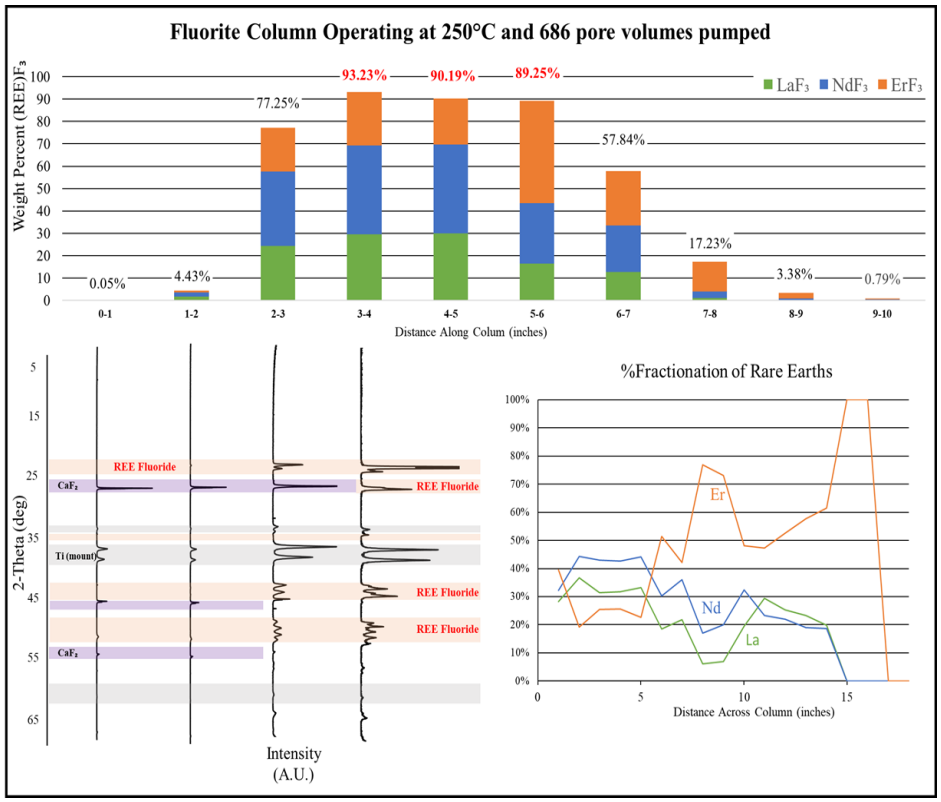

FIGURE 7.23 Demonstration of partial elemental fractionation along length of hydrothermal column.

Our initial tests are promising (Fig. 7.24). However, lacking during these initial tests were information on the scalability of the method and in-depth testing of synthetic or natural REE sources from coal or coal waste, along with other materials. For this Phase 1 study, we have so far investigated the point of Nd breakthrough, defined as the complete saturation of the fluorite system with Nd and thus unable to sequester any additional Nd. We unfortunately to date have not been able to complete further breakthrough tests with other REE, nor complete tests with synthetic and natural feedstocks. This has largely been a combined results of staffing and facility operation complications. Below we detail results of Nd breakthrough experiment and planned future tests.

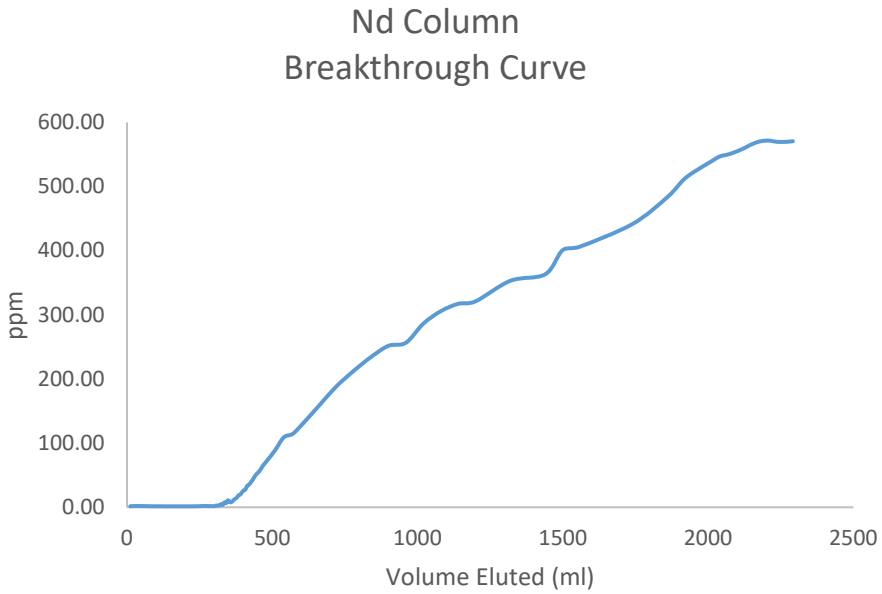

FIGURE 7.24 Nd breakthrough curve for fluorite column at 900 pst, 200 C and 12 ml/hr. Breakthrough demonstration was with a purposefully small fluorite volumes and high Nd load that might be expected in natural feedstocks.

Nd breakthrough experiments were completed at purposely small fluorite volumes and elevated Nd concentrations. Figure 7.18 shows the results of the successful experiment. Run conditions were otherwise 900 psi at 200 C with a flow rate of 12 ml/hour. For this first experiment where precise Nd concentrations are not needed, we employed UV-vis spectroscopy to detect Nd breakthrough. The breakthrough pattern is nearly linear in terms of continual rise in eluant concentration after initial breakthrough suggesting that some fluorite sites were available for reaction until the initial starting concentration was reached in the eluant indicating that no further reactions were taking place.

We initially ran similar tests using sulfate solutions; however, we observed clogging and subsequent over pressure issues leading to failure of the Teflon lining. We were unsure of the cause of the over pressure situation and without detailed investigation beyond the time we had available, could not differentiate between volumetric expansion of the fluorite during conversion to fluorocerite, or other clogging issues. Ultimately, we concluded that over pressurization was a result of failure of the pressure regulator in the system. By then we had switched to a chloride-based solution fearing a sulfate solution was the issue.

This thus leaves some unresolved questions and motivates future experiments. Briefly, experiments we would like to undertake are:

Similar breakthrough experiments using Er and or other REE

- Experiments with sulfate solution
- Synthetic feedstocks mimicking real feedstocks (e.g., acid mine drainage, coal leachate, humate leachate, uranium in situ recovery leachate or ion column eluant)
- Examination of fluocerite solids to better characterize material produced to inform further processing.

Finally, we have compiled a short list of potential direct to market paths for REE-fluorite materials. Some of the list below represent mixed fluorides, while others require single element REE-fluorides. Further, there is active research ongoing into the efficient conversion of REE-fluorides to REE-oxides, which have additional industrial uses (Chong and Riley, 2022).

Current uses for REE-fluorides include

- Solid powder lubricants in high temperature environments
- Nanocrystals and nanocoatings
- Anhydrous fluorides are precursor to REE metals production
- Fiber optics
- Polishing compounds

Other extraction/separation pathways

Other potential REE extraction and separation techniques showing promises are outlined below.

- Lanmodulin protein-based separation of REE pregnant solution show some light/heavy REE selectivity, allowing for possible separation. Possibly scalable akin to ion exchange (Cotruvo et al., 2018)
- Arthrobacter nicotianae used on North Dakota lignite coal recovered 80% total REEs, and over 90% middle and heavy REEs (Park et al., 2020).
- Bioleaching of coal using Shewanella oneidensis MR-1 in Alaska achieved 98.4% recovery with a very cheap and low waste process (Sachan, 2019).
- Ion exchange REE extraction methods recover less than 20% of total REE, though they can be improved with the addition of acid to aid in leaching (Eteriho-Ikelegbe et al., 2021)
- Use of Roseobacter sp. AzwK-3b to fix REE from REE pregnant solution (Bonoficio and Clairke, 2016).
- REE extraction from coal ash using weak mineral acid, netrualization and formation of aqueous solution for further processing (Joshi et al., 2015). Potentially environmentally friendly and could be ideal precursor step.
- Extraction of REE using supercritical CO_2 is effective but prohibitively expensive (Das et al., 2018). Additional work is being done by Sandia National Laboratory (has patent pending).
- Flash joule heating enhances extractability of REE with more dilute acid than otherwise would be required (Deng et al., 2022).

- Systematic separation of REE using ionic liquids using an aqueous biphasic solution. Added benefit is that there is additional elemental selectivity of transition metals and actinides that are also CM (Li et al., 2022).

7.3.9 SNL Environmentally Benign Extraction (G. Xu)

Two different leaching methods involving food grade citric acid have been tested. In the 0.5M citric acid leaching, 0.5 g powder was leached by 30 g of acid solution in oven at 70 ˚C for one week. Table 7.8 shows that the extraction efficiency for REEs varies from less than 5% to 62% depending on the sample composition. The most promising sample is coal #2 which contains 258 ppm of total REEs and of which 62% can be extracted with 0.5M citric acid.

TABLE 7.8 REE contents measured by microwave multi-acid digestion and extraction efficiency using 0.5M citric acid.

		Sc (ppm)	La (ppm)	Ce (ppm)	Pr (ppm)	Nd (ppm)	Sm (ppm)	Eu (ppm)	Gd (ppm)	Tb (ppm)	Dy (ppm)	Ho (ppm)	Er (ppm)	Tm (ppm)	Yb (ppm)	Lu (ppm)	Y (ppm)	REE-Y-Sc (ppm)	extraction efficiency
Coal #1	some residue observed	3.97	15.43	32.59	1.11	18.67	3.05		3.19		2.94		1.53		1.29		10.73	94.5	51.9%
Coal #2	near complete digestion	3.11	59.13	114.37	9.50	53.56	5.50		4.69		2.10		1.00		0.82		4.11	257.9	61.6%
Coal #9	near complete digestion	14.95	60.92	129.05	12.83	70.66	10.76		10.74		6.24		2.93		2.41		21.40	342.9	15.2%
Coal #10	near complete digestion	2.45	2.82	8.51	0.00	6.13	0.96		0.75		0.76		0.47		0.43		0.00	23.3	56.7%
Coal #26	some residue observed	1.01	12.25	21.46	0.00	12.08	1.66		1.66		1.35		0.83		0.71		5.92	58.9	4.8%
Coal #31	some residue observed	1.30	0.00	0.00	0.00	2.56	0.85		0.64		0.84		0.53		0.48		0.69	7.9	51.4%
NIST 1632e std	hot plate digestion	3.44	5.89	11.86	1.41	7.17	1.13	0.25	1.28	0.18	1.04	0.22	0.64	0.09	0.58	0.09	5.95	41.2	

In another set of leaching tests, the mixture of citric acid and $MgSO_4$ was used to extract critical minerals from beach placer sample Far2. As shown in Table 7.9 the combination of diluted citric acid (0.1M) with MgSO4 can significantly increase the extraction efficiency to 62% for REEs. Results also show that citric acid is more effective than ascorbic acid at same concentration for REE extraction. Table 7.10 shows major elements, Zr and Ti concentration in the leachate. A few percents of iron are leached out. However, both Zr and Ti concentrations in the leachate are very low, less than 1%, indicating unable to leach from zircon and ilmenite and/or anatase. Therefore, it is inferred that majority of REEs leached are from iron oxides.

TABLE 7.9 Leaching efficiency for REEs for beach placer sample Far2.

0.1M $MgSO_4$	4%
0.1M citric acid	38%
0.1M citric acid + 0.05M $MgSO_4$	55%
0.1M citric acid + 0.1M $MgSO_4$	56%
0.1M citric acid + 0.2M $MgSO_4$	62%
0.1M ascorbic acid	12%
0.1M ascorbic acid + 0.1M $MgSO_4$	22%

TABLE 7.10 Leachate major elements, Zr and Ti compositions for beach placer sample Far2.

	Ca (%)	Mg (%)	Fe (%)	K (%)	Na (%)	Si (%)	Al (%)	Zr (ppm)	Ti (ppm)
Far2 sandstone ore deposit at 70 °C for one week									
0.1M citric acid	0.21	0.36	1.55	0.17	0.00	0.87	0.88	17.1	52.0
0.1M citric + 0.1M MgSO4	0.24	-	1.84	0.18	0.01	0.89	0.95	18.6	125.9
0.1M ascrobic acid	0.21	0.16	2.23	0.08	BDL	0.37	0.25	16.2	21.9
0.1M ascrobic + 0.1M MgSO4	0.21	-	3.15	0.08	BDL	0.39	0.33	18.6	74.4

Not reported due to added $MgSO_4$

7.4 Summary of findings

- Much of the required infrastructure (highways, railroads, power transmission lines, etc.) needed for economic development is available in the region, mostly near Farmington, Gallup, Grants, Raton, and other populated areas. However, infrastructure in less-populated, rural New Mexico, especially the tribal lands, is not as well developed. Many areas in rural New Mexico do not have paved roads, available running potable water, internet, cell phone, etc. Many federal, state, and tribal agencies are addressing these deficiencies.
- Three samples of clinker were dated by $^{39}Ar/^{40}Ar$ methods to establish the age of pyrometamorphism. The age of the coal deposits are Late Cretaceous in age. The age of the clinker deposit was completely reset during pyrometamorphism. The pyrometamorphism of this coal seam happened in the recent past and not several to 10's of million years ago.
- A preliminary correlation of descriptive drill logs, geophysical logs, laboratory chemical analyses, and pXRF chemical analyses was examined as part of this project. In theory some elements such as U, Th, and K should correlate with gamma logs because concentrations of these elements produce the variability in the gamma logs. If other elements correlate well with U, Th, or K, then those elements should also correlate with the gamma logs. However, preliminary results indicated downhole plots of the handheld pXRF geochemistry cannot be directly correlated with the geophysical survey for hole H-16. Additional study using a more precise pXRF and additional drill holes is planned for phase 2. If the correlation between certain elements and the gamma logs is correct, then this correlation is important in developing machine learning techniques to map and predict the presence of certain elements, particularly critical minerals, in the subsurface across the basins.

8.0 TECHNOLOGY INNOVATION CENTER (TASK 6)

A long-range plan to compile information about critical minerals was developed for the USGS Earth MRI program and revised this year. This plan will guide future endeavors to examine critical minerals in New Mexico. See https://geoinfo.nmt.edu/staff/McLemore/projects/mining/REE/documents/NMBGMR_CM_Plan23v1_001.pdf. This plan will develop a Critical Minerals Research Center at NMT to study and develop innovative advances in exploration, mining, processing, environmental science, permitting, and other technologies. Partners include members from the Earth and Environmental Science, Mineral Engineering and Material Engineering Departments, Petroleum Research Recovery Center, Los Alamos National Laboratory, and Sandia National Laboratory. Funding will be provided through industry, Federal government grants, and state appropriations.

9.0 STAKEHOLDER OUTREACH, EDUCATION, AND WORK FORCE DEVELOPMENT (TASK 7)

9.1 Purpose (V.T. McLemore)

As our society shifts and adapts to new carbon-free technologies to reduce greenhouse gases, we have new opportunities to engage with communities to share information about the importance of mining to solve societies' challenges. Carbon-free technologies ultimately mean a reduction in coal, oil, and gas production in the San Juan and Raton Basins. However, these new carbon-free technologies also will require more and, in some cases, new minerals production, such as rare earth elements (REE), copper, and other critical minerals. Can the San Juan and Raton Basins supply some of those new resources, perhaps even from coal? That is the essence of the CORE-CM San Juan River and Raton Basins project. But how do we engage the communities to contribute to these new possibilities and encourage new industries to replace the jobs from current coal, oil, and gas production? Inclusive engagement to make changes that engage stakeholders and flip the script from apathetic to exciting, limiting to expansive, and frustrating to encouraging. Everyone needs to be a part of that discussion—we are smarter as a group than as individuals. Communication is a vital component of this process.

NMT has engaged in stakeholder outreach and education throughout the San Juan and Raton basins CORE-CM project and the USGS Earth MRI projects. The CORE-CM project has included training (including retraining/uptraining) of the next generation of technicians, skilled workers, and STEM professionals, to secure domestic feedstocks and material component production. Staff, especially Dr. McLemore has a history of mentoring minority (BIPOC) students, and mindfully contributes to diversity in the geoscience and mining engineering workforce (see Student Theses (nmt.edu)).

Section 9 is about outreach and education—what we have done and what we would like to do in the future. It describes how we have informed and educated stakeholders and the public about the importance of critical minerals and REE in our society and why these minerals have to be mined. Section 9 also covers how we have and will inform others about the results of our San Juan and Raton Basins CORE-CM project.

- Some of the questions that need to be addressed include:
- What did we learn during the CORE-CM project?
- What are the critical minerals and REE resource potential in coal and related strata in the San Juan and Raton Basins?
- What other opportunities are there in minerals production in the San Juan and Raton Basins?
- What will San Juan and Raton Basins look like without coal, oil, and gas production?
- What will San Juan and Raton Basins feel like without coal, oil, and gas production?
- What will you see in the future in the San Juan and Raton Basins?
- What do you want to preserve, no matter what else happens?
- What else is important?
- What obstacles might get in the way of achieving the end of coal, oil, and gas production in the San Juan and Raton basins, while maintaining a sustainable way of life in the area?
- What can we improve?

9.2 Audience (V.T. McLemore)

The audience for this outreach effort includes all stakeholders and the public. Residents of many small communities in rural New Mexico are concerned about mineral resources in their communities and the CORE-CM project will aid in their understanding of those resources and the potential effects and consequences of extracting these resources or not extracting them. Tribal communities want to be included in discussions and participate in future technologies. Technical data presented in the CORE-CM project will increase our understanding of ore formation, mineral resource potential, production, consumption, disposal, and how minerals and mineral extraction interact with the environment. State and federal government decision makers, mining companies, and the public require this information for land use decisions, remediation prioritization and to determine if some of these deposits can be mined.

9.3 Workforce development plan (C. Connolly)

An effective workforce development plan can add to the flexibility and longevity of organizations by promoting a goal-oriented approach to management. Workforce development plans should include objectives that support organizational goals, and identify workforce demographics and environmental factors. Strong workforce development plans should assess strengths, needs, workforce training, mentorship, and should include provisions to ensure engagement and retention along with methods to improve and modify the structure of the workforce development model based on data.

9.3.1 Foundation supports

Analysis of an organization's short- and long-term goals must be the foundation of a workforce development plan. Research that involves staffing, safety, training protocols, operations management, worker retention, and organizational growth should be addressed. The objectives of the plan can and should be modified based on additional information. Goals should be shared with management and the workforce, regularly evaluated, and changed when needed.

9.3.2 Background Research

Asset mapping that includes worker demographics, local infrastructure data, and information about the environment is necessary for developing a useful workforce plan. Workforce age, gender, diversity, education, experience, career goals, and growth potential provide essential statistics for planning workforce development. Infrastructure such as paved roads and bridges, access to clean drinking water, stores, affordable housing, schools, medical care, restaurants, and entertainment offerings build communities and provide environmental support to attract and retain workers.

9.3.3 Invest in the Workforce

Development plans should also invest in the workforce by matching the compatibility of worker skills with required job tasks and training. Alignment of workers to the proper job can be accomplished through interview questions, background checks, skills assessments, job training

and certification, and performance reviews. Regular performance evaluations can aid productivity, chart growth, and encourage continuing education and training, to help plan future progress. Educational workforce supports that include mentorship, cross-training, internal and external learning opportunities, and technology integration can prepare workers to assume leadership roles. These supports help employers fill gaps when necessary, and plan for leadership succession.

9.3.4 Worker Training, Development, Retention, and Growth

Workforce plans should also include provisions for worker on-board training, and growth by encouraging employees to communicate their concerns and methods for management to respond. The workforce plan should include measures that provide a safe work environment and protocols to report unsafe conditions anonymously. It should also outline definite methods for career path training and advancement for workers to provide flexibility and promote work-life balance. Employee retention is also aided by encouraging a culture of workplace community and camaraderie. Shared employee events, publicly recognizing employee accomplishments, and rewarding workers for service can boost morale and increase retention. As part of the interview process and annual employee evaluations, a workforce development plan may be tailored to suit the organization's needs by allowing workers and supervisors to collaboratively set short and long-term goals. Another approach is to enable groups working within a sector the freedom to create and evolve projected team goals with the approval of management. Adapting workplace practices, based on employee feedback, improves organizational competitiveness and encourages employee engagement.

9.3.5 Summary

The workforce plan, along with clear objectives and responsiveness to feedback, provides direction for the organization by setting realistic individual and team goals. Investment in the workforce through training, recognition of accomplishments, team building, and paths to leadership improve employee morale and engagement. Workforce plan implementation builds a culture of safety, ownership, and pride, which leads to improved employee commitment and organization coherence.

9.4 What has been accomplished (C. Connolly and V.T. McLemore)

9.4.1 New Mexico State and Regional Education

The NMT Team has completed many outreach and training activities relating to the CORE-CM project, as described below.

9.4.2 Project web page

More information can be found on the project web page https://geoinfo.nmt.edu/staff/McLemore/REEinCoalWeb.html.

9.4.3 Historical archives

Archiving data and housing geological collections is an important role the Bureau of Geology plays in improving our understanding of the geology of New Mexico. For the past 35 years, coal data from drill holes and outcrop measurements, and coal quality data have been collected, interpreted and entered into the National Coal Resource Data System (NCRDS) through a cooperative grant program with the U.S. Geological Survey. These data are geographically located by latitude and longitude and the Public Land Survey System (township and range). Data can be obtained by request or searching our archives online (Data, Archives, & Collections (nmt.edu)). Drill core and cuttings of numerous holes are available in our core facility and have been used to evaluate critical minerals potential.

9.4.4 Earth Matters

New Mexico Earth Matters is a free, semi-annual newsletter, written for New Mexicans interested in the state's water, landscapes, and earth resources. In each issue, Earth Matters takes a deeper look at an earth science topic that's important to New Mexico in less-technical language. The winter issue in 2023 examined the importance of critical minerals (https://geoinfo.nmt.edu/publications/periodicals/earthmatters/23/n1/em_v23_n1.pdf). Older issues have also examined REE (https://geoinfo.nmt.edu/publications/periodicals/earthmatters/11/n2/em_v11_n2.pdf) and potash (https://geoinfo.nmt.edu/publications/periodicals/earthmatters/8/n2/em_v8_n2.pdf).

9.4.5 Rockin' Around New Mexico

We have created critical minerals and REE research-based activities that have been shared during the annual NMBGMR/NMT summer geology teacher workshop-"Rockin' Around New Mexico". The Rockin' teacher training is part of the NMT Master's in Science Teaching degree program. K-12 certified educators can also take the Rockin' Around New Mexico course for professional development. Up to 30 teachers from school districts throughout New Mexico (including tribal communities) and adjacent states attend the Rockin' Around New Mexico workshop (Fig. 9.1, 9.2). Educators are considered to be multipliers of information shared at the Rockin' workshop since they teach lessons learned to their students. Critical minerals and REE lessons with a focus on extraction of critical minerals and REE from coal and coal fly ash, the impact of critical minerals and REE to the economy of New Mexico, and hazard mitigation in the form of carbon sequestration have been taught at Rockin' and made available to teachers at the workshop through notebooks, data collection and in-person or virtual classroom experiences. Information is also shared on our NMBGMR Education webpage. Lessons and activities created for the Rockin' Around New Mexico workshop on our NMBGMR website for free public use and distribution (Dr. Virginia McLemore (nmt.edu)). Rockin' Around New Mexico teachers visited the Navajo coal mine in 2022 and the Lee Ranch coal mine in 2024.

FIGURE 9.1 K-12 grade educators learn about subsurface mapping during Rockin' Around NM 2022 as part of an activity taught by NMBGMR Petroleum Geologist Luke Martin (center; photograph by Cynthia Connolly).

FIGURE 9.2 Rockin' Around New Mexico teachers collect coal samples at the Lee Ranch mine (photograph by Cynthia Connolly).

9.4.6 Lite Geology

Lite Geology is an online, biannual NMBGMR education periodical written for K-12 grade teachers that includes articles, classroom activities, teachers' resources, web links, and geological and scientific events (Fig. 9.3). *Lite Geology* publications with critical minerals and REE related articles include:

Issue 47 with an article on potash (https://geoinfo.nmt.edu/publications/periodicals/litegeology/47/lg_v47.pdf)

Issue 50 with an article on Rare Earth Element Deposits in the Gallinas Mountains, Lincoln County, New Mexico (https://geoinfo.nmt.edu/publications/periodicals/litegeology/50/lg_v50.pdf)

Issue 51 includes an article on Rare Earth Elements and Critical Minerals in Late Cretaceous Coal and Related Strata in the San Juan and Raton Basins, New Mexico (https://geoinfo.nmt.edu/publications/periodicals/litegeology/51/lg_v51.pdf)

Issue 53 includes an article on Climate Change and the Need for Copper (https://geoinfo.nmt.edu/publications/periodicals/litegeology/53/lg_v53.pdf)

Issue 54 is entirely on the San Juan Basin critical minerals resources (https://geoinfo.nmt.edu/publications/periodicals/litegeology/54/lg_v54.pdf).

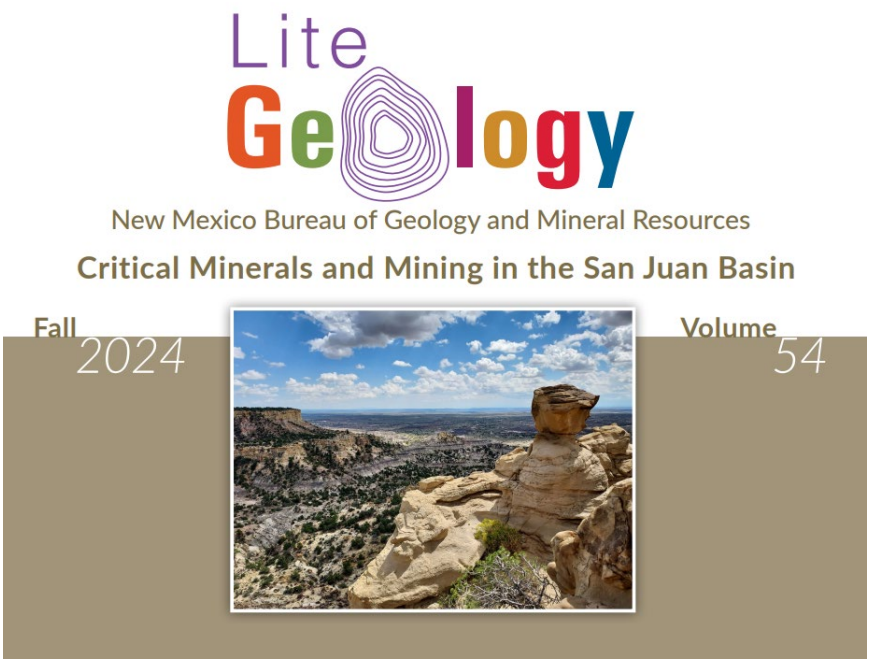

FIGURE 9.3 Cover photo of Lite Geology Volume 54, featuring Critical Minerals and Mining in the San Juan Basin. (Photograph by Kevin Hobbs).

9.4.7 Post Cards from the Field

Post cards from the field are short descriptions of field activities from NMBGMR staff and are generally posted on the NMBGMR Facebook page (https://www.facebook.com/NMBGMR).

- SME conference 2024

- https://geoinfo.nmt.edu/geoscience/research/postcards/home.cfml?id=702&title=Society+of+Mining+Metallurgy+and+Exploration+Inc+Annual+Conference+20240)
- Eureka copper mine, Nacimiento Mountains mining district, Rio Arriba County, New Mexico https://geoinfo.nmt.edu/geoscience/research/postcards/home.cfml?id=693&title=Eureka+copper+mine+Nacimiento+Mountains+mining+district+Rio+Arriba+County+New+Mexico
- NM Bureau of Geology hosts the USGS during sample collection at the Copper Flat Mine near Hillsboro New Mexico https://geoinfo.nmt.edu/geoscience/research/postcards/home.cfml?id=653&title=NM+Bureau+of+Geology+hosts+the+USGS+during+sample+collection+at+the+Copper+Flat+Mine+near+Hillsboro+New+Mexico
- Are mine dumps in NM a source for critical minerals? https://geoinfo.nmt.edu/geoscience/research/postcards/home.cfml?id=654&title=Are+mine+dumps+in+NM+a+source+for+critical+minerals

9.4.8 Lesson plans

Lessons plans were developed for teaching mineral identification of critical minerals and for gold panning for all ages (Dr. Virginia McLemore (nmt.edu)).

9.4.9 Displays and exhibits in local and regional museums, Earth Science days and other events

An exhibit on Critical Minerals in New Mexico was set up for the Legislature and Earth Science days at the Round House in February 2024 and 2025, the New Mexico Mining Association annual meeting in August 2024, and the New Mexico Mineral Symposium in November 2024 and 2025. The raw critical minerals along with the products they are used in were displayed. A display of Critical Minerals was also at the NMBGMR Museum in 2023-2024.

9.4.10 Magdalena Science Café

Magdalena high school students collected samples from Magdalena district, NM mine wastes as part of their extracurricular activity. Chemical analyses of samples they collected are in Appendix 7.

9.4.11 Field trips with teachers

NMGBMR economic geology group led a field trip to the Nacimiento copper mine near Cuba, NM for New Mexico Science Teacher Association teachers and discussed mining and the environmental effects of mining (https://geoinfo.nmt.edu/news/home.cfml?id=718&title=NMSTA+K12+teacher+tour+to+Nacimiento+copper+mine).

9.4.12 Field trips with community groups

We led a field trip for the Corrales Art Society to the Zuni Mountains to expose artist to geology and different geologic media that goes into various art forms. Artists collected geologic materials including clay, fluorite, mica, and copper. We also led a field trip to the Magdalena district for the Mining History Association (web).

9.4.13 Field trips with Cub Scouts

We led a field trip to the Hidee mine, Idaho Springs, Colorado for a Denver Cub Scout troop to expose scouts and their parents to mining and gold panning.

9.4.14 EarthScope interns

EarthScope offers a variety of paid summer internships for undergraduate students from community (Geo-Launchpad | EarthScope Consortium), two-year and four-year colleges (Home - RESESS (unavco.org)). This program teams undergraduate students with university research groups so the students can participate in research projects. In 2023, two students worked with the NMBGMR Economic Geology Group on critical minerals and in 2024, four students are working with our group. This year (2025), two additional students interned with our group. These students select a research project that they can complete during the summer and present a poster on their research at either GSA or AGU annual conference. The interns are paid a salary, travel and housing expenses; the program is supported by the National Science Foundation, USGS, and NASA. One of the interns from 2024 is now a graduate student in the Earth and Environmental Science Department at New Mexico Institute of Mining and Technology working on her Master's degree and is funded by a USGS Earth MRI project!

9.4.15 Tribal engagement

We have conducted previous work with the Navajo and Jicarilla Apache Nations: (https://geoinfo.nmt.edu/geoscience/research/home.cfml?id=145&project=REE+in+Coal+and+associated+strata+in+the+San+Juan+and+Raton+basins+New+Mexico) and Jicarilla Apache Tribe (heavy mineral sandstones, https://geoinfo.nmt.edu/publications/openfile/details.cfml?Volume=587).

Some of our students are members of Native American Tribes (https://geoinfo.nmt.edu/news/home.cfml?id=701&title=Bureau+researchers+and+students+win+honors+at+Society+for+Mining+Metallurgy+and+Exploration+annual+meeting).

9.4.16 Technical workshops

We headed a panel on Mining Innovations and Challenges in New Mexico at the 1st Annual Consortium for Energy Sustainability and Advanced Management workshop (CESAM). We plan to continue with this consortium.

9.4.17 Public field trips

Field trips were conducted by the PI (Virginia McLemore) and other staff members as part of the outreach activities. Cub scouts in the Denver area toured the Hidee gold mine in Central City, Co.; mine safety and gold panning were included. Teachers toured the Nacimiento mine in Sandoval County. Students from NMT and San Juan College toured the Navajo and humate mines in the San Juan Basin; Chino copper mine in Silver City, and Morenci copper mine in Morenci, Az.; mine safety was included. Tours of Lake Valley mines in Sierra County were conducted as part of the New Mexico Mineral Symposium in November 2024 and 2025. Tours of the Kelley mines near Magdalena were conducted as part of the Notional History Association annual conference in 2023.

9.4.18 Other Publications

A short summary of the project was written for Gold Pan NMIMT Alumni Newsletter (https://nmt.edu/advancement/goldpan_archives/2022_Summer_GoldPan_Digital2.pdf)

9.4.19 Participation in geologic and mining engineering conferences

Students and staff contributed displays, presentations and posters at geologic and mining engineering conferences throughout the project.

Geological Society of America (GSA)
Society of Mining, Metallurgy, and Exploration, Inc. (SME)
New Mexico Mining Association (NMMA)
New Mexico Geological Society (NMGS)
Mining History Association (MHA)
American Exploration and Mining Association (AEMA)
New Mexico Mineral Symposium (presented poster on Beach placer sandstones)
U.S. Geological Survey Earth MRI and Data preservation workshops

9.4.20 Workforce development

Another aspect of this project is the training of the future workforce. Students at NMT and San Juan College were hired to work on this project. Undergraduate and graduate students assisted in data collection and entry. Students learned to understand the importance of critical minerals, structure of databases, inventory of samples, creation of metadata, and online mapping tools. Existing data were collected, reviewed, and evaluated. Many of the presentations and publications mentioned in this report were written by students to showcase their research. These are skills that the current and future work force must master. The data is available online for public access (Appendix 2).

9.4.21 Mineral kits for teachers

Mineral kits were prepared for teachers attending Rockin Around New Mexico with lesson plans. The mineral kits included samples of various critical minerals, identification

guidelines, lesson plans, locations in New Mexico where the minerals were collected, and uses of critical minerals.

9.4.22 Field notes on the geology of New Mexico

In celebration of Earth Science Week, we began collaborating with the staff at KUNM in 2009 to create a week-long series on the geology of New Mexico. We have posted podcasts and scripts of these radio spots. KUNM, 89.9 FM is a public radio station that broadcasts from the campus of the University of New Mexico in Albuquerque, NM. In 2022, McLemore presented Critical Minerals in New Mexico (oral https://geoinfo.nmt.edu/events/esweek/2022/audio/ESW_Friday_Virginia_McLemore.mp3, text https://geoinfo.nmt.edu/events/esweek/2022/scripts/ESW_2022_McLemore.pdf) . In 2020, McLemore presented on the Importance of Mining in New Mexico (oral https://geoinfo.nmt.edu/events/esweek/2020/audio/ESW2%20Virginia.mp3, text https://geoinfo.nmt.edu/events/esweek/2020/scripts/ESW2-McLemore_Importance_of_NM.pdf).

10.0 LESSONS LEARNED, CHALLENGES, FRUSTRATIONS, AND DATA GAPS

- A gap analyses is required for the entire project and will be performed in phase 2, if funded.
- Other coal fields in New Mexico should be examined, sampled and analyzed.
- No agreed upon method of geochemically analyzing coal and coal ash accurately.
- Lack of access to coal samples and ash at power plants. Additional samples are required to characterize many of the coal fields (Table 3.1). Better resource estimation of critical minerals around areas such as coal mines requires more refined sampling spatially, which will help to better understand distribution of critical minerals across the basin.
- Stratigraphic data from electric logs should be integrated with pXRF analyses and geologic models to improve the spatial distribution understanding of critical minerals.
- Cretaceous beach-placer sandstone deposits should be re-examined for their critical minerals potential.
- Throughout our work to measure REE in surface water, we have identified a significant gap of REE data for surface water.

11.0 CONCLUSIONS

Most chapters include at the end a significant findings section, which summarizes the conclusions of sections in that chapter. The executive summary includes the important conclusions for this project. Ultimately, the economic potential of critical minerals and REE in the San Juan and Raton basins and adjacent areas will most likely depend upon production of more than one commodity, maybe even from coal, humate, beach-placer, uranium, and clinker deposits.

12.0 REFERENCES

Acheampong-Mensah, A.S., 2024, Geochemistry of critical minerals in mine waste at Hillsboro and Steeple Rock districts, New Mexico: M.S. thesis, New Mexico Institute of Mining and Technology, Socorro, 64 p.

Affolter, R.H., 2009, Quality characterization of Cretaceous coals from the Colorado Plateau coal assessment area; in Chapter G of Geologic assessment of coal in the Colorado Plateau: Arizona, Colorado, New Mexico, and Utah: U.S. Geological Survey, Professional Paper 1625

Affolter, R.H. et al., 2011, USGS data series 635: Geochemical Database of Feed Coal and Coal Combustion Products (CCPs) from Five Power Plants in the United States: U.S. Geological Survey (USGS).

Araya, A., 1993, A study of the sulfur distribution and minor and major-element geochemistry of a high-volume bituminous coal seam in northwestern New Mexico [Ph.D. Dissertation]: New Mexico Institute of Mining and Technology, Socorro, 266 p.

Anderson, O.J., 1987, Geology and coal resources of Atarque Lake 1:50,000 quadrangle, New Mexico: New Mexico Bureau of Mines and Mineral Resources Geologic Map 61, 2 sheets.

Averitt, P., 1973, Coal. In D.A. Brobst & W.P. Pratt (Eds.), United States Mineral Resources (pp. 133–142). U.S. Geological Survey Professional Paper 820. https://pubs.usgs.gov/pp/0820/report.pdf

Asafo-Akowuah, J., McLemore, V.T., and Zutah, W., New Mexico Abandoned Uranium Mines Study: Jeter, Lucky Don, and Little Davie mines, Socorro County, New Mexico, Socorro, New Mexico, May 2017

Badonie, M., Newcomer, J., Shaver, S., and McLemore, V.T., 2023, REE in coal and associated strata in the San Juan and Raton Basins, New Mexico: Minexchange, 2023 Society of Mining, Metallurgy and Exploration, Inc., Annual Conference Technical Program, preprint 23-055, 5 p. https://geoinfo.nmt.edu/staff/McLemore/documents/23-055.pdf, accessed April 23, 2025.

Baker, L., 1989, Vertical distribution of trace elements in coal seams from the San Juan and Raton basins, New Mexico: M.S. thesis, New Mexico Institute of Mining and Technology, Socorro, 443 p.

Bamburak, J.D., Nicolas, M.P.B., Hatcher, J. and Yang, X.M., 2013, Rare-earth element potential of the Gammon Ferruginous Member of the Upper Cretaceous Pierre Shale in southwestern Manitoba; *in* Report of Activities 2013, Manitoba Mineral Resources: Manitoba Geological Survey, p. 123–128.

Beaumont, E.C., 1973, Stratigraphic distribution of coal in San Juan Basin; in Strippable low–sulfur coal resources of the San Juan Basin in New Mexico and Colorado: New Mexico Bureau of Mines and Mineral Resources Memoir 25, p. 15–30.

Beisner, K.R., Travis, R.E., Alvarez, D.A., Barber, L.B., Fleck, J.A., Jasmann, J.R., 2024, Temporal variability and sources of PFAS in the Rio Grande, New Mexico through an arid urban area using multiple tracers and high-frequency sampling: Emerging Contaminants, Vol. 10, Issue 3; https://doi.org/10.1016/j.emcon.2024.100314.

Bing, D. et al., 2022. Rare earth elements from waste. Sci. Adv.8, 3132, DOI:10.1126/sciadv.abm3132

Bonificio, W.D., and Clarke, D.R., 2016, Rare-earth separation using bacteria. Environmental Science and Technology Letters, 3(4), 180-184.
Borden, R., 2001, Geochemical evolution of sulfide-bearing waste rock soils at the Bingham Canyon Mine, Utah: Geochemistry: Exploration, Environment, and Analysis 1(1): 15-21.
Brower. D, 2021, How to Remove Uranium From Drinking Water. EarthWater Alliance, https://www.earthwateralliance.org/filtering-systems-for-uranium-and-radioactive-particles/#:~:text=Reverse%20osmosis%20will%20reduce%20uranium,alumina%20can%20also%20be%20utilized. (accessed 2023-10-31)
Breit, G.N., 2016, Resource potential for commodities in addition to uranium in sandstone-hosted deposits: Reviews in Economic Geology, v. 18, p. 323-338.
Briggs, P.H., 2001, The Determination of Forty Elements in Geological and Botanical Samples by Inductively Coupled Plasma-Atomic Emission Spectrometry, U.S. Geological Survey Open File Report 02-223-G, Analytical Methods for Chemical Analysis of Geologic and Other Materials, U.S. Geological Survey.
Brister, B.S. and Hoffman, G.K., 2002, Fundamental geology of San Juan Basin energy resources; in Brister, B.S. and Price, L.G., eds., New Mexico energy, present and future: Decision-makers field conference 2002, San Juan Basin, 156 p.
Caldwell, S., 2018, Paragenesis of uranium minerals in the Grants mineral belt, New Mexico: applied geochemistry and the development of oxidized uranium mineralization: M.S. thesis, New Mexico Institute of Mining and Technology, Socorro, 202 p.
Campbell, K.M., Seal, R.R., Piatak, N.M., Azain, J.S., Morrison, J.M., White, S.J., Manning, A.H., Walton-Day, K., Holloway, J.M., and Wang, B., 2025, Earth Mapping Resources Initiative protocols—Sampling hard-rock mine waste and perpetual mine water sources: U.S. Geological Survey Scientific Investigations Report 2025–5068, 22 p., https://doi.org/10.3133/sir20255068.
Cannon, W.F., Kimball, B.E., and Corathers, L.A., 2017, Manganese, *in* Schulz, K.J., DeYoung, J.H., Jr., Seal, R.R., II, and Bradley, D.C., eds., Critical mineral resources of the United States—Economic and environmental geology and prospects for future supply: U.S. Geological Survey Professional Paper 1802, p. L1–L28. https://doi.org/10.3133/pp1802L.
Carnevale, J., 2023, Greek God Uranus: Family & Symbols - Study.Com., https://study.com/learn/lesson/greek-god-uranus-mythology.html (accessed 2023-10-31).
Carpenter, M.B. and Keane, C.M., 2016, The geoscience handbook 2016: Alexandria, Virginia, American Geosciences Institute (AGI) Data Sheets, 5th edition, 480 p.
Chenoweth, W.L., 1974, Uranium occurrences of the Nacimiento-Jemez region, Sandoval and Rio Arriba Counties, New Mexico, *in* Siemers, C.T., Woodward, L.A., and Callender, J.F., eds., Ghost Ranch: New Mexico Geological Society Guidebook 25, p. 309–313, https://doi.org/10.56577/FFC-25.309
Collins, G.E., and Nye, T.S., 1957, Exploration drilling in the Ladron Peak area, Socorro County, New Mexico: U.S. Atomic Energy Commission, Technical Memorandum Report DAO-4-TM-8, 25 p.
Committee on Critical Mineral Impacts of the U.S. Economy, 2008, Minerals, Critical Minerals, and the U.S. Economy: Committee on Earth Resources, National Research Council, ISBN: 0-309-11283-4, 264 p., http://www.nap.edu/catalog/12034.html
Cotruvo Jr., J.A., Featherston, E.R., Mattocks, J.A., Jackson, V.Ho, and Laremore, T.N., 2018. Lanmodulin: A Highly Selective Lanthanide-Binding Protein from a Lanthanide-

Utilizing Bacterium. Journal of the American Chemical Society, 140 (44), 15056-15061. http://doi.org/10.1021/jacs.8b09842.
Committee on Uranium Mining in Virginia, Committee on Earth Resources; National Research Council., Washington (DC): National Academies Press (US), 2011, Uranium Mining in Virginia: Scientific, Technical, Environmental, Human Health and Safety, and Regulatory Aspects of Uranium Mining and Processing in Virginia. Washington (DC): National Academies Press (US); 2011 Dec 19. 6, Potential Environmental Effects of Uranium Mining, Processing, and Reclamation. Available from:, (accessed 2023-09-25) https://www.ncbi.nlm.nih.gov/books/NBK201052/
Coveney, R.M., Jr. and Glascock, M.D., 1989, A Review of the Origins of Metal-Rich Black Shales Central USA with an Inferred Role for Basinal Brines: Applied Geochemistry, v. 4, p. 347–367.
Cox, D.P., and Singer, D.A., eds., 1986, Mineral deposit models: U.S. Geological Survey Bulletin 1693, 379 p., https://doi.org/10.3133/b1693
Craddock, P.R., van le Doan, T., Bake, K., Polyakov, M., Charsky, A.M., and Pomerantz, A.E., 2015, Evolution of kerogen and bitumen during thermal maturation via semi-open pyrolysis investigated by infrared spectroscopy: Energy and Fuels, v. 29, https://pubs.acs.org/doi/full/10.1021/ef5027532
Craddock, P.R. and Sauerer, B., 2022, Robust determination of kerogen properties in organic-rich mudrocks via Raman spectroscopy: Organic Geochemistry, v. 169, 104381, https://doi.org/10.1016/j.orggeochem.2022.104381
Dai, S. and Finkelman, R.B., 2018, Coal as a promising source of critical elements: Progress and future prospects: International Journal of Coal Geology, v. 186, p. 155-164.
EMNRD Coal Water Quality Sample & Parameter, 2019
Das, S., G. Gaustad, G., Sekar, A. and Williams, E., 2018, Techno-economic analysis of supercritical extraction of rare earth elements from coal ash: J. Clean. Prod., vol. 189, p. 539–551, doi: 10.1016/j.jclepro.2018.03.252.
Davis, B., 1998, What is a sample? What does it represent? Australian Institute of Geoscientists Bulletin, v. 22, p. 39-34.
Tan, K.H., Humic Matter in Soil and the Environment: Principles and Controversies, 2014, CRC Press, Boca Raton, FL, 2014, ISBN: 9781482234459
Desborough, G.A., Poole, F.G., Hose, R.K. and Green, G.N., 1984, Metalliferous oil shale in the Upper Devonian Gibellini Facies of the Woodruff Formation in the Southern Fish Creek Range, Nevada, *in* A.L. Bush, ed., Contributions to Mineral Resources Research, 1984: U.S. Geological Survey Bulletin 1694, p. 91–104.
Dodbiba, G., and Fujita, T. 2023. Trends in extraction of rare earth elements from coal ashes—A review: Recycling 2023, v. 8, no. 17, https://doi.org/10.3390/recycling8010017.
Dorr, J.V.N., 1965, Manganese: New Mexico Bureau of Mines and Mineral Resources, Bulletin 87, p. 183–195. https://doi.org/10.58799/B-87
Downing, B., 2008, ARD sampling and sample preparation: http://technology.infomine.com/enviromine/ard/sampling/intro.html
du Bray, E., 2007, Time, space, and composition relations among northern Nevada intrusive rocks and their metallogenic implications: Geosphere, v. 3, p. 381–405.
Dyni, J.R., 2006, Geology and resources of some world oil-shale deposits: U.S. Geological Survey Scientific Investigations Report, 2005–5294, 42 p.

EPA Method 200.8: Creed, J.T., Brockhoff, C.A., Martin, T.D., 1994, Determination of Trace Elements in Waters and Wastes by Inductively Couples Plasma – Mass Spectrometry. U.S. Environmental Protection Agency, Cincinnati, Ohio: Method 200.8, Revision 5.4.

EPA Method 200.7: Martin, T.D., Brockhoff, C.A., Creed, J.T., 1994, Determination of Metals and Trace Elements in Water and Wastes by Inductively Coupled Plasma-Atomic Emission Spectrometry. U.S. Environmental Protection Agency, Cincinnati, Ohio: Method 200.7, Revision 4.4.

EPA Method 120.1: Conductance (Specific Conductance, µmhos 25°C) by Conductivity Meter, 1982, Methods for the Chemical Analysis of Water and Wastes (MCAWW) (EPA/600/4-79/020).

EPA Method 150.1: pH (Electrometric), 1982, Methods for the Chemical Analysis of Water and Wastes (MCAWW) (EPA/600/4-79/020).

EPA Method 310.1: Alkalinity (Titrimetric, pH 4.5) by Autoanalyzer, 1978, Methods for the Chemical Analysis of Water and Wastes (MCAWW) (EPA/600/4-79/020).

EPA Method 300.0: Pfaff, J.D., 1993, Determination of Inorganic Anions by Ion Chromatography. U.S. Environmental Protection Agency, Cincinnati, Ohio: Method 300.0, Revision 2.1.

Essary, J., 2025, Extraction of alumina from mineral resources found at New Mexico mine sites (M.S. thesis): New Mexico Institute of Mining and Technology, Socorro,

Eterigho-Ikelegbe, O., Harrar, H. and Bada, S., 2021, Rare earth elements from coal and coal discard – A review: Miner. Eng., vol. 173, p. 107187, doi: 10.1016/j.mineng.2021.107187.

Farnham, L.L., 1961, Manganese deposits of New Mexico: U.S. Bureau of Mines, Information Circular 8030, 176 p.

Fassett, J. E., and Hinds, J. S.,1971, Geology and fuel resources of the Fruitland Formation and Kirtland Shale of the San Juan Basin, New Mexico and Colorado (U.S. Geological Survey Professional Paper 676, 76 p.). U.S.

Finkelman, R.B., Dai,S., and French, 2019, The importance of minerals in coal as the hosts of chemical elements: A review: International Journal of Coal Geology, v. 212, 17 p.

Fire, S., Robledo, V., McLemore, V.T., 2024, Stratigraphic analysis for correlativity of geophysical and geochemical properties with lithology: Rare Earth Element Occurrence in the Late Cretaceous Fruitland Formation (abstr.), *in:* 2024 New Mexico Geological Society Annual Spring Meeting, April 19, 2024, Macey Center, Socorro, NM, Kelley, Shari, McCrory, Tom, *ed(s)*, p. 19-20. ISSN: 2834-5800 https://doi.org/10.56577/SM-2024.2990

Flint, E.P., Clarke, W.F., Newman, E.S., Shartsis, L., Bishop, D.L., and Wells, L.S., 1946, Extraction of alumina from clays and high-silica bauxites: Journal of Research of the National Bureau of Standards, 36(RP1691), p. 68–106.

Folk, R.L., 1974, Petrology of Sedimentary rocks: Austin, Texas, Hemphill Pub. Co., 182 p.

Force, E.R. and Cannon, W.F., 1988, Depositional model for shallow-marine manganese deposits around black shale basins: Economic Geology, v. 83, p. 93–117. https://doi.org/10.2113/gsecongeo.83.1.93

Geboy, N.J., Engle, M.A., and Hower, J.C., 2013, Whole-coal versus ash basis in coal geochemistry—A mathematical approach to consistent interpretations: International Journal of Coal Geology, v. 113, p. 41–49. http://dx.doi.org/10.1016/j.coal.2013.02.008

Gibellini Vanadium Project, 2019, https://www.mining-technology.com/projects/gibellini-vanadium-project/ Accessed on 6/14/2019.
Goddard, E.N., 1966, Geologic map and sections of the Zuni Mountains fluorspar district, Valencia County, New Mexico: U.S. Geological Survey Miscellaneous Geologic Investigations Map 454, scale 1:31,680, https://doi.org/10.3133/i454
Goudarzi, G.H., 1984, Guide to preparation of mineral survey reports on public lands: U. S. Geological Survey, Open-file Report 84-787, 50 p., http://pubs.usgs.gov/of/1984/0787/report.pdf
Gromet, L.P., Dymek, R.F., Haskin, L.A., Korotev, R.L., 1984, Geochinica et Cosmochimica Acta, v. 48, p. 2469-2482, PII: 0016-7037(84)90298-9
Harben, P., Austin, G., Hoffman, G., McLemore, V., Caledon, M., and Barker, J., 2008, Industrial Minerals, a Staple in the Economy of New Mexico: Colorado Geological Survey, Resource Series 46, p. 11-156.
Harrer, C.M., 1965, Iron; *in* Mineral and water resources of New Mexico: New Mexico Bureau of Mines and Mineral Resources, Bulletin 87, p. 176-183.
Hermassi, M., Granados, M., Valderrama, C., Ayora, C., Cortina, J.L., 2022, Recovery of rare earth elements from acidic mine waters: An unknown secondary resource. Science of The Total Environment, Vol. 810; https://doi.org/10.1016/j.scitotenv.2021.152258
Hoffman, G. K., 1996, Coal resources of New Mexico, New Mexico Bureau of Mines and Mineral Resources, Resource Map, v. 20, 22 p., 1 sheet, scale 1:1,000,000.
Hoffman, G.K., 2017, Coal, *in* McLemore, V.T., Timmons, S., and Wilks, M., eds., Energy and mineral resources of New Mexico: New Mexico Bureau of Geology and Mineral Resources Memoir 50B, and New Mexico Geological Society Special Publication 13B, 80 p.
Hoffman, G.K., Campbell, F.W., and Beaumont, E.C., 1993, Quality assessment of strippable coals in northwestern New Mexico: Fruitland, Menefee, and Crevasse Canyon Formation coals in San Juan Basin and Moreno Hill Formation coals in Salt Lake field: New Mexico Bureau of Mines and Mineral Resources Bulletin 141, 84 p.
Hoffman, G. and Hereford, J. 2009. Mining history of the Carthage coal field, Socorro County, New Mexico; *in* Lueth, V., Lucas, S.G., Chamberlin, R.M. eds., Geology of the Chupadera Mesa: New Mexico Geological Society, Guidebook 60, 407-414 p. https://doi.org/10.56577/FFC-60
Hoffman, G.K., Jones, G.E., 1998, Availability of coal resources in the Fruitland Formation, San Juan Basin, northwest New Mexico, New Mexico Bureau of Geology and Mineral Resources Open-File Report 438, p. 5.
Hoffman, G.K., and Jones, G.E., 2011, Coal Availability Study – Standing Rock Area, San Juan Basin Northwest New Mexico. New Mexico Bureau of Geology and Mineral Resources, Open-file Report 540, 31 p.
Holland, H.D., 1979, Metals in black shales-A reassessment: Economic Geology, v. 74, p. 1676–1680.
Houston, R.S. and Murphy, J.F., 1970, Fossil beach placers in sandstones of Late Cretaceous age in Wyoming and other Rocky Mountain states: Wyoming Geological Association, 22nd Guidebook, p. 241–249.
Houston, R.S. and Murphy, J.F., 1977, Depositional environment of Upper Cretaceous black sandstones of the western interior: U.S. Geological Survey, Professional Paper 994-A p. A1–A29.

Howard, E.V., 1967, Metalliferous occurrences in New Mexico: Phase 1, state resources development plan: State Planning Office, Santa Fe, 270 p.Hayes, T.S., Cox, D.P., Piatak, N.M., and Seal, R.R., II, 2015, Sediment-hosted, stratabound copper deposit model: U.S. Geological Survey Scientific Investigations Report 2010–5070–M, 147 p., https://doi.org/10.3133/sir20105070M

Hu, Z. and Gao, S., 2008, Upper crustal abundances of trace elements: a revision and update. Chemical Geology, v. 253, p. 205-221.

Huyck, H.L.O., 1990, When is a metalliferous black shale not a black shale? *in* R. Grauch and H.L.O. Huyck, eds., Metalliferous Black Shales and Related Ore Deposits-1988, Working Group Meeting of IGCP 254: U.S. Geological Survey Circular 1058, p. 42–56.

John, D.A., and Taylor, R.D., 2016, By-products of porphyry copper and molybdenum deposits: Reviews in Economic Geology, v. 18, p. 137–164.

Joshi, P.B., Preda, D.V., Skyler, D.A., Tsinberg, A., Green, B.D., and Marinelli, W.J., 2015, Recovery of Rare Earth Elements and Compounds from Coal Ash, U.S. Patent No. 8,968,688. Washington, DC: U.S. Patent and Trademark Office.

Kelley, S., Engler, T., Cather, M., Pokorny, C., Yang, C.-H., Mamer, E., Hoffman, G., Wilch, J., Johnson, P., and Zeigler, K., 2014, Hydrologic assessment of oil and gas resource development of the Mancos Shale in the San Juan Basin, New Mexico, New Mexico Bureau of Geology and Mineral Resources OFR-566, 65 pp.

Kelley, V.C., 1949, Geology and economics of New Mexico iron ore deposits: University of New Mexico, Publications in Geology, no. 2, 246 p.

Kendrick (1985), M.S. thesis, New Mexico Institute of Mining and Technology, Socorro,

Koch, G.S., Jr and Link, R.F., 1971, Statistical analysis of geological data: Dover Publications, Inc., New York, 438 p., ISBN 0-486-64040-X

Kowallis, B.J., Christiansen, E.H., Deino, A.L., Zhang, C. and Everett, B.H., 2001, The record of Middle Jurassic arc volcanism in the Carmel and Temple Cap formations of southwestern Utah: Geological Society of America Bulletin, v. 113, p. 373–387.

Lai, C.H., Chen, C.Y., Removal of metal ions and humic acid from water by iron-coated filter media, Chemosphere, Volume 44, Issue 5, 2001, Pages 1177-1184, ISSN 0045-6535, DOI: 10.1016/S0045-6535(00)00307-6.

Langman, J.B., Sprague, J.E., and Durall, R.A., 2012, Geologic framework, regional aquifer properties (1940s–2009), and spring, creek, and seep properties (2009–10) of the upper San Mateo Creek Basin near Mount Taylor, New Mexico: U.S. Geological Survey Scientific Investigations Report 2012–5019, 96 p.

LaPoint, D.J., 1979, Geology, geochemistry, and petrology of sandstone copper deposits in New Mexico [Ph.D. dissertation]: Boulder, University of Colorado, 333 p.

LaPoint, D.J., 1989, A model for the diagenetic formation of sandstone copper deposits in sedimentary rocks of Permian and Triassic age, in New Mexico, U.S.A., *in* Boyle, R.W., Brown, A.C., Jefferson, C.W., Jowett, E.C., and Kirkham, R.V., eds., Sediment-hosted stratiform copper deposits: Geological Association of Canada Special Paper 36, p. 357–370.

Lara, A., Rivera, E., Park, Y.H., Rivera, R., Fowler, T., and Jones, J., Natural clays with an inherent uranium component that nevertheless sequester uranium from contaminated water, Journal of Environmental Science and Health, Part A, 54:2, 101-109, DOI: 10.1080/10934529.2018.1530536, November, 2018

Large, R., 2012, Future potential for metal resources from black shales: Ni, Mo, Zn, Cu, U, V, Ag, Au, PGE: http://new.aig.org.au/wp-content/uploads/2012/12/Ross-Large-Future-Potential-for-Metal-Resources-from-Black-Shales.pdf

Lawton, T.F., and N.J. McMillan, 1999, Arc abandonment as a cause for passive continental rifting: Comparison of the Jurassic Mexican Borderland rift and the Cenozoic Rio Grande rift: Geology, v. 27, p. 779–782.

Le Maitre, R. W. (1989) A Classification of Igneous Rocks and Glossary of Terms. Recommendations of the IUGS Commission on the Systematics of Igneous Rocks. Oxford: Blackwell.

Lempke, J., Frey, B., Goehring, B., McLemore, V., 2023, Rare Earth Elements in Humates Mined in the San Juan Basin, Socorro, New Mexico. NMGS spring meeting abstract.

Leventhal, J.S., 1993, Metals in black shales, *in* Organic Geochemistry: Principles and applications, M.H. Engel and S.A. Macko, eds.: Plenum Press, New York, p. 581–583.

Leventhal, J.S. and Hosterman, J., 1982, Chemical and mineralogical analyses of Devonian black shale samples from Kentucky, Ohio, Virginia, and Tennessee: Chemical Geology, v. 37, p. 239–264.

Li, M.Y.H., Zhou, M.-F., and William-Jones, A.E., 2019, The genesis of regolith-hosted heavy rare earth element deposits: Insights from the world-class Zudong deposit in Jiangxi Province, South China: Economic Geology, v. 114, no. 3, p. 541–568, https://doi.org/10.5382/econgeo.4642

Li, Y., 2018, Preliminary geochemical evaluation of long-term leaching tests on uranium-bearing waste materials from the Grants Mining District in New Mexico: M.S. thesis, New Mexico Institute of Mining and Technology, Socorro, 202 p.

Li, X., van de Ven, J. J., Li, Z., and Binnemans, K. (2022). Separation of rare earths and transition metals using ionic-liquid-based aqueous biphasic systems. Industrial & Engineering Chemistry Research, 61(17), 5927-5935.

Lindgren, W., Graton, L.C., and Gordon, C.H., 1910, The ore deposits of New Mexico: U.S. Geological Survey Professional Paper 68, 361 p., https://doi.org/10.3133/pp68

Lottermoser, B. G. (2010). Acid Rock Drainage: Principles and Practice. *Springer,* Berlin, Heidelberg.

Loukola-Ruskeeniemi K., H. Arkimea, M.-L. Airo, S. Vuorianen, E. Hyvonen, J. Lerssi and J. Vanne, 2013, Genetic Model for the Talvivaara Ni-Cu-Zn-Co Deposit and Ore Potential of Black Shale Units in Finland, *in* E. Jonsson ed., Sveriges Geologiska Undersökning: Uppsala Mineral Deposits for a High-Tech World, p. 600–603.

Marsh, E.E., Hitzman, M.W., and Leach, D.L., 2016, Critical elements in sediment-hosted deposits (clastic-dominated Zn-Pb-Ag, Mississippi Valley-type Zn-Pb, sedimentary rock-hosted stratiform Cu, and carbonate-hosted polymetallic deposits): A review, *in* Verplanck, P.L., and Hitzman, M.W., Rare earth and critical elements in ore deposits: Reviews in Economic Geology, v. 18, https://doi.org/10.5382/Rev.18.12

McDonough, W.F. and Sun, S.S. (1995) The composition of the Earth. *Chemical Geology*. 120, 223-253.

McLemore, V. T., 1983, Uranium and thorium occurrences in New Mexico: distribution, geology, production, and resources; with selected bibliography: New Mexico Bureau of Mines and Mineral Resources, Open-file Report OF-182, 950 p., also U.S. Department of Energy Report GJBX-11(83).

McLemore, V.T., 1985, Evaluation of mineral-resource potential in New Mexico: New Mexico Geology, v. 7, no. 2, p. 50-53.
McLemore, V.T., 1989, Base and precious metal deposits in the Zuni Mountains, Cibola County, New Mexico, *in* Anderson, O.J., Lucas, S.G., Love, D.W., and Cather, S.M., Southeastern Colorado Plateau: New Mexico Geological Society Guidebook 40, p. 317–320, https://doi.org/10.56577/FFC-40.317
McLemore, V.T., 1993, Geology and geochemistry of the mineralization and alteration in the Steeple Rock district, Grant County, New Mexico and Greenlee County, Arizona: Ph.D. dissertation, University of Texas at El Paso; also New Mexico Bureau of Mines and Mineral Resources, Open File Report 397, 526 p. https://doi.org/10.58799/OFR-397
McLemore, V.T., 2007, Uranium resources in New Mexico. Society for Mining, Metallurgy, and Exploration Inc. (SME) preprint, 2007 annual meeting.
McLemore, V.T., 2010, Use of the New Mexico Mines Database in uranium reclamation studies: Society for Mining, Metallurgy and Exploration Transactions, 10 p., http://geoinfo.nmt.edu/staff/McLemore/documents/10-125. pdf.
McLemore, V.T., 2010a, Distribution, Origin, and Mineral Resource Potential of Late Cretaceous Heavy Mineral, Beach-Placer Sandstone Deposits, San Juan Basin, New Mexico: New Mexico Geological Society Guidebook 61, p. 197-212.
McLemore, V.T., 2010b, Use of the New Mexico Mines Database in Uranium Reclamation Studies: Society of Mining, Metallurgy and Exploration Transactions, v. 328.
McLemore, V.T., Hill, B., Khalsa, N., and Lucas Kamat, S.A., 2013, Uranium resources in the Grants uranium district, New Mexico: An update. New Mexico Geological Society Guidebook, 64th Field Conference.
McLemore, V.T., 2013, Geology and mineral resources in the Zuni Mountains mining district, Cibola County, New Mexico: Revisited, *in* Zeigler, K., Timmons, J.M., Timmons, S., and Semken, S., eds., Geology of Route 66 Region: Flagstaff to Grants: New Mexico Geological Society Guidebook 64, p. 131–142, https://doi.org/10.56577/FFC-64.131
McLemore, V.T., 2017, Mining districts and prospect areas of New Mexico: New Mexico Bureau of Geology and Mineral Resources, Resource Map 24, 65 p., scale 1:1,000,000, https://doi.org/10.58799/RM-24 (accessed 31 January 2025).
McLemore, V.T., 2017, Heavy mineral, beach-placer sandstone deposits at Apache Mesa, Jicarilla Apache Reservation, Rio Arriba County, New Mexico; *in* The Geology of the Ouray-Silverton Area, Karlstrom, K.E., Gonzales, D.A., Zimmerer, M.J., Heizler, M., and Ulmer-Scholle, D.S.: New Mexico Geological Society 68th Annual Fall Field Conference Guidebook, p.. 123-132.
McLemore, V.T., 2018a, Mineral-Resource Potential of proposed U.S. Bureau of Land Management exchange of lands with New Mexico State Land Office: New Mexico Bureau of Geology and Mineral Resources, Open-file Report OF-598, 152 p., https://geoinfo.nmt.edu/publications/openfile/details.cfml?Volume=598
McLemore, V.T., 2018b, Mineral-Resource Potential of Sabinoso Wilderness Area and Rio Grande Del Norte National Monument in Northeastern New Mexico: New Mexico Bureau of Geology and Mineral Resources, Open-file Report OF 599, 55 p., https://geoinfo.nmt.edu/publications/openfile/details.cfml?Volume=599
McLemore, V.T., 2019, Critical minerals in New Mexico: SME Annual Meeting, Preprint 19-132, 6 p., https://geoinfo.nmt.edu/staff/McLemore/projects/documents/19_132.pdf

McLemore, V.T., 2020, Critical minerals in New Mexico; work needed to realize resources: Mining Engineering, v. 72, no. 2, pp. 31-31, https://me.smenet.org/abstract.cfm?preview=1&articleID=9501&page=31

McLemore, V.T., 2020, Uranium Resources in New Mexico. New Mexico Bureau of Geology & Mining Resources, https://geoinfo.nmt.edu/resources/uranium/nmresources.html accessed 2023-09-15

McLemore, V.T., 2025, Critical minerals in the Cuba manganese deposits, Cuba Manganese mining district, Sandoval County, New Mexico: New Mexico Geological Society Guidebook 72, p. 221-226, https://doi.org/10.56577/FFC-75.221

McLemore, V.T., Asafo-Akowuah, J. and Robison, A., 2016, Assessment of Rare Earth Elements at Apache Mesa (Stinking Lake), Jicarilla Apache Reservation, Rio Arriba County, New Mexico: Final report to Jicarilla Indian Tribe, NMBG Open-file report 587, http://geoinfo.nmt.edu/publications/openfile/details.cfml?Volume=587 .

McLemore, V.T. and Austin, G.S., 2016, Industrial minerals and rocks, in McLemore, V.T., Timmons, S., and Wilks, M., eds., Energy and Mineral Resources of New Mexico: New Mexico Bureau of Geology and Mineral Resources, Memoir 50E, and New Mexico Geological Society, Special Publication 13E. 128 p.

McLemore, V.T. and Chenoweth, W.L., 1989, U resources in New Mexico: New Mexico Bureau of Mines and Minerals Resources, Resource Map 18, 36 p.

McLemore, V.T. and Chenoweth, W.C., 2017, Uranium resources; *in* McLemore, V.T., Timmons, S., and Wilks, M., eds., Energy and Mineral deposits in New Mexico: New Mexico Bureau of Geology and Mineral Resources Memoir 50 and New Mexico Geological Society Special Publication 13, 80 p.

McLemore, V.T., Wilton, T., and Pelizza, M.S., 2016, In situ recovery of sandstone-hosted uranium deposits in New Mexico: past, present, and future issues and potential. New Mexico Geology, 38(4), 68-76.

McLemore, V.T., and Chenoweth, W.L., 2017, Uranium Resources, In McLemore, V.T., Timmons, S., and Wilks M., (Eds.), Energy and Mineral Resources of New Mexico*:* New Mexico Bureau of Geology and Mineral Resources, and New Mexico Geological Society, Special Publication 13C, Memoir 50C, p. 1-80.

McLemore, V. T., Donahue, K., Krueger, C. B., Rowe, A., Ulbricht, L., Jackson, M. J., Breese, M. R., Jones, G., and Wilks, M., 2002, Database of the uranium mines, prospects, occurrences, and mills in New Mexico: New Mexico Bureau of Geology and Mineral Resources, Open file Report 461, CD-ROM, http://geoinfo.nmt.edu/publications/openfile/details.cfml?Volume=461

McLemore, V.T., Frey, B., Trivitt, A., Owen, E.J., Motlagh, Z.K., Best, M.B., Jones, D.S., Kelley, R., Acheampong-Mensah, A.S., Leo-Russell, M., Sarpong, L., Nipah, S., Otoo, R., Regier, C., Lamery, A., and Badonie, M., 2025a, Geochemistry of critical minerals in mine wastes in the Hillsboro, Black Hawk, and Steeple Rock mining districts, southwestern New Mexico: New Mexico Bureau of Geology and Mineral Resources Open-file Report OF-639, https://geoinfo.nmt.edu/publications/openfile/details.cfml?Volume=639

McLemore, V.T. and Gysi, A., 2023, Critical minerals in New Mexico: Earth Matters, winter 2023, https://geoinfo.nmt.edu/publications/periodicals/earthmatters/23/n1/em_v23_n1.pdf

McLemore, V.T. and Lueth, V., 2017, Metallic Mineral Deposits; *in* McLemore, V.T., Timmons, S., and Wilks, M., eds., Energy and Mineral deposits in New Mexico: New Mexico Bureau of Geology and Mineral Resources Memoir 50 and New Mexico Geological Society Special Publication 13, 92 p.

McLemore, V.T. and Owen, E.J., 2024, Geochemistry of critical minerals in mine wastes in New Mexico: Mining Engineering, v. 24, p. 23–30.

McLemore, V.T., 2025, Critical minerals in the Cuba manganese deposits, Cuba Manganese mining district, Sandoval County, New Mexico: New Mexico Geological Society Guidebook 72, p. 227-234, https://doi.org/10.56577/FFC-75.227.

McLemore, V.T., and Hoffman, G., 2017, Mineral-resource potential in New Mexico: report for the State Land Office, 110 p.

McLemore, V.T., Hoffman, G., Smith, M., Mansell, M., and Wilks, M., 2005a, Mining districts of New Mexico: New Mexico Bureau of Mines and Mineral Resources, OF-494, CD-ROM.

McLemore, V.T., Krueger, C.B., Johnson, P., Raugust, J.S., Jones, G.E., Hoffman, G.K. and Wilks, M., 2005b, New Mexico Mines Database: Mining Engineering, February, p. 42-47.

McLemore, V.T., Roybal, G.H., Broadhead, R.F., Chamberlin, R.M., North, R.M., Osburn, J.C., Arkell, B.W., Colpitts, R.M., Bowie, M.R., Anderson, K., Barkers, J.M., and Campbell, F.W., 1984, Preliminary report on the geology and mineral-resource potential of the northern Rio Puerco Resource Area in Sandoval and Bernalillo Counties and adjacent part of McKinley, Cibola, and Santa Fe, Counties, New Mexico: New Mexico Bureau of Mines and Mineral Resources, Open-file Report OF-211, 817 p. https://doi.org/10.58799/OFR-211

McLemore, V.T., Broadhead, R.F., Barker, J.M., Austin, G.S., Klein, K., Brown, K.B., Murray, D., Bowie, M.R., and Hingtgen, J.S., 1986, A preliminary mineral-resource potential of Cibola County, northwestern New Mexico: New Mexico Bureau of Mines and Mineral Resources Open-file Report 230, 403 p.

McLemore, V.T., Smith, K.S., Russell, C.C., editors, 2014, Management Technologies for Metal Mining Influenced Water, volume 6: Sampling and monitoring for the mine life cycle: Society for Mining, Metallurgy, and Exploration, Inc., Littleton, CO.

McLemore, V.T., Timmons, S., and Wilks, M., eds., 2017, Energy and Mineral deposits in New Mexico: New Mexico Bureau of Geology and Mineral Resources, Memoir 50 and New Mexico Geological Society, Special Publication 13, 6 volumes.

McLemore, V.T., and Lueth, V., 2017, Metallic mineral deposits, *in* McLemore, V.T., Timmons, S., and Wilks, M., eds., Energy and Mineral Resources of New Mexico: New Mexico Bureau of Geology and Mineral Resources Memoir 50D / New Mexico Geological Society Special Publication 13, 92 p., https://geoinfo.nmt.edu/publications/monographs/memoirs/50/D/home.cfm

McLemore, V.T., Owen, E.J., and Newcomer, J., 2024, Critical minerals in sediment-hosted, stratabound copper deposits in the Nacimiento and Zuni Mountains, northwestern New Mexico: Preliminary results: New Mexico Geological Society Guidebook 72, p. 147-164, nmgs.nmt.edu/publications/guidebooks/downloads/74/74_p0307_p0317.pdf.

McLemore, V.T., Owen, E., Badonie, M., Shaver, D., and Newcomer, J., 2024a, Rare earth elements (REE) and other critical minerals in Late Cretaceous Coal and related strata in the San Juan and Raton Basins, New Mexico: Preliminary Observations: Society of

Mining, Metallurgy and Exploration, Inc., Annual Conference, Preprint 24-78, 10 p. https://geoinfo.nmt.edu/geoscience/research/documents/145/McLemore%20et%20al%20REE%20and%20other%20CMs%20in%20Late%20Cretaceous%20coal%20and%20related%20strata%20in%20San%20Juan%20and%20Raton%20Basins%20NM%20SME%202024%20preprint.pdf, accessed April 23, 2025.

McLemore, V.T. and Owen, E.J., 2025, Critical minerals in Late Cretaceous coal beds of the San Juan Basin, New Mexico New Mexico Geological Society Guidebook 72, 227-234, https://doi.org/10.56577/FFC-75.227.

McLemore, V.T., Owen, E.J., and Newcomer, J., 2024b, Critical minerals in sediment-hosted, stratabound copper deposits in the Nacimiento and Zuni Mountains, northwestern New Mexico—Preliminary results: New Mexico Geological Society, Guidebook 72, p. 147–164. nmgs.nmt.edu/publications/guidebooks/downloads/74/74_p0307_p0317.pdf, accessed April 23, 2025

Migdisov, A.A., Williams-Jones, A.E., and Wagner, T., 2009, An experimental study of the solubility and speciation of the Rare Earth Elements (III) in fluoride- and chloride-bearing aqueous solutions at temperatures up to 300°C: Geochimica et Cosmochimica Acta, v. 73, p. 7087–7109, doi:10.1016/j.gca.2009.08.023.

Migdisov, A.A., and Williams-Jones, A.E., 2014, Hydrothermal transport and deposition of the rare earth elements by fluorine-bearing aqueous liquids: Mineralium Deposita, v. 49, p. 987–997, doi:10.1007/s00126-014-0554-z.

Migdisov, A., Guo, X., Nisbet, H., Xu, H., and Williams-Jones, A.E., 2019, Fractionation of REE, U, and Th in natural ore-forming hydrothermal systems: Thermodynamic modeling: The Journal of Chemical Thermodynamics, v. 128, p. 305–319, doi:10.1016/j.jct.2018.08.032.

Motlagh, Z.K. and McLemore, V.T., 2025, Geochemistry of critical minerals in mine waste in Grant, Sierra, and Socorro Counties, New Mexico: SME preprint 25-039, 9 p.

Munroe, E. A., 1999, Geology and geochemistry of waste rock piles in the Hillsboro mining district, Sierra County, New Mexico: M.S. thesis, New Mexico Institute of Mining and Technology, Socorro, 144 p.

Murphy, E., Moxness, L., and Kruger, N., 2023, Elevated critical mineral concentrations associated with the Paleocene-Eocene thermal maximum, Golden Valley Formation, North Dakota: North Dakota Geological Survey Report of Investigation RI-133, https://www.dmr.nd.gov/dmr/sites/www/files/documents/Survey/RI133/RI-133%20Elevated%20Critical%20Mineral%20Concentrations%20Associated%20with%20the%20Paleocene-Eocene%20Thermal%20Maximum%2C%20Golden%20Valley%20Formation%2C%20North%20Dakota.pdf

Nakamura, N., 1974, Determination of REE, Ba, Fe, Mg, Na, and K in carbonaceous and ordinary chondrites: Geochimica et Cosmochimica Acta, v. 38, p. 757–775.

Neuendorf, K.K.E., Mehl, J.P., Jr., and Jackson, J.A., 2005, Glossary of Geology (5th ed.). American Geological Institute.

Newcomer, R.W., Nybo, J.P. and Newcomer, J.R., 2021, Humate in the Upper Cretaceous Fruitland Formation in northwestern New Mexico, *in:* New Mexico Geological Society, 71st Annual Fall Field Conference, September 2021, Geology of Mount Taylor, Frey, Bonnie A.; Kelley, Shari A.; Zeigler, Kate E.; McLemore, Virginia T.; Goff, Fraser;

Ulmer-Scholle, Dana S., New Mexico Geological Society, Guidebook, p. 153-158. https://doi.org/10.56577/FFC-71.153

New Mexico Energy, Minerals and Natural Resources Department, 1986-2025, Annual Resources Report: New Mexico Energy, Minerals and Natural Resources Department, Santa Fe, various paginated, http://www.emnrd.state.nm.us/ADMIN/publications.html

New Mexico Energy, Minerals and Natural Resource Department, 2024, 2023 Annual Report New Mexico Mining Act Reclamation Program: Report to the New Mexico Mining Commission, 15 p. https://www.emnrd.nm.gov/officeofsecretary/wp-content/uploads/sites/2/emmrd_annual_report_2024.pdf, accessed April 23, 2025

Newton, B.T., 2004, Geologic Controls on Shallow Groundwater Quality in the Socorro Basin, New Mexico [Master's Thesis]: New Mexico Institute of Mining and Technology, 163 p.

North, R.M., and McLemore, V.T., 1986, Silver and gold occurrences in New Mexico: New Mexico Bureau of Mines and Mineral Resources Resource Map 15, 32 p., scale 1:1,000,000.

Osburn, J.C., 1983, Coal resources of Socorro County, New Mexico. In C.E. Chapin & J.F. Callender (Eds.), Socorro Region II (pp. 223-226). New Mexico Geological Society 34th Annual Fall Field Conference Guidebook. https://nmgs.nmt.edu/publications/guidebooks/downloads/34/34_p0223_p0226.pdf

Ottea, J.M., and Uhl, B.H., 2020, Copper-mineralized fossil wood from the Nacimiento mining district, Sandoval County, New Mexico: Rocks and Minerals, v. 95, no. 6, p. 548–554, https://doi.org/10.1080/00357529.2020.1791629

Otoo, R. McLemore, V.T., and Owen, E.J., 2025, Minimum concentrations of critical minerals for exploration—how good is good enough: SME preprint 25-058, 5 p.

Otoo, R. McLemore, V.T., and Owen, E.J., 2025, Minimum concentrations of critical minerals for exploration—how good is good enough: Mining Engineering, v. 77, no. 8, p. 20-25.

Owen and McLemore, 2024 Mineralogy and Geochemistry off Heavy Mineral Beach-Placer Sandstones in New Mexico. SME pre-print.

Park, D. et al., "A biosorption-based approach for selective extraction of rare earth elements from coal byproducts," Sep. Purif. Technol., vol. 241, p. 116726, Jun. 2020, doi: 10.1016/j.seppur.2020.116726.

Pearce, A.R., 2020, Implications of cryptic, nonstoichiometric uranium mineralization on the formation and leachability of sandstone-hosted uranium ores, Grants district, New Mexico: Ph.D. dissertation, New Mexico Institute of Mining and Technology, Socorro, 201 p.

Phillips, J.S., 1960, Sandstone-type copper deposits of the western United States [Ph.D. dissertation]: Cambridge, Harvard University, 320 p.

Quinby-Hunt, M.S., Wilde, P., Orth, C.J. and Berry, W.B.N., 1989, elemental geochemistry of black shales-statistical comparison of low-calcic with other shales, in Metalliferous Black Shales and Related Ore Deposits-Program and Abstracts, R. Grauch and J.S. Leventhal eds.: U.S. Geological Survey Circular 1037, p. 8–15.

Quirico, E., Rouzaud, J.N., Bonal, L., and Montagnac, G., 2005, Maturation grade of coals as revealed by Raman spectroscopy: Progress and problems: Spectrochimica Acta Part A: Molecular and Biomolecular Spectroscopy, v. 61, p. 2368-2377, https://doi.org/10.1016/j.saa.2005.02.015

Rigali, M.J. and Krumhansl, J.L., 2019, Metals in oil and gas-bearing shales: Are they potential (future) ore deposits? *in* Dewers, T., Heath, J., and Marcelo Sánchez M., eds., Shale:

Subsurface Science and Engineering. American Geophysical Union, p. 59-67. https://agupubs.onlinelibrary.wiley.com/doi/chapter-epub/10.1002/9781119066699.ch4
Rollinson, H.R., 1993, Using geochemical data: evaluation, presentation, interpretation: Longman Scientific and Technical, John Wiley and Sons, New York, 352 p.
Rudnick, R.L. and Gao, S., 2003, The Composition of the Continental Crust, in Holland, H.D. and Turekian, K.K., Eds., Treatise on Geochemistry, v. 3, The Crust, Elsevier-Pergamon, Oxford, 65 p., https://doi.org/10.1016/B978-0-08-095975-7.00301-6
Sachan, A., 2019, Enhanced Bioweathering of Coal for Rare Earth Element Extraction and Concentration," M.S., University of Alaska Fairbanks, https://scholarworks.alaska.edu/bitstream/handle/11122/10536/Sachan_A_2019.pdf?sequence=1&isAllowed=y
Saehwa, C., and Riley, B.J., 2022. Thermal conversion in air of rare-earth fluorides to rare-earth oxyfluorides and rare-earth oxides. Journal of Nuclear Materials, 561, 153538, doi.org/10.1016/j.jnucmat.2022.153538.
Schrader, F.C., 1906, Copper deposits of the Zuni Mountains, New Mexico: Science, v. 23, p. 916.
Schulz, K.J., DeYoung, J.H., Jr., Seal, R.R., II, and Bradley, D.C., eds., 2017, Critical mineral resources of the United States—Economic and environmental geology and prospects for future supply: U.S. Geological Survey Professional Paper 1802, 797 p., http://doi.org/10.3133/pp1802.
Scott, C. and Kolker, A., 2019, Rare earth elements in coal and coal fly ash: U.S. Geological Survey Fact Sheet, 4 p., https://doi.org/10.3133/fs20193048
Shomaker, J.W., Beaumont, E.C., and Kottlowski, F.E., 1971, Strippable low-sulfur coal resources of the San Juan Basin in New Mexico and Colorado. New Mexico Bureau of Mines and Mineral Resources Memoir 25
SEC Technical Report Summary, 2023, Pre-Feasibility Study - Greenbushes Mine, Western Australia.
Smith, K.S. 2007. Strategies to predict metal mobility in surficial mining environments, J.V. DeGraff, editor, Understanding and Responding to Hazardous Substances at Mine Sites in the Western United States: Ch. 3. Reviews in Engineering Geology, Vol. 17, Boulder, CO, Geological Society of America. p. 25–45.
Smith, K.S., Huyck, H.L.O. 1999. An overview of the abundance, relative mobility, bioavailability, and human toxicity of metals, *in* The Environmental Geochemistry of Mineral Deposits. Part A, Vol. 6A, Chapter 2, Plumlee, G., Logsdon, M., eds., Reviews in Economic Geology: Society of Economic Geologists, Inc., Chelsea, MI. p. 29-70.
Smith, K.S., Ramsey, C.A., and Hageman, P.L., 2000, Statistically-based sampling strategy for sampling the surface material of mine-waste dumps for use in screening and prioritizing historical dumps on abandoned mines lands; *in* ICARD 2000; Proceedings from the 5th international conference on acid rock drainage: Society for Mining, Metallurgy, and Exploration, Inc., Littleton, Colo., p. 1453-1461. http://crustal.usgs.gov/minewaste/minewaste.pubs.html
Smith, L.N. and Lucas, S.G., 1991, Stratigraphy, sedimentology, and paleontology of the lower Eocene San Jose Formation in the central portion of the San Juan Basin, northwestern New Mexico: New Mexico Bureau of Mines and Mineral Resources, Bulletin 126, 49 p. https://doi.org/10.58799/B-126

Snyder, G.T., Riese, W.C., Franks, S., Fehn, U., Pelzmann, W.L., Gorody, A.W., and Moran, J.E., 2003, Origin and history of waters associated with coalbed methane:129I, 36Cl, and stable isotope results from the Fruitland Formation, Colorado and New Mexico: Geochimica et Cosmochimica Acta, v. 67, no. 23, p. 4529–4544.

Sonke, JE., (2006) Lanthanide−Humic Substances Complexation. II. Calibration of Humic Ion-Binding Model V. Environ. Sci. Technol. v. 40, p.7481-7487.

Soulé, J.H., 1956, Reconnaissance of the "red bed" copper deposits in southeastern Colorado and New Mexico: U.S. Bureau of Mines Information Circular 7740, 74 p.

Standard Methods: Clesceri, L.S., Rice, E.W., Greenberg, A.E., eds., 2005, Standard Methods for the Examination of Water & Wastewater, 21st (Centennial) Edition, American Public Health Association, American Water Works Association, Water Environment Federation, ISBN: 0-87553-047-8.

Strzelecki, A.C., Migdisov, A., Boukhalfa, H., Sauer, K., McIntosh, K.G., Currier, R.P., Williams-Jones, A.E., and Guo, X., 2022, Fluocerite as a precursor to rare earth element fractionation in ore-forming systems: Nature Geoscience, v. 15, p. 327–333, doi:10.1038/s41561-022-00921-6.

Tabet, D.E., 1979, Geology of Jornada del Muerto coal field, Socorro County, New Mexico. New Mexico Bureau of Mines and Mineral Resources, Circular 168. https://geoinfo.nmt.edu/publications/monographs/circulars/downloads/168/Circular_168.pdf

Tabet et al., 1995, https://ugspub.nr.utah.gov/publications/reports_of_investigations/RI-225.pdf

Takaya, Y., Yasukawa, K., Kawasaki, T. et al., 2018, The tremendous potential of deep-sea mud as a source of rare-earth elements: Nature Sci Rep 8, p. 5763 https://doi.org/10.1038/s41598-018-23948-5

Talbott, L.W., 1974, Nacimiento pit: A Triassic strata-bound copper deposit, *in* Siemers, C.T., Woodward, L.A., and Callender, J.F., eds., Ghost Ranch: New Mexico Geological Society Guidebook 25, p. 301–303, https://doi.org/10.56577/FFC-25.301

Tan, K.H., Humic Matter in Soil and the Environment: Principles and Controversies, 2014, CRC Press, Boca Raton, FL, 2014, ISBN: 9781482234459

Taylor, S.R., and McLennan, S.M., 1985, The Continental Crust—Its Composition and Evolution: Oxford, Blackwell Science Publishers, 312 p.

Thomsen, M., 2024, Rare earth elements in seafloor metal precipitate deposits from nodules, crusts and pelagic sediments with modern versus paleo examples as potential new sources of world-class critical mineral ore bodies: (99+) Rare Earth Elements in Seafloor Metal Precipitate Deposits from Nodules, Crusts and Pelagic Sediments with Modern Versus Paleo Examples as Potential New Sources of World-Class Critical Mineral Ore Bodies

Tsosie, R., Addressing Long-Standing Water Contamination Issues in Dine Communities using Indigenous and Western Scientific Approaches, University of Montana - Missoula, July 2020

U.S Department of Energy - Office of Nuclear Energy, Nuclear Fuel Facts: Uranium., Office of Nuclear Energy. https://www.energy.gov/ne/nuclear-fuel-facts-uranium#:~:text=Uranium%20was%20discovered%20in%201789,uran%E2%80%9D%20after%20the%20planet%20Uranus . (accessed 2023-10-31).

U.S. Executive Order No. 13,817, 2017, Presidential executive order on a federal strategy to ensure secure and reliable supplies of critical minerals:

https://www.whitehouse.gov/presidential-actions/presidential-executiveorder-federal-strategy-ensure-secure-reliable-supplies-critical-minerals/.
U.S. Bureau of Mines, 1927-1990, Minerals Yearbook: Washington, D.C., U.S. Government Printing Office, variously paginated.
U.S. Geological Survey, 1902-1927, Mineral resources of the United States (1901-1923): Washington, D.C., U.S. Government Printing Office, variously paginated.
U.S. Geological Survey, 1965, Mineral and water resources of New Mexico: New Mexico Bureau of Mines and Mineral Resources, Bulletin 87, 437 p.
U.S. Geological Survey, 2025, Mineral commodity summaries 2025: https://pubs.usgs.gov/periodicals/mcs2025/mcs2025.pdf.
U.S. Geological Survey National Produced Waters Geochemical Database v 2.3, 2019.
Verplanck, P.L., Van Gosen, B.S., Seal, R.R, and McCafferty, A.E., 2014, A deposit model for carbonatite and peralkaline intrusion-related rare earth element deposits: U.S. Geological Survey Scientific Investigations Report 2010–5070-J, 58 p. https://doi.org/10.3133/sir20105070J
Water Quality Portal (WQP), 2021, Washington (DC): National Water Quality Monitoring Council, United States Geological Survey (USGS), Environmental Protection Agency (EPA). https://doi.org/10.5066/P9QRKUVJ.
Wellmer, F.W., 1989, Statistical evaluations in exploration for mineral deposits: Springer-Verlag, New York, 379 p., ISBN 3-540-61242-4
Winston, R.B., 2000, Graphical User Interface for MODFLOW, Version 4: U.S. Geological Survey Open-File Report 00-315, 27 p., https://doi.org/10.3133/ofr00315EPA data resource
Woodward, L.A., 1987, Geology and mineral resources of Sierra Nacimiento and vicinity, New Mexico: New Mexico Bureau of Mines and Mineral Resources Memoir 42, 86 p., https://doi.org/10.58799/M-42
Woodward, L.A., Kaufman, W.H., Schumacher, O.L., and Talbott, L.W., 1974, Strata-bound copper deposits in Triassic sandstone of Sierra Nacimiento, New Mexico: Economic Geology, v. 69, p. 108–120, https://doi.org/10.2113/gsecongeo.69.1.108
World Nuclear Association, What is Uranium? How does it Work? World Nuclear Association. https://world-nuclear.org/information-library/nuclear-fuel-cycle/introduction/what-is-uranium-how-does-it-work.aspx (accessed 2023-09-25)

APPENDIX 1. ACRONYMS, CONVERSIONS, AND GLOSSARY

Acronyms

ARD	Acid rock drainage
AML	Abandoned Mine Lands
AMLB	Abandoned Mine Lands Bureau
BLM	U.S. Bureau of Land Management
BSE	Backscattered electron imaging
Earth MRI	Earth Mineral Resources Initiative
EO	Presidential Executive Order
GeMS	Geologic Map Schema
ICP-MS	Inductively coupled plasma mass spectrometry
MRDS	Mineral Resource Data System
MILS	Minerals Industry Location System
SQLS	MS SQL Server
NMBGMR	New Mexico Bureau of Geology and Mineral Resources
NMGRL	New Mexico Geochronology Research Laboratory
NMGS	New Mexico Geological Society
NMSHD	New Mexico State Highway Department
NMT	New Mexico Tech (New Mexico Institute of Mining and Technology)
PI	Principal investigator
QA/QC	Quality assurance and quality control
REE	Rare earth elements
REEY	Rare earth elements and Y
USBM	U.S. Bureau of Mines
USGS	U.S. Geological Survey
VAG	Volcanic arc granite
WAG	Within plate granite
WDS	Wavelength dispersive spectroscopy
XRD	X-ray diffraction
XRF	X-ray fluorescence

Conversions

1 ounce (troy) = 31.1034768 grams.
1 troy ounce per short ton = 34.2857 ppm = 34.2857 grams per metric tonne
1 gram per metric tonne = 0.0292 troy ounces per short ton
1 kilogram (kg) = 32.151 ounces (troy) =2.205 pounds
1 ounce (avoirdupois) = 28.3495 grams
1 inch (in) = 2.54 centimeters
1 foot (ft) = 0.3048 meters
1 cubic foot (cu ft) = 0.028 cubic meters
1 yard (yd) = 91.44 centimeters =0,9144 meters
1 meter (m) = 39.370 inches =3.28083 feet =1.094 yards

1 mile (mi) = 1.6093 kilometers =1609.3 meters
1 kilometer (km) = 0.621371 miles =3280 feet =1000 meter
1 acre (ac) = 0.4047 hectares
1 hectare (ha) = 2.471 acres =10,000 square meters =0.00386 square miles
1 square kilometer (sq km) = 247.1 acres =100 hectares =0.3861 square miles
1 square mile (sq mi) = 640 acres =258.99 hectares =2.59 square kilometers
1 liter (l) = 0.220 gallons =0.880 quarts
1 liter (l) = 1000 cubic centimeters =61.025 cubic inches
1 kilogram (kg) = 2.2045855 pounds
1 metric ton (1000 kg)= 0.9842 long tons =1.102311 short tons =2204.622 pounds
1 long ton (l t) = 1.01605 tonne =2240 pounds (lb)
1 short ton (s t) = 0.90718474 tonne =2000 pounds (lb)
1 pound (lb) = 0.45359237 kilograms
Degrees Fahrenheit (°F) - 32x5/9 = Degrees Celsius (°C)

APPENDIX 2. PROJECT PUBLICATIONS, THESES, AND PRESENTATIONS

Badonie, M.N. and McLemore, V.T., 2022, REE in coalbeds in the San Juan-Raton coal basins (abstr.): New Mexico Geological Society, Spring Meeting, https://nmgs.nmt.edu/meeting/abstracts/view.cfm?aid=2838. Poster at https://geoinfo.nmt.edu/staff/McLemore/documents/NMSG.Poster2022COPY2.pdf.

Badonie, M.N. and McLemore, V.T., 2023, Rare earth elements and critical minerals in coal and related strata in the San Juan Basin in northern New Mexico (abstr.): New Mexico Geological Society, Spring meeting, https://nmgs.nmt.edu/meeting/abstracts/view.cfm?aid=2939

Badonie, M., Newcomer, J., Shaver, S., and McLemore, V.T., 2023, REE in coal and associated strata in the San Juan and Raton Basins, New Mexico: Minexchange, 2023 SME Annual Conference Technical Program, preprint 23-055, 5 p., https://geoinfo.nmt.edu/staff/McLemore/documents/23-055.pdf

Byrd, Aurora K., McLemore, Virginia T., and Kazemi Motlagh, Zohreh, 2025, Critical Minerals Potential of Late Cretaceous Heavy Mineral Beach-Placer Sandstone Deposits of Northern New Mexico (abstr.): Geological Society of America, Annual Conference

Detsoia, B., Frey, B., McLemore, V., Jones, J., and Tsosie, R., 2024, Humates Used as a Filtering Medium for Uranium: SME Annual Conference, poster

Detsoi, Brianna, 2024, Humate used as a filtration Medium for Uranium, Senior Thesis, B.S. Chemistry, New Mexico Institute of Mining and Technology, 12 p.

Essary, J., McLemore, V., and Fuierer, P., 2024, Extracting Aluminum Oxide From Kaolinite (abstr.): New Mexico Geological Society Spring Meeting, April

Essary, J., Fuierer, P., and McLemore, V.T., 2024, Extraction of aluminum: Lite Geology, v. 54, p. 2-3.

Essary, J., 2025, Extraction of alumina from mineral resources found at New Mexico mine sites (M.S. thesis): New Mexico Institute of Mining and Technology, Socorro

Fire, S., Robledo, V., and McLemore, V.T., 2024, Stratigraphic Analysis for Correlativity of Geophysical and Geochemical Properties With Lithology: Rare Earth Element Occurrence in the Late Cretaceous Fruitland Formation (abstr.): New Mexico Geological Society Spring Meeting, April

Leo-Russell, M.R. and McLemore, V.T., 2023, A review of lithium as a critical industrial material and engagement prospects in New Mexico (abstr.), New Mexico Geological Society, Spring meeting, https://nmgs.nmt.edu/meeting/abstracts/view.cfm?aid=2926

Lempke, J.J., Frey, B., and McLemore, V., 2024, Rare earth elements and major constituents in surface water from Lee Ranch Mine (abstr.): New Mexico Geological Society Spring Meeting, April

Lempke, J., Frey, B., Goehring, B., and McLemore, V.T., 2023, Rare earth elements in humates mined in the San Juan Basin (abstr.): New Mexico Geological Society, Spring meeting, abstract https://nmgs.nmt.edu/meeting/abstracts/view.cfm?aid=2954 presentation https://nmgs.nmt.edu/meeting/presentations/2023/2926/NMGS-Presentation-Lithium_LeoRussell-McLemore_1.pdf

Lempke, J., Frey, B., Goehring, B., and McLemore, V.T., 2023, Rare earth elements in humates mined in the San Juan Basin (abstr.): New Mexico Geological Society, Spring meeting, https://nmgs.nmt.edu/meeting/abstracts/view.cfm?aid=2954

McLemore, V.T., 2020, Critical minerals in New Mexico; work needed to realize resources: Mining Engineering, v. 72, no. 2, pp. 31-31, https://me.smenet.org/abstract.cfm?preview=1&articleID=9501&page=31
McLemore, V.T., 2022, Rare Earth Elements (REE) in Late Cretaceous coal and beach-placer sandstone deposits in the San Juan Basin, New Mexico: Preliminary Observations (abstr.): Geological Society of America, Annual Conference, October, https://gsa.confex.com/gsa/2022AM/meetingapp.cgi/Paper/378264, presentation https://geoinfo.nmt.edu/staff/McLemore/documents/McLemoreGSA22Wed10-12-22.pdf
McLemore, V.T., 2022, Rare earth elements (REE) in Late Cretaceous coal and beach-placer sandstone deposits in the San Juan Basin, New Mexico: Preliminary results: presentation at the DOE National Energy Technology Laboratory Resource Sustainability Project Review Meeting, Oct. 25-27, 2022 https://geoinfo.nmt.edu/staff/McLemore/documents/McLemoreDOE22Tues10-25-22.pdf
McLemore, V.T., 2023, Critical minerals in New Mexico, (abstr.), New Mexico Geological Society, Spring meeting, https://nmgs.nmt.edu/meeting/abstracts/view.cfm?aid=2892\
McLemore, V.T., 2023, Rare Earth Elements and Critical Minerals in Late Cretaceous Coal and Related Strata in the San Juan and Raton Basins, New Mexico: Lite Geology, v. 51, https://geoinfo.nmt.edu/publications/periodicals/litegeology/51/lg_v51.pdf
McLemore, V.T., 2023, Industrial minerals in the San Juan Basin, New Mexico: Forum on the Geology of Industrial Minerals, presentation, https://geoinfo.nmt.edu/staff/McLemore/documents/fgim23-ppt_sm.pdf
McLemore, V.T., 2025, Critical minerals in the Cuba manganese deposits, Cuba Manganese mining district, Sandoval County, New Mexico: New Mexico Geological Society Guidebook 72, p. 221-226, https://doi.org/10.56577/FFC-75.221
McLemore, V.T., 2025, How do critical minerals (elements) occur in nature? Lite Geology, v. 56, p. 8-11, https://geoinfo.nmt.edu/publications/periodicals/litegeology/56/lg_v56.pdf
McLemore, V.T. and Gysi, A., 2023, Critical minerals in New Mexico: Earth Matters, winter 2023, https://geoinfo.nmt.edu/publications/periodicals/earthmatters/23/n1/em_v23_n1.pdf
McLemore, V., Owen, E., Badonie, M., Shaver, D., and Newcomer, J., 2024, Rare Earth Elements (REE) And Other Critical Minerals In Late Cretaceous Coal And Related Strata In The San Juan Basin, New Mexico: Preliminary Observations (abstr.): Geological Society of America, Annual Meeting, https://gsa.confex.com/gsa/2023AM/top/papers/index.cgi?username=392235&password=680673&personid=227838
McLemore, V.T. and Owen, E.J., 2024, Geochemistry of critical minerals in mine wastes in New Mexico: Mining Engineering, November, p. 23-30, Geochemistry of critical minerals in mine wastes in New Mexico - November 2024, Volume 76, Issue 11 - Mining Engineering Online
McLemore, V.T. and Owen, E.J., 2024, Energy and mineral resources in the San Juan Basin area of New Mexico: Lite Geology, v. 54, p. 8-10.
McLemore, V.T. and Owen, E.J., 2025, Critical minerals in Late Cretaceous coal beds of the San Juan Basin, New Mexico New Mexico Geological Society Guidebook 72, 227-234, https://doi.org/10.56577/FFC-75.227.
McLemore, V.T., Owen, E., Badonie, M., Shaver, D., and Newcomer, J., 2024a, Rare earth elements (REE) and other critical minerals in Late Cretaceous Coal and related strata in

the San Juan and Raton Basins, New Mexico: Preliminary Observations: Society of Mining, Metallurgy and Exploration, Inc., Annual Conference, Preprint 24-78, 10 p. https://geoinfo.nmt.edu/geoscience/research/documents/145/McLemore%20et%20al%20REE%20and%20other%20CMs%20in%20Late%20Cretaceous%20coal%20and%20related%20strata%20in%20San%20Juan%20and%20Raton%20Basins%20NM%20SME%202024%20preprint.pdf, accessed April 23, 2025.

McLemore, V.T., Owen, E.J., and Newcomer, J., 2024, Critical minerals in sediment-hosted, stratabound copper deposits in the Nacimiento and Zuni Mountains, northwestern New Mexico: Preliminary results: New Mexico Geological Society Guidebook 72, p. 147-164, nmgs.nmt.edu/publications/guidebooks/downloads/74/74_p0307_p0317.pdf.

McLemore, V.T., Boakye, R., and Motlah, Z.K., 2026, Critical minerals potential of uranium deposits in New Mexico: SME preprint, 9 p., in press.

Otoo, R. McLemore, V.T., and Owen, E.J., 2025, Minimum concentrations of critical minerals for exploration—how good is good enough: SME preprint 25-058, 5 p.

Otoo, R. E., McLemore, V. T., and Owen, E. J. (2025). Minimum concentrations of critical minerals for exploration: How good is good enough? Mining Engineering, 77(8).

Owen, E.J. and McLemore, V.T., 2023, Distribution of REE in selected deposits in New Mexico: Forum on the Geology of Industrial Minerals, presentation, https://geoinfo.nmt.edu/staff/McLemore/documents/ejo.FGIM23AustinDistributionofREEinselectedNMdeposits0.1.pdf

Owen, E.J and McLemore, V.T., 2023, Mineralogy and geochemistry of heavy mineral beach-placer sandstones in New Mexico: SME Annual Conference, Preprint 24-060, 8 p., https://geoinfo.nmt.edu/geoscience/research/documents/145/Owen%20&%20McLemore%20Mineralogy%20and%20geochem%20of%20heavy%20mineral%20sandstones%20NM%20SME%202024%20preprint.pdf

Owen, E.J. and McLemore, V.T., 2024, Earth briefs: Heavy-mineral sandstones as a source of critical minerals in New Mexico: Lite Geology, v. 54, p. 4-6.

Powell, M., Guangping Xu, Mark J Rigali, Virginia McLemore, Shuya We[2] and Robert Happney, 2023, Microwave Digestion for Rare Earth Elements (REE) Quantification in Coal and Coal Ash (abstr.): Goldschmidt2023 conference, July, 2023

Powell, Matt, Xu, Guangping, Huang, Shichun, Duggan, Brian, Alexander, Benjamin, Wang, Ping, McLemore, Virginia T., Owen, Evan, Wei, Shuya, 2025, Critical Mineral Resource in Heavy Mineral Beach-Placer Sandstone Deposits in New Mexico (abstr.): Geological Society of America, Annual Conference

Shaver, D., 2023, Coal mining history of New Mexico (abstr.): Mine History Association annual meeting, Socorro, NM, June 2023, https://geoinfo.nmt.edu/staff/McLemore/documents/CoalMiningHistoryNewMexico.pdf

Shaver, D.R., McLemore, V.T., and Owen, E., 2023, **A**lteration and geochemistry of clinkers in the San Juan Basin, New Mexico (abstr.): New Mexico Geological Society, Spring meeting, https://nmgs.nmt.edu/meeting/abstracts/view.cfm?aid=2933

Shaver, D. and McLemore, V., 2024, Alteration and Geochemistry of Clinkers in the San Juan Basin, New Mexico: SME Annual Conference, Preprint 24-008, 8 p., https://geoinfo.nmt.edu/geoscience/research/documents/145/Shaver%20&%20McLemore%20Alteration%20and%20Geochemistry%20of%20Clinkers%20in%20the%20San%20Juan%20Basin%20NM%20SME%202024%20preprint.pdf

APPENDIX 3. MINING DISTRICTS IN AND SURROUNDING THE SAN JUAN AND RATON BASINS

See separate file. Data from McLemore (2017).

APPENDIX 4. LIST OF SOPS AND PLANS

See https://geoinfo.nmt.edu/staff/McLemore/REEinCoalWeb.html for copies as they are completed

Number	Name	Description
HASP	Health and Safety Plan (HASP)	Health and safety plan for field and laboratory work (https://geoinfo.nmt.edu/staff/McLemore/documents/HASP_v2.pdf)
FSP	Field Sampling Plan (FSP)	Field sampling plan (https://geoinfo.nmt.edu/staff/McLemore/documents/samplingplan_v3.pdf)
SOP 1	Data management	entering, reporting, verification, and validation of data to the database
SOP 2	Photography	procedures taking photographs in the field and laboratory
SOP 3	GPS surveying	Procedures for use of handheld GPS surveying
SOP 4	Sampling outcrops, rock piles, and drill core	field procedures for taking surface solid samples
SOP 17	Drillhole logging	procedures for drilling, logging, and sampling of subsurface samples (solids) (https://geoinfo.nmt.edu/staff/McLemore/documents/SOP17DrillholeLoggingupdated.pdf)
SOP 6	Soil paste pH and paste conductivity	laboratory procedures for soil paste pH and paste conductivity
SOP 7	Field measurements of water	field procedures for measuring water flow, pH, conductivity, alkalinity, temperature when collecting water samples
SOP 8	Surface water and seep sampling	field procedures for collecting samples of surface and seep water samples
SOP 9	Petrographic analysis	laboratory procedures for describing petrographic samples
SOP 10	Electron microprobe analyses	laboratory procedures use for analyses using the electron microprobe
SOP 12	X-ray diffraction (XRD) analyses	laboratory procedures for mineralogical analyses by x-ray diffraction (XRD)

APPENDIX 5. DESCRIPTION OF SAMPLES

See separate file.
This appendix includes detailed descriptions of samples.

APPENDIX 6. XRD FILES

See separate file.
This includes the XRD diffractograms.

APPENDIX 7. CHEMICAL ANALYSES (SOLID)

See separate file.
This appendix includes chemical analyses of the samples.

APPENDIX 8. PXRF DATA

See separate file.
This appendix includes pXRF chemical analyses of the samples.

APPENDIX 9. GEOCHEMISTRY OF WATER SAMPLES

See separate file.
This appendix includes pXRF chemical analyses of the samples.

APPENDIX 10. PARTICLE SIZE ANALYSES

See separate file.
This appendix includes chemical analyses of water samples.

APPENDIX 11. ELECTRON MICROPROBE AND ANALYSES

See separate file.
This appendix includes microprobe data.

APPENDIX 12. USGS PRODUCED WATER DATA

See separate file.
This appendix includes USGS produced water data.

APPENDIX 13. GEOCHRONOLOGY

See separate file.
This appendix includes geochronology data.

APPENDIX 14. ENDOWMENTS OF CRITICAL MINERALS IN COAL FIELDS IN THE SAN JUAN AND RATON BASINS

See separate file.
This appendix includes endowment data.

APPENDIX 15. SONOASH CEMENTITIOUS PRODUCTS MEMO

See separate file.

APPENDIX 16. ZERO WASTE COAL

See separate file.

APENDIX 17. BATCH CAPACITY TEST AND COLUMN TESTS

See separate file.